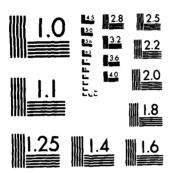
AD-A143 300 PROCEEDINGS OF THE INTERNATIONAL CONFERENCE ON RECENT ROYANCES IN STRUCTU. (U) SOUTHAMPTON UNIV (ENGLAND) INST OF SOUND AND VIBRATION RESERR. H PETYT ET R... 1984 1/5 UNCLASSIFIED

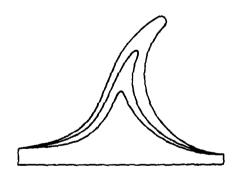


MICROCOPY RESOLUTION TEST CHART NATIONAL BUREAU OF STANDARDS-1963-A

DTIC FILE COPY



RECENT ADVANCES IN STRUCTURAL DYNAMICS



VOLUME I

DTIC APR 27 24

Approved for public release; distribution unlimited

INSTITUTE OF SOUND & VIBRATION RESEARCH UNIVERSITY OF SOUTHAMPTON

84 04 26 051

COMPONENT PART NOTICE

THIS PAPER IS A COMPONENT PART OF THE FOLLOWING COMPILATION REPORT:

Proceedings of the International Conference on Recent Advances in Structural (TITLE): _ Dynamics (2nd) held at the University of Southampton (England) on

9-13 April 1984. Volume 1.

AD#:

(SOURCE): Southampton Univ., (England) Ins. of Sound and Vibration Research

TO ORDER THE COMPLETE COMPILATION REPORT USE AD-A143 300

TITLE:

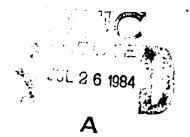
THE COMPONENT PART IS PROVIDED HERE TO ALLOW USERS ACCESS TO INDIVIDUALLY AUTHORED SECTIONS OF PROCEEDINGS, ANNALS, SYMPOSIA, ETC. HOWEVER, THE COMPONENT SHOULD BE CONSIDERED WITHIN THE CONTEXT OF THE OVERALL COMPILATION REPORT AND NOT AS A STAND-ALONE TECHNICAL REPORT.

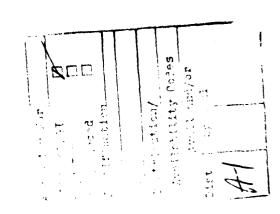
THE FOLLOWING COMPONENT PART NUMBERS COMPRISE THE COMPILATION REPORT:

run .	11166	
AD-P003 638 AD-P003 639		Wave Propagation in Circularly Curved Beams and Rings. Calculation of Natural Frequencies of Specially Orthotropic Multilayered Thin Circular Cylinders.
AD-P003 640		Dynamic Response of Layered Orthotropic Cylindrical Shells Subjected to Pressure and Axial Loadings.
AD-P003 641		Amplitude Growth in Vibrations of Arms With Increasing Length.
AD-P003 642		Seismic Stress Fields for Nuclear Elbows Using Toroidal Elasticity Theory.
AD-P003 643		Vibrational Power Transmission From a Short Source Beam to a Long Finite Receiver Beam via a Vibration Isolator.
AD-P003 6444		Prediction of Smoothed Frequency Responses Using General Orthogonal Polynomials.
AD-P003 645		Dynamic Analysis of Systems of Bars Encased in Encased in Elastic Medium.
AD-P003 646		Auxiliary Mass Doamper for Cardan Suspended Gyro.
AD-P003 647		Alleviation of Observation Spillover in Continuous Structures.
AD-P003 648		A New Beam Finite Element with Seven Degrees of Freedom at Each Node for the Study of Coupled Bending-Torsion Vibrations.
AD-P003 649		A Boundary Element Program for the Calculation of Coupled Flexure Torsion Constants for Beams of any Cross Section Shape.
AD-P003 650		A Comparative Study of Soil Spring and Finite Element Models Application to Nuclear Power Station.
AD-P003 651		Dynamic Response of Crane Structure.
AD-P003 652		State Space Approach to Mechanical Vibration.

COMPONENT PART NOTICE (CON'T)

AD#:	TITLE:	
AD-P003	653	Non-Stationary Division by the Space Time
		Finite Element Method in Vibration Analysis.
AD-P003	654	Application of the Method of Integral Equations
ADP003	4	to the Vibration of Plates.
AD-P003	222	Use of Strain Energy Density as a Basis for Finite Element Model Development.
AD-P003	646	Analysis of Dynamic Stress Characteristics of
AD-FOO5	050	Hollow Shell Type Blades.
AD-P003	657	Some Recent Advances in Dynamic Response of Shells.
AD-P003		Calculation of Eigenvalues Using Substructures
ر 100 ــــــــــــــــــــــــــــــــــ	0,0	and Dynamic Condensation.
AD-P003	659	The Improvement of Free-Mode Methods in Component
1ED-1007	4))	Mode Synthesis Techniques and Its Accuracies.
AD-P003	660	Locality Principle in Structural Dynamics.
AD-P003		Nonlinear Analysis of Plate and Shell Vibrations.
AD-P003		Nonstationary Random Response of Nonlinear
		Structures to Nonstationary Random Excitation.
AD-P003	663	Extension of Transfer Matrix Methodology to
		Nonlinear Problems.
AD-P003	664	Modal Synthesis of Large Structures with
-	•	Nonlinear Joints from Vibration Tests.
AD-P003	665	An Averaging Technique for the Analysis of
-		Oscillations in Abruptly Nonlinear Systems.
AD-P003	666	The Numerical Solution of Discontinuous
		Structural Systems.
AD-P003	667	A Finite Element Method for Nonlinear Forced
		Vibrations of Beams.
AD-P003	668	Snap-Through of Initially Buckled Beams under
		Uniform Random Pressure.
AD-P003	669	Accurate Nonlinear Equations and a Perturbation
		Solution for the Free Nonplanar Vibrations of
		Inextensional Beams.
AD-P003	670	Parametric Vibration in Large Blades Rotating in
	15.	a Gravitational Field.
AD-P003		Damped Vibrations of a Jointed Cantilever Beam.
AD-P003	0/2	The Effect of Small Clearances and Friction-Loaded
		Constraint Points on Bending Wave Energy
AD DOO:	(72	Transmission in a Long Beam.
AD-P003	013	Review of Air-Blast Response of Beams and Plates.





in down int has been approved Finding Lieuse and sale; its

SECURITY CL	ASSIFICATION	OF THIS PAGE

	D50057 50000				
	REPORT DOCUME				
1a REPORT SECURITY CLASSIFICATION Unclassified		16. RESTRICTIVE M	IARKINGS		
28. SECURITY CLASSIFICATION AUTHORITY	3. DISTRIBUTION/AVAILABILITY OF REPORT				
2b. DECLASSIFICATION/DOWNGRADING SCHED	DULE		or public r	elease; dist	ribution
		unlimited			
4. PERFORMING ORGANIZATION REPORT NUM	BER(S)	5. MONITOFING OR	IGANIZATION RI	EPORT NUMBER(S)
63. NAME OF PERFORMING ORGANIZATION	66. OFFICE SYMBOL	7a. NAME OF MONI	TORING ORGAN	IZATION	
University of Southampton	(If applicable)	Acoustics ar	nd Sonic Fa	tigue Group	
6c. ADDRESS (City, State and ZIP Code)	<u> </u>	7b. ADDRESS (City,	State and ZIP Cod	le)	
Southampton, S09 5NH		AFWAL/FIBEI			1
England		Wright-Patt	erson AFB,	OH 45433	
8e. NAME OF FUNDING/SPONSORING ORGANIZATION	8b. OFFICE SYMBOL (If applicable)	9. PROCUREMENT I	NSTRUMENT ID	ENTIFICATION NU	MBER
0. ADDOSC (Ch. Ch.) - 1710 C. (1)	<u> </u>				
8c. ADDRESS (City, State and ZIP Code)		10. SOURCE OF FUI	PROJECT	TASK	WORK UNIT
		ELEMENT NO.	NO.	NO.	NO.
	· · · - · · · · · · · · · · · · · · · ·				9
11. TITLE (Include Security Classification) Recent Advances in Structural	Dynamics, Vol I	1	ļ		
12. PERSONAL AUTHOR(S)		<u>. </u>	L		-
					1)
13a. TYPE OF REPORT 13b. TIME C Conference Proceedings FROM		14. DATE OF REPOI	RT (Yr., Mo., Day)	15. PAGE CO 392	DUNT
16. SUPPLEMENTARY NOTATION		<u> </u>		372	
No Air Force designated number	was used				
17. COSATI CODES	18. SUBJECT TERMS (C	ontinue on reverse if ne	cessary and identi	fy by block number	4
FIELD GROUP SUB. GR.					, e
	<u> </u>	_			
19. ABSTRACT (Continue on reverse if necessary and This report contains the Secon	d identify by block number	Conformed	coccodings	on Pacent Ad	vances in
Structural Dynamics held 9-13	April 1984 at t	ne Institute o	of Sound an	d Vibration	Research,
The University of Southampton,					
	K				1
					Y
					4
					,
					j
20. DISTRIBUTION/AVAILABILITY OF ABSTRAC	:T	21. ABSTRACT SECU	IRITY CLASSIE!	CATION	
					A
UNCLASSIFIED/UNLIMITED 🖳 SAME AS RPT.	LI DTIC USERS LI	Unclassifie		, 	
228. NAME OF RESPONSIBLE INDIVIDUAL		22b. TELEPHONE Nº /Include Area Co		22c. OFFICE SYME	, 1
Howard F. Wolfe		(513) 255-5229		AFWAL/FIBED	
DD FORM 1473, 83 APR	EDITION OF 1 JAN 73 I	S OBSOLETE.		ssified	
			SECURIT	Y CLASSIFICATIO	N OF THIS PAG

(2)

PROCEEDINGS OF THE SECOND INTERNATIONAL CONFERENCE ON

RECENT ADVANCES IN STRUCTURAL DYNAMICS

9-13 April, 1984

University of Southampton, England

Edited by M.Petyt and H.F.Wolfe

VOLUME 1

ORGANISATION

The Conference was organised by the

Institute of Sound and Vibration Research

in collaboration with the

Air Force Wright Aeronautical Laboratories, Wright-Patterson Air Force Base

and the

European Office of Aerospace Research and Development, London, England.

ORGANISING COMMITTEE

Local Members

Dr. M. Petyt Dr. J.K. Hammond Dr. J.G. Walker

Professor R.G. White Dr. R.J. Pinnington Mrs. M.Z. Strickland

Dr. F.J. Fahy Mr. K.T. Brown

International Members

H.F. Wolfe Professor B.L. Clarkson Mr. D.C.G. Eaton

Major J.E. Marsh Professor M. Heckl Dr. C. Mei

Colonel C.F. Fisher Professor M. Lalanne Mr. J. Soovere

Professor A.C. Nilsson

PREFACE

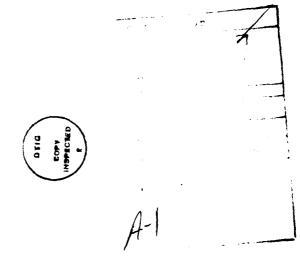
This conference follows the very successful first event in the series organised by the Institute of Sound and Vibration Research in July 1980. The second conference has support from the Air Force Wright Aeronautical Laboratories in the USA, the European Office of Aerospace Research and Development and has the continuing objective of reviewing advances which have been made in theoretical and experimental structural dynamics.

Dynamic structural analysis now benefits greatly from the availability of large computational facilities, either for theoretical work or signal processing. Most work is, however, based upon the assumption of linear behaviour, an assumption which is often not valid in practice. Although the balance of the conference is biased towards linear vibration, a section on nonlinear vibration is included which has attracted contributions on a variety of problems.

Generally, the conference papers cover a wide range of topics and it is hoped that this will stimulate discussion and promote liaison between the participants.

I hope that you enjoy the conference both technically and socially.

K.G. While



Editors' Preface

We should like to thank all authors for their contributions. Due to the high standard of the papers we accepted more than for the previous Conference. Many were suitable for more than one session. In selecting which one, we have tried to establish an interesting and well balanced programme.

Our thanks also go to the members of the organizing committees for their help in many ways.

m.Petyk. H. F. Wolfe

CONTENTS

		Page No
	1. ANALYTICAL METHODS	
1.	Wave propagation in circularly curved beams and rings C.A. Fettahlioglu and G.M. Yehodian	1
2.	Calculation of natural frequencies of specially orthotropic multilayered thin circular cylinders C.B. Sharma and M. Darvizeh	15
3.	Dynamic response of layered orthotropic cylindrical shells subjected to pressure and axial loadings O.A. Fettahlioglu and A.M. Sayed	25
4.	Amplitude growth in vibrations of arms with increasing length S. Bergamaschi, A. Sinopoli and A. Repaci	37
5.	Seismic stress fields for nuclear elbows using toroidal elasticity theory H.A. Lang	47
6.	Vibrational power transmission from a short source beam to a long finite receiver beam via a vibration isolator R.J. Pinnington	55
7.	Prediction of smoothed frequency responses using general orthogonal polynomials M.E. Gaylard	65
8.	Dynamic analysis of systems of bars encased in elastic medium S.M. Aljaweini and J.J. Tuma	73
9.	Invited paper - Transmission of waves through localized discontinuities; evaluation of two approaches G. Maidanik	83
	2. VIBRATION CONTROL	
10.	Auxiliary mass damper for Cardan suspended gyro J. Rosenberg and A. Kahana	87
11.	Alleviation of observation spillover in continuous structures A.V. Metcalse and J.S. Burdess	97

3. FINITE ELEMENT AND BOUNDARY ELEMENT METHODS

12.	A new beam finite element with seven degrees of freedom at each node for the study of coupled bending-torsion vibrations A. Potiron, D. Gay and C. Czekajski	109
13.	A boundary element program for the calculation of coupled flexure torsion constants for beams of any cross section shape C. Czekajski, D. Gay and A. Potiron	119
14.	A comparative study of soil spring and finite element models application to nuclear power station K.M. Ahmed	127
15.	Dynamic response of crane structure Chen Wei-zhang	139
16.	State space approach to mechanical vibration ${\it Hu~longwu~and~Yan~Junqi}$	151
17.	Non-stationary division by the space time finite element method in vibration analysis $C.I.\ Bajer$	161
18.	Application of the method of integral equations to the vibration of plates J. Scheuren	171
19.	Use of strain energy density as a basis for finite element model development A.H. Patel and R. Alí	179
20.	Analysis of dynamic stress characteristics of hollow shell type blades J. Thomas and S.H. Abdulrahman	189
21.	Some recent advances in dynamic response of shells R.K. Kapania and T.Y. Yang	199
	4. COMPONENT MODE SYNTHESIS TECHNIQUES	
22.	Calculation of eigenvalues using substructures and dynamic condensation N. Petersmann	211
23.	The improvement of free-mode methods in component mode synthesis techniques and its accuracies 2.W. Wang and M. Petyt	221
24.	Locality principle in structural dynamics A.K. Belyaev and V.A. Palmov	229

5. NON LINEAR ANALYSIS TECHNIQUES

25.	Invited paper - Nonlinear analysis of plate and shell vibrations A. Leissa	241
26.	Nonstationary random response of nonlinear structures to nonstationary random excitation C.W.S. To	· 261
27.	Extension of transfer-matrix methodology to non-linear problems J.W. David and L.D. Mitchell	271
28.	Modal synthesis of large structures with nonlinear joints from vibration tests L. Jezequel	281
29.	An averaging technique for the analysis of oscillations in abruptly non-linear systems R.K. Miller and M.A. Heidari	297
30.	The numerical solution of discontinuous structural systems W.K.D. Borthwick	307
	6. NON LINEAR DYNAMICS OF BEAMS	
31.	A finite element method for nonlinear forced vibrations of beams C. Mei and K. Decha-Unphai	319
32.	Snap-through of initially buckled beams under uniform random pressure P. Seide	329
33.	Accurate nonlinear equations and a perturbation solution for the free nonplanar vibrations of inextensional beams A. Luongo, G. Rega and F. Vestroni	341
34.	Parametric vibration in large blades rotating in a gravitational field A.D.S. Barr and T. Webster	351
35.	Damped vibrations of a jointed cantilever beam H. Wissbrok	361
36.	The effects of small clearances on friction loaded constrained points on bending wave energy transmission in a long beam M.J.H. Fox	373
37.	Review of air-blast response of beams and plates J. Ari-Gur. D.L. Anderson and M.D. Olson	383

7. TESTING TECHNIQUES

38.	Invited paper - Application of modal synthesis concepts to spacecraft design verification A. Bertram	395
39.	A flexible multichannel measurement system for dynamic analysis H. Van der Auweraer, P. Van Herck, R. Snoeys	415
40.	Limitations on the identification of discrete structural dynamic models A. Berman	427
41.	Foolproof methods for frequency response measurements H.G.D. Goyder	437
42.	An investigation of the behaviour of the simultaneous three axis vibration system G.K. Hobbs	447
43.	Recent experimental devices to obtain the dynamic parameters of bridges W.C. McCarthy, K.R. White and A.G. Arroyo	457
44.	The experimental measurement of flexural wave power flow in structures W. Redman-White	467
	8. MODAL AND DATA ANALYSIS OF NON LINEAR SYSTEMS	
45.	Recent advances in reduction methods in nonlinear structural dynamics S.R. Idelsohn and A. Cardona	475
46.	Feasibility of using modal analysis techniques for nonlinear multi-degree of freedom systems C. Nopporn, R. Singh and H. Busby	483
47.	Modal analysis and identification of structural non-linearity G.R. Tomlinson and N.E. Kirk	495
48.	Time domain analysis of nonlinear vibration data S.F. Masri, R.K. Miller, H. Sassi and T. Caughey	511
49.	Extended damping models for vibration data analysis J.A. Fabunmi	521
	9. NON LINEAR DYNAMICS OF PLATES	
50.	Non-stationary responses of non-linear rectangular plates during transition through parametric resonance, Part I: Theory G. Ostiguy	535

51.	Non-stationary responses of non-linear rectangular plates during transition through parametric resonance, Part II: Experiment G. Ostiguy	547
52.	Nonlinear dynamic analysis of anisotropic rectan- gular plates by a new method M. Sathyamoorthy	559
53.	Large amplitude vibration of an initially stressed bimodulus thick plate L.W. Chen and C.J. Lin	567
54.	Nonlinear multimode response of clamped rectangular plates to acoustic loading C. Mei and D.B. Paul	577
	10. RESPONSE TO SEISMIC EXCITATION	
55.	Steel fibrous concrete under seismic loading L. Minnetyan and G.B. Batson	589
56.	Inelastic analysis of short highway bridges subjected to strong ground motions M. Saiidi, J.D. Hart and B.M. Douglas	599
57.	Elastic-plastic response of rooftop frames to distributed and concentrated shock load: experimental results and predictions using a numerical technique M.S.J. Hashmi	609
	11. RANDOM VIBRATION	
58.	Invited paper - Researches in random vibration J.D. Robson	621
59.	Some closed-form solutions in random vibration of Timoshenko beams I. Elishakoff and D. Livshits	639
60.	Random vibration of discrete, periodic coupled frame-wall systems G. Oliveto and A. Santini	649
	12. ROAD VEHICLES	
61.	Dynamic analysis of vehicles with nonlinear suspension properties J.A. Lyons and L. Minnetyan	665

62.	stationary, nonlinear random vibration with particular application to the problem of vehicles on rough ground R.F. Harrison and J.K. Hammond	073
	13. RAILWAY VEHICLES	
63.	Invited paper - Dynamic modelling of railway track and wheelsets S.L. Grassie	681
64.	Two theoretical models for wave propagation in rails $\textit{W. Scholl}$	701
65.	Dynamics and stability of train-track systems R. Bogacz and K. Popp	711
66.	Assessment of the generating mechanisms and characteristics of wheel/rail noise via study of a rolling disc N.S. Ferguson and R.G. White	725
67.	On the acoustically optimal design of railway wheels H. Irretier and O. Mahrenholtz	733
	14. AEROSPACE STRUCTURES AND/OR FATIGUE	
68.	Galileo spacecraft modal test and evaluation of testing techniques Jay-Chung Chen	751
69.	Acoustic fatigue life of adhesive bonded structures subjected to acoustic loads H.F. Wolfe and I. Holehouse	765
70.	Dynamic response and acoustic fatigue of stiffened composite structures J. Soovere	777
71.	Sonic fatigue design method for the response of CFRP stiffened-skin panels 1. Holehouse	789
72.	Prediction of the dynamic properties of carbon- glass fibre sandwich hybrid laminated composites R.D. Adams, R.G. Ni and D.X. Lin	801

73.	Life time prediction based on the combined use of finite element and modal analysis data E. Verdonck and R. Snoeys	811	•
	15. MACHINERY		-
74.	Noise energy radiated from rod-like structures L.C. Chow and J.M. Cuschieri	827	•
75.	Using a scale model to investigate the post fracture structural vibrations and noise of a 200 tonne power press G. Stimpson	837	Ď
76.	Active force control in machinery noise J.M. Cuschieri	847	
77.	Modelling the relation between structural vibrations and radiated sound P. Sas, P. Vandeponseele, R. Snoeys	855	•
	16. DAMPING		*
78.	Development of the aerospace structures technology damping design guide J. Soovere, M.L. Drake, V.R. Miller and L.C. Rogers	869	, •
79.	Continuum modelling of damping in large space structures S. Abrate and C.T. Sun	879	-
80.	Determination of receptances of locally damped structures	889	

1. ANALYTICAL METHODS

WAVE PROPAGATION IN CIRCULARLY CURVED BEAMS AND RINGS

Omer A. Fettahlioglu* and Giora M. Yehodian**

*New York Institute of Technology **Polytechnic Institute of New York

1. INTRODUCTION

The first comprehensive treatment of inextensional vibrations of circularly curved beams was presented by Lamb [1] using Hamilton's principle. For other early investigations concerning the incomplete circular ring undergoing inextensional deformations reference may be made to Den Hartog [2,3] and Archer [4]. A myriad of authors have treated various aspects of the problem that no attempt will be made here to provide extensive survey. Seidel and Erdelyi [5] derived the frequency equation of a thick free ring by considering the bending, shear and extensional strain energies together with the translational and rotational kinetic energies. They calculated the frequencies by specializing their frequency equation to inextensional deformation for a free complete ring. Rao and Sundararajan [6] adopting the same procedure as was done for the Timoshenko beam [7] examined the inextensional vibrations of a free ring including the effects of shear deformation and rotatory inertia, and determined the natural frequencies of a stiffened ring. Veletsos and Austin [8] presented an analysis of the free vibrational characteristics of circular arches vibrating in their own planes. Their study which is based on Flügge's equations for cylindrical shells accounts for the extensibility of the arch axis but neglects the effects of rotatory inertia and shearing deformation. In a later paper; Austin and Veletsos [9] presented a method of analysis based on Federhofer's system of differential equations which includes the effects of rotatory inertia and shearing deformation. Their governing equations were solved numerically by a combination of a Holzer type iterative procedure and an initial value integration.

The present theory which deals with the problem in its general form has been developed previously by the first author [10] from variational considerations using Hamilton's principle to derive the exact equations of motion for thin circularly curved beams and rings, together with consistent boundary, discontinuity and initial conditions in terms of the radial and tangential midsurface displacements, and the rotation of the normal. The theory accounts for the effects of extensional, flexural and shearing deformations, and rotatory inertia. The effects of distributed elastic foundtions in the directions of the radial and tangential displacements and the rotation are also incorporated into the equations of motion.

The vibration and wave propagation analyses on which the present investigation is based properly begin with the resolution of the foregoing equations of motion into three-uncoupled sixth order homogeneous differential equations in terms of the radial and tangential midsurface displacements, and the rotation. Using the classical form for the traveling wave solution, the frequency equation is derived in closed-form, in terms of the flexural, transverse shearing and extensional stiffnesses as well as the three spring constants of the elastic foundations as precisely identifiable parameters. The frequency equation reduces to that found by Rao [6] neglecting the effects of extensibility and elastic foundations; and it coincides with Lamb's equation [1] deleting the effects of extensibility and transverse shear.

Exact solutions for the three deformations are derived from the three uncoupled homogeneous differential equations in terms of six independent

constants of integration. The response of curved beams with various end conditions (fixed-fixed and hinged-hinged) are then formulated by means of the exact deformations and stress resultants.

Exact solutions are also derived for the phase velocities of the propagating elastic waves in rings and curved beams. The governing dispersion relations are derived and illustrated in terms of short and long wave lengths, cutoff frequencies and standing waves.

With the exception of Graff [11], little attention has been given to wave propagation in rings with or without the effects of extensibility and/or shearing deformation. Dispersion curves and frequency spectra wherein the effects of curvature, extensibility and shearing deformation on the wave propagation characteristics of curved beams may be assessed, are generally not available in the literature.

2. DERIVATION OF GOVERNING EQUATIONS

A thin circular ring element (Fig. 1) that is symmetrical about the plan of its centroidal axis is considered to be deformed in the plane of its initial curvature with normals preserved in the process (Bernoulli-Euler hypothesis).

The strain of a fiber at a distance z from the centroidal axis resulting from bending of the ring accompanied by stretching of its centre line is expressed in the form

$$\varepsilon_{\theta} = \varepsilon_0 - z(\phi'/R) \tag{1}$$

where prime denotes differentiation with respect to θ and ϕ is the relative rotation of the deformed element. In accordance with the linearized strain-displacement relations of the Sanders' [12] thin-shell theory reduced to one dimension, the extensional strain of the centre line and the total rotation of the deformed element are, respectively,

$$\varepsilon_0 = (v'-w)/R$$
 and $\chi = (w'+v)/R$ (2)

The total rotation depends not only on the relative rotation of cross sections of the ring element, but also on the shear as follows:

$$\chi = (w' + v)/R = \phi + \psi \tag{3}$$

where ϕ is the relative rotation when the shearing deformation is neglected and ψ is the angular deformation due to shear at the neutral axis in the same cross section.

With the use of Hooke's law and the strain distribution defined by Eq. (1), the thrust and the bending moment become, respectively,

$$T = \iint E \epsilon_{\theta} dA = (EA/R)(v'-w)$$
 (4)

$$M = \iint E \epsilon_{\theta} z dA = -(EI/R) \phi'$$
 (5)

where, A and I are the cross sectional area and the moment of inertia of the cross section, respectively.

The shear stress resultant is given by Timoshenko in the form

$$N = kAG\psi = (kAG/R) (w'+v-R\phi)$$
 (6)

where k is the form factor for shear, depending on the shape of cross section.

For thin-ring kinematics given by (1) and the load system illustrated in Fig. 1, the tangential and radial motions are coupled, as described by the following system of differential equations which were derived in [10] using Hamilton's principle:

$$a(v'-w)+c(w''+v'-R\phi')-k_1Rw=\rho AR\ddot{w}$$

$$a(v''-w')-c(w'+v-R\phi)-k_2Rv=\rho AR\ddot{v}$$

$$bR^2\phi''+cR(w'+v-R\phi)-k_3R\phi=\rho IR\ddot{\phi}$$
(7)

The constants a, b, and c are defined as

$$a=EA/R$$
; $b=EI/R^3$; $c=kAG/R$ (8)

The dots denote differentiation with respect to time, and ρ is the mass density of the ring.

The consistent boundary conditions at each end of the curved beam are

$$c(w'+v-R\phi)=\overline{N}$$
 or $\delta w=0$
$$a(v'-w)=\overline{T}$$
 or $\delta v=0$ (9)
$$-bR^2\phi'=\overline{M}$$
 or $\delta \phi=0$

where \overline{N} , \overline{T} , and \overline{M} are the values of the stress resultants at the boundaries.

The vibration and wave propagation analyses on which the present treatise is based, properly begin with the resolution of the foregoing equations of motion (7) into three-uncoupled sixth order homogeneous differential equations. Since each of the normal modes of free vibration of a thin curved beam executes a simple harmonic motion with an associated natural frequency, the period and phase of motion are the same for all points in the curved beam. Therefore, the time dependence of the beam variables can be removed by assuming that their spatial and temporal variations are separable in the following form:

$$v(\theta,t) = V(\theta) \cdot e^{i\omega t};$$
 $w(\theta,t) = W(\theta) \cdot e^{i\omega t};$ $\phi(\theta,t) = \phi(\theta) \cdot e^{i\omega t}$ (10)

The substitution of (10) into (7) and the elimination of W,V and Φ , successively (considering the operational coefficients of the variables W,V, and Φ) with the notation of D=d/d θ , yields

$$\{D^{6} + \alpha_{1}D^{4} + \alpha_{2}D^{2} + \alpha_{3}\}V(\theta) = 0$$

$$\{D^{6} + \alpha_{1}D^{4} + \alpha_{2}D^{2} + \alpha_{3}\}W(\theta) = 0$$

$$\{D^{6} + \alpha_{1}D^{4} + \alpha_{2}D^{2} + \alpha_{3}\}\phi(\theta) = 0$$

$$(11)$$

where, in the absence of elastic foundations [13], $k_1=k_2=k_3=0$ in (7),

$$\alpha_{1} = [2 + 2\Omega Z + X\Omega Z]; \quad \alpha_{2} = [\Omega^{2} Z^{2} (1 + 2X) + \Omega (Z - XZ - 1) + 1]$$

$$\alpha_{3} = [X\Omega^{3} Z^{3} - \Omega^{2} Z^{2} (1 - X) - \Omega^{2} Z + \Omega (Z + 1)]$$
(12)

in which the measures of transverse shearing and extensional deformations respectively, are

$$X=E/kG$$
 and $Z=b/a=I/AR^2$ (13a,b)

The dimensionless circular frequency, $\boldsymbol{\Omega}$ is given in terms of dimensional circular frequency, $\boldsymbol{\omega}$ in the form

$$\widetilde{\Omega}^2 = \Omega = \omega^2 R^4 (\rho A / EI) \tag{14}$$

In the absence of the effects of shearing and extensional deformations, X=0 and Z=0, respectively, the operator in (11) reduces to the form: $\{D^6+2D^4+(1-\Omega)D^2+\Omega\}$ which, then, coincides with the statics solution given in [10] for $\Omega=0$.

3. SOLUTION FOR FREE RING

The normal modes of a complete ring in the form

$$W(\theta) = A_1 \exp(-in\theta); \ V(\theta) = A_2 \exp(-in\theta); \ \Phi(\theta) = A_3 \exp(-in\theta)$$
 (15)

give the frequency equation from (11) as follows:

$$\beta_1 \Omega^3 + \beta_2 \Omega^2 + \beta_3 \Omega + \beta_4 = 0 \tag{16}$$

where,
$$\beta_1 = XZ^3$$
; $\beta_2 = -[n^2Z^2(1+2X) + Z^2(1+X) + Z]$
 $\beta_3 = [n^4Z(2+X) + n^2(1+XZ-Z) + Z+1]$; $\beta_4 = -n^2(n^2-1)^2$

which reduces to the form given by Lamb [1] for the case of inextensibility (Z=0), neglecting the transverse shear effect. (16) rewritten in terms of mode number is: $n^6 - \alpha_1 n^4 + \alpha_2 n^2 - \alpha_3 = 0$.

The roots of the frequency equation (16) give the solutions of the propagating elastic waves of the following form for the vector of the deformations, v, w and ϕ

$$\tilde{\mathbf{y}} = \tilde{\mathbf{A}} \exp[\mathbf{i}(\mathbf{y}\mathbf{\tau} - \mathbf{\theta})\lambda]$$
 (17)

where, the dimensionless wave number, λ and phase velocity, γ are

$$\lambda = Rm$$
; $\gamma = \Omega^*/\lambda$ (18)

in which m is the dimensional wave number; and Ω^* is related to the dimensional circular frequency, ω as follows:

$$\Omega^* = (t/\tau)w = wR(\rho/E)^{\frac{1}{2}} = (\Omega Z)^{\frac{1}{2}}$$
 (19)

The term $(E/\rho)^{\frac{1}{2}}$ is the bar velocity. The dimensionless time, τ in terms of the dimensional time, t is chosen to be: $\tau = (t/R)(E/\rho)^{\frac{1}{2}}$. Accordingly, (16) reduces to a cubic in γ^2 or a quadratic in λ^2 , respectively,

$$\lambda^{4}(XZ)\gamma^{6} - \lambda^{2}[\lambda^{2}Z(1+2X) + Z(1+X) + 1]\gamma^{4} + [\lambda^{4}Z(2+X) + \lambda^{2}(1+XZ-Z) + Z + 1]\gamma^{2} - Z(\lambda^{2}-1)^{2} = 0$$
(20)

$$Z[X\gamma^6 - (1+2X)\gamma^4 + \gamma^2(2+X) -1]\lambda^4 - \{[1+Z(1+X)]\gamma^4$$

$$-(1+XZ-Z)\gamma^2 -2Z] \lambda^2 + [(1+Z)\gamma^2 - Z] = 0$$
 (21)

An horizontal asymptote, $\gamma = 1.0$ (bar velocity) is obtained from (21) for $\lambda \to \infty$, neglecting the shearing deformation (X=0); a second horizontal asymptote, $\gamma = X^{-\frac{1}{2}}$ (shear velocity) is also obtained from a study of the behavior of the phase velocity with respect to the wave number for various physically realistic values of X (measure of shear deformation), X>1.

4. CURVED BEAM OF GENERAL BOUNDARY CONDITIONS

The general solution of (11) in the form

$$\widetilde{\mathbf{y}}_{\mathbf{i}} = \{\mathbf{V}, \mathbf{W}, \mathbf{\phi}\}^{\mathrm{T}} = \widetilde{\mathbf{A}}_{\mathbf{i}} \mathbf{e}^{\mathrm{r}\boldsymbol{\theta}}$$
 (22)

gives the auxiliary equation

$$r^{6} + [2+\Omega Z(2+X)]r^{4} + [\Omega^{2}Z^{2}(1+2X) + \Omega(Z-XZ-1) + 1]r^{2} + [X(\Omega Z)^{3} - (\Omega Z)^{2}(1-X) - \Omega^{2}Z + \Omega(Z+1)] = 0$$
(24)

The roots of this polynomial (23) are functions of Ω ; and the elimination of the arbitrary constants from the six boundary conditions (three for each end) gives the frequency values [13]. The behavior of the roots of (23) is determined by substituting the value of Ω calculated from Lamb's "classical" inextensional solution as an upper bound [1]; the result is 3 pairs of complex-conjugate roots as follows: p_1+q_1i , p_1-q_1i , $-p_1+q_1i$, $-p_1-q_1i$, p_5+q_5i , p_5-q_5i . Therefore, the general soluton of (11) for steep arches ($\alpha > 180^{\circ}$) is of the form

 $V = \{\exp(p_1\theta)[F_1\cos q_1\theta + F_2\sin q_1\theta + F_3\theta\cos q_1\theta + F_4\theta\sin q_1\theta]\}$

+
$$\exp(p_5\theta)[F_5\cos q_5\theta + F_6\sin q_5\theta]$$
}

$$W = \{\exp(p_1\theta)[C_1\cos q_1\theta + C_5\sin q_1\theta + C_3\theta\cos q_1\theta + C_4\theta\sin q_1\theta]$$
 (24)

+
$$exp(p_5\theta)[C_5cosq_5\theta+C_6sinq_5\theta]$$
}

 $\Phi = (\exp(p_1\theta)[H_1\cos q_1\theta + H_2\sin q_1\theta + H_3\theta\cos q_1\theta + H_4\theta\sin q_1\theta]$

+
$$\exp(p_5\theta)[H_5\cos q_5\theta + H_6\sin q_5]$$
}

The eighteen constants of integration are not all independent. The conditions that insure that the equations of motion (7) are identically satisfied by the substitution of the foregoing deformations (24) by means of (10) yield after substantial algebra the admissible deformations in terms of six independent constants of integration: F_i , $i=1,\ldots,6$. The relations which connect the twelve dependent constants to the six independent constants are

$$\begin{split} & H_{1} = \{ H_{11} cosq_{1}\theta + H_{21} sinq_{1}\theta \} F_{1} \; ; \; \; H_{2} = \{ H_{12} cosq_{1}\theta + H_{22} sinq_{1}\theta \} F_{2} \\ & H_{3} = \{ H_{13} cosq_{1}\theta + H_{23} sinq_{1}\theta + H_{33}\theta cosq_{1}\theta + H_{43}\theta sinq_{1}\theta \} F_{3} \end{split}$$

$$H_{4}=\{H_{14}\cos q_{1}\theta+H_{24}\sin q_{1}\theta+H_{34}\theta\cos q_{1}\theta+H_{44}\theta\sin q_{1}\theta\}F_{4}$$
(25)

$$H_{5} = \{ H_{55} cosq_{5}\theta + H_{65} sinq_{5}\theta \} F_{5} ; H_{6} = \{ H_{56} cosq_{5}\theta + H_{66} sinq_{5}\theta \} F_{6}$$

$$C_1 = \{C_{11}\cos q_1\theta + C_{21}\sin q_1\theta\}F_1 ; C_2 = \{C_{12}\cos q_1\theta + C_{22}\sin q_1\theta\}F_2$$

$$C_3 = \{C_{13} \cos q_1 \theta + C_{23} \sin q_1 \theta + C_{33} \theta \cos q_1 + C_{43} \theta \sin q_1 \theta\} F_3$$

 $C_4 = \{C_{14} \cos q_1 \theta + C_{24} \sin q_1 \theta + C_{34} \theta \cos q_1 + C_{44} \theta \sin q_1 \theta\} F_4$

 $C_5 = \{C_{55}\cos q_5\theta + C_{65}\sin q_5\theta\}F_5 ; C_6 = \{C_{56}\cos q_5\theta + C_{66}\sin q_5\theta\}F_6 \}$

where, the coefficients of the trigonometric functions, H_{ij} and C_{ij} for i,j = 1...,6 are given in the Appendix.

For shallow arches (angular span, α <180°), the behavior of the auxiliary equation (23) is characterized by three distinct pairs of complex-conjugate roots which require some adjustments in the deformation expressions (24) pertaining to the steep region. The solution for the shallow region given in [13] is not the scope of this paper.

5. NUMERICAL ANALYSIS

Numerical results presented herein are obtained by the computer program RADA[14] which is capable of performing dynamic response analyses of rings and curved beams with general boundary conditions.

5.1 Case of a Free Ring

The variation of the normalized frequency, $\widetilde{\Omega}/\widetilde{\Omega}_C$, i.e., the ratio of the frequency determined herein to that given by Lamb [1], $\Omega_C = n^2(n^2-1)^2/(n^2+1)$, with respect to $Z = I/AR^2$, is presented in Fig. 2 and 3 for a free ring.

The frequency spectrum exhibits clearly the effects of shearing and extensional deformations over that of rotatory inertia in causing a deviation from the frequencies given by the classical formula of Lamb. This behavior is more pronounced with higher modes. An increase in the value of X = E/kG which implies that the ring is more flexible in shear, causes the natural frequencies of free rings to deviate more and more from the "classical" formula. The present results are compared with those of Rao [6] and with the experimental values of Kuhl given in [5]. The curve of variation of Ω^* = $\Omega^2 Z^2 = \omega R(\rho/E)^{\frac{1}{2}}$ versus R/t (radius to thickness ratio) for a thin ring reveals that the present results are closer to the experimental values than those of Rao, since Rao neglected the effect of extensibility. An additional advantage of the present investigation is that the two higher-branch frequencies are also obtained and presented in Table 1, which is not possible with the Rayleigh's method employed by Den Hartog [2,3] and the inextensional "classical" solution given by Lamb [1].

The variation of the phase velocity with respect to the wave number is described in Fig. 4 corresponding to two values of the measure of extensibility, Z, for a fixed value of transverse shear deformation. Both branches approach the bar velocity ($\gamma=1$) as the wave number becomes very large; however, the upper branch representing the longitudinal mode is nearly equal to the bar velocity for any wave number except in the immediate vicinity of $\lambda=0$, which corresponds to very long wave length limit. The longitudinal mode is not influenced by the change in the measure of extensibility, Z. The lower branch representing the flexural mode is extremely sensitive to a change in the measure of extensibility: decreasing Z lowers the phase velocity considerably such that for the limiting case of inextensibility (Z=0) the velocity tends to zero; thus, the flexural mode becomes insignificant and the longitudinal mode governs. When the effect of transverse shear deformation, X, is taken into account, the flexural wave (lower branch) approaches the shear velocity ($\gamma=X^{-\frac{1}{2}}$) faster as Z becomes larger. Furthermore, the longi-

tudinal mode does still approach the bar velocity ($\gamma=1$) as before; but, the propagating wave is also influenced by the shear mode which appears as the higher branch. This branch approaches the bar velocity as λ increases; however, it tends to infinity as λ tends to zero, at a much faster rate with increasing Z. Table 2 presents exact numerical results for the phase velocity corresponding to various levels of X and Z effects for numerous wave numbers.

5.2 Arches with General Boundary Conditions

The deformations (V,W, and Φ) which are the solutions of the differential equations (11) are given by (24). The stress resultants are then obtained in exact form by the substitution of (24) into (4), (5), and (6) and are presented in [13]. Arches of any boundary conditions can then be analyzed in a consistent manner accounting the combined effects of extensional and/or shearing deformations.

The boundary conditions at both edges of the fixed and two-hinged arches are: V=W= Φ =0 and V=W=M=0, respectively. These conditions yield six simultaneous homogeneous algebraic equations in terms of the frequency, the roots of the auxiliary equation (23) and the six independent constants of integration, F_i (i=1...6). The determinant of the coefficient matrix must vanish for a nontrivial solution of the boundary equations. In this analysis an upper-bound frequency is calculated from Lamb's inextensional formula, thus permitting the explicit solution of the auxiliary equation. With the assumed value of Ω and the calculated values of the roots of (23), the condition of the vanishing of the determinant is checked. By systematically varying Ω and calculating the value of the determinant, the convergence to the correct values of the natural frequencies is accomplished.

The variation of the fundamental frequency with respect to the angular span, α is exhibited in Fig. 6 for both fixed and two-hinged arches. The effects of extensibility and transverse shear are illustrated in Table 3 for the fixed arch, wherein, an increase in each of the measures of extensional and shearing deformations causes a decrease in frequencies.

Acknowledgment

The authors would like to thank Dr. Carl J. Turkstra, Chairman and Dr. Ping Chun Wang, Professor of the Department of Civil and Environmental Engineering at Polytechnic Institute of New York for their helpful discussions and support.

$\widetilde{\Omega}_1$					$\widetilde{\Omega}_2$ $(10^3$			
Х	0	.0	3	.0	0	. 0	3.	0
n Z	0.00	0.001	0.00	0.001	0.00	0.001	0.00	0.001
2	7.2	7.17	7.19	7.1	50	5	50	5
3	58.6	57.5	57.4	55.6	100	10	100	10
4	213	208	210	199	170	17	170	17
5	554	540	548	504	260	26	260	26
6	1192	1150	1175	1044	370	37	370	37

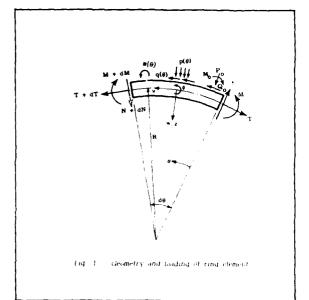
Table 2

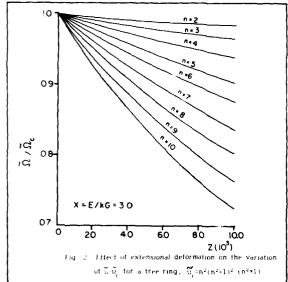
Effects of shearing and extensional deformations on phase velocities of a free ring.

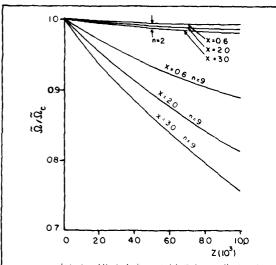
γ										
X	0.00		1.0		2.0		3.0			
λZ	10 ³	10 ²	10 ³	10 2	10 ³	10 2	10 3	10 2		
40	0.371	0.784	0.292	0.68	0.333	0.582	0.317	0.51		
80	0.625	0.93	0.554	0.82	0.494	0.662	0.45	0.56		
160	0.848	0.981	0.735	0.9	0.617	0.694	0.53	0.572		
184	0.887	0.985	0.773	0.92	0.638	0.698	0.54	0.574		

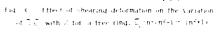
 ${\bf Table~3} \\ {\bf Effects~of~shearing~and~extensional~deformations~on~frequencies~of~fixed-arch.}$

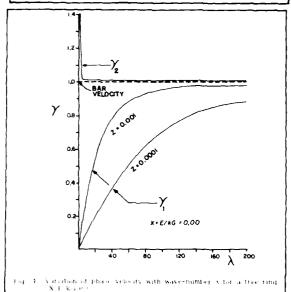
$\widetilde{\Omega}$									
α	220)°	260°						
Z	3.0	0.0	3.0	0.0					
0.000	2.451	2.452	1.43	1.44					
0.0005	2.448	2.449	1.425	1.43					
0.0007	2.446	2.447	1.424	1.43					
0.001	2.444	2.445	1.42	1.425					

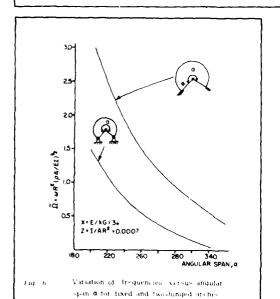


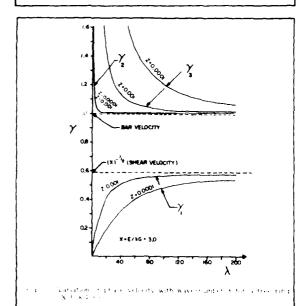












6. APPENDIX

$$\begin{split} & H_{11} = -(h_1h_3 + h_2h_4)/(h_3^2 + h_4^2); & H_{12} = (h_1h_4 + h_3h_2)/(h_3^2 + h_4^2) \\ & H_{13} = -\{1/(h_3^2 + h_4^4)\}\{(h_3/q_1 + h_4/P_1)(h_2 + h_4H_3) + h_4(h_3/P_1 - h_4/q_1)H_{43}\} \\ & H_{14} = -\{1/(h_4^2 + h_3)\}\{(h_3/P_1 - h_4/q_1)(h_2 + h_4H_4) + h_4(h_3/q_1 + h_4/P_1)H_{34}\} \\ & H_{21} = -(h_1h_4 - h_2h_3)/(h_3^2 + h_4^2); & H_{22} = -(h_1h_3 - h_2h_4)/(h_3^2 + h_4^2) \\ & H_{23} = -\{1/(h_3^2 + h_4^2)\}\{(h_4/P_1 + h_3/q_1)(h_2 + h_4H_3) + h_4(h_4/P_1 + h_3/q_1)H_{43}\} \\ & H_{24} = -\{1/(h_3^2 + h_4^2)\}\{(h_4/P_1 + h_3/q_1)(h_2 + h_4H_3) + h_4(h_4/q_1 - h_3/P_1)H_{34}\} \\ & H_{23} = -(h_1h_3 + h_2h_4)/(h_3^2 + h_4^2); & H_{34} = (h_1h_4 - h_2h_3)(h_3^2 + h_4^2) \\ & H_{33} = -(h_1h_4 - h_2h_3)/(h_4^2 + h_3^2); & H_{44} = -(h_2h_4 + h_1h_3)/(h_3^2 + h_4^2) \\ & H_{43} = -(h_1h_4 - h_2h_3)/(h_4^2 + h_3^2); & H_{44} = -(h_2h_4 + h_1h_3)/(h_3^2 + h_4^2) \\ & H_{55} = -h_{12}\{(1 + X + h_{11})(h_3 + h_3 + K) + 2h_{10}(1 + X) X P_5 q_5\} \\ & H_{56} = -h_{12}\{(1 + X + h_{11})(1 + X) h_{10} - 2X P_5 q_6 \| h_9(1 + X) + R\}\} \\ & H_{66} = -h_{12}\{2(1 + X) h_{10} X P_5 q_5 + (1 + X + X P_5^2 - X q_5^2 + X \Omega Z - 1)\{h_9(1 + X) + R\}\} \\ & H_{66} = -h_{12}\{2(1 + X) h_{10} X P_5 q_5 + (1 + X + X P_5^2 - X q_5^2 + X \Omega Z - 1)\{h_9(1 + X) + R\}\} \\ & C_{13} = -h_{13}\{P_1(C_{34} + h_7 H_{13}) - q_1(C_{43} + h_6 H_{23}) + h_8 H_{33}\} \\ & C_{14} = -h_{13}\{P_1(C_{34} + h_7 H_{13}) - q_1(C_{43} + h_6 H_{23}) + h_8 H_{33}\} \\ & C_{24} = -h_{13}\{P_1(C_{34} + h_7 H_{13}) + q_1(C_{34} + h_6 H_{23}) + h_8 H_{34}\} \\ & C_{24} = -h_{13}\{P_1(C_{34} + h_7 H_{23}) + q_1(C_{34} + h_6 H_{13}) + h_8 H_{44}\} \\ & C_{23} = -h_{13}\{P_1(C_{34} + h_7 H_{23}) + q_1(C_{34} + h_6 H_{13}) + h_8 H_{44}\} \\ & C_{24} = -h_{13}\{P_1(C_{34} + h_7 H_{23}) + q_1(C_{34} + h_6 H_{13}) + h_8 H_{44}\} \\ & C_{24} = -h_{13}\{P_1(C_{34} + h_7 H_{23}) + q_1(C_{34} + h_6 H_{13}) + h_8 H_{43}\} \\ & C_{24} = -h_{13}\{P_1(C_{34} + h_7 H_{23}) + q_1(C_{34} + h_6 H_{13}) + h_8 H_{43}\} \\ & C_{35} = -h_{15}\{q_5(1 + h_9 H_5 + h_1 h_6 + h_2 h_9 + q_1 (h_1 h_3 + h_2 h_4) + P_1 R(h_1 h_4 -$$

 $\begin{array}{l} h_8 = 2XZR(q_1^2 + P_1^2); \ h_9 = R\{XZ(P_5 - q_5 + \Omega Z) - 1\}; \ h_{10} = 2P_5q_5XZR \\ h_{11} = X(P_5 - q_5 + \Omega Z) - 1; \ h_{12} = (1/\{(h_9 + h_9X + R)^2 + (1 + X)^2 h_{10}^2)\} \\ h_{13} = \{1/(P_1^2 + q_1^2)\}; \ h_{14} = 1/\{(X + 1)(P_1^2 + q_1^2)(c^2 + d^2)\}; \ h_{15} = 1/(P_5^2 + q_5^2) \end{array}$

7. REFERENCES

- 1. H. LAMB 1889 Proceedings of the London Mathematical Society, Vol. XIX, pp 365-376. On the Flexure and Vibrations of a Curved Bar.
- 2. J.P. DEN HARTOG 1928 Journal of Applied Mechanics, TRANS. ASME, Vol. 50, APM-50-6. Vibrations of Frames of Electrical Machines.
- 3. J.P. DEN HARTOG 1928 Journal of Applied Mechanics, TRANS. ASME, Vol. 50, APM-50-11. Vibrations of Frames of Electrical Machines.
- 4. R.R. ARCHER 1960 Int. Journal Mech. Sciences: Pergamon Press Vol. 1, pp. 45-56. Small Vibrations of Thin Incomplete Circular Rings.
- 5. B.S. SEIDEL and E.A. ERDELYI 1964 Journal of Engineering and Industry, TRANS. ASME, Series B, Vol. 86, pp. 240-244. On the Vibration of a Thick Ring in Its Own Plane.
- 6. SS. RAO and V. SUNDARARAJAN September, 1969 Journal of Applied Mechanics, Design, Data, and Methods, TRANS. ASME, pp. 620-625. In-Plane Flexural Vibrations of Circular Rings.
- 7. S. TIMOSHENKO 1921 Philosophical Magazine, Series 6, Vol. 41, pp. 744. On the Correction Shear of the Differential Equation for Transverse Vibration of Prismatic Bars.
- 8. A.S. VELETSOS and W.J. AUSTIN April, 1972 Journal of the Engineering Mechanics Division, ASCE, Vol. 98, No. EM2, Proc. Paper 8806, pp. 311-329. Free In-Plane Vibration of Circular Arches.
- 9. W.J. AUSTIN and A.S. VELETSOS August, 1973 Journal of the Engineering Mechanics Division, ASCE, No. EM4, Proc. Paper 9913, pp. 735-753. Free Vibration of Arches Flexible in Shear.
- 10. O.A. FETTAHLIOGLU and T.K. STEELE May 19-23, 1980 Proceedings of the Fourth International Conference on Pressure Vessel Technology, Vol. II, Paper No. C85/80, pp. 185-192. Thermal Deformations and Stresses in Circularly Curved Thin Beams and Rings.
- 11. K.F. GRAFF 1971 International Journal of Mech. Sciences: Pergamon Press, Vol. 13, pp. 107-111. On Dispersion of Elastic Waves in Rings.
- 12. J.L. SANDERS 1963 Q. Appl. Math., pp. 21-36. Nonlinear Theories of Thin Shells.
- 13. G.M. YEHODIAN 1984 Engineer's Thesis, Polytechnic Institute of New York. A Treatise on In-plane Vibrations and Elastic Propagating Waves in Rings and Curved Beams.
- O.A. FETTAHLIOGLU and G.M. YEHODIAN 1983 New York Institute of Technology - Ring and Arch Dynamic Analysis (NYIT-RADA).





CALCULATION OF NATURAL FREQUENCIES OF SPECIALLY ORTHOTROPIC MULTILAYERED THIN CIRCULAR CYLINDERS

C. B. Sharma and M. Darvizeh

University of Manchester Institute of Science and Technology Manchester M60 1QD

INTRODUCTION

AD-P003 639 It is of great technical importance to investigate the dynamic characteristics of thin walled circular cylindrical shells with some complicating parameters because of their use as basic elements in modern lightweight structures. It is immensely useful to obtain the natural analytical frequencies for specially orthotropic multilayered cylindrical shells serving as complete structures or structural components. In the recent past many new areas in this field have been explored [1] and as such the dynamic response of such composite materials and structures will continue to be of considerable interest in the industrial applications.

Previous analyses of this problem were mainly confined to the simply supported boundary conditions e.g. Dong [2], Bert et al [3], Stavsky and Lowey [4], Greenberg and Stavsky [5] etc., owing, perhaps, to the computational complexity) The procedures employed were also not so easy to handle as regards calculation of vibration characteristics in general and natural frequencies in particular. It is the main aim of this paper to present a simple theoretical analysis for determining the natural analytical frequencies of thin walled circular cylindrical shells with layers of homogeneous isotropic or specially orthotropic material symmetrically situated about the shell mid-surface with a variety of end conditions viz: clamped-free, clamped-supported, clamped-clamped etc. The theory governing the response is based on the Love-Timoshenko hypothesis regarding deformation and is capable of handling a shell structure comprised of an arbitrary number of thin bonded layers which can have different thicknesses and elastic material properties.[6].

The procedure adopted for the solution of governing equations is a simple one. It is an application of the Rayleigh-Ritz approximate variational procedure. Various boundary conditions are incorporated via the approximation of the longitudinal modal forms by the characteristic functions of a vibrating beam. These functions were successfully used by one of the authors in dealing with the vibration characteristics of isotropic thin circular cylinders [7]. Procedure yields a cubic frequency equation. Out of the three roots of this cubic (which is solved exactly) two are several orders higher that the third one and are not of any immediate practical interest. For various reasons the lowest or fundamental natural frequency of the structure and the mode (or modes) associated with it, are usually of most interest to the analyst and the designer.

An extensive computer exploration is carried out for natural frequencies for various shell geometrical and material parameters. To ensure a check on the validity of the present analysis and its computational implementation the case of free vibration characteristics of homogeneous isotropic cylinders is deduced as a particular case of the anlaysis given in this paper. The results obtained thus are compared with the results of previous analytical $[\delta]$ and experimental [9] investigations and it was found that the two sets of analytical results were identical and agreed very well with the observed results for the boundary conditions considered. Calculations are also carried out for threelayered orthotropic plywood shells and sandwich shells with the inner and outer layer made of steel and the middle layer of a solid plywood board. Graphical

illustrations of these and various other results are given for various boundary conditions.

2. THEORETICAL CONSIDERATIONS

The formulation is on the basis of a thin shell theory with axial and circumferential co-ordinates represented by x and θ respectively. The deformation of shell reference surface is expressed in terms of displacements u, v, w in the axial, circumferential and radial directions respectively, with positive normal direction outwards. Using Timoshenko-Love theory, the strain components ϵ_{x} , ϵ_{θ} , $\gamma_{x\theta}$ and the changes of curvature κ_{x} , κ_{θ} and $\kappa_{x\theta}$ are given as

$$\varepsilon_{x} = \varepsilon'_{x} + z\kappa_{x}$$
, $\varepsilon_{\theta} = \varepsilon'_{\theta} + z\kappa_{\theta}$, $\gamma_{x\theta} = \gamma'_{x\theta} + 2z\kappa_{x\theta}$

where

$$\begin{split} \varepsilon_{x}^{\dagger} &= \partial u/\partial x, \quad \varepsilon_{\theta}^{\dagger} &= (1/a) \; (\partial v/\partial \theta + w), \quad \gamma_{x\theta}^{\dagger} &= \partial v/\partial x + (1/a)\partial u/\partial \theta \\ \kappa_{x}^{\dagger} &= \partial^{2} w/\partial x^{2}, \quad \kappa_{\theta}^{\dagger} &= (1/a^{2}) \; (\partial^{2} w/\partial \theta^{2} - \partial v/\partial \theta), \\ \kappa_{x\theta}^{\dagger} &= (1/a) \; (\partial^{2} w/\partial x \partial \theta - \partial v/\partial x) \end{split}$$

and a is the shell radius.

2.1 Expressions for strain and kinetic energies

The general forms of the strain energy U and the kinetic energy T for laminated orthotropic cylindrical shells are given as in reference [2].

$$U = \frac{1}{2} \int_{0}^{L} \left[A_{11} \varepsilon_{x}^{'} + 2A_{12} \varepsilon_{x}^{'} \varepsilon_{\theta}^{'} + A_{22} \varepsilon_{\theta}^{'} + A_{66} \gamma_{x\theta}^{'} \right]^{2} + 2B_{11} \varepsilon_{x}^{'} \kappa_{x}$$

$$+ 2B_{12} (\varepsilon_{x}^{'} \kappa_{\theta} + \varepsilon_{\theta}^{'} \kappa_{x}) + 2B_{22} \varepsilon_{\theta}^{'} \kappa_{\theta} + 4B_{66} \gamma_{x\theta}^{'} \kappa_{x\theta}$$

$$+ D_{11} \kappa_{x}^{2} + 2D_{12} \kappa_{x} \kappa_{\theta} + D_{22} \kappa_{\theta}^{2} + 4D_{66} \kappa_{x\theta}^{2} \right] \text{ ad}\theta dx \qquad (2)$$

and

$$T = \frac{1}{2} \int_{0}^{2\pi} \int_{0}^{L} \rho_{T} [\dot{u}^{2} + \dot{v}^{2} + \dot{w}^{2}] \text{ ad}\theta dx$$
 (3)

where the shell stiffnesses $A_{i,j}$, $B_{i,j}$, and $D_{i,j}$ are defined as

$$(A_{ij}, B_{ij}, D_{ij}) = \sum_{k=1}^{n} Q_{ij}^{(k)} ((h_k - h_{k-1}), \frac{1}{2} (h_k^2 - h_{k-1}^2), \frac{1}{3} (h_k^3 - h_{k-1}^3))$$

$$\frac{1}{3} (h_k^3 - h_{k-1}^3)$$
(4)

and L being the shell length and $\rho_{\, T}$ the mass density per unit of surface area, i.e.

$$\rho_{\rm T} = \int \rho(z) dz = \sum_{k=1}^{n} \rho_{\rm T}(h_k - h_{k-1}).$$
 (5)

In equations (4) and (5) h_k and h_{k-1} are the distances measured from the reference surface to the outer and inner surface of the kth laminate respectively and $Q_{ij}^{(k)}$ are the elastic moduli of the k'th laminate.

2.2 Modal forms and variational formulation

It is reasonable to suppose that the modal forms of cylindrical shells are periodic in the circumferential direction and have a harmonic time dependence of frequency ω . Hence one can postulate that a general relation for the displacements u, v, w can be written in the form

(u, v, w) =
$$(A\phi'_{m}(x) \cos p\theta, B\phi_{m}(x) \sin p\theta, C\phi_{m}(x) \cos p\theta)$$
 (6)

where $\phi_m(x)$ represents unknown axial mode function, dash denotes differentiation with respect to the argument and A, B, C are amplitude coefficients.

Upon substitution of modal forms (6) into the energy expressions (2) and (3) and applying Rayleigh-Ritz variational procedure, one obtains as a consequence a homogeneous system of linear simultaneous equations for the generalised amplitude coefficients A, B and C. Condition for the existence of a non-trivial solution set for this system (i.e. letting the determinant of the coefficient matrix vanish) one obtains a cubic equation in the frequency parameter $\Delta(=\omega)$ as

$$\det [a_{i,j}] = 0$$
, $i, j = 1.2.3$ (7)

where a. = c.; + $\alpha\Delta\delta_{ij}$, δ_{ij} being the Kronecker delta and the parameter α =- $\rho_T a^2 N_m^2 I_2$ (an expression involving integral of the characteristic orthogonal functions $\phi_m(x)$) for the first row and $\rho_T a^2$ for the second and third rows of the symmetric matrix $[a_{ij}]$. The expression for the matrix elements c. are given as follows:

$$c_{11} = N_{m}^{2} (a^{2}N_{m}^{2} A_{11} + p^{2}I_{2}A_{66})$$

$$c_{12} = pN_{m}^{2} \{I_{1}(aA_{12} - B_{12}) - I_{2}(aA_{66} - 2B_{66})\}$$

$$c_{13} = N_{m}^{2} \{I_{1}(aA_{12} - p^{2}B_{12}) + a^{2}N_{m}^{2} B_{11} + 2p^{2}I_{2}B_{66}\}$$

$$c_{22} = (p^{2}/a^{2})\{a^{2}A_{22} - 2a B_{22} + D_{22}\} + N_{m}^{2} I_{2}\{a^{2}A_{66} - 4aB_{66} + 4D_{66}\}$$

$$c_{23} = (p/a)(aA_{22} - B_{22}) - a(p^{3}/a^{3})(aB_{22} - D_{22})$$

$$+ pN_{m}^{2} \{aI_{1}(aB_{12} - D_{12}) - 2I_{2}(aB_{66} - 2D_{66})\}$$

$$c_{33} = A_{22} + N_{m}^{2} \{2I_{1}(aB_{12} - p^{2}D_{12}) + a^{2}D_{11} + 4p^{2}I_{2}D_{66}\}$$

$$- (p^{2}/a^{2})(2aB_{22} - p^{2}D_{22}).$$
(8)

Here N 's represent the eigenvalue properties of the characteristic functions $\phi_m(x)$ and integrals I and I involving these functions and their derivatives (with respect to the argument) are given by

$$I_{1} = (1/L) \int_{0}^{L} \phi_{m}^{*}(x) \phi_{n}(x) dx \cdot I_{2} = (1/L) \int_{0}^{L} \phi^{*2}(x) dx.$$
 (9)

The cubic equation (7), for each pair of axial and circumferential wave numbers m and p respectively, gives three roots for the frequency parameter, Δ , that correspond to motion that is predominantly radial, axial or circumferential.

Since the radial frequency is much lower that the other two, and as most shell vibrations include radial excitation, it is the lowest of the frequency triplet that is of most structural interest both to the analyst and the designer.

2.2 Special case of an isotropic cylinder

Free vibration analysis of istotropic cylindrical shells is deduced as a particular case of the foregoing analysis for a laminated orthotropic shell. Following the usual notations and defining

$$(A_{ij}, B_{ij}, D_{ij}) = \int_{-h/2}^{h/2} (1, z, z^2) Q_{ij} dz$$
 (10)

with

$$Q_{11} = Q_{22} = E/(1-v^2), Q_{12} = Ev/(1-v^2), Q_{66} = E/2(1+v)$$
 (11)

and

$$\rho_{\rm T} = \begin{cases} h/2 \\ \rho \, dz = \rho h \end{cases} \tag{12}$$

the foregoing analysis is reduced to one for the special case of an isotropic cylinder.

2.3 Boundary conditions

The choice of axial modal forms $\phi_m(x)$ is made to satisfy a prescribed set of end conditions. To approximately achieve this the characteristic functions of a vibrating beam are introduced in a general form

$$F_{m}(N_{m}x) = \cosh N_{m}x - \cos N_{m}x - cm \left(\sinh N_{m}x - \sin N_{m}x\right)$$
 (13)

where the properties and the numerical values of these functions and the associated parameters N and c are found tabulated in reference [10] for various end conditions. For the three sets of boundary conditions considered here, viz, clamped-free, clamped-supported and clamped-clamped, $\phi_m \equiv F_m$ and $\phi^*_m \equiv N_m F^*_m$ are to be taken in equation (6). It may, however, be remarked that these general form choices for the axial mode function ϕ_m in equation (6) are satisfactory within certain limitations inherent in the variational procedure.

The values of the integrals I_1 and I_2 given in equation (9) are of immense interest when ϕ_n 's are represented by the characteristic beam functions given by equation (13). These have been calculated [11] and the expressions for I_1 and I_2 corresponding to various end conditions can be found in reference [7].

3. RESULTS AND DISCUSSION

The discussion of numerical results of multi-layer specially orthotropic thin cylinders with clamped-free, clamped-supported and clamped-clamped edges is presented in what follows. The results are given in graphical forms.

3.1 Clamped-free cylinders

To start with cantilever cylindrical shells are to be analysed. As indicated $\phi_m \equiv F_m(N_m x)$ is taken in here and appropriate values of characteristic parameters given in [10] are used.

3.1.1 Homogeneous isotropic case

This problem has received ample attention and it is also not the main aim of the present paper. But to ensure a check on the validity of the present analysis and its computational implementation the case of free vibration characteristics of homogeneous isotropic cylinders is deduced following the procedure given in the section 2.2. The results of frequency variation with the circumferential wave number, p are illustrated in the Figure 1 for a given shell whose geometrical and material parameters are listed on the Figure 1 itself. Three different curves correspond to first three axial modes (m=1,2,3) and follow the well known pattern of a frequency increase with an increase in the axial wave number, m. For a fixed axial wave number, the natural frequency vs circumferential wave number curve normally contains a dip which is due to the decrease in membrane part and the increase in bending part of the strain energy as p is increased. The lowest values of the frequency for m≈1,2 and 3 correspond to p=5,8 and 10 respectively. The agreement with the experimental results of reference [9], which are shown as broken lines (m=1,2), is apparently very good. It can thus be inferred that the homogeneous isotropic cases can be directly deduced from the general case.

3.1.2 Three-layered orthotropic case

Figure 2 analyses a three layered orthotropic ply-wood shell (geometrical and material parameters given on the Figure 4). Frequency vs circumferential wave number curves are again drawn for m=1,2,3. The pattern is similar to that displayed in the previous Figure. As would be expected, lowest frequencies and the corresponding p-values are different from the previous case. By taking zero the inner and outer layer thicknesses a shell made of solid wood board can be analysed. These particular kind of shells were considered because the material property data was easily available.

Natural frequencies of a sandwich type of three-layered cylindrical shell, consisting of inner and outer steel layers and the middle layer made of plywood, are plotted with the circumferential wave number, p in Figure 3 where all the relevant geometrical and material properties are also listed. The minimum frequencies for the axial modes m=1,2,3 correspond to p=2,3,4 respectively. Since the parameters are arbitrary so these can be chosen by the user to the necessary advantage.

Figure 4 shows a logarithmic plot of frequency against the dimension-less geometrical parameter $\lambda (= Lh^{\frac{1}{2}} h_{\overline{2}})$ for several values of $p \ge 1$ and m=1,2,3. Clearly the minimum frequency always occurs for m=1. Modal behaviour of a cylindrical shell consists of looking at the minimum natural frequency (which is the envelope of frequency curves drawn for constant values of p). Each value of p provides one member of a festoon like family of curves. Each curve takes its turn to provide the lowest member of the family over a particular range of values of λ , and indeed it adopts this special role precisely in its transition region, where the bending and stretching effects are of the same order. Also it is clear from looking at the frequency envelope that the fundamental natural frequency decreases with increasing λ , with all other parameters remaining the same. These frequency envelopes are similar to those drawn by Forsberg [12]. But it should be noted in particular that non-dimensional geometrical parameter, λ , used here is more useful measure of the length (see for example [13]) than the dimension-less ratios l/a and a/h used in [12] separately. important point brought out clearly by the Figure 4 (as in [14]) is that the circumferential mode number p corresponding to the fundamental mode depends strongly on the shell geometry, i.e. on the value of the dimension-less group

3.2 Clamped-supported cylinders

In Figures 5-7 variation of frequency against the circumferential wave number is plotted for clamped-supported shells and pattern of these graphs is similar to those in Figures 1-3 for the clamped-free case. Figure 5 deals with a three-layered isotropic cylinder (geometrical and material parameters are listed in the Figure). As can be seen that lowest frequency for the first three axial modes m=1,2,3 correspond to p=9,11,13 respectively. Figure 6,7 correspond to the same shell parameters as Figures 2,3 respectively. Overall natural frequencies are a little exaggerated because of the end x=L being supported (amounting to the introduction of a const.aint) rather than free as in the previous case. This point is also brought out clearly by comparing the Figure 5 for a clamped-supported shell with its counterpart Figure 4 for a clamped-free shell (all the parameter being identical). Overall pattern of the Figure 6 is the same as that of Figure 4.

3.3 Clamped-clamped cylinders

Figures 9-11 depict the behaviour pattern of natural frequencies against the circumferential wave number, p for a shell clamped at both the ends and these can now be compared with their counterparts given by the Figures 5-7 respectively. It is found that all other parameters being the same, the frequencies in a clamped-clamped case are a little higher than the corresponding frequencies in a clamped-supported or indeed for a clamped-free case. Figure 12 has the identical parameters to the Figures 4 and 6. Frequency envelopes made by festoon type of curves also emphasize the point that the frequencies for a clamped-clamped case are higher either than that for a clamped-supported or a clamped-free case, all shell parameters being identical.

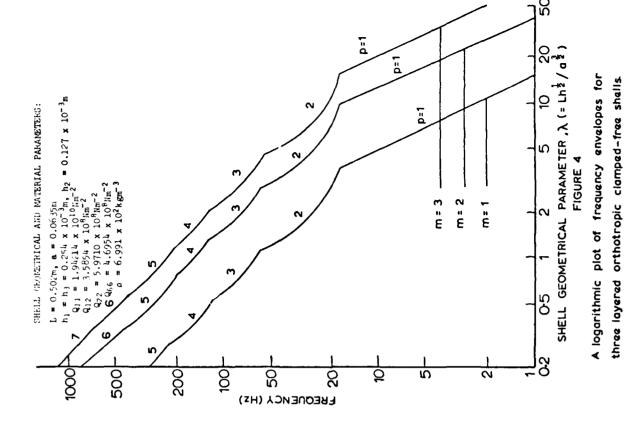
Comparing the groups of Figures 5 and 9; 2, 6 and 10; and 3, 7 and 11 who have identical shell parameters, it can be seen that for sufficiently high circumferential wave numbers the influence of change in the boundary conditions at the end x=L is not felt and the frequency parameters are more or less equal to each other in that region for the various groups.

4. CONCLUDING REMARKS

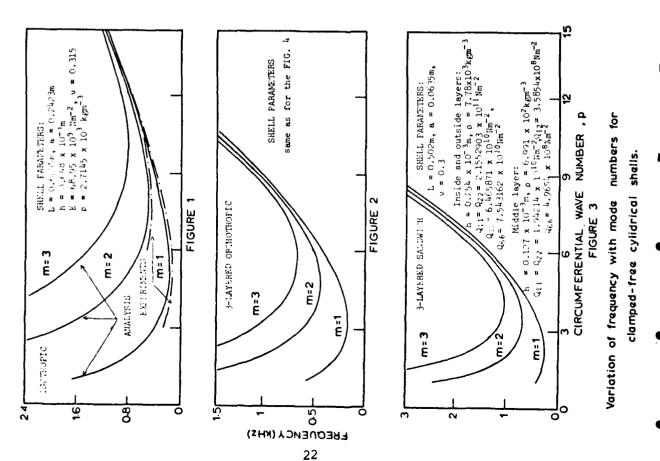
The dynamic response of laminated specially orthotropic thin circular cylindrical shells is analysed based on Timoshenko-Love theory by the use of Rayleigh-Ritz variational procedure. The approach is simple and straightforward and provides a powerful tool to calculate the natural frequencies for a variety of boundary conditions viz clamped-free, clamped-supported, clamped-clamped etc. Paper also studies the influence of boundary conditions on the modal behaviour of cylindrical snells. An example of isotropic cylinder is studied as a particular case of the present analysis which yielded results which agreed well with some existing experimental results. Similar comparision was not possible for orthotropic cylinuers because of non-availability of previous results for the boundary conditions considered. Although available shell parameters were used but the analysis is capable of handling all sorts of shell geometrical and material parameters. The main aim of the paper has been to give the designer a simple useful predictive tool for the natural frequency of such shells with a variety of boundary conditions. Computer time required is minimal because it only needs solution of a cubic to calculate matural frequencies. It is hope; that this paper will provide a small step in the direction of problem solution in this area because of the easy adaptability of the method discussed.

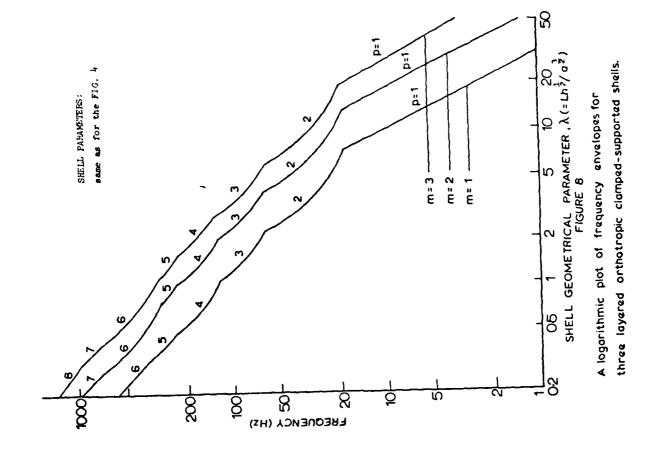
REFERENCES

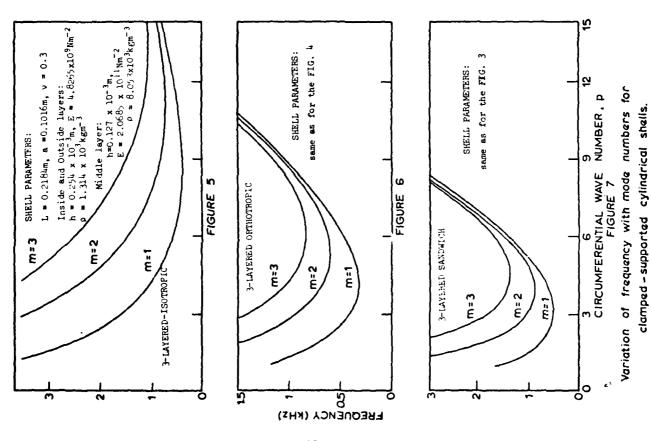
- 1. A.W. LEISSA 1973 Vibration of Shells. NASA SP-288.
- 2. S.B. DONG 1968 Journal of Acoustical Society of America 44, 1628-1635. Free Vibration of laminated orthotropic cylindrical shells.
- 3. C.W. BERT, J.L. BAKER and D.M. EGLE 1969 Journal of Composite Materials 3, 480-490. Free vibrations of multilayer anisotropic cylindrical shells.
- 4. Y. STAVSKY and R. LOWEY 1971 Journal of Sound and Vibration 15, 235-256. On Vibrations of heterogeneous orthotropic cylindrical shells.
- 5. J.B. GREENBERG and Y. STAVSKY 1980 Acta Mechanica 36, 15-29. Buckling and vibration of orthotropic composite cylindrical shells.
- 6. M. DARVIZEH 1983 M.Sc. Dissertation, University of Manchester. Natural frequencies of laminated orthotropic thin circular cylinders.
- 7. C.B. SHARMA 1980 Recent Advances in Structural Dynamics 1, 61-72, ISVR, University of Southampton. An analytical vibration study of thin circular cylinders.
- 8. C.B. SHARMA 1974 Journal of Sound and Vibration 35, 55-76. Calculation of natural frequencies of fixed-free circular cylindrical shells.
- 9. J.L. SEWALL and E.C. Naumann 1968 An Experimental and Analytical Study of Thin Cylindrical Shells With and Without Longitudinal Stiffeners NASA TND-44705.
- 10. D. YOUNG and R.P. FELGAR JR 1949 Tables of Characteristic Functions Representing Normal Modes of Vibration of a Beam. University of Texas Publication N.4913.
- 11. C.B. SHARMA 1978 Journal of Sound and Vibration <u>56</u>, 475-480. Calculation of integrals involving characteristic beam functions.
- 12. K. FORSBERG 1964 AIAA Journal 2, 2150-2157. Influence of boundary conditions on the modal characteristics of thin cylindrical shells.
- 13. C.R. CALLADINE 1982 Journal of Sound and Vibration, <u>82</u>, 345-369. Natural frequencies of cooling tower shells.
- 14. C.R. CALLADINE 1982 Theory of Shell Structures. Cambridge University Press.

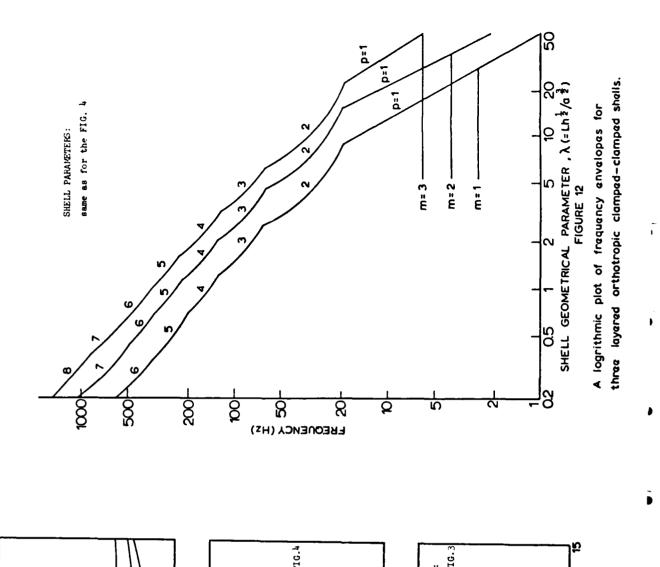


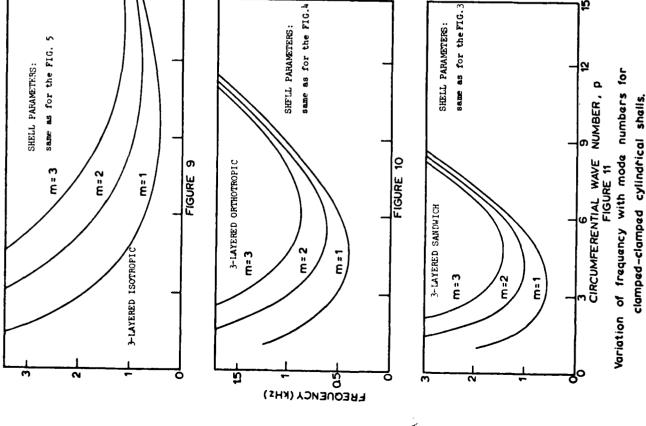
Ì













DYNAMIC RESPONSE OF LAYERED ORTHOTROPIC CYLINDRICAL

SHELLS SUBJECTED TO PRESSURE AND AXIAL LOADINGS

O.A. Fettahlioglu* and A.M. Sayed**

New York Institute of Technology* and Polytechnic Institute of New York**

1. INTRODUCTION

This paper presents a study of the dynamic response of layered orthotropic cylindrical shells subjected to uniform pressure and/or axial loading, accounting for the influence of the change in the meridional slope (the so-called pressurization effect), the transverse shear deformation and the rotatory inertia.

Earlier analytical efforts were restricted to cylindrical shells either considering a single-layer orthotropic construction or excluding some of the above-mentioned effects. Mirsky obtained solutions in terms of infinite series for the axisymmetric vibrations of single-layer, orthotropic cylinders neglecting the effect of pressurization [1, 2]. Dong formulated the problem of the free vibration of laminated orthotropic cylindrical shells in terms of second-order, partial differential equations involving the three orthogonal displacements as dependent variables; however, he did not consider the effects of pressurization, rotatory inertia or the transverse shear deformation. He obtained closed-form solutions for frequencies of the free vibration of simply-supported cylindrical shells and presented an iterative procedure for the case of general boundary conditions [3]. In a later paper [4], Dong showed the determination of the frequencies of axisymmetric and asymmetric vibrations of laminated, orthotropic shells of revolution by the finite-element method. Dym studied the effects of pressurization and of deletion of the in-plane inertia on the vibrations of a single-layer orthotropic cylindrical shell, but he neglected the effect of transverse shear deformation, [5]. Penzer and Kraus presented an exact solution for the free vibration of single-layer orthotropic shells having arbitrary boundary conditions, considering the effects of normal pressure, axial load, rotation including the centrifugal and coriolis forces and torque [6]. Their solution does not account for the layered orthotropic construction and the transverse shear deformation. Bert and Chen [7] presented an analysis for the propagation of free harmonic waves in fluid conveying, single-layer cylindrical shells of orthotropic material by placing emphasis upon the difference between the behavior of pipe constructed of fiber glass-epoxy composite material and that of steel pipe, neglecting the transverse shear deformation. In a later paper [7], Bert and Chen extended the shear deformable analog of Sanders' theory to cylindrical shell vibration accounting for bending-stretching coupling. Thus, in this investigation, this coupling is also included as the arbitrarily prescribed orthotropic shell element is considered. The analysis is presented in much more detail in [8, 9, 10 and 11], in which asymptotic solutions for the static stress and deformation in orthotropic shells of revolution including thermal loading, stability and the extension to wave propagation are also treated.

In this treatise, the governing equations of motion for the axisymmetric vibrations of thin, orthotropic layered cylindrical shells are obtained from those for general nonhomogeneous shells of revolution given in [8, 11] by specializing them to the cylindrical shell geometry. The equations of motion of the orthotropic cylinder herein are obtained in terms of a new system of six coupled first-order partial differential equations, accounting the influence of the change in the meridianal slope (the pressurization effect), the transverse shear deformation and the rotatory inertia. The fundamental dependent variables, in terms of which the equations of motion are presented, are taken as those quantities that appear in the appropriate boundary conditions of the classical theory on an axisymmetric circular edge. The governing equations of motion are in such form that no derivatives of the shell or orthotropic material

properties appear in the coefficients of these equations.

The system of equations is cast into a vector equation involving only one derivative with respect to the space variable, the dimensionless arclength, providing a substantial mathematical reduction. The form of the vector equation is such that the asymptotic and stepwise integration techniques are directly applicable to their solution.

The frequency equation of the simply supported orthotropic layered cylindrical shell with properties varying through the wall thickness but remaining constant along the meridian is derived in exact closed-form accounting for the effects of pressurization and shearing deformation. This frequency equation is a sixth degree polynomial in Ω including all the effects, and reduces to a fourth degree polynomial in Ω neglecting the effect of transverse shear deformation. In the limiting case of a single-layer isotropic cylinder without the pressurization effect, the frequency equation reduces to that given by Steele [12].

The variation of the natural frequencies is also treated by considering the order of magnitude of the terms in the frequency equation, associated with a large parameter introduced into the coefficients of the equations of motion. The approximate solutions are then obtained in closed-form by grouping the frequencies into regions of membrane wave, bending wave and a transition region from membrane to bending wave. These solutions which are quite accurate for thin cylinders, are relatively simple and in compact form, enabling the frequency analysis using a pocket computer. The numerical results confirm that the present approximate solutions are in excellent agreement with the exact solutions presented herein.

The frequency spectrum exhibited in the figures clearly indicates the fact that the pressure and/or axial loading have significant effects on the natural frequencies for both isotropic and orthotropic layered cylindrical shells. The transverse shear deformation is also seen to have a considerable effect, only, on a higher branch curve which represents the shear mode; a decrease in its value increases the frequency. The behavior of the composite shell is also significantly affected by the relative values of the various elastic constants.

2. DERIVATION OF EQUATIONS

The equations of axial, radial and moment equilibrium are [13]:

$$d/ds (rV) = -rp_{V}; \quad d/ds (rH) = N_{\theta} - rp_{H}$$

$$d/ds (rM_{\phi}) = M_{\theta} \cos\phi + rH \sin\phi - rV \cos\phi$$
(1)

where P_V and P_H are the axial and radial components of the surface loading. The compatibility equations are [13]:

$$\frac{d\chi/ds}{ds} = \kappa_{\phi}; \quad \frac{d}{ds} h = \epsilon_{\phi} \cos\phi - \chi \sin\phi + \mu/E_{\phi} t_{\phi} Q \sin\phi$$

$$\frac{dv}{ds} = \epsilon_{\phi} \sin\phi + \chi \cos\phi - (\mu/E_{\phi} t_{\phi}) Q \cos\phi$$
(2)

where χ is the rotation of the meridian, h and v are the radial and axial displacements, and E_0/μ is the equivalent transverse shear modulus.

The well known constitutive relations for a layered orthotropic shell are:

$$N_{\phi} = C_{11} \epsilon_{\phi} + C_{12} \epsilon_{\theta} + K_{11} \kappa_{\phi} + K_{12} \kappa_{\theta}$$

$$\begin{split} &N_{\theta} = C_{12} \, \varepsilon_{\phi} + C_{22} \, \varepsilon_{\theta} + K_{12} \, \kappa_{\phi} + K_{22} \, \kappa_{\theta} \\ &M_{\phi} = D_{11} \, \kappa_{\phi} + D_{12} \, \kappa_{\theta} + K_{11} \, \varepsilon_{\phi} + K_{12} \, \varepsilon_{\theta} \\ &M_{\theta} = D_{12} \, \kappa_{\phi} + D_{22} \, \kappa_{\theta} + K_{12} \, \varepsilon_{\phi} + K_{22} \, \varepsilon_{\theta} \end{split} \tag{3}$$

The typical notation is employed (See Fig. 1). For a layered shell, Fig. 2, the elastic parameters are computed from the formulas

where, F_{ij} are the elastic properties. With the kinematic relations

$$\varepsilon_{\theta} = h/r$$
 ; $\kappa_{\theta} = \chi \cos \phi / r$ (5)

and the relation: $N_{\phi} = H \cos \phi + V \sin \phi$ all the equations may be reduced to the following matrix equation for the axisymmetric deformation of the shell of revolution, in which the axial and radial motions are coupled:

$$-\frac{1}{\lambda}\frac{\partial}{\partial x} \quad y + A \cdot y + \frac{1}{\lambda^2} \quad F \cdot \frac{\partial^2}{\partial \tau^2} \quad y = 0$$
 (6)

where, λ is a large parameter and c_0 is a reference parameter

$$\lambda = [R/c_0]^{\frac{1}{2}} \text{ and } c_0 = t_0 [12(1-v_0^2)]^{-\frac{1}{2}}$$
 (7)

of the cylindrical shell of radius ${\tt R}$ and the dimensionless arclength and time are chosen to be

$$x = s/R$$
; $\tau = (t*/\lambda R) (E_o/m_o)^{\frac{1}{2}}$ (8)

in which, m_0 , E_0 , t_0 and v_0 are the reference values of the mass density, Young's modulus, the shell thickness and Poisson's ratio, respectively; t^* is the time and s is the arclength.

The vector stress and deformation quantities are

$$\mathbf{y}^{\mathrm{T}} = \begin{bmatrix} \frac{\mathsf{M}}{\mathsf{p}} & \frac{\mathsf{H}\lambda}{\mathsf{E}_{\mathsf{o}}\mathsf{t}_{\mathsf{o}}} & \frac{\mathsf{H}\lambda}{\mathsf{E}_{\mathsf{o}}\mathsf{t}_{\mathsf{o}}} & \frac{\mathsf{V}\lambda}{\mathsf{E}_{\mathsf{o}}\mathsf{t}_{\mathsf{o}}} & \frac{\mathsf{X}}{\mathsf{X}} & \frac{\mathsf{h}}{\mathsf{R}} & \frac{\mathsf{v}}{\mathsf{R}} \end{bmatrix}$$
(9)

The matrix A_{ij} is given in [8, 11]. The non-zero elements of the F matrix are

$$F_{14} = (1/12\lambda^2) (t_o/c_o)^2$$
; $F_{25} = 1$ and $F_{36} = 1$ (10)

The propagation of traveling waves is considered in the form

$$y(x,t) = \bar{y}(x) e^{i\Omega t \lambda}$$
(11)

where the dimensionless frequency, Ω is related to the circular frequency, ω as follows: $\Omega = (t*/\tau) \omega = \omega R \lambda \left(\frac{m_0}{E_0} \right)^{\frac{1}{2}}$ in which $\left(\frac{E_0}{m_0} \right)^{\frac{1}{2}}$ is the bar velocity. Then, the frequency in cycles per second is $f = (\Omega/2\pi R \lambda) \left(\frac{E_0}{m_0} \right)^{\frac{1}{2}}$.

The substitution of (11) into (6) yields

V = h = 0 at both ends.

$$-\frac{1}{\lambda} \frac{\partial}{\partial x} \bar{y} + (A - \Omega^2 F) \cdot \bar{y} = 0$$
 (12)

where \bar{y} must satisfy the end conditions. For cylindrical shells with simply supported ends $\bar{y}^T(o) = \bar{y}^T(\ell) = [0, H(\frac{\lambda}{E_0 t_0}), 0, \chi \lambda^{-1}, 0, v/R]$ which implies $M_{\phi} = \frac{1}{2} \left(\frac{\lambda}{E_0 t_0} \right)$

Exact solutions in closed-form are obtainable for orthotropic layered cylindrical shells of constant thickness and material properties along the axial direction since the coefficients of the equation (12) are constant. For simply supported ends without axial constraint, the spatial dependence in the axial direction is taken to be proportional to $\exp(-i \, m \chi \lambda)$, where m is the dimensionless wave number. The explicit form of the soluton is

$$\tilde{y} = \alpha e^{-imx\lambda}$$
 (13)

where, α is the eigenvector whose components are the amplitudes of the stress resultants and deformations. The substitution of (13) into (12) yields

$$(im\underline{I} + \underline{A} - \Omega^2\underline{F}) \cdot \underline{\alpha} = 0$$
 (14)

which is an homogeneous system of equations whose nontrivial solutions are given by the characteristic equation as follows:

$$|\operatorname{im} I + A - \Omega^2 F| = 0 \tag{15}$$

 $\underline{\alpha}$ is the corresponding eigenvector of the matrix $(\underline{A} - \Omega^2 \underline{F})$. The imaginary part of \underline{y} will satisfy the simple-support conditions at x = 0 and $x = \ell$ if $m\lambda \ell = n\pi$ for n = 1, 2, 3... Hence, $m = n\pi/\lambda \ell$.

The characteristic equation (12) takes the following form:

$$\begin{vmatrix} im & 1 & 0 & \rho R/E_{o}t_{o}c_{o} - (\Omega t_{o}/\lambda c_{o})^{2}/12 & 0 & 0 \\ (c_{o}/t_{o})B_{14} & im & B_{13}/\lambda & 0 & B_{11} - \Omega^{2} & 0 \\ 0 & 0 & im & 0 & 0 & -\Omega^{2} \\ (c_{o}/t_{o})^{2}B_{44} & 0 & (c_{o}/t_{o})B_{34}/\lambda & im & -(c_{o}/t_{o})B_{14} & 0 \\ 0 & \frac{\mu}{\lambda^{2}} & 0 & (\mu\rho/E_{o}t_{o})-1 & im & 0 \\ (c_{o}/t_{o})B_{34}/\lambda & 0 & B_{33}/\lambda^{2} & 0 & -B_{13}/\lambda & im \end{vmatrix}$$
(16)

in which t is the wall thickness, E $/\mu$ is the equivalent transverse shear modulus and ρ is the pressurization effect defined by the relation

$$\rho = V_o + p_o R/2 \tag{17}$$

The elements of B_{ij} are given in terms of the elastic parameters (4) in [8, 11].

A typical element of B_{ij} is

$$B_{11} = [\beta^{-1}(2c_{12}K_{11}K_{12} - c_{12}^2D_{11} - c_{11}K_{12}^2) + c_{22}]/E_ot_o$$

where,
$$\beta = C_{11}D_{11} - K_{11}^2$$

For the special case of a single-layer isotropic shell, B_{ij} , reduce to the following form:

$$B_{11} = 1$$
 ; $B_{12} = 0$; $B_{13} = 0$; $B_{14} = 0$
 $B_{21} = 0$; $B_{22} = 1/12$; $B_{23} = 0$; $B_{24} = 0$ (18)
 $B_{31} = 0$; $B_{32} = 0$; $B_{33} = 1 - 0^2$; $B_{34} = 0$
 $B_{41} = 0$; $B_{42} = 0$; $B_{43} = 0$; $B_{44} = 12(1 - 0^2)$

The expansion of the determinant (16) yields a sixth degree polynomial in Ω including the effects of pressurization and transverse-shear deformation as follows:

$$A \Omega^{6} + B \Omega^{4} + C \Omega^{2} + D = 0$$
 (19)

where

$$A = \mu (B_{33}B_{44} - B_{34}^2)/12\lambda^6$$

$$\begin{split} \mathbf{B} &= (\mathbf{B}_{33}\mathbf{B}_{44} - \mathbf{B}_{34}^2) \left[(\mathbf{c}_0/\mathbf{t}_0)^2 \lambda^{-2} \left((\mu \rho/\mathbf{E}_0\mathbf{t}_0)^{-1} \right) - \mu \lambda^{-6} \left(\mathbf{R}^2 \rho/\mathbf{E}_0\mathbf{t}_0^3 \right) - (\mathbf{m}^2/12\lambda^4) \right] \\ &+ (\mu/12\lambda^6) \left(\mathbf{B}_{11}\mathbf{B}_{34}^2 + 2 \mathbf{B}_{13}\mathbf{B}_{14}\mathbf{B}_{34} - \mathbf{B}_{14}^2\mathbf{B}_{33} \right) + \mu \lambda^{-4} \left[\mathbf{m}^2\mathbf{B}_{33} - (\mathbf{B}_{44/12}) \right] \\ &+ (\mathbf{B}_{13}^2 + \mathbf{B}_{11}\mathbf{B}_{33} + \mathbf{m}^2\lambda^2)\lambda^{-2} \end{split}$$

$$\begin{split} c &= \mu \lambda^{-6} (R^2 \rho / E_o t_o^3) \ [-B_{13} B_{14} B_{34} + B_{14}^2 B_{33} - B_{11} B_{34}^2 + B_{13}^2 B_{44} + B_{11} B_{33} B_{44} \\ &+ B_{44} m^2 \lambda^2] + m^2 \lambda^{-4} (R^2 \rho / E_o t_o^3) \ [B_{33} B_{44} - B_{34}^2] + (c_o / t_o)^2 \lambda^{-2} \ [(\mu \rho / E_o t_o)^{-1}] \ x \\ &= [B_{13} B_{14} B_{34} + B_{11} B_{34}^2 - B_{13} B_{34} - B_{14}^2 B_{33} - B_{13}^2 B_{44} - B_{11} B_{33} B_{44} - m^2 B_{44}] \\ &- \mu \lambda^{-6} B_{13} B_{14} B_{34} + \mu m^2 \lambda^{-4} [B_{11} B_{33} + B_{14/12}^2 + B_{11} B_{44/12} + \lambda^2 + B_{13}^2] \\ &+ (c_o / t_o) \ m^2 \lambda^{-2} (B_{14} B_{33} - B_{13} B_{34}) + m^4 \lambda^{-2} (B_{33} + B_{44/12}) + m^2 \ (c_o / t_o) \ \lambda^{-2} \\ &= [(\mu \rho / E_o t_o) \ -1] \ (B_{13} B_{34} - B_{14} B_{33}) \end{split}$$

$$\begin{split} \text{D} &= \{ -\text{m}^2 [-\text{m}^2 - \text{B}_{14} \ (\text{c}_{\text{o}}/\text{t}_{\text{o}})] \ [-\text{m}^2 + \text{B}_{14} \ (\text{c}_{\text{o}}/\text{t}_{\text{o}}) \ ((\mu\rho/\text{E}_{\text{o}}\text{t}_{\text{o}})\text{-}1)] + [-\text{m}^4\text{B}_{11} \ \mu/\lambda^2 \\ &+ \text{m}^2 \ \text{B}_{11}\text{B}_{44} \ (\text{c}_{\text{o}}/\text{t}_{\text{o}})^2 \ ((\mu\rho/\text{E}_{\text{o}}\text{t}_{\text{o}})\text{-}1)] + (\text{m}^2/\lambda^4) \ (\text{R}^2\rho/\text{E}_{\text{o}}\text{t}_{\text{o}}^3) \ [-\lambda^{-4}\text{B}_{14}^2 \ \mu \\ &- \text{m}^2 \ \text{B}_{44} - \mu \ \text{B}_{11}\text{B}_{44} \} \end{split}$$

For the limiting case of a single-layer isotropic cylindrical shell, (19) takes the following form:

$$\Omega^{6} \ \left[\mu (1-\upsilon^{2})^{2}/\lambda^{6}\right] + \Omega^{4} \ \left\{\left[-m^{2} \ (1-\upsilon^{2})/\lambda^{4}\right] \ (-\mu-1) \ - \ \left[(1-\upsilon^{2}) \ \mu/\lambda^{4}\right] \ \left[m \ + \ (1-\upsilon \)/\lambda \ \right]$$

$$- [(1-\upsilon^{2}) \mu/\lambda^{6}] [\upsilon^{2} + 12(1-\upsilon^{2}) (R^{2}\rho/E t^{3})] + (1-\upsilon^{2})/\lambda^{2} [(\mu\rho/E t) -1]$$

$$+ \Omega^{2} \{(m^{4}/\lambda^{2}) [\mu+2(1-\upsilon^{2})] + m^{2} \mu(1+\upsilon^{2})/\lambda^{4} + [(\mu\rho/E t) -1] [-(\upsilon^{2}/\lambda^{2})$$

$$- (1-\upsilon^{2})/\lambda^{2} - m^{2}] + 12(1-\upsilon^{2}) (R^{2}\rho/E_{o}t_{o}^{3}) [(m^{2}(1-\upsilon^{2})/\lambda^{4}) + (\mu\upsilon^{2}/\lambda^{6})$$

$$+ 12\mu(1-\upsilon^{2}) (R^{2}\rho/E t^{3}) [m^{2} + (1-\upsilon^{2})/\lambda^{2}]/\lambda^{4} \} + \{-m^{6} + m^{2} [(\mu\rho/E t) -1]$$

$$- [12m^{2} (1-\upsilon^{2}) (R^{2}\rho/E_{o}t_{o}^{3}) (\lambda^{2} + \mu)/\lambda^{4}] - m^{4}\mu/\lambda^{2} = 0$$

$$(20)$$

When $\rho=0$ (19) reduces to that given by Steele [12].

3. APPROXIMATE SOLUTIONS

The curves of variation of the natural frequencies Ω as a function of the wave number m can be developed by a series of order-of-magnitude approximations with respect to the large parameter λ . This is done in what follows by neglecting the pressurization effect. For m and Ω both O(1), and using the fact that λ is a large number, (19) yields the bending waves analogous to those in an Euler-Bernoulli beam on an elastic foundation

$$\Omega^{2} = (t_{o}/c_{o})^{2}/B_{44}[(m^{2} + B_{14}c_{o}/t_{o})^{2} + (c_{o}/t_{o})^{2} B_{11}B_{44}]$$
 (21)

which reduces for the case of isotropy to $\Omega^2 = m^4 + 1$ as given by Steele [12].

For m << 1, the frequency equation (19) yields

$$m^{2} = (\Omega/\lambda)^{2} \left[B_{13}^{2} B_{44} + (B_{11} - \Omega^{2}) \left(B_{33} B_{44} - B_{34}^{2} \right) \right] / B_{44} (B_{11} - \Omega^{2})$$
(22)

For the case of isotropy, (22) becomes

$$m^2 = (\Omega/\lambda)^2 [1 - (1 - v^2)\Omega^2] / (1 - \Omega^2)$$
 (23)

Tracing back, one can obtain this result by assuming all the transverse shear and bending stresses to be negligible. Consequently, this gives the "membrane waves." The ordinate to orgin (m=0) obtained from (22) is

$$\Omega^2 = B_{11} + (B_{13}^2 B_{44}) / (B_{33} B_{44} - B_{34}^2)$$
 (24)

which reduces to the ring mode, $\Omega = (1-v^2)^{-\frac{1}{2}}$ for the isotropic cylinder.

Furthermore, for $\Omega \ge O(\lambda)$, the frequency Equation (19) takes the following form:

$$\Omega^{6}(\mu/12\lambda^{6}) \left[B_{33}B_{44} - B_{34}^{2}\right] + \Omega^{4}(1/\lambda^{4}) \left[\left(-\lambda^{2}(c_{o}/t_{o})^{2} - m^{2}/12\right) \left(B_{33}B_{44} - B_{34}^{2}\right)\right] - \mu m^{2}(B_{33} + B_{44/12}) + \Omega^{2}(1/\lambda^{2}) \left[B_{33} \left(m^{2} + (c_{o}/t_{o}) B_{14}\right)^{2} + m^{4} B_{44/12}\right] + m^{2}(\left(c_{o}/t_{o}\right)^{2} B_{44}\lambda^{2} + \mu m^{2}) - m^{2} \left[m^{2} + (c_{o}/t_{o}) B_{14}\right]^{2} = 0$$
(25)

The ordinate to orgin (m=o) is

$$\Omega^{2} = \frac{1}{2} \left\{ \frac{12}{\mu} \lambda^{4} \left(\frac{c}{t_{o}} \right)^{2} + \left[\frac{144}{\mu^{2}} \lambda^{8} \left(\frac{c}{t_{o}} \right)^{4} + \frac{48}{\mu} \lambda^{4} \left(\frac{c}{t_{o}} \right)^{2} + \frac{B^{2} B}{B_{34}^{2} - B_{33} B_{44}} \right] \right]^{\frac{1}{2}} \right\}$$
(26)

which reduces to the form

$$\Omega^2 = \lambda^4 / (1 - \upsilon^2) \mu \tag{27}$$

representing the shear mode of isotropic cylindrical shells [12].

Moreover, for $\Omega > O(\lambda^2)$, (19) resolves into two equations:

$$m^2 - \mu(\Omega/\lambda)^2 = 0 \tag{28}$$

$$m^4 - m^2 (B_{33} + B_{44/12}) (\Omega/\lambda)^2 + (B_{33}B_{44} - B_{34}^2) (\Omega/\lambda)^4/12 = 0$$
 (29)

For the case of isotropy, (29) reduces to the following form:

$$m^2 = (\Omega/\lambda)^2 (1-v^2) \tag{30}$$

The positive real values of Ω resulting from all the approximations studied can be evaluated using a pocket computer. The values are exhibited in Fig. 3 and 4 in correlation with those corresponding to the exact solution (19). The numerical results support the fact that the approximate solution may be used in lieu of the exact solution.

The quantity $\pi/\lambda \ell$ is small, except for very short cylinders whose length is in the magnitude of $(Rt)^{\frac{1}{2}}$. For λ very large (that is, very thin shell), the curve of variation of Ω versus \bar{m} in the transition region from membrane to bending wave becomes very flat and a large number of natural frequencies are found near $\Omega = (B_{11})^{\frac{1}{2}}$ ($\Omega = 1$ for the case of isotropy). In fact, if just the membrane solution is used, an infinite number of natural frequencies approaching the limit $\Omega = (B_{11})^{\frac{1}{2}}$ can be determined; however, in the range $(B_{11})^{\frac{1}{2}} < \Omega <$ the value of Ω given by (20), referred to as a "zone of silence" none can be found. Since the cylindrical shell has an ample number of natural frequencies in the range $\Omega = O(B_{11})$, for most problems the higher branch and the deviation of the bending solution curve for large Ω are not important. Therefore, the transverse shear deformation and rotatory inertia effects may be neglected.

Furthermore, for $\Omega<(B_{11})^{\frac{1}{2}}$, the analysis for general boundary conditions can be performed as in the static case. The membrane solution is determined from the conditions on the axial force, V or axial displacement, v. The "dynamic edge-effect" solution provides the constants to satisfy the conditions on H or h and M or χ . The mode shape is essentially "membrane" with the edge-effect correction. Moreover, for $\Omega>(B_{11})^{\frac{1}{2}}$, the membrane solution is still valid but the solutions which give the "dynamic edge-effect" for $\Omega<(B_{11})^{\frac{1}{2}}$ become short wavelength bending solutions [8].

4. AXISYMMETRIC STABILITY LIMIT

A "classical" stability limit for orthotropic layered cylindrical shells is derived by the first author in [8] from the frequency equation (19) by setting Ω equal to zero and minimizing ρ in the resulting equation with respect to the wave number, m.

$$d\rho/dm = 0$$
 yields $m^2 = \pm (c_0/t_0)(B_{14}^2 + B_{11}B_{44})^{\frac{1}{2}}$

which gives the minimum value of the pressurization parameter, ρ defined by (17), as follows:

$$\rho = -(2E_o t_o^2/R) \left[B_{14} + (B_{14}^2 + B_{11}^2 B_{44})^{\frac{1}{2}} \right] / B_{44}$$
 (31)

Indeed, (31) reduces to the well-known classical stability limit for homogeneous and isotropic cylinders. In fact, (31) is only a special case of the more general stability limits for orthotropic layered shells of revolution given in [9] by the first author.

NUMERICAL ANALYSIS

Numerical results presented herein are obtained by the computer program DAS [14] which is capable of performing dynamic analyses of orthotropic layered shells of revolution.

The properties of the isotropic and orthotropic cylindrical shells for the base curves (solid lines) are listed in Tables 1 and 2, respectively.

TABLE 1 - Isotropic Cylinder

Length L(cm)	Radius R(cm)	Thickness t(cm)	E (Pa)	Poisson's ratio υ	μ
254	152.4	0.635	6895×10 ⁷	0.30	3.0

TABLE 2 - Orthotropic Cylinder (L = 254 cm; R = 152.4 cm)

Layer	Thickness (cm)	Ε (På)	E _θ (Pa)	υφθ	μ
1 (Inner)	0.254	6895×10 ⁷	3448×10 ⁷	0.30	
2 (Middle)	0.254	4137x10 ⁷	2069x10 [']	0.30	3.0
3 (Outer)	0.254	2758×10′	1379x10'	0.30	

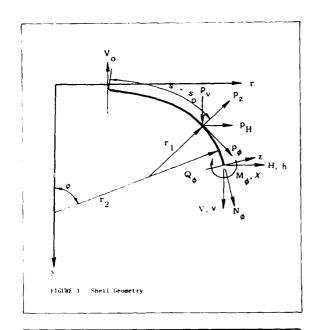
The variation of the frequency with respect to the wave number is presented in Fig. 3, 5 and 6 for the isotropic, and Fig. 4 and 7 through 9 for the orthotropic cases. The figures demonstrate clearly that the pressurization has a significant effect on the natural frequencies especially for the m>0.1 range of the membrane and bending (lower branch) waves. The higher branch of the bending wave (shear mode) is not affected by the pressurization. The effect of internal pressurization ($\rho>0$ and/or V>0 for m>0.1) is to stiffen the cylinder with respect to the frequency, thus causing frequencies to increase; however, the external pressurization ($\rho<0$ and/or V<0) has an adverse effect on the frequency.

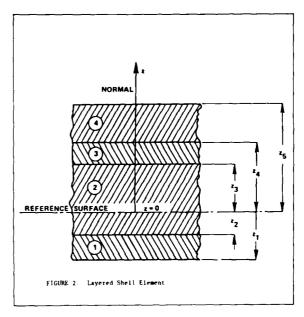
TABLE 3. Natural frequencies for isotropic cylinder

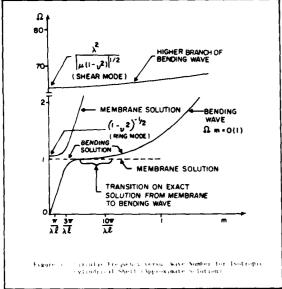
TABLE 4. Natural frequencies for orthotropic cylinder

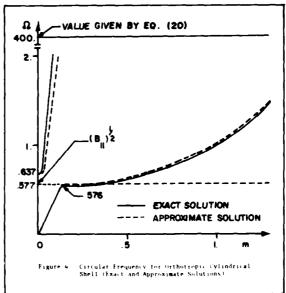
R/t	m	Ω_{1}	f ₁ (Hz)	R/t	m	Ω_{1}	f ₁ (Hz)
120	1.04	1.337	71.7	100	1.04	1.056	75.9
240	1.04	1.345	25.5	200	1.04	1.043	26.5
480	1.04	1.342	18.0	300	1.04	4.872	10.7

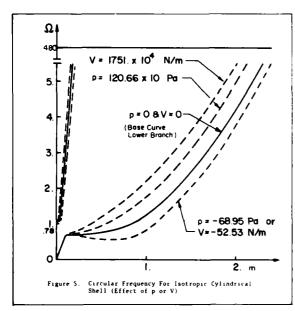
Tables 3 and 4 describe the effect in the change of the ratio of radius to thickness (R/t) on the frequencies given by the lower branch; increasing R/t ratio lowers the frequency values. The inclusion of transverse shear deformation does not influence the lower branches of the membrane and bending waves. The reversal of the sequence of lamination in Table 2 increases frequencies considerably for m>0.1, Fig. 9. The replacement of the values of E_{φ} with E_{θ} in Table $(E_{\theta}>E_{\varphi})$ produces a large increase in Ω . An increase in the shear deformation (the shell is more flexible in shear) decreases frequencies of the higher branch of bending wave (shear mode).

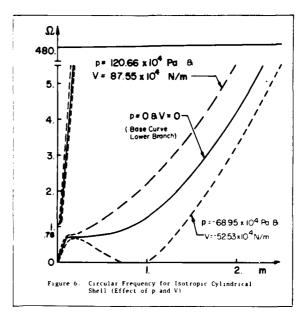


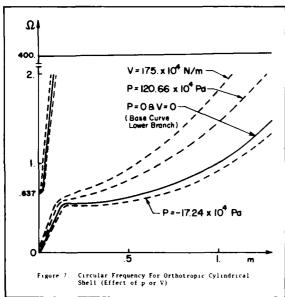


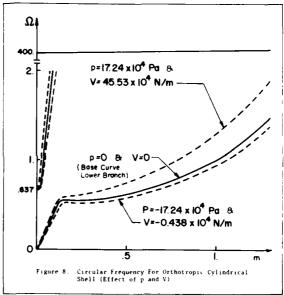


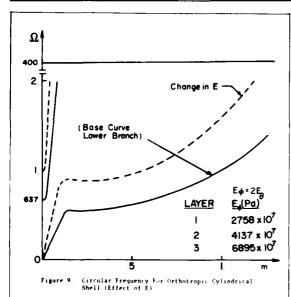










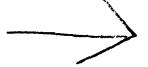


Acknowledgement

The authors would like to thank Dr. Carl J. Turkstra, Chairman of the Department of Civil and Environmental Engineering at Polytechnic Institute of New York for his helpful discussions and support throughout this research work.

REFERENCES

- I. MIRSKY 1964 Journal of Acoustical Society of America, 36 (11).
 Axisymmetric Vibrations of Orthotropic Cylinders.
- 2. I. MIRSKY 1966 Journal of Acoustical Society of America, 39 (3). Three-dimensional and Shell-theory Analysis for Axisymmetric Vibrations of Orthotropic Shells.
- 3. S.B. DONG 1968 Journal of Acoustical Society of America, 44 (6). Free Vibration of Laminated Orthotropic Cylindrical Shells.
- 4. S.B. DONG and L.G. SELNA 1970 Journal of Composite Materials, 4. Natural Vibrations of Laminated Orthotropic Shells of Revolution.
- 5. C.L. DYM 1971 AIAA Journal, 1201-1203. Vibrations of Pressurized Orthotropic Shells.
- 6. L.E. PENZES and H. KRAUS 1972 AIAA Journal, 1309-1313. Free Vibration of Prestressed Cylindrical Shells having Arbitrary Homogeneous Boundary Conditions.
- 7. C.W. BERT and T.L.C. CHEN 1975 Trans. ASME, Journal of Pressure Vessels Technology, Paper 75 PVP-18. Wave Propagation in Fluid-Conveying Piping Constructed of Composite Material.
- 8. O.A. FETTAHLIOGLU 1972 Ph.D. Thesis, Polytechnic Institute of Brooklyn, New York. Static, Buckling and Vibration Characteristics of Orthotropic Nonhomogeneous Shells of Revolution.
- 9. O.A. FETTAHLIOGLU and C.R. STEELE 1974 Journal of Applied Mechanics, Series E, 41. Asymptotic Solutions for Orthotropic Nonhomogeneous Shells of Revolution.
- 10. O.A. FETTAHLIOGLU and P.C. WANG 1977 Proc. Third International Conference on Pressure Vessel Technology, Tokyo. Asymptotic Solutions for Thermal Stress and Deformation in Orthotropic Nonhomogeneous Shells of Revolution.
- 11. O.A. FETTAHLIOGLU and P.C. WANG 1983 AIAA/ASME/ASCE/AHS 24th Structures, Structural Dynamics and Materials Conference, Lake Tahoe, Nevada. Paper AIAA-83-0893-CP. Axisymmetric Vibrations of Pressurized Orthotropic Nonhomogeneous Shells of Revolution.
- 12. C.R. STEELE 1971 Int. J. Solids and Structures 7 (9), 1171-1198. Beams and Shells with Moving Load.
- 13. E. REISSNER 1950 Proc. Third Symposium on Applied Mathematics.
 McGraw Hill, New York, 27-52. On Axisymmetrical Deformations of Thin
 Shells of Revolution.
- 14. O.A. FETTAHLIOGLU and A.M. SAYED 1982 Polytechnic Institute of New York and New York Institute of Technology, User's Manual. Dynamic Analysis of Shells (PINY/NYIT - DAS).



AMPLITUDE GROWTH IN VIBRATIONS OF ARMS WITH INCREASING LENGTH

S. Bergamaschi

Institute of Applied Mechanics. University of Padua. Italy

A. Sinopoli

Institute of Architecture. University of Venice. Italy

A. Repaci

Department of Mathematics. Polytechnic of Turin. Italy

ABSTRACT.

The Timoshenko theory of flexural vibrations of beams and the WKB method are adopted to evaluate the amplitude changes of the free vibrations of beams, the length of which varies linearly with time. It is found that the change is dependent only on the length increase (or decrease). Results are also given for the frequency modifications.

1. INTRODUCTION

Some mechanical systems are required to change their length while in operation. This is the case of manipulator arms or deployable antennas, the length of which can be varied by amounts equal to many times the initial (or final) span. In such cases it can be expected that the amplitudes of the flexural vibrations originated by the manoeuvres are not constant; in particular, it has been observed that when the length of a mechanical arm is increased to reach same target, undesired vibrations are originated, so that the successive phase of the operation has to be delayed until the oscillatory motion is damped by dissipative forces [1]. Thus, the study of the dynamics of beams with variable length seems to be interesting in technical problems, in order to decide if the addition of dampers is required.

The problem seems to have some interest also from the point of view of the techniques of solution, because the use of the methods usually adopted for beams of constant length cannot be extended to this case. Further, to the knowledge of the authors, only a few works have been devoted to the analytical investigation of strings and beams with variable length.

In the present case, the problem can be simplified, because it is plausible to assume that the velocity at which the length is changed is small, if $mean}$ sured in units of the fundamental periods of the free vibrations; therefore, the use of a perturbation method (the WKB method) is allowed.

Two other hypotheses are inherent in the mathematical model which will be presented in the following paragraph:

a) it is assumed that the initial or final configuration of the arm is such that it cannot be considered as slender, so that shear and rotatory iner tia can have non negligible effects. Accordingly, the Timoshenko theory will be adopted;

- b) the effect of weight is not taken into account. This is partly because some preliminary computations carried out with the Euler-Bernoulli model have shown that, for masses up to about 100 Kg and length increases equal to 4 times the initial one, the weight effect is negligible. The other reason is that some very interesting systems with variable length have been designed to be used during space missions. Among others, this is the case of the deployable boom which will be mounted on the Space Shuttle to provide the initial gravity gradient at the beginning of the deployment in future missions of tethered satellites [2].
- 2. MATHEMATICAL MODEL AND METHOD OF SOLUTION.

According to [3], the equations of motion are:

$$\begin{cases} \mu \frac{\partial^{2} y^{*}}{\partial t^{2}} + \frac{\partial y^{*}}{\partial x} = 0 \\ -\frac{\partial M^{*}}{\partial x} + I_{o} \frac{\partial^{2} \beta^{*}}{\partial t^{2}} + y^{*} = 0 \\ \frac{\partial 6^{*}}{\partial x} = \frac{M^{*}}{EI} \qquad (0 \le x \le \ell(t)) \end{cases}$$

$$V^{*} = -KAG\alpha^{*}$$

$$\frac{\partial y^{*}}{\partial x} = \alpha^{*} + \beta^{*}$$

The meaning of the symbols are given in the table at the end.

Eqs.(1) constitute a system with constant coefficients, but defined in a time dependent domain. To reduce the problem to one with time independent boundary conditions, the following substitution is made:

$$x = s \cdot \ell(t) \qquad (0 \le s \le 1) \tag{2}$$

so that it can be written:

$$\begin{cases}
\mu \ell & \frac{\partial^2 y^*}{\partial t^2} + \frac{\partial v^*}{\partial s} = 0 \\
- & \frac{\partial M^*}{\partial s} + I_O \ell \frac{\partial^2 \beta^*}{\partial t^2} + \ell v^* = 0 \\
& \frac{\partial \beta^*}{\partial s} = \ell \frac{M^*}{EI} \qquad (0 \le s \le 1)
\end{cases}$$

$$v^* = - KAG(\frac{1}{\ell} \frac{\partial y^*}{\partial s} - \beta)$$

where the field of definition is constant, but the coefficient ℓ depends on time.

It is now assumed that the length is changed linearly with time (which seems quite plausible in most applications), so that:

$$\ell(t) = \ell_0 + \dot{\ell}t \tag{4}$$

with $\dot{\ell}$ = constant. As noted in the introduction, the hypothesis is also made that:

$$\frac{T_{0}^{\ell}}{\ell(t)} \ll 1 \tag{5}$$

is valid at any instant; in other words, the time interval during which the length is changed must be much longer that the period T of the fundamental mode in the configuration with maximum length. In this case the system is a diabatic, so that eq.(4) can be rewritten as:

$$l(t) = l_0 + \varepsilon \dot{l}t$$
 (6)

and perturbation methods can be adopted for its solution. In the present in vestigation, system (3) is solved by means of the WKB method [4], looking for solutions having the form:

$$y''(s,t) = y(s,\tau) e^{i\frac{\psi(\tau)}{\varepsilon}} x''(s,t) = \beta(s,\tau) e^{i\frac{\psi(\tau)}{\varepsilon}}$$

$$y''(s,t) = y(s,\tau) e^{i\frac{\psi(\tau)}{\varepsilon}} x''(s,t) = y(s,\tau) e^{i\frac{\psi(\tau)}{\varepsilon}}$$

$$y''(s,t) = y(s,\tau) e^{i\frac{\psi(\tau)}{\varepsilon}}$$

$$y''(s,t) = y(s,\tau) e^{i\frac{\psi(\tau)}{\varepsilon}}$$

$$y''(s,t) = y(s,\tau) e^{i\frac{\psi(\tau)}{\varepsilon}}$$

$$(7)$$

where ε is a small parameter, $\tau = \varepsilon t$ is the slow time and:

$$y(s,\tau) = \sum_{On}^{\infty} y_n(s,\tau) \varepsilon^n, \beta(s,\tau) = \sum_{On}^{\infty} \beta_n(s,\tau) \varepsilon^n$$

$$(8)$$

$$M(s,) = \sum_{On}^{\infty} M_n(s,\tau) \varepsilon^n, V(s,\tau) = \sum_{On}^{\infty} V_n(s,\tau) \varepsilon^n, \psi(\tau) = \sum_{1}^{\infty} v_n(\tau) \varepsilon^n$$

Substituting eqs.(7) in (3), it is easily found:

$$\begin{cases} \mu \ \ell \ \varepsilon^{2} \left(\ddot{y} + \frac{2i}{\varepsilon} \ \dot{y} \dot{\psi} + \frac{i}{\varepsilon} \ \dot{y} \dot{\psi} - \frac{1}{\varepsilon^{2}} \dot{y} \dot{\psi}^{2} \right) + V' = 0 \\ - M' + \varepsilon^{2} I_{O} \ell \left(\ddot{\beta} + \frac{2i}{\varepsilon} \ \dot{\beta} \dot{\psi} + \frac{i}{\varepsilon} \ \beta \ddot{\psi} - \frac{1}{\varepsilon^{2}} \ \beta \dot{\psi}^{2} \right) + \ell V = 0 \\ \beta' = \frac{\ell}{EI} M \\ y' = \frac{1}{KAG} (KAG\beta - V) \end{cases}$$

$$(9)$$

where the dots and the apices mean, respectively, differentiation with respect to τ and to s.

Introducing eqs.(6) and (8) in (9) and separating the contributions pertaining to different orders of ϵ and, for each order, real quantities from imaginary ones, it is found that the 0-th order contribution is exclusively real and is given by:

$$\begin{cases}
-\mu \, \mathcal{L}_{O} \, \mathbf{y}_{O} \, \stackrel{\bullet}{\mathbf{v}}_{O}^{2} + \mathbf{V}_{O}^{1} = 0 \\
-\mathbf{M}_{O} \, -\mathbf{I}_{O} \, \mathcal{L}_{O} \, \mathbf{\beta}_{O} \, \stackrel{\bullet}{\mathbf{v}}_{O}^{2} + \mathcal{L}_{O} \, \mathbf{V}_{O} = 0 \\
\beta_{O}^{1} = \frac{\mathcal{L}_{O}}{EI} \, \mathbf{M}_{O} \\
\mathbf{y}_{O}^{1} = \frac{\mathcal{L}_{O}}{KAG} \, (KAG \, \beta_{O} - \mathbf{V}_{O})
\end{cases}$$
(10)

When dealing with perturbation methods, it is frequent that the complete n-th order solution can be found only if some information about the n+1-th order is available. In this case, further information about eqs.(10) is provided by the imaginary part of the first order expansion, which gives:

$$\begin{cases} 2\dot{y}_{0}\dot{\psi}_{0} + y_{0}\psi_{0} = 0\\ 2\dot{\beta}_{0}\dot{\psi}_{0} + \beta_{0}\psi_{0} = 0 \end{cases}$$
(11)

Eqs.(11) can be satisfied by: $\dot{y} = \dot{\beta} = \ddot{\psi} = 0$; therefore, it appears that eqs.(10) constitute the usual system governing the vibrations of a beam with length ℓ_{o} . In particular: $\dot{\psi}_{o}(\tau) = \text{const} = \omega$. The real part of the first order is:

and from the imaginary part of the second order:

$$y_1 = -\frac{\bar{\psi}_1}{2\psi_0} y_0 \qquad \beta_1 = -\frac{\psi_1}{2\psi_0} \beta_0$$
 (13)

if the initial phase is $\psi_0(0)$. After some algebraic manipulation on eqs.(12), it is also found:

$$M_{1} = -\left(\frac{\mathring{\psi}_{1}}{2\psi_{0}} + \frac{\mathring{\ell}}{\ell_{0}} \tau\right) M_{0}$$

$$V_{1} = \frac{\mathring{\ell}}{\ell_{0}} \tau KAG \beta_{0} - \left(\frac{\mathring{\psi}_{1}}{2\psi_{0}} + \frac{\mathring{\ell}}{\ell_{0}} \tau\right) V_{0}$$
(14)

Eqs.(13) and (14) give the first order corrections as functions of the 0-th order quantities and the unknown frequency variation. To determine ψ_1 it must be remembered that system (10) admits exponential solutions:

$$y_{o}(s) = y_{oo}e^{\lambda s}$$
, $\beta_{o}(s) = \beta_{oo}e^{\lambda s}$, $M_{o}(s) = M_{oo}e^{\lambda s}$, $V_{o}(s) = V_{oo}e^{\lambda s}$ (15)

and, that, for each vibration mode and for each value of λ in any mode:

$$\beta_{OO} = \frac{KAG\lambda^{2} + \mu \ell_{O}^{2} \dot{\psi}^{2}_{O}}{KAG\lambda \ell_{O}} \quad y_{OO} \quad M_{OO} = \frac{EI(KAG\lambda^{2} + \mu \ell_{O}^{2} \psi_{O}^{2}) \lambda}{KAG \ell_{O}^{2}} \quad y_{OO} \quad V_{OO} = \frac{\mu \ell_{O} \dot{\psi}^{2}_{O}}{\lambda} \quad y_{OO} \quad (16)$$

Introducing eqs.(13), (14) and (16) in (12), one can write:

$$\frac{\dot{\psi}_{1n}}{\psi_{on}} = -\left(1 - \frac{KAG}{\mu \ell_{o}^2 \psi^2}\right) \frac{\dot{\ell}_{\tau}}{2\ell_{o}}$$
 (17)

Finally:

$$\frac{y_{1n}}{y_{on}} = \left(1 - \frac{\kappa AG \lambda_n^2}{\mu \ell_o^2 \psi_o^2}\right) \frac{\ell_T}{4\ell_o}$$
(18)

and similar formulas for β_{1n} , M_{1n} and V_{1n} can easily be found from eqs.(13) and (14). Thus, it is seen that the first order corrections of any mode are the sum of two different contributions pertaining, for the same value of n, to the two different values of λ^2 which can be found equating to zero the determinant of the coefficients of system (10).

COMPUTATIONS AND RESULTS

It is now convenient to introduce non dimensional parameters. Let it be:

$$b^{2} = \frac{EI}{\mu \ell^{4}} \dot{\psi}^{2} \qquad p = \frac{KG}{E} \qquad q = \frac{A\ell^{2}}{I}$$
 (19)

so that the biquadratic equation relating λ to $\overset{\bullet}{\psi}_{\Omega}$ can be written as:

$$\lambda_{n}^{2} = \frac{b_{n}^{2}}{2pq} \left\{ -(p+1) + [(p-1)^{2} + \frac{4p^{2}q^{2}}{b_{n}^{2}}]^{\frac{1}{2}} \right\}$$
 (20)

If: $(p-1)^2 + \frac{4 p^2 q^2}{b^2} > (p+1)^2$ let us write: (case a)

$$\alpha_{n}^{2} = \frac{1}{2pq} \left\{ -(p+1) + \left[(p-1)^{2} + \frac{4 p^{2}q^{2}}{b_{n}^{2}} \right]^{\frac{1}{2}} \right\}$$
 (21)

and in the opposite case : $\alpha_n^{*2} = -\alpha_n^2$ (case b)

Further:

$$\beta_{n}^{2} = -\frac{1}{2pq} \left\{ p+1 + \left[(p-1)^{2} + \frac{4 p^{2} q^{2}}{b_{2}^{2}} \right]^{\frac{1}{2}} \right\}$$
 (22)

So that the amplitude corrections are:

$$K_{\alpha n} = \left(\frac{y_{1n}}{y_{\alpha n}}\right)_{\alpha_n} = (1 - p q \alpha_n^2) \frac{\Delta \ell}{4\ell_0} \qquad (case a)$$

or:

$$\kappa_{\alpha, n} = (\frac{y_{1n}}{y_{0n}})_{\alpha, n} = (1 + pq\alpha_n^{2}) \frac{\Delta \ell}{4\ell_0} \qquad \text{(case b)}$$

and:

$$\kappa_{\beta_{n}} = (\frac{y_{1n}}{y_{0n}})_{\beta_{n}} = (1 + p q \beta_{n}^{2}) \frac{\Delta \ell}{4\ell_{0}}$$
(25)

The values of the adimensionalized frequency b, needed to compute α , α' and β are found solving the frequency equation. If the arm is assumed to have a clamped end, while the other is free, the boundary conditions of the 0-th or der problem are:

$$y_{o}(0) = \beta_{o}(0) = M_{o}(1) = V_{o}(1) = 0$$
 (26)

and the frequency equations corresponding to a cantilever, both in case a) and b), are given in [5]. For sake of brevity, in the following, formulas are given only for case a) because the changes in case b) are obvious. Therefore:

$$y_0(s) = y_{01} + y_{02}$$
 (27)

with:

$$y_{01} = C_1 \sinh b\alpha s + C_2 \cosh b\alpha s$$

$$y_{02} = C_3 \sin b\beta s + C_4 \cos b\beta s$$
(28)

Now, from eqs.(17) and (18) it can be seen that, for each n, at the first order of ϵ there are both two values of the frequency and the amplitude corrections, depending if α or β values are substituted for $\lambda.$ Thus, K is the correction to the exponential part of the solution, while the trigonometric part is changed by Kg. Accordingly, the following quantity has been taken to measure the change of amplitude vibration during the length variation in any mode:

$$a(\tau) = \frac{K_{\alpha} y_{01} + K_{\beta} y_{02}}{Y_{0}}$$
 (29)

A simple computer program has been implemented to find the five lowest roots of the frequency equation corresponding to conditions (26) and to evaluate a at the free end of the cantilever. In the computations, it has been assumed that the arm is made of steel, so that: $E = 2.1 \cdot 10^{11} \text{N/m}^2$ and v = 0.3; further, the Cross section has been considered to be a thin walled hollow circle and the pertinent shear coefficient has been computed with the formulas of Cowper [6]. The value of p has been held constant in any computation, while the slenderness ratio q has been considered as a variable parameter. Some preliminary runs showed complete agreement with the results at the end of [5].

The main result of this investigation is shown in fig.1, from which it is apparent that a changes linearly with the length increase.

This result is valid for any vibration mode and for any value of p and q, so that it can be concluded that the amplitude change with length is a purely geometrical feature, being completely independent from characteristics of the 0-th order solution different from vibration amplitude.

In fig.2 the ratio K_{β}/K is shown for four values of q as a function of the mode number. It is interesting to note that for slender arms the two amplification factors are almost equal and of opposite signs, while as rotary inertia and shear forces increase, K can change sign, so that the exponential and the trigonometric part of the vibration can be changed by very different amounts.

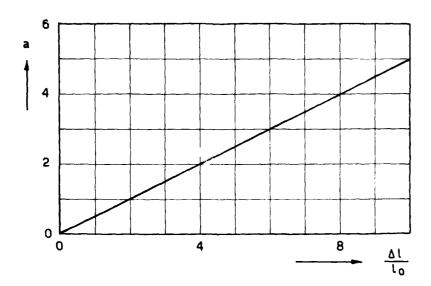
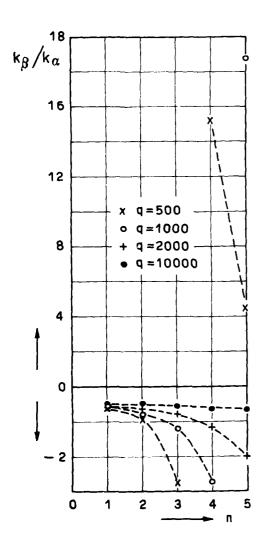


FIG.1 - Amplitude as a function of length change



Figs.3 and 4 show,respectively, the adimensionalized frequency modifications of y_{01} and y_{02} up to mode five. As $\Delta\omega_{1\alpha}$ is positive, corresponding to frequency in crease, it is seen from fig.3, that the frequency of the upper modes can decrease if the arm is sufficiently thick. On the contrary, $\Delta\omega_{1\beta}$ is negative, and from Fig.4 it can be seen that the frequency modifications corresponding to β are negative in any case. In both cases, the asymptotic values tend to those given by the Euler-Bernoulli theory and the effects of rotary inertia and shear forces are apparent for q < 2000.

In conclusion, beats are present in the vibration, due to the proximity of $(\omega + \Delta \omega_{\alpha})_n$ to $(\omega + \Delta \omega_{\beta})_n$, and their amplitude variation is slower and slower as long as q tends to infinity.

FIG.2 - Ratio of the amplification factors for the first five modes.

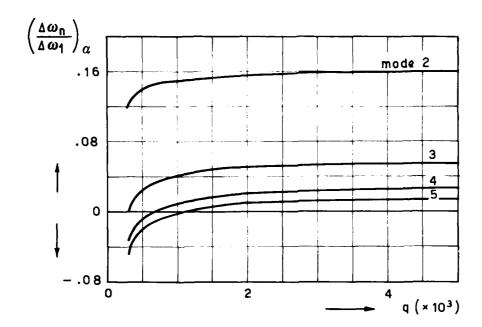


FIG.3 - Frequency change corresponding to $\alpha.$ The values are given with respect to the change of the first mode.

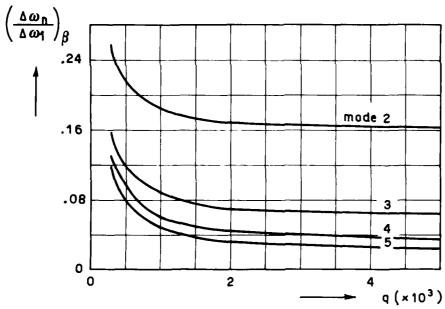


FIG.4 - Adimensionalized change of the upper modes, corresponding to $\boldsymbol{\beta}.$

4. REFERENCES

- 1. F. GIORDANA and G. RUGGIERI 1983 Polytechnic of Milan, Italy. Private communication.
- 2. V.V.A.A. 1977 Spacelab Satellites for A.M.P.S. ESA Phase A Final Report, Vol. III, ESTEC Ref. TF/GD-DD/cs 5063.
- 3. C.L. DOLPH 1954 Quarterly Jn. of Applied Mathematics, Vol. II, pp. 175-187. On the Timoshenko Theory of Transverse Beam Vibrations.
- 4. C.M. BENDER and S.A. ORSZAG 1978 Advanced Mathematical Methods for Scientists and Engineers. McGraw-Hill: New York.
- 5. T.C. HUANG 1961 ASME Journal of Applied Mechanics, pp. 579-584. The Effect of Rotatory Inertia and of Shear Deformation on the Frequency and Normal Mode Equations of Uniform Beams with Simple End Conditions.
- 6. G.R. COWPER 1966 ASME Journal of Applied Mechanics, pp. 335-340. The Shear Coefficient in Timoshenko's Beam Theory.

LIST OF SYMBOLS

a(τ) :	amplitude change
A :	area of the cross section
b :	adimensionalized frequency
E :	Young modulus
G:	shear modulus
I:	moment of inertia of the cross section
I :	moment of inertia of a beam with unit length
I : K°:	shear coefficient
κ _α , κ _β :	amplification factors corresponding to α and β values of
a p	the wave number
l(t):	length of the beam
l _o :	initial length of the beam
M*(s,t) :	bending moment
p :	ratio to measure the relative effect of rotary inertia
	for given shear and flexural rigidity
q:	slenderness ratio
s _. :	adimensionalized space variable
V [*] (s,t) :	shear force
$y^*(s,t) : \alpha^*(s,t) :$	beam deflection
	slope due to shear
β*(s,t) :	slope due to bending
Δωηα' Δωηβ :	frequency modifications of mode n
$\lambda : n_{\mathcal{D}}$	adimensionalized wave number
μ:	mass per unit length
τ:	slow time
ψ(τ) :	phase angle



SEISMIC STRESS FIELDS FOR NUCLEAR ELBOWS USING TOROIDAL ELASTICITY THEORY

H. A. Lang

Director - LANG-Research West Santa Monica, California, USA AD-P003 642

ABSTRACT

Toroidal elasticity, first introduced at London, England (1980) is a new tool of stress analysis. It merges a toroidal geometry with the fully three dimensional theory of elasticity. For isotropic materials, it includes both stress and strain compatibility relations in order to ensure that the deformations are properly determined and topologically correct. Since the theory is complete, all three components of displacement, all six components of strain, and all six components of stress may be determined.

The compatibility equations, though rigorously correct, are lengthy. To apply the theory to a large number of boundary value problems, the method of successive approximation has been adopted. All equations are expanded in powers of 1/R (where R is the toroidal radius). This leads to a set of working equations appropriate for the solution of problems.

In the present paper the methods of toroidal elasticity are extended to the problem of determining the stress fields in a hollow circular elbow or pipe bend under the action of seismic accelerations.

The seismic accelerations are represented by equivalent body forces X,Y,Z acting in arbitrary directions. The seismic forces may also be viewed as upper bounds obtained from seismic response curves.

Calculations are made for parameters $s_b = 0.35$ and $s_a = 0.30$, corresponding to major elbows of nuclear plants.

NOTATION

r,
$$\phi$$
, θ = toroidal coordinates

 $\sigma_{\mathbf{r}}$, σ_{ϕ} , σ_{θ} = normal stress components

 $T_{\mathbf{r}\phi}$, $T_{\mathbf{r}\theta}$, $T_{\phi\theta}$ = shear stress components

 R = toroidal radius

 a = inner radius

 b = outer radius

 $\mathbf{s} = \frac{\mathbf{r}}{R}$
 $\mathbf{q} = 1 + \mathbf{s} \cos \phi$
 \mathbf{X} , \mathbf{Y} , \mathbf{Z} = Seismic forces (per unit volume)

 $\nabla_{0}^{2} = \frac{\partial^{2}}{\partial \mathbf{s}^{2}} + \frac{1}{\mathbf{s}} \frac{\partial}{\partial \mathbf{s}} + \frac{1}{\mathbf{s}^{2}} \frac{\partial^{2}}{\partial \phi^{2}}$
 $\mathbf{\Phi} = \sigma_{\mathbf{r}} + \sigma_{\phi} + \sigma_{\theta}$

 $\frac{\partial}{\partial g} = \cos \phi \frac{\partial}{\partial s} - \frac{\sin \phi}{s} \frac{\partial}{\partial \phi}$

2. INTRODUCTION

Toroidal elasticity (as used in this paper) refers to the application of the classical theory of elasticity to a toroidal geometry as typified by solid circular ring sectors, pipe elbows, and curved pipe bends. The term "toroidal elasticity" was first introduced in [1] where it was emphasized that the theory was complete because of the inclusion of both stress and strain compatibility equ tions. This means that the theory is topologically correct and can be used to extermine stresses, strains, and displacements everywhere in an elbow.

Because the rigorously correct compatibility equations are lengthy, it is desirable to apply the method of successive approximations. All equations are expended in powers of 1/R (where R is the toroidal radius). The result is a set of working equations appropriate for the solution of many boundary value problems.

The method of successive approximation has been applied to the determination of stress fields for

- (1) twist of elbows, pipe bends and ring sectors.
- (2) in-plane bending of elbows under the action of pressure and end-bending moments.
- (3) in-plane bending of elbows under the action of end normal force and end shear force.
- (4) out-of-plane bending under the action of end bending moments and end twisting moments.
- (5) out-of-plane bending under the action of end shear force.

There exists a total of 16 solved problems for ring sectors and for pipe elbows under end loads and pressure.

In addition to these statically loaded problems, two problems involving seismic accelerations in a solid circular ring sector were solved [2], [3].

The specific objective of the present paper is to determine the stress fields for an elbow arising from two of the three constant components X, Y, Z induced by seismic accelerations. The three components X, Y, Z may be viewed as:

- 1 Equivalent body forces -X, -Y, -Z
- 2 Extreme or upper bounds obtained from seismic response curves
- 3 Derived from displacements \mathbf{u}_0 sin ωt , \mathbf{v}_0 sin ωt and \mathbf{w}_0 sin ωt so that $\mathbf{X} = -\mathbf{u}_0$ ω^2 , $\mathbf{Y} = -\mathbf{v}_0$ ω^2 and $\mathbf{Z} = -\mathbf{w}_0$ ω^2 (where the time term sin ωt is omitted everywhere)

As shown in Figure 1, the components in the toroidal elastic frame of reference are related to the components X, Y, Z by the direction cosine scheme.

	X	Y	Z
F _r	cos φ cos θ	$\cos \phi \sin \theta$	sin ¢
. . φ	- $\sin \phi \cos \theta$	- $\sin \phi \cos \theta$	cos φ
\mathbf{F}_{θ}	- sin θ	cos θ	0

In the present paper, only the field of stress due to components X and Y will be considered. The Z component, which requires separate discussion, is deferred to another paper.

The stress field of the X component can be derived from the stress field for the Y component by a simple substitution. Therefore, it is only necessary to consider the Y component in detail.

The stresses are given by a converging series such that $S(total) = S(0) + S(1) + S(2) + \dots$ (where S is any stress)

The working equations consist of terms on the RHS which may be called equilibrium functions or compatibility functions. These functions are developed in the body of the paper.

3. STRESS FIELD FOR INITIAL STATE (0)

The equations of motion are

$$\frac{\partial(\sigma_{\mathbf{r}}\mathbf{s})}{\mathbf{s}\partial\mathbf{s}} + \frac{1}{\mathbf{s}} \frac{\partial T_{\mathbf{r}\phi}}{\partial\phi} - \frac{\sigma_{\phi}}{\mathbf{s}} = (\mathbf{Y}\mathbf{R} \sin \theta) \cos \phi$$

$$\frac{\partial\sigma_{\phi}}{\mathbf{s}\partial\phi} + \frac{1}{\mathbf{s}^2} \frac{\partial(T_{\mathbf{r}\phi}\mathbf{s}^2)}{\partial\mathbf{s}} = -(\mathbf{Y}\mathbf{R} \sin \theta) \sin \phi$$

$$\frac{\partial(T_{\mathbf{r}\theta}\mathbf{s})}{\mathbf{s}\partial\mathbf{s}} + \frac{1}{\mathbf{s}} \frac{\partial T_{\phi\theta}}{\partial\phi} = (\mathbf{Y}\mathbf{R} \cos \theta)$$
(1)

These equations are satisfied by the initial field of stress given by:

$$\sigma_{\mathbf{r}}(0) = (\mathbf{YR} \sin \theta) \cdot \mathbf{s} \cos \phi \qquad \qquad \sigma_{\phi}(0) = (\mathbf{YR} \sin \theta) \cdot \mathbf{s} \cos \phi$$

$$\sigma_{\theta}(0) = (\mathbf{YR} \sin \theta) \cdot 2\mathbf{v} \mathbf{s} \cos \phi \qquad \qquad T_{\mathbf{r}\phi}(0) = 0 \qquad (2)$$

$$T_{\mathbf{r}\theta}(0) = (\mathbf{YR} \cos \theta) \cdot \frac{1}{2} \cdot \mathbf{s} \qquad \qquad T_{\phi\theta}(0) = 0$$

The expression for σ_{θ} is based on the initial condition, ℓ_{θ} = 0. It can be shown that the initial stress field satisfies all six conditions of strain compatibility and, therefore, represents an allowable field of deformation.

To continue the analysis, it is convenient to omit the multiplier (YR sin θ) from the first four stresses. We also omit the multiplier (YR cos θ) from the last two stresses. Thus

$$\mathbf{\Theta}_{0} = (\sigma_{\mathbf{r}} + \sigma_{\phi} + \sigma_{\theta})_{0} = 2(1 + \nu) \text{ s cos } \phi$$
 (3)

The equilibrium functions for the next state of stress are

$$N_{0}(1) = \left[(\sigma_{\theta} - \sigma_{r}) \cos \phi + T_{r\theta} \right]_{0} = vs - \left(\frac{1 - 2v}{2} \right) s \cos 2\phi$$

$$N_{0}(2) = \left[(\sigma_{\phi} - \sigma_{\theta}) \sin \phi \right]_{0} = \frac{(1 - 2v)}{2} s \sin 2\phi$$

$$N_{0}(3) = -\left[2 T_{r\theta} \cos \phi + \sigma_{\theta} \right]_{0} = -(1 + 2v) s \cos \phi$$

The compatibility functions for the next state of stress are

$$V_{0}(1) = \frac{\partial \sigma}{\partial q} = 1$$

$$V_{0}(2) = \frac{\partial \sigma}{\partial q} = 1$$

$$V_{0}(3) = \frac{\partial \sigma}{\partial q} + \frac{1}{1+\nu} \frac{\partial \Phi}{\partial q} = 2(1+\nu)$$

$$V_{0}(4) = 0$$

$$V_{0}(5) = \frac{\partial T_{r\theta}}{\partial q} + 2\cos\phi = \frac{5}{2}\cos\phi$$

$$V_{0}(6) = -\frac{T_{r\theta}}{s} - 2\sin\phi = -\frac{5}{2}\sin\phi$$

4. STRESS FIELD FOR STATE (1)

The equations of motion are:

$$\left(\frac{1}{s} \frac{\partial (\sigma_{\mathbf{r}} \mathbf{s})}{\partial \mathbf{s}} + \frac{1}{s} \frac{\partial T_{\mathbf{r}\phi}}{\partial \phi} - \frac{\sigma_{\phi}}{\mathbf{s}}\right)_{1} = N_{0} (1)$$

$$\left(\frac{1}{s} \frac{\partial \sigma_{\phi}}{\partial \phi} + \frac{1}{s^{2}} \frac{\partial (T_{\mathbf{r}\phi} \mathbf{s}^{2})}{\partial \mathbf{s}}\right)_{1} = N_{0} (2)$$

$$\left(\frac{\partial (T_{\mathbf{r}\theta} \mathbf{s})}{\mathbf{s} \partial \mathbf{s}} + \frac{1}{s} \frac{\partial T_{\phi\theta}}{\partial \phi}\right)_{1} = N_{0} (3)$$

All terms on the LHS refer to the stress state (1).

A solution is readily found to be

$$\sigma_{\mathbf{r}}(1) = \frac{v}{4} \left[\mathbf{s}^2 + \frac{\mathbf{s_a}^2 \mathbf{s_b}^2}{\mathbf{s}^2} - (\mathbf{s_a}^2 + \mathbf{s_b}^2) \right] - (1 - 2v) \left[\frac{\mathbf{s}^2}{4} - \frac{\mathbf{B_2}}{\mathbf{s}^4} - \mathbf{C_2} - \frac{2\mathbf{D_2}}{\mathbf{s}^2} \right] \cos 2\phi$$

$$\sigma_{\phi}(1) = -\frac{v}{4} \left[\mathbf{s}^2 + \frac{\mathbf{s_a}^2 \mathbf{s_b}^2}{\mathbf{s}^2} + (\mathbf{s_a}^2 + \mathbf{s_b}^2) \right] - (1 - 2v) \left[\frac{\mathbf{s}^2}{4} + 2\mathbf{A_2}\mathbf{s}^2 + \frac{\mathbf{B_2}}{\mathbf{s}^4} + \mathbf{C_2} \right] \cos 2\phi$$

$$T_{r\phi}(1) = -(1 - 2\nu) \left[A_2 s^2 - \frac{B_2}{s^4} + C_2 - \frac{D_2}{s^2} \right] \sin 2\phi$$

$$\sigma_{\theta}(1) = d_0 - \frac{(1 + \nu)s^2}{2} - (1 - 2\nu) \left(d_1 s^2 + \frac{d_2}{s^2} \right) \cos 2\phi$$

$$T_{r\theta}(1) = \left(\frac{9 + 8\nu}{16} \right) \left[-s^2 - \frac{s_a^2 s_b^2}{s^2} + (s_b^2 + s_a^2) \right] \cos \phi$$

$$T_{\phi\theta}(1) = \left[\left(\frac{11 - 8\nu}{16} \right) s^2 - \frac{9 + 8\nu}{16} \left(\frac{s_a^2 s_b^2}{s^2} \right) - \frac{9 + 8\nu}{16} (s_b^2 + s_a^2) \right] \sin \phi$$
(5)

In the above, the boundary conditions determine A_2 , B_2 , C_2 and D_2

The boundary conditions are $\sigma_r = 0$ at $s = s_a$, s_b and $T_{r\phi} = 0$ at $s = s_a$, s_b

We find

$$A_{2} = -\frac{1}{4} \frac{(s_{b}^{4} + 4s_{a}^{2}s_{b}^{2} + s_{a}^{4})}{(s_{b}^{2} - s_{a}^{2})^{2}} \qquad C_{2} = \frac{1}{4} \frac{(s_{b}^{2} + s_{a}^{2})(s_{b}^{4} + s_{a}^{4} + s_{a}^{2}s_{b}^{2})}{(s_{b}^{2} - s_{a}^{2})^{2}}$$

$$B_{2} = \frac{3}{4} \frac{s_{a}^{4}s_{b}^{4}(s_{a}^{2} + s_{b}^{2})}{(s_{b}^{2} - s_{a}^{2})^{2}} \qquad D_{2} = -\frac{1}{2} \frac{s_{a}^{2}s_{b}^{2}(s_{b}^{4} + s_{a}^{4} + s_{a}^{2}s_{b}^{2})}{(s_{b}^{2} - s_{a}^{2})^{2}} \qquad (6)$$

The compatibility equations for stress state (1) are:

$$\left(\nabla_{0}^{2} \sigma_{\mathbf{r}} - \frac{4}{\mathbf{s}^{2}} \frac{\partial \mathbf{r}_{\varphi}}{\partial \phi} - \frac{2}{\mathbf{s}^{2}} (\sigma_{\mathbf{r}} - \sigma_{\phi}) + \frac{1}{1 + \nu} \frac{\partial^{2} \mathbf{\theta}}{\partial \mathbf{s}^{2}}\right)_{1} = -V_{0}(1)$$

$$\left(\nabla_{0}^{2} \sigma_{\theta} + \frac{4}{\mathbf{s}^{2}} \frac{\partial \mathbf{r}_{\varphi}}{\partial \phi} + \frac{2}{\mathbf{s}^{2}} (\sigma_{\mathbf{r}} - \sigma_{\phi}) + \frac{1}{1 + \nu} \left(\frac{1}{\mathbf{s}} \frac{\partial \mathbf{\theta}}{\partial \mathbf{s}} + \frac{1}{\mathbf{s}^{2}} \frac{\partial^{2} \mathbf{\theta}}{\partial \phi^{2}}\right)\right)_{1} = -V_{0}(2)$$

$$\left(\nabla_{0}^{2} \sigma_{\theta}\right)_{1} = -V_{0}(3)$$

$$\left(\nabla_{0}^{2} \mathbf{r}_{\varphi} + \frac{2}{\mathbf{s}^{2}} \frac{\partial}{\partial \phi} (\sigma_{\mathbf{r}} - \sigma_{\phi}) - \frac{4\mathbf{r}_{\varphi}}{\mathbf{s}^{2}} + \frac{1}{1 + \nu} \left[\frac{1}{\mathbf{s}} \frac{\partial^{2} \mathbf{\theta}}{\partial \mathbf{s} \partial \phi} - \frac{1}{\mathbf{s}^{2}} \frac{\partial \mathbf{\theta}}{\partial \phi}\right]\right)_{1} = -V_{0}(4)$$

$$\left(\nabla_{0}^{2} \mathbf{r}_{\varphi} - \frac{\mathbf{r}_{\varphi}}{\mathbf{s}^{2}} - \frac{2}{\mathbf{s}^{2}} \frac{\partial \mathbf{r}_{\varphi}}{\partial \phi}\right)_{1} = -V_{0}(5)$$

$$\left(\nabla_{0}^{2} \mathbf{r}_{\varphi} - \frac{\mathbf{r}_{\varphi}}{\mathbf{s}^{2}} + \frac{2}{\mathbf{s}^{2}} \frac{\partial \mathbf{r}_{\varphi}}{\partial \phi}\right)_{1} = -V_{0}(6)$$

These are satisfied by the solution of Equations (5) provided that

$$2d_1 = 4A_2 v - 1$$
 and $d_2 = -2D_2 v$ (7)

To complete the solution for $\boldsymbol{\sigma}_{\boldsymbol{\theta}}(\boldsymbol{1}),$ we take

$$d_0 = -\frac{v}{4} (s_a^2 + s_b^2)$$
.

The equation for d_0 follows from the boundary condition $T_{r\theta}(2) = 0$ for $s = s_a$, s_b .

5. STRESS FOR STATE (2)

The algebraic details for the determination of the six stresses for state (2) are reasonably lengthy. Space limitations require the omission of this stress state. However, the complete mathematical development for stress state (2) can be found in [4].

6. STRESS RATIOS

Since expressions for all unknown coefficients have been determined in the body of the paper, the field of six stresses may be summarized (by Equation number). Thus

The stress field resulting from the X-seismic component can be determined by replacing the multiplier YR sin θ by XR cos θ and by replacing the multiplier XR cos θ by - XR sin θ . The equations in square brackets represent stress ratios.

Calculations for the stress ratios on the inner and outer surfaces of an elbow or pipe bend are determined using s $_{\rm a}$ = 0.30 and s $_{\rm b}$ = 0.35. These two values correspond closely to major nuclear elbows. They were determined for elbows of heat exchangers and steam generators based on a specific design for a breeder reactor plant.

Because of the boundary conditions, T vanishes. Moreover, T = 0.175 YR cos θ on the outer surface and T = 0.15 YR cos θ on the inner surface.

The remaining stresses are given in Table 1 and have been computed for seven values of the circumferential angle, ϕ . Maximum values are underlined.

7.	Table 1. Stress Ratios
	Padial Strong (g /VP gin A or g /VP cos A)

Radial Stress ($\sigma_{\mathbf{r}}/\mathrm{YR}$ sin θ or $\sigma_{\mathbf{r}}/\mathrm{XR}$ cos θ)								
φ°	0	30	60	90	120	150	180	
Outer Surface	0.35	0.3031	0.175	0	-0.175	-0.3031	<u>-0.35</u>	
Inner Surface	0.30	0.2598	0.150	0	-0.150	-0.2598	-0.30	
	Circumferential Stress $(\sigma_{\phi}/YR \sin \theta \text{ or } \sigma_{\phi}/XR \cos \theta)$							
φ°	0	30	60	90	12Ŏ	150	180	
Outer Surface	0.6892	0.6423	-0.0424	-0.4030	-0.3924	-0.1494	-0.0108	
Inner Surface	-0.1880	-0.0001	0.3462	0.4242	0.0462	-0.5197	- <u>0.7880</u>	
Meridional Stress $(\sigma_{\theta}/YR \sin \theta \text{ or } \sigma_{\theta}/XR \cos \theta)$								
	Meridio	nal Stres	s (o _A /YR :	$\sin \theta$ or	σ _θ /XR cos	θ)		
φ	Meridio	nal Stres 30	s (σ _θ /YR : 60	sin θ or 90	σ _θ /XR cos 120	θ) 150	180	
φ° Outer Surface	_		. °1		-		180 -0.4427	
	0	30	60	90	120	150		
Outer Surface	0 0.2627 -0.0078	30 0.3439 0.0248	60 -0.0571 0.0723	90 -0.2337 0.0390	120 -0.2671 -0.1077	150 -0.2008 -0.2870	<u>-0.4427</u>	
Outer Surface	0 0.2627 -0.0078	30 0.3439	60 -0.0571 0.0723	90 -0.2337 0.0390	120 -0.2671 -0.1077	150 -0.2008 -0.2870	<u>-0.4427</u>	
Outer Surface	0 0.2627 -0.0078 Shear	30 0.3439 0.0248 Stress (T	60 -0.0571 0.0723 φθ/YR cos	90 -0.2337 0.0390 θ or - T	120 -0.2671 -0.1077 $\phi\theta$ /XR sin	150 -0.2008 -0.2870 θ)	<u>-0.4427</u> <u>-0.3678</u>	

MAXIMUM STRESSES

From Table 1, it is possible to determine the maximum stresses and their location. For the Y seismic component only

Maximum circumferential stress = -0.788 YR (at ϕ = 180°, θ = 90°, s = s_a)

Maximum meridional stress = -0.4427 YR (at ϕ = 180°, θ = 90°, s = s_h)

For the X seismic component only

Maximum circumferential stress = -0.7881 XR (at ϕ = 180°, θ = 0°, s = s₂)

Maximum meridional stress = -0.4427 XR (at ϕ = 180°, θ = 0°, s = s_h)

For both X and Y seismic components

Maximum circumferential stress = -0.788R $\sqrt{X^2 + Y^2}$

(at
$$\phi = 180^{\circ}$$
, $s = s_a$, $\tan \theta = \frac{Y}{X}$)

For equal X and Y seismic components

Maximum circumferential stress = -1.114 YR (at ϕ = 180°, s = s_a, θ = 45°)

Maximum stresses σ_r and $\tau_{r\phi}$ are located (very nearly) at the geometric mean radius s = $\sqrt{s_a s_b}$

CONCLUSION

The six stress components for stress states (0) and (1) have been determined in the paper. The method of successive approximations, as mentioned previously, can be continued but the algebraic details become lengthy. The steps for the determination of stress state (2) are detailed in [4].

The maximum value of θ for an elbow is 90°. However, this value can be decreased or increased to correspond to a curved pipe bend or a partial elbow.

The stresses σ_{φ} and σ_{θ} at the outside and inside surfaces of an elbow are readily determined by computer routines for both X and Y seismic components. Two computer routines (in Fortran), incorporating stress state (2) as well as stress states (0) and (1), have been established.

REFERENCES

- H.A. LANG 1980 Fourth International Conference on Pressure Vessel Technology, London, England. Proceedings, vol. 2, 251-260. Stress Analysis of Pressurized Elbows for Nuclear Components using Toroidal Elasticity.
- 2. H.A. LANG 1982 Strain Analysis for Engineering Design (to be submitted). Seismically Induced Stress Fields in a Circular Ring Sector.
- 3. H.A. LANG 1982 Strain Analysis for Engineering Design (to be submitted). Stress Fields Produced by a Vertical Seismic Force Acting on a Circular Ring Sector.
- 4. H.A. LANG 1983 International Journal of Pressure Vessels and Piping (to be submitted). Seismic Stress Fields in a Hollow Circular Elbow or Pipe Bend.

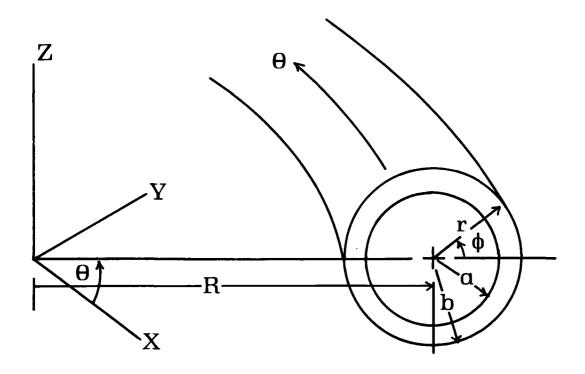


Figure 1. Toroidal Coordinates and Seismic Axes X, Y, Z

AD-P003 643



VIBRATIONAL POWER TRANSMISSION FROM A SHORT SOURCE BEAM TO A LONG FINITE RECEIVER BEAM VIA A VIBRATION ISOLATOR

R.J. Pinnington Institute of Sound and Vibration Research University of Southampton

1.0 INTRODUCTION

In many engineering situations machines have to be mounted upon a flexible foundation, and as a vibration control measure compliant isolators are used to mechanically decouple the two systems from each other. The effectiveness of this vibration isolation is most completely described in terms of the vibrational power transmission to the flexible foundation.

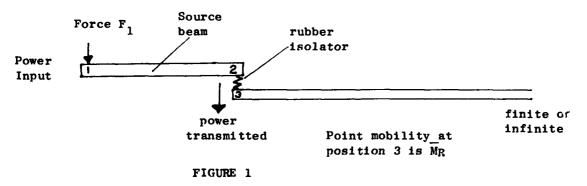
For large complex foundations it is difficult and often unnecessary to predict detailed narrow band power transmission. A rather more practical approach is to predict the frequency averaged power transmission in terms of a few controlling parameters namely; the frequency averaged point mobilities of the machine and foundation structures, and the stiffness and damping of the isolator. In |1| this method was used to analyse the low frequency problem, where the machine was represented by a rigid mass and the foundation represented by a long finite beam.

In this paper the higher frequency vibration is considered, where the machine can vibrate in the natural modes of vibration. For simplicity the machine is represented by a simple free-free beam excited at one end. This is connected at the undriven end via a rubber spring to long finite beam, (the finite but large flexible foundation). This configuration was chosen as the analysis renders a simple algebraic solution for the frequency average power transmission. However, the results are more generally applicable, as the solution requires only the frequency average mobility of the two systems at the coupling point.

The theoretical formulae are compared with some experimental measurements of a short finite beam coupled via an isolator to an "infinite beam" and a long finite beam.

2.0 THEORY

The system under consideration is shown in Figure 1.



The short source beam is driven at the free end by a pure force of magnitude F_1 . End (2) of the beam is connected by a damped spring, of complex stiffness K(1+in), to the long receiver beam.

The point mobility at one end of the source beam before coupling is defined in [1] as:

$$\overline{M}_2 = S_n + iS_i - iS \tag{1}$$

where

$$S_{r} = \frac{S \cos \varepsilon}{1 - \sin \varepsilon \sin \theta}, \qquad S_{i} = \frac{S \sin \varepsilon \cos \theta}{1 - \sin \varepsilon \sin \theta}$$
 (2)

S is the real component of the point mobility at the end of an equivalent semi-infinite source beam, $G=2k\ell-\frac{\pi}{2}$ is the phase change in a wave making a return journey from the end of the finite source beam (at length ℓ and wavenumber k). E is the damping parameter, controlling the peak value of the point mobility S at resonance (when sin@=1) i.e. from Equation 1,

$$\hat{S} - 2S/\cos \epsilon$$
 (3)

It is shown in [2] that the transfer mobility \overline{M}_{12} between points 1 and 2 is related to the real component of the point mobility S_r by the expression,

$$|\mathbf{M}_{12}|^2 = \hat{\mathbf{S}} \, \mathbf{S}_{\mathbf{r}} \, \sin \varepsilon. \tag{4}$$

Likewise for the uncoupled receiver beam the point mobility at one end is given in general as:

$$\overline{M}_{12} = Q_r + iQ_i - iQ \tag{5}$$

where

$$Q_{r} = \frac{Q \cos \beta}{1 - \sin \beta \sin \theta}, \qquad Q_{i} = \frac{Q \sin \beta \cos \theta}{1 - \sin \beta \sin \theta}$$
 (6)

where Q is the real component of the point mobility of an equivalent semi-infinite receiver beam. B and 9 are the damping and phase parameters, similarly defined as for the source beam above. Q is the resonance peak value of the receiver beam mobility and is equal to

$$\hat{Q} = 2Q/\cos\beta \tag{7}$$

The vibration and power transmission between two systems coupled at a single point as is Figure 1, can be written in terms of the point and transfer

$$P_{tr} = \frac{1}{2} |F_1|^2, \quad \frac{|M_{12}|^2}{\left|\overline{M}_2 + \overline{M}_R + \frac{\omega}{V} (1+i\eta)\right|^2}. \quad \text{Re } \{\overline{M}_R\}$$
 (8)

The vibrational power transmission is calculated by substituting for \overline{M}_2 , \overline{M}_{12} and \overline{M}_L using Equations 1-7, and performing the following algebra.

The Power Transmission averaged over several receiver beam resonances. < P>

Power transmission occurs between the two beams due to resonances in both systems. The receiver is assumed to be much larger than the source and so for each source beam resonance, $(0 < 9 < 2\pi)$, there are many receiver beam resonances. It is therefore assumed that for each receiver beam resonance (i.e.) for an interval 0< θ < 2π , θ , and hence the source beam mobility, remains constant. The averaged power transmission due to each receiver resonance <P> , can be found by averaging equation 8 over an interval of 0< θ < 2π , as follows.

First, substituting equation (5) and (1) into (8) gives
$$P_{tr} = \frac{1}{2} |F_1|^2 \cdot \frac{|M_{12}|^2 \cdot Q_r}{(S_r + \frac{\eta \omega}{K} + Q_r)^2 + (S_1 + C + Q_1)^2}$$
(9)

where $C=(S+Q-\omega/K)$.

By substituting from Equation (6) for $\mathbf{Q_r}$ and $\mathbf{Q_i}$, and by making use of the identity

$$Q_{\mathbf{r}}^2 + Q_{\mathbf{i}}^2 = Q^2 \cdot \frac{1 + \sin\beta\sin\theta}{1 - \sin\beta\sin\theta} , \qquad (10)$$

enables equation (9) to be written in terms of θ and β

$$P_{tr} = \frac{1}{2} |F_1|^2 \cdot \frac{|M_{12}|^2 \cdot Q \cos \beta}{a_1^2 + 2Q(S_r + \frac{\eta \omega}{K}) \cos \beta - \sin \beta \left[(a_1^2 - 2Q^2) \sin \theta - 2Q(S_1 + A) \cos \theta \right]}$$

where
$$a_1^2 = (Sr + \frac{\eta \omega}{K})^2 + (S_1 + C)^2 + Q^2$$
. (11)

Using the two angle formula

$$sin(A-B) = sinA.cosB - cosAsinB$$
 (12)

in Equation (11) gives

$$P_{tr} = \frac{1}{2} |F_1|^2 \cdot \frac{|M_{12}|^2 \cdot Q \cos \beta}{a_1^2 + 2Q(S_r + \frac{\eta \omega}{K}) \cos \beta - \sin \beta \left[a_1^4 - 4Q^2 (S_r + \frac{\eta \omega}{K})^2 \right]^{\frac{1}{2}} \sin(\theta - \gamma)}, (13)$$

where

$$\tan \gamma = \frac{2Q(S_1 + C)}{a_1^2 - 2Q^2}$$
 (14)

Now as Θ varies over an interval $0 < \Theta < 2\pi$, all the other terms in equation (13) remain approximately constant being functions of either \emptyset or ω . There is a peak in power transmission associated with a receiver mode whenever $sm(\Theta-\gamma)=1$. The average power transmission from each of these peaks < P >, is formed by averaging equation (13) over an interval $0 < \Theta < 2\pi$, i.e.

$$< P> = \frac{1}{2\pi} \int_{0}^{2\pi} P_{tr} d\theta$$

This integral is solved using a standard solution, see for example 3.

$$\frac{1}{2\pi} \int_{0}^{2\pi} \frac{d}{b-c \sin x} dx = \frac{d}{(b-c)^{\frac{1}{2}}}$$
 (15)

a,b,c are constants b>c.

Therefore,

$$\langle p \rangle = \frac{1}{2} |F_1|^2 \cdot \frac{|M_{12}|^2 \cdot Q}{a_1^2 + (S_r + \frac{\eta \omega}{K}) \cdot Q}$$
 (16)

Substituting for $|M_{12}|^2$ and a_1^2 in terms of S_r and S_1 using equations (2) and (4) respectively, gives

$$\langle P \rangle = \frac{1}{2} |F_1|^2 \cdot \frac{2S.S_r.tanc.Q}{(S_r^2 + S_1^2) + S_r(\hat{Q} + \frac{2\eta\omega}{K}) + 2S_1C + C_2^2Q_d^2},$$
 (17)

where

$$Q_d^2 = Q^2 + \frac{\eta_W}{\kappa} \hat{Q} + (\frac{\eta_W}{\kappa})^2.$$
 (18)

By making use of the identity

$$S_{r}^{2} + S_{i}^{2} = S^{2}. \frac{(1+\sin \epsilon \sin \theta)}{1-\sin \epsilon \sin \theta}$$
(19)

and substituting for S_r and S_i in terms of \emptyset , from equation (3), <P> becomes, after some manipulation

$$\langle P \rangle = \frac{1}{2} |F_1|^2. \frac{S \sin \varepsilon . 2SQ}{a_2^2 + S \cos \varepsilon \left\{ \hat{Q} + \frac{2\eta \omega}{K} \right\} - \sin \varepsilon \left[(a_2^2 - 2S^2) \sin \emptyset - 2SC \cos \emptyset \right]}$$
 (20)

where $a_2^2 = S^2 + Q_d^2 + C^2$.

Using the identity in Equation (12), the term in [] becomes after some manipulation.

$$\left[a_{2}^{4} - 4S^{2}Q_{d}^{2}\right]^{\frac{1}{2}} \sin(\theta - \gamma),$$

where

$$tan\gamma = \frac{2SC}{a_2^2 - 2S^2}.$$
 (21)

<P> therefore becomes

$$\langle P \rangle = \frac{1}{2} |F_1|^2 \cdot \frac{S \sin \epsilon \cdot 2SQ}{a_2^2 + S \cos \epsilon (\hat{Q} + \frac{2\eta \omega}{K}) - \sin \epsilon \left[a_2^4 - 4S^2 Q_d^2 \right]^{\frac{1}{2}} \sin(\theta - \gamma)}$$
(22)

<P>, as expressed in Equation (22) is of the same form as the real component of the source beam mobility S_{Γ} , Equation (2), except that <P> is a function of \mathcal{G} - γ rather than \mathcal{G} . This means that the maximum power is, in this case, input and transmitted at the resonance frequencies of the coupled system when \mathcal{G} - γ -1, rather than at the uncoupled resonance frequency when \mathcal{G} =1.

3.0 EXPRESSIONS FOR <P>, <P> AND <<P>>

The properties of <P> can be summarised in terms of its maximum value < \hat{P} >, when sin (\emptyset - γ) = 1; its trough value < \hat{P} >, when sin (\emptyset - γ)=-1, and the frequency averaged value <<P>>>.

These quantities are found by (i) assuming that 2the damping of the source beam is light, allowing sin ϵ to be written as $1-\frac{\cos 2\epsilon}{2}$. (ii) Assuming S $\neq Q_d$ at the frequency of maximum coupling (when (S+Q- ω /K) = 0, then the approximation may be made

$$\left|a_{2}^{2}-4S^{2}Q_{d}^{2}\right|^{\frac{1}{2}} = a_{2}^{2}-\frac{2S^{2}Q_{d}^{2}}{a_{2}^{2}}$$
 (23)

(iii) dividing the numerator and demoninator of equation (22) by a_2^4 . When $\sin(\theta-\gamma) = 1$, the peak value $\langle \hat{P} \rangle$ is

$$\langle \hat{P} \rangle = \frac{1}{2} |F_1|^2 \cdot \frac{S \sin \varepsilon}{\left(\frac{\cos \varepsilon}{t_d}\right)^2 + \left(\frac{\cos \varepsilon}{\cos \beta}\right) + \left(\frac{t_d^2}{4}, \left(\frac{Q_d}{Q}\right)^2\right)}$$
(1) (11) (111)

When sin(9-x) = -1 the trough value occurs

$$\langle P \rangle = \frac{1}{2} |F_1|^2 \cdot \frac{S \sin \varepsilon}{\left(\frac{4}{t_0^2}\right) + \left(\frac{\cos \varepsilon}{\cos \beta}\right)}$$
(1) (11)

The frequency average value is given by averaging equation (22) over an interval of $0< 9< 2\pi$, but it is also found to be the geometric mean <P> and <P̄>, namely

$$\langle \langle P \rangle \rangle = \frac{1}{2} |F_1|^2 \frac{S \sin \varepsilon}{\left(\frac{2\cos}{t_d}\right)^2 + \left(\frac{\cos \varepsilon}{\cos \beta} \cdot \frac{4}{t_d^2}\right) + \left(\frac{\cos \varepsilon}{\cos \beta}\right)^2 + \left(\frac{Q}{Q}\right)^2}$$
(26)

where t_d^2 is a kind of transmission coefficient for waves in the source beam at the connecting boundary with the isolator, and is defined as:

$$t_{d}^{2} = \frac{4QS}{a_{2}^{2}} = \frac{4QS}{S^{2} + Q_{d}^{2} + (S + Q - K)^{2}}$$
(27)

4.0 PARAMETERS CONTROLLING POWER TRANSMISSION

The three parameters which control the power transmission are in the denominator of Equation 24, they are: (i) $(\cos\epsilon/t_d)^2$ the coupling between the beams (ii) $(\cos\epsilon/\cos\beta)$ or $S\hat{Q}/\hat{Q}$ the relative damping of the two beams (iii) the isolator damping parameter ($t_d Q_d/2Q$). The largest of these three terms is therefore the controlling parameter in a particular frequency regime.

4.1 Heavy source beam damping and light receiver beam and isolator damping

Under this condition $\cos \epsilon/\cos \beta$ is the controlling parameter of Equation (24). It can be seen from Figure 2 that decreasing $\cos \beta$ (the receiver damping) or increasing the source beam damping, decreases the peak power transmission <P>, but leaves the trough value unaffected. In this condition the vibrational power input to the source beam is mainly dissipated there. With increasing frequency a point is reached when $(\cos \epsilon/t_d)^2 > \cos \epsilon/\cos \beta$ or $(\omega/K)^2 > \hat{SQ}$ (the break points in Figure 2). Above this frequency the source beam becomes uncoupled from the receiver beam and behaves as a velocity source driving the top of the isolator. The peak and trough power transmission are given from Equation (24) as

$$\langle \hat{P} \rangle = \frac{1}{2} |F_1|^2 .S\hat{S}(\omega/K)^2 .Q, \qquad \langle \hat{P} \rangle = \frac{1}{2} |F_1|^2 .S\hat{S}.(\omega/K)^2 .Q$$
 (28)
 $\hat{S} - S \cos \varepsilon/2.$

where

4.2 Light source beam damping or heavy isolator damping

Under this condition term (iii) in Equation (24) diminishes the low frequency response seen in Figures 3 and 4. Increasing the isolator damping and decreasing the receiver beam damping reducing the vibrational power transmission. If there is no isolator damping then then power transmitted equals the power input to the source beam, which is on average

$$<>_{tr} = \frac{1}{2} |F_1|^2 . S.$$
 (29)

With increasing frequency decoupling between the two beams occurs when $2\cos/t_d^2 > Q_d/Q$. (The break points in Figure 3).

Above this frequency the frequency averaged power transmission takes the values given in Equation (28).

5.0 EXPERIMENTAL RESULTS

An experiment was set up with the configuration shown in Figure 1 in order to test the theoretical predictions. The source beam was a 50cm x 3.2cm x 6mm aluminium alloy bar, with both sides damped with a constrained layer damping treatment. The receiver beam was of steel and had dimensions 6.2lm x 5cm x6mm. The isolator consisted of two adjacent blocks of natural rubber each 1cm x 1.2cm x 1.2cm. The dynamic stiffness was constant at 1.2 x 10⁵N/m until 2 KHz. The vibrational power input at end 1 of the source beam was measured using the force and acceleration signals from an impedance head, while the power transmitted to the receiver beam was measured from the acceleration on the beam using the expression,

 $P = \frac{1}{2} |V|^2 \times Re\{M_R\} / |M_R|^2$. as in |1|.

Figure 5 shows the vibrational power (normalised to the input force) input to the uncoupled source beam. The maximum power is input at the resonances and the frequency averaged value is given by Equation 29. Figure 6 shows the vibrational power input to the source beam and transmitted to the receiver beam when the receiver beam was semi-infinite. In practical terms this entailed the far end of the beam being embedded in a sand box.

The frequency averaged power input to the source beam is again equal to that of the uncoupled source beam (Figure 5, Equation 29). The frequency averaged power transmitted, Figs 6 and 7, were predicted from Equations 24-26 using the measured values for $\hat{S}, \hat{S}, \hat{Q}, Q$, ω/K . For frequencies less than 400 Hz it was found that the isolator (Case 4.2) (term iii Equation 24) controlled the power transmission (i.e. the source beam damping is ineffective).

Figure 8 shows the vibrational power input to the source beam and transmitted to the finite receiver beam (no sand box). It can again be seen that above 400Hz the two beams are only weakly coupled, the power input is not strongly influenced by the presence of the receiver beam. Figure 9 shows the frequency averaged power transmitted compared to that of the semi-infinite beam. Below the decoupling frequency (400Hz) it can be seen that slightly less power is transmitted to the finite beam than to the semi-infinite beam, the isolator damping being more efficient when the receiver beam is finite.

REFERENCES

- 1. R.J.PINNINGTON and R.G. WHITE, Power flow through machine isolators to resonant and non-resonant beams. JSV 75(2) 1981, 179-197.
- 2. R.J.PINNINGTON, 1980. Power transmission from rigid and resonant sources to resonant and non-resonant structures. ISVR Tech Report 114.
- 3. G.E.CARRIER, McKROOK and C.E.PEARSON. Functions of a complex variable. McGraw Hill, 1966.

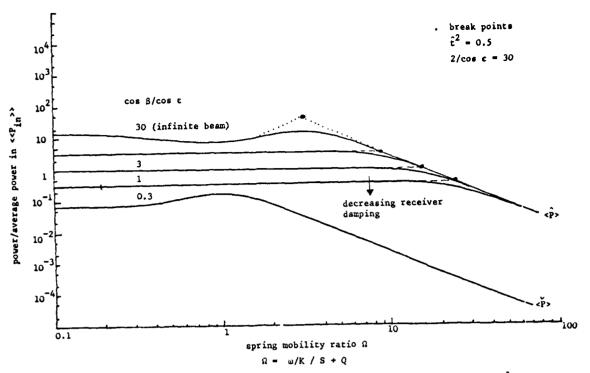


Fig. 2 The effect of the source-receiver damping ratio (cos β /cos ϵ) on peak $\langle \hat{P} \rangle$ and trough $\langle P \rangle$ power transmission.

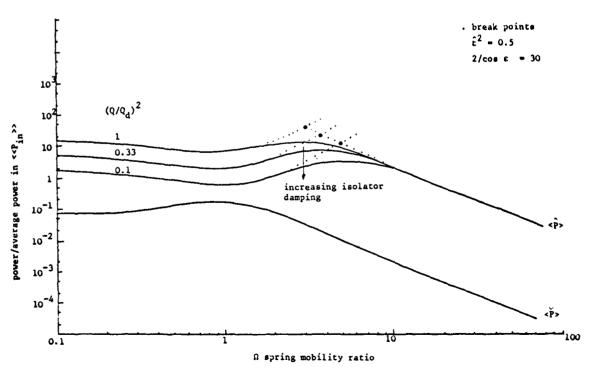


Fig.3 The effect of increasing the isolator damping on $\langle \hat{P} \rangle$ and $\langle \hat{P} \rangle$ when the source mobility is greater than the receiver mobility, i.e., S > Q.

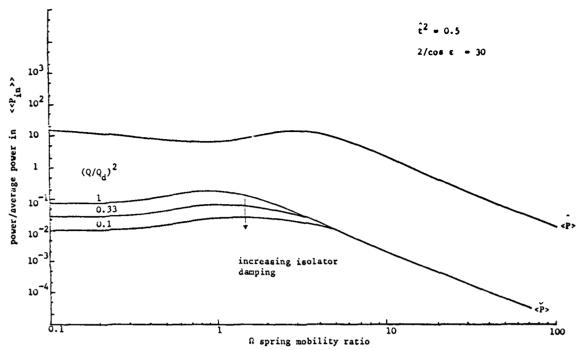


Fig.4 The effect of increasing the isolator damping on $\langle \hat{P} \rangle$ and $\langle \hat{P} \rangle$ when the source mobility is less than the receiver mobility, i.e., S < Q.



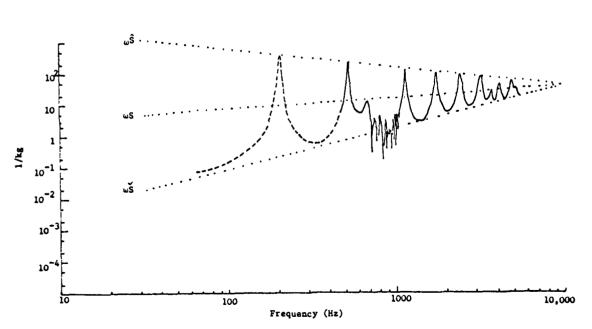


Fig. 5 Imaginary component of inertance at end 1 of the source beam

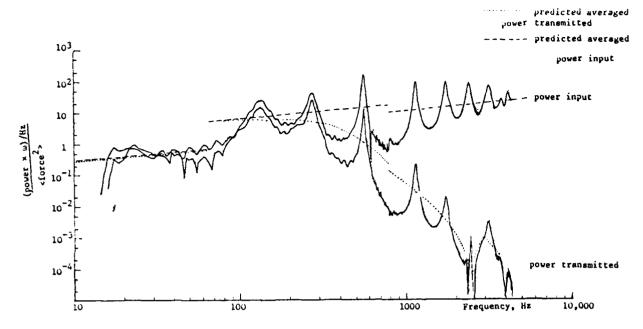


Fig. 6 Power $\times \omega$ input to source beam and transmitted to the semi-infinite receiver beam, unit force spectral density input, 10 Hz - 4 kHz.

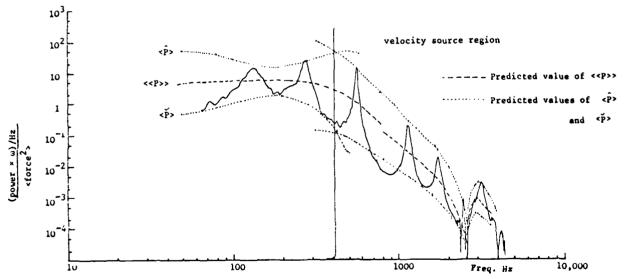


Fig. 7 Power × ω transmitted to the semi-infinite receiver beam unit force spectral density, 10 Hz

- 4 kHz.

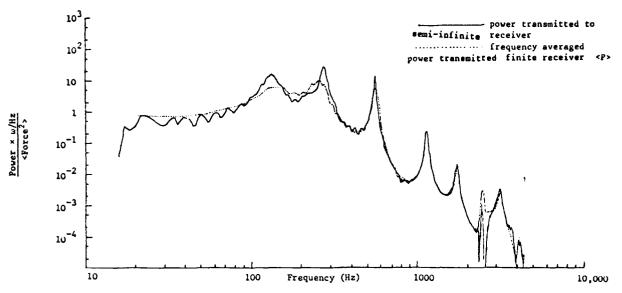
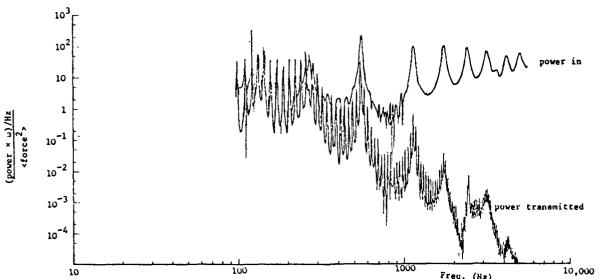


Fig. 9 Comparison of power $\times \omega$ transmitted to a semi-infinite beam and the frequency averaged power $\times \omega$ transmitted to a finite beam, for unit force spectral density input, 10 Hz -

4 kHz.



Freq. (Hz)

Fig. 8 Power × ω input to source beam and transmitted to finite receiver beam for unit input force spectral density, 100 Hz - 4 kHz.

PREDICTION OF SMOOTHED FREQUENCY RESPONSES USING GENERAL ORTHOGONAL POLYNOMIALS



M.E. Gaylard

Department of Mechanical Engineering
Brunel University

1. INTRODUCTION

Smoothed frequency responses describe vibration behaviour without regard to resonant-antiresonant detail. The object in this paper is to show how they can be predicted from information about stiffness coefficients and masses, using a series-expansion in general orthogonal polynomials (not just the Tchebyshev polynomials which were used in a previous paper [1]).

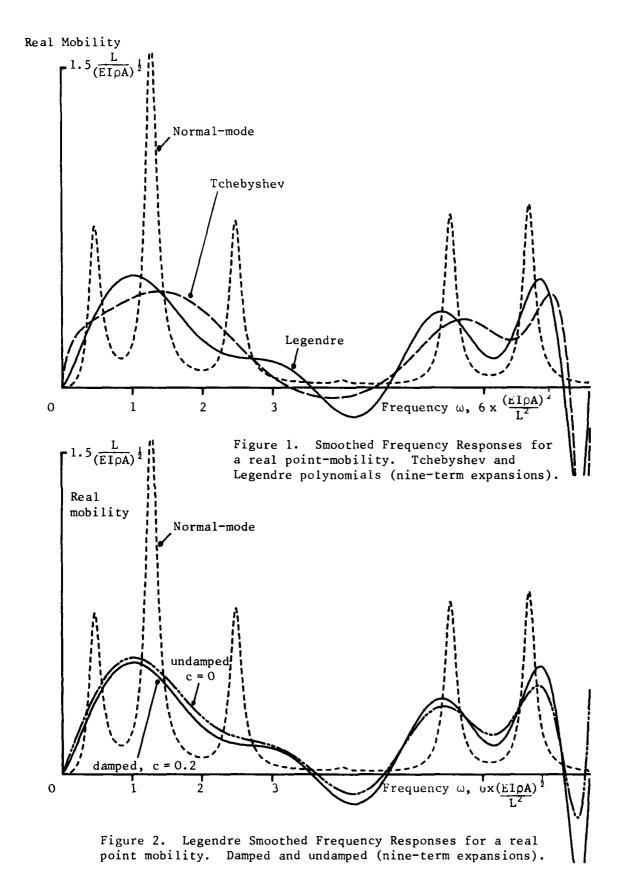
Resonant-antiresonant detail concerns sharpness, range, and location of resonant peaks and antiresonant notches in the true vibration response, and for many purposes constitutes the most important feature of that response. Nevertheless, there is some interest in the part of the vibration response that still can be examined when resonant-antiresonant detail is unknown, witness two known approaches: Statistical Energy Analysis 12 and the Mean-Value Method. 13.

A recently-introduced method [1] is to apply smoothing by means of an orthogonal polynomial fit. Using a series-expansion, there is heavier smoothing as fewer orthogonal polynomial terms are employed, but resonant-antiresonant detail can be recovered if the number of terms is sufficiently increased. Figures 1 and 2 of this paper show examples of smoothed frequency responses where nine orthogonal polynomial terms were used to describe a behaviour governed by six modes of vibration.

To obtain a smoothed frequency response, there is no need to establish the full response which contains resonant-antiresonant detail, nor is there any need to determine natural frequencies or modes of vibration. It suffices to know the elements of the stiffness matrix and mass matrix for the structure or other system under study. By considering real mobility versus frequency, the smoothed frequency response has a much weakened dependence on damping, compared with other measures such as, say, receptance versus frequency (unless many polynomial terms are used, or damping is heavy). Reference [1] gives details and theory for smoothed frequency responses relating to matrix-characterized structures, together with an example on a theoretical structure (a uniform clamped-clamped beam considered in seven equal elements, which also provides data for figures 1 and 2 in the present paper).

Reference [1] also suggests applications where it is reasonable to seek some advantage from a smoothed frequency response, compared with Statistical Energy Analysis [2] or normal-mode analysis. Such advantages concern volume of arithmetical working, simplified presentation of frequency-responses, disclaim of a detailed exactitude which may be spurious because of uncertain numerical data, certain possibilities relating to incompletely-characterized structures, and investigation of the known [4] relation between modal density and the real mobilities. However, the derivation and method in reference [1] is limited to one particular sort of orthogonal polynomial (Tchebyshev), and it is natural to enquire about the use of other polynomials.

The present paper includes a summary of the theoretical basis in reference [1], sufficient to introduce some new developments, namely the extension to the case of general orthogonal polynomials, the suggestion that it may be profitable to ignore damping so long as smoothed frequency responses



do not depend on too many orthogonal polynomial terms, and an example with Legendre polynomials for comparison with earlier results for the Tchebyshev case.

2. EXPANSION IN GENERAL ORTHOGONAL POLYNOMIALS

Consider the following series-expansion in polynomial functions $f_n(\underline{A})$ of a matrix \underline{A} ,

$$\operatorname{Re}(\underline{Y}) = (\phi_{0}(\omega) \cdot f_{0}(\underline{A}) + \phi_{1}(\omega) \cdot f_{1}(\underline{A}) + \dots + \phi_{v}(\omega) \cdot f_{v}(\underline{A})) \cdot \underline{M}^{-1}$$
(1)

which relates to a system with stiffness matrix \underline{K} , mass matrix \underline{M} , viscous damping which is assumed to take the special form $c\underline{M}$, and with vector \underline{x} of displacement-amplitudes. If there is excitation by sinusoidal forces at frequency ω rad.s with amplitudes recorded in vector \underline{F} , the matrix force equation is

$$(\underline{K} + j\omega c\underline{M} - \omega^2\underline{M}) \cdot \underline{x} = \underline{F}$$
 (2)

and a matrix of mobilities Y in $j\omega x = Y.F$ is given by

$$\underline{Y} = j\omega(\underline{K} + j\omega c\underline{M} - \omega^2 \underline{M})^{-1}$$

$$= j\omega(\underline{M}^{-1}\underline{K} + (j\omega c - \omega^2)\underline{I})^{-1}.\underline{M}^{-1}$$
(3)

Re(\underline{Y}) in equation (1) signifies a matrix whose elements are real parts of mobilities, and the $\phi_n(\omega)$ are scalar coefficients. Matrix \underline{A} is equal to $\underline{\underline{M}}^{-1}\underline{\underline{K}}$, or, in practice, is linearly related to $\underline{\underline{M}}^{-1}\underline{\underline{K}}$ for purposes of standardisation. The polynomial functions $f_n(\underline{A})$ are best computed by means of a recurrence relation which is given in equation (5) below.

The coefficients $\phi_n(\omega)$ are constant functions of n and ω , regardless of the rank and content of the N x N matrices \underline{K} , \underline{M} , \underline{A} etc., even if N = 1 (when all quantities reduce to scalars). This is easily shown, given a similarity transformation which diagonalises $\underline{M}^{-1}\underline{K}$ and consequently \underline{A} (i.e. a transformation like $\underline{X}^{-1}(\underline{M}^{-1}\underline{K})\underline{X} = \underline{\Lambda}$, a diagonal matrix). Consequently, determination of the coefficients $\phi_n(\omega)$ can proceed by reference to the scalar case, using a well-known method which requires that the scalar $f_n(A)$ are orthogonal polynomials in scalar A, that is,

where w(A) is a chosen weight function, and (a,b) is an interval which, in the present application, must be chosen to contain all of the eigenvalues of \underline{A} .

It is an important feature that any orthogonal polynomial of a continuous variable must [5] obey a recurrence relation:

$$f_n(A) = (c_1 + c_2.A).f_{n-1}(A) - c_3.f_{n-2}(A)$$
 (5)

where c_1 , c_2 , and c_3 are constants which depend on the sort of polynomial (Tchebyshev, Legendre, etc. [5], [6]), and may depend on n. In the present work, the same equation (5) is used for the matrix $f_n(\underline{A})$ as for the scalar $f_n(\underline{A})$.

For the scalar real mobility, equation (3) gives

Re(y) = Re(j
$$\omega$$
(k/m + j ω c - ω ²)⁻¹ · m⁻¹)
= Re(j ω (A - z)⁻¹ · m⁻¹) (6)

where
$$A = k/m$$
 (7)

and
$$z = \omega^2 - j\omega c$$
 (8)

(In practice, identities (7) and (8) are replaced by linear relations, thereby standardising A and z so that all values fall in some chosen interval, for example within the interval (a,b) = (-1,1), see reference [1]).

The orthogonality expressed in equation (4) permits the following determination for coefficients in a series-expansion,

$$\phi_{n}(\omega) = \frac{1}{h_{n}} \int_{a}^{b} \operatorname{Re}(y) \cdot f_{n}(A) \cdot w(A) \cdot dA$$

$$= \frac{-\omega}{m \cdot h_{n}} \cdot \operatorname{Im} \left(\int_{a}^{b} \frac{f_{n}(A) \cdot w(A)}{(A - z)} dA \right)$$
(9)

After equation (9), all that remains for determination of coefficients in matrix equation (1) is to evaluate integrals of the type

$$I_{n} = \int_{a}^{b} \frac{f_{n}(A).w(A)}{(A-z)} dA$$
 (10)

In reference [1], I_n was evaluated only for one sort of polynomial, the Tchebyshev polynomials $f_n(A) = T_n(A)$ with weight function $w(A) = (1 - A^2)^{-\frac{1}{2}}$, see [5] or [6]. A present development relates to the general case, when $f_n(A)$ is any orthogonal polynomial of a continuous variable. It concerns the reduction of an integral I_n to the simplest integral I_0 , by exploiting the same recurrence relation, equation (5), as governs the polynomials $f_n(A)$ in the integrand. Substituting with equation (5) in equation (10) gives

$$I_{n} = \int_{a}^{b} \frac{(c_{1} + c_{2}.A).f_{n-1}(A) - c_{3}.f_{n-2}(A)}{(A - z)} w(A).dA$$

$$= \int_{a}^{b} \frac{(c_{1} + c_{2} \cdot z) \cdot f_{n-1}(A) - c_{3} \cdot f_{n-2}(A)}{(A - z)} w(A) \cdot dA$$

$$+ \int_{a}^{b} \frac{c_{2} \cdot (A - z) \cdot f_{n-1}(A)}{(A - z)} w(A) \cdot dA$$

$$= (c_{1} + c_{2} \cdot z) \cdot I_{n-1} - c_{3} \cdot I_{n-2} + c_{2} \cdot \int_{a}^{b} f_{n-1}(A) \cdot w(A) \cdot dA$$
(11)

But orthogonality in equation (4) gives

$$\int_{a}^{b} f_{n-1}(A) \cdot w(A) \cdot dA = 0 \qquad (n = 2, 3, 4, ...)$$

$$= \frac{h_{0}}{f_{00}} \qquad (n = 1)$$

because $f_0(A) = a$ constant, $f_0(A) = a$ consequently the integrals in equation (10) obey the same recurrence relation as in equation (5), that is,

$$I_n = (c_1 + c_2.z).I_{n-1} - c_3.I_{n-2}$$
 $(n = 2,3,4,.....)$ (12)

and, by considering $f_1(A) = f_{11} \cdot A - f_{10}$, where f_{11} , f_{10} are constants, it is easily shown that

$$I_1 = f_1(z) \cdot I_0 + f_{11} \cdot \frac{h_0}{f_{00}}$$
 (13)

Both of equations (12) and (13) depend on
$$I_0 = f_{00} \cdot \int_a^b \frac{w(A) \cdot dA}{(A-z)}$$
 (14)

If the integral I in equation (14) can be evaluated, then all other integrals I, I, I, etc. in equations (10), (12) and (13) become straightforward, and complete the determination for coefficients $\phi_1(\omega)$ in matrix equation (1). From this general approach, two special cases (those of the Tchebyshev and Legendre polynomials) are selected for evaluation of I as follows.

For the Tchebyshev polynomials, $w(A) = (1 - A^2)^{-\frac{1}{2}}$, standardised interval (-1,1), contour integration (e.g. in [1]) gives

Tchebyshev
$$I_o = \frac{-j 2\pi}{(b-a) \cdot \sin(\alpha + j\beta)}$$
 whence, from equation (13), $I_1 = \frac{-j 2\pi \cdot \exp(j(\alpha + j\beta))}{(b-a) \cdot \sin(\alpha + j\beta)}$ (15)

where $\cos(\alpha + j\beta)$ is a standardised replacement for z in equation (8), and the constants in equations (4) and (5) are taken from references [5] or [6], namely

$$h_n = \pi/2$$
 $(n\neq 0)$, $c_1 = 0$, $c_2 = 2$, and $c_3 = 1$.

For the Legendre polynomials, weight function w(A) = 1, standardised interval (-1,1), one can use

$$(1-z) = r.\exp(j\theta)$$

 $(-1-z) = -r'.\exp(-j\theta') = r'.\exp(j(\pi-\theta'))$

in Legendre
$$I_0 = \int_0^1 \frac{dA}{(A-z)}$$

= $\ln(1-z) - \ln(-1-z)$
= $\ln(r/r') - j(\pi - \theta - \theta')$
with $I_1 = zI_0 + 2$ (16)

and constants taken from [5] or [6]: $h_n = (n + \frac{1}{2})^{-1}$, $c_1 = 0$, $c_2 = 2 - 1/n$, and $c_3 = 1 - 1/n$.

In practice, the expressions for I and I in equations (15) and (16) will contain another factor, introduced when equations (7) and (8) are replaced by linear transformations such that (a,b) is replaced by a standardised interval (-1,1). Figure 1 shows smoothed frequency responses which were computed from the alternative expressions for I_0 , I_1 in equations (15) and (16).

3. NEGLECT OF DAMPING

Damping influences the true frequency response through the range and sharpness of resonant-antiresonant detail, but has little or no influence upon an average magnitude for real mobilities, taken over a range of frequencies.

Smoothed frequency responses tend to remove the resonant-antiresonant detail, consequently it is reasonable to expect them to show small sensitivity to damping (but not if they relate to measures other than real mobility). The latter measure is a ratio with respect to an excitation-force for the in-phase part of a response-velocity. It has the property that a decrease in damping causes the resonant peaks to grow in height, but also to shrink in width, and causes the flanks of the peaks to decrease.

Insensitivity to damping can be exploited in the computation of the smoothed frequency responses in this paper, by arbitrarily setting damping equal to zero. The advantage is a simplification of arithmetic, because the need for complex arithmetic disappears in a practical computation with equations (12) to (16). The results will show some small differences from the case when damping is considered, but these differences are likely to be insignificant, given that the object of a smoothed frequency response is to ignore detail in the resonant-antiresonant behaviour. Figure 2 shows a comparison of cases when damping is considered and when it is ignored, for a smoothed frequency response using Legendre polynomials.

If a smoothed frequency response were calculated with sufficiently many polynomial terms, there would be a tendency to reproduce all of the resonant-antiresonant detail, and it then would be misleading to ignore damping.

4. EXAMPLE

Figures 1 and 2 show an example concerning a theoretical clamped-clamped uniform beam, taken from a previous paper [1] except that Legendre polynomials now are used in place of Tchebyshev polynomials. By considering seven identical beam elements, values were derived for 6 x 6 matrices of stiffnesses and masses, corresponding to natural frequencies 0.457, 1.256, 2.442, 5.448, and 6.552 times $1/L^2(EI/\rho A)^2$, where L,E,I, ρ and A are constants of the beam geometry or material. It happened that very little participation of the fourth mode of vibration was predicted for the point where both the excitation and response were considered (giving a point-mobility for the junction between the second and third elements from one end of the beam). Details of the mathematical model for the beam are given in reference [1]. Legendre smoothed frequency responses were established from equations (1), (10) - (12) and (16) of the present paper, using polynomials up to degree ν = 9 computed with BASIC on a Microtan personal microcomputer.

Figure 1 shows a comparison between two smoothed frequency responses, of the Legendre and Tchebyshev types. Both of these are to be judged in relation to a detailed frequency response which was calculated by normal-mode analysis after the necessary determinations of natural frequencies and modes, and which is included in the same figure. Both of the smoothed frequency responses in figure 1 show the following: a region of low response near an almost non-participating tourth mode of vibration; an embryonic appearance of resonant-antiresonant detail for the fifth and sixth modes; and a region of high response embracing the first three modes. (From the standpoint of computation, these modes are closer together than appears from figure 1. Computation relates most closely to a distribution of modes with respect to ω^2 , but figure 1 shows a distribution with respect to ω).

Figure 2 shows a Legendre smoothed frequency response, once for the case when damping is considered, and again for the case when damping is neglected. Excepting the latter case, all of the curves in figures 1 and 2 relate to a value c=0.2 for the damping coefficient in equation (2). Differences are perceptible between the damped and undamped smoothed frequency responses in figure 2, but are insignificant in comparison with differences between either of the smoothed frequency responses and the detailed response which was calculated by normal-mode analysis. The saving of arithmetic through neglect of damping approached three-fifths of the multiplications needed for a plot of each point on a smoothed frequency response when the values for the polynomial matrices f (A) were given. The latter matrices are constants of the structure, and their once-for-all determinations for a given structure by means of equation (5) are unaffected by damping.

5. DISCUSSION

The result of equations (9),(10) and (12) - (14) is that the smoothed frequency response in matrix equation (1) can be used with <u>any</u> system of orthogonal polynomials of a continuous variable, subject only to two conditions: first, the integral I in equation (14) can be evaluated; second, the chosen type of polynomial is satisfactory in numerical stability and in practical convergence of the smoothed frequency response on to the true frequency response as the degree \vee is increased.

At the time of writing, only the Tchebyshev polynomials of the first kind, T (A), and the Legendre polynomials have been investigated and shown satisfactory in a numerical example with a smoothed frequency response.

Smoothed frequency responses of low degree \vee (that is, with little or no display of resonant-antiresonant detail) can be approximated by setting damping equal to zero, unless the true damping is heavy, with a consequent simplification in part of the arithmetic.

The example in this paper concerns a point mobility, that is, where excitation is applied along the same coordinate as used for measuring response. However, determination of a smoothed frequency response for a real transfer mobility is not excluded (although the transfer case may be less important, and may need more polynomial terms to be considered, see reference [1]).

REFERENCES

- 1. M.E. GAYLARD In Press (Journal of Sound and Vibration) Smoothed frequency responses for matrix-characterized vibrating structures.
- 2. R.H. LYON 1975 Statistical Energy Analysis of Dynamical Systems. Cambridge, Massachusetts: M.I.T. Press.
- 3. E. SKUDRZYK 1980 Journal of the Acoustical Society of America 67, 1105-1135. The mean-value method of predicting the response of complex vibrators.
- 4. B.L. CLARKSON 1981 Journal of Sound and Vibration 77, 583-584. The derivation of modal densities from point impedances.
- 5. G. SZEGO 1967 Orthogonal Polynomials. Providence, Rhode Island: American Mathematical Society, third edition.
- 6. M. ABRAMOWITZ and I.A. STEGUN (Editors) 1968 Handbook of Mathematical Functions. New York: Dover.

1



DYNAMIC ANALYSIS OF SYSTEMS OF BARS ENCASED IN ELASTIC MEDIUM

S. M. Aljaweini and J. J. Tuma

Department of Civil Engineering
Arizona State University

1. INTRODUCTION

A general method is presented for the analysis of space frames encased fully or partially in elastic medium and subjected to time-dependent loads of harmonic variation, such as those arising from rotating or reciprocating machinery. Off-shore structures, pipelines, bridges, components of ships and aerospace structures are examples of such systems. The analysis is restricted to systems of straight linearly elastic bars of constant sections, which have two orthogonal axes of symmetry or are axial symmetrical. The time-independent mass of each bar is uniformly distributed along its axis. The material constants of each bar and of its surrounding medium are independent of time and are known from experiments. The sign convention of the transport method and of the stiffness method is used in the respective sections.

From the transport matrix formed by twelve dynamic parameters and twelve forcing functions of a single bar, the transcendental stiffness matrix is constructed and converted into an algebraic stiffness matrix, the elements of which are truncated series. Analytical expressions are presented for the calculation of the coefficients of each series, for the location of singularity points of each series and for the limits within which each series yields results of practical significance. Finally, a computer program is discussed which generates the finite element matrices as functions of their respective series, selects the element sizes within the predetermined range of accuracy, produces the frequency determinant, identifies the critical states and yields a complete response of the system. The historical background of this approach is summarized in [1], [2], [3].

2. TRANSPORT MATRIX EQUATIONS

Assuming small oscillation about the configuration of stable equilibrium, the free vibration of a finite bar LR of length ${\bf s}$ is defined by the transport matrix equations given in full form in Table 1 and in submatrix form below as

$$\begin{bmatrix}
\bar{S}_{R} \\
\bar{\Delta}_{R}
\end{bmatrix} = \begin{bmatrix}
\bar{t}_{RL} & \bar{c}_{RL} \\
\bar{d}_{RL} & \bar{s}_{RL}
\end{bmatrix} \begin{bmatrix}
\bar{S}_{L} \\
\bar{\Delta}_{L}
\end{bmatrix} = \begin{bmatrix}
\bar{t}_{LR} & \bar{c}_{LR} \\
\bar{d}_{LR} & \bar{s}_{LR}
\end{bmatrix} \begin{bmatrix}
\bar{S}_{R} \\
\bar{\Delta}_{R}
\end{bmatrix}$$

$$T_{RL} \quad \overline{H}_{L} \quad \overline{H}_{L} \quad \overline{H}_{R}$$
(1)

where \overline{H}_R and \overline{H}_L are the dimensionless state vectors of the right end R and of the left L, respectively, consisting of forces \overline{U} , \overline{V} , \overline{W} , moments \overline{X} , \overline{Y} , \overline{Z} , linear displacements $\overline{\phi}$, $\overline{\psi}$, $\overline{\theta}$ and \overline{T}_{RL} , \overline{T}_{LR} are the dimensionless transport matrices, the elements of which are the dynamic parameters T_{1u} , T_{2u} , ..., T_{3w} , T_{4w} , all shown in Table 1.

The shape parameters

$$\bar{\lambda}_{\mathbf{u}} = \mathbf{s}\lambda_{\mathbf{u}} = \mathbf{s}\sqrt{\frac{\mu\omega^2 - \mathbf{k}}{\mathbf{E}\mathbf{A}}}$$
 $\bar{\lambda}_{\phi} = \mathbf{s}\lambda_{\phi} = \mathbf{s}\sqrt{\frac{\rho\omega^2 - \mathbf{k}}{\mathbf{G}\mathbf{I}_{\mathbf{x}}}}$
(2)

TABLE 1 DIMENSIONLESS TRANSPORT MATRIX EQUATIONS

$1u = \cos \overline{\lambda} u$ $T_{2u} = \sin \overline{\lambda} u$ $T_{1\phi} = \cos \overline{\lambda} \phi$	$T_{2v} = 1/2 \text{ (sinh } \overline{\lambda}_{v}$	$T_{2w} = 1/2 \left(\sinh \overline{\lambda}_{w} + \sin \overline{\lambda}_{w} \right)$
$T_{2\phi} = \sin \overline{\lambda}_{\phi}$		
Ū _R ∇ _R	T _{1u} T _{1v} -T _{4v} T _{1w} T _{4w}	$\begin{bmatrix} -T_{2U} & & & & & \\ & -T_{2V} & & -T_{3V} & & & & \\ & & -T_{2W} & & T_{3W} & & & & \end{bmatrix} \begin{bmatrix} \overline{U}_L \\ \overline{V}_L \\ \overline{W}_L \end{bmatrix}$
¬¬R	T _{1¢} T _{2w} T _{1w}	$\begin{array}{cccccccccccccccccccccccccccccccccccc$
ū _R	-T _{2v} T _{1v} T _{2u} -T _{4v} T _{3v}	$\begin{array}{cccccccccccccccccccccccccccccccccccc$
₩R ₩R ₩R	-T _{4w} -T _{3w} T _{2φ} T _{3w} T _{2w}	
	-T _{3v} T _{2v} ,	τ _{2u}
₹ _L	т _{1v} т _{4v} т _{1w} т _{1w} -т _{4w} т _{1ф}	T_{2w} T_{3w} \overline{X}_{R}
Ψ _L	-T _{2w} T _{1w}	$\begin{array}{cccccccccccccccccccccccccccccccccccc$
u v v v v v v v v v v v v v v v v v v v	-T _{2u} T _{4v} T _{3v}	$\begin{array}{cccccccccccccccccccccccccccccccccccc$
€ 	T _{4v} T _{3v} T _{4w} -T _{3w} -T _{2φ} -T _{2w} -T _{3v} -T _{2v}	$\begin{array}{cccccccccccccccccccccccccccccccccccc$

$$\bar{\lambda}_{v} = s\lambda_{v} = s\sqrt[4]{\frac{\mu\omega^{2} - k_{v}}{EI_{z}}} \qquad \bar{\lambda}_{w} = s\lambda_{w} = \sqrt[4]{\frac{\mu\omega^{2} - k_{w}}{EI_{y}}}$$
(3)

which appear as arguments in the dynamic parameters are functions of mass per unit length $\mu,$ mass polar moment of inertia per unit length $\rho,$ angular frequency $\omega,$ moduli of elastic medium $k_u,$ $k_{\varphi},$ $k_v,$ $k_w,$ functions of the normal section A, I, I, and the elastic constants E, G.

3. STIFFNESS MATRIX EQUATIONS

In terms of the sign convention and notation of the stiffness method, the lower submatrix equations in (1) yield

$$S_{LR} = \underbrace{d_{RL}^{1-1} s_{RL}}_{k_{LL}} \Delta_{L} - \underbrace{d_{RL}^{1-1} \Delta_{R}}_{k_{LR}} \qquad S_{RL} = -\underbrace{d_{LR}^{1-1} s_{LR}}_{k_{RR}} \Delta_{R} + \underbrace{d_{LR}^{1-1} \Delta_{L}}_{k_{RL}}$$
(4)

where S_{LR} , S_{RL} are the end reactions, Δ_L , Δ_R are the end displacements and k_{LL} , k_{LR} , k_{RL} , k_{RR} are the stiffness submatrices shown in full form in Table 2.

Once the dynamic stiffness matrix equations are available for all bars of the system, the analysis based on the conditions of dynamic joint equilibrium follows the pattern of static analysis and leads eventually to the frequency determinant equation.

In addition to the treatment of joint loads, the distributed mass bars are able to account for the dynamic loads acting between the joints as

$$\begin{bmatrix} S_{LR} \\ S_{RL} \end{bmatrix} = \begin{bmatrix} k_{LL} & k_{LR} \\ k_{RL} & k_{RR} \end{bmatrix} \begin{bmatrix} \Delta_{L} \\ \Delta_{R} \end{bmatrix} + \begin{bmatrix} S_{LO} \\ S_{RO} \end{bmatrix}$$
(5)

where

$$S_{LO} = -k_{LR} \Phi_{R\Delta} \qquad S_{RO} = -k_{RL} \Phi_{L\Delta}$$
 (6)

and $\boldsymbol{\Phi}_{L\Delta},~\boldsymbol{\Phi}_{R\Delta}$ are the absolute load functions given in Table 3.

4. EXPANSION OF STIFFNESS FACTORS

Since the stiffness factors in Table 2 are linear combinations of circular and hyperbolic functions, the solution of the frequency determinant, even in cases of frames with a few joints, is a monumental task, requiring a large amount of computer time. Kolousek [2], while investigating the free vibration of free bars, conceived the idea to expand the stiffness factors into series of McLaurin's type. Since each factor is a fraction, the numerator and denominator of which are transcendental functions, the expansion requires a synthetic division of two power series or a generation of a series, which is equivalent to the quotient series. The latter is used below.

The dimensionless parts of the stiffness factors in Table 2 are in series form,

TABLE 2 ABSOLUTE STIFFNESS MATRIX EQUATION

= EA λ	u cot $\overline{\lambda}_{\mathbf{u}}$	$D_{V} = (1-\cosh \overline{\lambda}_{V})$	$\cos \overline{\lambda}_{\mathbf{v}})^{-1}$	K _{1¢} ≠ GI	$x^{\lambda_{\phi}} \cot \overline{\lambda_{\phi}}$
= EA λ	u csc Xu	$\csc \overline{\lambda}_{\mathbf{U}}$ $\vartheta_{\mathbf{W}} = (1-\cosh \lambda_{\mathbf{W}} \cos$		$(\cos \overline{\lambda}_W)^{-1}$ $K_{2\phi} = GI_X \lambda_{\phi} \csc \overline{\lambda}_{\phi}$	
= EIz	$\lambda_{\mathbf{y}}$ (cosh $\overline{\lambda}_{\mathbf{y}}$ sin $\overline{\lambda}_{\mathbf{y}}$ - si	$nh\ \overline{\lambda}_{\mathbf{v}}\ cos\ \overline{\lambda}_{\mathbf{v}})\ D_{\mathbf{v}}$	K _{4v} = EI _{z \(\lambda\)\(\lambda\) (s}	inh $\overline{\lambda}_{\mathbf{v}}$ - sin $\overline{\lambda}_{\mathbf{v}}$)	D _V
= EI _z	$\lambda_{\mathbf{V}}^{2}$ sinh $\overline{\lambda}_{\mathbf{V}}$ sin $\overline{\lambda}_{\mathbf{V}}$ D		$K_{5v} = EI_Z \lambda_v^2$ (co	$\cosh \overline{\lambda}_{\mathbf{V}} - \cos \overline{\lambda}_{\mathbf{V}})$	D _v
= EI _z	$\lambda_{\mathbf{v}}^{3}$ (cosh $\overline{\lambda}_{\mathbf{v}}$ sin $\overline{\lambda}_{\mathbf{v}}$ + si	nh $\overline{\lambda}_{\mathbf{V}}$ cos $\overline{\lambda}_{\mathbf{V}}$) D	κ _{6ν} = ΕΙ _Ζ λ _ν (s		D _v
= EIy	λ_{W} (cosh $\overline{\lambda}_{W}$ sin $\overline{\lambda}_{W}$ - si	nh $\overline{\lambda}_{\mathbf{u}}$ cos $\overline{\lambda}_{\mathbf{u}}$) $\mathbf{D}_{\mathbf{u}}$	K _{4w} = EI _y λ _w (s	inh $\overline{\lambda}_{W}$ - sin $\overline{\lambda}_{W}$)	D _w
- EIy	λ_W^2 sinh $\overline{\lambda}_W$ sin $\overline{\lambda}_W$ D_W	f	$K_{5w} = EI_y \lambda_w^2$ (co	$ \cosh \ \overline{\lambda}_{W} - \cos \ \overline{\lambda}_{W}) $	D _w
= EI _y	$\lambda_{\mathbf{W}}^{3}$ (cosh $\overline{\lambda}_{\mathbf{W}}$ sin $\overline{\lambda}_{\mathbf{W}}$ + si	nh $\overline{\lambda}_{W}$ cos $\overline{\lambda}_{W}$) D_{W}	K _{6w} = EI _y λ _w 3 (s	inh $\overline{\lambda}_{\mathbf{W}}$ + sin $\overline{\lambda}_{\mathbf{W}}$)	D _w
U _{LR}	Γ _{κ1u}		-K _{2u}		T u,]
V _{LR}	K _{3v}	K _{2v}	-K _{6v}	K _{5v}	٧٢
W _{LR}	К _{Зพ}	^{-K} 2w	-K _{6w}	-K _{5w}	WL
X _{LR}		K _{1∳}	-к	2∳	∳ر
YLR	-K _{2w}	K _{Iw}	K _{5w}	K _{4w}	ψ _ι
Z _{LR}	K _{2v}	K _{1v}	-k _{5v}	K _{4v}	. PL
U _{RL}	-K _{2u}		K _{lu}		u _R
Y _{RL}	^{-K} 6v	-K _{5v}	K _{3v}	-K _{2v}	V _R
W _{RL}	-K _{6w}	K _{5w}	K _{3w}	K _{2w}	w _R
x _{RL}		-K _{2∳}	K	14	∳ _R
Y _{RL}	-K _{5w}	K _{4w}	K _{2w}	Klm	ΨR
Z _{RL}	K _{5v}	-K _{4v}	K _{2v}	K _{1v}	θ _R

TABLE 3 ABSOLUTE LOAD FUNCTIONS

 P_x, P_y, P_z = concentrated loads (N)

s,a,b = segments (m)

 p_x, p_y, p_z = intensities of distributed loads (N/m)

 $A_{1u}^{\lambda}, A_{2u}^{\lambda}, \dots, A_{3w}^{\lambda}, A_{4w}$ and $B_{1u}^{\lambda}, B_{2u}^{\lambda}, \dots, B_{3w}^{\lambda}, B_{4w}^{\lambda}$ are the dynamic parameters defined in Table 1 for the segments a and b, respectively.

[⊕] Lu	=	-	$\frac{A_{2} u^{P} x}{\lambda_{u} EA}$	
ΦLv	=	-	$\frac{A_{4v} P_{y}}{\lambda_{v}^{3} EI_{z}}$	

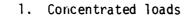
$$\Phi_{Lw} = -\frac{A_{4w}P_z}{\lambda_w^3 EI_y}$$

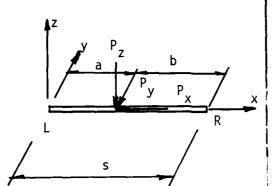
$$\Phi_{L\psi} = 0$$

$$\Phi_{L\psi} = -\frac{A_{3w}P_z}{\lambda_w^2 EI_y}$$

$$A_{3v}P_v$$

$$\Phi_{L\theta} = -\frac{A_{3v}P_y}{\lambda_v^2 EI_z}$$





$$R_{u} = \frac{B_{2u}P_{x}}{\lambda_{u}EA}$$

$$P_{RV} = -\frac{4V y}{\lambda_V^3 EI_2}$$

$$\Phi_{RW} = -\frac{B_{4W}P_z}{\lambda_W^3 EI_y}$$

$$\Phi_{R\psi} = \frac{B_{3w}P_z}{\lambda_w EI_y}$$

$$\Phi_{R\theta} = -\frac{B_3 v^P y}{\lambda_V EI_z}$$

$$\Phi_{Lu} = -\frac{1}{\lambda_u^2} \frac{1}{EA} P_x$$

$$\Phi_{LV} = -\frac{T_{1}v^{-A_{1}v}}{\lambda_{v}^{+}EI_{z}} \mathcal{F}_{z}$$

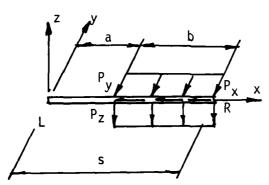
$$\Phi_{Lw} = -\frac{1}{\lambda_W^+ EI_y} P$$

$$\Phi_{\mathsf{L}\Phi} = 0$$

$$\phi_{L\psi} = -\frac{\Gamma_{4w}^{-A}_{4w}}{\lambda_{w}^{3} EI_{y}} P_{1}$$

$$\Phi_{L\theta} = -\frac{T_{4v} - A_{4v}}{\lambda_v^3 EI_z} P_y$$

2. Uniform loads



$$\Phi_{Ru} = -\frac{31u}{\lambda_u^2 EA} P_X$$

$$\Phi_{RV} = -\frac{B_{IV}^{-1}}{\lambda_{V}^{4} EI_{Z}} P_{Y}$$

$$\Phi_{RW} = -\frac{B_{1W}^{-1}}{\lambda_{W}^{4} EI_{Z}} P_{Z}$$

$$\Phi_{DA} = 0$$

$$\Phi_{R\psi} = \frac{B_{4w}}{\lambda_w^* EI_y} P_z$$

$$|\Phi_{R\theta}| = -\frac{B_{4V}}{\lambda_V^{5} EI_2} P_y$$

$$\bar{K}_{ju} = C_{j0} + \sum_{r=1}^{\infty} C_{jr} \left(\frac{\bar{\lambda}^{2}_{u}}{10}\right)^{r} \qquad \bar{K}_{j\phi} = C_{j0} + \sum_{r=1}^{\infty} \left(\frac{\bar{\lambda}^{2}_{\phi}}{10}\right)^{r}$$
(7)

$$\bar{K}_{kv} = C_{k0} + \sum_{r=1}^{\infty} C_{kr} \left(\frac{\bar{\lambda}_{v}^{4}}{100} \right)^{r}$$

$$\bar{K}_{kw} = C_{k0} + \sum_{r=1}^{\infty} \left(\frac{\bar{\lambda}_{w}^{4}}{100} \right)^{r}$$
(8)

where
$$C_{jr} = (10)^r \bar{C}_{jr}$$
, $C_{kr} = (100)^r \bar{C}_{kr}$ and $j = 1, 2, k = 1, 2, ..., 6$

The coefficients \bar{C}_{jr} are well known and the coefficients \bar{C}_{kr} can be determined automatically by the generating matrix equation given below. Their numerical values are listed in Tables 4 and 5.

$$\begin{bmatrix} \bar{c}_{k0} \\ \bar{c}_{k1} \\ \bar{c}_{k2} \\ \bar{c}_{k3} \\ \cdot \\ \cdot \end{bmatrix} = \frac{1}{D_0} \begin{bmatrix} N_{k0} \\ N_{k1} - D_1 \\ N_{k2} - D_2 - D_1 \\ N_{k3} - D_3 - D_2 - D_1 \\ \cdot \\ \cdot \\ \cdot \end{bmatrix} \begin{bmatrix} 1 \\ \bar{c}_{k0} \\ \bar{c}_{k1} \\ \bar{c}_{k2} \\ \cdot \\ \cdot \end{bmatrix} . \tag{9}$$

where \mathbf{D}_0 , \mathbf{D}_1 , ..., are the coefficients of the initial denominator series and \mathbf{N}_{k0} , \mathbf{N}_{k1} , ..., are the coefficients of the initial numerator series.

The singularities of the stiffness factors, given by the zero values of their denominators, are for

$$j = 1, 2$$
 $\overline{\lambda} = \pi, 2\pi, 3\pi, ...$ $k = 1, 2, ..., 6$ $\overline{\lambda} = 4.730043, 7.853203, 10.995608, ...$

of which only the first ones are considered significant and are used as the radii of convergence of the respective series.

TABLE 6 ADMISSIBLE RANGE

Factor	Number of Terms	Range of	Error	
	2	$0 \leq \overline{\lambda} \leq 0.4$,	
K,	3	$0 \leq \overline{\lambda} \leq 0.8$	$\varepsilon \leq 5.8(10)^{-4}$	
	4	$0 \leq \overline{\lambda} \leq 1.1$		
	2	$0 \leq \overline{\lambda} \leq 1.3$	•	
K _k	3	$0 \leq \overline{\lambda} \leq 2.0$	$\varepsilon \leq 1.4(10)^{-3}$	
	4	$0 \leq \overline{\lambda} \leq 2.5$		

TABLE 4 NUMERICAL VALUES Cjr

r	Clr	C _{2r}
0	1.000 000 (E+00)	1.000 000 (E+00)
1	-3.333 333 (E+00)	1.666 667 (E+00)
2	-2.222 222 (E+00)	1.944 440 (E+00)
3	-2.116 402 (E+00)	2.050 265 (E+00)
4	-2.116 402 (E+00)	2.099 868 (E+00)
5	-2.137 780 (E+00)	2.133 605 (E+00)
6	-2.164 404 (E+00)	2.163 347 (E+00)
7	-2.192 595 (E+00)	2.192 328 (E+00)
8	-2.221 461 (E+00)	2.221 393 (E+00)
9	-2.250 788 (E+00)	2.250 767 (E+00)

TABLE 5 NUMERICAL VALUES Ckr

	C _{3r}
1 -9.523 810 (E-01) -5.238 095 (E-01) -3.	.200 000 (E+01)
	.714 286 (E+O1)
	.648 732 (E+00)
3 -3.196 602 (E-02) -1.487 972 (E-01) -4.	.934 361 (E-01)
4 -6.373 130 (E-03) -2.962 389 (E-02) -1.	.377 192 (E-01)
5 -1.272 857 (E-03) -5.915 478 (E-03) -2.	.749 213 (E-02)
	.492 613 (E-02)
7 -5.079 765 (E-05) -2.360 708 (E-04) -1.	.097 306 (E-03)
8 -1.014 808 (E-05) -4.716 092 (E-05) -2.	.192 147 (E-04)
9 -2.027 329 (E-06) -2.621 314 (E-06) -3	.343 481 (E-06)
r C _{4r} C _{5r}	C _{6r}
	.200 000 (E+01)
	.285 714 (E+01)
	.295 712 (E+00)
	.844 299 (E-01)
	.374 831 (E-01)
	.748 592 (E-02)
	.491 528 (E-03)
	.097 083 (E-03)
	.191 697 (E-04)
	.378 457 (E-05)

Table 6 shows the range of $\bar{\lambda}$'s for which the respective stiffness factor may be approximated by two, three and four terms of its series, so that the truncation error remains below a prescribed value. The three-term approximation is used as the simplest and most efficient numerical model.

5. FINITE ELEMENT GENERATOR

Once the truncated stiffness factors are available for all bars of the system, the remaining part of the analysis consists of the following steps:

- (a) The algebraic determinant of the system stiffness matrix is solved for the apparent natural frequencies and the shape parameters $\bar{\lambda}_u^{}$, $\bar{\lambda}_v^{}$, $\bar{\lambda}_v^{}$, $\bar{\lambda}_v^{}$, $\bar{\lambda}_v^{}$, corresponding to these frequencies, are calculated for all bars.
- (b) If these values fall in the prescribed range given in Table 6, the truncation error remains in the prescribed range and the apparent frequencies are the true values.
- (c) If the values of the shape parameters $\bar{\lambda}_{u}'$, $\bar{\lambda}_{v}'$, and $\bar{\lambda}_{v}'$, $\bar{\lambda}_{w}'$, are above 0.8 and 2.0, respectively, the corresponding members must be divided so that their parameters remain in the selected range. The required number of elements in a particular bar is given as

$$n = \overline{\lambda}_{11}^{\dagger}/0.8 \qquad n = \overline{\lambda}_{0}^{\dagger}/0.8 \qquad n = \overline{\lambda}_{V}^{\dagger}/2.0 \qquad n = \overline{\lambda}_{W}^{\dagger}/2.0 \qquad (10)$$

where the largest n in (10) defines the minimum number of elements in a particular bar, required to meet the desired accuracy.

- (d) With the required number of elements known, the new system stiffness matrix is constructed and the frequency determinant is solved for the natural frequencies.
- (e) The steady state response analysis follows the procedure outlined in Sec. 3. Since all factors are functions of the forcing frequency, all stiffness factors and load functions are calculated by their transcendental formulas introduced in Table 2 and in (6).

The procedure described above was programmed in FORTRAN IV listed in [1] and its application is illustrated by a numerical example.

6. NUMERICAL EXAMPLE

A reinforced concrete rigid frame partially encased in elastic foundation and acted on by concentrated loads of Ω = 350 rad/s,

$$P_{3y} = (3560 \sin \Omega t) kN$$
 $P_{4x} = (890 \sin \Omega t) kN$

is shown in Fig. 1. The moduli of foundation are

$$k_{y} = 3.8(10)^{7} Pa$$
 $k_{y} = k_{y} = 1.9(10)^{7} Pa$

The procedure of analysis follows the steps of Sec. 5. The first three natural frequencies obtained by using the three-term truncated stiffness factors are

$$\omega_1' = 329 \text{ rad/s}$$
 $\omega_2' = 390 \text{ rad/s}$ $\omega_3' = 408 \text{ rad/s}$

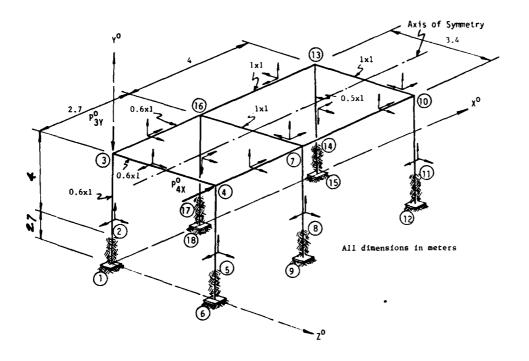


Figure 1. Rigid Frame

The extreme values of the shape factors corresponding to these frequences are,

for
$$\omega_1$$
, $\bar{\lambda}_u^{\,\prime} \leq 0.410$, $\bar{\lambda}_{\varphi}^{\,\prime} \leq 0.958$, $\bar{\lambda}_v^{\,\prime} \leq 3.371$, $\bar{\lambda}_w^{\,\prime} \leq 2.383$ for $\omega_2^{\,\prime}$, $\bar{\lambda}_u^{\,\prime} \leq 0.486$, $\bar{\lambda}_{\varphi}^{\,\prime} \leq 1.136$ $\bar{\lambda}_v^{\,\prime} \leq 3.671$, $\bar{\lambda}_w^{\,\prime} \leq 2.595$ for $\omega_3^{\,\prime}$, $\bar{\lambda}_u^{\,\prime} \leq 0.509$, $\bar{\lambda}_{\varphi}^{\,\prime} \leq 1.189$ $\bar{\lambda}_v^{\,\prime} \leq 3.756$, $\bar{\lambda}_w^{\,\prime} \leq 2.656$

As some of the shape parameters exceed the permissible range, the finite element generator calls automatically for a new system, by dividing the members with

$$\bar{\lambda}_{\phi}^{\dagger} \geq 0.8$$
 $\bar{\lambda}_{v}^{\dagger} \geq 2.0$ $\bar{\lambda}_{w}^{\dagger} \geq 2.0$

into two elements.

The determinant equation of this new system yields

$$\omega_1$$
 = 325 rad/s ω_2 = 386 rad/s ω_3 = 404 rad/s

and the corresponding shape parameters fall in the admissible range.

The calculations of the joint displacements and of end reactions of particular members follows the procedure outlined in Sec. 5e. Since the forcing Ω is above ω_1 and below ω_2 , the critical state is avoided.

ACKNOWLEDGEMENTS

This paper is based on the dissertation by S. M. Aljaweini, submitted to the Graduate School of Arizona State University, in partial fulfillment of the requirement for the degree of Doctor of Philosophy in Civil Engineering. The

investigation was performed under the direction of J. J. Tuma as a part of the institutional research program in the area of space structural dynamics.

REFERENCES

- 1. S. M. ALJAWEINI 1983 Ph.D. Thesis, Arizona State University, Dynamic analysis of bars encased in elastic medium.
- 2. V. KOLOUSEK 1973 Dynamics of Engineering Structures, London, Butterworth.
- 3. J. J. TUMA and F. Y. CHENG 1983 Dynamic Structural Analysis, New York, McGraw-Hill.



TRANSMISSION OF WAVES THROUGH LOCALIZED DISCONTINUITIES; EVALUATION OF TWO APPROACHES

G. Maidanik and L. J. Maga

David Taylor Naval Ship Research and Development Center Bethesda, Maryland 20084, USA

Many a complex dynamic system of interest to structural acousticians admit, at least on a phenomenonological basis, to modeling by a cascade of coupled basic one-dimensional (BOD) dynamic systems. A basic dynamic system is one in which a single wavevector needs to be specified to define propagation in it. Two approaches are discussed for describing the transmission of waves through the coupling junctions; a coupling junction specifies the coupling between two adjacent BOD dynamic systems. The transmission between BOD dynamic systems that are singly, doubly, and triply removed from each other are cited as examples. The evaluation is carried out in terms of the two approaches. Similarities and differences in the evaluations by the two approaches are emphasized and discussed.

2. VIBRATION CONTROL

AUXILIARY MASS DAMPER FOR CARDAN SUSPENDED GYRO



J. Rosenberg*, A. Kahana**

A.D.A. P.O.Box 2250, Haifa, ISRAEL

AD-P003 646

1. . INTRODUCTION

The article deals with a spin stabilized platform. In order to isolate the system from external moments it is suspended through its center of mass by means of a cardan. Deviation from ideal suspension, such as friction effects in the bearings and in the surrounding environment together with external disturbances, generate vibrations in the natural frequencies of the system. These vibrations should be suppressed by means of damping effects. should not impair the isolation of the platform from its environment (as in the case of damping in the cardan bearings). The simplest model of a cardan suspended gyro involves only one natural frequency, termed the nutation. Several methods for nutation damping are discussed in the literature: (1) Connecting a ring partially filled with mercury to the gyro rotor [1,2,3]. The mercury serves as an auxiliary mass damper. Such dampers that are connected to the rotor are known to cause instability [4,5,6] if the lateral inertia of the system is higher than the polar inertia. (2) Active damping by means of a control system [7]. This method may require high energy sources for its actuators. (3) Using an impact mass damper attached to the platform [8]. In this method energy is dissipated when non-elastic collision occurs. While such damper may prove to be efficient and no tuning is necessary, there is no analytic solution and it is hard to obtain parameters (such as coefficient of restitution) for numerical simulation. Any conclusion concerning the use of such damper should allow for possible damage to the system owing to the impact effect. (4) Adding an auxiliary mass which is connected to the gimbal system by means of a spring and a viscous dash-pot. This method has been extensively used in rotating machine damping and more recently in the aerospace industry in the damping of dual spin satellite [2,9]. In such cases the damper inertia is neglected in comparison with the platform inertia. This results in a simplified model, in which the nutational frequency is taken to be the forced frequency. In the following, the interaction between the stabilized platform and the damper is considered. This causes the appearance of three natural frequencies instead of the nutational frequency.

2. STATEMENT OF PROBLEM

The equation of motion for a two axis Gyro assuming small angles are as follows (for detailed discussion see any advanced dynamics textbook e.g. [10])

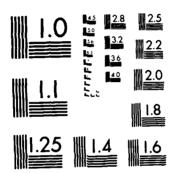
$$\vec{A\Theta} + \vec{h\Psi} = My$$

$$\vec{A\Psi} - \vec{h\Theta} = Mz$$
(1)

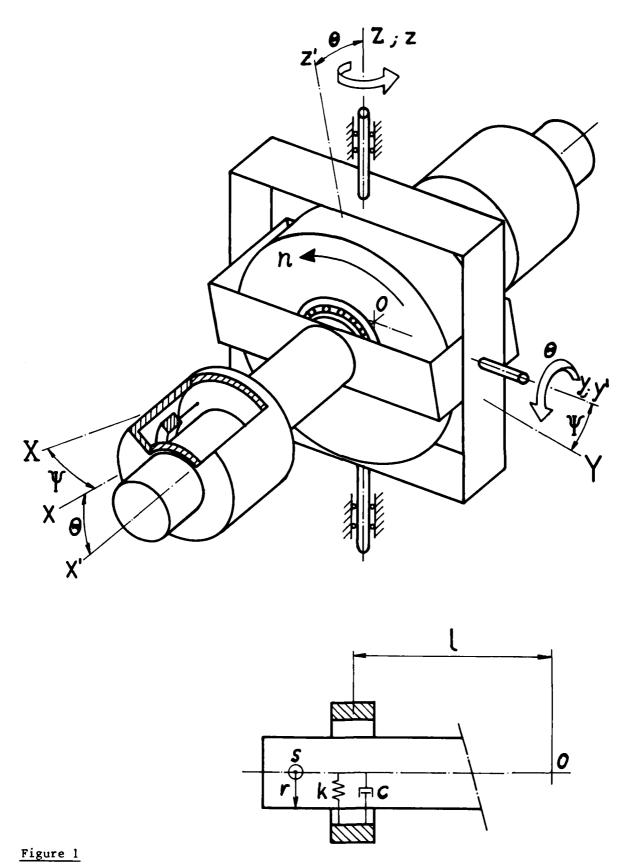
where A is the transverse moment of inertia of the rotor and the platform, h - the momentum of the rotor defined as h = nJ where n is the spin and J is the polar moment of inertia of the rotor. My and Mz are external moments. O and Y are the angular coordinates of the system defined in figure 1. Using complex variables:

- (*) Research Associate.
- (**) Research Engineer.

PROCEEDINGS OF THE INTERNATIONAL CONFERENCE ON RECENT ADVANCES IN STRUCTU.. (U) SOUTHAMPTON UNIV (ENGLAND) 1981 OF SOUND AND VIBRATION RESEAR.. H PETYT ET AL. 1984 AD-A143 300 2/5 UNCLASSIFIED NL.



MICROCOPY RESOLUTION TEST CHART NATIONAL BUREAU OF STANDARDS-1963-A



Schematic description of cardan suspended gyro with an auxiliary mass damper.

$$\eta = \Theta + i\Psi
M = My + iMz$$

i = √~

we obtain

$$\ddot{\eta} - ip\dot{\dot{\eta}} = \frac{M}{A} \tag{2}$$

with the homogeneous solution

$$\eta_{\mu} = \eta_{\alpha} e^{i\lambda t}$$

$$\lambda_1 = 0 \quad \lambda_2 = P$$

 $p=\frac{h}{A}$ is the nutation frequency. By introducing viscous damping f* at the gimbal bearings or the surrounding environment, we modify equation (2) to vield

$$\ddot{\eta} - ip\eta + f\eta = \frac{M}{A}$$
 (3)

where $f = \frac{f^*}{A}$ and the homogeneous solution

$$\eta_{H} = \eta_{o} e^{ipt} e^{-ft}$$
 (4)

On one hand, increasing the external damping f increases the rate at which nutational frequency is suppressed, on the other, such damping impairs the isolation of the platform from external excitations.

Adding an auxiliary mass damper which is connected to the platform by means of a spring (K) and dashpot (C) as shown in figure 1, results in the following equations of motion:

$$\ddot{\Theta} + f\dot{\Theta} + p\dot{\Psi} = \omega_{n}^{2}\varepsilon\alpha + 2\zeta\omega_{n}\varepsilon\dot{\alpha}$$

$$\ddot{\Psi} + f\dot{\Psi} - p\dot{\Theta} = \omega_{n}^{2}\varepsilon\beta + 2\zeta\omega_{n}\varepsilon\dot{\beta}$$

$$\ddot{\alpha} + \ddot{\Theta} + \omega_{n}^{2}\alpha + 2\zeta\omega_{n}\dot{\alpha} = 0$$

$$\ddot{\beta} + \ddot{\Psi} + \omega_{n}^{2}\beta + 2\zeta\omega_{n}\dot{\beta} = 0$$
(5)

where ω_n (= $\sqrt{\frac{K}{m}}$) is the natural frequency of the damper; ζ (= $\frac{C}{2m \ \omega n}$) is its damping ratio; ε (= $\frac{ml^2}{A}$) is the nondimensional inertia of the damper. I is the typical length (shown in figure 1), and α and β are small angles defined as α = r/l; β = s/l where r and s are coordinates of the centre of mass of the auxiliary mass (m) relative to the platform.

Using complex variables

$$\eta = \Theta + i\Psi$$

$$\gamma = \alpha + i\theta$$

and substituting in eq. (5) yields:

$$\ddot{\eta} + (f-ip)\dot{\eta} - \omega_n^2 \varepsilon \gamma - 2\zeta \omega_n \varepsilon \dot{\gamma} = 0$$

$$\ddot{\gamma} + \ddot{\eta} + \omega_n^2 \gamma + 2\zeta \omega_n \dot{\gamma} = 0$$
(6)

Assuming the solution:

$$\eta = \eta_0 e^{i\lambda t}; \gamma = \gamma_0 e^{i\lambda t}$$

we obtain the following polynomial for the eigenvalues:

$$\lambda^3 + \lambda^2 \left[-p - i(2\zeta \omega_n (1+\varepsilon) + f) \right] + \lambda \left[-\omega_n^2 (1+\varepsilon) + 2ip\zeta \omega_n - 2\zeta f \omega_n \right] + \omega_n^2 (if + p) = 0 \tag{7}$$

Thus, the solution for the platform equations of motion is given by

$$\eta = \sum_{j=1,3} \eta_j e^{i\lambda_j^j t} e^{-\lambda_{im}^j t}$$
(8)

where λ_{r}^{j} (j=1,3) are the natural frequencies of the system and λ_{lm}^{j} (j=1,3) are magnitudes indicating the quality of the damping of the system. Positive λ_{lm} means suppressed vibrations while negative values for λ_{lm} signify instability.

ANALYSIS

Using the Routh Hurwitz stability criterion, the polynomial (7) has been analyzed. It can be shown (Appendix A) that the system is always stable, i.e., that as the parameters $f,\epsilon,\omega_n,\zeta,P$ are physical quantities whose values are always positive, λ_{im} will be positive. The quality of the damper is a function of λ^j_{im} (j=1,3). The higher the value of λ_{im} the better the damping. Optimum damping is obtained when the minimum of the λ^j_{im} (j=1,3) attains its largest value.

In the analysis, the gyro system is characterized by given (constant) p and f. The optimization is performed on the damper parameters ε , ω_n and ζ . Results are shown in figures 2, 3 and 4 for a gyro system characterized by a nutation frequency p = 377 rad/sec and inherent damping (due to the bearings etc.) of f = $\frac{f*}{A}$ = 0.9 l/sec.

The optimum value for λ_{im} was found to be 50.1/sec. The optimum damper was found to have the following parameters $\zeta=0.3$; $\epsilon=0.05$; $\omega_{n}=340$ rad/sec.

The system (5) has been analyzed using the CSMP simulation program with initial values for θ (=1.0 rad/sec). the results are shown in figures 5 and 6, in which the effect of the damper on the behavior of the system is simulated.

4. EXPERIMENTAL

An experimental auxiliary mass damper was designed using a ring (m) supported by wire springs and immersed in oil as schematically shown in figure l. Experiments were conducted by applying a pulsed load to the platform and measuring the decay rate of the system using noncontact displacement gauges (figure 7). Modified Prony method was used for the analysis of the experimental results [11]. In this method curve fitting yields the natural frequencies as well as the corresponding damping ratios, amplitudes and phase shifts. The computer code is capable of interpreting constant deformation (DC level) which is inherent in this type of loading and also purely exponential variations (as in the case of highly damped systems).

By varying the mass of the ring, the rigidity of the wire springs and the oil viscosity, optimum values were obtained. The gyro system had the same parameter values as those used in the theoretical analysis.

The optimum λ_{im} obtained was about 20.1/sec. The values of the optimum damper parameters (ε, ω_n) were found to be in close agreement with the theoretical values. The value of the optimum damping ratio ζ was found to be 0.1 (figure 8) which differs from the theoretical value. The discrepancy is thought to be due to the following reasons: (1) Nonlinear effects are neglected in the modeling of the oil chamber as a linear dash-pot (2) the theoretical model assumes an idealized two-degree gyro which means infinite rigidity of the rotor and gimbal bearings etc. Adding more degrees of freedom would complicate the analysis but might yield a better agreement with the experimental values.

REFERENCES

- 1. Kyle T. Alfriend 1974 J. Spacecraft Vol. 11 No. 7 469-474. Stability of a Dual-spin Satellite with two dampers.
- 2. Kyle T. Alfriend 1974 J. Spacecraft Vol. 11 No. 7 456-462. Partially filled viscous ring nutation damper.
- 3. Prescott D. Crout and Horance L. Newkirk 1970 5th Aerospace Mechanisms Symposium NASA Cal.-Tech. Lockheed. 1-16. Dynamic behaviour of the Mercury Damper.
- 4. W.R. Haseltine 1962 Journal of the Aerospace Sciences 543-549. Passive damping of Wobbling satellites: General stability Theory and example.
- 5. T.M. Spencer 1974 J. Spacecraft 463-467 Energy-sink analysis for asymmetric Dual Spin Spacecraft.
- I Porat 1979 Israel Journal of Technology Vol. 17 pp. 201-206. Axisymmetric Auxiliary mass notation damper.
- 7. D.L. Mingory at al 1971 J. Spacecraft Vol. 8 No. 5 448-455. Semi passive and Active Nutational dampers for Dual-spin spacecraft.
- 8. E.A. Privalov 1979 Appl. Mech. Vol. 15 No. 6 514-518. Selection of the parameters of a shock absover for vibration of a Gyroscope.
- Gordon A. Haines and Cornelius T. Leondes 1973 The Journal of the Astronautical Sciences Vol. XXI No. 1 1-25. Eddy Current nutation dampers for Dual-Spin satellite.
- 10. Jr. Cannon 1967 Dynamic of Physical systems. New York: McGraw Hill.
- 11. J. Rosenberg Some Modifications In the Prony Method for the spectral Analysis of Damped Vibrations to be published.

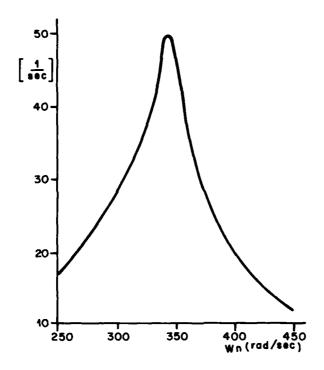


Figure 2

The damping quality λ_{im} (min) vs. natural frequency of the damper for gyro paramaeters p = $377\frac{rad}{sec}$; f = 0.9 $1/_{sec}$ and damper parameters ε = 0.05; ζ = 0.3.

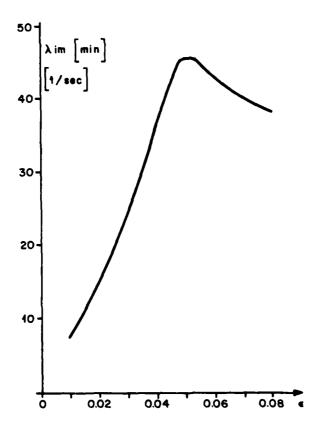


Figure 3

The damping quality λ_{im} (min) vs. damper inertia ϵ for gyro parameter p = $377\frac{rad}{sec}$; f = 0.9 $^{1}/_{sec}$ and damper parameters ω_{n} = 340 $\frac{rad}{sec}$; ζ = 0.3.

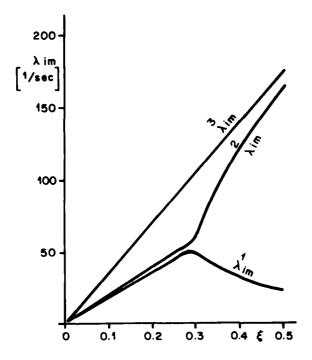


Figure 4

The damping quality λ_{im} vs. the damping rate ζ for gyro parameters $p = 377 \frac{rad}{sec}$; $f = 0.9 \frac{1}{sec}$ and damper parameters $\omega_n = 340 \frac{rad}{sec} \varepsilon = 0.05$.

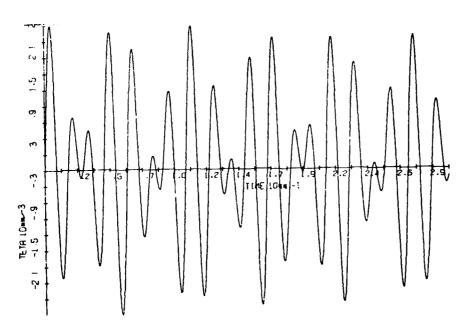


Figure 5

CSMP simulation of Eq. (5) having initial conditions for Θ and damping ratio $\zeta = 0$. (Other parameters values are $p = 377 \frac{\text{rad}}{\text{sec}}$; $\varepsilon = 0.05$; f = 0.9).

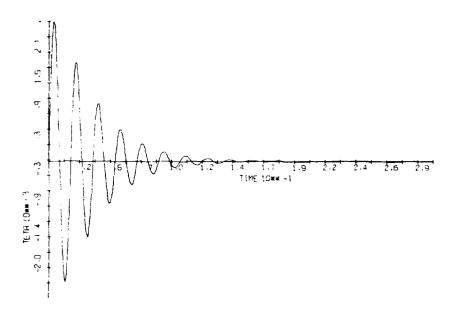


Figure 6

CSMP simulation of Eq.(5) with initial conditions for $\hat{\theta}$ and damping ratio $\zeta=0.3$. (Other parameter's values as in Fig. 5).

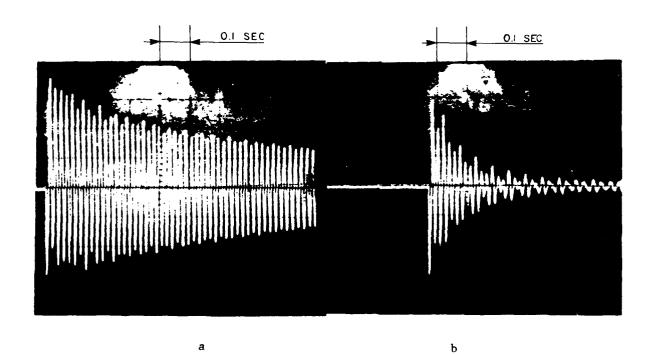


Figure 7

- (a) Response of the experimental system to pulsed load without a damper.
- (b) Response of the experimental system to pulsed load with a damper having $\zeta = 0.1$ and $\varepsilon = 0.04$.

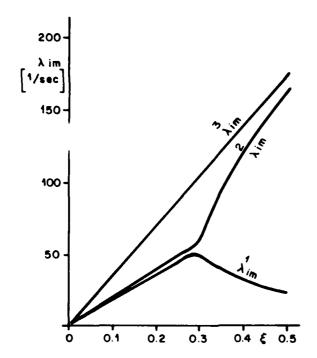


Figure 4

The damping quality λ_{im} vs. the damping rate ζ for gyro parameters p=377 $\frac{\text{rad}}{\text{sec}}$; f=0.9 $^{1}/_{\text{sec}}$ and damper parameters $\omega_{\text{n}}=340$ $\frac{\text{rad}}{\text{sec}}$ $\epsilon=0.05$.

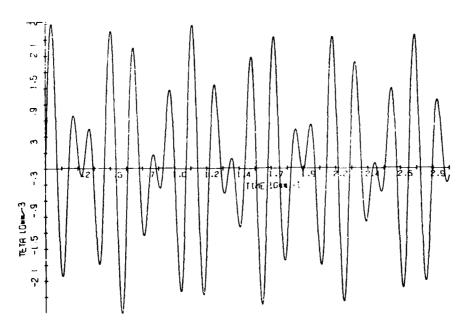


Figure 5

CSMP simulation of Eq. (5) having initial conditions for Θ and damping ratio $\zeta = 0$. (Other parameters values are $\rho = 377\frac{\rm rad}{\rm sec}$; $\varepsilon = 0.05$; f = 0.9).

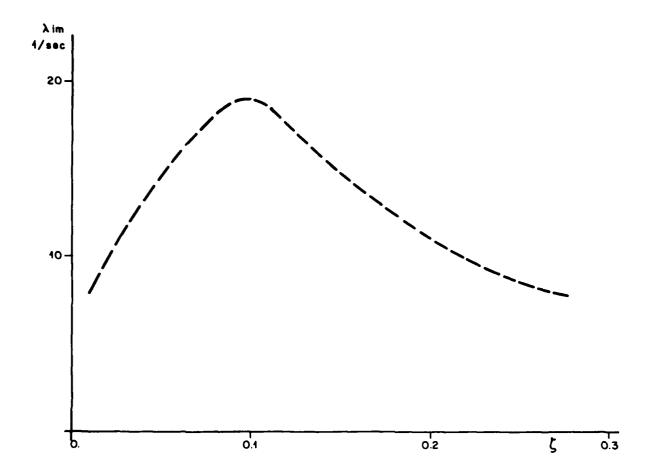


Figure 8

Experimental results obtained for the quality of damping (λ_{im}) vs. damping ration ζ . [Gyro parameters: p=377 $\frac{\text{rad}}{\text{sec}}$; f=0.9 $\frac{1}{\text{sec}}$, damper parameters ω_{n} =340 $\frac{\text{rad}}{\text{sec}}$ sec

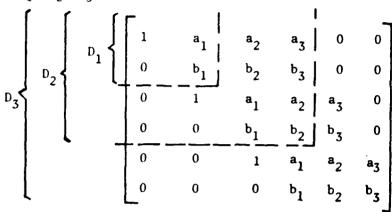
Appendix A

STABILITY OF THE SYSTEM

Routh Hurwitz criterion for a 3rd order polynomial with complex coeficients can be stated as follows:

The polynomial

 $\lambda^3[a_0+ib_0]+\lambda^2(a_1+ib_1)+\lambda(a_2+ib_2)+(a_3+ib_3)=0$ is stable, if the values of the minors D_1 , D_2 , D_3 of the determinant



are: $p_1 < o$; $p_2 > o$; $p_3 < o$.

In the analysed model (eq. (7)) the minors have the following values:

$$\begin{split} & p_1 = -p < 0 \\ & p_2 = 2\zeta\omega_n f^3 + 8\zeta^2\omega_n^2\varepsilon f^2\omega_n^2\varepsilon f^2 + 8\zeta^2\omega_n^2 f^2 + 8\zeta^3\omega_n^3\varepsilon^2 f + \\ & + 4\zeta\omega_n^3\varepsilon^2 f + 16\zeta^3\omega_n^3\varepsilon f + 6\zeta\omega_n^3\varepsilon f + 8\zeta^3\omega_n^3 f + 2\zeta\omega_n^3 f + \\ & + 2\zeta p^2\omega_n f + 4\zeta^2\omega_n^4\varepsilon^3 + 12\zeta^2\omega_n^4\varepsilon^2 + 12\zeta^2\omega_n^4\varepsilon + \\ & + 4\zeta^2 p^2\omega_n^2\varepsilon + 4\zeta^2\omega_n^4 > 0 \\ & p_3 = -4\zeta^2\omega_n^4 f^5 - 16\zeta^3\omega_n^5\varepsilon f^4 - 4\zeta\omega_n^5\varepsilon f^4 - 16\zeta^3\omega_n^5 f^4 - 16\zeta^4\omega_n^6\varepsilon^2 f^3 \\ & - 16\zeta^2\omega_n^6\varepsilon^2 f^3 - \omega_n^6\varepsilon^2 f^3 - 32^4\omega_n^6\varepsilon f^3 - 24\zeta^2\omega_n^6\varepsilon f^3 \\ & - 16\zeta^4\omega_n^6 f^3 - 8\zeta^2\omega_n^6 f^3 - 8\zeta^2 p^2\omega_n^4 f^3 - 16\zeta^3\omega_n^7\varepsilon^3 f^2 \end{split}$$

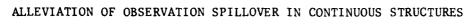
$$\begin{array}{l} -4 \zeta \omega_{n}^{7} \varepsilon^{3} f^{2} - 48 \zeta^{3} \omega_{n}^{7} \varepsilon^{2} f^{2} - 8 \zeta \omega_{n}^{7} \varepsilon f^{2} - 48 \zeta^{3} \omega_{n}^{7} \varepsilon f^{2} - 4 \zeta \omega_{n}^{7} \varepsilon f^{2} \\ -24 \zeta^{3} P^{2} \omega_{n}^{5} \varepsilon f^{2} - 4 \zeta P^{2} \omega_{n}^{5} \varepsilon f^{2} - 16 \zeta^{3} \omega_{n}^{7} f^{2} - 16 \zeta^{3} P^{2} \omega_{n}^{5} f^{2} \end{array}$$

$$-4\zeta^2\omega^8\varepsilon_n^4f^{-16}\zeta^2\omega_n^8\varepsilon^3f^{-24}\zeta^2\omega_n^8\varepsilon^2f^{-16}\zeta^4P^2\omega_n^6\varepsilon^2f$$

$$-8\zeta^{2}P^{2}\omega_{n}^{6}\varepsilon^{2}f-16\zeta^{2}\omega_{n}^{8}\varepsilon f-32\zeta^{4}P^{2}\omega_{n}^{6}\varepsilon f$$

$$-16\zeta^{4}P^{2}\omega_{n}^{6}f-8\zeta^{3}P^{4}\omega_{n}^{5}\varepsilon$$
 - $(2\zeta\omega_{n}^{4}-2\zeta P^{2}\omega_{n}^{2})^{2}f$ < 0

Therefore the system is stable.



A. V. Metcalfe and J. S. Burdess

Departments of Engineering Mathematics and Mechanical Engineering, The University of Newcastle upon Tyne

1. INTRO WICTION

The design of controllers for complex structures is a challenging problem with an expanding range of applications which include the control of large scale space structures. The purpose of the control system may be to enable the structure to carry out a specific task or to combat vibration. Two examples are the attitude control of a space telescope and the control of vibration in helicopters. Feedback control techniques are often used because of their great flexibility and insensitivity to unexpected disturbances. However such controllers usually require knowledge of the displacements and velocities of the significant modes of the structure and direct measurement of these may be impossible. A theoretical solution to this problem is to construct estimates of these variables from a modest number of sensor signals by using an auxilary system known as an observer, [4].

The practical situation is less clear cut. There are inherent problems if many degree of freedom structures or distributed parameter structures are modelled by a reduced number of modes or a finite number of modes respectively. The most serious of these is the fact that lightly damped high frequency modes may lead to instability via the observer. The mechanism behind this phenomenum is as follows. The controller may affect modes which have been ignored in the model: this effect is called control spillover. Motions of these modes contaminate sensor outputs, this effect is called observation spillover, with the result that the closed loop system may become unstable. Engineers are aware of these problems, see [5] for example, but in many cases there is sufficient natural damping in the system to prevent instability. For structures such as spacecraft natural damping may be very small, of the order of 0.005 [6], and a satisfactory technique to alleviate spillover is crucial.

Several remedies for the spillover problem have been proposed, notably by Balas [1,6,7]. These can be loosely divided into three main groups: redesign of the structure and controller with relocation of actuators and sensors, signal filtering techniques, and the use of what Balas describes as additional feedthrough terms in the controller design [7]. The first group includes such strategies as locating actuators and sensors at the zeros of the mode shapes of the residual modes. Whilst this may work for some special cases in general it will prejudice the controllability and observability of the system. Signal filtering introduces the attendant problems of phase distortion and delay. Now consider the use of additional feedthrough terms. Assume the system can be realistically described by N + Q + B modes, a controller can be designed for the N modes when the $Q + \beta$ residual modes are ignored, and observation spillover from the Q modes is causing instability. Use of additional feedthrough terms offers the possibility of removing this spillover without increasing the controller order. However the design procedure requires a model including all N + Q modes and the resulting modification to the original controller may adversely affect the remaining β modes. Also implementation may require additional sensors.

The contamination of the input to the observer by observation spillover is the cause of stability problems. In this paper we propose a method of estimating such contamination and of making allowance for it. Our suggestion is that this can be done by augmenting the observer with a further dynamic system which can be described as a disturbance observer. We have described the use of such a device for the active control of vibration in [8].

THEORY

Consider a structure which can be described by N + R modes with modal damping. The N modes will form the controlled subsystem and the remaining R modes are the residual modes. The structure and sensor outputs can be described by the equations $\frac{1}{2} \frac{1}{2} \frac$

$$\dot{\mathbf{v}}_{\mathbf{N}} = \mathbf{A}_{\mathbf{N}} \mathbf{v}_{\mathbf{N}} + \mathbf{B}_{\mathbf{N}} \mathbf{f} \tag{1a}$$

$$\dot{\mathbf{v}}_{\mathbf{R}} = \mathbf{A}_{\mathbf{R}} \mathbf{v}_{\mathbf{R}} + \mathbf{B}_{\mathbf{R}} \mathbf{f} \tag{1b}$$

$$y = C_N v_N + C_R v_R \tag{1c}$$

where v_N , v_R are vectors representing the displacements and velocities of the controlled and residual modes respectively. The vectors f and y represent the control forces and sensor outputs respectively. The dimensions of v_N , v_R , f and y are 2N, 2R, m and p respectively and A_N , A_R , B_N , B_R , C_N and C_R are matrices of the appropriate dimensions. The matrix B_R represents the control spillover and the matrix C_R represents the observation spillover.

Assume that the reduced order model (A_N, B_N, C_N) is controllable and observable; conditions for these properties in flexible structures are presented in [6]. An observer and feedback control law can be designed for the reduced order model by, for examples, optimal control [9] or modal control [10] methods. The resulting controller is described by the equations,

$$\hat{v}_{N} = (A_{N} - LC_{N})\hat{v}_{N} + B_{N}f + Ty$$
 (2a)

$$f = Gv_N$$
 (2b),

where v_N is the observer state vector and an estimate of v_N .

This would be satisfactory if \mathbf{C}_R were zero but if there is any spillover there will be an undesirable input $\mathbf{C}_R\mathbf{v}_R$ into the observer.

The proposal is to estimate this input and apply a cancelling signal u. This can be done with the aid of a disturbance observer [8]. The ensuing control system can be represented by

$$\hat{v}_{N} = (A_{N} - LC_{N})\hat{v}_{N} + B_{N}f + LC_{N}v_{N} + LC_{R}v_{R} + Lu$$
 (3a)

$$f = Gv_N$$
 (3b)

where u is the output of the disturbance observer which is a dynamic system represented by

$$\dot{z} = Tz + \hat{\mathbf{Q}v}_{N} \tag{4a}$$

$$\varepsilon = z - \hat{Sv_N} \tag{4b}$$

$$u = -K_{\varepsilon} \tag{4c}$$

the dimensions of the vectors z, ϵ and u being p. Differentiation of (4b) and use of (3a), (3b), (4a) and (4c) yields

$$\dot{\varepsilon} = (T + SLK)\varepsilon - SLC_N(v_N - \hat{v}_N) - SLC_Rv_R + (TS + Q - SA_N - SB_NG)\hat{v}_N$$
(5)

Now choose the matrices T, S and K so that (T + SLK) has eigenvalues with large negative real parts and set Q such that

$$TS + Q - SA_N - SB_NG = 0$$
 (6).

The motivation for such choices is that if the observer error (v $_{\rm N}$ - v $_{\rm N}$) is small then in the steady state

$$(T + SLK)_{\varepsilon} = SLC_{R}v_{R}$$
 (7)

and

$$u = -K\varepsilon \simeq -K(T + SLK)^{-1}SLC_{p}v_{p}$$
 (8)

Consideration of (8) in isolation suggests that SLK should be large compared with T to make u approximately opposite to $C_R v_R$; however the effect of the disturbance observer on the complete system, consisting of structure and controller, must be considered.

Define e as the observer error

$$e = v_N - \hat{v}_N \tag{9}$$

and describe the structure and controller by the state space equation

$$\begin{pmatrix} \mathbf{v}_{N} \\ \mathbf{e} \\ \mathbf{\varepsilon} \\ \mathbf{v}_{R} \end{pmatrix} = \begin{pmatrix} A_{N} + B_{N}G - B_{N}G & 0 & 0 \\ 0 & A_{N} - LC_{N} & LK & -LC_{R} \\ 0 & -SLC_{N} & T + SLK - SLC_{R} \\ B_{R}G & -B_{R}G & 0 & A_{R} \end{pmatrix} \begin{pmatrix} \mathbf{v}_{N} \\ \mathbf{e} \\ \mathbf{\varepsilon} \\ \mathbf{v}_{R} \end{pmatrix}$$
 (10).

In the case when the dimension of y is one T and K are scalar quantities which we denote by t and k. This is less restrictive than it might appear at first sight since the system (A_N, B_N, C_N) is observable with one point displacement sensor, provided it is located away from the mode

shapes which are to be controlled and the closed loop system has no repeated eigenvalues [6]. It is shown in the appendix that if k tends to infinity and all other parameters stay finite then the eigenvalues of

the system matrix in (10) tend to those of the matrices

$$A_N + B_N G$$
, A_R and $A_N - LC_N$ Ik $-SLC_N$ $t + SLk$ (11)

We have tested the procedure described in this section for several cases with the dimension of y set as one and N and R being one or two. A disadvantage was the tendency for large values of k to move the real parts of some of the eigenvalues of the partitioned matrix in (11) to the right. However the real parts did remain negative and the practical interpretation was that the observer took longer to converge onto the true values. It was possible to compensate for this undesirable effect by making t large and negative but such remedial action had a tendency to reintroduce instabilities in the residual modes. These findings are illustrated by Example 1.

When the dimension of y is greater than one the situation is more complex. We demonstrate the stabilisation of a system where the dimension of y is two in Example 2.

EXAMPLES

We demonstrate the use of the noise observer and compare it with other approaches to the spillover problem in two examples.

Example 1

Consider a two mode structure and assume a controller is needed for the first mode only. There is no requirement for any control over the second mode save that it should remain stable. In particular take

$$A_{N} = \begin{pmatrix} 0 & 1 \\ -100 & -.1 \end{pmatrix} \qquad B_{N} = \begin{pmatrix} 0 \\ 1 \end{pmatrix} \qquad C_{N} = \begin{pmatrix} 1 & 0 \end{pmatrix} \qquad L = \begin{pmatrix} 20 \\ 0 \end{pmatrix}$$

$$G = \begin{pmatrix} 0 & -10 \end{pmatrix}$$

$$A_{R} = \begin{pmatrix} 0 & 1 \\ -200 & -.1 \end{pmatrix} \qquad B_{R} = \begin{pmatrix} 0 \\ .3 \end{pmatrix} \qquad C_{R} = \begin{pmatrix} -.3 & 0 \end{pmatrix} .$$

Notice that $\mathbf{C}_{\mathbf{N}}$ and $\mathbf{C}_{\mathbf{R}}$ imply that only displacement is measured. The closed loop eigenvalues are

and we see that the system is unstable. Set up a disturbance observer with

$$S = (-1 \ 0) \ T = t \ K = k$$
.

The following Table 3.1 gives the positions of the system eigenvalues for varying t and k.

<u>t</u>	<u>k</u>				Eigen	values		
-100 -100 -100 -100 -100 0 -20 -40	0 20 30 40 100 10	-100; -516; -717; -918; -2119;	-5.1 -5.1	<pre>± j8.1; ± j8.8; ± j8.7; ± j8.7; ± j8.6; ± j8.6; ± j8.7; + j8.7;</pre>	-10.5 -1.9 -1.4 -1.1 52 07 89	; 3.6; ; 9.6; ; 9.8; ; 9.8; ; 19.9; ; 19.5; ; 19.5;	.011 004 013 034 037 016	± j14.2 ± j14.1 ± j14.1 ± j14.1 ± j14.2 ± j14.2 ± j14.2

Table 3.1 Closed Loop Eigenvalues for Example 1 with Disturbance Observer

An obvious alternative approach is to reduce either the feedback or observer gains i.e. the elements of G or L. In this example if L is reduced to

$$L = \begin{pmatrix} 2.8 \\ 0 \end{pmatrix}$$

the eigenvalues of the system without the disturbance observer become

$$-5.1 \pm j8.7$$
; $-1.4 \pm j9.9$; $-.004 \pm j14.1$.

The approach described by Balas in [7] is not applicable to this example. It requires the dimension (p) of y to exceed twice the number of residual modes from which spillover is to be removed. For p to equal two a velocity measurement must also be made rendering an observer redundant.

Example 2

Consider the four mode system described by the matrices,

$$A_{N} = \begin{pmatrix} 0 & 1 & 0 & 0 \\ -100 & -.1 & 0 & 0 \\ 0 & 0 & 0 & 1 \\ 0 & 0 & -400 & -.2 \end{pmatrix} \qquad A_{R} = \begin{pmatrix} 0 & 1 & 0 & 0 \\ -600 & -.2 & 0 & 0 \\ 0 & 0 & 0 & 1 \\ 0 & 0 & -1000 & -.3 \end{pmatrix}$$

$$B_{N} = \begin{pmatrix} 0 \\ 1 \\ 0 \\ -.5 \end{pmatrix} \qquad B_{R} = \begin{pmatrix} 0 \\ -.3 \\ 0 \\ .2 \end{pmatrix} \qquad C_{N} = \begin{pmatrix} 1 & 0 & 0 & 0 \\ 0 & 0 & 1 & 0 \\ 0 & 0 & 1 & 0 \end{pmatrix}$$

$$C_{R} = \begin{pmatrix} 0 & 1 & 0 & 0 & 0 \\ 0 & 0 & 0 & 1 & 0 \\ 0 & 0 & 1 & 0 \end{pmatrix}$$

A controller is designed for the two lower frequency modes with

The closed loop eigenvalues are:

and the system is unstable. It can be stabilised by using a disturbance observer with

$$S = \begin{pmatrix} 0 & 0 & 0 & 0 \\ -1 & 0 & 1 & 0 \end{pmatrix} \qquad T = \begin{pmatrix} 0 & 1 \\ 360 & -180 \end{pmatrix} \qquad K = \begin{pmatrix} 40 & -20 \\ -5 & -10 \end{pmatrix} .$$

The closed loop eigenvalues become:

The stablisation does not depend on accurate knowledge of A_R , B_R and C_R in so much as the system appears to remain stable for changes in these matrices which would reduce the spillover if there were no disturbance observer. Here we consider spillover as measured by the maximum of the real parts of the system eigenvalues.

One alternative approach for removing the spillover is to reduce the gains in the matrix L. If L is changed to

$$L = \begin{cases} 2.5 & 0 \\ 0 & 0 \\ 0 & 3 \\ 0 & 0 \end{cases}$$

the closed loop eigenvalues become:

Since only one of the residual modes is causing spillover and p=2 the approach by Balas can be used. It does not guarantee system stability as the modifications to the controller may adversely affect the ignored residual mode. In this example the controller is modified to

$$\hat{\mathbf{v}} = \mathbf{A}_{\mathbf{N}} \hat{\mathbf{v}}_{\mathbf{N}} + \mathbf{B}_{\mathbf{N}} \mathbf{f} + \mathbf{L} (\mathbf{y} - \hat{\mathbf{y}}) + \mathbf{\Psi} \mathbf{B}_{\mathbf{Q}} \mathbf{f}$$

$$\mathbf{f} = \mathbf{G} \hat{\mathbf{v}}_{\mathbf{N}} + \mathbf{\Phi} (\mathbf{y} - \hat{\mathbf{y}})$$

where

$$\hat{y} = C_N \hat{v}_N \qquad B_Q = \begin{pmatrix} 0 \\ -.3 \end{pmatrix}$$

$$\phi = \begin{pmatrix} .057 & -.0049 \\ .487 & .0096 \\ -.205 & .0057 \\ -2.287 & -.1372 \end{pmatrix} \qquad \phi = (10.09 & -239.8) .$$

The closed loop eigenvalues become:

Figure 3.1 shows envelopes for the displacements of the four modes with the disturbance observer (dotted line) and the innovations feedthrough of Balas (broken line). Initial displacements were set at one and initial velocities and observer states were set at zero.

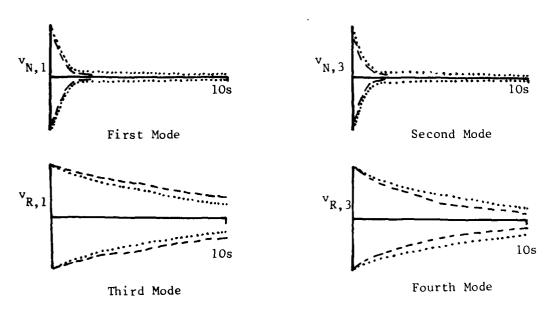


Figure 3.1 Envelopes for Modal Displacements.

4. CONCLUSION

If there are a finite number (R) of residual modes the use of innovations feedthrough, described by Balas in [7], enables complete removal of observation spillover when certain conditions are satisfied. Of these the requirement for 2R sensors may restrict its use. Complete removal of observation spillover depends on accurate knowledge of the matrices describing the residual modes although the modified controller may still stabilise the system when these are incorrectly estimated. Also elimination of observation spillover may increase the control spillover but this will not make the system unstable. Balas compares his approach with that of designing a reduced order controller in [7].

In practical applications there are likely to be a large or infinite number of residual modes of which Q may be causing instabilities. Application of innovations feedthrough to these Q modes does not guarantee that the system eigenvalues will not be moved. In fact the modified controller may increase spillover in the other β residual modes, but it is hoped that this will not make the system unstable. For example spillover could be exchanged from modes with very little natural damping to different frequency modes with greater natural damping. The use of the disturbance observer described in this paper is an alternative to Balas' approach, the disturbance observer having an advantage of not requiring at least 2Q sensors.

The disturbance observer can be used in situations where there is only one point sensor although in the example we considered it was no improvement on reduction of the observer gains. Nevertheless it may have applications. If N is large the matrix L will have many elements. If an observer has been made and spillover is found to be a problem it might be more convenient to augment the observer with a disturbance observer than to change all the observer gains. Secondly whilst the performance of two strategies may be similar when judged by the position of eigenvalues the behaviour of the states of interest may differ in the two cases leading to a distinct preference for one or the other.

5. APPENDIX

It is assumed that p = 1. First consider the case of N = R = 1. Then L and $\mathbf{C_p}$ are of the form

$$L = \begin{bmatrix} 1 \\ 1 \\ 2 \end{bmatrix} \qquad C_R = (c_1 \quad c_2)$$

The characteristic polynomial of the system described by (10) is

$$\phi(\lambda) = \begin{bmatrix} A_{N} + B_{N}G - \lambda I & -B_{N}G & 0 & 0 & 0 \\ 0 & A_{N} - LC_{N} - \lambda I & 1_{1}k & -1_{1}c_{1} & -1_{1}c_{2} \\ & & & 1_{2}k & -1_{2}c_{1} & -1_{2}c_{2} \\ 0 & -SLC_{N} & t - \theta k - \lambda & \theta c_{1} & \theta c_{2} \\ B_{R}G & -B_{R}G & 0 & A_{R} - \lambda I \end{bmatrix}$$
(12)

$$= \begin{bmatrix} 0 & 0 & 0 & 0 \\ 0 & 0 & 0 & 0 \\ 0 & -1_{1}c_{1} & -1_{1}c_{2} \\ 0 & -1_{2}c_{1} & -1_{2}c_{2} \\ t - \lambda & \theta c_{1} & \theta c_{2} \\ 0 & a_{66} & a_{67} \\ 0 & a_{76} & a_{77} \end{bmatrix} + \begin{bmatrix} 0 & 0 & 0 \\ 0 & 0 & 0 \\ 1_{1}k & 0 & -1_{1}c_{2} \\ 0_{7x4} & 1_{2}k & 0 & -1_{2}c_{2} \\ -\theta k & 0 & \theta c_{2} \\ 0 & a_{66} & a_{67} \\ 0 & a_{76} & a_{77} \end{bmatrix}$$

Since the third determinant is zero there are no terms in ϕ which involve the product c_1k . A similar expansion applied to the second determinant shows there are no terms involving the product c_2k . Now consider the determinant (12) with c_1 , c_2 set equal to zero and c_2k . Now consider the zero. The resulting polynomial has a common factor $(t - \theta k - \lambda)$ and as c_2k , c_3k , c_4k , c_5k , and c_5k are all stable the other factor is a polynomial of degree 6 with all its coefficients strictly positive. It follows that c_5k has k appearing in all the coefficients except that of c_5k . The coefficient of c_5k does not involve c_5k or c_5k so the effect of c_5k and c_5k becomes negligible as k tends to infinity. The required result follows and the proof generalises for any values of N and R.

6. REFERENCES

- 1. M.J. BALAS 1982 IEEE Transactions on Automatic Control AC-27, 522-535. Trends in large space structure control theory: fondest hopes, wildest dreams.
- 2. C.E. KAPLOW and J.R. VELMAN 1980 Journal of Guidance and Control 3, 227-233. Active local vibration isolation applied to a flexible space telescope.
- 3. G. SCHULZ 1979 Automatica 15, 461-466. Active multivariable isolation for a helicopter.
- 4. D.G. LUENBERGER 1971 IEEE Transactions on Automatic Control AC-16, 596-602. An introduction to observers.
- 5. R.W. ELLIS and C.D. MOTE Jr. 1979 Transactions of the ASME: Journal of Dynamic Systems, Measurment and Control 101, 44-48. A feedback vibration controller for circular saws.

- 6. M.J. BALAS 1978 IEEE Transactions on Automatic Control AC-23, 673-679. Feedback control of flexible systems.
- 7. M.J. BALAS 1980 International Journal of Control 32, 983-1003. Enhanced modal control of flexible structures via innovations feedthrough.
- 8. J.S. BURDESS and A.V. METCALFE 1983 Ninth ASME Vibrations Conference 12th-14th September, Dearborn, Michigan, USA. The active control of forced vibration produced by arbitrary disturbances.
- 9. H. KWAKERNAAK and R. SIVAN 1972 Linear Optimal Control Systems. Wiley
- 10. B. PORTER and R. CROSSLEY 1972 Modal Control. Taylor & Francis.

3. FINITE ELEMENT AND BOUNDARY ELEMENT METHODS

A NEW BEAM FINITE ELEMENT WITH SEVEN DEGREES OF FREEDOM
AT EACH NODE FOR THE STUDY OF COUPLED BENDING-TORSION VIBRATIONS

A. Potiron and D. Gay

Department of Mechanics National Institute of Applied Sciences

C. Czekajski

Department of Structures
National School of Aeronautics and Space
Toulouse (France)

AD-P003 648

1. INTRODUCTION

The subject matter of the first part or this study is the derivation of coupled bending-torsion relations characterizing the dynamical behaviour of unsymetrical cross-section beams. This allows for the further definition of a beam element with seven degrees of freedom per node. The numerical results obtained with the FEM are compared to experiment in some section shape cases.

In order to characterize the displacement field of considered beams, the method of integrated displacements allows us to consider the so-called secondary effects: longitudinal warping inertia, and shear deformation due to both shearing forces and nonuniform warping. The literature on dynamical flexure and torsion of beams is extensive. Cowper for flexure and Gay-Boudet for torsion introduce integrated displacements. We extend in the following this notion to the study of coupled bending-torsion of an homogeneous straight beam.

BASIC THEORY

2.1 Displacement Field

 Ω is the domain occupied by the cross-section. Γ is the boundary, and G is the centroid. In the plane of the section, the principal axis are noted Gx_2, Gx_3 . $C(c_2, c_3)$ is the shear center, as defined by Trefftz [3] (figure 1).

The displacement of any point M of the beam is noted $X_M(x_i)$, with components X_i (i=1,2,3). Let us define the seven displacement parameters:

Three angular parameters:
$$\theta_{i}(x_{1},t) = \frac{1}{I_{i}} \int_{\Omega} (GM \times X_{M}) \cdot x_{i} d\Omega$$
 (1-a)

Three linear parameters:
$$U_{i}(x_{1},t) = \frac{1}{S} \int_{\Omega} \vec{X}_{M} \cdot \vec{x}_{i} d\Omega$$
 (1-b)

A warping parameter:
$$\dot{\Theta}(x_1,t) = \frac{1}{I_{\Phi}} \int_{\Omega} \Phi . X_1 d\Omega$$
 (1-c)

 $\Phi(x_2,x_3)$ is the Saint-Venant warping function defined in C, and $I_{\Phi}=\int\limits_{\Omega}\Phi^2~d\Omega$ is the quadratic warping moment.

Hence, the displacement field takes the form of:

$$\vec{X} = \vec{U} + \vec{GM} \times \vec{\theta} + \vec{\Phi} \vec{O} \vec{x}_1 + \vec{\eta}$$
 (2)

According to the above definitions, necessary orthogonality conditions hold in the domain Ω for the functions 1, x_2 , x_3 , Φ , η_1 , together with:

$$\int_{\Omega} \eta_2 \ d\Omega = \int_{\Omega} \eta_3 \ d\Omega = \int_{\Omega} (x_2 \eta_3 - x_3 \eta_2) \ d\Omega = 0$$
 (3)

2.2 Equations of Motion

Assuming the lateral surface of the beam free of any force, we take into account as first hypothesis (H.1) the assumption that normal stresses σ_{22} and σ_{33} are expected to be negligible compared to σ_{11} . Then, the principle of virtual work associated with the displacement field (2) leads to the classical set of motion equations:

$$\rho S \vec{U},_{tt} = \vec{F},_1 + \vec{p}$$
 (4-a,b,c)

$$\rho[I]\vec{\theta},_{tt} = \vec{M},_{1} + \vec{m} + \vec{x}_{1} \times \vec{F}$$
 (5-a,b,c)

And the seventh motion equation is the bimoment one:

$$\rho I_{\phi} \dot{\theta},_{tt} = B_{1} + b + (M_{1} - GJ\theta_{1},_{1}) - c_{2}F_{3} + c_{3}F_{2}$$
 (6)

2.3 Constitutive Equations

In order to obtain a technical formulation for the constitutive equations, we assume as second hypothesis (H.2) that the change in the deformation $\vec{\eta}$ of two infinitely near adjacent cross sections is neglected in order to evaluate the longitudinal and shear stresses σ_{1j} , j=1,2,3. Thus, starting from the Hooke's law for a linear elastic body, the constitutive equations below are deduced from integrations over the domain of the section:

$$u_{1,1} = \frac{F_1}{ES}$$
; $\theta_{2,1} = \frac{M_2}{EI_2}$; $\theta_{3,1} = \frac{M_3}{EI_3}$; $\theta_{1,1} = \frac{B}{EI_{\Phi}}$ (7-a,b,c,d)

Moreover, noting that the first component η_1 of $\vec{\eta}$ (2) is essentially due to the shear forces F_2 , F_3 and nonuniform warping moment noted $M_{\text{nuw}} = (M_1 - GJ\theta_1, 1)$, we obtain the three followed coupled relations written in matrix form:

$$\begin{bmatrix} \theta_{1,1} - \dot{\theta} \\ u_{2,1} - \theta_{3} - c_{3} \dot{\theta} \\ u_{3,1} + \theta_{2} + c_{2} \dot{\theta} \end{bmatrix} = \begin{bmatrix} K_{11} - K_{12} - K_{13} \\ -K_{21} & K_{22} - K_{23} \\ -K_{31} - K_{32} & K_{33} \end{bmatrix} \begin{bmatrix} M_{\text{nuw}} / G(I_{1} - J) \\ F_{2} / GS \\ F_{3} / GS \end{bmatrix}$$
 (8-a,b,c)

In (8) appear nine shear coefficients with the symmetry properties:

$$K_{23} = K_{32}$$
 ; $K_{1j} = K_{j1} \frac{I_1 - J}{S}$, $j = 2, 3$ (9-a,b,c)

Starting from the local equilibrium of continuous media, we show that the shear coefficients K_{ij} can be computed after solving three Poisson's problems in the cross section, namely:

$$\nabla^2 \mathbf{g} = \mathbf{f}(\mathbf{x}_2, \mathbf{x}_3) \text{ over } \Omega, \text{ with successively } \mathbf{f} = \mathbf{x}_2, \mathbf{x}_3, \Phi.$$

$$\partial \mathbf{g}/\partial \mathbf{n} = 0 \text{ along the boundary } \Gamma \qquad (10-a,b,c)$$
with
$$\int_{\Omega} \mathbf{g} \ d\Omega = 0$$

For the complete expressions of K_{ij} , see appendix A. The effective calculus of all bending-torsion constants involved in the aforementioned relations (I_i , J, I_{ϕ} , K_{ij} , c_i) has been performed by means of a boundary element method [4].

3. FINITE ELEMENT FORMULATION

For the setting up of a finite element formulation, let us first look at the technical expressions of potential and kinetic energies.

3.1 Potential Strain Energy $V(x_1,t)$

For a beam element of length $d\mathbf{x}_1$, and according to H.1, the general form of strain energy:

$$dV = \{\frac{1}{2} \int_{\Omega} \sigma_{ij} \epsilon_{ij} d\Omega \} dx_1$$

reduces to:

$$V_{1} = \frac{1}{2} \int_{\Omega} (\sigma_{11} \varepsilon_{11} + 2\sigma_{12} \varepsilon_{12} + 2\sigma_{13} \varepsilon_{13}) d\Omega \qquad (11)$$

Consideration of (2) and H.2 leads to the practical expressions:

$$V_{,1} = V_{\sigma,1} + V_{\tau,1}$$
 (12)

in which:

$$V_{\sigma,1} = \frac{1}{2} \left\{ \frac{F_1^2}{ES} + \frac{M_2^2}{EI_2} + \frac{M_3^2}{EI_3} + \frac{B^2}{EI_{\Phi}} \right\}$$
 (13-a)

$$V_{\tau,1} = \frac{1}{2} \{K_{22} \frac{F_2^2}{GS} + K_{33} \frac{F_3^2}{GS} + K_{11} \frac{M_{\text{nuw}}^2}{G(I_1 - J)} \dots$$

... +
$$\frac{(GJ\theta_1, 1)^2}{GJ}$$
 - $(K_{23}+K_{32})\frac{F_2F_3}{GS}$ - $\frac{M_{nuw}}{G(I_1-J)}\{F_2(K_{12}+\frac{I_1-J}{S}K_{21}) + ...$

...
$$F_3(K_{13} + \frac{I_1 - J}{S} K_{31})$$
 (13-b)

3.2 Kinetic Energy

In the same way, we retain the simple expression:

$$T_{,1} = \frac{1}{2} \rho S(\vec{v}_{,t})^2 + \frac{1}{2} \rho I_{\phi} \mathring{\theta}_{,t}^2 + \frac{1}{2} \rho \{\vec{\theta}_{,t}\}^T | I | \{\vec{\theta}_{,t}\}$$
 (14)

3.3 Definition of the Element

Seven displacements per node k characterize the motion of the two-nodes beam element. In a matricial form:

$$\{\mathbf{w}_{\mathbf{k}}\} = [\mathbf{u}_1, \mathbf{u}_2, \mathbf{\theta}_3, \mathbf{u}_3, \mathbf{\theta}_2, \mathbf{\theta}_1, \mathbf{0}]_{\mathbf{k}}^{\mathsf{T}}$$

Substituting the static case for the quasi-static dynamical one leads to an interpolation matrix [A] not detailed here, allowing a displacement field in the form of:

$$\{W(x_1,t)\} = [A(x_1)] {\stackrel{e}{W}(t)}$$
 (15)

where
$$\{\mathring{W}(t)\} = \{\mathring{W}_1(t)\}$$

3.4 Stiffness Matrix

Introducing the displacement field (15), the element strain energy is obtained after integration of (13) over the length ℓ of the element, and written in the matrix form:

$$2V = \{ \stackrel{e}{W} \}^T [D] \{ \stackrel{e}{W} \}$$

We detail in Appendix B the stiffness matrix [D] in the simplified case $i \neq j \rightarrow K_{ij} \sim 0$. It can be noted that, for symetrical section shape cases and for uniform warping (Saint-Venant torsion), this stiffness matrix reduces to the classical one derived by Przemieniecki [5].

3.5 Mass Matrix

The calculus of the kinetic energy for the whole element by means of (15) leads to the form:

$$2T = {\stackrel{e}{W}, {}_{t}}^{T} [M] {\stackrel{e}{W}, {}_{t}}$$

in which [M] is a consistent mass matrix, reached after very heavy calculus. In the much more simpler case of lumped mass approximation, the kinetic energy reduces to:

$$2T = \rho \frac{\ell}{2} \sum_{k=1,2} \{ \sum_{j=1,2,3} (Su_{kj,t}^2 + I_j \theta_{kj,t}^2) + I_{\phi} \dot{\theta}_{k,t}^2 \}$$

from which a simple diagonal mass-matrix is easily derived.

4. APPLICATIONS

Numerical and experimental tests have been performed on several cantilever beams. For the dynamical flexure and torsion of a rectangular section beam, numerical values of frequencies provided by FEM and analytical ones are in good agreement with the experiment, especially for high frequencies. The dynamical torsion of an I-section beam has been likewise investigated. In such a case, exact analytical values of torsional constants cannot be reached, needing a previous computational work. The results for dynamical case are detailed in reference [6], and some of them are recalled in appendix C. In a same manner, we have also tested two U-section beams (thick and thin). Here coupling between flexure and torsion occurs, and the whole theory above applies. We shall present both numerical and experimental frequencies. Rather good agreement can be noted for all tests, the rank of the modes concerned depending on the number of elements of the discretization.

CONCLUSION

The study of coupled bending-torsion can be performed with acceptable accuracy by means of the formulation above, starting from the definition of seven displacements parameters in each section of the beam. The finite element derived allows a simple numerical prediction of the dynamical behaviour of beams with any cross sections. Nevertheless, we must keep in mind that an accurate computation of coupled bending-torsion constants is the first stage when using this element.

NOMENCLATURE

- E, G Young's and shear modulus.
- S, I_1, I_2, I_3 Cross section area and quadratic moments of inertia in G.
- I d Quadratic warping moment.
- J Saint-Venant's torsional rigidity.
- F_1, F_2, F_3 Normal and shear forces.
- M_1, M_2, M_3 Torsion torque and bending moments.
- \vec{v} , $\vec{\theta}$ Linear and angular displacement vectors (components: u_i and θ_i).
- \dot{x}_i Unit vectors of principal axis.
- ρ Mass per unit volume.
- (), Partial derivative with respect to x_i .
- (), tid. with time t.
- ∂ / ∂ n Outward normal derivative along the boundary Γ .
- \overrightarrow{p} , \overrightarrow{m} , \overrightarrow{b} Distributed forces, moments and bimoment along the beam.
- [I] Diagonal inertia matrix of cross section.
- n Complementary displacement vector.

REFERENCES

- G.R. COWPER 1966 Journal of Applied Mechanics. June 335-340.
 The Shear Coefficient in Timoshenko Beam Theory.
- 2. D. GAY and R. BOUDET 1980 Journal of Mechanical Design 102 627-632. A Technical Theory of Dynamical Torsion for Beams of Any Cross Section Shapes.
- 3. E. TREFFTZ 1935 Z.Angew.Math.Mech. 15 220-225. Über den Schubmittelpunkt in Einem Durch Eine Einzellast Gebogenen Balken.
- 4. C. CZEKAJSKI, D. GAY and A. POTIRON 1984 Second International Conference on Recent Advances in Structural Dynamics.
 Southampton. A Boundary Element Program for the Calculation of Coupled Flexure-Torsion Characteristics for Beams of Any Cross-Section Shapes.
- 5. J.C. PRZEMIENIECKI 1968 Theory of Matrix Structural Analysis Mc Graw-Hill.
- 6. A. POTIRON, D. GAY and C. CZEKAJSKI 1983 Design and Production Engineering Technical Conference of ASME. Dearborn(Michigan) ASME paper n° 83-DET-87. Limitation of Simplified Hypothesis Concerning Thin-Walled Beam Characteristics if Accurate Prediction of Torsional Oscillations is Requested.

Appendix A

4

Shear Coefficients Kii

Solutions of (10-a,b,c) allow the knowledge of the functions $g_{i,0}$ (i=1,2,3) verifying over the domain Ω of the cross-section:

$$\nabla^2 g_{10} = \frac{Sc_3}{I_{\phi}} \Phi - \frac{S}{I_3} x_2$$

$$\nabla^2 g_{20} = -\frac{Sc_2}{I_{\phi}} \Phi - \frac{S}{I_2} x_3$$

$$\nabla^2 g_{30} = \frac{I_1 - J}{I_{\phi}} \Phi$$

with $\partial g_{i0}/\partial n = 0$; i=1,2,3 along the boundary Γ .

Then, the Kij are deduced in the form of:

$$K_{11} = -\frac{1}{I_{\Phi}} \int_{\Omega} \Phi g_{30} d\Omega$$

and for i, j=2,3; $i \neq j$; k=j-1:

$$K_{jj} = \frac{1}{I_i} \int_{\Omega} x_j g_{k0} d\Omega + (j-i) \frac{c_i}{I_{\phi}} \int_{\Omega} \Phi g_{k0} d\Omega$$

$$K_{ji} = -\frac{1}{I_{j}} \int_{\Omega} x_{j} g_{k_{0}} d\Omega + (j-i) \frac{c}{I_{\phi}} \int_{\Omega} \Phi g_{k_{0}} d\Omega$$

$$K_{j1} = \frac{I_{1} - J}{SI_{\Phi}} \int_{\Omega} \Phi g_{k0} d\Omega$$

$$\frac{\mathbf{I}_{1}-\mathbf{J}}{\mathbf{S}} \quad \mathbf{K}_{1}\mathbf{j} = -\frac{1}{\mathbf{I}_{i}} \int_{\Omega} \mathbf{x}_{j} \quad \mathbf{g}_{30} \quad d\Omega + (i-j) \quad \frac{\mathbf{c}_{i}}{\mathbf{I}_{\Phi}} \int_{\Omega} \Phi \mathbf{g}_{30} \quad d\Omega$$

The properties of symetry of the $\kappa_{i\,j}$ are shown by means of the Green-Gauss theorem, and we find:

$$K_{23} = K_{32}$$
 ; $K_{j1} = \frac{I_1 - J}{S} K_{1j}$

Appendix B

Stiffness Matrix [D]

We introduce the following dimensionless notations:

$$\alpha = 1 + K_{11} \frac{J}{I_1 - J}$$
; $\lambda^2 \ell^2 = \frac{GJ \ell^2}{\alpha E I_{\phi}}$; $k_1 = \frac{\lambda \ell \sinh \lambda \ell}{\cosh \lambda \ell - 1}$

$$I_{\phi} k_{0} = \{\frac{1}{\phi_{1}} (\alpha k_{1}-2) + \frac{\alpha}{I_{\phi}} (\frac{I_{3}c_{3}^{2}}{1+\phi_{3}} + \frac{I_{2}c_{2}^{2}}{1+\phi_{2}}) (k_{1}-2)\}^{-1}$$

$$\Phi_1 = 12 K_{11} \frac{EI_{\phi}}{G(I_1 - J) \ell^2}; \beta_1 = \alpha \frac{k_0 I_{\phi}}{\Phi_1} (2 - k_1)$$

$$j=2,3 \rightarrow \Phi_{j} = 12 K_{jj} \frac{EI}{GS l_{2}}$$
; $\beta_{j} = \alpha k_{0} \frac{I_{j} c_{j}^{2}}{1+\Phi_{j}}$ (2-k₁)

Then, the symetry properties of [D] leads to the following terms, in the simplified case : $i\neq j\to K_i\,j^{=0}$.

$$d_{1}^{1} = d_{8}^{8} = -d_{8}^{1} = -d_{1}^{8} = \frac{ES}{\ell} \quad ; \quad \text{others } d_{j}^{1} = d_{1}^{j} = d_{8}^{j} = d_{8}^{j} = 0$$

$$d_{2}^{2} = d_{9}^{9} = -d_{9}^{2} = \frac{12 EI_{3}}{\ell^{3} (1 + \Phi_{3})} \quad (1 + \beta_{3})$$

$$d_3^2 = d_{10}^2 = -d_{10}^9 = -d_9^3 = \frac{\ell}{2} d_2^2$$

$$d_4^2 = d_{11}^9 = -d_{11}^2 = -d_9^4 = -\frac{12 \text{ EI}_3}{\ell^3 (1+\Phi_3)} \beta_2 c_3/c_2 = -\frac{12 \text{ EI}_2}{\ell^3 (1+\Phi_2)} \beta_3 c_2/c_3$$

$$d_5^2 = d_{12}^2 = -d_9^5 = -d_{12}^9 = -d_4^3 = -d_{10}^4 = d_{11}^3 = -\frac{\ell}{2} d_4^2$$

$$d_6^2 = d_{13}^9 = -d_{13}^2 = -d_9^6 = \frac{12 \text{ EI}_3}{\ell^3 (1 + \ell_3)} \beta_1 c_3$$

$$d_7^2 = d_{14}^2 = -d_9^7 = -d_{14}^9 = k_0 GJ \frac{I_{3} C_{3}}{1+\Phi_{3}}$$

$$d_3^3 = d_{10}^{10} = \frac{EI_3}{\ell(1+\Phi_3)} (4+\Phi_3+3\beta_3)$$

$$d_5^3 = d_{12}^3 = d_{12}^{10} = -\frac{\ell}{2} d_4^3$$

$$d_6^3 = -d_{13}^3 = d_{10}^6 = -d_{13}^{10} = \frac{\ell}{2} d_6^2$$

$$d_7^3 = d_{14}^3 = d_{10}^7 = d_{14}^{10} = \frac{\ell}{2} d_7^2$$

$$d_{10}^3 = \frac{EI_3}{9.(1+\Phi_3)} (2-\Phi_3+3\beta_3)$$

$$d_{4}^{4} = d_{11}^{11} = -d_{11}^{4} = \frac{12 \text{ EI}_{2}}{\ell^{3} (1+\theta_{2})} (1+\theta_{2})$$

$$d_5^4 = d_{12}^4 = -d_{12}^{11} = -d_{11}^5 = -\frac{\lambda}{2} d_4^4$$

$$d_{6}^{4} = d_{13}^{11} = -d_{13}^{4} = -d_{11}^{6} = -\frac{12 \text{ EI}_{2}}{\ell^{3} (1 + \Phi_{0})} \beta_{1} c_{2}$$

$$d_7^4 = d_{14}^4 = d_{11}^7 = -d_{14}^{11} = -k_0 GJ \frac{I_2 c_2}{1+\Phi_2}$$

$$d_5^5 = d_{12}^{12} = \frac{EI_2}{g(1+\phi_2)} (4+\phi_2+3\beta_2)$$

$$d_6^5 = -d_{13}^{12} = -d_{13}^5 = d_{12}^6 = -\frac{\ell}{2} d_6^4$$

$$d_7^5 = d_{14}^5 = d_{14}^{12} = d_{12}^7 = -\frac{2}{2} d_7^4$$

$$d_{10}^5 = -\frac{\ell}{2} d_{10}^4$$

$$d_{12}^{5} = \frac{EI_{2}}{\ell(1+\phi_{2})} (2-\phi_{2}+3\beta_{2})$$

$$d_6^6 = d_{13}^6 = d_{13}^{13} = \beta_1 \frac{GJ}{\ell} \frac{k_1}{2-k_1} - 12\alpha \frac{EI_{\phi}}{\ell^3 \phi_1} (\beta_2 + \beta_3)$$

$$d_{7}^{6} = d_{14}^{6} = -d_{13}^{7} = -d_{14}^{13} = k_{0} I_{\Phi} \frac{GJ}{\Phi_{1}}$$

$$d_{7}^{7} = d_{14}^{14} = -\frac{GJk_{0}}{\alpha\lambda(ch\lambda\ell-1)} \left\{ \frac{I_{\Phi}}{\Phi_{1}} (sh\lambda\ell - \alpha\lambda\ell ch\lambda\ell) + \alpha \left(\frac{I_{2} c_{2}^{2}}{1+\Phi_{2}} + \frac{I_{3} c_{3}^{2}}{1+\Phi_{3}} \right) \dots \right\}$$

$$\dots$$
 (sh λ l - λ lch λ l)}

$$d_{1+}^{7} = \frac{GJk_0}{\alpha\lambda(ch\lambda\ell-1)} \left\{ \frac{I_{\phi}}{\Phi_1} \left(sh\lambda\ell - \alpha\lambda\ell \right) + \alpha \left(\frac{I_2 c_2^2}{1+\Phi_2} + \frac{I_3 c_3^2}{1+\Phi_3} \right) \left(sh\lambda\ell - \lambda\ell \right) \right\}$$

Appendix C

The study of natural torsional frequencies of a cantilever beam performed by means of the finite element procedure has been compared to the experimental datas. The results concerning the relative error are shown on table I below.

wh 0.0355	MODE N°	1	2	3	4	5	6	7	8	9	10
D:0;100	ERROR %	0.	0.9	ο.	0.7	-1.	-0.9	-1.6	-1.3	0.1	2.

Table 1.

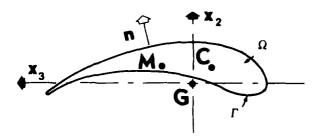


Figure 1.

A BOUNDARY ELEMENT PROGRAM FOR THE CALCULATION OF COUPLED FLEXURE TORSION CONSTANTS FOR BEAMS OF ANY CROSS SECTION SHAPE

C. Czekajski

Department of Structures National School of Aeronautics and Space

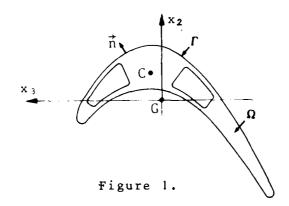
D. Gay and A. Potiron

Department of Mechanics
National Institute of Applied Sciences
Toulouse (France)

AD-P003 649

1. , INTRODUCTION

The study of coupled flexure-torsion of beams by means of a finite element procedure to needs the foregoing knowledge of a set of coefficients to be introduced in the corresponding program. The constants involved by the theory [1] are as follows:



- a) Center of inertia G and corresponding principal axis Gx_2 and Gx_3 for the cross section (figure 1).
- b) Quadratic moments of inertia for flexure I_2 and I_3 .
- c) Quadratic moment for torsion (in principal axis) I1.
- d) Constant of torsional rigidity J.
- e) Center of shear C (co-ordinates c2 and c3 in principal axis).
- f) Quadratic warping moments I_{ϕ} and I_{ϕ} respectively in G and C.
- g) Shear coefficients for coupled flexure-torsion (nine constants $k_{\,i\,\,\dot{j}}$ [1]).

BOUNDARY FORMULATIONS

2.1 Classical Torsion Characteristics

The numerical treatment of cases a,b,c is classical. The calculus of torsional rigidity J has already been performed by several numeri-

cal methods (finite differences, finite elements, boundary elements). For example, it can be deduced from the warping function ϕ of the Saint-Venant problem:

$$\begin{cases} \nabla^2 \phi = 0 \text{ inside } \Omega. \text{ (figure 1)} & (1-a) \\ \partial \phi / \partial n = x_3 n_2 - x_2 n_3 \text{ along the boundary } \Gamma. (1-b) \\ \text{and } \int_{\Omega} \phi d\Omega = 0 \rightarrow \int_{\Gamma} \phi x_2 n_2 d\Gamma = 0 & (1-c) \end{cases}$$

in this last case, the boundary element method is particularly wellsuited, since it can be shown that:

$$J = \int_{\Gamma} \left\{ \frac{1}{3} \left(x_2^3 n_2 + x_3^3 n_3 \right) - \phi \overrightarrow{\nabla} \phi \cdot \overrightarrow{n} \right\} d\Gamma$$

Moreover, this approach reduces the localization of the center of shear $C(c_2, c_3)$ as follows:

$$c_{2} = -\frac{1}{I_{2}} \int_{\Omega} \phi x_{3} d\Omega = -\frac{1}{2} \int_{\Gamma} \frac{(3\phi x_{3}^{2} n_{3} + x_{3}^{3} x_{2} n_{3}) d\Gamma}{\int_{\Gamma} x_{3}^{3} n_{3} d\Gamma}$$

$$c_3 = \frac{1}{I_3} \int_{\Omega} \phi x_2 d\Omega = \frac{1}{2} \int_{\Gamma} \frac{x_2^2 n_2 (3\phi - x_2 x_3) d\Gamma}{\int_{\Gamma} x_2^3 n_2 d\Gamma}$$

2.2 Quadratic Warping Moment

In the same manner, the case f) can also be treated on the boundary as:

$$I_{\phi} = \int_{\Omega} \phi^2 d\Omega = -\int_{\Gamma} g_3 \overrightarrow{\nabla} \phi \cdot \overrightarrow{n} d\Gamma \qquad \text{and} \qquad I_{\phi} = I_{\phi} - \left\{ \frac{1}{I_2} \left(\int_{\Omega} x_3 \phi d\Omega \right)^2 + \frac{1}{I_3} \left(\int_{\Omega} x_2 \phi d\Omega \right)^2 \right\}$$

where appears a function g3 described later.

2.3 Shear Coefficients

Treatment of case g) (shear coefficients) implies a special adaptation of the boundary element method to the solving of the following Poisson problem:

$$\nabla^2 \mathbf{g} = \mathbf{f}(\mathbf{x}_2, \mathbf{x}_3) \quad \text{inside } \Omega$$

$$\partial \mathbf{g}/\partial \mathbf{n} = 0 \quad \text{along } \Gamma$$
(2-a)

$$\partial g/\partial n = 0$$
 along Γ (2-b)

and
$$\int_{\Omega} g d\Omega = 0$$
 (2-c)

where $f(x_2,x_3)$ takes the successive forms:

$$f(x_2, x_3) = x_2 \text{ or } x_3 \text{ or } \phi(x_2, x_3)$$

Then, the shear coefficients $k_{\,\hat{1}\,\hat{j}}$ are shown to be obtained as linear combinations $\left[\,l\,\right]$ of the nine integrals:

$$C_{ij} = \int_{\Omega} g f(x_2, x_3) d\Omega$$
 (3)

Adaptation of the BEM for each form of f(x2,x3) in problem (2):

a) $f(x_2, x_3) = x_2$

The Poisson's problem is reduced to a Laplace one in the form of:

$$\nabla^{2}(g_{1}-u) = 0 \text{ inside } \Omega$$

$$\partial g_{1}/\partial n \text{ and } \partial u/\partial n \text{ known along } \Gamma$$
(4)

and the condition of unicity $\int\limits_{\Omega} g_1 \ d\Omega$ = 0 can be turned into:

$$\int_{\Gamma} g_1 x_2 n_2 d\Gamma + \frac{1}{8} \int_{\Gamma} x_2^4 n_2 d\Gamma = 0$$
 (5)

In this way, the BEM provides the purely boundary form (6) in every point i on the boundary Γ (i = 1,N):

$$ag_{i} = au_{i} - \int_{\Gamma} (g_{1} - u) \frac{\partial Log r}{\partial n} d\Gamma + \int_{\Gamma} Log r \left(\frac{\partial g_{1}}{\partial n} - \frac{\partial u}{\partial n} \right) d\Gamma$$
 (6)

The coefficient "a" depending on the smoothness of the boundary $\lfloor 3 \rfloor$. In this way, we can write a system of N+1 equations with N unknowns which is solved in the sense of the minimal least squares.

b)
$$f(x_2, x_3) = x_3$$

In a same way, the particular solution retained is $u=\frac{1}{6}x_3^3$. Then the condition of unicity $\int\limits_{\Omega}g_2d\Omega=0$ turns into:

$$\int_{\Gamma} g_2 x_2 n_2 d\Gamma + \frac{1}{6} \int_{\Gamma} x_3 x_2^3 n_2 d\Gamma = 0$$
 (7)

c) $f(x_2, x_3) = \phi(x_2, x_3)$

In the general case of any cross sectional shapes, the warping function ϕ can be reached only in a numerical form, after solving the problem (1). Thus, the simplification above does not hold any more, the integral formulation of the problem (2) being [3]:

$$ag_{3i} = \int_{\Gamma} \frac{\partial g}{\partial n}^{3} \quad Log \quad r \quad d\Gamma \quad -\int_{\Gamma} \frac{\partial Log \quad r}{\partial n} \quad g_{3} \quad d\Gamma \quad -\int_{\Omega} \varphi \quad Log \quad r \quad d\Omega$$
 (8)

To avoid the calculus of the surface integral in the formulation above, we have changed the problem (2) into a biharmonic one:

$$\nabla^{4}\mathbf{g}_{3} = 0 \text{ inside } \Omega$$
 (9-a)
$$\partial \mathbf{g}_{3}/\partial \mathbf{n} = 0 \text{ along } \Gamma$$
 (9-b)

with the condition of unicity $\int\limits_{\Omega}\mathbf{g}_3$ $\mathrm{d}\Omega$ = 0 rewritten in the form of:

$$\int_{\Gamma} g_3 x_2 n_2 d\Gamma + \frac{1}{6} \int_{\Gamma} \phi x_2^3 n_2 d\Gamma - \frac{1}{24} \int_{\Gamma} x_2^4 x_3 n_2 d\Gamma = 0$$
(9-c)

The boundary formulation of (9-a) is:

$$ag_{3\hat{1}} = \int_{\Gamma} \{Ag_{3} - B \frac{\partial g}{\partial n}^{3} + C\phi - D \frac{\partial \phi}{\partial n}\} d\Gamma \qquad (10)$$

in which:
$$A = \overrightarrow{\nabla} \{ \nabla^2 (r^2 \log r) \} . \overrightarrow{n}$$

$$B = \nabla^2 (r^2 \log r)$$

$$C = \overrightarrow{\nabla} (r^2 \log r) . \overrightarrow{n}$$

$$D = r^2 \log r$$
(11)

In (10), φ and $\partial\varphi/\partial n$ are known from the solution of (1). Then, we obtain a system of N+1 equations with N unknowns values of the function g_3 , solved in the sense of minimal least squares.

The following step consists in the evaluation of auxilliary coefficients $C_{i\,j}$ (3), boundary forms of which are as follows:

$$C_{jj} = \frac{1}{2} \int_{\Gamma} g_{j-1} x_{j}^{2} n_{j} d\Gamma + \frac{1}{30} \int_{\Gamma} x_{j}^{5} n_{j} d\Gamma , j=2,3$$

$$C_{23} = C_{32} = \frac{1}{2} \int_{\Gamma} g_{1} x_{3}^{2} n_{3} d\Gamma + \frac{1}{24} \int_{\Gamma} x_{3}^{4} x_{2} n_{3} d\Gamma$$

$$C_{21} = C_{12} = \frac{1}{2} \int_{\Gamma} g_{3} x_{2}^{2} n_{2} d\Gamma + \frac{1}{24} \int_{\Gamma} \varphi x_{2}^{4} n_{2} d\Gamma - \frac{1}{120} \int_{\Gamma} x_{2}^{5} x_{3} n_{2} d\Gamma$$

$$C_{31} = C_{13} = \frac{1}{2} \int_{\Gamma} g_{3} x_{3}^{2} n_{3} d\Gamma + \frac{1}{24} \int_{\Gamma} \varphi x_{3}^{4} n_{3} d\Gamma + \frac{1}{120} \int_{\Gamma} x_{3}^{5} x_{2} n_{3} d\Gamma$$

$$C_{11} = -\int_{\Gamma} h \frac{\partial \varphi}{\partial n} d\Gamma$$

In the last integral above appears a function $h(x_2, x_3)$ which is shown to be the solution of the following problem:

$$\nabla^6 h = 0 \text{ inside } \Omega$$
$$\partial h/\partial n = 0 \text{ along } \Gamma$$

solved likewise by the BEM [4]. Then, the shear coefficients k_ij of the coupled bending-torsion with nonuniform warping are obtained as linear combinations of the aforementioned C_{ij} [1].

3. NUMERICAL RESULTS

Among several sections tested, we cite below the results concerning two particular shapes.

3.1 Rectangular Section

In that case, analytical results are known for flexure [5] and torsion with non uniform warping [6]. Table 1 shows the values obtained with 160 constant boundary elements along the whole boundary, for a rectangular b×h section, with h/b=3.

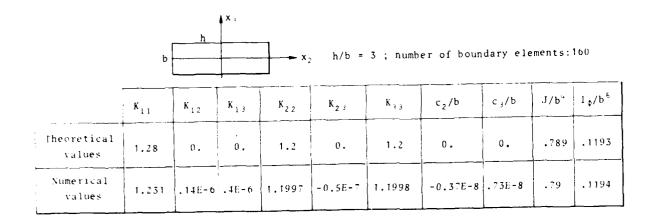


Table 1.

Improvement of accuracy is obtained either by increasing the number of boundary elements, or by means of higher order elements.

3.2 USection Shape

For this shape, no analytical values are available. Varying the number of elements, we have obtained the following results (table 2).

Number of Boundary Elements	J(m")	Ι _φ (m ⁶)	c ₂ (m)
80	2.586E-6	2.929E-9	-0.02481
120	2.584E-6	2.913E-9	-0.02475
160	2.582E-6	2.906E-9	-0.02473

Table 2.

The section's characteristics are given in figure 2, in which are also noted the shear coefficients values, and the convergence obtained. The rather slow rates of convergence for the shear coefficient of nonuniform warping k_{11} and for the coupling flexure-torsion shear coefficient k_{13} are due to successive computation of three functions, each of them being approximated by lower values. It can also be observed that the Timoshenko's shear coefficients $k_{2\,2}$ and $k_{3\,3}$ are quite stable.

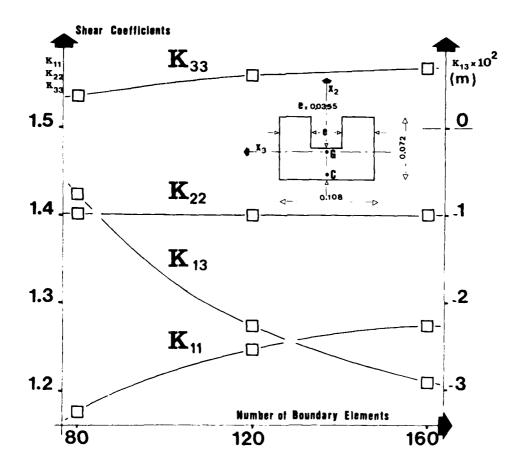


Figure 2.

4. CONCLUSION

The main feature of the presented work consists in the introduction of auxilliary functions allowing the conversion of surface integrals into boundary integral expressions.

Accuracy of computed results has been tested on several symetric [2] as well as assymetric section shapes, and the constants obtained compared with analytical ones when previously known. Furthermore, experiment has been performed in the dynamical domain for beams for which analytical values could not be reached, with good agreement even for high order modes.

We finally note that the aforementioned adaptation of the boundary element method allows a considerable time saving (order of 80% in our study) compared with the classical finite element method.

REFERENCES

- 1. A.POTIRON, D. GAY and C. CZEKAJSKI 1984 Second International Conference on Recent Advances in Structural Dynamics.

 Southampton. A New Beam Finite Element with Seven Degrees of Freedom at Each Node for the Study of Coupled Bending-Torsion Vibrations.
- 2. C. CZEKAJSKI, S. LAROZE and D. GAY 1982 Symposium on Advances and Trends in Structural and Solid Mechanics. Washington. NASA CP 2245. Application of a Boundary Element Method to the Study of Dynamical Torsion of Beams.
- 3. C.A. BREBBIA and S. WALKER 1980 Boundary Element Techniques in Engineering. London-Boston: Newnes-Butterworths.
- 4. C. CZEKAJSKI and D. GAY 1983 National School of Aeronautics and Space. ENSAE Technical Report. Résolution d'un Problème Tri-Harmonique par la Méthode des Equations Intégrales.
- 5. G.R. COOPER 1966 Journal of Applied Mechanics, 33,335-340. The shear Coefficient in Timoshenko Beam Theory.
- 6. D. GAY and R. BOUDET 1980 Journal of Mechanical Design, 102, 627-632. A Technical Theory of Dynamical Torsion for Beams of Any Cross-sectional Shapes.



A COMPARATIVE STUDY OF SOIL SPRING AND FINITE ELEMENT MODELS APPLICATION TO NUCLEAR POWER STATION

K. M. Ahmed

National Nuclear Corporation Limited
Engineering Department
Booths Hall
Knutsford
Cheshire

INTRODUCTION

1

2

A nuclear power station is normally composed of several buildings some of which have their own separate foundation base mat or footing. When subjected to seismic excitation the response of these buildings is coupled through soil structure interaction effects. Two basic methods are commonly available to solve the structure-to-structure interaction effects: The direct finite element method as implemented by FLUSH, (1) and the lumped parameter finite element approach. A comparative study between the elastic half space solution as computed by the MODAN code (2) and the FLUSH code for the AGR island on a single base mat was reported in [5] and good agreement was obtained in the computed structural response. The objective of the study reported here is:

to assess the degree of conservatism in the seismic response based on analysis using linear soil coupling springs and dampers. Non-linear seismic analysis have been performed in recent years using both the embedded and surface-founded configurations. Results obtained in these non-linear analyses were compared to those with linear springs. The present paper addresses the work done at NNC with those comparisons and may be summarised as:

to compare the dynamic response of the coupled AGR structures obtained by the lumped parameter finite element approach with that of the direct finite element solution.

The analysis is limited to the behaviour of the Nuclear Island under the action of earthquake ground motion acting horizontally in the longitudinal direction. The free field ground motion used is the modified Parkfield accelerogram with 0.25 g peak acceleration [5].

STRUCTURAL IDEALISATION

The major structural components of the AGR Nuclear Island considered for this study to consist of the following:

Prestressed Concrete Pressure Vessel (PCPV), PCPV support system, PCPV internals, reactor building and its services annexes, fuel handling building complex.

The structural idealisations for both the finite element soil and the elastic half space soil models are shown in Fig 1 and 2 respectively. The idealisation of the structural components in each case consists of beam elements, with distributed mass, lumped masses, rigid links and linear-damped-spring elements drawn with such generality that configurations with a shallowly-embedded base mat can also be effectively represented.

As shown in Fig 2, four sticks have been modelled to represent the Prestressed Concrete Pressure Vessel (PCPV) and its internals (gas baffle, graphite core, diagrid and supporting structure) and reactor building and its services annexes. Two sticks with shear spring connections to represent the fuel handling building complex. These sticks are connected by infinitively rigid members at the bottom and by three simulated spring damper elements. There are a total of 34 mass points and 34 beam elements and 47 nodes in this model. The reactor building stick consists of seven mass points and six beam elements. $K_{\mbox{\scriptsize Coup}}$ represents the equivalent soil spring including soil coupling between the buildings and $C_{\mbox{\scriptsize Coup}}$ represents the equivalent radiation coupling damping constant.

3 HALF SPACE APPROACH

In this approach, the effect of the foundation medium (soil) is represented by the frequency independent foundation impedance. The foundation impedance can be simulated by a mechanical analogue composed of equivalent spring and dampers. The equivalent dampers represent the effect of radiation damping. The material damping of the foundation medium is generally neglected since it is small compared with the radiation damping. This lumped parameter soil spring approach is generally used for structures supported at or near the surface of soils which may be idealised as a uniform elastic half space.

3.1 Soil Configurations

The necessary requirements specified for this part of the project was that the choice of the soil models should be such that they represent a wide range of soil properties, representing also an envelope of the soil profile for the Heysham II site. Thus specific information regarding soil layering, material anisotropy, depth dependent properties and water table is neglected. A set of two idealised site configurations was selected to sample local soil profiles encountered in Heysham II site. The idealised configurations consisted of semi-infinite single horizontal homogenous soil layers. The four basic parameters used in this study to define the material properties of the sandstone materials are:

shear wave velocity	Vs
damping ratio	β
Poisson's ratio	ν
mass density	0

The other important properties - Young's modulus E, shear modulus G and compression wave velocity $V_{\rm p}$ - may be evaluated from the following expressions based on elastic theory:

E =
$$2 \rho V_s^2 (1 + \nu)$$

G = ρV_s^2 (1)
 $v_p = v_s \left\{ 2 (1 - \nu)/(1 - 2\nu) \right\}^{\frac{1}{2}}$

Within the scope of this study, the two most important soil parameters which affect the coupled seismic response are taken to be the shear wave velocity and the damping ratio. An increase in the shear wave velocity of the soil increases the natural frequencies of the combined soil structure system. The effect of the Poisson's ratio and material density are shown to be insignificant for the evaluation of the overall response. The values assigned to the soil material parameters resulted from an iterative process 'Equivalent Linear Method' on a soil column typical of Heysham II site under an SSE level of excitation.

These parameters are listed as follows:

	Shear wave velocity (M/S)	Damping ratio
1 1	1133	0.011
! ! ! ! 2 !	1527	0.017

The above soil properties correspond to soil properties for layer 12 and layer 26 respectively for the soil model shown in Fig 1.

3.2 Derivation of Coupling Flexibility Matrix

The interaction model is shown schematically in Fig 2. The interacting structures were idealised as lumped mass cantilevers supported on soil springs and connected by coupling springs. The coupling springs take into account the isolated soil spring constants. The coupling stiffness matrix was derived by computing first the flexibility coefficients base on the geometric relationships of the three foundations resting on the surface of a homogenous isotropic, linear elastic half space and then inverting it. The expressions for the displacement of the footings in terms of the corresponding forces may be expressed as:

$$d = F f$$

$$\approx \approx \infty$$
(2)

where

$$d = \left\{u1, v1, \theta1, u2, v2, \theta2, u3, v3, \theta3\right\}$$

displacements and rotations of the foundations

$$f = \left\{ f_{u1}, f_{v1}, f_{\theta_1}, f_{u2}, f_{v2}, f_{\theta_2}, f_{u3}, f_{v3}, f_{\theta_3} \right\}$$
= corresponding forces and moments

and

[F] = flexibility matrix

The terms of the above flexibility matrix are functions of the elastic properties of the isotropic and homogeneous foundation media (Young's modulus and Poisson's ratio), the dimensions of the footings, and the distance between the foundations. The elements of the 3 x 3 submatrices on the leading diagonals of equation (3) represent the independent uncoupled foundations and maybe evaluated either numerically (using the procedure for coupling terms described below) or by using the inverse of the expressions for soil spring stiffnesses given in [3]. The remaining terms of the flexibility matrix which represent the coupling between the three foundations were obtained in this investigation by using a numerical procedure as described below.

The coupling terms of the flexibility matrix were evaluated by computing the displacements resulting from unit loads applied to rigid foundations in the directions corresponding to the degrees of freedom for foundation one, two and three. For these unit loads applied in the horizontal, vertical and rotational directions for each foundation a pressure distribution as shown in Fig 3 is assumed. The resulting displacements at the first footing were evaluated numerically using the solutions provided by Poulos and Davis [4]. The displacements at the centres of all other foundations, computed as described above. were then averaged and normalised by the total load applied at the first footing to obtain the corresponding flexibility coefficients. It may be noted that in the flexibility matrix given by equation (2). the coefficients representing the coupling between the horizontal degrees of freedom at one foundation with the vertical and rotational degrees of freedom at other footings were also considered. these coupling flexibility matrix coefficients were determined from physical considerations and these are depicted in Fig 4. The term r_o in Fig 4 is the radius of a circular foundation equal in area to that of the actual foundation.

As mentioned earlier, the diagonal terms of the flexibility matrix in equation (3) can also be computed using a numerical procedure similar to that described above, where each foundation was assumed to rest independently on the surface of an elastic half space. For concentrated load applied at the centre of each foundation, the displacements at the centres of all other elements can be computed using an assumed pressure distribution. The corresponding flexibility terms for the elements can be obtained by averaging these displacements and normalised by the applied load. The resulting coupling flexibility matrix of the soil-structure-interaction is shown in Fig 4 and by inverting this matrix the coupling stiffness matrix is obtained.

3.3 Analysis Procedure

The Nuclear Island has been assumed in this document to have complete structural symmetry about the vertical plane YZ passing through the fuel handling building complex and since the exciting motion is in the direction X, normal to this plane and consequently antisymmetric to it, then the response of the system must be antisymmetric about YZ plane. Thus it is only necessary to consider only one-half of the structural idealisations. The antisymmetric behaviour of the separate three base mats can be ensured by the antisymmetric transformation of both the stiffness and damping matrices thus:

$$\begin{bmatrix} K \end{bmatrix} = \begin{bmatrix} T \end{bmatrix}^{t} \begin{bmatrix} K \end{bmatrix} \text{ soil} \begin{bmatrix} T \end{bmatrix}, \begin{bmatrix} C \end{bmatrix} = \begin{bmatrix} T \end{bmatrix}^{t} \begin{bmatrix} C \end{bmatrix} \text{ soil}$$
 (4)

in which the antisymmetric transformation matrix is

$$[C] = [\alpha] [K] [\alpha]$$

in which

$$\begin{bmatrix} \alpha \end{bmatrix} = \begin{bmatrix} \alpha_{\mathbf{u}1} & \alpha_{\mathbf{v}1} & \alpha_{\theta1} & \alpha_{\mathbf{u}2} & \alpha_{\mathbf{v}2} & \alpha_{\theta2} & \alpha_{\mathbf{u}3} & \alpha_{\mathbf{v}3} & \alpha_{\theta3} \end{bmatrix}$$

and

$$\alpha_{ui} = \sqrt{\frac{C_{ui}}{K_{ui}}}, \quad \alpha_{i} = \sqrt{\frac{C_{vi}}{K_{vi}}}, \quad \alpha_{\theta i} = \sqrt{\frac{C_{\theta i}}{K_{\theta i}}}$$

where C_{ui} , C_{0i} , C_{0i} are the radiation coefficient for horizontal, vertical and velocity modes of isolated foundation raft 'i'

and the displacement vector for the rafts being

 $\left\{ \begin{array}{cccc} u_1 & v_1 & \theta_1 & u_2 & \theta_2 \\ \end{array} \right\}$ where <code>[K]</code> and <code>[C]</code> are the stiffness and damping matrices of soil the soil respectively.

For each soil condition considered in this document sets of time-history response curves were obtained . These results were then combined to produce envelope curves of floor response spectra. From the calculated time-history response of the system, floor response spectra have been generated for 5% critical damping and the maximum peak ground acceleration was set equal to 0.25 g.

DIRECT FINITE ELEMENT APPROACH

The finite element FLUSH analysis is one of the well established methods used to perform the soil-structure interaction analysis. In this method, the entire soil-structure system is modelled by a finite element model. The advantage of the finite element analysis is that the non-linear soil properties and other type of material behaviour can be approximately included in the analysis. One of the limitations of the FLUSH analysis is that, although an attempt is made to simulate the three-dimensional effect, the model is basically a two-dimensional model. The direct finite element method (FLUSH) in its present form cannot study the torsional response of a soil-structure system as a result of the non-vertically incident seismic waves, or the lack of symmetry of the structural configuration. Above all, the two-dimensional characteristics of the FLUSH analysis may result in under-estimation of the response of an isolated structure, while exaggerating the interaction effect of multi structures.

Figure 1 outlines one-half of the finite element model of the AGR island and consists of 446 solid elements, two void elements, 90 beam elements and 662 nodal points. The earthquake ground motion is prescribed at the base of the foundation i.e. at the top of layer 12 (see Fig 1).

The peak acceleration of the Modified Parkfield wave was normalised to 0.25 g. One-dimensional deconvolution is used to compute iteratively by Equivalent Linear Analysis strain compatible shear moduli and damping values in the different soil layers as well as the rigid base acceleration. The damping values of the soil layers were up to 20% whilst for the sandstone strata were about 2%. The model is equipped with transmitting boundary on the right hand side of the model to represent the lateral soil to infinity and viscous boundaries are used by FLUSH to model the out-of-plane energy dissipation through the soil. A complete interaction analysis is performed in one step using transfer functions in the frequency domain and fast numerical Fourier transformations to obtain the time history response of the structure to the horizontal base acceleration computed from the deconvolution processes. The depth of the rigid base underlying layer 26 which is non-existing in reality is chosen large enough not to influence the structural response.

RESULTS OF THE ANALYSES

The dynamic analyses of the soil-structure-interaction analyses were performed using both the modal superposition procedure as implemented in the MODAN code for the lumped parameter approach and the complex response method as implemented in the FLUSH code for the finite element model. In the lumped parameter approach all modes up to 35 Hz were considered in the analyses whilst for the finite element procedure a cut-off frequency of 33 Hz was utilised. The soil profile used for this exercise corresponds to soil type 2 corresponding to

layer 26 as stated in sub-section 3.1. Four locations of interest are chosen for this study for comparing the dynamic responses and these are:

PCPV vault floor, +0.15 m (node 251)

reactor building at 0.0 m (node 317)

fuel shielded block at +32.0 m (node 606)

fuel shielded block at +0.0 m (node 616)

Horizontal seismic soil-structure interaction analysis results obtained using the direct finite element method and the frequency-independent lumped parameter approach are compared for the above locations in terms of 5% floor response spectra. In Fig 5 to 8 inclusive the finite element solution is displayed as solid curves whilst that of the lumped parameter approach is shown as dotted curves. The separation distance between the foundation base mats is taken to be 25 mm which in essence represents a typical separation distance between the various foundations of the AGR Nuclear Island.

Figure 5 depict the comparative study of the 5% damping floor response spectrum for one location on the Prestressed Concrete Pressure Vessel and its primary circuit. For locations on the PCPV, reactor building and the fuel handling building complex, the spring - dashpot method predicts a maximum peak spectral accelerations of the order 10 to 46% higher than the finite element FLUSH method particularly in the period range of 0.15 seconds to 0.35 seconds.

The differences in spectral amplitude between the FLUSH - direct finite element approach and the soil spring solution can be attributed to the following items:

- (1) foundation input motions which characterize the process by which the seismic waves are scattered by the presence of embedded foundation are not included in the soil spring approach analysis
- (2) hysteretic damping is not included in the soil spring method
- (3) the structural damping for the soil spring method was based upon one dominate natural mode of vibration
- (4) the use of free field input motions in the seismic soilstructure-interaction analysis will result in much more conservative structural responses as compared with those obtained by using embedded input motion. This is mainly because of iltering effect of the dominate natural periods of ground motion takes place.

Overall, however, the agreement between the FLUSH and the soil spring approach response spectra appears to be quite reasonable. The adoption of two extreme values of soil conditions for the overall evaluation of the seismic response of the AGR plant on a layered site should be used with some care.

6 CONCLUSION

The effects of through soil coupling on the seismic response of the AGR plant have been determined through comparison studies using surface-founded and embedded models. Currently, the results generated from MODAN analysis for linear surface-founded models are conservative in comparison with the embedded plant analysis using FLUSH. This conservatism in surface-founded models may be removed by using more accurate soil material damping in addition to radiation damping simulation. This can be achieved either through the use of non-linear modelling or hysteretic soil media or by representing the soil region as a linear viscoelastic half-space as used in CLASSI computer code.

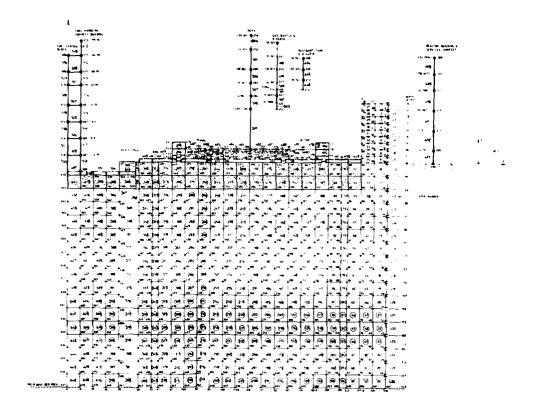
In view of the differences in modelling the soil and foundations and also in the treatment of damping, the two approaches lumped parameter finite element (MODAN) and direct finite element (FLUSH) - have predicted comparable responses.

7 REFERENCES

- 1. JOHN LYSMER et al 1975 Report No. EERC 73-30. FLUSH a computer program for approximate 3-D analysis of soil structure interaction problems.
- 2. A User's Guide to MODAN 1973 C92/SDS/151/501. Issue A.
- 3. F.E. RICHART, J.R. HALL and R.D. WOOD 1970 Vibration of soils and foundations. Englewood: Prentice Hall.
- 4. H.G. POULOS and E.H. DAVIS 1974 Solutions for soil and rock mechanics. New York: John Wiley.
- K.M. AHMED 1980 Seismic response of the AGR Island: Phase 2 Part 1.
 Soil structure interaction effects. NNC Report No. C92/SDS/151/006.

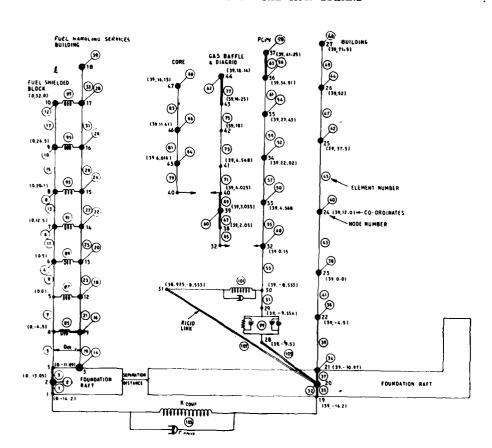
Acknowledgement

The author would like to thank the National Nuclear Corporation Limited for their kind permission to present this paper.



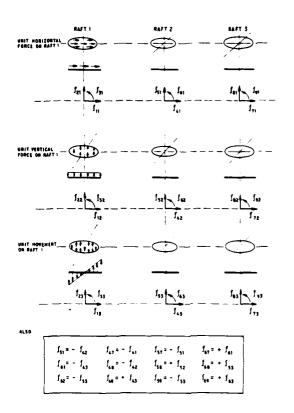
FINITE ELEMENT MODEL OF THE AGR ISLAND

: TG 1



SPRING-DASHPOT - MODEL OF THE AGR ISLAND

FIG 2

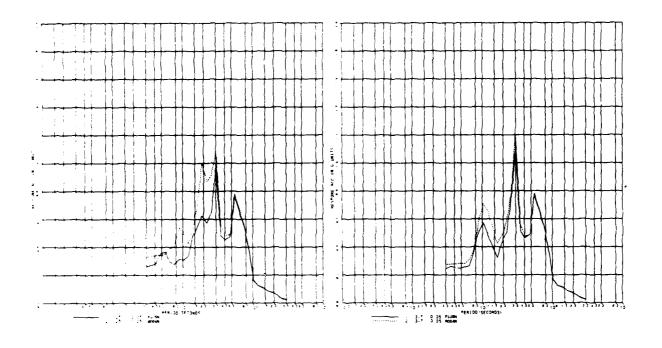


TYPICAL UNIT LOADING AND FLEXIBILITIES

FLEXIBILITY MATRIX FOR SOIL FOUNDATION

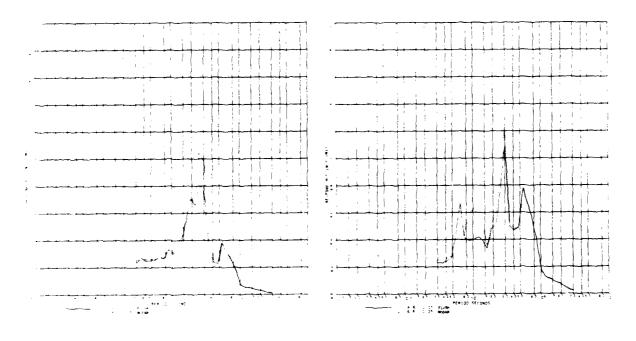
FIG 4

FIG 3



IDMPARISON OF MORITOWTAL FLOOR RESPONSE SPECTRA SETTEEN FIG 5 THE FINITE SILDMENT AND THE LUMPED PARAMETER RETRODS FOR THE PURP FAULT FLOOR, MOVIES IN MODE 1510

COMPARISON OF ROBLEONTAL FLOOR RESPONSE SPECTRA SETWERS FIG.
THE FINITE SLEMENT AND THE COMPED PARAMETER WITHOUS FOR THE
REACTOR SUILDING, D.J. x (NODE 317)



IOMPARISON OF AURICONTAL FLOOR RESPONSE SPECTRA SETVEEN THE FINITE SLEMENT AND THE LUMPED PARAMETER METHODS FOR THE SHIPLING SLOCK -32.0 g. NODE 906) THE FINITE ELEMENT AND THE LIMPED PARAMETER SETTIONS FOR THE SHEELDED SLOCK J.J 2 (VODE 516)

71G 1

 \leftarrow



DYNAMIC RESPONSE OF CRANE STRUCTURE

Chen Wei-zhang

Marine and Transportation Institute of Shanghai

1. INTRODUCTION

The vibration of a crane structure, when a load on the ground is hoisted, is the dynamic response of the space structure to the hoisting excitation. It is a composition of all natural modes. The degree of structural response depends on the hoisting speed, the elasticity distribution and the mass distribution of the crane structure-wire rope-load system, and the state of operation.

In the current crane design specifications of many countries and areas, such as BS 2573 of UK, Din 15018 of GFR, JIS 8821 of Japan, and F.E.M. of Europe, one dynamic load factor Kd is applied to take this dynamic influence into account, i.e., hoisted load multiplied by Kd is treated as static one. The factor Kd is either given directly or defined as a linear function of hoisting speed Vh according to the category, rank, and hoisting grade of the crane. By this method the complicated response of each crane can not be fully reflected, therefore, great attention has been paid to dynamic analysis in crane profession all along.

In the beginning of 1950's a great deal of research in this field was carried on in the University of Leeds, Britain for the sake of revising the steel structure design specification of the bridge crane (BS 466). Later on scholars of GFR, USSR and GDR published references [1],[2],[3] in succession. They analyzed the dynamic behaviour of bridge cranes before and after the load to be hoisted was lifted up. The essence of crane structural response to hoisting excitation began to be revealed. But restricted by calculating means, a good deal of simplification was adopted so that some limitations were brought about.

In the references mentioned above crane structures are all simplified as spring-mass systems with single degree of freedom (DOF). Not only is it difficult to choose an assumed mode shape for a crane structure which has complex geometry, but also the generalized single DOF system based on the assumed mode shape can not display the coumpound response of the actual system made up of multiple modes. For this reason equivalent dynamic response can not be achieved. In the above dynamic models the vibration of a structure was entirely described by the displacement of the mass, and the ratio of the maximum dynamic displacement to the static one defined as the hoisting dynamic load factor. This means that the shape of the dynamic displacement and the distribution of the inner forces of the structure are considered similar to those of the same structure under the static load, merely amplified Kd times in values. In fact, the actual structures are of indefinite Subjected to hoisting excitation there will happen compound vibration composed by indefinite natural modes with different frequencies. Since the degree of each natural mode's response to the same excitation differs from others, and the distribution of

inner forces corresponding to one natural mode is totally different from that under a static load, the maximum dynamic and the static inner forces of various sections of an actual structure are not of the same proportion, that is, a united dynamic load factor does not exist. This has already been verified by a lot of experiments [4].

The hoisting wire ropes of many cranes, such as wheel cranes, gantry cranes, bridge unloaders with rope-trolley, and container cranes, are wound round a lot of wheels and joined to winding reels. Thus, the tensile excitation of hoisting ropes will exert influence on the joints and every place on which wheels are installed. Similar difficulty is present in determining equivalent forces of the generalized models as mentioned in the preceding paragraph.

Some cranes possess other wire rope systems besides hoisting rope system, such as the luffing rope system, the trolley-driving rope system, etc. These wire rope systems compose a kind of special elements in structure and have an effect upon the stiffness and stiffness distribution of the structure. Wire rope elements have peculiar properties different from structural elements. Therefore, it is necessary to develop their unique element stiffness matrices, and coordinate transformation matrices. These facts, however, have never been reflected in the above references.

In this paper I try to transform the crane structure of indefinite DOF into a space model with definite DOF by using finite element method and lumped mass method. The amount of joints (nodes) may be decided according to the level of complexity of the actual structure and to the required calculating accuracy. So it is not difficult to let the model approach the actual structure and reflect the response of structural modes of higher frequencies. The model with definite DOF is far more superior to the simple DOF model.

Based on this model, we can set up its differential equations of free vibration and then use subspace iteration method to solve the large generalized eigenvalue problem. Finally the dynamic response of two phases in the lifting course can be calculated by employing mode superposition method. The maximum dynamic and static inner forces of each end of every element and corresponding dynamic factors can be obtained. The whole calculation is carried out on digital computer.

2. THE DIFFERENTIAL EQUATION FOR FREE VIBRATION OF SPACE FRAME STRUCTURE POSSESSING WIRE ROPE ELEMENTS

The differential equation for free vibration of a multiple DOF system may be written in matrix form

$$\mathbf{M} \overset{\cdot \cdot \cdot}{\mathbf{Y}} + \mathbf{K} \mathbf{Y} = \mathbf{0} \tag{1}$$

in which M, K are system mass and stiffness matrix respectively, and \ddot{Y} , Y are generalized acceleration and displacement vector separately.

There are six DOF corresponding to a joint in a space model.

If the structure is modeled to have n DOF (n=6n_j), where n_j denotes the amount of joints of the model), M, K are n×n square matrices and \ddot{Y} , Y are n×1 vectors.

Equation (1) shows that the crucial process involved in arriving at it is generating M and K of the system.

Through the use of the finite element method K is easy to determine, but it must be noted that common engineering structures have no wire ropes so that wire rope elements have never been discussed in ordinary finite element method. But in crane structures wire ropes exist universally. In static analysis, the static tensile forces of wire ropes are known constants and may be considered as external forces to exert on the corresponding joints. But in dynamic analysis, they vary with the vibration of the load and every joint concerned, round which wire ropes are wound. This kind of tensile forces can not be simply considered as external forces; they are elastic forces of wire ropes, and wire rope elements must be treated as components of structures. Their stiffness matrix.

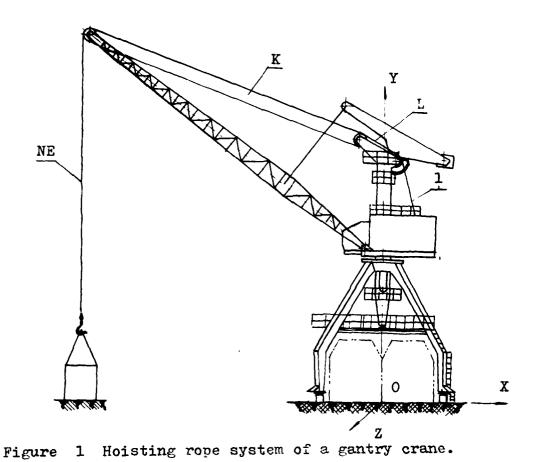
Wire rope elements are a kind of special elements different from common ones. First, wire ropes are flexible components; they have only axial stiffness but no transverse and torsional stiffness. For this reason, though every joint of a wire rope element has six displacement components, there is only one force component --axial force. Second, all elements of the same wire rope system are linked together. The tensile force of each branch in the system is equal everywhere on condition that the resistance of wheels and the rigidity of the rope are neglected. So the tensile forces of all elements in the same system vary simultaneously during the whole vibration history, and their values are in definite proportions to each other. The proportions are equal to the ratios of the branches of the elements. These mean that the displacement of any joint, round which the wire rope is wound, will produce elastical tensile forces of all wire rope elements in the same wire rope system. Therefore, stiffness matrix of wire rope element is more complicated than that of common element, and its transformation and summation to the system stiffness matrix are also out of the ordinary.

These are discussed in detail as follows.

If some wire rope system of a crane is divided into NE elements (Fig. 1). Take two arbitrary elements, the Kth element and the Lth element, for example (Fig. 2). Their joints are labeled i(k), j(k) and i(1), j(1). The system coordinate system is 0-XYZ, and element coordinate systems are $\overline{O}_k - \overline{X}_k \overline{Y}_k \overline{Z}_k$ and $\overline{O}_1 - \overline{X}_1 \overline{Y}_1 \overline{Z}_1$ respectively. The origin of the element coordinate system is placed at the i-end with the \overline{X} -axis along the element from i toward j. Now, let us look into the relation between the joint displacements of element L and the joint forces of element K. Since wire rope elements have only axial joint forces, the relation must be set up referring to truss elements.

Denote the joint displacements of element L as $\overline{U}_i(1)$ and $\overline{U}_i(1)$. The elongated value of the element is

$$L^{\bullet}-L = \overline{U}_{j}(1) - \overline{U}_{i}(1)$$



 $\overline{X}_{i}^{(k)}$ $\overline{I}_{w}^{(k)}$ $\overline{I}_{w}^{(k)}$ \overline{Z}_{k} $\overline{U}_{i}^{(1)}$ $\overline{U}_{j}^{(1)}$ $\overline{U}_{j}^{(1)}$ \overline{Z}_{1} \overline{X}_{1}

Figure 2

If the amount of wire rope branches of the element is $I_W(1)$, as a result of the displacements, the elongated value of the whole wire rope system is given by

$$L_{\mathbf{W}}^{\bullet} - L_{\mathbf{W}} = I_{\mathbf{W}}(1) (L^{\bullet} - L)$$

$$= I_{\mathbf{W}}(1) (\overline{U}_{j}(1) - \overline{U}_{j}(1))$$
(2)

The elastic force of every wire rope branch is

$$N_{\mathbf{W}} = \frac{E_{\mathbf{W}}A_{\mathbf{W}}}{L_{\mathbf{W}}} \left(L_{\mathbf{W}}^{\bullet} - L_{\mathbf{W}} \right) \tag{3}$$

where A_W is the section area of the wire rope, and E_W is the modulus of elasticity of the wire rope material. L_W is the total length of the whole wire rope in the system.

Let $\mathbf{I}_{\mathbf{W}}(\mathbf{k})$ be the amount of branches of element K. The joint forces of element K are

$$\overline{X}_{j}(k) = \frac{E_{W}A_{W}}{L_{W}} (L_{W}^{\bullet} - L_{W}) I_{W}(k)$$

$$= -\frac{E_{W}A_{W}}{L_{W}} I_{W}(1) I_{W}(k) \overline{U}_{j}(1) + \frac{E_{W}A_{W}}{L_{W}} I_{W}(1) I_{W}(k) \overline{U}_{j}(1)$$

$$\overline{X}_{j}(k) = \frac{E_{W}A_{W}}{L_{W}} I_{W}(1) I_{W}(k) \overline{U}_{j}(1) - \frac{E_{W}A_{W}}{L_{W}} I_{W}(1) I_{W}(k) \overline{U}_{j}(1)$$
(4)

As wire rope elements have no other stiffness, other stiffness coefficients are all zero. Thus, the relation between the joint forces of element K and the joint displacements of element L may be written in matrix form as follows.

$$\begin{bmatrix}
\overline{X}_{1}(k) \\
\overline{Y}_{1}(k) \\
\overline{Z}_{1}(k) \\
\overline{M}_{X_{1}}(k) \\
\overline{M}_{X_{1}}(k) \\
\overline{M}_{X_{1}}(k) \\
\overline{M}_{X_{1}}(k) \\
\overline{X}_{1}(k) \\
\overline{X}_{2}(k) \\
\overline{M}_{X_{1}}(k) \\
\overline$$

or

in which \overline{F}_k , \overline{D}_l are the joint force vector of element K and the joint displacement vector of element L separately, and \overline{K}_{wkl} is named the element stiffness matrix of element K corresponding to joint displacements of element L.

The relation of joint forces and joint displacement of element K is merely a special form of the general relation above mentioned. In this case, all we have to do is to change symbol "1" in equation (5) into symbol "k".

It is evident that element K has element stiffness matrix corresponding to the joint displacements not only of its own (k=1), but also of all other elements in the same wire rope system (l=1,2, \dots , NE but l \neq k).

Equation (5) may be expressed with system coordinates as

$$T_{k} F_{k} = \overline{K}_{Wkl} T_{l} D_{l}$$
 (6)

where \mathtt{T}_k is transformation matrix of element K, and \mathtt{T}_{l} is that of element L.

As we all know, $T_{\bf k}$ and $T_{\bf l}$ are all orthogonal matrices. Premultiplying two sides of Equation (6) by $T_{\bf k}{}^T$, we obtain

$$F_k = T_k^T \overline{K}_{wkl} T_l D_l$$

Let
$$T_k^T \overline{K}_{wkl} T_l = K_{wkl}$$

then
$$F_k = K_{wkl} D_l$$
 (7)

in which K_{Wkl} is the element stiffness matrix of element K corresponding to the joint displacements of element L in system coordinates.

The next step is to partition K_{wkl} and system stiffness matrix K_s according to numbers of the joints, and add the partitions of K_{wkl} which have nonzero terms to the corresponding positions of K_s with the aid of subsymbols.

In a wire rope system, forming and adding element stiffness to the K_S should be carried on $(NE)^2$ times, i.e., they must be done corresponding to permutation of every value of k and l, here $k=1, 2, \ldots, NE$ and $l=1, 2, \ldots, NE$.

How to determin system mass matrix is presented in most modern dynamic texts. In this paper, the lumped mass method is adopted instead of the consistent mass method. The advantages of the former over the latter are:

- (1) The former is more simple and can be directly perceived.
- (2) Any desired accuracy can be achieved with the former method merely by increasing joints properly. Increasing joints will increase DOF of the system, and a greater computational effort is required. But it does not cause much difficulty if a digital computer with large memory capacity is used.

3. EMPLOYING SUBSPACE ITERATION METHOD TO SOLVE THE LARGE GENERALIZED EIGENVALUE PROBLEM

Determining the harmonic solution of equation (1) leads to the following generalized eigenvalue problem

$$K X = p^2 M X \tag{8}$$

In the vibration of a crane structure excited by hoisted load, the major components are those of lower frequencies. A small subset of lower eigenvalues and corresponding eigenvectors of the system are important from the point view of engineering. In this case, the subspace iteration method is very effective. If m lower eigenpartners are needed, a q-dimensional subspace should be adopted, where

$$q = min (2m, m+8)$$
.

Since the eigenvalues in a subspace is determined by the requirements of stagnation points of Rayleigh quotient, and the requirements may turn into another generalized eigenvalue problem, whose order is reduced to q. The following five steps may be followed in iteration cycles after preparing initial matrix composed by q assumed modes.

(1) Use the following equation to make an inverse iteration with the aim of strengthening the components of lower frequencies in the subspace represented by $\rm X_{k-1}$

(2) Compute the projection of the original stiffness matrix in the subspace represented by $\overline{\bf X}_k$ using the equation

$$K* = \overline{X}_{k}^{T} K \overline{X}_{k}$$

(3) Compute the projection of the original mass matrix in the same subspace by the equation

$$M^* = \overline{X}_{k}^T M \overline{X}_{k}$$

(4) Use the QL method to solve generalized eigenvalue problem

$$K * B_k = M * B_k P_k^2$$

and obtain q eigenvalues of the subspace, which compose the matrix $P_{K\bullet}^{\bullet}$

(5) Calculate corresponding eigenvactors by using

$$X_k = \overline{X}_k B_k$$

The above steps are carried on until m lower eigenpartners converge with enough accuracy.

4. COMPUTE THE DYNAMIC RESPONSE OF CRANE STRUCTURE IN TWO PHASES OF LIFTING COURSE WITH THE MODE SUPERPOSITION METHOD

The equation for the motion of multiple DOF system subjected to exciting forces is

$$M \ddot{Y} + K Y = F (t) \tag{9}$$

Using m modes $X_n(i)$ ($i=1,2,\ldots,m$) normalized with respect to M, to transform equation (9) from physical coordinates Y to normal coordinates Y_n , we will obtain

in which $Y_n = X_n^{-1} Y$, $\ddot{Y}_n = X_n^{-1} \ddot{Y}$ (the displacement vector and the acceleration vector of normal coordinates separately), and X_n is the mode matrix whose columns are normalized modes and whose order is $n \times m$.

Since diagonal matrix P2 is uncoupled, equation (10) can be written as m independent equations

$$\ddot{y}_{ni} + p_1^2 y_{ni} = f_{ni}(t)$$
 (i = 1, 2, 3, . . . , m)

. Each modal response due to F(t) and intial conditions Y_{O} and Y_{O} can be calculated by

$$y_{ni} = y_{oni} \cos p_i t + \frac{\dot{y}_{oni}}{p_i} \sin p_i t + \frac{1}{p_i} \int_0^t f_{ni}(c)$$

$$\sin p_i(t-c)dc \qquad (11)$$

where y_{onj} , \dot{y}_{onj} are the ith elements of initial displacement and initial velocity vector of normal coordinates respectively, and p_i is the square root of the ith element of the diagonal matrix \dot{P}^2 .

The total response of the system can be obtained by superposing m modal responses as shown in the following equations:

$$Y = X_n Y_n; \dot{Y} = X_n \dot{Y}_n$$

The duration which begins when the tensile force of the hoisting rope appears and ends when the load leaves the ground is termed the first phase of the lifting course. In this phase the response of the structure-wire rope-load system is merely due to the tensile force of hoisting rope, which is produced by the operation of the hoisting mechanism, and all initial conditions are zero.

Let V(t) denote the velocity of the end of the hoisting wire which is wound on the reel. The tensile force produced by drawing rope in (Fig. 3) of each wire rope branch is

$$S(t) = \frac{E_W A_W}{L_W} \int_0^t V dt$$

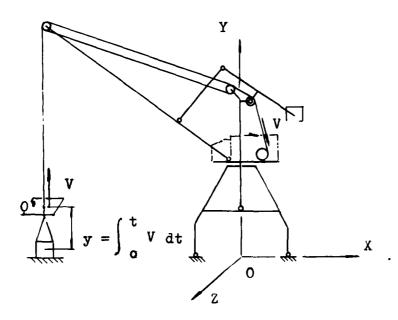


Figure 3 The motion of the load's coordinate origin caused by drawing rope into the reel.

The exciting tensile force of the kth element in hoisting rope is

$$S_k(t) = I_w(k) S(t) = I_w(k) \frac{E_w A_w}{L_w} \int_0^t V dt$$

Then we transform it into system coordinates. The excitation vector of system coordinates F(t) can be assembled. We solve the response in this phase by using the mode superposition method to obtain joint displacement, joint velocities and inner forces of the elements (which include elastic inner forces of wire rope elements) of the system.

The criterion for the end of this phase is that the inner force of the last hoisting rope element, on which the load is hung, is equal to the gravity of the load, namely, this phase ends when the following equation comes true

$$S_1(t) + N_1(t) = Q_1$$
 (13)

where $S_1(t)$ = exciting tensile force of the last element $N_1(t)$ = elastic tensile force of the last element Q_1 = the gravity of the load

The second phase in the lifting course begins when the load is lifted from the ground. In this phase, since the load is hung on the flexible component, which has no transverse and torsional stiffness, some measure must be adopted to prevent the system stiffness matrix from being abnormal. One measure is to introduce restraints to eliminate the DOF of three rotary motions of the load, which we are not interested in.

Two swinging motions of the load may be simplified as the vibration of a simple pendulum (Fig. 4), so that the pendular stiffness coefficients is given by

$$k_{wii22} = k_{wii33} = k_{wjj22} = k_{wjj33} = Q_1/L$$

 $k_{wij22} = k_{wij33} = k_{wji22} = k_{wji33} = -Q_1/L$ (14)

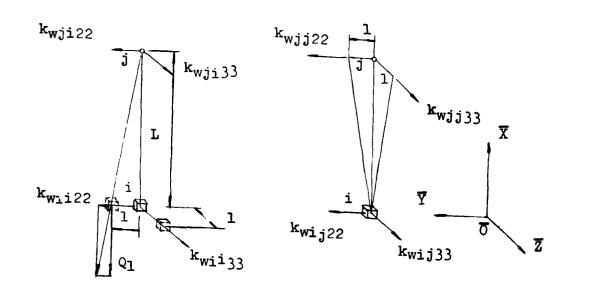


Figure 4

After coordinates' transformation, they have to be added to the system stiffness matrix.

The initial conditions of the second phase are the dynamic parameters of the first phase at the moment when the load leaves the ground. They are initial displacements, initial velocities and tensile exciting forces of the wire rope. Notice that since the load has been lifted, the exciting force vector becomes instant in this phase, and the gravity Q1 of the load must be added to the corresponding place of the vector. Similarly, an initial load velocity Vh, which is down-ward vertically, must be added to the initial velocity vector because the origin of coordinates for the load moves up with lifting velocity (Fig. 3) at the begenning of this phase; generally it has reached the normal value by then.

We calculate the dynamic response of the system and obtain joint displacements and inner forces of coresponding elements in this phase. Then the dynamic factors of the inner forces of every element can be evaluated by maximum dynamic forces divided by corresponding static ones.

5. CONCLUDING REMARKS

The vibration of a struture excited during the course of hoisting the load is one of the main dynamic responses of the

crane structure. It effects the dynamic operational performance and the strength of the crane structure greatly. With the aim o. designing cranes for good operational and economical performances, it is necessary to foresee the character of free vibration and the response to hoisting excitation of the designed crane. It is oversimplified to use a single dynamic load factor to reflect this dynamic effect, and the determinations of the factor in the present crane design specifications and current approximate formulae are too sketchy. We think it is reasonable to set up the multiple DOF model of a complex crane structure, using the finite element method and the lumped mass method. Through the use of this model, we can evaluate the compound response of multiple modes. It can reflect the influence of the vibration with higher frequencies. This model has incomparable superiority over a single DOF model. In line with the character of crane structures, the influence of wire rope elements must be considered. This is necessary not only to estimate accurately the stiffness and the stiffness distribution of the system, but also to determine precise inner forces history and the exact time when the load leaves the ground. This paper makes a detailed study of the element stiffness matrices and the transformation matrices of wire rope elements. The results of computing practical instances indicate that either the natural frequencies or the dynamic factors of inner forces got by this method are more approximate to the actual situation, and the different dynamic factors of inner forces of the different parts in the structure can be fully reflected.

REFERENCES

- 1. R. NEUGERAUER 1957 Der Stahlbau H $\frac{1}{2}$, 16-21. Dynamische Kräfte in Laufkranen beim Anheben und Abbremsen.
- 2. M.M. GOHBELK 1959 Metal Structure of Crane Designed after the Phenomenon of Fatigue. USSR: Machine Engineering Press.
- F. KURTH and G. PAJER 1965 Unstetigförderer. Berlin: Veb Verlage Technik.
- 4. A.N. DUKILSKY 1971 Handbook of Cranes Vol. 1. Leningrad: Machine Engineering Press.





Hu Zongwu and Yan Junoi

AD-P003 65

Department of Mechanical Engineering Shanghai Jiao Tong University

1. ABSTRACT

The State Space Nethod originating from modern control theory is an effective direct integrating method. It is also applicable to approaching dynamic response of mechanical system. Its theoretical basis, means of calculation, computer program and main characteristics are described in this paper.

Setting up a mathematical model for the travelling mechanism of an overhead travelling crane, the authors have tried to find the dynamic response of the system in different conditions using the state space method. The result shows that this method is a stable and accurate theoretical calculating method suitable for all time-varying loads. It helps to get directly the time response of a mechanical system and analyse its dynamic characteristics.

2. INTRODUCTION

At present there are two commonly used methods of solving equations of motion of linear system: The Mode Summation Nethod and the Direct Integrating Method. Mode Summation Method, however, requires extraction of eigenvalues and eigenvectors. Besides, the modal matrix can be used to translate coordinates and uncouple the equations on condition that the assumption of proportional or modal damping is made for the damping vibration of the system, this has limited its application. The classical numerical integrating method also has limitation due to its poor stability. By contrast, the state space method is an effective directly integrating method which can be used to give dynamic time response of system. It can be adopted for arbitrary damping matrices and requires no extraction of eigenvalues and eigenvectors, neither does it need to translate generalized coordinates into normal coordinates for uncoupling equations. Besides, this method provides good stability and excellent accuracy. It can conveniently get time response under various complicated loads.

While working on & Crane Design Rule >> , the authors used the state space method in approaching dynamic response in different conditions of heavy mechanical system such as the travelling mechanism of overhead travelling crane, and got quite satisfactory results. In this paper the means of calculation, error analysis and computer programs in this respect are given.

3. THEORETICAL INFERENCE

3.1 State Equations of System

There are n differential equations for an n-freedom decrees system, which can be expressed in matrix form as

$$V\ddot{x} + C\dot{x} + Kx = Q \tag{1}$$

where x is the column vector of the absolute displacements, P, C, K are mass, damping and stiffness matrices respectively (all of order nxn), C is the in-

put column vector (order r), which is the forcing function of time t.

Take state variables Z as follows

$$Z_1 = X_1, \ldots Z_n = X_n, \qquad Z_{n+1} = \dot{X}_1, \ldots Z_{2n} = \dot{X}_n$$

and rewrite the equations of motion (1) in terms of Z, we have

$$\begin{pmatrix} \dot{\mathbf{z}}_1 \\ \vdots \\ \dot{\mathbf{z}}_{2n} \end{pmatrix} = \begin{pmatrix} 0 & \mathbf{I} \\ \cdots & \cdots & \cdots \\ -\mathbf{M}^{-1}\mathbf{K} & -\mathbf{M}^{-1}\mathbf{C} \end{pmatrix} \begin{pmatrix} \mathbf{Z}_1 \\ \vdots \\ \mathbf{Z}_{2n} \end{pmatrix} + \begin{pmatrix} 0 \\ \cdots \\ \mathbf{M}^{-1} \end{pmatrix} \{ \mathbf{C} \} \tag{2}$$

which can be simplified as:

$$\dot{\mathbf{Z}} = \mathbf{F} \mathbf{Z} + \mathbf{G} \mathbf{Q} \tag{3}$$

where F is called coefficient matrix (a square matrix of order n), G is called control matrix (order $2n \times r$). Equation (3) is called state equation of system.

3.2 Solution of State Equation

We will just consider the constant coefficient system. Theoretical calculations and experimental results show that all common mechanical systems can be dealt with in this way and the accuracy reached is satisfactory.

According to the modern control theory (1), the solution of equation (3) is

$$Z(t) = e^{F(t-t_0)} Z(t_0) + \int_{t_0}^{t} e^{F(t-t_1)} GG(t_1) dt_1$$
 (4)

The expression (4) is also called state transition equation which describes the transition from initial state $Z(t_0)$ to state Z(t) at time t. e^{Ft} is called matrix exponential and can be represented by the Taylor series,

$$e^{Ft} = I + Ft + \frac{F^2 t^2}{2!} + \dots + \frac{F^k t^k}{k!} + \dots = \sum_{k=0}^{\infty} \frac{F^k t^k}{k!}$$
 (5)

In order to get a numerical solution, we can select a sufficiently small time interval T during which the column vector (t) is considered to be constant and represented by (KT), its value at the preceding instant. The input function can also be assumed to be linear or parabolical for higher accuracy, and the expression (4) will be different after discretization, namely,

$$C(kT + t_1) = C(kT) \qquad C \leq t_1 \leq T$$
 (6)

then the solution (4) can be rewritten in a difference form as

$$Z((k+1)T) = e^{FT} Z(kT) + \int_{0}^{T} e^{Ft_1} dt_1 \cdot G(kT)$$
 (7)

Let

$$A(A) = e_{A_1} = \sum_{k=0}^{k=0} \frac{k_1}{k_1}$$

$$B(T) = \left(\int_{0}^{T} e^{rt} dt_{1} \right) G = T \left(\sum_{k=0}^{\infty} \frac{r^{k} r^{k}}{(k+1)!} \right) G$$

Substituting these into the equation (7), we have

$$Z \{(k-1)T\} = A(T)Z(kT) + B(T)C(kT)$$
(8)

This is a recurrence formula. Using it recursively will give the values of the state vectors of system at time $t=T,\ 2T,\ \ldots,\ KT,\ \ldots$

3.3 Determining the Latrix Exponential eft

In recent years the state space method has rapidly developed. Different methods for determining matrix exponential have been but forward, such as the Laplace transform method, the diagonal matrix method, the awaiting—determinative coefficient method, the matrix series method, etc. Here, we will only deal with the approximate method of matrix series available for computer calculations.

Formula (5) is the Taylor series definition of the matrix exponential. This series is always convergent for all arbitrary matrix F and all finite

time interval T, so it can be truncated at k=m. Then
$$e^{FT} = \sum_{k=0}^{m} \frac{F^k T^k}{k!} = W$$

Cwing to the development of matrix technique, the truncation error can be calculated as the function of time interval T, and controlled effectively. But the number m of the truncated terms in the matrix series can be taken by the empirical formula [2]

$$m = 3 \parallel F \parallel T + 6$$
 (9)

where

$$\| F \| = \sum_{i,j=1}^{n} |f_{i,j}|$$

The calculation of travelling mechanism of everhead travelling crane has proved that formula (3) is more enough to assure the accuracy required in engineering (significant figures $d \ge 0$). In order to be fitted for recursive calculation of the computer, $\Lambda(T)$ and B(T) are rewritten as the inlay-multiplied formulas

$$\Lambda(T) \stackrel{!}{=} I + \bar{r} T \left(I + \frac{\bar{r} T}{2} \left(I + \frac{\bar{r} T}{3} \left(I + \dots + \frac{\bar{r} T}{m-1} \left(I + \frac{\bar{r} T}{m} \right) \dots \right) \right) \right)$$
 (10)

$$B(T) \stackrel{!}{=} T \left(I + \frac{FT}{2} \left(I + \frac{FT}{3} \left(I + \dots + \frac{FT}{m-1} \left(I + \frac{FT}{m}\right) \dots\right)\right)\right) G$$
 (11)

These two formulas are very alike. One can use the same program to get A(T) and B(T), and the intermediate result of calculating, which is obtained in calculating A(T) can also be used to get B(T). This reduces the time for calculating quite much. A(T) and B(T) are determined only once for a given problem.

For a mechanical system, especially for such a heavy mechanical system as a crane, using coneral engineering units will make the values of elements in F and the number m too big, and make the time for calculation too long. Desides, the computer may be stopped because of the spillover before " is obtained. Therefore, we take centisecond $(\frac{s}{100})$ or millisecond $(\frac{s}{1000})$ as the unit of time to reduce the figure of each element in F and the || F || T can be controlled within the limit of no more than one hundred (3).

3.3 <u>Error Analysis</u>

brors occur at two stages. One kind of errors are the truncation errors produced while er is determined. Because of the convergency of matrix series, this kind of errors can be calculated by choosing appropriate m and thus can be controlled effectively. That is why the state space method provides higher accuracy. Another kind of errors are produced when equation (8) is recursively used. In this case a stair function which changes after every time interval T is substituted for practical input, and because of the limitation of register length of the computer each calculation has a round-off error. These two factors are contradictary to each other. The smaller is the time interval T, the closer the stair function approaches to the practical input, and on the other hand, the more recursively calculating times are for the response in a given time progress. As a result, the accumulated round-off errors will be increased, and the time required for calculating will be prolonged. Since the maximum peaked dynamic load of an overhead travelling crane appears at the very instant just after the machine is started, the round-off errors needn't be taken into consideration, and T can be talten as small as possible.

A. THE CALCULATION OF DYNAMIC RESPONSE OF TRAVELLING MECHANISM OF CVERHEAD TRAVELLING CRAME

2.1 Tatheratical Lodel

Figure 1 shows a travelling mechanism of an overhead travelling crane, which can be simplified as a six freedom degrees system as shown in Fig. 2. The physical parameters are indicated on the figures too.

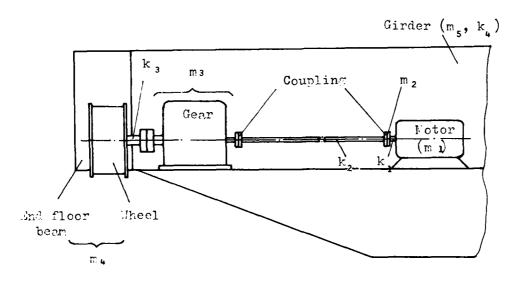
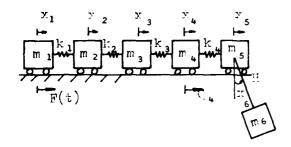
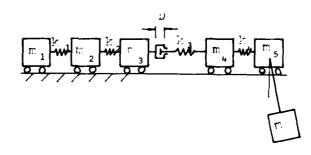


Fig. 1 Travelling mechanism of an overhead travelling crane





- (a) Mithout transmission clearance
- (b) With transmission elemence

Fig. 2 Technical model of the travelling mechanism

All rotational masses, tersional stiffnesses, as well as the continuously distributed mass and electricity are replaced by rectilineal masses and stiffnesses in the direction in which the canno travels. Here mg is the mass of hoisting load, H is the length of the carrying rone. m_A , m_5 , k_4 , are equivalent masses and equivalent stiffnesses relating to the metal structure. All of them can be calculated using the energy method, by which we get following approximate formulas:

$$m_{\Lambda} = m_8 + C \cdot 3m_9$$
 (12)

$$m_5 = \frac{1}{2}m_7 + 0.2m_9 \tag{13}$$

$$K_{A} = \frac{2\pi^{A}}{L^{3}} FJ_{y} = 195 \frac{EJ_{y}}{L^{3}}$$
 (14)

where

m7-mass of the crane tralley

me-mass of end floor beams and the travelling equipment

mo-mass of girder

 J_{y}^{\prime} -moment of inertia of the cross-sectional area in the middle of girder

L -span

After the generalized coordinates x1...x6 are selected, the differential equations of the system may be written according to the Lagrange's equation.

kinetic energy

$$T = \frac{1}{2} \sum_{i=1}^{5} m_i \dot{x}_i^2 + \frac{1}{2} m_6 (\dot{x}_5^2 + H^2 \dot{x}_6^2 + 2H \dot{x}_5 \dot{x}_6)$$

potential energy

$$U = \frac{1}{2} \sum_{i=1}^{4} k_i (x_i - x_{i+1})^2 + m_5 SH(1 - \cos x_6)$$

generalized force

$$\zeta_2 = \zeta_3 = \zeta_5 = Q_6 = 0$$

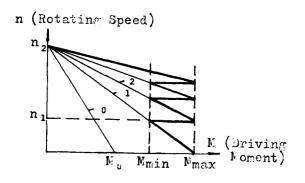
resistance to motion

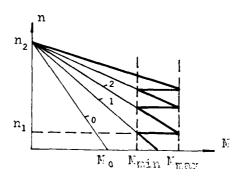
$$C_4 = -0.02G \cdot sgn(x_4)$$

where G - total weight of the crane

$$sgn(\dot{x}_4) = \begin{cases} -1 & \text{when} & \dot{x}_4 < 0 \\ 0 & \text{when} & \dot{x}_{\Lambda} = 0 \\ 1 & \text{when} & \dot{x}_{\Lambda} > 0 \end{cases}$$

Driving force $C_1 = F(t)$, it depends on mechanical characteristics of the electric motor which are shown in Fig. 3. (a) and (b) are two possible ways of starting. In Fig. 3 the curve "O" shows the preparatory stage. It produces the prepressing torque K_0 , but can not start the mechanism. When the system is in the stage "2",





(a) Sudden starting

(b) Smooth starting

Fig. 3 Mechanical characteristics of electric motor

$$F(t) = M(t) \frac{i}{R} = \frac{V_{\text{max i}}}{R} \frac{n_2}{n_2 - n_1} - \frac{9.55 \ V_{\text{max i}}^2}{(n_2 - n_1)R^2} \dot{x}_1 \tag{15}$$

where

i-transmission ratio of the mechanism

R-radius of wheel

Obviously, when $n_1 = 0$, equation (15) is fit for the curve "1" in Fig. 3(a).

Because F(t) is expressed relating to \dot{x}_1 , the final result reflects the influence of vibration feedback on motor driving torque. (If the mode summetion method is used, the matrix made of coefficients of \dot{x} can not become diagonal due to the increase of terms of \dot{x} and it is difficult to consider vibration-feedback.) Similarly, the dynamic response of system, whose damping can not be neglected, is also obtained conveniently by using the state space method without making assumption of proportional or model damping.

Now the motion equations of the system can be written in matrix form (1), and

$$\mathbf{F} = \begin{pmatrix} \mathbf{m}_1 & & \\ & \mathbf{m}_2 & & \\ & & \mathbf{m}_3 & & \\ & & & \mathbf{m}_5 & \\ & & & & \mathbf{1} \end{pmatrix}$$

$$K = \begin{pmatrix} K_1 & -K_2 & & & & & & & \\ -K_1 & K_1 + K_2 & -K_2 & & & & & & \\ & -K_2 & K_2 + K_3 & -K_3 & & & & & \\ & & -K_3 & K_3 + & K_4 & -K_4 & & & & \\ & & & -K_4 & K_4 & -m6g/H & & & \\ & & & & K_4/m_5 & -K_4/m_5 & g/H(1 + m6/m_5) \end{pmatrix}$$

$$C = \begin{pmatrix} \frac{\text{Imax i}}{R} & \frac{n_2}{n_2 - n_1} \\ & 0 \\ & C \\ -C \cdot O2G \cdot \text{sgn } (\dot{x}_4) \\ & 0 \\ & C \end{pmatrix}$$

In damping matrix C all of elements are "C" except that $C_{11} = \frac{9.55 \text{ Mmax i}^2}{(n_2 - n_1)R_2}$ With the introduction of state variables $Z_1 \dots Z_{12}$, the equations can be written in state space form (3).

4.2 Several Operating Conditions

4.2.1 Sudden Starting:

Then the crane is in busy condition, the system is considered to start directly in the light of curve "l" in Fig. 3(a). Because the transmission clearance D exists in the gear train as shown in Fig. 2(b), the starting procedure is divided into two stages. In the first stage only m_1 , m_2 , m_3 are moved. Then $m_3 = D$, the second stage begins, and all masses are moved. If D is very small and can be neglected, the value of D is considered as D = 0.

4.2.2 Smooth Starting:

At first the system is in the preparatory stage, then starts successively in the light of Fig. 3(b). In this way not only the clearance is removed before the starting, but also the mechanism is prepressed. After proper revising the program used in condition 4.2.1 can be used for this condition. The system enters directly into the second stage without passing through the first stage, and the static deformations of the system under the prepressing torque are taken as the initial values of state variables and their initial velocities remain to be zero (static prepressing).

4.2.3 Normal Braking:

The procedure is divided into two stores. The first store is from the storting of braking to the disappearance of clearance ($|x_4-x_3|=D$). In this stage it is supposed that $K_3=0$. If $|x_4-x_3|$ is equal to or bigger than D, then the last part of the program used in condition 4.2.1 or 4.2.2 can also be used here.

From the three operating conditions described above we can see that the selection of state variables has much flexibility and state space method can get time response directly, so it is convenient to analyse the system, whose parameters and input functions are variable, and the computer program is fairly simple.

5. DIGITAL COMPUTATION

A problem about dynamic response of travelling mechanism of overhead travelling crane has been programmed ($\mathbb{B}.310$ program) and solved using the digital computer.

The main parameters of crane are:

Hoisting mass 20000/5000 kg, number of spans 5, rated torque of electric motor is 77 M-F, starting torque may be 120 or 160 N-M, rotational speed n_1 (see Fig. 3) 427 r.y.m., transmission ratio of the mechanism i = 24.6, radius of wheel R = 0.3m. Other parameters are given as follows

m ₁ (kg)	540 560	K ₁ (N/m)	1.21 x 10 ⁹
m ₂ (kg)	250	K ₂ (H/m)	3.55 x 10 ⁶

Span (m)	10.5	16.5	22.5	2 °• 5	31.5
m <u>/</u> (200)	3250	4480	5790	8360	10260
m ₅ (kg)	528C	6020	6800	8350	9500
K _V (E/m) x 10 ⁶	12.36	8.25	4.13	3.22	2.30

Four chloulated enerating conditions are

- (1) Smooth starting: the prepressing force $F_0 = \frac{\Gamma_0 \hat{1}}{R} = 3200 \text{ M}$
- (2) Subject starting: the prepressing Tence $F_0=0$ the transmission elemence D=0

- (3) Sudden starting: D = 0.002m (or the angle clearance at the high speed gear = 10°)
- (4) Sudden starting: D = 0.000m (or the angle clearance at the high speed gear = 40°)

The following table illustrates the results from the calculations of dynamic coefficients (peak to rated ratio) [4]. In the table, dynamic coefficient of spring K_1 is over the curve and spring K_4 is below it. We have also calculated the dynamic response of transmission gear testbed using the same program. The results of the calculations are approaching the experiment results.

Dyna-Cperating mic condi- coeffi- tion	Smooth starting		Sudden starting without transmission clearance		Sudden starting with transmission clearance		
cient					$D = 0.002^{m}$		D = 0.008m
Span(m)	M=120	M=160	K=120	N=160	M=120	M=160	N = 160
10•5	2.25	3.CO	2•59	3•34	2.90	3•98	5.08
-	1.94	3.02	2.58	5.52	3.21	4.02	7.52
16.5	2.25	2.98	2.60	3.34	2.82	3•97	5.18
	1.92	2.94	2.41	3•35	2.88	3.71	6.16
22.5	2.22	2.97	2.59	3•32	2.86	3•99	
	1.64	2.49	1.92	2.76	2.21	2.95	
28.5	2.26	3.06	2.66	3.42	2.97	4.08	
	1.33	2.02	1.47	2.17	1.64	2.27	
31.5	2.28	3.09	2.69	3.46	2.91	4.13	
	1.10	1.72	1.15	1.77	1.25	3•73	

6. CONCLUSION

The state space method can serve the purpose of predication of dynamic response of mechanical system. It is a very efficient numerical integrating method, which can be used to consider all the factors relating to velocity (such as the vibration feedback and damping) without the difficulties in uncoupling equations as in the mode summation method.

The state space method gets solution of motion equations directly in time domain. The response at each instant depends only on the values of state variables at this instant and the input at the preceding instant. Thus the transition from one state to another is flexible. This is important for approaching mechanical systems with various conditions. Thanks to the development of matrix technique, excellent accuracy and stability can be obtained. Koreover, the state space method based on time domain means makes it possible to predict and control the time domain parameters.

REFERENCES

- 1. S.M. SHINNER 1978 Modern Control System Theory and Application. Mass. Addison-Wesley.
- 2. J.A. CADZOW and H.R. MARTENS 1970 Discrete-time and Computer Control Systems. Prentice-Hall.
- 3. YAN JUN-QI 1980 Masters Thesis, Shanghai Jiao Tong University. State Space Method Approach to Dynamic Characteristics of Travelling Mechanism of Overhead Travelling Crane.
- 4. HU ZHONG-WU 1977 Materials Handling Equipment, 2(3). Dynamic Load and Dynamic Coefficient of Crane Transmission Mechanism. China



NON-STATIONARY DIVISION BY THE SPACE TIME FINITE ELEMENT METHOD IN VIBRATION ANALYSIS

C.I. Bajer

Department of Civil Engineering, Engineering College Zielona Góra, Poland

1. | INTRODUCTION

Commonly known methods of integration of the motion equation require the same partition of the structure into finite elements in each time step. The stiffness, mass and damping matrices formulated at the begining are valid throughout the whole time period of computations. If non-linear problems are considered the global matrix formulation is performed in each step. In plasticity problems for example the influence of the plastic regions is taken into account while element matrices are computed. Different functions are integrated in different parts of the element area. Also in the case of a beam or a plate placed on the unilateral foundation the construction in each moment is described by different differential equations. If the partition is stationary the line which limits the area of the soil-structure contact does not coincide with the division mesh. It should be emphasized that in the static analysis the structure is divided into elements choosing characteristic points or some characteristic curves, for example in places where material properties or thickness are changed. The same procedure should be introduced into the dynamic analysis. In this case the coincidence of the mesh edges and characteristic curves should be assured in each moment of the time. Only non-stationary division of the structure can satisfy that condition. It also enables the solution of quite new class of problems. The cases involving a moving support require the changeable node location. In simple load cases a traveling point force can be always placed in the joint.

Correctly formulated non-stationary division can only be performed by the space-time finite element method [1],[2],[3]. Space-time finite element is a finite element in which additionally the time dimension is considered. Therefore a beam element has two dimensions in space and time and it has a rectangular shape. A plate element becomes a rectangular prism /Fig. 1 a/. But non-rectangular space-time elements are also possible /Fig. 1 b/.

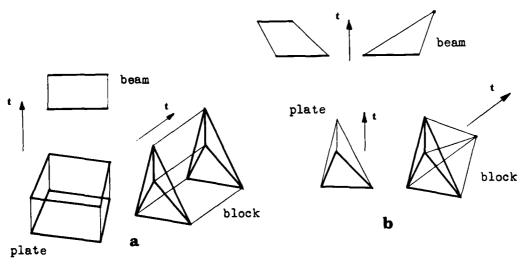


Fig. 1 Rectangular and non-rectangular space-time elements

Introduction of the idea of such elements enables the arbitrary division of the time space and is especially usefull in the case of the time division condensation in regions of greater stiffness of the construction. The case of a beam placed on the unilateral foundation is schematically ilustrated in Fig. 2.

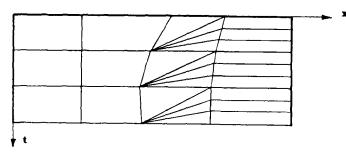


Fig. 2 Non-rectangular elements in a beam vibration modelling

Below the main principles of the space-time finite element method will be presented. The discussion will involve the derivation of stiffness, mass and damping matrices, the stability and accuracy analysis. In addition the solution for selected test problems will be described.

2. QUADRANGULAR BEAM ELEMENT

2.1 General formulation

Let $\underline{f}(x,t)$ be a displacement vector with elements w and θ (w - deflection, θ_x - angle of rotation). Let the strain vector be $\varepsilon_x(x,t)$ which has the form

$$\mathcal{E}_{\mathbf{x}} = \left\{ \begin{array}{c} \boldsymbol{\beta} \\ \boldsymbol{\lambda} \end{array} \right\} = \left\{ \begin{array}{c} \frac{\partial \mathbf{w}}{\partial \mathbf{x}} + \boldsymbol{\Theta}_{\mathbf{x}} \\ \frac{\partial \boldsymbol{\Theta}_{\mathbf{x}}}{\partial \mathbf{x}} \end{array} \right\} = \left[\begin{array}{c} \frac{\partial}{\partial \mathbf{x}} & 1 \\ 0 & \frac{\partial}{\partial \mathbf{x}} \end{array} \right] \cdot \underline{\mathbf{f}} = \boldsymbol{\partial}_{\mathbf{x}} \cdot \underline{\mathbf{f}}$$

$$\tag{1}$$

β - mean angle of shear deformation,

- curvature.

Strains can be dependent on the nodal displacement vector \mathbf{o}

$$\mathbf{\mathcal{E}}_{\mathbf{x}} = \mathbf{\partial}_{\mathbf{x}} \, \mathbf{N} \, \mathbf{\delta} \tag{2}$$

Matrix N is the shape matrix. Deformations of the element in time $\pmb{\mathcal{E}}_t$ can be determined as velocity

$$\mathcal{E}_{t} = \frac{\partial}{\partial t} \, \underline{\mathbf{f}} = \frac{\partial}{\partial t} \, \mathbf{N} \, \, \mathbf{\delta} \tag{3}$$

Strains inside the element in the case of Kelvin-Voigt model can be expressed by the relation

$$\mathbf{G}_{\mathbf{x}} = \left(\mathbf{E} + \mathbf{\eta}_{\mathbf{w}} \frac{\partial}{\partial \mathbf{t}}\right) \boldsymbol{\mathcal{E}}_{\mathbf{x}} \tag{4}$$

where

$$\mathbf{E} = \operatorname{diag}\left[\frac{\operatorname{GA}}{\operatorname{K}}, \operatorname{EI}\right] \tag{5}$$

is the elastic matrix, G - shear modulus, A - cross section area, K - shape factor for cross section, EI - flexural stiffness and γ_w is an internal damping

coefficient. The momentum of the material point σ_t (with the mass density $\bar{\rho}$) equals

$$\boldsymbol{\delta}_{t} = -m \boldsymbol{\mathcal{E}}_{t}$$
, $m = \operatorname{diag} \left[\bar{\rho} A, \bar{\rho} I \right]$ (6)

m - matrix of elementary inertia coefficients.

Denoting η_z as the external damping coefficient the virtual four-work of internal forces in the volume of element can be equated to the four-work of external forces.

$$\int_{V} \left(\delta \mathcal{E}_{x}^{T} \delta_{x} + \delta \mathcal{E}_{t} \delta_{t} \right) dV = \delta \delta F - \int_{V} \delta \underline{f}^{T} \gamma_{z} \frac{\partial \underline{f}}{\partial t} dV$$
 (7)

Considering (1),(2),(3) and (4) it can be written

$$(K + M + W + Z) \delta = F$$
 or $K^* \delta = F$ (8)

where

$$\mathbf{K} = \int_{\mathbf{V}} (\mathbf{\partial}_{\mathbf{x}} \mathbf{N})^{\mathrm{T}} \mathbf{E} \mathbf{\partial}_{\mathbf{x}} \mathbf{N} \, \mathrm{dV} \tag{9}$$

$$\mathbf{M} = -\int_{V} \left(\frac{\partial}{\partial t} \mathbf{N}\right)^{\mathrm{T}} \mathbf{m} \frac{\partial}{\partial t} \mathbf{N} dV \tag{10}$$

$$\mathbf{W} = \int_{\mathbf{V}} (\mathbf{a_x} \mathbf{N})^{\mathrm{T}} \mathbf{v} = \frac{\partial}{\partial \mathbf{t}} \partial_{\mathbf{x}} \mathbf{N} \, \mathrm{d} \mathbf{v} \tag{11}$$

$$\mathbf{Z} = \int_{\mathbf{V}} \mathbf{N}^{\mathrm{T}} \, \mathbf{y}_{\mathbf{z}} \, \frac{\partial}{\partial \mathbf{t}} \, \mathbf{N} \, d\mathbf{V} \tag{12}$$

The global matrix $K^{\mathbf{x}}$ for the time layer 'i' can be splitted into submatrices in a form

$$\mathbf{K}_{\hat{\mathbf{i}}}^{\mathbf{x}} = \begin{bmatrix} \mathbf{A}_{\hat{\mathbf{i}}} & \mathbf{B}_{\hat{\mathbf{i}}} \\ \mathbf{C}_{\hat{\mathbf{i}}} & \mathbf{D}_{\hat{\mathbf{i}}} \end{bmatrix}$$
 (13)

Matrices K, M, W and Z are called stiffness, mass, internal damping and external damping matrices, respectively. The analysis of the joint connection in several succesive time layers leads to the global matrix in a form

$$\begin{bmatrix} \mathbf{A}_1 & \mathbf{B}_1 \\ \mathbf{C}_1 & \mathbf{D}_1 + \mathbf{A}_1 & \mathbf{B}_2 \\ & \mathbf{C}_2 & \mathbf{D}_2 + \mathbf{A}_3 & \mathbf{B}_3 \end{bmatrix} \cdot \begin{bmatrix} \mathbf{d}_1 \\ \mathbf{d}_2 \\ \mathbf{d}_3 \end{bmatrix} = \begin{bmatrix} \mathbf{F}_1 \\ \mathbf{F}_2 \\ \mathbf{F}_3 \end{bmatrix}$$

$$(14)$$

For one time layer the equation (8) has the form for which the step by step solution is possible:

$$C_{i-1} \int_{i-1} + (D_{i-1} + A_i) \int_{i} + B_i \int_{i+1} = F_i$$
 (15)

In such a case the whole consideration can be reduced to the problem of the determination of the shape matrix N for the space-time element.

2.2 The first model of quadrangular_element

Let us assume the element of nodes arbitrary located in the time space. Let the diffection in the area of element be defined by a polynomial

$$w(x,t) = ax^3t + bx^2t + cxt + dt + ex^3 + fx^2 + gx + h$$
 (16)

Let the angle of rotation is

$$\Theta_{\mathbf{x}}(\mathbf{x},\mathbf{t}) = -\left(\frac{\partial \mathbf{w}}{\partial \mathbf{x}} + \mathbf{r} \frac{\partial^{3} \mathbf{w}}{\partial \mathbf{x}^{3}}\right) \tag{17}$$

where

$$\Upsilon = \frac{D}{H}$$
 , $D = EI$, $H = \frac{GA}{K}$

The vector of nodal displacements can be determined from (16) and (17) and then unknown parameters a,b,c,...,h can be computed. It is easy to form the shape matrix. But such a procedure provides only the nodal value conformance. We should assure the conformance of displacements on the edges of the elements.

2.3 The second model of quadrangular element

To provide the displacement continuity on edges the shape function defined in local coordinates ξ, τ is introduced:

$$N_{i} = \begin{bmatrix} (m_{1} - \mu m_{2}) \frac{1}{2} (1 + \tau \tau_{i}) & \frac{3}{3} (m_{2} - \mu m_{3}) \frac{\partial x}{\partial \xi} \frac{1}{2} (1 + \tau \tau_{i}) \\ -\frac{\frac{5}{3} i}{\frac{\partial x}{\partial \xi}} m_{1}^{(1)} (1 - \mu) \frac{1}{2} (1 + \tau \tau_{i}) & -(m_{2}^{(1)} - \mu m_{1}^{(1)}) \frac{1}{2} (1 + \tau \tau_{i}) \end{bmatrix}$$

$$i=1,2,3,4$$
(18)

where:

$$m_{1} = m_{1} (\xi_{0}) = \frac{1}{4} (-\xi_{0}^{3} + 3 \xi_{0} + 2)$$

$$m_{2} = m_{2} (\xi_{0}) = \frac{1}{4} (-\xi_{0}^{3} - \xi_{0}^{2} + \xi_{0} + 1)$$

$$m_{3} = m_{3} (\xi_{0}) = \frac{1}{4} (-\xi_{0}^{3} + \xi_{0})$$

$$m_{1}^{(1)} = m_{1}^{(1)} (\xi_{0}) = \frac{3}{4} (-\xi_{0}^{2} + 1)$$

$$m_{2}^{(1)} = m_{2}^{(1)} (\xi_{0}) = \frac{1}{4} (-3 \xi_{0}^{2} - 2 \xi_{0} + 1)$$

$$\xi_{0} = \xi_{1}^{2}, \quad \mu = \frac{3r}{1+3r}, \quad \gamma = \frac{D}{H(\frac{3x}{3\xi})^{2}}, \quad D = EI, \quad H = \frac{GA}{K}$$

Functions of matrix $N(\xi,T)$ are transformed to global coordinates x,t by the linear relations

$$x = \sum_{i=1}^{4} \overline{N}_{i}(\xi, \tau) x_{i} \qquad t = \sum_{i=1}^{4} \overline{N}_{i}(\xi, \tau) t_{i} \qquad (19)$$

where:

$$\overline{N}_{i} = \frac{1}{4} \left(1 + \xi \xi_{i} \right) \left(1 + \tau \tau_{i} \right) \tag{20}$$

 $\mathbf{x_i}$, $\mathbf{t_i}$ - nodal coordinates in global coordinate system, $\mathbf{z_i}$, $\mathbf{\tau_i}$ - nodal coordinates in local coordinate system.

2.4 Stability analysis

During the examination of the solution, schemes approximated by non-rectangular mesh in some cases led to non-stability. A simple mesh was taken for the test computations (Fig. 3).

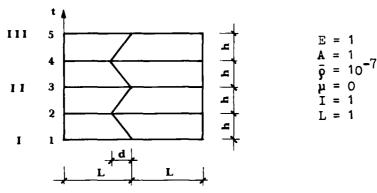


Fig. 3 A mesh of the simple test problem

Each second layer of joints was eliminated and thus regular super-elements were obtained. The transient matrix T satisfying the relation

was formulated. As shown for example in [4] the scheme (21) is stable when the spectral radius of matrix T, $\rho(T)$, satisfies the condition

$$\varrho(T) \leqslant 1 \tag{22}$$

The relationship between the spectral radius ρ and the value of the mesh point dislocation 'd' (Fig. 3) for the first and the second model of quadrangle is shown in Fig. 4 and Fig. 5, respectively.

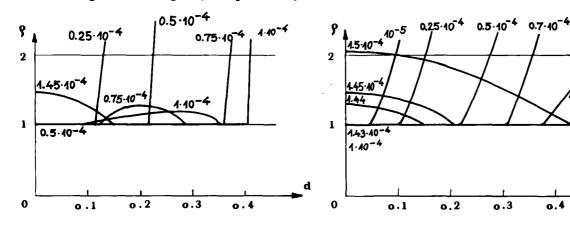


Fig. 4 The stability for the first model of quadrangle

Fig. 5 The stability for the second model of quadrangle

Better properties of the second model are evident. Two parameters can be introduced to express the stability condition for any type of a beam and without restrictions for stiffness and mass density:

$$\mathbf{\xi} = \frac{\mathbf{d}}{\mathbf{h}} \frac{1}{\sqrt{\mathbf{E}}} \tag{23}$$

$$\mathcal{J} = \frac{h}{\sqrt{12}} \omega \tag{24}$$

The second parameter can be evaluated from the definition describing the extremal time step 'h' for the conditionally stable formulation of the method.

$$\omega_{h_{ex}} = \sqrt{12}$$
 (25)

 ω - the highest modal frequency. Fig. 6 can be depicted in terms of the parameters z and z.

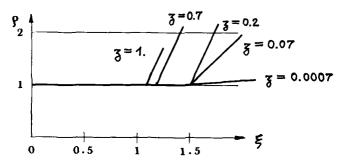


Fig. 6 Stability condition for different values of 3

It is also interesting whether the vertical displacement of the joint (parallel to Ot axis) changes the spectral radius value. To determine the value of $\rho(T)$ the test problem shown in Fig. 7 was solved.

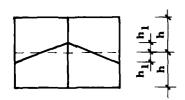


Fig. 7 The scheme of the test problem

Let us assume the dimensionless parameter

$$y = \frac{h_1}{h}$$
, $0 \le y \le 1$ (26)

Fig. 8 presents the influence of the vertical displacement h_1 on the spectral radius value.

It should be emphasized that in addition to the tests described above there exist other successful test that will not be discussed here.

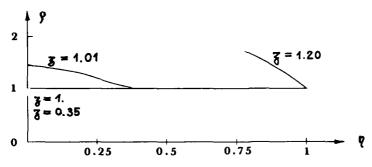


Fig. 8 The extension of the stability range in the case of the vertical displacement of the joint (Fig. 7)

3. TRIANGULAR BEAM ELEMENT

To form a correctly formulated shape function we must ensure the conformance of displacements on edges in the neighbour elements. The assumption of displacement distribution varying cubically along the element sides allows the evaluation of displacements in additional 6 mid-side nodes. Then a polynomial of sufficiently high order can be assumed to expres displacement distribution in the element area.

The displacements on edges are expressed in terms of the nodal values by the form

$$\underline{\mathbf{f}}_{\mathbf{k}}(\mathbf{\xi}) = \left\{ \begin{array}{l} \mathbf{w} \\ \mathbf{\theta}_{\mathbf{x}} \end{array} \right\} = \mathbf{N}_{1}^{\mathbf{k}} \, \mathbf{f}_{1}^{\mathbf{k}} + \mathbf{N}_{2}^{\mathbf{k}} \, \mathbf{f}_{j} \tag{27}$$

Expresions N_i^k are related to local coordinate ξ as follows:

$$\mathbf{N_i^k} = \begin{bmatrix} \mathbf{N_{11i}} & \mathbf{N_{12i}} \\ \mathbf{N_{21i}} & \mathbf{N_{22i}} \end{bmatrix}$$
 (28)

$$N_{11i} = m_1 - \mu m_3 \cos^2 \alpha_k$$

$$N_{12i} = \frac{1}{2} \xi_{i} 1_{k} (m_{2} - \mu m_{3}) \cos \alpha_{k}$$

$$N_{21i} = -\xi_{i} m_{1}^{(1)} (1 - \mu) \frac{2}{1_{k}} \cos \alpha_{k}$$

$$N_{22i} = -(m_{2}^{(1)} - \mu m_{1}^{(1)}) \cos^{2} \alpha_{k} + \frac{1}{2} (1 + \xi \xi_{i}) \sin^{2} \alpha_{k}$$
(29)

l, is the lengh of the side 'k' and α_k is the angle between the axis Ox and the edge of the triangle. The system of coordinates is x,ct, where c is the speed of the wave propagation in an elastic medium. The distribution of displacements inside the element is expressed by the polynomials:

$$\mathbf{f}(\mathbf{x},\mathbf{t}) = \begin{cases} \mathbf{w} \\ \mathbf{\theta}_{\mathbf{x}} \end{cases} = \begin{cases} \mathbf{a}_{1} \mathbf{x}^{3} + \mathbf{a}_{2} \mathbf{x}^{2} \mathbf{t} + \mathbf{x} \mathbf{t}^{2} + \mathbf{a}_{3} \mathbf{t}^{3} + \mathbf{a}_{4} \mathbf{x}^{2} + \mathbf{a}_{5} \mathbf{x} \mathbf{t} + \mathbf{a}_{6} \mathbf{t}^{2} + \mathbf{a}_{7} \mathbf{x} + \mathbf{a}_{8} \mathbf{t} + \mathbf{a}_{9} \\ \mathbf{b}_{1} \mathbf{x}^{3} + \mathbf{b}_{2} \mathbf{x}^{2} \mathbf{t} + \mathbf{x} \mathbf{t}^{2} + \mathbf{b}_{3} \mathbf{t}^{3} + \mathbf{b}_{4} \mathbf{x}^{2} + \mathbf{b}_{5} \mathbf{x} \mathbf{t} + \mathbf{b}_{6} \mathbf{t}^{2} + \mathbf{b}_{7} \mathbf{x} + \mathbf{b}_{8} \mathbf{t} + \mathbf{b}_{9} \end{cases}$$
(30)

The evaluation of displacements in all nine nodes enables the determination of unknown parameters a_1, \ldots, a_g and b_1, \ldots, b_g . Shape matrix can be easily formulated when all nodal displacements are determined in terms of the displacement values in three joints. The stability analysis for the time space partition is presented in Fig. 9. The partition scheme is the same as shown in Fig. 3. Each quadrangle

in the mesh is divided into two triangles.

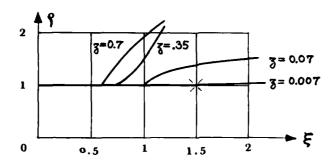


Fig. 9 The result of the stability analysis for the triangular element

4. EXAMPLE OF APPLICATION

Non-stationary division was used in vibration analysis of a beam placed on the unilateral foundation and subjected to traveling force (Fig. 10).

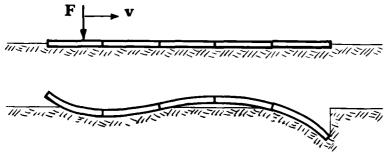


Fig. 10 The scheme of a beam on the unilateral foundation

The partition of the beam was carried out in the points limiting the base-structure contact area. In each step the displacements of the beam were analysed and the points of zero diffection were found. In the partition into elements the coincidence between the mesh joints and points limiting the contact area was assumed (Fig. 11). In the area of the solid interaction the time division was condensed (as shown in Fig. 2).

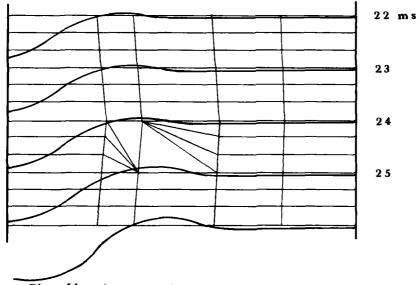


Fig. 11 Accommodation of the partition into elements to the shape of the contact area

To simplify the solution algorithm the constant total number of the degrees of freedom was assumed. Possible introduction of the numerical damping instead of the damping matrices formulation considerably shortens the time of computation.

5. CONCLUSIONS

The method described above can be successfully extended to other types of structure. In the case of beam vibrations the results differ only by few per cent as compared to the results obtained with the use of the rectangular mesh (even if the slope of the oblique edge is close to the permissible value).

When high frequences dominate the stability and accuracy require the assumption of small time integration step. The contact area changes slowly and then in succesive steps only elements neighbouring with the contact area boundary are modified. The geometry of the rest is unchanged.

REFERENCES

- 1. Z. KACZKOWSKI 1975 J. Technical Phisics 16, 1. The method of finite space-time elements in dynamics of structures.
- 2. Z. KĄCZKOWSKI 1979 Archiwum Inżynierii Lądowej 25, 3. General formulation of the stiffness matrix for the space-time finite elements.
- 3. Z. KĄCZKOWSKI and J. LANGER 1980 Archiwum Inżynierii Lądowej <u>26</u>, 1. Synthesis of the space-time element method.
- 4. J. LEGRAS 1971 Méthodes et techniques de l'analyse numérique. Dunod, Paris.



APPLICATION OF THE METHOD OF INTEGRAL EQUATIONS TO THE VIBRATION OF PLATES

J. Scheuren

Institut für Technische Akustik Technische Universität Berlin AD-P003

INTRODUCTION

The calculation of the vibrations of an elastic continuum normally starts from the mathematical formulation of the problem in terms of a boundary value problem. This means, that the field variables describing the vibrations have to satisfy a differential equation and certain conditions on the boundary surrounding the region under consideration. Analytical solutions of such boundary value problems exist only in some cases with special geometric configurations. So, normally one has to solve the problem by numerical methods.

In many cases it is convenient to replace the differential equation and the boundary conditions by the appropriate integral equation containing explicitely the boundary values of the field variables which yield a unique solution. The representation of the sound pressure $p(x_i)$ within a volume V as a function of the sources q in V and the values of the pressure and its normal derivative on the surrounding surface S is a widely used example of such an integral equation [1], [2]

$$p(\mathbf{x}_{i}) = -\frac{1}{4\pi} \iiint_{\mathbf{V}} q(\mathbf{x}_{qi}) \frac{e^{-jkr}}{r} dv_{q}$$

$$-\frac{1}{4\pi} \oiint_{\mathbf{S}} p(\mathbf{x}_{qi}) \frac{\partial}{\partial n_{q}} \frac{e^{-jkr}}{r} ds_{q}$$

$$+\frac{1}{4\pi} \oiint_{\mathbf{S}} \frac{\partial p(\mathbf{x}_{qi})}{\partial n_{q}} \frac{e^{-jkr}}{r} ds_{q}$$
(1)

The quantity

$$r = | x_i - x_{qi} |$$
 (2)

represents the distance between the source point x_q and the field point x_i , q represents the sources of the sound field, given by the right-hand-side of the inhomogeneous wave equation

$$\Delta p + k^2 p = q \tag{3}$$

and the wavenumber k is given by the angular frequency $\boldsymbol{\omega}$ and the phase velocity c of the medium under consideration

$$k = \frac{\omega}{C}$$

The derivatives $\partial/\partial n$ have to be taken along the surface norma

pointing out of the volume V. The index q should illustrate that those derivatives and the integrations refer to the variables \mathbf{x}_{qi} . The above equations suppose harmonic time dependence and this assumption shall be valid furtheron.

All solutions of equation (1) are solutions of (3), differing in the boundary values on S. Equation (1) therefore can be taken as starting point for the numerical evaluation of the boundary value problem [3], [4].

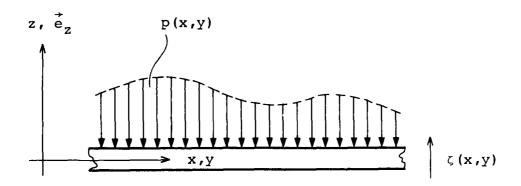
In the following, an analogous relationship will be given for the flexural vibrations of plates.

INTEGRAL-RELATIONSHIP FOR FLEXURAL WAVES

The equation of motion governing the flexural vibrations of thin, homogeneous plates is given by [5]

$$L(\zeta) = \Delta \Delta \zeta - k^{4} \zeta = -\frac{p}{D} = q$$
 (4)

where ζ is the displacement of the plate, p is the exciting pressure distribution, which actuates the plate surface, D is the bending stiffness of the plate and k the flexural wave number.



To get a unique solution of this equation within a given area S, it is necessary to specify suitable boundary conditions on the edge-contour C. They may consist of the specification of two of the four field variables given by displacement, bending angle, bending moment and shear force. They also may specify linear combinations of those as represented by force or moment impedances.

The edge-contour C may be of arbitrary shape, including N corner points with smooth curves between them.

The integral representation of boundary value problems supposes the considered differential operator to be self-adjoint and can always be obtained by application of the generalized Greenformula belonging to this operator. In the present case, this formula can be derived easily from the frequently used relation for the Laplace-operator Δ , which, in the two-dimensional case, yields

$$\iint\limits_{S} (w\Delta u - u\Delta w) dS = \oint\limits_{C} (w \frac{\partial u}{\partial n} - u \frac{\partial w}{\partial n}) d1$$

Replacing u by Δu and subtracting from the so obtained equation the one obtained by interchanging u and w gives

$$\iint_{S} (\mathbf{w} \Delta \Delta \mathbf{u} - \mathbf{u} \Delta \Delta \mathbf{w}) \, d\mathbf{S} = \oint_{C} (\mathbf{w} \frac{\partial (\Delta \mathbf{u})}{\partial \mathbf{n}} - \frac{\partial \mathbf{w}}{\partial \mathbf{n}} \Delta \mathbf{u} + \Delta \mathbf{w} \frac{\partial \mathbf{u}}{\partial \mathbf{n}} - \frac{\partial (\Delta \mathbf{w})}{\partial \mathbf{n}} \mathbf{u}) \, d\mathbf{I}$$
(5)

The vector \vec{n} defining the direction of the normal derivatives $\partial/\partial n$ is perpendicular to the edge-contour C and points out of the area S of the considered plate. The integration along this contour has to be carried out in the mathematically positive sense, which means that the considered area S of the plate lies on the "left" of the integration path.

Taking into account eq. (4), one can write for the left-handside of eq. (5)

$$\iint_{S} (\mathbf{w} \Delta \Delta \mathbf{u} - \mathbf{u} \Delta \Delta \mathbf{w}) \, dS = \iint_{S} (\mathbf{w} L(\mathbf{u}) - \mathbf{u} L(\mathbf{w})) \, dS \tag{6}$$

Substituting in (6) w by the displacement $\zeta(x_i) = \zeta(x,y)$ and u by the Green's function $g(x_i; x_{qi})$, which is defined as a solution of

$$L(g(x_{i},x_{qi})) = \frac{1}{D} \delta(x_{i} - x_{qi})$$
 (7)

one obtains

$$\iint_{S} (\zeta L(g) - gL(\zeta)) dS = \frac{1}{D} \alpha(x_{qi}) \zeta(x_{qi})$$

$$- \iint_{S} q(x_{i}) g(x_{i}; x_{qi}) dS$$
(8)

The function $\alpha(\mathbf{x}_i)$ is given by

$$\alpha(\mathbf{x_i}) \zeta(\mathbf{x_i}) = \iint_{S} \zeta(\mathbf{x_{qi}}) \delta(\mathbf{x_i} - \mathbf{x_{qi}}) dS_q$$

and the index q again indicates that the integration refers to x_{qi} . The value of α depends on the position of x_i

$$\alpha(\mathbf{x}_i) = \begin{cases} 1 & \text{if } \mathbf{x}_i \text{ lies in S} \\ 0 & \text{if } \mathbf{x}_i \text{ lies out of S} \end{cases}$$
 (9)

Inserting ζ and g into the right-hand-side of (5) and interchanging x_i and x_{gi} , one obtains from (5) with (6) and (8)

$$\frac{1}{D} \alpha (\mathbf{x_i}) \zeta (\mathbf{x_i}) = \iint_{S} \mathbf{q}(\mathbf{x_{qi}}) \mathbf{g}(\mathbf{x_{qi}}; \mathbf{x_i}) dS$$

$$+ \oint_{C} \zeta (\mathbf{x_{qi}}) \frac{\partial}{\partial \mathbf{n_q}} (\Delta_{\mathbf{q}} \mathbf{g}(\mathbf{x_{qi}}; \mathbf{x_i})) dl_{\mathbf{q}} - \oint_{C} \frac{\partial \zeta (\mathbf{x_{qi}})}{\partial \mathbf{n_q}} \Delta_{\mathbf{q}} \mathbf{g}(\mathbf{x_{qi}}; \mathbf{x_i}) dl_{\mathbf{q}} (10)$$

$$+ \oint_{C} \Delta_{\mathbf{q}} \zeta (\mathbf{x_{qi}}) \frac{\partial \mathbf{g}(\mathbf{x_{qi}}; \mathbf{x_i})}{\partial \mathbf{n_q}} dl_{\mathbf{q}} - \oint_{C} \frac{\partial}{\partial \mathbf{n_q}} (\Delta_{\mathbf{q}} \zeta (\mathbf{x_{qi}})) \mathbf{g}(\mathbf{x_{qi}}; \mathbf{x_i}) dl_{\mathbf{q}}$$

This is the integral relation belonging to the differential equation (4). With the exception of the not yet specified Green's function it corresponds to eq. (1). Complete analogy is obtained by determining g as the Green's function of an infinite plate. It again only depends on the distance $r = |x_i - x_{qi}|$ and is given by [5]

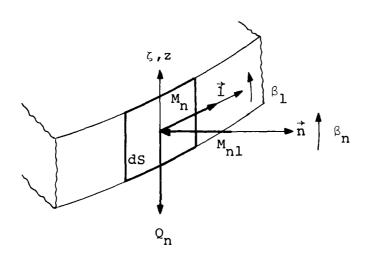
$$g(r) = \frac{-j}{8k^2D} (H_o^{(2)}(kr) - H_o^{(2)}(-jkr))$$
 (11)

where $H_{O}^{(2)}$ is the zero-order Hankel function of the second kind.

Eq. (10) immediately shows how the pressure distribution p = -Dq, the quantities ζ and $\Delta \zeta$ and their normal derivatives on C contribute to the displacement of the point x, on S. Its evaluation, however, supposes the knowledge of those quantities, which therefore have to be determined first. But before discussing this, eq. (10) will be transformed in order to contain only such field variables, that appear in the formulation of physical boundary conditions.

3. INTRODUCTION OF PHYSICAL FIELD VARIABLES

The mathematical description of the vibrational state of a thin plate normally uses, besides the displacement and the rotation of a plate element, the shear forces and the moments acting upon it. They are functions of the position and the direction of the surface element they are applied to. Given this direction by \vec{n} , they satisfy the following relations [5], [6], [7]



$$\beta_{\mathbf{n}} = \frac{\partial \zeta}{\partial \mathbf{n}} \tag{12}$$

$$\beta_1 = \frac{\partial \zeta}{\partial 1} \tag{13}$$

$$M_{n} = -D \left(\frac{\partial^{2} \zeta}{\partial n^{2}} + \mu \frac{\partial^{2} \zeta}{\partial l^{2}} \right)$$
 (14)

$$M_{n1} = - (1 - \mu) D \frac{\partial^2 \zeta}{\partial n \partial I}$$
 (15)

$$Q_{n} = D \frac{\partial (\Delta \zeta)}{\partial n}$$
 (16)

where μ is the Poisson's ratio of the plate material.

The above equations show that the displacement ζ , the bending angle β_n and the shear force Q_n may be substituted directly into eq.(10). In order to be able to replace the expression $\Delta \zeta$ in (10) by the field variables defined above, the integral containing $\Delta \zeta$ has to be transformed. Introducing the torsional moment M_{nl} in accordance with (14) and (15) one obtains

$$\Delta \zeta \frac{\partial \mathbf{g}}{\partial \mathbf{n}} = - \mathbf{D} \left(\mathbf{M}_{\mathbf{n}} \frac{\partial \mathbf{g}}{\partial \mathbf{n}} + \mathbf{M}_{\mathbf{n}1} \frac{\partial \mathbf{g}}{\partial \mathbf{1}} \right) + (1 - \mu) \left(\frac{\partial}{\partial \mathbf{1}} \left(\frac{\partial \zeta}{\partial \mathbf{1}} \frac{\partial \mathbf{g}}{\partial \mathbf{n}} \right) - \frac{\partial}{\partial \mathbf{n}} \left(\frac{\partial \zeta}{\partial \mathbf{1}} \frac{\partial \mathbf{g}}{\partial \mathbf{1}} \right) \right)$$

The same transformation of the integral in eq. (10) containing Δg makes vanish the last term after the subtraction prescribed by (10). The term before neither contributes to the integral over C since the gradients of the displacements ζ and g are continuous functions even in the corner points.

$$\oint_{C} \frac{\partial}{\partial 1} \left(\frac{\partial \zeta}{\partial 1} \frac{\partial g}{\partial n} - \frac{\partial \zeta}{\partial n} \frac{\partial g}{\partial 1} \right) d1 =$$

$$= - \overrightarrow{e}_{z} \oint_{C} \frac{\partial}{\partial 1} (\operatorname{grad} \zeta \times \operatorname{grad} g) d1 = 0$$

here denotes the unit vector in the z-direction. The remaining terms only contain the field variables defined above.

Next, the field variables belonging to the Green's function g are introduced. They are obtained by replacing ζ by g in eqs.(12) to (16) and shall be characterized by the symbol "~", e.g.

$$\tilde{\zeta} = g$$
 and $\tilde{\beta}_n = \frac{\partial \tilde{\zeta}}{\partial n} = \frac{\partial g}{\partial n}$.

Thus, with Dq = -p, eq. (10) yields

$$\alpha \zeta = -\iint_{S} p \tilde{\zeta} dS$$

$$+ \oint_{C} \zeta \tilde{Q}_{n} d1 - \oint_{C} Q_{n} \tilde{\zeta} d1$$

$$+ \oint_{C} \beta_{n} \tilde{M}_{n} d1 - \oint_{C} M_{n} \tilde{\beta}_{n} d1$$

$$+ \oint_{C} \beta_{1} \tilde{M}_{n1} d1 - \oint_{C} M_{n1} \tilde{\beta}_{1} d1$$

$$+ \int_{C} \beta_{1} \tilde{M}_{n1} d1 - \oint_{C} M_{n1} \tilde{\beta}_{1} d1$$
(17)

To bring this integral relationship to it's final form, it shall be taken into account that the independent specification of torsional moments on C overdetermines the boundary value problem under consideration because of the neglection of shearing deformations in Kirchhoff's plate theory [7], [8]. It is therefore necessary to replace the torsional moments by an equivalent shear force distribution on C. This is done by partial integration of the last integral in eq. (17). In contrast to the transformations leading

to eq. (17). the discontinuity of \mathbf{M}_{ns} in the corner points here yields additional terms.

$$\oint_C M_{n1} \tilde{\beta}_1 d1 = - \oint_C \frac{\partial M_{n1}}{\partial 1} \tilde{\zeta} d1 + \sum_{i=1}^{N} F_i \tilde{\zeta}_i$$

The quantities F_i are point forces actuating on the corner points and directed i opposite to the z-axis. If l_i , i = 1,...,N denotes the values of the parameter l in these corner points, they are given by

$$F_i = F(i_i) = M_{n1} (i_i - 0) - M_{n1} (i_i + 0)$$
 (18)

while

$$\zeta_{i} = \zeta (l_{i}) \tag{19}$$

specify the associated displacements. With the resulting shear force

$$Q_{rn} = Q_n - \frac{\partial M_{n1}}{\partial 1}$$
 (20)

the described transformation of the last two integrals of eq. (17) finally yields

$$\alpha \zeta = - \iint_{S} p \tilde{\zeta} dS$$

$$+ \oint_{C} \zeta \tilde{Q}_{rn} dl - \oint_{C} Q_{rn} \tilde{\zeta} dl$$

$$+ \oint_{C} \beta_{n} \tilde{M}_{n} dl - \oint_{C} M_{n} \tilde{\beta}_{n} dl$$

$$+ \sum_{i=1}^{N} \zeta_{i} \tilde{F}_{i} - \sum_{j=1}^{N} F_{i} \tilde{\zeta}_{j}$$

$$(21)$$

4. DISCUSSION

Given the influence functions $\tilde{\zeta}$, $\tilde{\beta}_n$, \tilde{M}_n , \tilde{Q}_n and \tilde{F}_i in terms of the Green's function g, eq. (21) specifies how the knowledge of the exciting pressure p on S and the four field variables on C enables the computation of the displacement in any point of the plate. At the same time it includes the relationship for the determination of the boundary values not prescribed by the arrangement under investigation, which always is given in form of an integro differential equation for the displacement ζ on the edge contour C.

Thus it is possible to evaluate the forms of vibration of thin plates with arbitrary shape for all kinds of excitation. The special case of vanishing excitations may be used to determine the natural frequencies and the associated modes of vibration for a given plate-arrangement. By the combination of integral relations for adjacent areas to a system of integro differential equations it is in addition possible to solve problems with regions of constant, but different parameters.

The advantage of the presented relation as starting point of a numerical treatment lies in the fact, that the equations to solve are reduced to a one-dimensional formulation. This means, that the number of values to be computed is only proportional to n, if n points have to be regarded on C to obtain a sufficient resolution.

REFERENCES

- 1. LORD RAYLEIGH 1896 Theory of Sound, § 293. Now York, Dover (reprint 1945).
- P.M. MORSE and K.U. INGARD 1968 Theoretical Acoustics.
 New York: McGraw-Hill.
- 3. H.A. SCHENCK 1968 The Journal of the Acoustical Society of America, Vol. 44, number 1, pp 41 58. Improved Integral Formulation for Acoustic Radiation Problems.
- 4. M.N. SAYHI, Y. OUSSET and G. VERCHERY 1981 Journal of Sound and Vibration, Vol. 74, number 2, pp. 187 204. Solution of Radiation Problems by Collocation of Integral Formulations in Terms of Single and Double Layer Potentials.
- 5. L. CREMER and M. HECKL 1973 Structure-Borne Sound. Berlin: Springer.
- 6. A.E.H. LOVE 1927 A Treatise on the Mathematical Theory of Elasticity. New York, Dover.
- 7. I. SZABO 1977 Höhere Technische Mechanik. Berlin: Springer
- 8. R.D. MINDLIN 1951 Journal of Applied Mechanics, Vol. 18, pp. 31 38. Influence of Rotatory Inertia and Shear on Flexural Motions of Isotropic, Elastic Plates.

USE OF STRAIN ENERGY DENSITY AS A BASIS FOR FINITE ELEMENT MODEL DEVELOPMENT

A.H. Patel and R. Ali

Department of Transport Technology University of Technology, Loughborough

The paper examines the use of strain energy density distribution within deformed structures as a criterion for the development of progressively refined finite element models. This criterion has been used to study the dynamic characteristics of a cantilever beam and a diesel engine sump pan. The technique has been used to identify regions within the deformed structure which need a more comprehensive modelling consideration.

INTRODUCTION

In recent years several investigators have put forward theses for the consideration of the variation in strain energy density, SED, of a structure under analysis as a criterion for the development of progressively refined finite element mesh [1,2,3,4]. The basis of these theses is the minimisation of the total potential energy or the maximisation of the total strain energy[5]. However the class of problems for which the SED criterion has been considered so far is limited to elastostatic problems. For this class of problems the criterion has proved to be most effective in providing guidelines for mesh refinement [3]. It is our belief that the same criterion can be extended to elastodynamic problems.

The method relies on a preliminary analysis of the structure with a coarse mesh for the determination of the nodal stress vector which is subsequently used to evaluate the nodal SED [2]. A contour plot of the SED allows the analyst to identify regions within the structure which may require a more comprehensive modelling consideration for acceptable results. The use of elements that can approximate linear SED functions has, however, necessitated the need for numerical evoluation of second order variations of the SED distribution within the deformed structure.

2. THEORY

In a dynamic problem, according to, Rayleigh's principle the best possible solution will be obtained by minimising the difference between the exact mode shapes and those resulting from the finite element analysis. Since the SED distribution within a structure is a function of the deformed shape and consequently varies according to the deformation, it follows that for static and dynamic problems, the object is to accurately predict this distribution and as a result the internal energy of the deformed structure. A distinct implication of this method is that each mode of vibration would have to be treated individually thus necessitating the need for a different mesh for each mode of vibration.

In a Ritz finite element solution one is concerned with obtaining the best approximation to the displacement vector and thereby the internal energy of the analysed structure. Hence for this solution the primary concern is minimisation of the energy in the error which can be represented by the inner product as

$$U(\underline{u} - \underline{u}^h, \underline{u} - \underline{u}^h)$$

where u is the exact displacement vector

 \underline{u}^h is the displacement vector obtained from a finite element analysis.

Assuming that $U(u,u^h)$ is equal to $U(\dot{u}^h,\dot{u}^h)$, the energy in the error can be shown [6] to be equal to the error in the energy

$$U(\underline{u} - \underline{u}^{h}, \underline{u} - \underline{u}^{h}) = U(\underline{u}, \underline{u}) - U(\underline{u}^{h}, \underline{u}^{h})$$
 (1)

where the right hand side of equation(1) represents the error in the energy. For the equation of elasticity, the energy inner product, the internal energy of the deformed structure is given by the following

$$U(\underline{u},\underline{u}) = \int_{V} \sigma^{\mathsf{T}} \varepsilon dV = \int \varepsilon^{\mathsf{T}} [E]^{\mathsf{T}} [dV = \int (\underline{D}\underline{U})^{\mathsf{T}} [E]^{\mathsf{T}} (\underline{D}\underline{U}) dV$$
 (2)

where σ is the stress vector, ε is the strain vector, [E] is the elastic matrix and D is a first order differential operator relating displacements to strains.

Since equation (2) represents the strain energy content of the domain, V, the right hand side of equation (1) represents the difference in the total strain energy between the exact and the finite element solution. Hence the minimisation of the energy in the error is equivalent to minimising the total strain energy difference between the exact and the finite element solution. In addition, since the SED is the integrand of the total strain energy, the finite elements must be positioned such that the best possible approximation to the exact SED function is obtained and the difference between the exact and the approximate total strain energy is minimised.

The next question that arises is how should the finite elements be positioned to give the minimum difference between the exact and the approximation obtained from the finite element analysis of the SED function within the deformed structure. The answer to this question is given by the error estimate for an interpolant in approximation theory where the difference between the exact solution, V, and it's interpolant is given by

$$|V-V_I|_e \leq C_i h_e^k |D^k V| \tag{3}$$

where C_i is a constant, h^k is a representative element size, D^k is a differential operator of order k and k-1 is the degree of the interpolant that can be approximated by the element e.

For constant strain elements, the SED can only be constant and thus equation (3) states that the error in the SED function is proportional to the size of the element times the first variation in the SED. This implies that the error of the approximated SED function will be greater where the exact SED function varies rapidly because in these regions piecewise approximation of the continuous function by constant values of the constant strain elements gives a lower average of the exact SED and hence a lower value of the approximated strain energy content of that region. For the SED distribution to be better approximated in regions where the SED varies rapidly smaller elements must be used in comparison with regions where the variation is not so great. The method used for orientating the elements for the minimisation of the variation within an element of the exact SED distribution is described in [7]. Generally the elements are spaced between selected contours so that the exact SED function can be approximated by piecewise constant values. Hence if the SED field obtained from two consecutive refinements in a particular region does not change in that region then the best possible solution has been obtained. In practise, however, the use of smaller elements in regions of rapid SED variation generally has the effect of producing a larger gradient in that region and as such the use of subsequent SED contour plots resulting from the refined grid show that further refinement is needed in that region. For this reason it has been found that the initial analysis should be made with elements of comparable size if possible and further refinements should be based

on the contour plot of only the initial mesh until a solution parameter other than SED converges.

Quadratic elements can approximate both constant and linear SED functions and hence in view of equation (3) the problem becomes one of approximating the exact SED distribution with piecewise linear values. This suggests that smaller elements should be used where the variation in the SED gradient is greatest and larger elements where it is least. This second variation in SED is difficult to evaluate numerically and can be further complicated by elements that can approximate different SED functions in different directions. For most problems, however, it is found that in regions where the second variations in SED are high, the first variations are also high. Accordingly both linear and quadratic element refinements can be based on the first variation in the SED field.

Ecer [8] has suggested a further guideline for producing refined meshes for dynamic problems based on the minimisation of the variations in the strain energy content between elements by selectively reducing the size of those elements whose strain energy content is above a selected norm. Using this criterion he was able to successfully produce refined finite element meshes for modelling a wheelwell. In spite of his apparent success, the authors feel that this method is not universally applicable as shown below.

Consider a bar of unit thickness with a tapered section carrying an axial load as shown in figure 1. It was modelled with constant strain triangular elements. The actual SED distribution plot for this load case is shown in figure 2. For this problem it is noticed that elements in section A have a higher strain energy content than those in section B or C and thus according to Ecer's criterion, section A would have to be redefined with smaller elements. The refined mesh, however, will fail to produce any significant change in the displacement of the bar since the constant SED field in section A can be exactly represented by any number of constant strain elements. The region of the bar which needs redefining with smaller elements is that part of the bar which is tapered since the linear SED function in that region cannot be accurately represented by the constant values of the SED which the constant strain elements can approximate. It is suggested that the reason for Ecer's success in modelling the wheelwell was due to the fact that regions of high strain energy content were also regions of rapid SED variation.

3. FINITE ELEMENT ANALYSIS

Using the first variation in SED as a criterion for mesh refinement two dynamic problems were studied. As has been stated previously, different modes of vibration require refinement in different regions. Accordingly the analyses for the two problems were limited to the study of one or two modes of vibration only to demonstrate the effectiveness of the criterion for mesh refinement. For each problem the number of master degrees of freedom was kept constant and these were chosen automatically [9].

3.1 Cantilever Beam

The cantilver beam analysed is shown in figure 3. The elastic modulus of the material of the beam and it's thickness were $2.09 \times 10^{11} \text{ N/m}^2$ and 0.15m respectively. Since the width of the beam is less than a tenth of the length of the beam, shear deformation was neglected. The frequency of vibration for the first mode of this beam from classical theory is 31.3 Hz.

This problem was solved by using constant strain triangular elements which are known to yield poor results and provide considerable scope for mesh refinement. The initial mesh, a contour plot resulting from the initial mesh, a refined mesh produced from the information afforded by the contour plot and a uniform mesh for

the same case are shown in figure 4. The results obtained from the three meshes are given in table ${\tt l}$.

The results in table I indicate that value of the frequency obtained from the initial and the uniform mesh are relatively poor in comparison to that obtained from the mesh synthesized from the information provided by the contour plot inspite of the larger number of elements used for the uniform mesh.

3.2 Diesel Engine Sump Pan

For the analysis of the free vibration characteristics of a diesel engine sump pan an initial model was developed. The elastic modulus, Poisson's ratio and density of the pressed mild steel plate of mean thickness 1.2mm were taken to be $2.0 \times 10^{11}~\text{N/m}^2$, 0.3 and $7800~\text{Kg/m}^3$ respectively. The initial model consisted of 3 and 4 noded facet shell elements. Advantage was taken of the symmetric nature of the sump and only half of the structure was analysed. This is shown in figure Sa. Agreement between the theoretical and measured values of the frequencies for the first four modes of vibration was fairly statisfactory. Discrepancies between the two results were noted for the higher modes and accordingly this technique was applied to the fifth and sixth modes. Experimentally measured results for these modes of vibration [10] are shown in figure 5 and table 2. The results obtained from the initial analysis are also shown in table 2. It was noted from the initial analysis that although the corresponding theoretical mode shapes tended to have the same general shapes as those measured experimentally, the frequencies obtained for the fifth and the sixth modes did not compare well with test results. The order of the error encountered was 30% and 42% respectively. This suggested that besides the geometric differences between the finite element model and the actual sump pan, certain other factors such as the element displacement formulation were responsible for these large differences. It was thought that refinement of the initial mesh on the basis of the SED criterion, whilst maintaining the same topology, would allow the error in the predicated frequencies to be minimised to a level accountable by the differences in the geometry of the model and the actual sump.

The SED contour plots for the modes in conflict with test results are shown in figures 6b, 6c. Although the contour plots suggested that the element concentration in the Z direction should be increased, it was believed that the out of plane displacement function of the elements could predict the deflection in the Y - Z plane with sufficient accuracy without involving significant inplane deflections of the elements. As pointed out previously since one is concerned with the second variation in SED for out of plane deflections, it is not necessarily true to assume that refinement in the Z direction will yield a better set of results. It was believed that although the concentration of the contours in the X direction is not as great as in the Z direction, the bending deformation of the elements of the groove in the X-Y plane would require them to assume a quadratic form of in plane displacement along the line of discontinuities. elements cannot represent this since their displacement formulation allows only linear displacements. Hence several other meshes based on the refinement of the base of the pan in the X direction were produced. These are shown in figure 7. The results obtained from the finite element analysis of these meshes are given intable 2.

The predicted results from the refined grids show a tendency to converge rapidly with increasing number of elements in the X direction. However, there is still a large discrepancy between the two sets of results. It is believed that this error is largely attributable to the geometric differences between the model and the actual pan. A better set of results would be those obtained using elements that allowed quadratic in plane deflections. Accordingly the analysis of the initial mesh was repeated using 6 and 8 noded facet shell elements. The results obtained from this analysis are given in table 2. These results indicate

that the refined mesh using 3 and 4 noded elements, with the base refined in the manner shown in figure 7c gave results which were comparable to those obtained using higher order elements which are known to be able to best predict the deflected shape of the sump pan. The difference between the two sets of results was found to be due to the need for refinement of the flange [11] and further refinement of the base. It can be seen that the error in the frequencies of the refined mesh with respect to results obtained using 6 and 8 noded elements has been successfully reduced.

4. CONCLUSIONS

The criterion examined in this paper offers a guideline for mesh refinement for the reduction of errors in the prediction of vibration frequencies. This has been demonstrated for the case of a cantilever beam and for the selected modes of vibration of a diesel engine sump pan. From the SED contour plots obtained from a preliminary analysis it has been possible to systematically produce refined grids for the problems studied. Although the errors in predicated frequencies for the diesel engine sump pan, using 3 and 4 noded elements, were considerably reduced by mesh refinement based on the selected criterion, this problem has demonstrated the need for numerical evaluation of second order variations in the SED function when using quadratic elements in modelling the structure. However with a degree of intervention from the user it has been possible to demonstrate that the first variation in the SED can provide guidelines for finite element mesh refinement when using quadratic elements for modelling purposes.

REFERENCES

- M.S. SHEPHARD, R.H. GALLAGHER and J.F. ABEL 1980 International Journal of Numerical Methods in Engineering 15, 1021-1039. Synthesis of near optimum finite element meshes with interactive computer graphics.
- 2. M.S. SHEPHARD 1979 Ph.D Thesis, Cornell University. Finite element grid optimisation with interactive computer graphics.
- 3. D.J. TURKE and G.M. McKNIECE 1974 Computers and Structures 4, 499-519, Guidelines for selecting finite element grids based on optimisation study.
- 4. R.J. MELOSH and P.V.MARCAL 1977. International Journal of Numerical Methods in Engineering 11. An energy basis for mesh refinement of structural continua.
- 5. O.C. ZIENKIEWICZ 1977. The Finite Element Method. London: McGraw-Hill.
- 6. G. STRANG and G.J. FIX 1973. An Analysis of the Finite Element Method. Englewood Cliffs N.J.: Prentice-Hall.
- 7. E.R.A.OLIVERA 1971 Proc. 3rd Conference on Matrix Methods in Structural Mechanics. W.P.A.F.B. Ohio Optimization of finite element solutions.
- 8. A. ECER 1978 SDRC Technical Report. A case study for evaluation of finite element modelling in dynamic analysis of thin shell structures.
- 9. PAFEC 75 1976. Theory and Results. Nottingham: Pafec Ltd..
- 10. A.G. KEIGHTLEY 1980 University of Loughborough, Technical project report. Finite element modelling of the Perkins 4.236 sump pan.

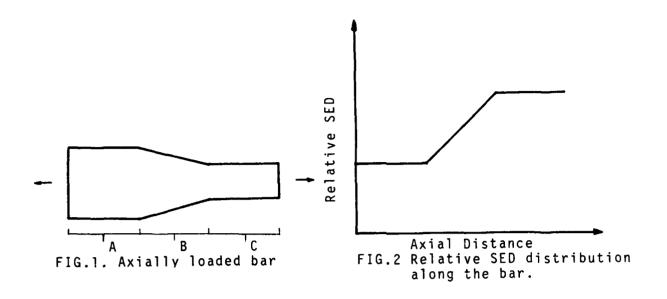
11. G.L. TURNER 1983 Ph.D Thesis University of Loughborough. Finite element modelling and dynamic substructuring for prediction of diesel engine vibration.

TABLE 1
Predicated frequencies for the first mode of vibration of a cantilever beam.

Mesh	Number of Elements	Frequency Hz
Initial (Fig.4a)	80	45.9
Synthesised (Fig.4c)	190	35.9
Uniform (Fig.4d)	240	37.2
<u> </u>	<u> </u>	

TABLE 2
Predicted frequencies for different mesh topologies.

Mode		Frequ	uency Hz			
No.	Experimental	Initial Mesh	Initial Mesh	3,4 noded Elements		
		,,,,,,,,,,,,,,,,,,,,,,,,,,,,,,,,,,,,,,,	6,8 noded		Second Re fineme nt	Third Refinement
5	417	541	476	516	513	510
6	494	703	525	601	576	569



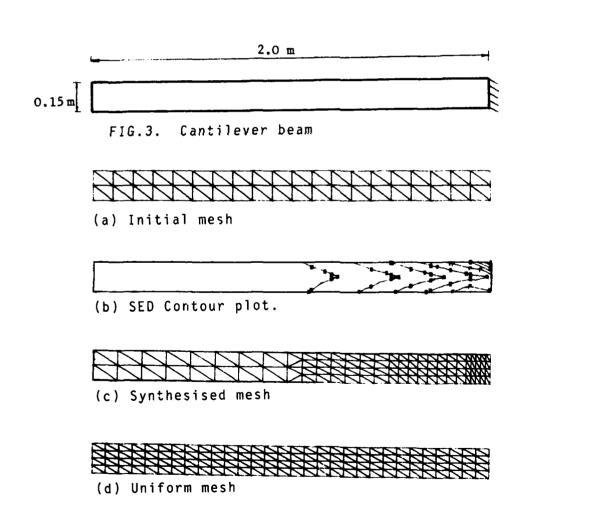
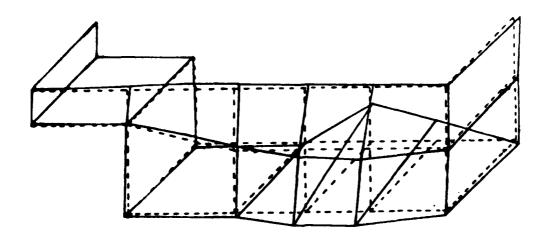
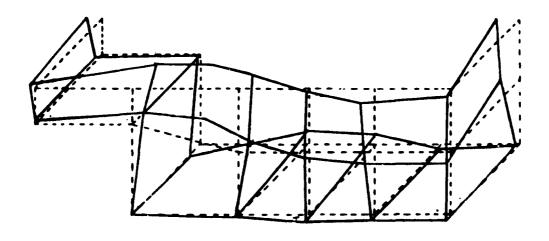


FIG.4. Element meshes for the Cantilever beam

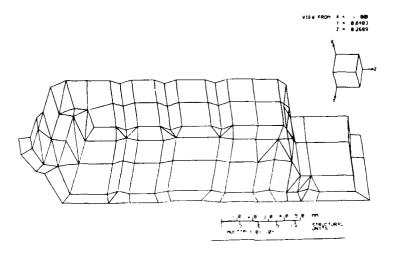


(a) Fifth Mode

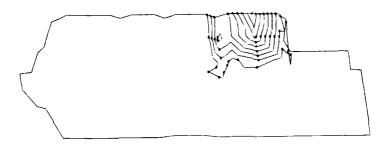


(b) Sixth Mode

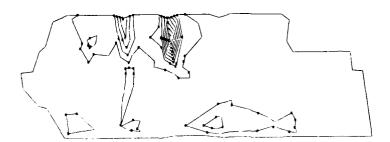
FIG.5. Modes of vibration of the Sump Pan



(a) Initial Mesh

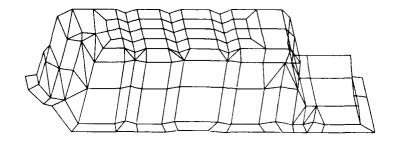


(b) Contour plot of the fifth Mode

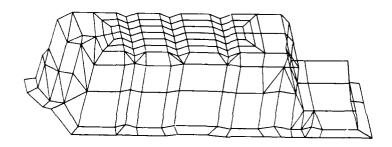


(c) Contour plot of the sixth Mode

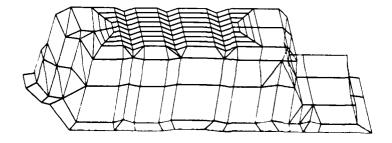
FIG.6. Initial finite element model



(a) First refinement



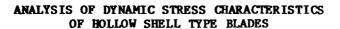
(b) Second refinement



(c) Third refinement

FIG.7. Refined finite element model







J Thomas and S H Abdulrahman

Department of Mechanical Engineering University of Surrey, Guildford, Surrey, UK

1. ABSTRACT

A superparametric parabolic shell element specially adapted for dynamic conditions is utilised to analyse the vibration characteristics and dynamic stresses in a hollow aerofoil and symmetrical shell type turbine blades. The efficiency of the element developed is investigated and is shown to be superior to other available elements. Various results are presented to establish the dependence of the frequency on the geometric parameters. Relative principal stress distributions on a hollow turbine blade, for various modes of vibration, are presented indicating the variation of the point of maximum dynamic stresses with mode order. These points are the critical points where the fatigue cracks may originate leading to the final destruction.

2. INTRODUCTION

The continuous advancement in technology in the fields of aeronautics and space, demands high performance and reliability of every engineering components. In turbomachinery the blades have been of interest to designers for a few decades as they are subjected to severe dynamic environments. The need to obtain higher efficiency has necessitated the working temperature of the gas turbines to the limits of the materials used in these turbines. The use of hollow blades where gases at a lower temperature can be passed through to maintain the temperature within safe limits become an essential part in the design feature of the blades. It is essential to have an understanding of the dynamic behaviour of such blades at the design stage.

Several analytical and numerical methods have been developed, one of the most successful one's being the finite element method. A number of different types of elements were developed and used by various authors in the study of the behaviour of thin shells. Some of the early attempts were to use flat plate elements, cylindrical and doubly curved elements developed from thin shell theory. The development of three dimensional isoparametric element gave a more realistic method of analysing the dynamic characteristics of shells.

The three dimensional isoparametric element with numerical integration was successfully used by Ergatoudis, Irons and Zienkiewicz [1,2] representing the geometry as shell segments. This element gave good results for most of the problems, but it was found to be overstiff when applied to thin shell situations. Zienkiewicz, Taylor and Too [3] modified and improved the element to overcome the overstiffness and relaxed the element by using the reduced integration technique which was presented by Too [4]. Thomas and Mota Soares (5,6) developed the superparametric parabolic shell element such that it became applicable to non-linear dynamic analysis of shells and dynamic analysis of prestressed and rotating shell structures.

Ucmaklioglu [7], Ucmaklioglu and Gill [3] have studied the application of isoparametric eight noded and ten-noded finite elements to represent shell structures having geometries with deep curvatures or with sharp connections. Attention was given to the effect of different numbers of integration points on the performance of these elements. Finally, the element was applied to predict

PROCEEDINGS OF THE INTERNATIONAL CONFERENCE ON RECENT ADVANCES IN STRUCTU. (U) SOUTHAMPTON UNIV (ENGLAND) INST OF SOUND AND VIBRATION RESEAR. H PETYT ET AL. 1984 ND-R143 300 3/5 UNCLASSIFIED NL



MICROCOPY RESOLUTION TEST CHART NATIONAL BUREAU OF STANDARDS-1963-A the natural frequencies of oval cross-section and aerofoil cross-section hollow blading. Al-Jumaily [9] and Al-Jumaily and Faulkner [10] developed an analytical technique in which closed form solutions based on thin shell theory was used to investigate the vibration characteristics of straight long hollow symmetrical blades of uniform cross-section. Surana [11] was the first to introduce the development of isoparametric transition finite elements in connection with cross-sectional properties of stress analysis of beams. Later Surana [12] extended the concept and applied the transition isoparametric element for axisymmetric stress analysis. Furthermore Surana [13] presented an isoparametric formulation for three dimensional transition elements and applied it to solid elements and curved shell elements. It was also applied to three dimensional stress analysis problems to demonstrate its accuracy.

A superparametric parabolic shell element is used in the investigations presented in this paper. Reduced integration technique and an eigenvalue economiser is used to reduce the overall matrix size in the resulting eigenvalue problem. A smoothing technique is used in the evaluation of the stresses at the nodal points of the element based on the values at the gaussian points used in the integration process.

3. THEORETICAL CONSIDERATIONS

A typical superparametric parabolic shell element with nodes at four corners and one at midpoints on each side is shown in Fig.1. The element is referred to a set of curvilinear local non-dimensional coordinates ξ,η,ζ and a global catesian coordinates x,y,z. Also a local set of cartesian coordinates x',y',z' are uniquely defined. The coordinates x,y,z are related to the coordinates x',y',z' by a variable transformation matrix θ .

The displacements U,V,W within each element in directions x,y,z,respectively are given by,

where $N_i(\xi,\eta)$ are the shape functions, U_i,V_i,W_i are the displacements at Node i and α_i,β_i are the rotations about the unit vectors V_{li} and $-V_{2i}$ respectively.

The global coordinates x,y,z are related to the curvilinear coordinates by

$$\begin{cases} x \\ y \\ z \end{cases} = \sum_{i=1}^{n} N_{i}(\xi, \eta) \begin{cases} x_{i} \\ y_{i} \\ z_{i} \end{cases} + \sum_{i=1}^{n} N_{i}(\xi, \eta) \frac{\zeta}{2} \overrightarrow{V}_{3i}$$
(2)

where x_i, y_i, z_i are the coordinates at node i and \vec{v}_{3i} is the thickness vector at node i.

The equation (1) can be written as
$$\begin{cases} \mathbf{V} \\ \mathbf{V} \end{cases} = \begin{bmatrix} \mathbf{N} \\ \mathbf{I} \end{bmatrix} \begin{bmatrix} \mathbf{N}_2 \\ \mathbf{N}_3 \end{bmatrix} \begin{bmatrix} \mathbf{N}_3 \\ \mathbf{N$$

3.1 Dynamic Stiffness and Mass Matrices

The strain energy of an element can be expressed as.

S.E. =
$$\frac{1}{2} \int_{\text{vol}} \left\{ \varepsilon' \right\}^{\text{T}} \left[D' \right] \left\{ \varepsilon' \right\} d\text{vol}$$
(5)

The elastic properties [D'] and the strain vector \mathbf{e}' can be decomposed into two parts, inplane and out of plane, such that,

S.E. =
$$\frac{1}{2} \int_{\text{vol}} \left[\left\{ \varepsilon_{\text{m}}' \right\}^{\text{T}} \left[D_{\text{m}}'' \right] \left\{ \varepsilon_{\text{m}}' \right\} + \left\{ \varepsilon_{\text{s}}' \right\}^{\text{T}} \left[D_{\text{s}}' \right] \left\{ \varepsilon_{\text{s}}' \right\} \right]_{\text{dvol}} \dots (6)$$

On transforming the local displacement vector to global coordinate system, the strain can be written as

strain can be written as $\{\varepsilon'\} = [G][\theta] \{V\}$ (7) Using equations (1),(3) and (7) the strain energy of the element be expressed as

S.E =
$$\frac{1}{2} \left\{ q \right\}^T \int_{\text{Vol}} \left[B_L \right]^T \left[D' \right] \left[3_L \right]^T \text{ dvol } \left\{ q \right\}$$
(8)

where $B_L = [G][\Theta]^T[N]$ The stiffness matrix of the element is $[K] = \int_{\text{Vol}} [B_L][D][B_L]$ dvol

It is more convenient to define the submatrix of the stiffness matrix in the

 $K_{ij} = \int_{-1}^{+1} \int_{-1}^{+1} \int_{-1}^{+1} \left[B_{i} \right] \left[D_{j} \right] \left[J \right] d\xi d\eta d\zeta$

[J] is the Jacobian of the transformation from the global cartesian to curvilinear coordinates. This equation is numerically integrated using Gaussian quadrature using a 2 x 2 array of Gaussian points.

The kinetic energy of the element is given by

$$K.E. = \frac{1}{2} \left\{ \dot{\mathbf{q}} \right\}^{T} \int_{vol} \rho \left[\mathbf{N} \right]^{T} \left[\mathbf{N} \right] dvol \left\{ \dot{\mathbf{q}} \right\}$$
(11)

On transforming the volume from the cartesian to the curvilinear coordinate axes system the mass matrix of the element can be expressed as,

$$[M] \approx \int_{-1}^{+1} \int_{-1}^{+1} \int_{-1}^{+1} \rho[N]^{T}[N][J] d\xi d\eta d\zeta$$

 $M_{ij} = \int_{-1}^{+1} \int_{-1}^{+1} \int_{-1}^{+1} \rho \left[N_{i} \right]^{T} \left[N_{j} \right] \left[J \right] d\xi d\eta d\zeta$ and the submatrix as

This equation is integrated numerically using a 3 x 3 Gaussian mesh

The eigenvectors giving the nodal displacements and the eigenvalues giving the frequencies of vibration of the whole structure are obtained by solving the eigenvalue problem generated by the assembly of the element matrices to represent the whole structure.

3.2 Stress Evaluation

The strain components in the orthogonal local axes system for a shell is given by

$$\{ \boldsymbol{\varepsilon'} \} = \left[\boldsymbol{\varepsilon_{x}'} \quad \boldsymbol{\delta_{y}'} \quad \boldsymbol{\delta_{y}'} \quad \boldsymbol{\delta_{y}'} \quad \boldsymbol{\delta_{x}'} \quad \boldsymbol{\delta_{x}'} \quad \boldsymbol{\delta_{x}'} \quad \boldsymbol{\delta_{x}'} \quad \boldsymbol{\delta_{y}'} \quad \boldsymbol{\delta_{y}'} \quad \boldsymbol{\delta_{y}'} \quad \boldsymbol{\delta_{z}'} \right]^{T}$$

$$= \left[\boldsymbol{\delta_{x}'} \quad \boldsymbol{\delta_{y}'} \quad \boldsymbol{\delta_{y}'} \quad \boldsymbol{\delta_{y}'} \quad \boldsymbol{\delta_{x}'} \quad \boldsymbol{\delta_{x}'} \quad \boldsymbol{\delta_{x}'} \quad \boldsymbol{\delta_{z}'} \quad \boldsymbol{\delta_{y}'} \quad \boldsymbol{\delta_{z}'} \right]^{T} \qquad (13)$$

The stress corresponding to these strains are defined by

where {ε' represents any initial strains.

Using equations (3) and (9) the equation (15) can be expressed as,
$$\{\sigma'\} = [D'][B']\{q\}$$
 (16)

The values of {q} for the whole structure are available as the eigenvectors of the eigenvalue problem solved for the free vibration of the structure. Using these eigenvalues the local stress components at any point within the structure can be evaluated from the equation (16) by assigning the coordinate values of the point under consideration. However the principal stresses at those points are of more importance than the components of the stresses along the coordinate axes. The stress calculation give a more accurate value at the Gaussian points used in the intregration process. The stresses at the nodal points can, however, be obtained by using a smoothing technique.

4. RESULTS AND DISCUSSIONS

The superparametric parabolic shell element developed was applied to the study of vibration characteristics of hollow blades in the first instance. The cross-sectional views of the blades and dimensions are given in Fig 2 and Fig 3.

Table 1 shows the frequencies of vibration of a hollow blade of aerofoil cross-section shown in Fig 2. The length of the blade is 0.2m. The fast convergence characteristics of the superparametric element clearly indicates that better results can be obtained with fewer number of elements than that would be required from an isoparametric element. Fig 4 shows the modeshape of vibration of the hollow aerofoil blade for the first six modes. From the figure it can be seen that there is considerable distortions in the cross-section of the blade which would induce high stresses at various points across its section.

Table 2 shows the comparison of frequency values obtained by the present element and those obtained by using isoparametric element for a blade of 0.4m length. It can be seen that the convergence is very rapid as the number of elements increases and also that the results obtained from a 9×3 superparametric elements are better than that obtained by a 9×10 isoparametric element. Fig 5 shows the modeshape of vibration of an aerofoil blade of length 0.4m and of cross-section shown in Fig 2. The nodal lines show a very different pattern from that of Fig 4 which was for a blade of length 0.2. The comparison of Fig 4 and Fig 5 illustrates the effect of blade length or the aspects ratio on the vibration characteristics of the blades.

Table 3 compares the calculated values of the frequencies of vibration of a hollow blade of symmetrical cross-section shown in Fig 3. The calculated results are obtained from a mesh of 8 x 5 having an overall degree of freedom of 600. The theoretical results show good agreement with the experimental results for all modes considered. Fig 6 shows the modeshape of the corresponding modes of vibration. The distortions in the cross-section of the blade under certain modes of vibration is illustrated.

The relative stress distributions in the blade of hollow symmetric cross-section shown in Fig 3 are given in Fig 7. The values of the stresses given are the principal stresses at the nodal points of the element mesh. The absolute value of the stresses cannot be obtained until the absolute value of the eigenvectors can be obtained which in turn requires the magnitude and characteristics of the forces applied to the blade. However the relative stress distributions given in the figure would indicate the points of high stresses and those points where fatigue cracks are likely to originate under continued operation. This would give the designer a good estimate of the durability of the machinery under operating conditions.

REFERENCES

- 1. I. ERGATOUDIS, B.M. IRONS and O.C. ZIENKIEWICZ 1968 Institute of Civil Engineering, Proc. Symp. on Arch Dams. Three Dimensional Analysis of Arch Dams and their Foundations.
- 2. I. ERGATOUDIS, B.M. IRONS and O.C. ZIENKIEWICZ 1968 Int. Journal of Solid Structures Vol.4, 31-42. Curved, Isoparametric, 'Quadrilateral' Elements for Finite Element Analysis.
- O.C. ZIENKIEWICZ, R.L. TAYLOR and J.M. TOO 1971 Int. Journal of Num. Meth. in Engineering Vol.3. Reduced Integration Technique in General Analysis.
- 4. J.M. TOO 1971 Ph.D. Thesis, University College, Swansea. Two Dimensional Plates, Shells and Finite Prism Isoparametric Elements and Their Applications.
- J. THOMAS and C.A. MOTA SOARES 1973 ASME Paper No. 73-DET-94 Design Engineering Technical Conference. Finite Element Analysis of Rotating Shells.
- 6. J. THOMAS and C.A. MOTA SOARES 1976 Cambridge University, International Conference on Vibrations in Rotating Machinery. Dynamic Analysis of Rotating Turbine and Compressor Blading.
- 7. M. UCMAKLIOGLU 1978 Ph.D. Thesis, University of Durham. Vibration of Shells with Application to Hollow Blading.
- 8. P.A.T. GILL and M. UCMAKLIOGLU 1979 Journal of Sound Vibration Vol.65, No.2, 259-273. Isoparametric Finite Elements for Free Vibration Analysis of Shell Segments and Non-Axisymmetric Shells.
- 9. A.M. AL-JUMAILY 1977 Ph.D. Thesis, Ohio State University. Vibration of Complex Structures by Matching Spatially Dependent Boundary Conditions of Classical Solutions.
- 10. A.M. AL-JUMAILY and L.L. FAULKNER 1978 ASME Trans. Vol.100, No.1, 183-187. Vibration Characteristics of Hollow Symmetrical Blades Based on Thin Shell Theory.
- 11. K.S. SURANA 1979 Int. Journal Num. Meth. Engineering Vol.14, 475-497. Isoparametric Elements for Cross-sectional Properties and Stress Analysis of Beams.
- 12. K.S. SURANA 1980 Int. Journal Num. Meth. Engineering Vol.14. Transition Finite Elements for Axisymmetric Stress Analysis.
- 13. K.S. SURANA 1980 Int. Journal Num. Meth. Engineering Vol.15. Transition Finite Elements for Three Dimensional Stress Analysis.

TABLE.1. Variation of natural frequencies (Hz) of free vibration of hollow aerofoil blade (length, a = 0.2m, width, b · 0.2m, wall thickness, h = 0.002m) Cross-section shown in Fig.2)

TABLE 2. Variation of natural frequencies (Hz) of free vibration of hollow aerofoil blade (length, a = 0.4 m, width, b = 0.2 m, wall thickness, h = 0.002 m; cross-section shown in Fig.2)

		Frequencies (Hz)	s (Hz)	
Mode No.	Super-pa (Mesh, I	Super-parametric element (Mesh, DOF, Master DOF)	يد	Isoparametric element Ucmaklioglu
	(9 x 1, 135, 27)	(9 x 2, 270, 54)	(9 x 3, 405, 81)	(9 × 10,600,160
	418.019	394.418	383.573	384
7	627.396	606.735	598.864	265
٤	880.293	770.283	756.205	797
4	1060.966	960.654	922.984	1052
s	1202.134	1127.040	1078.040	1070
٠	1783.598	1218.925	1183.694	•
7	1914.847	1658.200	1560.143	1
∞	2145.031	1673.061	1603.043	ı
6	2419.801	1916.117	1829.751	1
10	3582.219	2050.423	1945.154	,

		Frequencies (Hz)	(Hz)	
MODE	Superpa (mesh,	Superparametric element (mesh, DOF, Master DOF)	it)F)	Isoparametric element Ucmaklioglu
8	(9 x 1,135,27)	(9 x 2, 270, 54)	(9 x 3,405,81)	(9×10,600,160)
-	214.566	200.256	196.695	199
2	298.629	277.896	270.304	244
2	482.470	450.002	439.313	470
4	734.217	569.988	524.436	545
s	881.345	723.963	717.836	ı
9	1034.149	851.547	829.690	861
7	1246.410	887.487	844.757	1
00	1763.774	1007.722	927.125	1
6	1846.506	1090.304	1055.317	1
10	2156.448	1523.556	1079.567	1

TABLE 3 Comparison of natural frequencies of symmetrical hollow cantilever blades of cross-section in Fig. 3 a = 0.3048 m, b = 0.0762 m, h = 0.00085 m R₁ = 0.0508 m, R₂ = 0.0762, C₂-C₁ = 0.0317 m E = 2.07 x 10¹¹ N/m², p = 7834 kg/m³

0	Geometrical r	odes
•	Displacement	node

MODE No.	Theoretical freq. (Hz) (8x5, 600)	Experimental freq. (Hz)	Error
1	152.305	148	2,82
2	474.204	486	2.4B
3	705.016	-	-
4	707.289	711	-0.0052
S	813.035	793	2.46
6	816.731	813	0.0045
•	1082.985	1065	1.66
8	1460.789	1441	1.35
9	1739.594	1756	-1.10
10	1864.552	1845	1.04
11	1972.412	-	-
12	2016.144	2039	-1.12
1 3	2051.921	2066	-0.0068
14	2481.543	2428	2.15

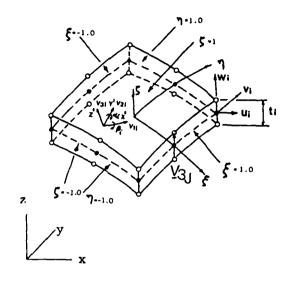


Fig. 1 Super-parametric parabolic shell element

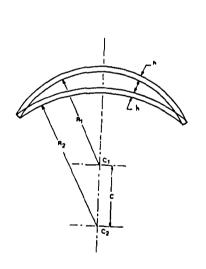
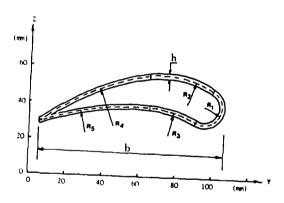
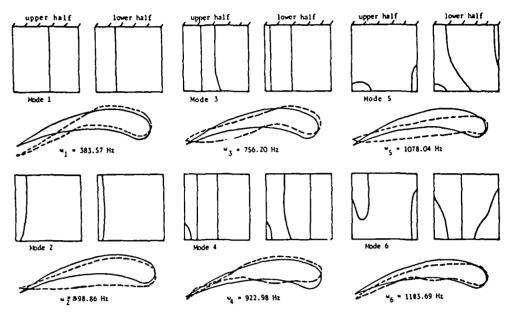


Fig. 3 Crescent cross-section hollow blading



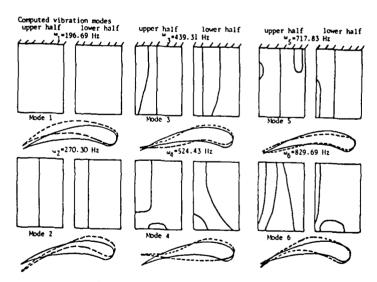
Subscript	Radius R (mm)	ofcen Y(men) 2(men	tre
1	17.4	186.1 38.	
:	91.9	143.0 -22.4	
5	127.0	117.0 -85.6	,
,	331.8	188.5 -257.	4
5	253.7	109.0 -212.	5

Fig. 2 Geometry of the cross-section of the aerofoil hollow blade



Finite element model of $(9 \times 3, 405, 81)$

Fig. 4 Vibration modes of aerofoil hollow blade of 0.2 m



Finite element model of (9 \times 3, 405, 81)

Fig. 5 Vibration modes of aerofoil hollow blade of 0.4 m

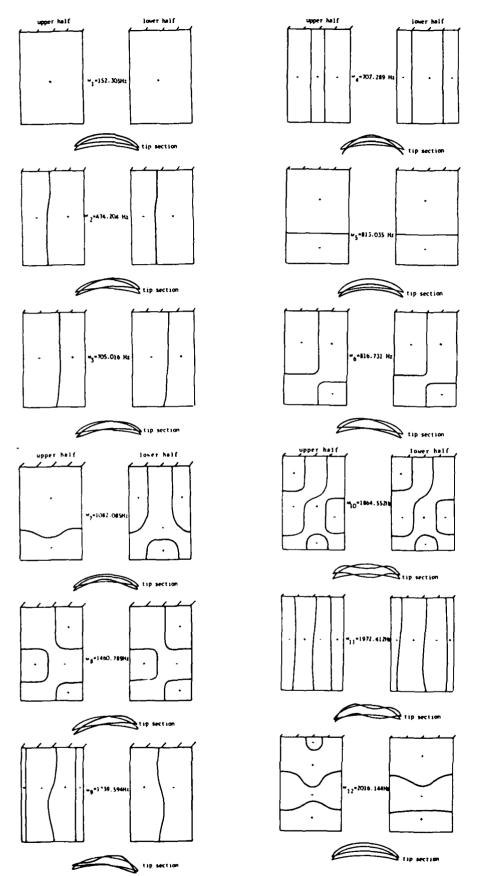
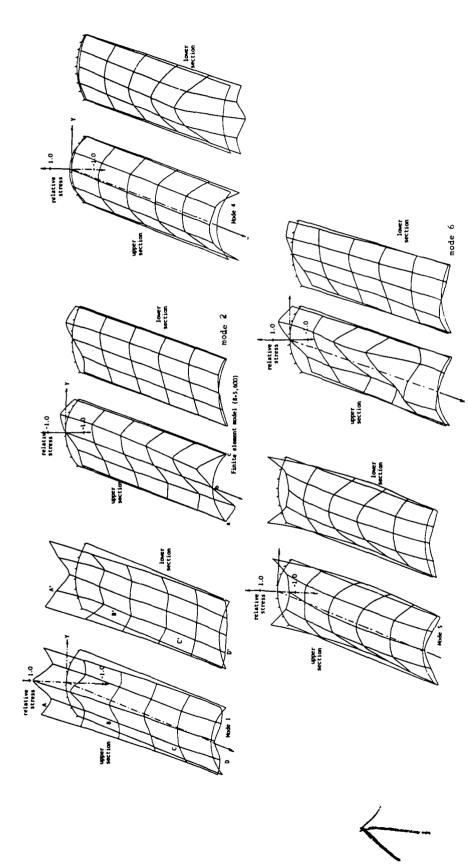


Fig.6. Vibration Modes of hollow blades of cross-section shown in Fig. 3



Relative dynamic stress distribution of symmetrical hollow blade (a=0.3048m, b=0.0762 m, R_1 =0.0508m, R_2 =0.0762m) Fig. 7.

AD-P003 657.



SOME RECENT ADVANCES IN DYNAMIC RESPONSE OF SHELLS

Rakesh K. Kapania and T.Y. Yang

School of Aeronautics and Astronautics Purdue University, West Lafayette, Indiana 47907 U.S.A.

1. \ INTRODUCTION

Thin shell structures, during their operational life, are often subjected to dynamic loads that can be both deterministic and nondeterministic. For a cost effective and reliable design it is important that an accurate dynamic response analysis be performed. An account of the analytical methods for shell analyses was given, for example, by Soedel [1].) For complex shell geometries and complex loading conditions, the finite element method has become an attractive option as a method of analysis.

Many investigators have used the finite element method to study the deterministic response of shells. A brief review of these efforts was given by Chang, Yang, and Soedel [2]. They used the modal superposition method to study the transient response of a series of examples. An alternative to the above method is to use the direct integration methods to solve the governing equations of motion [3]. Suryoutomo, Gould and Basu [4] employed this method to study the transient response of revolution shells. Both these studies used the rotational-type shell elements for modeling the shells.

In this study, both the aforementioned methods were used in conjunction with a 48 d.o.f. doubly curved quadrilateral shell element [5] for the transient analyses of shells. These developments were first verified through comparison of results with those of a spherical cap [2,4] and were subsequently applied to perform a time domain (Monte-Carlo simulation) analysis of a cooling tower under wind loads.

The development in the research of random response of continuous structures has had a long history [6]. A review of the applications of the analytical methods to perform random response of shells is given in reference [7]. In the previous analytical studies, the shapes of the shell structures were generally cylindrical or spherical and the correlation function of the loads were generally purely random in time and space or random in time only. It was possible to find the statistics of the responses in an analytical fashion. For more complex shell geometry and more complex correlation function of the loads which are random both in time and space, numerical methods may be desirable. An apparent choice appears to be the development of a basic formulation that uses finite elements to model the complex shell and Gaussian quadrature to integrate the cross-spectral density function. An account of the efforts in finite element developments before 1972 on the studies of the random responses of continuous structures was given by Olson and Lindberg [8].

Olson and Lindberg [8] developed a consistent finite element method for analyzing the random response of complex structures. The method was based on the standard modal approach using the mode shapes obtained from finite element solution. A linear polynomial representation over each finite element of the excitation cross spectral density function was introduced. Thus the spatial integrations involved in evaluating the modal force cross spectral matrix could be carried out in closed form. Dey [9] used a lumped load method to convert the pressure cross spectral density into the matrix of the cross spectral density of nodal forces. The approach assumed that the same random force acts on the entire contributing area around a node with full correlation.

Thus far, the application of the finite element methods to random response problems has not included shell elements [8,9]. In this study, the random response problem was formulated using the 48 d.o.f. quadrilateral doubly curved shell element [5]. Here, the displacement shape functions were used to formulate the consistent or work-equivalent generalized nodal loads based on the random distributed pressure. Gaussian quadrature was used which allows the use of the spectral density function in its original form instead of an approximate linear polynomial form [8]. The displacement shape functions were used to interpolate the spectral density values at an arbitrary pair of points within two individual shell elements from the element nodal values. In reference [9], the random forces acting on the area associated with each nodal point were assumed to be fully correlated. Such assumption was not made in this study.

The present formulation and integration procedures were first verified through comparison of results with those of a simply supported cylindrical panel under purely random loads [10] and were subsequently applied to study response of a cooling tower subjected to wind loads. Results were obtained, based on quasi-steady aerodynamic theory and Davenport's spectrum [11].

2. METHOD OF ANALYSIS

2.1 The Shell Finite Element

The shell finite element used in the present study is shown in Fig. 1. The element is a quadrilateral defined by lines of principal curvature; thus it is rectangular in the local curvilinear coordinate system. The equations are specialized to general shells whose reference surfaces are a portion of an axisymmetric surface. An array of eight mapping points specifies a cubic variation of R and Z in the meridional direction. The element possesses 12 d.o.f.'s at each of the four vertices: u; $\partial u/\partial \xi$; $\partial u/\partial \eta$; $\partial^2 u/\partial \xi \partial \eta$; v; $\partial v/\partial \xi$; $\partial v/\partial \eta$; $\partial^2 v/\partial \xi \partial \eta$; w; $\partial w/\partial \xi$; $\partial w/\partial \eta$ and $\partial^2 w/\partial \xi \partial \eta$. The displacement components u, v, and w are in meridional, circumferential and normal-to-surface directions, respectively. The displacement functions for u, v and w were assumed to be of the same form, each consisting of a bicubic Hermite polynomial in ξ and η directions. The detailed derivation of the stiffness, mass and incremental stiffness matrices can be found in [5] where the element was applied to perform static, vibration and buckling analyses of cooling towers and other shells of revolution.

2.2 Deterministic Response Analysis

The equations of motion for an elastic, viscously damped system subjected to dynamic loads may be written as

$$[K]{q} + [C] {\dot{q}} + [M] {\dot{q}} = {F(t)}$$
 (1)

in which $\{q\}$ is the vector of the system's nodal degrees-of-freedom, the dot represents differentiation with respect to time; [K], [M] and [C] are, respectively, the stiffness, mass and damping matrices, and $\{F\}$ is the vector of the generalized nodal forces. The vector $\{q\}$ can be determined by using either modal superposition or the direct integration method [3]. Both methods were employed in this study. For the latter case, Wilson- θ method with θ =1.4 was used.

2.3 Random Response Analysis

The basic method for computing cross spectrum of random response of a continuous structure subjected to stationary, correlated (in time and space) distributed loads was given by, among others, Lin [6]. The cross spectral density of a response quantity q at two points \mathbf{r}_1 and \mathbf{r}_1 , is given as

$$\phi_{qq} (\vec{r}_1, \vec{r}_2; \omega) = \sum_{j} \sum_{k} f_{j}(\vec{r}_1) f_{k}(\vec{r}_2) H_{j}(\omega) H_{k}^{*}(\omega) I_{jk}(\omega)$$
(2)

where $f_{i}(\vec{r})$ is the <u>j</u>th undamped natural mode, and

$$H_{j}(\omega) = m_{j}^{-1} (\omega_{j}^{2} - \omega^{2} + 2i\zeta_{j}^{2} \omega\omega_{j}^{2})^{-1}$$
(3)

is the complex admittance for jth mode, the symbols m_j, ω_j ζ_j are the generalized mass, natural frequency and effective damping for the jth mode. The cross-spectral density function for the generalized forces for the modes j and k is

$$I_{jk} = \int_{D} \int_{D} \phi_{pp} (\vec{\rho}_{1}, \vec{\rho}_{2}; \omega) f_{j} (\vec{\rho}_{1}) f_{k} (\vec{\rho}_{2}) d\vec{\rho}_{1} d\vec{\rho}_{2}$$
(4)

where the integrations are extended over the entire domain D and ϕ_{pp} $(\stackrel{\rightarrow}{\rho}_1,\stackrel{\rightarrow}{\rho}_2;\omega)$ is the cross-spectral density of the random excitation pressure and must be known.

Once the spectral density $\phi_{qq}(\omega)$ is obtained, many important statistics of q(t) can be determined. For a Gaussian random process, the response is also a Gaussian process. For this, it is sufficient to determine only up to second order statistics, i.e. mean and standard deviation. For a zero-mean excitation, the response is also a zero-mean process. For a non-zero mean excitation, the response can be obtained by superimposing two components: (a) static component due to the mean value of excitation; and (b) dynamic component due to the zero mean fluctuating part of the excitation. The variance or standard deviation of the response is given as

$$\sigma_{\mathbf{q}}^{2} = \int_{-\infty}^{\infty} \phi_{\mathbf{q}\mathbf{q}}(\omega) d\omega \tag{5}$$

Because of the difficulties encountered in performing the integration in equation (4), it may be desirable to use the finite element method. In this method, the matrix of cross-spectral densities of various nodal quantities is given as

$$[\Phi_{\mathbf{q}\mathbf{q}}(\omega)] = [H(\omega)][\Phi_{\mathbf{p}\mathbf{p}}(\omega)][H^{\star}(\omega)]$$
(6)

where $[H(\omega)]$ is the matrix of frequency response functions and $[\phi_{pp}(\omega)]$ is the matrix of the cross-spectral densities of the generalized nodal forces. A method of determining this, using Gaussian quadrature procedure, is presented here.

For the present element, the consistent load vector, after using Gaussian quadrature procedure based on MxN grid points, is given as

$$\{F(t)\} = \sum_{i=1}^{NE} [T]_{i} \sum_{k=1}^{M} \sum_{\ell=1}^{N} [N_{i}(r_{k\ell})] \{p_{i}(r_{k\ell};t)\}$$

$$R_{\theta_{i}}(r_{k\ell})R_{\phi_{i}}(r_{k\ell})|J_{i}(r_{k\ell})|W_{k}W_{\ell}$$
(7)

where i is the element number; NE is the number of elements; [T] transforms all the 48 nodal quantities including the consistent nodal loads from element curvilinear coordinates to global coordinates; p(ξ , n;t) is a 3xl column vector containing the distributed loads associated with u, v, and w related d.o.f.'s, respectively; R₀ and R₀ are the radii of curvature in corcumferential and meridional directions, respectively; |J| is the Jacobian of the coordinate transformation; r_{kl} represents the location of the Gaussian integration point at (ξ _k, n_l); and W_k and W_l are the two weight factors.

The correlation matrix for the generalized nodal forces can be obtained by taking the expectation (denoted by E) of the cross product of the generalized

force vectors at two instants. For the present case, it is given as

$$[R_{FF}(t_{1},t_{2})] = \sum_{i=1}^{NE} [T]_{i} \sum_{k=1}^{M} \sum_{\ell=1}^{N} [N_{i}(r_{k\ell})] R_{\theta_{i}}(r_{k\ell}) R_{\phi_{i}}(r_{k\ell}) |J_{i}(r_{k\ell})|$$

$$W_{k}W_{\ell} \sum_{j=1}^{NE} \sum_{m=1}^{M} \sum_{n=1}^{N} E[\{p_{i}(r_{k\ell};t_{1})\}\{p_{j}(r_{mn};t_{2})\}^{T}[N_{j}(r_{mn})]^{T}$$

$$[T]_{j}^{T} R_{\theta_{j}}(r_{mn}) R_{\phi_{i}}(r_{mn}) |J_{j}(r_{mn})| W_{m}W_{n}$$
(8)

In this study, the tangential loads are neglected. Thus the 3x3 matrix [R] resulting from E[{p_i}{p_j}^T] contains all zero terms for R₃₃ or R_{pp}, which is the correlation function for the normal pressure. For the stationary normal pressure, the correlation function R_{pp}(t₁,t₂) is independent of the time origin and is a function of time shift $\tau(=t_2-t_1)$ only. The left hand side of equation (8) becomes [R_{FF}(τ)].

The matrix of cross-spectral densities of the generalized nodal forces can be obtained by taking the Fourier transform of the $R_{FF}(\tau)$ matrix [6]. Thus, taking the Fourier transformation of equation (8) and eliminating the shape functions and correlating coefficients for tangential loads related to u and v displacements give

$$[;_{pp}(\omega)] = \sum_{i=1}^{NE} \sum_{k=1}^{M} \sum_{\ell=1}^{N} \sum_{j=1}^{NE} \sum_{m=1}^{M} \sum_{n=1}^{N} [T]_{i} \{N_{3}(r_{k\ell})\} R_{\theta_{i}}(r_{k\ell}) R_{\phi_{i}}(r_{k\ell})$$

$$|J_{i}(r_{k\ell})| W_{k} W_{\ell} \{N_{3}(r_{mn})\}^{T} [T]_{j}^{T} R_{\theta_{j}}(r_{mn}) R_{\phi_{j}}(r_{mn}) W_{m} W_{n}$$

$$|J_{j}(r_{mn})| \phi_{pp}(r_{k\ell_{i}}; r_{mn_{j}}; \omega)$$
(9)

where the 48x3 matrix [N] is reduced to a 48x1 column vector and the 3x3 matrix [R] is reduced to one term, all related to w-displacement only. In equation (9), if the cross spectral density of the normal pressure field, $\phi_{pp}(r_{k\ell_i}; r_{mn_i}; \omega)$,

which correlates the Gauss point (ξ_k,η_ℓ) in element i to Gauss point (ξ_m,η_n) in element j is available, the matrix $[\Phi_{DD}(\omega)]$ can be obtained.

The matrix of frequency response functions $[H(\omega)]$ can be obtained either using the direct complex matrix inversion method or using the modal superposition method. Both the methods are described in detail in references [6,10]. The relative merits of the two methods are given in [7].

The cross-spectral density matrix of the displacements, $[\phi_{u_1u_2}]$, and the stress resultants, $[\phi_{\sigma_1\sigma_2}]$ for two arbitrary points, r_1 in element i and r_2 in element j can be obtained by using the 48x3 matrix [N] of displacement functions, the 48x6 strain displacement matrix [B]^T, and the 6x6 stress-strain matrix [D], for the present 48 d.o.f. shell element [5]. The two matrices are given as [7]

$$[\phi_{\mathbf{u}_1\mathbf{u}_1}(\mathbf{r}_1;\mathbf{r}_2;\omega)] = [\mathbf{N}(\mathbf{r}_1)]_{\mathbf{i}}^{\mathbf{T}} [\mathbf{T}]_{\mathbf{i}} [\phi_{\mathbf{q}_1\mathbf{q}_1}(\omega)] [\mathbf{T}]_{\mathbf{j}}^{\mathbf{T}} [\mathbf{N}(\mathbf{r}_2)]_{\mathbf{j}}$$
(10)

$$[\ddagger_{\sigma_1\sigma_2}(\mathbf{r}_1;\mathbf{r}_2;\omega)] = [D] [B(\mathbf{r}_1)]_{\mathbf{i}}^{\mathbf{T}} [T]_{\mathbf{i}} [\phi_{\mathbf{q}_{\mathbf{i}}\mathbf{q}_{\mathbf{j}}}(\omega)] [T]_{\mathbf{j}}^{\mathbf{T}} [B(\mathbf{r}_2)]_{\mathbf{j}} [D]$$
(11)

Equations (10) and (11) thus convert the matrix of the cross spectral densities of generalized nodal displacements [ϕ (ω)] for elements i and j to the cross $q_i q_j$

spectral densities of the displacements and stress resultants at two desired locations: \mathbf{r}_1 in element i and \mathbf{r}_2 in element j.

EVALUATIVE EXAMPLES

3.1 Step Response of a Spherical Cap

A clamped aluminum spherical cap under a step pressure as shown in Fig. 2 was considered. This problem was previously analyzed by using direct integration method in [4] and the modal superposition method in [2]. Due to the axisymmetric nature of the problem only a segment need be modeled. In this scudy, a segment subtending an angle of 5° in the circumferential direction was modeled using a 10x1 mesh. Natural frequencies for the first 7 meridional nodes were found to be in excellent agreement with those obtained by Chang, Yang and Soedel [2]. These 7 modes were used to perform the time history response analysis. The results are shown in Figure 2 along with those obtained using the Wilson- θ direct integration integration method ($\Delta t = 1.0 \times 10^{-5}$ sec.). Both sets of results are in good agreement with each other and also with those of references [2,4].

3.2 A Simply Supported Cylindrical Panel Subjected to Purely Random Loads

The geometric and material data for the cylindrical panel considered is shown in Fig. 3. An analytical solution for this example was given by Nemat-Nasser [10]. In this study, a 4x4 mesh of equal sized elements was used. The results for various natural frequencies for the circumferential wave number n=1, 2,3,4 and the meridional mode number m=1,2,3 were found to be in good agreement with the analytical solution [10] and are given in reference [7]. Response spectral densities were obtained using equations (6), (9), (10), and (11) based on 5x5 Gauss points. Both the direct complex matrix inversion and the modal superposition methods were used. The auto-spectral densities of the normal displacement at the center point with those of reference [10] are shown in Figure 3. The agreement among the three sets of solutions is good. The results for the spectral densities for various stress-resultants were also obtained [7] and excellent agreement was observed between the present results and those of reference [10].

APPLICATIONS

After the above numerical evaluations, the present developments were applied to study the probabilistic response of a fixed base cooling tower subjected to wind loads. The results were obtained using both the frequency domain analysis and the time domain analysis (Monte-Carlo Simulation).

4.1 Frequency Domain Analysis

The cooling tower considered is shown in Figure 4 [4]. Three wind velocities at the throat were considered: 22.35; 33.53; and 44.7 m/sec. The velocity was assumed to vary logarithmically along the height [11]. The cross-spectral density ϕ_{pp} of the pressure field for two points (θ_1,z_1) , and $^{'}\theta_2,z_2)$ was determined from the quasi-steady aerodynamic theory,

$$\phi_{\mathbf{p}\mathbf{p}}(\theta_1, \mathbf{z}_1; \theta_2, \mathbf{z}_2; \omega) = \nu^2 \tilde{\mathbf{V}}_{\mathbf{z}_1} \tilde{\mathbf{V}}_{\mathbf{z}_2}^2 \cdot \mathbf{C}_{\mathbf{p}}(\theta_1) \mathbf{C}_{\mathbf{p}}(\theta_2) \phi_{\mathbf{v}\mathbf{v}}(\theta_1, \mathbf{z}_1; \theta_2, \mathbf{z}_2; \omega)$$
(12)

where \overline{V}_z is the mean wind velocity at height z; ρ is the air density; and $C_p(\theta)$ gives the external normal pressure distribution in θ , which were taken from those obtained from experimental measurements performed on a full scale cooling tower [12]. For the cross spectral density of the velocity fluctuation ϕ_{VV} , Davenport's spectrum was used [7,11]. The wind pressure on the cooling tower was assumed to be symmetrical $(C_p(\theta)=C_p(-\theta))$ about the windward direction $(\theta=0)$ at all times.

Thus only half of the shell need be analyzed. This assumption may, however, not be accurate when the cooling tower is in the wake of other towers or surrounded by other structures in the vicinity. In that case, one has to model the whole shell.

In this study, a 5x5 finite element mesh as shown in Fig. 1 was used to model half of the shell. All the elements have the same subtending angles. The five element layers have the height ratio, starting from base, of 1:2:3:4.08:2.42. The probabilistic response analysis was performed using equations (6) and (9-11) and based on a 4x4 gridpoints for Gaussian quadrature. The damping factor ζ_j was assumed as 0.02 for all modes. Only modal superposition method was used and the 15 lowest natural frequencies and the corresponding modes as given in [7] were used. The results for the auto-spectral densities for the normal displacement at both the top and the throat at θ =0 were obtained for the three wind velocities [7]. The results corresponding to wind velocity of 44.70 m/sec. are shown in Figure 4. Both the curves show a peak at about 0.10 rad./sec. which is due to the peak in the input wind spectra and also show 9 dominant peaks with frequency values corresponding to the natural frequencies of the tower.

The mean values of the responses of the cooling tower were obtained by performing a static analysis based on a static pressure distribution

$$p(z,\theta) = \frac{1}{2} \tilde{V}_{z}^{\theta} \left\{ C_{p}(\theta) - C_{p_{i}} \right\}$$
(13)

where the uniform internal coefficient C $_{\ p_{_{\dot{\mathbf{1}}}}}$ due to internal suction was assumed as

0.4 [12]. The mean values for the normal displacement at the top and throat (at 0=0) were found to be 30.48 and 45.2 mm/ respectively for the wind velocity of 44.7 m/sec. The corresponding values of the standard deviation were found to be 7.62 and 9.91 mm, respectively. The values of the standard deviation were obtained using the trapezoidal rule to integrate the spectral densities following equation (5). The peak and the gust response factors were obtained, respectively, as 3.68 and 1.92 mm at the top and 3.59 and 1.80 mm at the throat. The contours of the mean and standard deviation of the normal displacement and meridional stress resultant are given in [7].

4.2 <u>Time Domain Analysis</u>

Time domain or the so-called Monte-Carlo simulation approach is an alternative to the aforementioned frequency domain analysis method for determining the response statistics. In this technique, a set of sample functions of the random excitation are generated. A deterministic time history response of the shell structure is then performed based on these sample functions. The response statistics can then be obtained by processing an ensemble of the time history responses. For ergodic random processes, however, the required statistics can be obtained from a single, relatively longer, sample function. Such an assumption is made here.

In this study, the sample function of the dynamic component of the pressure at any point on the cooling tower was generated using the ARIMA (Auto-Regressive Integrated Moving Average) models given by Reed and Scanlan [13]. According to this model, the dynamic component of the pressure on a cooling tower is given as

$$p(t) = t_1 p(t-\Delta t) + t_1 p(t-\Delta t) + a(t)$$
 (15)

where ; and \ddagger are the autoregressive parameters; \triangle t was taken as 1 second [13] and a(t) is a Gaussian random shock with mean zero and variance $\frac{1}{a}$. This variance is related to the variance $\frac{1}{p}$ of the pressure fluctuations according to Yule-Walker relation [13].

Based on the values of ϕ_1 and ϕ_2 taken from [13] and the variation of σ_D^2

around the cooling tower taken from [14], a sample function of the excitation pressure was simulated by generating a set of random variables with mean zero and variance σ_a^2 . The response of the cooling tower was then determined for a mean wind velocity of 44.7 m/sec. at the throat and varying logarithmically in the height. The time history of the normal displacement at the top and throat are shown in Figure 5 for 500 seconds of seconds of response. The rms and the peak values of the response were found to be 3.85 and 12.04 mm (t=125.1 seconds) at top and 6.23 and 15.24 mm (t=122.15 seconds) at the throat. The spectral density of the response can be found using the fast Fourier transform.

5. SUMMARY AND CONCLUSIONS

In this study, efforts were made to perform the deterministic and nondeterministic response analyses of shells of revolution using a 48 d.o.f. quadrilateral shell element [5]. For the deterministic analysis, both modal superposition and direct integration methods were used. For the random response analysis, a Gaussian integration scheme was presented to calculate the matrix of the cross spectral densities of the generalized nodal forces. Evaluative examples with highly accurate results were presented. The developments are then applied to study the probabilistic response of a cooling tower subjected to wind loads. These developments can be extended to study the probabilistic response of a general class of thin shells such as hulls of ships and submarines, skin of flight vehicles and earth-based thin shell structures.

ACKNOWLEDGEMENT

This research was supported by the National Science Foundation through grant CEE-8024883. The authors gratefully acknowledge the help from Drs. S.C. Liu, M.P. Gaus, Y.K. Lin and A.J. Schiff.

REFERENCES

- W. SOEDEL 1981 Vibrations of Shells and Plates. New York: Marcel-Dekker, Inc.
- 2. Y.B. CHANG, T.Y. YANG and W. SOEDEL 1983 Journal of Sound and Vibration 86, 523-538. Linear dynamic analysis of revolutional shells using finite elements and modal expansion.
- 3. K.J. BATHE and E.L. WILSON 1976 Numerical Methods in Finite Element Analysis. Englewood Cliffs: Prentice-Hall, Inc.
- 4. H SURYOUTOMO, P.L. GOULD and P.K. BASU 1977 Computers and Structures 7, 425-433. Direct dynamic analysis of shells of revolution using high-precision finite element.
- 5. T.Y. YANG and R.K. KAPANIA 1983 Journal of Engineering Mechanics 109, to appear in Oct. Shell elements for cooling tower analysis.
- 6. Y.K. LIN 1976 Probabilistic Theory of Structural Dynamics. Huntington: Bobert E. Krieger Publishing Company.
- 7. T.Y. YANG and R.K. KAPANIA 1983 Purdue University, School of Aeronautics and Astronautics, Report submitted to National Science Foundation, Wind effects on complex thin shells.
- 8. M.D. OLSON and G.M. LINDBERG 1971 Journal of Aircraft 8, 847-855. Jet noise excitation of an integrally stiffened panel.
- 9. S.S. DEY 1979 Computer Methods in Applied Mechanics and Engineering 20, 173-194. Finite element method for random response of structures due to

stochastic excitation.

- 10. S. NEMAT-NASSER 1968 American Institute of Aeronautics and Astronautics Journal 6, 1327-1331. On the response of shallow thin shells to random excitations.
- 11. E. SIMIU and R.H. SCANLAN 1978 Wind Effects on Structures: An Introduction to Wind Engineering. New York: John Wiley and Sons, Inc.
- 12. N.J. SOLLENBERGER, R.H. SCANLAN, and D.P. BILLINGTON 1980 Journal of the Structural Division 106, 601-621. Wind loading and response of cooling towers.
- 13. D.A. REED and R.H. SCANLAN 1983 Journal of Structural Engineering 109, 538-554. Time series analysis of cooling tower wind loading.
- 14. H. RUSCHEWEYH 1975/76 Journal of Wind Engineering and Industrial Aerodynamics $\underline{1}$, 335-340. Wind loading on hyperbolic natural draught cooling tower.

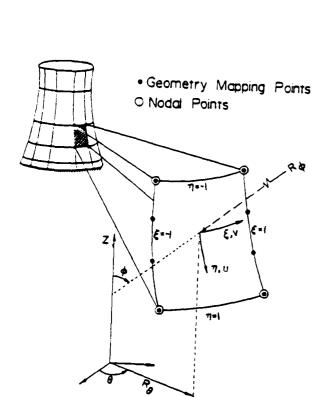


Figure 1. The 48 d.o.f. Doubly-Curved Quadrilateral General Shell Element.

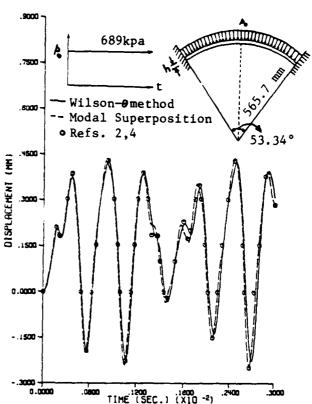


Figure 2. Step Response of a Clamped Aluminum Spherical Cap (E=72.345 G Pa, ρ =2631 kg/m³, and ν =0.3, h=10.4 mm).

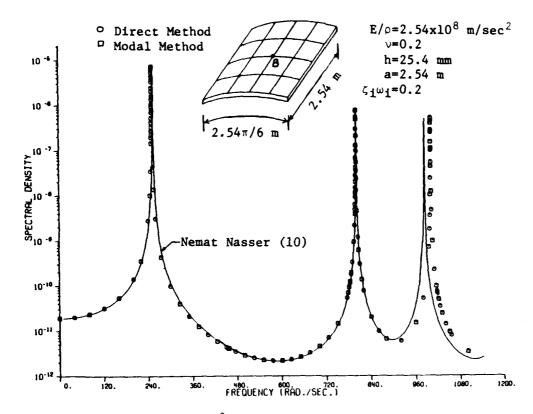


Figure 3. Auto-spectral Density (mm²-Sec./Rad.) of the Normal Displacement at the Center Point B of the S.S. Cylindrical Panel Due to Purely Random Loads.

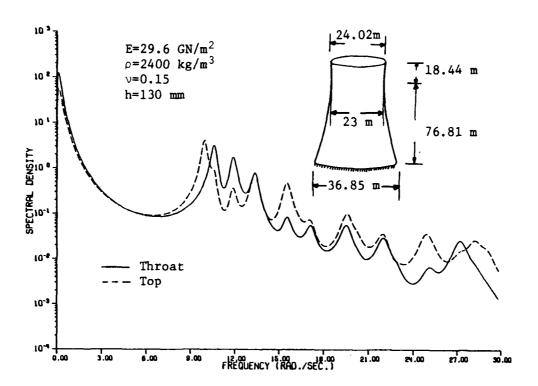


Figure 4. Autospectral Density of the Normal Displacement (mm^2 -Sec/Rad) at the Top and Throat of a Concrete Cooling Tower Due to Wind Velocity of 44.7 m/sec. at Throat.

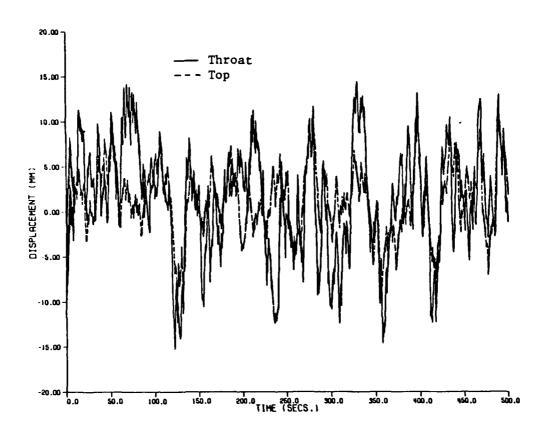


Figure 5. Time History Response of the Normal Displacement at the Top and Throat of a Cooling Tower Due to Simulated Wind Pressure at a Velocity of 44.70 m/sec. at Throat.

4. COMPONENT MODE SYNTHESIS TECHNIQUES



CALCULATION OF EIGENVALUES USING SUBSTRUCTURES AND DYNAMIC CONDENSATION

N. Petersmann

Institut für Mechanik, Universität Hannover Hannover, West Germany

1. \ INTRODUCTION

For the calculation of the dynamic behaviour of complex elastic structures in general the Finite Element method is used. In order to yield good approximations of the system behaviour, the physical model is divided in a large number of finite elements. Consequently, an excessive number of degrees of freedom appear in the idealisation of a complicated structure, but because of the used computer storage capacity it is not always useful, sometimes even impossible, to deal with the resulting large matrices.

In static problems these difficulties are overcome by using substructure techniques and static condensation. The complete structure involving an excess number of degrees of freedom is divided into smaller substructures, where the size of the substructures may be determined by physical considerations or by an admissible number of degrees of freedom. For each of these substructures condensation is carried out so that the behaviour of the substructure is described only by the boundary degrees of freedom and, if necessary, also the degrees of freedom of special interest e.g. force acting points. After assembling the substructures, the complete system contains far fewer degrees of freedom; this makes it possible to solve large systems without any loss of accuracy.

This paper deals with the application of a similar method to dynamic problems: subdivision of the complete structure into appropriate substructures, exact reduction of the number of degrees of freedom to the number of boundary degrees of freedom, and calculation of the eigenvalues and eigenvectors with the thus reduced number of equations.

2. DYNAMIC CONDENSATION

After the division of the complete structure in suitable substructures, only one of these is analysed. The degrees of freedom are separated into the remaining boundary, or master coordinates, and in the interior slave coordinates, which have to be eliminated. Thus the substructure eigenvalue equation is partitioned:

$$\left(\begin{bmatrix} \frac{K_{mm0}}{K_{sm}} + \frac{K_{ss}}{K_{ss}} \\ \frac{K_{sm}}{K_{sm}} + \frac{K_{ss}}{K_{ss}} \end{bmatrix} - \lambda \begin{bmatrix} \frac{M_{mm}}{M_{sm}} + \frac{M_{ss}}{M_{ss}} \\ \frac{M_{sm}}{M_{ss}} + \frac{M_{ss}}{M_{ss}} \end{bmatrix}\right) \left\{ -\frac{x_{m}}{x_{s}} \right\} = \left\{ -\frac{0}{0} \right\}, \tag{1}$$

where [K] denotes the stiffness and [M] the mass matrix. Using the second part of this matrix equation, a transformation between master and slave coordinates can be calculated:

$$\{x_{s}\} = -[K_{ss} - \lambda M_{ss}]^{-1} \cdot [K_{sm} - \lambda M_{sm}] \{x_{m}\}.$$
 (2)

This transformation relation allows a reduction of the substructure eigenvalue problem to an equation of the order m, where m denotes the number of master

coordinates [1]:

$$[D(\lambda)] \{x_m\} = \{0\}$$

with the abbreviations:

$$[D(\lambda)] = [D_{mm} - D_{ms} D_{ss}^{-1} D_{sm}]$$

$$[D_{mm}] = [K_{mm} - \lambda M_{mm}], [D_{ms}] = [K_{ms} - \lambda M_{ms}], \text{ e.t.c.}$$
(4)

This λ -dependent condensed dynamic stiffness matrix can be evaluated for each substructure and then added up to the overall dynamic stiffness matrix. Now, the resulting homogeneous simultaneous system of equations has to be solved. The solution of this system of equations is possible only if the determinant of the matrix $[D(\lambda)]$ becomes zero. This is only true, if λ coincides with the eigenvalues of the complete structure. Because of the λ -dependency of the matrices $[D_{mm}]$, $[D_{ms}]$ e.t.c., only an iterative solution is possible. The matrices [K] and [M] for each substructure have to be stored and in each iteration step, and for each substructure, the matrix $[D_{ss}(\lambda)]$ has to be inverted and then the matrix $[D(\lambda)]$ has to be evaluated. Consequently, this method is unfavourable and many authors have tried to avoid the λ -dependency between the master and slave degrees of freedom in the transformation relation (2) by simply setting λ to zero:

$$\{x_{s}\} = -[K_{ss}^{-1} K_{sm}] \cdot \{x_{m}\}.$$
 (5)

This means using a static transformation for the calculation of an approximate dynamic system behaviour [2]. The method must be used with care, because the results of the above approximation depend on the frequency as well as on the choice of the master and slave coordinates, and error estimations are necessary [3].

IMPROVEMENTS

A better way of attaining the dynamic condensed stiffness matrix $[D(\lambda)]$ for each substructure is possible using the substructure slave eigenvalue problem. The slave eigenvalue problem is obtained from the substructure eigenvalue problem, deleting all terms belonging to the master coordinates. Physically this can be interpreted as a substructure with fixed boundaries:

$$([K_{ss}] - \sigma[M_{ss}]) \{\varphi\} = 0.$$

$$(5)$$

The solution yields the eigenvalues $[\Sigma]$ and the eigenvectors $[\phi]$, where the eigenvectors are normalized in the following form:

$$\left[\phi\right]^{T}\left[K_{ss}\right]\left[\phi\right] = \left[\Sigma\right], \quad \left[\phi\right]^{T}\left[M_{ss}\right]\left[\phi\right] = \left[I\right].$$
 (6)

For a structure, with fixed boundaries, the motion of points within the structure can be described by modal superposition of the eigenvectors $\{x_s\} = [\phi] \cdot \{a\}$, where $\{a\}$ are unknown modal coefficients. By releasing the fixed boundaries an additional term is added to the description of $\{x_s\}$, namely, the static relation between $\{x_s\}$ and $\{x_m\}$, $\{x_{s2}\} = -[K_{ss}] \{x_m\}$. Therefore, $\{x_s\}$ becomes

$$\{x_s\} = \{x_{s1}\} + \{x_{s2}\} = [\phi] \cdot \{a\} - [A] \{x_m\},$$
 (7)

with $[A] = [K_{ss}^{-1} K_{ss}]$. To determine the modal coefficients $\{a\}$, the original transformation matrix (2) is employed and the result is:

$$\{a\} = [E(\lambda)][R]\{x_m\}, \tag{8}$$

where
$$[R] = [\phi^T M_{sm} - \Sigma^{-1} \cdot \phi^T \cdot K_{sm}]$$
 and $[E(\lambda)] = \lambda [\Sigma - \lambda I]^{-1}$.

This yields a new transformation relationship

$$\{x_{e}\} = ([\phi][E(\lambda)][R] - [A])\{x_{m}\},$$
 (9)

where only the diagonal matrix $[E(\lambda)]$ is frequency dependent, while the other matrices are constant and need only to be calculated once. Using this new transformation and the orthogonality relation (6) to evaluate the first part of eq. (1), the dynamic condensed stiffness matrix can be written as:

$$[D(\lambda)] = [K_c] - \lambda([M_c] + [R]^T [E(\lambda)][R]), \qquad (10)$$

with the abbreviation

$$[K_c] = [K_{mm} - K_{ms}A]$$

 $[M_c] = [M_{mm} - M_{ms}A - A^TM_{sm} + A^TM_{ss}A].$

The great advantage of this equation is the constance of the used matrices. $[K_C]$ and $[M_C]$ are constant and symmetric mxm matrices. The mxs matrix [R] is constant and the only nonconstant matrix is the diagonal matrix $[E(\lambda)].$ The matrices $[K_C]$ and $[M_C]$ are identical to those used in the quasistatic condensation. The coupling between the master and slave stiffness and mass properties are accounted for in the residual matrix [R] and the relation between the slave eigenfrequencies and the actual frequency is accounted for in the diagonal matrix $[E(\lambda)].$ It is obvious, that the product $[R^T][E(\lambda)][R]$ is symmetric, so that only the upper or lower triangle need to be calculated.

The same results can be obtained firstly by simply replacing the matrix $[D_{SS}]^{-1}$ in eq.(4) by the well known relation [4]

$$[D_{SS}]^{-1} = [K_{SS} - \lambda M_{SS}]^{-1} = \phi[\Sigma - \lambda I]^{-1} \phi^{T}$$
 (11)

and then extensively rearranging the equation (3) using the orthogonal relation in eq.(6) or, secondly, by the application of the reciprocal theorem as shown in [5].

4. SPECIAL ASPECTS

To consider some basic properties, the application of the dynamic condensation is performed on a single substructure; in general this is not advantageous. The investigated example is a simple plane frame, consisting of 6 finite beam elements with three generalized displacements of each node, see Fig. 1, and the overall number of the degrees of freedom is 12. The three displacement

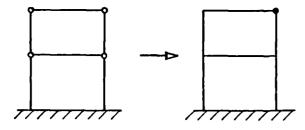


Fig. 1: Condensation from 12 to 3 degrees of freedom

coordinates of node 4 are selected as master coordinates, and the dynamic condensation is carried out so that the complete information of the system is condensed to the 3×3 matrix $[D(\lambda)]$. The solution of eq.(3) requires that the

determinant of the matrix $[D(\lambda)]$ must vanish. Therefore, the determinant values are plotted against the frequency λ from 0 to 100 Hz, Fig. 2. This curve differs from other determinant value curves by having asymptotic singularities.

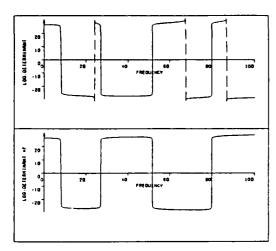


Fig. 2: Original and smoothed determinant curve

These discontinuities are caused by the eigenvalues of the slave system appearing in the frequency dependent matrix $[E(\lambda)]$. The obvious disadvantage of these singularities is that determinant search methods cannot be employed. More important than the effect of overflow, which can be avoided by dividing the elements of the stiffness matrix by a common factor, is the effect that the discontinuities at the slave eigenfrequencies can lead to wrong results. This difficulty can be avoided by multiplying the determinant values with the expression

$$F = \prod_{i=1}^{s} (\sigma_i - \lambda),$$

which does not affect the actual eigenvalues, but smoothes the curve making it possible to apply determinant search algorithms Fig. 2.

To obtain the eigenvalues of the condensed system, it is not necessary to evaluate the determinant curve. Using the Sturm sequence check, one can always calculate the number of eigenvalues below a trial value λ_{t} . It is also true for structures of the present type, where a subdivision in slave and master coordinates has been performed, and the slave system is supposed to be fixed [6]:

$$J_{+} = J_{0} + s\{D(\lambda_{+})\}$$
 (12)

 J_{t} is the wanted number of eigenvalues corresponding to frequencies less than the trial value λ_{t} . J_{0} is the known number of the slave eigenvalues corresponding to frequencies less than λ_{t} , known because the slave eigenvalues have already been calculated. $s\{D(\lambda_{t})\}$ is the number of negative signs of the elements of the diagonal matrix [d], when $[D(\lambda_{t})]$ is decomposed by the Gauss elimination into the product $[L][d][L]^{T}$. This decomposition is also required for the calculation of the determinant value of $[D(\lambda)]$, because $\det[D(\lambda)] = \prod_{t=1}^{T} d_{t}i$. So, two valuable pieces of information can be obtained by decomposing $[D(\lambda_{t})]$, firstly, the number of eigenvalues corresponding to frequencies less than the trial value λ_{t} and, secondly, the determinant value of $[D(\lambda_{t})]$. Once the isolation of the eigenfrequencies has been performed, using the modified Sturm sequence check, a determinant search algorithm can be applied to the smoothed determinant curve.

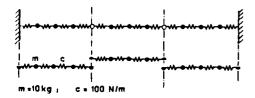
A further point of interest is the frequency dependent diagonal matrix $[E(\lambda)]$ in the master-slave transformation, eq. (9). The fixed boundary vibration of the structure is strongly influenced by the difference between the actual vibrating frequency λ and the eigenvalues $[\Sigma]$ of the slave system. By investigating the expression $\lambda/(\sigma_i-\lambda)$, and if the frequency domain of interest is known, it is possible to estimate how many of the eigenvalues σ_i of the substructure have to be considered. The same observation can be made in the third term of the dynamic condensed stiffness matrix, eq.(10). The elements of this term can be written as:

$$d_{ij}^{3} = \sum_{k=1}^{s} r_{ik} r_{jk} e_{k}(\lambda), \text{ with } e_{k}(\lambda) = \lambda/(c_{k} - \lambda).$$
(13)

For large values of σ_k , compared to λ , the expression $e_k(\lambda)$ tends to zero and a further consideration of this element is not necessary. This means that the summation in eq.(13) can be carried out for k = 1 to t, with t < s, rather that for k = 1 to s. By looking at the evaluation of the elements r_{ik} of the matrix [R], the effect of negle ting the last s-t elements of $[E(\lambda)]$ can be seen to be identical with the computation of only the slave eigenvalues and -vectors up to t. Depending on the desired accuracy, a considerable amount of calculation time and computer storage can be saved, and in the following examples it is shown that very good results can be obtained using only a few slave eigenpairs. In this context, it is notable that the order of the dynamic condensed stiffness matrix is not affected by the alteration of the number of the applied slave eigenpairs, it is only dependent on the number of the used master coordinates. This differs from the methods of component mode synthesis, where more considered substructure modes increases the number of generalised coordinates and the order of the resulting problem [7]. Another important point is the retention of the original coordinates, making it possible to easily manipulate the mass and stiffness properties of the structures. Additional masses or springs can be directly added to the dynamic condensed stiffness matrix and no new calculations of the substructure eigenproblem are necessary.

EXAMPLES

With the proposed method some examples are calculated to show the advantage of the dynamic condensation applied to substructures, especially identical ones. The first example deals with a simple spring-mass system. It consists of three identical substructures, shown in Fig. 3, with the master coordinates defined at the end of the substructures, making it possible to connect the substructures and support the system. The results are compared with the results of a complete



eigenvalues (s-2)											
subroutine	.689	2.67	5.85	10.0	14.8	20.0	25.1	30.0	34.1	37.3	39.3
condensation	.689	2.57	5.85	9.99	14.8	20.0	25.1	30.0	34.0	37.3	39.3

Fig. 3: Mass-spring system

Table 1: Comparison of calculated eigenvalues

eigenproblem solution. The slight difference between some values is only due to the ending of the iteration once a certain &-value is reached. The substructure eigenvalues are identical to the 2nd, 5th and 7nd eigenvalue of the complete structure, and, inspite of the discontinuities of the determinant value curve, a solution was possible. The results were obtained using a polynomial iteration, where the zero point of an estimation polynomial was employed to yield a better approximation to the actual eigenvalue. The second example deals with a two dimensional beamlike structure, Fig. 4. The structure is divided into

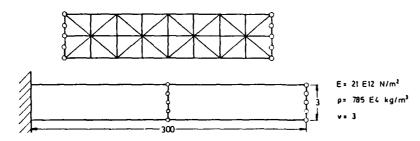


Fig. 4: Beamlike structure consisting of two identical substructures

2 identical substructures. The master degrees are defined, as before, at the joints to connect the substructures and to support the complete structure. One substructure consists of 32 plane stress triangular elements with a quadratic displacement function, 170 degrees of freedom with 10 masters at each boundary and 150 slave coordinates. The complete structure contains 320 dof's expressed in 20 master coordinates. The eigenvalues are calculated using different numbers of substructure modes and eigenvalues for the computation of the matrix [R], and also the Guyan-condensation, without slave eigenvalues, is performed. The results obtained with the polynomial iteration are shown in Table 2 and it can be seen that, in this example, 8 slave eigenmodes and -values, of the 150 involved, are sufficient to obtain exact results in the investigated frequency range of 0-6500 Hz.

Eigenvalues in Hz	Nr. of included slave eigenvalues and -modes								
111 112	0	2	4 	6	8	10	15		
I	27.94	27.93	27.93	27.93	27.93	27.93	27.93		
2	176.9	175.6	175.6	175.6	175.6	175.6	175.6		
3	595.9	494.7	494.7	494.7	494.7	494.7	494.7		
4	1717	981.5	978.2	978.0	978.0	978.0	978.0		
5	4425	1644	1636	1636	1636	1636	1636		
6		2527	2481	2480	2480	2479	2479		
7		4425	3526	3524	3524	3523	3523		
8		4850	4425	4317	4316	4314	4314		
9			4801	4789	4788	4785	4785		
10			6331	6302	6299	6295	6295		

Table 2: Eigenvalues of the complete structure, computed with different numbers of slave eigenvalues and -modes.

For the calculation of the eigenvalues, between 3 and 6 iteration steps are necessary to yield accurate results for $\varepsilon=1.E-8$. The Guyan-condensation (no slave eigenpairs are included) yields only 5, instead of 10, eigenvalues and only the first two can be considered as a good approximation of the actual eigenvalues. Additional to the eigenvalue calculation, the eigenmodes are computed. After the isolation of the eigenvalues, an inverse vector iteration with shift is used to improve the estimated eigenvalue. The results are shown in Fig. 5 where 24 identical substructures from Fig. 4 are connected to the same structure as in the previous example, yielding an overall number of dof's of 3200 expressed in 240 master coordinates. The vector iteration is performed only with ten master coordinates, so the master displacements are directly available and the slave displacements can easily be found using the transformation relation, eq.(9). The convergence of the iteration was found to be very good, with only 2 to 5 iteration steps necessary to achieve the permissible error of less than $\varepsilon=1.E-8$ between successive iteration results.

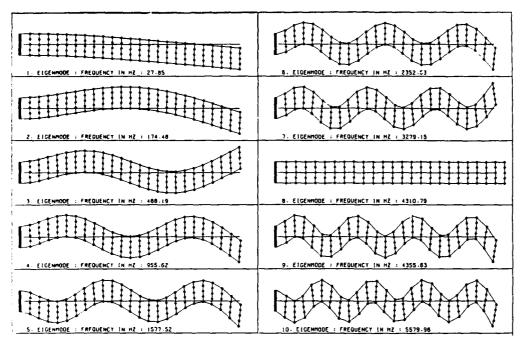


Fig. 5: Eigenmodes calculated using 24 identical substructures

The last example is made up of different substructures. The horizontal part of the frame like structure is built up of 12 identical substructures, I substructure is used for the corner and 12 identical substructures for the vertical part. The substructures are shown in Fig. 6. The lengths for this example were L1=665mm and L2=860mm and the material properties are the same as shown in Fig. 4.

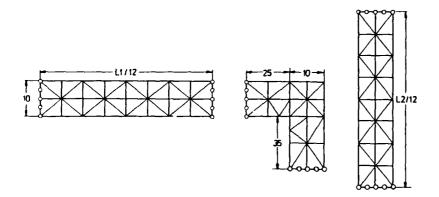
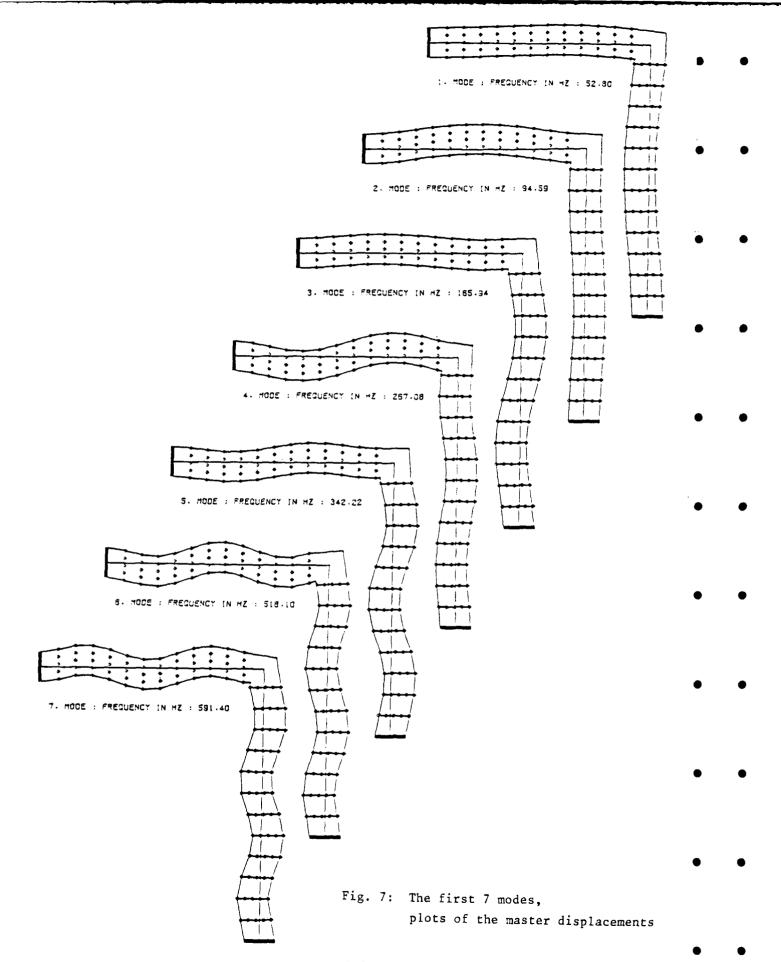


Fig. 6: The three substructures used

The overall number of the involved dof's is 3962 and the number of master dof's is 240. In the frequency range of 0 to 2500 Hz 17 eigenvalues were found. The results are obtained to the same accuracy both with the polynomial iteration, as well as with the vector iteration. The first five eigenpairs of each substructure are taken into account. In Fig. 7 the first seven modes are plotted. Only the master displacements are shown and marked with symbols. The substructure corner points are connected, for simplicity, by straight lines, although the actual lines are made up of four quadratic functions originating from the finite element idealisation.



6. CONCLUSIONS

Analogous to the condensation of substructures in statics, a dynamic condensation is performed which enables the description of the substructure behaviour by only a few remaining degrees of freedom. Contrary to the Guyan condensation, the choice of the master coordinates can be restricted, without any loss of accuracy, to the boundaries and to points of special interest. The frequency dependent coupling between master and slave coordinates is essentially expressed in constant matrices, which only need to be calculated once. The totally decoupled substructures can be analysed independently and a modification of any one substructure does not affect any other. Analysing the determinant value curve of the condensed dynamic stiffness matrix reveals the origin of the existent discontinuities. The application of determinant search techniques becomes possible by using a smoothing method not affecting the actual eigenvalues. Depending on the interesting frequency range of the complete structure, and on the fixed substructure eigenvalues, the expense of the required calculations of the substructure eigenvalues and -vectors can be substantially reduced without deteriorating the results. This method of dynamic condensation, applied to substructures, makes it possible to analyse systems with a large number of dof's, because the limited storage capacity of the computer is only used for each one of the substructures and not for the complete system. The use of identical substructures is very advantageous, because the substructure analysis only needs to be performed once. Further advantages are possible if the band nature of the substructure matrices, as well as the band nature of the overall dynamic stiffness matrix after the composition, can be maintained. Some examples, using identical and different substructures, have been computed. The results of the determinant search method, as well as that of the vector iteration method, have been obtained using only a few iteration steps and within a very short computation time.

REFERENCES

- 1. H. RÖHRLE 1980 Forschr.-Ber. VDI-Z., Reihel, Nr. 72. Reduktion von Freiheitsgraden bei Strukturdynamik-Auf-gaben.
- 2. R.J. GUYAN 1965 AIAA Journal 3(2), 380. Reduction of Stiffness and Mass Matrices.
- 3. M. GERADIN 1971 Journal of Sound and Vibration 19(2), 111-132. Error Bounds for Eigenvalue Analysis by Elimination of Variables.
- 4. P. LANCASTER 1966 Lambda-matrices and Vibrating Systems. Pergamon Press.
- 5. A.Y.T. LEUNG 1979 Int. J. Num. Meth. Engg. 14, 1241-1256. An Accurate Method of Dynamic Substructuring with Simplified Computation.
- 6. C.T. HOPPER and F.W. WILLIAMS 1977 J. Struct. Mech. 5(3), 255-278. Mode Finding in Nonlinear Structural Eigenvalue Calculation.
- 7. K.J. SCHMIDT 1980 Dissertation, Universität Hannover. Eigenschwingungsanalyse geikoppelter elastischer Strukturen.



THE IMPROVEMENT OF FREE-MODE METHODS IN COMPONENT MODE SYNTHESIS TECHNIQUES AND ITS ACCURACIES

Z.W. Wang and M. Petyt Institute of Sound and Vibration Research University of Southampton

AD-P003 659

ABSTRACT

Free-mode methods in component mode synthesis techniques are improved by the use of the concept of 'positive static' residuals, which are developed according to the theorems given in this paper. The technique of assembly of complicated structures is also presented. The convergence of the improved free-mode method is related to the so-called "eigenfrequency coefficient η ", which is generally greater than 1.0 and smaller than 1.4.

1.0 INTRODUCTION

To model a large and/or complicated structure and to reduce the storage and cost of computations, component mode synthesis techniques are playing a more and more important role and have been developed very rapidly. Generally, there are three categories of them ([1-5]):

- (a) Constraint-mode methods;
- (b) Free-mode methods;
- (c) Hybrid methods

This paper is only concerned with the second category.

1.1 Background

(1) Substructure Analysis The equation of motion of the $\mathbf{S}^{\mathbf{th}}$ substructure is as follows

$$\left[\mathbf{m}\right]_{\mathbf{s}} \left\{\ddot{\mathbf{x}}\right\}_{\mathbf{s}} + \left[\mathbf{k}\right]_{\mathbf{s}} \left\{\chi\right\}_{\mathbf{s}} = \left\{\begin{matrix}\mathbf{f}\mathbf{j}\\\mathbf{0}\end{matrix}\right\}_{\mathbf{s}} \tag{1.1}$$

where $\{\ddot{\chi}\}$ and $\{\chi\}$ are the vectors of physical accelerations and displacements respectively; $[m]_s$ and $[k]_s$ are the inertia and stiffness matrices of this substructure; $\{f_j\}$ is the vector of the reactions at the interface junctions; the inner coordinates are free.

Denoting the normal modes as $[\emptyset]_s$, then (1.1) becomes

$$\ddot{\mathbf{q}}_{\mathbf{s}} + [\Lambda]_{\mathbf{s}} {\mathbf{q}}_{\mathbf{s}} = [\mathbf{g}_{\mathbf{j}}]_{\mathbf{s}}^{\mathbf{T}} {\mathbf{f}_{\mathbf{j}}}_{\mathbf{s}}$$
(1.2)

where $\{q\}$ is the vector of corresponding generalised coordinates, $[\Lambda]_s$ is a diagonal matrix with eigenvalues of the substructure, $[\emptyset_j]_s$ is the part of $[\emptyset]_s$ corresponding to the coordinates of interface boundaries.

(1.2) is ready for coupling. The conditions of compatibility and equilibrium should be employed.

At the i'th junction where, say, the q'th, r'th and s'th substructures are joined together, the compatibility equations are

$$\{\chi_{i}\}_{q} = \{\chi_{i}\}_{r} = \{\chi_{i}\}_{s}$$
 (1.3)

and the equilibrium equation is

$$\{f_i\}_q + \{f_i\}_r + \{f_i\}_s = 0$$
 (1.4)

(2) Hou's Method.

Suppose only the first few lower frequency modes are employed, then

$$\{\chi_{j}\}_{s} = \left[\phi_{j}^{L}\right] \left\{q^{L}\right\}_{s} \tag{1.5}$$

in which "L" stands for the "Lower frequency modes" selected. Hou used this expression to assemble the structure. Since the contributions of all the higher frequency modes are lost, the convergence of the method is bad. The details of the coupling procedure is in $\begin{bmatrix} 6 \end{bmatrix}$.

(3) Rubin's Method.

Rubin [7] used the following expression

$$\{\chi_{\mathbf{j}}\}_{\mathbf{s}} \simeq \left[\mathbf{g}_{\mathbf{j}}^{\mathbf{L}}\right]_{\mathbf{s}} \{\mathbf{q}^{\mathbf{L}}\} + \left[\mathbf{G}_{\mathbf{j}\mathbf{j}}^{\mathbf{a}}\right]_{\mathbf{s}} \{\mathbf{f}_{\mathbf{j}}\}_{\mathbf{s}}$$
 (1.6)

where $\begin{bmatrix} G_{i,j}^a \end{bmatrix}_s$ is the matrix of the static residual flexibilities contributed by the deleted higher frequency modes. Therefore, the convergence is greatly improved. $\begin{bmatrix} G_{i,j}^a \end{bmatrix}_s$ is obtained by

$$\begin{bmatrix} G_{jj}^{a} \end{bmatrix}_{s} = \begin{bmatrix} G_{jj} \end{bmatrix}_{s} - \begin{bmatrix} G_{jj}^{L} \end{bmatrix}_{s}$$
(1.7)

where $[G_{jj}]_s$ is the total static flexibilities

 $\left[G_{\mathbf{j}\,\mathbf{j}}^{\mathrm{L}} \right]_{\mathbf{s}}$ is the static flexibilities caused by employed modes.

1.2 What are the problems in Rubin's method?

Although the properties of the convergence are very good, Rubin's method has some disadvantages. When rigid-body modes occur, $\begin{bmatrix} G_{j,j}^a \end{bmatrix}_s$ cannot simply be obtained by (1-7), because both $\begin{bmatrix} G_{j,j}^i \end{bmatrix}_s$ and $\begin{bmatrix} G_{j,j}^i \end{bmatrix}_s$ are infinite. Rubin proposed a method to calculate the residuals $\begin{bmatrix} 7 \end{bmatrix}$ which is rather complicated.

Besides, Rubin's method considers only static residual flexibilities, which, indeed, are the effects of the stiffness of higher frequency modes. Possibilities still exist that some of the effects of mass of higher frequency modes may be taken into account.

Furthermore, the coupling techniques for a complicated structure divided into more than two sub-parts is required.

2.0 TWO THEOREMS AND A NEW CONCEPT

2.1 Theorem 1

- (a) A dynamic stiffness matrix at a frequency* below its first eigenfrequency (including at a negative frequency) is always positive definite.
- (b) A dynamic stiffness matrix at frequencies beyond its last eigenfrequency is negative definite. The dynamic stiffness matrix of a continuum will never be negative definite.

*Here "frequency" or "eigenfrequency" is taken to mean its square, i.e. ω^2 , for convenience.

(c) A dynamic stiffness matrix at a frequency between its first eigenfrequency (including zero frequency if rigid-body modes exist) and the last one is non-singular, except at an eigenfrequency where it is singular.

2.2 Theorem 2

Residual flexibilities (dynamic or static) within the frequency range of interest are always finite.

2.3 The Concept of "Positive Static" and "Negative Static" Residual Flexibilities

Based on the above theorems, choose a suitable frequency ω_0^2 so that the dynamic stiffness matrix is non-singular. Then, the residuals still may be obtained by Equation (1.7), in which

$$\left[\mathbf{G}\right]_{\mathbf{S}} = \left[\mathbf{D}\right]_{\mathbf{S}}^{-1} \tag{2.1}$$

and

$$\left[\mathbf{G}_{\mathbf{j}\mathbf{j}}^{\mathbf{L}}\right]_{\mathbf{S}} = \left[\mathbf{\emptyset}_{\mathbf{j}}^{\mathbf{L}}\right]_{\mathbf{S}} \left\{\left[\Lambda\right]_{\mathbf{S}} - \omega_{\mathbf{o}}^{\mathbf{2}} \mathbf{I}\right\}^{-1} \left[\mathbf{\emptyset}_{\mathbf{j}}^{\mathbf{L}}\right]_{\mathbf{S}}^{\mathbf{T}}$$
(2.2)

where

$$\left[\mathbf{p}\right]_{\mathbf{s}} = \left[\mathbf{K}\right]_{\mathbf{s}} - \omega_{\mathbf{o}}^{2} \left[\mathbf{m}\right]_{\mathbf{s}} \tag{2.3}$$

Since ω^2 is a constant, the receptances at this frequency act like static flexibilities, as if the vertical axis were shifted to the right by an amount of ω^2 (or to the left if ω^2 is negative). Hence, they are called "positive static" flexibilities (or "negative static" flexibilities if ω^2_0 is negative).

For the latter, i.e. "negative static" flexibilities, they are almost equal to the real static ones if the $-\omega^2$ chosen is not far from the origin (see Figure 2.1). While "positive static" flexibilities are generally greater than the real static ones (Fig 2.2), since they take into account some of the contributions of the mass of the mode. In both figures, the curves are the spectrum of the receptance of a mode of a substructure (hence G_0 is its static flexibility (real)); λ 's are supposed to be the eigenfrequencies of the complete structure. If this mode is to be deleted and replaced by its value at ω^2 (in Rubin's method, it is G_0) then its contribution to different modes of the assembled structure is no longer varying but always equal to its value at ω^2 .

In the case of positive ω_0^2 , therefore, the contribution of this mode to the lower frequency modes (such as $\lambda_{\mathbf{r}}$ in Figure 2.2) is higher than it should be, and $\lambda_{\mathbf{r}}$ is expected to be smaller than the exact one, but not very much. On the other hand, the contribution to $\lambda_{\mathbf{t}}$, say, is lower, however, it is higher than that given by G_0 . Therefore the accuracy of the mode of $\lambda_{\mathbf{t}}$ is enhanced. "Negative static" flexibilities give nearly the same accuracy as Rubin's G_0 (see Fig 2.1).

3.0 COUPLING PROCEDURE

Using Equation (1.2), the uncoupled equation of the complete system is:

$$\begin{bmatrix} \Lambda^{L} - \lambda \mathbf{I} & \mathbf{0} \\ \mathbf{0} & \Lambda^{H} - \lambda \mathbf{I} \end{bmatrix} \qquad \begin{Bmatrix} \mathbf{q}^{L} \\ \mathbf{q}^{H} \end{Bmatrix} = \begin{bmatrix} \psi_{\mathbf{j}}^{L^{T}} \\ \psi_{\mathbf{j}}^{H} \end{bmatrix} \qquad \{\mathbf{f}_{\mathbf{j}}\}$$
(3.1)

where λ is the square of the frequency; subscripts "L" and "H" denote "Lower Frequency Modes to be kept" and "Higher Frequency Modes to be deleted", respectively, for all substructures. $[\psi]$ is an overall mode shape matrix which is composed of selected eigenvectors of all substructures; corresponding to each mode (columns) and the degrees of freedom of interface boundaries (rows); "T" denotes the transposed matrix.

Now $\{q^H\}$ will be deleted. The application of conditions of compatibility and equilibrium (1.3) and (1.4) to the expression (1.6) and to the second line of (3.1) gives

$$\{\mathbf{q}^{\mathbf{H}}\} = -\left[\Lambda^{\mathbf{H}} - \lambda \mathbf{I}\right]^{-1} \begin{bmatrix} \mathbf{q} \\ \mathbf{j} \end{bmatrix}^{\mathbf{T}} \begin{bmatrix} \mathbf{G}_{\mathbf{j}\mathbf{j}}^{\mathbf{W}} \end{bmatrix}^{-1} \begin{bmatrix} \mathbf{q} \\ \mathbf{L} \end{bmatrix}$$
(3.2)

where $\begin{bmatrix} G_j^w \end{bmatrix}$ is a matrix of overall residual flexibilities which consists of individual residual flexibility matrices of all substructures; corresponding to the degrees of freedom of interface boundaries. Hence, the transformation is formed:

$$\begin{cases}
\mathbf{q}^{\mathbf{L}} \\
\mathbf{q}^{\mathbf{H}}
\end{cases} = \begin{bmatrix}
\frac{\mathbf{I}}{-[\Lambda^{\mathbf{H}} - \lambda \mathbf{I}]^{-1} [\psi_{\mathbf{j}}^{\mathbf{H}}]^{\mathbf{T}} [G_{\mathbf{j}\mathbf{j}}^{\mathbf{w}}]^{-1} [\psi_{\mathbf{j}}^{\mathbf{L}}]} \\
= [\mathbf{s}] \{\mathbf{q}^{\mathbf{L}}\}$$
(3.3)

Substituting (3.3) into (3.1) and pre-multiplying $[S]^T$, the approximate equation of the assembled system is obtained as

$$([\Lambda^{L} - \lambda I] + [\psi_{\mathbf{j}}^{L}]^{T} [G_{\mathbf{j}\mathbf{j}}^{\mathbf{w}}]^{-1} [\psi_{\mathbf{j}}^{L}]) \{q^{L}\} = 0$$
(3.4)

4.0 THE ACCURACY OF THE METHOD

It was demonstrated in [8] that better convergence would be obtained if substructure modes are selected according to the ascending order of their eigenfrequencies. This conclusion is also applicable to free-mode methods. During the tests, substructure modes will be selected according to this order.

The basic method of research is comparing the approximate results to the results of the complete structural analysis which are considered as "exact". If the error is less than say 5%, the approximate results are considered as satisfactory.

To express the accuracy of a mode, an eigenfrequency coefficient η is used, which is defined as follows: the eigenfrequency coefficient η_i of the ith mode of the assembled structure is defined as

$$n_{\mathbf{i}} = \omega_{\mathbf{e}} / \lambda_{\mathbf{i}}^{\frac{1}{2}} \tag{4.1}$$

where λ_i is the ith eigenfrequency of the assembled structure; ω_e is the eigenfrequency of the last employed substructure mode (i.e. the highest eigenfrequency mode selected).

For different trials, the structure is assembled for different numbers of substructure modes, and three $\boldsymbol{\eta}_{\bm{i}}$ are chosen:

 $n_{\mbox{\scriptsize M}^-}$ of the last satisfactory mode, ie. M is the number of satisfactory modes;

 $\eta_{M=1}^{}$ - of the second last satisfactory mode; $\eta_u^{}$ - of the first unsatisfactory mode.

It is expected that η_{M} is greater than 1.0 but not more than 1.4, and η_{U} smaller than 1.0, since the spectrum of the receptance of a mode is a quadratic curve.

5.0 EXAMPLES

The authors used analytical modes of beams for substructure modes to analyse some beams and frameworks. The results show that the conclusions in Section 4 are correct. It will not be shown here due to the limitation of space. But it is important to apply this substructuring technique to finite element methods which are themselves approximate methods.

5.1 A Cantilever Beam

The data of this beam are shown in Figure 5.1. The $\eta-N$ relations are listed in Figure 5.2 where N is the number of total employed modes.

5.2 A Plane Framework (Fig 5.3)

In Figure 5.4, $\eta\text{-N}$ relations are plotted. Throughout all the trials, ω s are always taken as half of the values of $\omega_{\text{o}}s$.

All these figures and tables demonstrate that the conclusions in Section 4.2 of judging the accuracy of the improved free-mode method are basically correct. The existence of some discrepancies are not surprising because finite element methods themselves are approximate methods and the judging standard of 5% is used.

6.0 CONCLUSIONS

6.1 The following points are obtained:

- (1) The problem of calculating residuals is successfully solved by the theorems in Section 2. At the same time, partial compensations of mass for higher frequency modes of the assembled structure are obtained while there is little effect on lower frequency modes.
- (2) The use of the overall residual matrix $\begin{bmatrix} G_{jj}^w \end{bmatrix}$ makes it possible to assemble a complicated structure correctly.
- (3) If an eigenfrequency coefficient η_M is used, its value of the satisfactory highest frequency mode is about from 1.0 to 1.4; and η_u is usually smaller than 1.0.

6.2 Disadvantages:

Although free-mode methods have many advantages as stated by previous papers $\begin{bmatrix} 1-5 \end{bmatrix}$, its hidden disadvantages are exposed when a larger structure is sub-divided and analysed.

- (1) More substructure modes are needed for assembly if rigid-body modes occur in substructures.
- (2) The overall residual matrix will be very large if a greater number of interface degrees of freedom are produced.

6.3 Prospects:

Free-mode methods would have a very good future if the overall residual matrix can be obtained substructure by substructure.

Since "positive static" residual flexibilities are employed, the applications of free-mode methods to forced vibration would produce accurate results.

REFERENCES

- J.F. IMPERT, Finite Element Methods in the Commercial Environment <u>1</u>, 421-464. A Survey of Current Capability for Dynamic Analysis of Complex Structures.
- W.C. HURTY, J.P. COLLINS and G.C. HART 1971 Computers and Structures 1, 535-563. Dynamic Analysis of Large Structures by Modal Synthesis Techniques.
- 3. R.H. MACNEAL 1971 Computers and Structures 1, 581-601. A Hybrid Method of Component Mode Synthesis.
- 4. C. STAVRINIDIS Finite Element Methods in the Commercial Environment 1, 307-331. Paper 15. Theory and Practice of Modal Synthesis Techniques.
- 5. R.R. CRAIG Jr. 1965 AIAA 3, 678-685. Dynamic Analysis of Structural Systems Using Component Modes.
- 6. S.N. HOU Shock and Vibration Bulletin US Naval Research Lab. Proc. 40(4), 25-39. Review of Modal Synthesis Techniques and a New Approach.
- 7. S. RUBIN 1975 AIAA 13(8), 995-1006. Improved Component Mode Representation for Structural Dynamic Analysis.
- 8. Z.W. WANG 1982 M.Sc. Dissertation, University of Southampton. Accuracy of Constraint-mode Method in Component Mode Synthesis Techniques.

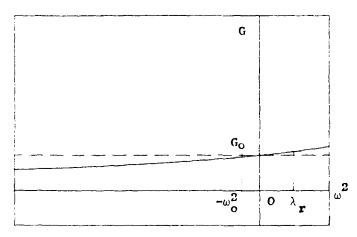


FIGURE 2.1 "Negative static" Flexibility

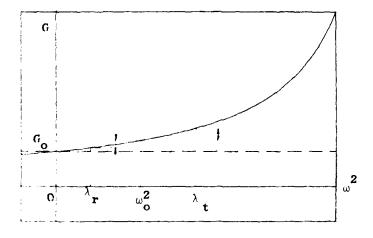


FIGURE 2.2 "Positive static" Flexibilities

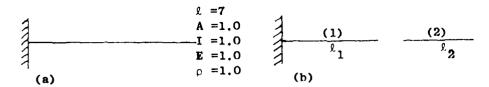


FIGURE 5.1 (a) A cantilever beam (b) The beam is divided into the two sub parts $\ell_1^{=4},\ \ell_2^{=3}$

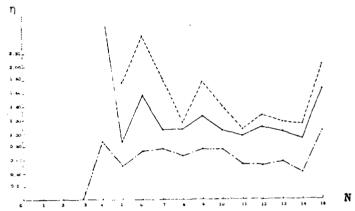


FIGURE 5.2: n-N Relations of the cantilever

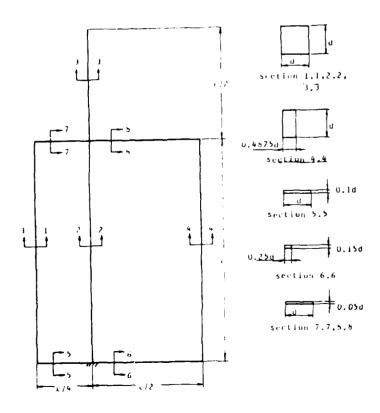
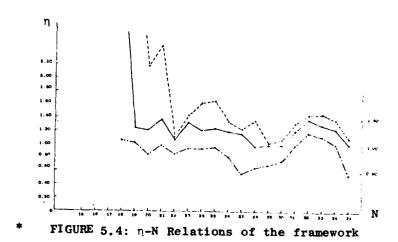


FIGURE 5.3 The Plane Framework, each beam being a substructure



* In both Figures 5.2 and 5.4 denotes $\eta_{\rm M}$ denotes $\eta_{\rm M-1}$ and denotes $\eta_{\rm u}$.

AD-P003 660



LOCALITY PRINCIPLE IN STRUCTURAL DYNAMICS

A.K.Belyaev and V.A.Palmov

Polytechnical Institute, Leningrad, USSR

I. INTRODUCTION

Det us consider a complicated mechanical object. For the study of its vibrational field it is sufficient to use a certain dynamic model. Theory of a medium with complex structure can be applied to this effect. The properties of the real object can be reflected in the medium with complex structure, the medium parameters are determined by rigidity and mass characteristics of the object resulting in certain integral characteristics and spectra. This enables one to avoid too much detailization of the object structure. The application of the theory of a medium with complex structure results in obtaining some generalized characteristics of the vibration field. This level of description can be considered sufficient for many cases. But sometimes it is necessary to find out the vibration state of a particular element of the object. It cannot be managed within the integral methods alone. The problem is that this particular element as such is not represented in the dynamical model. Thus to analyse the behaviour of a particular element one has to take into account both its particular structure and the conditions of its interaction with other elements. Trying to cover the entire complexity of a real object makes this task completely hopeless. Another possibility lies in precise consideration of a particular element alone. with the rest of the object being considered integrally. The present study is based upon this idea.

2. BOUNDARY PROBLEM OF THE DINAMICS OF A STRUCTURE

Here we use the methods described in [3] and [6]. So far we ignore damping characterizing all structures. We divide the structure by the system of surfaces into substructures V_n (n=I, 2,...N). The system of surfaces should be set either along the natural boundaries of the structures or along the exterior surface of the entire object.

Real displacement of a material point within the volume \mathbf{V}_n is denoted as $\underline{\mathbf{a}}_n(\underline{\mathbf{r}},\mathbf{t})$. The displacement field is normally found by expansion in the terms of natural modes $\underline{\mathbf{u}}_{nk}(\underline{\mathbf{r}})$ of the substructure \mathbf{V}_n

$$\underline{\mathbf{a}}_{n}(\underline{\mathbf{r}},\mathbf{t}) = \underline{\mathbf{v}}_{n}(\underline{\mathbf{r}},\mathbf{t}) + \sum_{k=1}^{\infty} \underline{\mathbf{u}}_{nk}(\underline{\mathbf{r}}) \mathbf{g}_{nk}(\mathbf{t})$$
 (I)

Here $g_{nk}(t)$ are generalized coordinates of the substructure V_n . Normal modes are required to satisfy zero kinematic conditions on the surfaces separating the substructures. As it is shown in [3] the best way to select the function \underline{v}_n is for it to meet the following requirement:

- the equations of static theory of elasticity;
- given kinematic conditions on the portion of the boundary involved:
- zero force value on the remaining portion of the boundary.

We place the following expansion (2) in correspondence with expansion (I) \sim

$$\underline{\mathbf{a}}_{\mathbf{n}}(\underline{\mathbf{r}},\mathbf{t}) = \underline{\mathbf{u}}_{\mathbf{n}}(\underline{\mathbf{r}},\mathbf{t}) + \sum_{k=1}^{\infty} \underline{\mathbf{u}}_{\mathbf{n}k}(\underline{\mathbf{r}})\mathbf{q}_{\mathbf{n}k}(\mathbf{t})$$
 (2)

In this expansion $\underline{u}_{nk}(\underline{r})$ are still normal modes, q_{nk} are generalized coordinates of the substructure V_n corresponding to them. The function \underline{u}_n coincides on the surface of the substructure V_n with real displacement \underline{a}_n , but is extremly smooth.

We take substructure $V_{\mathbf{S}}$ out of N substructures to be described accurately.

Kinetic energy of the entire structure V with expansions (I) and (2) considered is

$$T = \frac{1}{2} \int_{V} \rho \underline{\dot{a}} \cdot \underline{\dot{a}} dV = \frac{1}{2} \sum_{n=1}^{N} \sum_{k,r=1}^{\infty} \dot{q}_{nk} \dot{q}_{nr} \int_{V_{n}} \rho \underline{\dot{u}}_{nk} \cdot \underline{\dot{u}}_{nk} dV +$$

$$+\sum_{n=1}^{N}'\sum_{k=1}^{\infty}\dot{q}_{nk}\int_{\mathbf{v}_{n}}\rho\dot{\underline{u}}_{nk}\,dv + \frac{1}{2}\sum_{n=1}^{N}'\int_{\mathbf{v}_{n}}\rho\dot{\underline{u}}_{nu}\,dv +$$

+
$$\sum_{k,r=1}^{\infty} \dot{\epsilon}_{sk} \dot{\epsilon}_{sr} \int_{v_s} \rho \underline{u}_{sk} \cdot \underline{u}_{sr} dv +$$
+ $\sum_{k=1}^{\infty} \dot{\epsilon}_{sk} \int_{v_s} \rho \dot{\underline{v}}_{s} \cdot \underline{u}_{sk} dv + \frac{1}{2} \int_{v_s} \rho \dot{\underline{v}}_{s} \cdot \dot{\underline{v}}_{s} dv .$
(3)

The prime here means that the term number s is omitted. Even within each of the substructures V_n the density \emptyset and \underline{u}_n are highly oscillating functions. On the contrary \underline{u}_n is extremely smooth function and it changes very little within each substructure. So \underline{u}_n can be placed outside the integral sign. This operation will be performed for all substructures V_n except V_s . The result is

$$\begin{split} &\mathbb{T} = \frac{1}{2}\sum_{n=1}^{N} \left[\varrho \, \underline{\dot{\mathbf{u}}}_{n} \cdot \underline{\dot{\mathbf{u}}}_{n} + 2\varrho_{n} \underline{\dot{\mathbf{u}}} \cdot \sum_{k=1}^{\infty} \, \underline{\mathbf{U}}_{nk} \underline{\dot{\mathbf{q}}}_{nk} + \sum_{k=1}^{\infty} \, \underline{\mathbf{m}}_{nk} \underline{\dot{\mathbf{q}}}_{nk}^{2} \right] \, \mathbf{V}_{n} \, + \\ &+ \frac{1}{2} \int_{\mathbf{V}_{S}} \varrho \, \underline{\dot{\mathbf{v}}}_{s} \cdot \underline{\dot{\mathbf{v}}}_{s} \, \, \mathrm{d}\mathbf{V} + \sum_{k=1}^{\infty} \, \varepsilon_{sk} \, \int_{\mathbf{V}_{S}} \varrho \, \underline{\dot{\mathbf{v}}}_{s} \cdot \underline{\mathbf{u}}_{sk} \, \, \mathrm{d}\mathbf{V} + \frac{1}{2} \mathbf{V}_{s} \sum_{k=1}^{\infty} \, \underline{\mathbf{m}}_{sk} \varepsilon_{sk}^{2} \, . \end{split}$$

In the formula (4)

$$g_n = \frac{1}{V_n} \int_{V_n} g \, dV - \text{average density of the object in } V_n$$

$$\underline{\underline{U}}_{nk} = \frac{\underline{I}}{nV_n} \int_{V_n} Q \underline{\underline{u}}_{nk} dV$$
 - average displacement of the centre of

mass of substructure V_n , when it moves according to mode k. \underline{u}_n is the velocity \underline{u} of some middle point in V_n . To obtain the result (4) the orthogonality of the normal modes was used

$$\frac{1}{V_n} \int_{V_n} \rho_n \underline{u}_{nk} \cdot \underline{u}_{nr} \, dv = \underline{m}_{nk} \delta_{kr} ,$$

where $\delta_{\mathbf{kr}}$ is Kronecher delta.

The potential energy of structure V with expansions (I),(2) considered is

$$P = \frac{1}{2} \int_{\mathbf{V}} \mathbf{v} \underline{\mathbf{a}} \cdot \underline{\underline{\mathbf{c}}} \cdot \mathbf{v} \underline{\mathbf{a}} \ d\mathbf{V} = \sum_{n=1}^{N} \frac{1}{2} \int_{\mathbf{V}_{n}} \mathbf{v} \underline{\mathbf{u}}_{n} \cdot \underline{\underline{\mathbf{c}}} \cdot \mathbf{v} \underline{\mathbf{u}}_{n} \ d\mathbf{V} + \sum_{n=1}^{N} \sum_{k=1}^{\infty} \mathbf{q}_{nk}.$$

$$\int_{\mathbf{V_n}} \mathbf{v} \underline{\mathbf{u}_n} \cdot \underline{\mathbf{c}} \cdot \mathbf{v} \underline{\mathbf{u}_{nk}} \, d\mathbf{V} + \sum_{\mathbf{n}=1}^{\mathbf{N}} \sum_{\mathbf{k}, \mathbf{r}=1}^{\mathbf{m}} \mathbf{q_{nk}} \mathbf{q_{nr}} \, \frac{1}{2} \int_{\mathbf{V_n}} \mathbf{v} \underline{\mathbf{u}_{nk}} \cdot \underline{\mathbf{c}} \cdot \mathbf{v} \underline{\mathbf{u}_{nr}} d\mathbf{V} + \int_{\mathbf{k}=1}^{\mathbf{m}} \mathbf{v} \underline{\mathbf{v}_{sk}} \, d\mathbf{V} + \sum_{\mathbf{k}=1}^{\mathbf{m}} \mathbf{v} \underline{\mathbf{v}_{sk}} \int_{\mathbf{V_s}} \mathbf{v} \underline{\mathbf{v}_{s}} \cdot \underline{\mathbf{c}} \cdot \mathbf{v} \underline{\mathbf{u}_{sk}} \, d\mathbf{V} +$$

$$(5)$$

$$+ \sum_{k,r=1}^{\infty} \varepsilon_{sk} \varepsilon_{sr} \not \sim \int_{V_s} \underline{v}_{u_{sk}} \cdot \underline{\underline{c}} \cdot \underline{v}_{u_{sr}} dv ,$$

where $\underline{\underline{C}}$ is tensor of moduli of elasticity (tensor in 4 dimensions), \underline{v} is Hamiltonian operator, $\cdot \cdot$ is the symbol of double scalar multiplication [2]. Supposing that $\underline{\underline{u}}_n$ is smooth and the natural modes are orthogonal

$$\frac{1}{\sqrt{n}} \int_{\mathbf{n}} \nabla \underline{\mathbf{u}}_{nk} \cdot \underline{\underline{\mathbf{c}}} \cdot \nabla \underline{\mathbf{u}}_{nr} \, dV = C_{nk} \delta_{kr}$$

we obtain the following result

$$P = \frac{1}{2} \sum_{n=1}^{N} \left[(\sqrt{u})_{n} \cdot \cdot \underline{\underline{c}} \cdot \cdot (\sqrt{u})_{n} + 2(\sqrt{u})_{n} \cdot \cdot \sum_{k=1}^{\infty} \underline{\underline{c}}_{nk} q_{nk} + \sum_{k=1}^{\infty} \underline{\underline{c}}_{nk} q_{nk} \right] V_{n} + \frac{1}{2} \int_{V_{n}} V_{\underline{\underline{c}}} \cdot \cdot \underline{\underline{c}} \cdot \cdot v_{\underline{\underline{c}}} dV + \frac{1}{2} V_{\underline{\underline{c}}} \sum_{k=1}^{\infty} \underline{\underline{c}}_{sk} \underline{\underline{c}}_{sk}^{2},$$
(6)

where

$$\underline{\underline{C}}_n = \frac{\underline{I}}{\underline{V}_n} \int_{\underline{V}_n} \underline{\underline{C}} dV - \text{average value of the elasticity modules}$$
tensor in substructure \underline{V}_n ,

$$\underline{\underline{v}}_{nk} = \underline{\underline{v}}_{n} \int_{\mathbf{v}_{n}} \underline{\underline{c}} \cdot \underline{v}\underline{u}_{nk} dV$$
 - average value of stress tensor when substructure is under deformation according to normal mode k.

Equality $\int_{V_s} vv_s \cdot \cdot c \cdot \cdot vu_{sk} dV = 0$ proved in [3] that is a result of the definition v_s is considered in [6].

The work of external forces is written

$$W = \int_{O} \underline{\mathbf{F}} \cdot \underline{\mathbf{a}} \, dO + \int_{\mathbf{V}} \underline{\mathbf{k}} \cdot \underline{\mathbf{a}} \, d\mathbf{V} , \qquad (7)$$

here \underline{F} is external load on 0, 0 is external surface of the structure, \underline{k} is intensity of volume load. Substitution of expansions \underline{a} (I),(2) into (7) gives the following result

$$W = \sum_{n=1}^{N} \int_{Q_{n}} \underline{F} \cdot \underline{u}_{n} \, dQ + \int_{Q_{s}} \underline{F} \cdot \underline{v}_{s} \, dQ + \sum_{n=1}^{N} \int_{V_{n}} \underline{k} \cdot \underline{u}_{n} \, dV + \int_{Q_{s}} \underline{k} \cdot \underline{v}_{s} \, dV + \sum_{n=1}^{N} \int_{E=1}^{\infty} V_{n} Q_{nk} q_{nk} + \sum_{k=1}^{\infty} V_{s} Q_{sk} g_{sk}$$

$$(8)$$

In the last formula

$$Q_{nk} = \frac{I}{V_n} \left[\int_{V_n} \underline{k} \cdot \underline{u}_{nk} \, dV + \int_{O_n} \underline{F} \cdot \underline{u}_{nk} \, dO \right]$$

is generalized force for coordinate qnk.

The obtained expressions for T.P and W are considered below as Riemann sums of the corresponding volume and surface integrals. Replacing the sums with integrals we obtain

$$T = \frac{1}{2} \int (\langle \rho \rangle \dot{\underline{u}} \cdot \dot{\underline{u}} + 2\langle \rho \rangle \dot{\underline{u}} \cdot \sum_{k=1}^{\infty} \underline{\underline{U}}_{k} \dot{\underline{q}}_{k} + \sum_{k=1}^{\infty} \underline{\underline{m}}_{k} \dot{\underline{q}}_{k}^{2}) dV +$$

$$+ \frac{1}{2} \int \rho \dot{\underline{v}}_{s} \cdot \dot{\underline{v}}_{s} dV + \sum_{k=1}^{\infty} \dot{\underline{s}}_{sk} \int \rho \dot{\underline{v}}_{s} \cdot \underline{\underline{u}}_{sk} dV + \frac{1}{2} \underline{\underline{v}}_{sk}^{2} dV + \frac{1}{2} \underline{\underline{v}}_{sk}^{2}$$

$$W = \int_{\mathbf{V}-\mathbf{V}_{\mathbf{S}}} \underline{\mathbf{k}} \cdot \underline{\mathbf{u}} \ d\mathbf{V} + \int_{\mathbf{O}-\mathbf{O}_{\mathbf{S}}} \underline{\mathbf{F}} \cdot \underline{\mathbf{u}} \ d\mathbf{O} + \int_{\mathbf{V}-\mathbf{V}_{\mathbf{S}}} \sum_{\mathbf{k}=1}^{\infty} Q_{\mathbf{k}} Q_{\mathbf{k}} \ d\mathbf{V} + \int_{\mathbf{V}_{\mathbf{S}}} \underline{\mathbf{k}} \cdot \underline{\mathbf{V}}_{\mathbf{S}} \ d\mathbf{V} + \int_{\mathbf{V}_{\mathbf{S}}} \underline{\mathbf{k}} \cdot \underline{\mathbf{V}}_{\mathbf{S}} \ d\mathbf{V} + \int_{\mathbf{O}_{\mathbf{S}}} \underline{\mathbf{k}} \cdot \underline{\mathbf{V}}_{\mathbf{S}} \ d\mathbf{V} + \int_{\mathbf{V}_{\mathbf{S}}} \underline{\mathbf{k}} \cdot \underline{\mathbf{V}}_{\mathbf{S}} \ d\mathbf{V} + \int_{\mathbf{V}_{\mathbf{S}}} \underline{\mathbf{k}} \cdot \underline{\mathbf{V}}_{\mathbf{S}} \ d\mathbf{V} + \int_{\mathbf{O}_{\mathbf{S}}} \underline{\mathbf{k}} \cdot \underline{\mathbf{V}}_{\mathbf{S}} \ d\mathbf{V} + \int_{\mathbf{S}} \underline{\mathbf{k}} \cdot \underline{\mathbf{V}}_{\mathbf{S}} \ d\mathbf{V} + \int_{\mathbf{V}_{\mathbf{S}}} \underline{\mathbf{k}} \cdot \underline{\mathbf{V}}_{\mathbf{S}} \ d\mathbf{V}$$

In these formulae

$$\underline{\mathbf{u}} = \sum_{n=1}^{N} \mathbf{h}_{n} \mathbf{u}_{n} , \quad \langle \mathbf{g} \rangle = \sum_{n=1}^{N} \mathbf{h}_{n} \mathbf{g}_{n} , \quad \langle \underline{\underline{\mathbf{c}}} \rangle = \sum_{n=1}^{N} \mathbf{h}_{n} \underline{\underline{\mathbf{c}}}_{n}$$
 (IO)

etc. h_n is characteristic function of the substructure V_n , i.e. $h_n = I$, if a point belongs to V_n and $h_n = 0$ in the opposite case.

If we accept (IO) the pass-over from the Riemann sums to the integrals is accurate. However $\underline{u},\langle \rho \rangle,\langle C \rangle$ are supposed below to be continuous smooth approximations of the step functions (IO). But in this case the expressions T_*P_*W (9) become approximate. Function \underline{u} obtained in this way will be continuous function with the property of extreme smoothness within the entire volume of the structure. This function best corresponds to point displacement of the carrier structure and is identified with it.

Now we obtain the equations of the structural dynamics using Hamiltonian variational principle. The performance of this procedure results in the following system of the differential equations

in
$$\nabla - \nabla_{\mathbf{S}} = \nabla \cdot \left[\langle \underline{\mathbf{G}} \cdot \nabla \underline{\mathbf{u}} + \sum_{k=1}^{\infty} \underline{\mathbf{g}}_{k} \mathbf{q}_{k} \right] - \langle \mathbf{p} \rangle (\underline{\underline{\mathbf{u}}} + \sum_{k=1}^{\infty} \mathbf{U}_{k} \mathbf{q}_{k}) + \langle \underline{\mathbf{K}} \rangle = 0 \text{ (II)}$$

$$\mathbf{m}_{\mathbf{k}}\mathbf{q}_{\mathbf{k}} + 2\psi_{\mathbf{k}}\sqrt{\mathbf{m}_{\mathbf{k}}\mathbf{C}_{\mathbf{k}}} \mathbf{q}_{\mathbf{k}} + \mathbf{C}_{\mathbf{k}}\mathbf{q}_{\mathbf{k}} + \mathbf{\underline{z}}_{\mathbf{k}} \cdot \mathbf{v}\underline{\mathbf{u}} + \langle \boldsymbol{p} \rangle \underline{\mathbf{u}}_{\mathbf{k}} \cdot \underline{\mathbf{u}} = \mathbf{Q}_{\mathbf{k}} \quad (12)$$

$$m_{s}g_{sk}+2\psi_{k}\sqrt{m_{sk}G_{sk}}g_{sk}+G_{sk}g_{sk} = Q_{sk}-\frac{1}{V_{s}}\int_{S}\nabla_{s}u_{sk}dV \qquad (Th)$$

and the boundary condition on the structure surface

on
$$O-O_g$$
 $\underline{n} \cdot \left[\langle \underline{C} \rangle \cdot \cdot \nabla \underline{u} + \sum_{k=1}^{\underline{a}} \underline{z}_k q_k \right] = \underline{F}$ (15)

Here n is external normal to the surface 0. Continuity condition on O_8 in $\underline{u} = \underline{v}_8$ (I6) that occurs on internal boundary of substructure V_8 completes the boundary problem. The equations (I2),(I4) are written with structural damping considered, because it is the essential means of restriction of vibration amplitudes under resonances. Damping is written in a conventional way, i.e. by addition of components proportional to speed and damping factor ψ_k .

3. TRANSITION TO THE HOMOGENEOUS MEDIUM WITH COMPLEX STRUCTURE

The boundary problem obtained in this way is extremely difficult to be solved directly because it contains an infinite system of differential equations. Let us perform some simplifying procedures which enable one to arrive at the boundary problem suitable for immediate solution. These procedures follow mainly the work [6].

We admit that substructures deformations don't affect average stresses, i.e. $\mathbf{z}_{\mathbf{k}} = 0$. Let us consider stationary harmonic deformation of the structure

$$\frac{\underline{u}(\underline{r},t) = \underline{u}(\underline{r}) \exp(i\omega t)}{q_k(\underline{r},t) = q_k(\underline{r}) \exp(i\omega t)}$$
(17)

etc. Futher transformation will be performed over the amplitudes. Solving (I2) for $\boldsymbol{q}_{\boldsymbol{k}}$ we have

$$q_{\mathbf{k}} = \frac{\omega^{2}(\mathbf{p}) \, \underline{\mathbf{U}}_{\mathbf{k}} \cdot \underline{\mathbf{u}} + Q_{\mathbf{k}}}{\underline{\mathbf{u}}_{\mathbf{k}} (-\omega^{2} + 2\psi_{\mathbf{k}}\alpha_{\mathbf{k}}\mathbf{i}\omega + \alpha_{\mathbf{k}}^{2})}, \qquad (18)$$

where $q_k = \sqrt{C_k/m_k}$ is the natural frequency. Substitution of (18) into (II) yields the following equation

$$\nabla \cdot \left[\langle \underline{\mathbf{C}} \rangle \cdot \cdot \nabla \underline{\mathbf{u}} \right] + \omega^2 \underline{\mathbf{A}}(\omega) \cdot \underline{\mathbf{u}} + \underline{\mathbf{K}} = 0 , \qquad (19)$$

where

$$\underline{\underline{A}} (\omega) = \langle p \rangle \underline{\underline{E}} + \langle p \rangle^2 \sum_{k=1}^{\infty} \frac{\omega^2 \underline{\underline{U}_k} \underline{\underline{U}_k}}{\underline{\underline{m}_k} (-\omega^2 + 2\psi_k \alpha_k \underline{\underline{i}} \omega + \alpha_k^2)}$$

$$\underline{K} = \langle \underline{K} \rangle - \langle \rho \rangle \sum_{\underline{K}=1}^{\infty} \frac{Q_{\underline{k}}\underline{U}_{\underline{k}}}{\underline{m}_{\underline{k}}(-\omega^2 + 2\psi_{\underline{k}}\alpha_{\underline{k}}\underline{i}\omega + \alpha_{\underline{k}}^2)} . \tag{20}$$

here $\underline{\underline{A}}(\omega)$ is tensor of some mass inertia of the medium, $\underline{\underline{K}}$ is effective volume load. $\underline{\underline{A}}(\omega)$ acts as a tensor and differs in various directions. This property is unparalleled in mechanics [4]. However a real structure has such a complicated composition that it is impossible to find out its anisotropic axes of the substructure spectral properties. It makes us accept the hypothesis of the isotropy of the spectral properties of the object, namely isotropy of the tensor $\underline{\underline{A}}(\omega)$

$$\underline{\underline{A}}(\omega) = \underline{A}(\omega)\underline{\underline{E}} \quad . \tag{2I}$$

Taking into account (2I) the equation (I9) reads as follow

$$\nabla \cdot \left[(\underline{C} \cdot \nabla \underline{u}) + \omega^2 A(\omega) \underline{u} + \underline{K} = 0 .$$
 (22)

4. LOCALITY PRINCIPLE

Tensor $A(\omega)$ requires close study. We obtain its explicit expression [6]. For this purpose first invariant of the tensor is to be derived

$$I\left[\underline{A}(\omega)\right] = \underline{A}(\omega) \cdot \cdot \underline{E} = \underline{A}(\omega)\underline{E} \cdot \cdot \underline{E} = 3\underline{A}(\omega) . \qquad (23)$$

Obtaining of the first invariant based on the equation (20) yields the following result

$$A(\omega) = \langle \rho \rangle \left[I + \langle \rho \rangle \sum_{k=1}^{\infty} \frac{\underline{U}_{k} \cdot \underline{U}_{k} \omega^{2}}{3\underline{u}_{k} (-\omega^{2} + 2\psi_{k} \alpha_{k} i\omega + \alpha_{k}^{2})} \right] (24)$$

We pass over from the sum to the frequency integral. This is possible due to our assumption of high density natural frequencies α_k spectrum. We place the components in the above sum (24) in the ascending order of natural frequencies and introduce the symbol

 $\mathbf{M}(\alpha_{\mathbf{k}})\Delta\alpha_{\mathbf{k}} = \langle \rho \rangle \frac{\underline{U}_{\mathbf{k}} \cdot \underline{U}_{\mathbf{k}}}{3m_{\mathbf{k}}}$

Then replacing the sum by the integral we obtain

$$\mathbf{A}(\omega) = \langle \mathbf{p} \rangle \left[\mathbf{I} + \omega^2 \int_{0}^{\infty} \frac{\mathbf{M}(\alpha) \, d\alpha}{-\omega^2 + 2\psi \alpha i \omega + \alpha^2} \right] \quad . \tag{25}$$

The transition from the sum to the integral is provided on one hand by the high density of spectrum of freguencies α_k , on the other hand it is ensured by structural damping. The fact of

existence of structural damping is essential to perform the sum-to-the-integral transition. This is accounted for by the fact that in the absolutely elastic systems the influence of the boundary conditions is extended throughout the system. This is most explicit in the resonance vicinity. With structural damping present in the system, this relationship is not observed. The higher the structural damping in the system the more accurate is the transition of the sum (24) into the integral (25). It means that each value of the spectrum density has its own critical damping value, its being exceeded allows to replace the sum with the integral.

The possibility of the transition of the sum into the integral is extremely important, that is why it is given so much attention here. It was already mentioned above that the behaviour of a real object that is a body with distinct space heterogeneity can be described by the differential equation (22). Such an equation was obtained by the authors before for the cases of isotropic [1-3] and anisotropic [4] bodies. But the principle of obtaining of the equation was quite different in those works. It was assumed that there exists a certain linear elastic continuous medium (isotropic or anisotropic) that was named carrier medium. Each point of the carrier medium was connected with infinite set of oscillators which didn't interact with each other. The oscillators acted as dampers which provided high space absorption of vibration. It is interesting to note that not only the dynamics equation of the above mentioned works and the equation of this article (22) coincide, but the expressions of $A(\omega)$ there and in this article coincide as well. But the schemes of their obtaining are quite different. In this article using some natural assumptions we perform the pass-over from entire complexity of the real object to the equation that was obtained by consideration of the homogeneous medium with generalized rigidity and spectrum characteristics. The transition can be performed due to the possibility of replacement of the sum (24) with the integral (25), i.e. the simultaneous existence of the certain value of relative spectrum density and exceeding of a certain critical damping value to Which it corresponds. The above mentioned speculations allow us to formulate the locality principle. It reads as follows: each object with its own spectrum density has a certain critical damping value, which being

exceeded allows to describe the behaviour of the substructure V_s in the structure V by the following boundary problem (forced. vibrations are meant)

in
$$\nabla - \nabla_s$$

$$\nabla \cdot ((\underline{C}) \cdot \cdot \cdot \nabla \underline{u}) + \omega^2 \Lambda(\omega) \underline{u} + \underline{K} = 0$$
 (26)

in
$$\nabla - \nabla_{s}$$

$$\nabla \cdot (\langle \underline{c} \rangle \cdot \cdot \nabla \underline{u}) + \omega^{2} \underline{A}(\omega) \underline{u} + \underline{K} = 0$$
(26)
in ∇_{s}

$$\nabla \cdot (\langle \underline{c} \rangle \cdot \nabla \underline{u}) + \omega^{2} \underline{A}(\omega) \underline{u} + \underline{K} = 0$$
(27)
$$\nabla_{s} \underline{u}_{sk} (-\omega^{2} + 2\psi_{k} \alpha_{k} \underline{i} \omega + \alpha_{k}^{2}) \underline{g}_{sk} = \int (\underline{k} + g \omega^{2} \underline{v}_{s}) \cdot \underline{u}_{sk} d\nabla + \int \underline{F} \cdot \underline{u}_{sk} dO(28)$$

on
$$0-0_g$$
 $\underline{n} \cdot (\langle \underline{c} \rangle \cdot \cdot \underline{v}\underline{u}) = \underline{F} \quad v_s$ (29)

on
$$O_{s in}$$
 $\underline{u} = \underline{v}_{s}$ (30)

In other words we describe the behaviour of the structure element in question accurately, and the rest of the object integrally using for this purpose the mechanics of the medium with complex structure, where the microstructure is a set of oscillators. Thus, the vibration state of a particular element of a complicated dynamic structure depends mainly upon the particular composition of the element itself and upon certain generalized properties of the remote elements of the structure and does not depend upon their details. The locality principle works in the high frequency band first of all, because it is only there that the relative spectrum density is high. The locality principle is also absolutely valid for the systems with continuous spectrum, i.e. for infinite objects. In this case any damping value is sufficient.

5. REFERENCES

- V.A. PALMOV 1969 Journal of Applied Mechanics and Mathematics No.5. On a model of medium of complex structure (In Rus.)
- V.A. PALMOV 1976 Vibration of elastic-plastic bodies. Moscow: NAUKA. (In Russian)
- V.A. PALMOV 1979 Advances in Mechanics No.2 . Warsaw . The integral methods of study of vibration in complicated dynamic systems. (In Russian)
- A.K. BELYAEV 1978 Soviet Applied Mechanics (USA) 14, 5 4. Propagation of plane waves in an anisotropic medium having a complex structure.
- A.K. BELYAEV and V.A. PALMOV 1980 Recent advances in structural dynamics. Ed. by M. Petyt. I . Institute of Sound and Vibration Research, Southampton, England. Theory of vibroconductivity.
- A.I. STANKEVITCH 1979 Applied Mechanics 15, 10. Three-dimentional model for the study of dynamics in complicated mechanic systems. (In Russian)

5. NON LINEAR ANALYSIS TECHNIQUES



A.W. Leissa

Department of Engineering Mechanics Ohio State University Columbus, Ohio USA

AD-P003 661

1. INTRODUCTION

The subject of nonlinear vibrations has always been a difficult one. The primary difficulty lies in the solution of governing equations of motion which are nonlinear differential equations. Solution characteristics such as existence, uniqueness and superposition, which are taken for granted in linear vibration problems, are not guaranteed. Often the physical problem itself, including experiment, must be relied upon to suggest a reasonable nonlinear solution (which is typically not exact, but approximate).

Vibration analysis of one or two degree-of-freedom nonlinear problems arising from discrete systems is complicated enough, and numerous books and papers have been written dealing with such problems. Plates and shells are among the most complicated of a hierarchy of continuous systems (including also strings, beams, membranes and three-dimensional solids). Such problems are even more difficult, for one must deal with nonlinear partial differential equations, rather than ordinary ones. Consequently, the most common approach to nonlinear plate and shell vibration problems is to assume a mode shape, based upon physical understanding, intuition or the linear solution, which reduces the problem to one having a single degree of freedom. More complex solutions assume two or more modes in the response, which lead to more accurate results.

In plate or shell vibration problems, nonlinearity may arise in various ways; for example, (1) nonlinear stress-strain relations for the material, (2) nonlinear boundary conditions, such as nonlinear springs or partial slipping, (3) geometric nonlinearity in the strain-displacement relations, resulting from significantly large transverse displacements during vibration. Among these and other possible causes of nonlinearity, the literature of nonlinear vibrations of plates and shells deals almost exclusively with the third one. Furthermore, the geometric nonlinearity treated is typically quite restricted, and does not consider large inplane displacements.

In spite of the narrowness of the type of nonlinear behavior typically considered, considerable research on plate and shell vibrations has taken place in recent years. This is no doubt partly due to the physical importance of large amplitude, nonlinear effects, and partly due to the fascination and challenge in solving nonlinear problems. The recent increase in activity in nonlinear plate vibration during the past decade may be seen in Table 1. It should be mentioned that the relatively few references found in reference 1 before 1966 are the result of a more thorough literature search than those followed in preparing references 2, 3 and 4. Also appearing in recent years is an excellent book by Chia [5] which does much to organize and clarify the subject of large amplitude motions of plates.

The present paper has two major objectives: (1) to present an overview of the subject of nonlinear vibrations of plates and shells and (2) to summarize the recent literature in the subject. In regard to the latter objective, publications are referenced which have appeared in the past five years, with the exception of a few background references which extend further back in time. Length limitations have restricted the scope of the present work to free, undamped vibrations. While forcing and damping phenomena are also important, one must begin with a reasonable understanding of the free vibration problem before

Table 1. Publications dealing with nonlinear vibrations of plates

Period	Number of References	Source		
Before 1966	10	[1]		
1966–1972	24	[2]		
1973-1976	47	[3]		
1976-1980	58	[4]		

proceeding further.

2. FREE VIBRATIONS OF CLASSICAL PLATES

2.1 Fundamental Equations

Consider a plate of arbitrary shape as depicted in Figure 1. Its thickness (h) is assumed small in comparison with its lateral dimensions. The xy-plane lies at the undeformed middle surface, located at $z=\pm h/2$. Let the displacement components of a typical point within the plate be u,v,w in the x,y,z directions, respectively, while the body is undergoing deformation. Thus, u and v are inplane displacements and v is transverse with respect to the midplane.

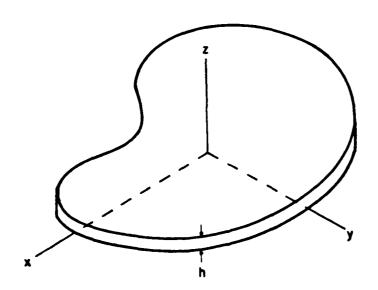


Figure 1. Plate of arbitrary shape, showing coordinates.

The classical equations of plate theory are 'ased upon the Kirchhoff hypothesis; viz., "normals to the midplane of the undeformed plate remain straight and normal to the midplane and unstretched in length during deformation." With this assumption the displacements may be written as

$$u = u_{0} - z \frac{\partial w}{\partial x}$$

$$v = v_{0} - z \frac{\partial w}{\partial y}$$

$$w = w_{0}$$
(1)

where, in general, u,v and w are functions of all three coordinates (x,y,z) and of time (t). The terms u,v and w are displacement components of a point at the midplane (z=0). Thus, the inplane displacements u and v are composed of two parts – stretching of the midplane (u and v) and bending, causing additional displacements proportional to both the local slopes and the distance of a point from the midplane. The strains $\varepsilon_x, \varepsilon_v$ and γ_{xv} may therefore be written as

$$\varepsilon_{\mathbf{x}} = \varepsilon_{\mathbf{x}_{0}} - z \frac{\partial^{2} \mathbf{w}}{\partial \mathbf{x}^{2}}$$

$$\varepsilon_{\mathbf{y}} = \varepsilon_{\mathbf{y}_{0}} - z \frac{\partial^{2} \mathbf{w}}{\partial \mathbf{y}^{2}}$$

$$\varepsilon_{\mathbf{xy}} = \varepsilon_{\mathbf{xy}_{0}} - 2z \frac{\partial^{2} \mathbf{w}}{\partial \mathbf{x} \partial \mathbf{y}}$$
(2)

where ε_{x_0} , ε_{y_0} and ε_{xy_0} are the midplane strains.

In the classical, <u>linear</u> theory of plates, the governing equation of transverse motion is uncoupled from the inplane equations. For relatively thin plates, inasmuch as the transverse vibration modes have considerably lower frequencies than the inplane modes, the inplane equations are usually ignored. Assuming an isotropic, homogeneous material, one uses the stress-strain equations, integrates over the plate thickness to obtain the bending moments, and substitutes into the transverse equation of motion to obtain

$$D\nabla^{4}w + \rho h \frac{\partial^{2}w}{\partial t^{2}} = N_{x} \frac{\partial^{2}w}{\partial x^{2}} + 2N_{xy} \frac{\partial^{2}w}{\partial x \partial y} + N_{y} \frac{\partial^{2}w}{\partial y^{2}}$$
(3)

where D = ${\rm Eh}^3/12(1-v^2)$ is the flexural rigidity, $\nabla^4=\nabla^2\nabla^2$ is the biharmonic differential operator, ρ is the plate mass per unit volume, and N_x, N_{xy}, N_y are the inplane stress resultants (i.e., forces per unit length, or stresses times thickness). For the classical, linear problem, assuming small transverse displacements, N_{xy} and N_y are stress resultants which are applied initially in the xy-plane and do not depend upon w or t.

In the case of large transverse displacements, additional inplane (or membrane) strains are caused by the stretching of the midplane. Then the midplane strains are given by

$$\varepsilon_{\mathbf{x}_{0}} = \frac{\partial \mathbf{u}_{0}}{\partial \mathbf{x}} + \frac{1}{2} \left(\frac{\partial \mathbf{w}}{\partial \mathbf{x}} \right)^{2}$$

$$\varepsilon_{\mathbf{y}_{0}} = \frac{\partial \mathbf{v}_{0}}{\partial \mathbf{y}} + \frac{1}{2} \left(\frac{\partial \mathbf{w}}{\partial \mathbf{y}} \right)^{2}$$

$$\varepsilon_{\mathbf{x}\mathbf{y}_{0}} = \frac{\partial \mathbf{v}_{0}}{\partial \mathbf{x}} + \frac{\partial \mathbf{u}_{0}}{\partial \mathbf{y}} + \frac{\partial \mathbf{w}}{\partial \mathbf{x}} \frac{\partial \mathbf{w}}{\partial \mathbf{y}}$$
(4)

where the last terms of equations (4) introduce nonlinearity into the problem, and where other nonlinear terms are considered to be higher order and therefore negligible.

The nonlinear equations of motion of the plate are a coupled, eighth order system of differential equations. This coupled system may be expressed solely in terms of the midplane displacements u_0 , v_0 and w (= w_0) (cf. [6]). However, it is often more convenient to utilize the inplane compatibility equation

$$\frac{\partial^{2} \varepsilon \mathbf{x}_{o}}{\partial \mathbf{y}^{2}} + \frac{\partial^{2} \varepsilon \mathbf{y}_{o}}{\partial \mathbf{x}^{2}} - \frac{\partial^{2} \gamma \mathbf{x} \mathbf{y}_{o}}{\partial \mathbf{x} \partial \mathbf{y}} = \left(\frac{\partial^{2} \mathbf{w}}{\partial \mathbf{x} \partial \mathbf{y}}\right)^{2} - \frac{\partial^{2} \mathbf{w}}{\partial \mathbf{x}^{2}} \frac{\partial^{2} \mathbf{w}}{\partial \mathbf{y}^{2}}$$
 (5)

which equations (4) identically satisfy. To reduce the number of dependent variables in the problem, it is also convenient to introduce an Airy stress function (ϕ) related to the inplane stress resultants by

$$N_{x} = h \frac{\partial^{2} \phi}{\partial y^{2}}, N_{y} = h \frac{\partial^{2} \phi}{\partial x^{2}}, N_{xy} = -h \frac{\partial^{2} \phi}{\partial x \partial y}$$
 (6)

With ϕ defined by equations (6), and if tangential accelerations $(\theta^2 u/\theta t^2)$ and $\theta^2 v/\theta t^2$ and body forces may be considered negligible, then the two inplane equations of motion (which are now equations of equilibrium) are identically satisfied by any choice of ϕ . Equations (3) and (5) then become

$$D\nabla^{4}w + \rho h \frac{\partial^{2}w}{\partial t^{2}} = h(\frac{\partial^{2}\phi}{\partial y^{2}} \frac{\partial^{2}w}{\partial x^{2}} + \frac{\partial^{2}\phi}{\partial x^{2}} \frac{\partial^{2}w}{\partial y^{2}} - 2 \frac{\partial^{2}\phi}{\partial x \partial y} \frac{\partial^{2}w}{\partial x \partial y})$$
 (7a)

$$\frac{1}{E}\nabla^{4}\phi = \left(\frac{\partial^{2}w}{\partial x \partial y}\right)^{2} - \frac{\partial^{2}w}{\partial x^{2}} \frac{\partial^{2}w}{\partial y^{2}}$$
 (7b)

Equations (7), along with the proper boundary conditions for the plate in question, constitute the governing equations which must be satisfied by the problem. Equations (7) are the dynamic form of the well known von Kármán plate equations [7]. One observes that the terms on their right-hand-sides are all nonlinear. Furthermore, the nonlinearity of the problem depends directly upon the magnitudes of the curvatures $(\partial^2 w/\partial x^2)$ and $\partial^2 w/\partial y^2$ or twist $(\partial^2 w/\partial x \partial y)$ of the deformed midsurface. However, since these quantities depend, in turn, upon the amplitudes of the vibration modes, it is traditional to speak of the "large displacement," nonlinear vibration problem.

A simplified set of equations accounting for the membrane stretching of the middle surface during transverse displacement of a plate was derived by Berger [8], and has been used by many analysts. These equations are based upon the assumption that the second invariant of the membrane strain tensor is negligible in comparison with the square of the first invariant. The resulting equations are considerably more simple than the von Kármán equations, but recent research has cast doubt upon the accuracy of the Berger equations.

Solution of the nonlinear equations, as well as experimental evidence, indicates that the large amplitude vibrations of plates may be characterized by a "hard" spring response. That is, the natural frequencies increase as the vibration amplitude is increased. Typically, significant frequency changes are found for plates having vibration amplitudes of the order of the plate thickness.

2.2 Rectangular Plates

To solve the nonlinear free vibration problem for a rectangular plate the most common procedure used is to begin by assuming a vibration mode shape for w. This mode shape should satisfy the boundary conditions relating to w. Thus, for example, the fundamental vibration mode of a plate having dimensions axb with all four edges simply supported (SSSS) can be represented by

$$w(x,y,t) = \sin \frac{\pi x}{a} \sin \frac{\pi y}{b} \tau(t)$$
 (8)

where $\tau(t)$ is a function of time to be determined. For the linear, small amplitude vibration problem equation (8) would yield the exact solution with $\tau(t) \approx A\sin\omega t + B\cos\omega t$, with A and B to be determined from the initial conditions. For the nonlinear problem, the assumed mode (8) is substituted into equation (7b), which permits one to solve for a corresponding ψ in terms of $\tau(t)$ and to satisfy the inplane boundary conditions on u and v. Finally, equation (7a) is satisfied approximately by means of the Galerkin procedure, which results in Duffing's equation for $\tau(t)$,

$$\frac{d^2\tau}{dt^2} + \omega_{\ell}^2 \tau + \alpha^2 \tau^3 = 0 \tag{9}$$

where ω_{ℓ} is the linear frequency. Equation (9) has a well known solution in terms of elliptic integrals. From such an analysis, curves showing the ratio of nonlinear to linear frequency (ω_n/ω_{ℓ}) as functions of the ratio of vibration amplitude to plate thickness may be plotted. Representative plots are shown in Figure 2 for a simply supported square plate having edges which are either completely constrained or movable in the inplane (x or y) directions. It is seen that frequency increases of approximately 6 and 40 percent are encountered for these two cases when the vibration amplitude equals the plate thickness.

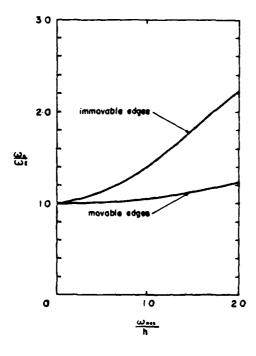


Figure 2. Ratio of nonlinear to linear frequency versus amplitude/thickness ratio for a simply supported square plate.

It should be remarked here that plots of the type shown in Figure 2 do not usually appear in the literature. What is typically shown for the ordinate is the ratio of nonlinear to linear period for the vibration cycle. While astronomers and (in some cases) physicists may be primarily interested in the periods of periodic motion, engineers are nearly always concerned with the frequencies. In reference 1 the ratio $\omega_{\hat{n}}/\omega_{\hat{n}}$ was used to avoid replotting the earlier work reported. However, it is hoped that $\omega_{\hat{n}}/\omega_{\hat{n}}$ will be used in the future literature of engineering vibrations.

A recent study by Kennedy [9] dealt with a plate having immovable simply supported edges. The nonlinear governing equations were written in finite difference form, using a 5x5 grid idealization, and the resulting nonlinear difference equations were solved for the time response (and frequency) by means of an analogue computer. The study showed that ω_n/ω_k depends upon the aspect ratio (a/b) as well as w_{\max}/h , which agrees with the earlier findings of Chu and Herrmann [10]. Specifically, ω_n/ω_k was found to increase with increasing a/b. Other studies using the Berger [8] simplified formulation of the problem have indicated that ω_n/ω_k did not depend upon a/b. It was also shown by Kennedy [9] that neglect of tangential inertia could lead to noticeable error in ω_n/ω_k in some cases (e.g., 3% error for a/b=3 and $w_{\max}/h=1$). Sathyamoorthy [6] used the Galerkin method on the displacement form of the von Karmán equations for the same problem and also found that ω_n/ω_k depends upon a/b.

Only a small amount of additional work on the nonlinear, free vibrations of rectangular plates, based upon classical theory, has taken place in recent years. Banerjee and Datta [11] used the method of conformal mapping to obtain solutions of the von Kármán equations (7) for square plates having movable or immovable clamped boundaries. Reddy [12] examined thin, simply supported square plates of isotropic material having square, central cutouts and presented frequencies for various cutout sizes. The finite element method was used. He showed that plates with cutouts exhibit larger ratios of linear to nonlinear frequencies $(\omega_n/\omega_{\hat{k}})$ for a given value of $w_{\rm max}/h$ than those without cutouts. Banerjee [13] studied the completely clamped square plate carrying a concentrated mass. Numerical results were obtained for the isotropic plate having immovable edges with a concentrated mass at its center. He determined that $\omega_n/\omega_{\hat{k}}$ is independent of the magnitude of the concentrated mass, which is contrary to the previous results presented by Ramachandran [14].

2.3 Circular Plates

For plates having circular boundaries (solid or annular), it is desirable to express the nonlinear governing equations (7) in polar coordinates. They become

$$DV^{4}w + h \frac{3^{2}w}{3t^{2}} = h \left[\left(\frac{1}{r} \frac{3}{3r} + \frac{1}{r^{2}} \frac{3^{2}\zeta}{3r^{2}} \right) \frac{3^{2}w}{3r^{2}} + \frac{3^{2}\zeta}{3r^{2}} \left(\frac{1}{r} \frac{3w}{3r} + \frac{1}{r^{2}} \frac{3^{2}w}{3r^{2}} \right) - 2\frac{3}{3r} \left(\frac{1}{r} \frac{3w}{3r} \right) \frac{3}{3r} \left(\frac{1}{r} \frac{3p}{3r} \right) \right]$$

$$(10a)$$

$$\frac{1}{E}x^4 := \left[\frac{3}{3r}\left(\frac{1}{r}\frac{3w}{3r}\right)\right]^2 - \frac{3^2w}{3r^2}\left(\frac{1}{r}\frac{3w}{3r} + \frac{1}{r^2}\frac{3^2w}{3r^2}\right)$$
 (10b)

where now the $\overline{\mathbf{v}}^4$ operator is taken in its polar coordinate form.

Sathyamoorthy [15] compared results obtained from the von Kármán formulation (equations (10)) with those from the simplified Berger [8] equations for the fundamental mode (which is axisymmetric) of thin, isotropic, circular plates having rigidly clamped (immovable) edges. These are summarized in Table 2

below, where ω_n/ω_ℓ is compared for various values of w_/h. One observes that the results from the two formulations of the problem do not differ greatly, with only 0.8 and 1.5 per cent differences of ω_n/ω_ℓ when w_max/h is 1 and 2, respectively.

Table 2.	Frequency	ratio	versus	amplitude,	bу	two	theories.
----------	-----------	-------	--------	------------	----	-----	-----------

w	ω _n /ω _ℓ				
h	von Kármán	Berger			
0	1.0000	1.0000			
0.5	1.0434	1.0460			
1.0	1.1647	1.1740			
1.5	1.3405	1.3580			
2.0	1.5361	1.5588			

Karmaker [16] also used the von Kármán equations to analyze circular plates having clamped, immovable edges, with concentrated mass M added at the center. He arrived at the following nonlinear frequency-amplitude formula:

$$\omega^{2} = \frac{50.2}{(\frac{\rho ha^{4}}{D} + \frac{15}{4} \frac{Ma^{2}}{D})} [(\frac{w_{max}}{h})^{2} + 2.1]$$
(11)

where a is the plate radius. Setting M=0 and using equation (11) to compute $\frac{1}{n}$ for w $\frac{1}{n}$ and 2, one obtains 1.21 and 1.70, respectively, which are significantly different than the corresponding values in the first column of Table 1.

The effects of elastic rotational edge constraint upon the axisymmetric nonlinear vibrations of circular plates having immovable edge supports were examined by Venkateswara Rao and Kanaka Raju [17] by means of the finite element method. Other axisymmetric results were obtained by Reddy, Huang and Singh [18], also using a finite element approach.

2.4 Other Shapes

A few authors have presented recent results for the nonlinear vibrations of elliptical plates. In two similar publications Sathyamoorthy and Chia [19,20] followed the standard procedure using the Galerkin method with the von Kármán equations to analyze elliptical plates having clamped, immovable boundaries. They presented the interesting result that the frequency ratio ω_n/ω_{ℓ} is virtually unaffected by the ratio of major to minor axis (a/b) of the ellipse. Inasmuch as, following the same procedure, significant differences in ω_n/ω_{ℓ} have been found for rectangular plates having different aspect ratios (see Section 2.2), one could assume that the surprising result for elliptical plates may be due to the simple, one term polynomial assumption used for the transverse displacement (w).

Karmaker [16] solved the same problem by the same method, but included a concentrated mass at the center of the plate. Interestingly enough, if his

results are specialized to the case of zero added mass, it is found that ω_n/ω_ℓ increases with increasing a/b, for a fixed value of w /h. This increase of ω_n/ω_ℓ with increasing slenderness is consistent with the previously mentioned results for rectangles (Section 2.2).

The parallelogram plate was analyzed by Sathyamoorthy [21,22] for the case when all edges are clamped and movable. From studying the numerical results presented one observes a drastic change in $\omega_n/\omega_{\hat{k}}$ for a given aspect ratio (a/b) as the skew angle is increased. For example, for a rhombic plate, $\omega_n/\omega_{\hat{k}}$ is shown to decrease from 1.203 to 1.020 for w_0/h=1.5 as the angle is increased from 0°(square) to 30°. This result is rather surprising, considering that the rhombus is a more slender shape than the square.

Banerjee and Datta [11] also used the conformal mapping approach with the von Kármán equations to solve the problems of simply supported regular polygonal plates having 3,4,...,8 sides which are either movable or immova`le. Their results were presented as the nondimensional frequency parameter $\omega a^2 \sqrt{\epsilon/Eh}$ versus w/h. If these results are replotted as ω_n/ω_ℓ versus w/h, one finds that, for a given set of edge conditions, the curves for the various polygonal plates virtually coincide. Chaudhuri [23] analyzed the equilateral triangular plate by the use of trilinear coordinates and the Galerkin method, along with the von Kármán equations.

3. COMPLICATING EFFECTS IN PLATE VIBRATIONS

3.1 Anisotropic Material

For a plate composed of material which is generally anisotropic with respect to a rectangular coordinate system the first term (D 4 w) of equation (7a) is replaced by

$$D_{1} \frac{\partial^{4} w}{\partial x^{4}} + D_{2} \frac{\partial^{4} w}{\partial x^{3} \partial y} + D_{3} \frac{\partial^{4} w}{\partial x^{2} \partial y^{2}} + D_{4} \frac{\partial^{4} w}{\partial x \partial y^{3}} + D_{5} \frac{\partial^{4} w}{\partial y^{4}}$$
(12)

where D_1,\ldots,D_5 are constant coefficients depending upon the material properties. The other governing equation (7b) is then correspondingly generalized, with its first term ($\nabla^4 \phi/E$) replaced by five terms similar in form to expression (12). For an orthotropic material the two equations are somewhat simplified with, for example, $D_2=D_4=0$ in expression (12). However, this simplification permits the widely-used approximate solution procedure described previously in Section 2.2 to be followed; for an assumed mode shape w(x,y,t) the orthotropic generalization of equation (7b) may be solved exactly for $\phi(x,y,t)$, and the Galerkin procedure followed with the generalization of equation (7a) to yield equation (9).

Several publications have recently appeared dealing with the nonlinear vibrations of orthotropic plates of rectangular shape [6,13,24-26]. These papers typically describe plates having the same conditions along all four edges; that is, clamped or simply supported, and movable or immovable with respect to inplane displacements. Work is generally lacking for nonuniform edge conditions (e.g., a CCCF plate), elastic edge supports, point supports and discontinuous edge conditions. Banerjee[13] considered the effects of a concentrated added mass. Varadan and Pandalai [26] treated clamped orthotropic plates having added stiffness, the latter being treated as being either discrete or "smeared out." Prathrap and Pandalai [27] studied the effects of transverse isotropy (i.e., the transverse shear modulus is different than the inplane shear modulus).

Plates having other shapes, but made of rectangularly orthotropic material, have also received recent attention by Sathyamoorthy and Chia. These include parallelogram (or skew) [22,28,29], circular [30,31] and elliptical [19,32] shapes.

Material orthotropy may be expressed in terms of any orthogonal, curvilinear coordinate system (e.g., elliptic-hyperbolic coordinates). In the case of polar orthotropy, the orthotropic stress-strain relations relate to radial (r) and circumferential (θ) directions, and the differential operator appearing in the generalization of the von Kármán equations becomes considerably more complicated than expression (12), and includes variable coefficients. Circular and annular plates having polar orthotropy axes concentric with their boundaries yield nonlinear vibration modes of the form $w(r,\theta)=F(r)\cos\theta$, where n is an integer, and where n=0 yields the axisymmetric modes. A few researchers have recently obtained results for circular [33,34] and annular [35] plates having polar orthotropy.

3.2 <u>Initial Inplane Stresses</u>

Inplane stresses may exist within a plate in static equilibrium, either by virtue of edge loadings or internal, self-equilibrating stress states (e.g., residual stresses from cold working). In this case the theoretical problem is changed by the addition of the expression

$$N_{x}^{*} \frac{\partial^{2} w}{\partial x^{2}} + 2N_{xy}^{*} \frac{\partial^{2} w}{\partial x \partial y} + N_{y}^{*} \frac{\partial^{2} w}{\partial y^{2}}$$
 (13)

to the right-hand-side of equation (7a). Here N $_{\rm x}^{*}$, N $_{\rm xy}^{*}$, and N $_{\rm xy}^{*}$ identify the initial inplane stress resultants which, in general, are constant with respect to time but not with respect to x or y. These are distinguished from and supplementary to N $_{\rm x}$, N $_{\rm xy}^{*}$ and N (eqs. (3) and (4)) which are the vibratory inplane stress resultants caused by large amplitude displacements. As in linear vibration problems, the effect of positive N $_{\rm x}^{*}$ or N $_{\rm x}^{*}$ (i.e., tension) is to increase the natural frequencies, whereas negative N $_{\rm xy}^{*}$ or N $_{\rm xy}^{*}$ (i.e., compression), or positive or negative N $_{\rm xy}^{*}$ (shear) causes the frequencies to decrease. As a frequency approaches zero, the plate approaches a buckling state.

Massalas, Soldatos and Tzivanidis [36] examined the large amplitude vibrations of a simply supported rectangular plate subjected to uniform compressive stress in one direction. Straightforward application of the Galerkin method with an assumed mode in the form of equation (8) yielded the same form of differential equation (9) as without initial stresses. Putnick, Matkowsky and Reiss [37] analyzed the same problem by means of the perturbation method and showed that, as $N_{\rm x}$ is increased, a critical value of $N_{\rm x}$ is reached at which the primary vibration mode bifurcates to a secondary mode. This secondary bifurcation phenomenon has been observed by a number of people for the large amplitude buckling behavior of plates.

3.3 Variable Thickness

For a plate having variable thickness, the simple term $D\nabla^4 w$ in equation (7a) is replaced by

$$\nabla^{2}(\mathbf{D}\nabla^{2}\mathbf{w}) - (1-\mathbf{v})\left(\frac{\partial^{2}\mathbf{D}}{\partial \mathbf{y}^{2}} \frac{\partial^{2}\mathbf{w}}{\partial \mathbf{x}^{2}} - 2 \frac{\partial^{2}\mathbf{D}}{\partial \mathbf{x}\partial \mathbf{y}} \frac{\partial^{2}\mathbf{w}}{\partial \mathbf{x}\partial \mathbf{y}} + \frac{\partial^{2}\mathbf{D}}{\partial \mathbf{x}^{2}} \frac{\partial^{2}\mathbf{w}}{\partial \mathbf{y}^{2}}\right)$$
(14)

Since $D = Eh^3/12(1-v^2)$, if h is a function of x and/or y, expression (14) becomes, in general, quite complicated with terms having variable coefficients. However, the usual solution procedure may still be straightforwardly followed. That is, assuming a mode shape for w and solving equation (7b) for ϕ , the Galerkin method can still be applied to yield an equation in the form of (9).

One recent paper by Banerjee and Das [38] analyzed the simply supported rectangular plate having parabolic thickness variation in one direction, with

immovable edges.

For circular plates having thickness variation expressed in polar coordinates, expression (14) is replaced by another relatively complicated form, but the solution procedure using the Galerkin method is, in principle, the same. Two recent papers analyzed circular plates having thickness varying linearly in the radial direction [39,40], with the edge supported elastically. One [39] used the Berger equations, the other [40] a finite element approach. It was shown [39] that plates with radially decreasing thickness have larger ω_n/ω_ℓ than constant thickness ones, and conversely for plates with radially increasing thickness.

3.4 Elastic Foundation

If a plate is attached to (or embedded in) an elastic foundation, the transverse displacement is resisted by a restoring force from the foundation. When the stiffness of the foundation is linear, a term kw is added to the left-hand-side of equation (7a), where k is the foundation stiffness (in dimensions of force per unit area per unit displacement, or F/L^3). For the classical, small amplitude vibration problem it is easily shown (cf. [1], p. 1), that although the frequencies are increased by the foundation stiffness, the eigenvalues are the same, with or without the foundation. However, for the nonlinear, large amplitude problem the situation is somewhat more complicated.

Massalas, Soldatos and Tzivanidis [36] considered a more general elastic foundation having linear and cubic restoring force terms (i.e., $k_1w + k_3w^3$), thus obtaining two sources of nonlinearity in the large amplitude vibration problem for a simply supported rectangular plate. However, they ignored inplane compatibility (eq. (7b)) completely in their solution.

3.5 Shear Deformation and Rotary Inertia

Consideration of shear deformation, in addition to the usual bending deformation, adds to the flexibility of a plate. Mathematically, the additional flexibility is typically added to the theory by replacing the slopes $\partial w/\partial x$ and $\partial w/\partial y$ in equations (1) by the new variables ψ_x and ψ_y , which are the bending slopes in the two directions (x and y). Thus, the total slope in a given direction at any point of the midsurface is comprised of two parts – bending and shear – and ψ_x and ψ_y are independent of w. Rotary inertia is added to the translational inertia of a plate by inclusion of proper terms in the rotational equations of motion. The result is that the fourth order equation of motion (7a) is replaced by three equations, each of second order, and the eighth order system of equations (7) becomes one of tenth order in the four variables ϕ_x , ψ_x and ψ_y . Both shear deformation and rotary inertia effects decrease the natural frequencies, and this decrease may become significant for plates having length-to-thickness ratios of ten or less.

Considerable recent research in nonlinear plate vibrations has included shear deformation and rotary inertia. Systems of equations have been derived (cf. [21,28,41-43]). Numerical results have been obtained for thick rectangular [27,44,45], circular [15,18,30,31,36,44,46,47], elliptical [32,44,48] and skew [21,29] shaped plates. It has been shown (cf. [46,49]) that the effects of shear deformation and rotary inertia upon the frequency ratio $\omega_n/\omega_{\hat{\chi}}$ become less significant as the amplitude ratio w_{max}/h increases.

3.6 Laminated Composite and Other Nonhomogeneous Plates

A plate having material properties which are not uniform throughout is nonhomogeneous (or heterogeneous). Material properties may vary in the inplane (x and y) or transverse (z) directions. They may vary continuously (e.g., rubber or styrofoam, or metals subjected to nonuniform, high temperatures) or stepwise

(e.g., a layered plate comprised of two homogeneous materials). Of particular importance in modern technology is the laminated composite plate comprised of layers of fibers (e.g., glass, boron, carbon) embedded in matrix materials (e.g., epoxy). Each layer may be regarded as an orthotropic lamina, and the fibers may be arranged in parallel-, cross- or angle-ply orientations with respect to each other and/or the sides of the plate. While the vibrations of plates having continuous nonhomogeneity have received little attention, laminated composite plates have been studied intensively in recent years. A recent survey article [50] discussed approximately 60 publications on vibrations of composite plates which appeared during the past 15 years.

In the case of a typical, laminated composite plate the orthotropic stress-strain equations must be written for each layer. These equations must then be tensorially transformed into the plate coordinate system. Integration over the thickness to obtain the bending moments $(M_{\rm x},\,M_{\rm y},\,M_{\rm xy})$ and inplane stress resultants $(N_{\rm x},\,N_{\rm y},\,N_{\rm xy})$ must be done in a piecewise manner. For symmetrically laminated (i.e., layers stacked symmetrically with respect to the midplane), the resulting equations for parallel— and cross-ply plates take the same form as those of an orthotropic plate, whereas for angle-ply plates they are those of a generally anisotropic plate (see Section 3.1). However, unsymmetric stacking sequences yield coupling between bending and stretching even for the case of linear, small amplitude vibrations. Large amplitudes cause additional coupling. Generalizations of the dynamic von Karman equations for large amplitude motions to composite plates of the general (i.e., unsymmetrically laminated) type were first presented by Whitney and Leissa [51,52]. Chia's recent book [5] devotes considerable attention to the nonlinear analysis of composite plates.

In recent years Nigoyi and Meyers [24] demonstrated a perturbation method of solution for the orthotropic plate equations on a series of glass-, boron- and graphite-epoxy rectangular plates. Sathyamoorthy and Chia used assumed mode approaches to analyze skew [29] and elliptical [19] plates comprised of boron- and glass-epoxy materials, respectively. Reedy and Chao [53-55] developed finite eleme t methods and demonstrated their use on a number of representative cross-ply and angle-ply rectangular plates having various edge conditions. Results were also obtained for composite rectangular plates having rectangular cutouts [12].

3.7 Initial Imperfections

Consider finally a plate which is not perfectly flat; in its static, unloaded condition, the midplane is assumed to deviate from flatness by a maximum amount which is of the order of the plate thickness. This initial imperfection in flatness (also called "geometric imperfection") is assumed to vary smoothly (e.g., sinusoidally or quadratically) between the plate edges. To accommodate the initial imperfection in the von Karman equations (7), w is replaced by $w + w^*$, where w^* is the imperfection shape.

In the case of a rectangular plate with initial imperfection subjected to inplane initial stresses and undergoing free vibration [56] the problem is non-linear, even for small vibratory displacements. Initial imperfections of the order of the plate thickness may result in much larger frequencies in the unloaded case. A typical plot of frequency versus initial, uniaxial compressive stress is shown in Figure 3 for simply supported square plates having various imperfection amplitudes ($w_{\max}^*/h=0$, 0.25, 0.5). With increasing initial stress, the fundamental plate frequency may first decrease and then increase, as shown.

Several recent works have studied the effects of imperfections on the large amplitude frequencies of plates. For rectangular plates, Celep [49] considered shear deformation and rotary inertia, whereas Massalas, Soldatos and Tzivanidis [36] included uniaxial initial stress and an elastic foundation. For circular

plates, Hui [57] showed that initial imperfections may change the large amplitude vibratory behavior from a hard spring to a soft spring type of response. Other work on circular plates with initial imperfections includes both theoretical and experimental results [58-60].

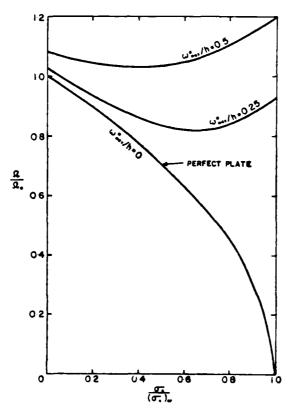


Figure 3. Effect of initial uniaxial compression and initial imperfection upon rectangular plate frequency.

4. SHELLS

4.1 Background Information

A shell is the generalization of a plate. That is, one dimension (the thickness, h) is small compared with the others. However, the midsurface of a shell is curved. Indeed, three components of curvature (one of them being the twist of the midsurface) are required to specify completely the shape of the shell. Plates, as discussed in the previous sections of this paper, may be considered both physically and mathematically to be special cases of shells - when all curvatures are zero.

Typically, shells are more difficult to analyze than plates. To begin with, shells may have an infinite number of curvatures of a variety of types (e.g., circular cylindrical, noncircular cylindrical, conical, spherical, ellipsoidal, toroidal, hyperbolic paraboloidal). Further, shell vibrations are typically governed by sets of eighth order differential equations, compared with the simple, fourth order equation used for typical (linear) plate vibration analysis, and a large number of different shell theories have been developed (cf., reference 61). More parameters must also be considered for shells than plates. However, all the complicating effects which may be present in plate vibrations may also be present for shells. The relative complexities of plate and shell vibrations are discussed in detail elsewhere [62].

As an example, consider a shallow shell panel having constant radii of curvature R_χ and R_γ in the x and y directions, and constant twist $R_{\chi\gamma}$. That is, the equation of the midsurface is given by the quadric function

$$z = -\frac{1}{2}(\frac{x^2}{R_x} + \frac{2xy}{R_{xy}} + \frac{y^2}{R_y})$$
 (15)

Due to the curvature and twist, normal displacements (w) cause additional strains w/R_x , w/R_y and $2w/R_{xy}$ in the midsurface which are added to the right-hand-sides of equations (4). The nonlinear governing equations of motion and compatibility, (7a) and (7b), then have the terms

$$-\frac{1}{R_{y}}\frac{\partial^{2}\phi}{\partial x^{2}} + \frac{2}{R_{xy}}\frac{\partial^{2}\phi}{\partial x\partial y} - \frac{1}{R_{x}}\frac{\partial^{2}\phi}{\partial y^{2}}$$
 (16a)

$$-\frac{1}{R_{x}}\frac{\partial^{2}w}{\partial x^{2}} + \frac{2}{R_{xy}}\frac{\partial^{2}w}{\partial x\partial y} - \frac{1}{R_{y}}\frac{\partial^{2}w}{\partial y^{2}}$$
(16b)

respectively, added to their right-hand-sides.

The free vibration characteristics of shells are considerably different from those of plates. For example, the newcomer to the subject is typically surprised to find that the fundamental (i.e., lowest frequency) mode of a circular cylindrical shell typically includes many sine waves around its circumference. In the case of large amplitude, nonlinear vibrations, plate behavior is typically of the hardening type (i.e., frequency increasing with vibration amplitude); for shells, it may be either hardening, or initial softening followed by hardening (cf., reference 63). A range of initial softening was also seen to appear in plates with initial imperfections (see Section 3.7), which are actually shells having very shallow curvature. In both cases the initial soft spring response can be seen mathematically as the result of a second degree term in τ added to the first and third degree terms of equation (9).

4.2 Recent Research

Research activity in nonlinear vibrations of shells has <u>decreased</u> in recent years, which is the opposite of what was found for plates (i.e., Table 1). For example, 25 references dealing with the nonlinear free vibrations of circular cylindrical shells were found to have been written before 1972 [61]. However, the literature search for the present study uncovered only 7 references for the same topic for the last 6 years. Doubtless, the decrease is part of an overall decline of the past decade in the number of shell vibration papers appearing.

Massalas and Kafousias [64] analyzed long, shallow shell panels of circular cylindrical curvature resting on a nonlinear, massless, elastic foundation, having the straight edges clamped. Shallow cylindrical panels were also studied by Ilina and Kuzemko [65], with an attached elastic foundation having both stiffness and mass. The problem was partially uncoupled by assuming the foundation response function to be of the same form as for a previously solved linear problem. Novikov [66] used a nonlinear vibration analysis of axially loaded circular cylinders to determine lower bounds for their buckling loads. Ramachandran [67] considered orthotropic cylindrical shells having a wall thickness which varies linearly in the axial direction, both in a vacuum and in an incompressible fluid. Veda [68] also took up cylindrical shells as part of a nonlinear study of conical shells.

Considerable interest has been shown recently in circular cylindrical shells having initial imperfections (i.e., deviations of the middle surfaces from

being perfect circular cylinders). An extensive work by Singer and Prucz [69] modified previous work for axially compressed, isotropic, homogeneous shells to accommodate axial and circumferential stiffeners. This was done by "smearing out" the stiffeners into an "equivalent" orthotropic shell. Nonlinear equations were obtained similar to those of equations (7) with added expressions (16); however, certain simplifying assumptions were made to linearize them. It was shown that small imperfections in the orthotropic shells change the frequencies to a smaller extent than for isotropic shells. More recent work by Watawala and Nash [70,71] solved the nonlinear equations for the isotropic, unloaded shell, with or without an internal fluid. It was observed that imperfections typically increase the vibration frequencies; however, if the vibration mode shape is the same as the imperfection shape, the frequencies first decrease with increasing imperfection amplitude, and subsequently begin to increase at an imperfection amplitude of the order of the thickness or less. It was also shown that the variation of frequency with vibration amplitude could be either of the hardening or softening types. Kovalchuk and Krasnopolskaya [72] made a theoretical study of the double resonances found for a single vibration mode shape when a circumferential imperfection is present. They found that the difference between the resonant frequencies depends upon the magnitude of the imperfection, and that only a single frequency exists when an axially symmetric imperfection is present.

Conical shells were analyzed by Veda [68]. Finite elements were used, and the method of weighted residuals was applied to the time variables to yield non-linear algebraic equations for frequency as a function of amplitude. Conical frustrums were considered for all apex angles varying between a cylindrical shell and an annular plate. Both simply supported and clamped edges were treated. The nonlinear frequency versus amplitude plots showed initial soft spring response at small amplitudes in all cases except for the annular plate, followed by a subsequent hard spring response.

Shallow spherical shells of polar orthotropic material having clamped circular boundaries were investigated by Varadan and Pandalai [73]. They found that for very shallow curvature the frequency-amplitude plots are hard spring responses, whereas for larger curvatures they are initially soft, subsequently becoming hard. It was also shown that for $E_{\rm r}/E_{\theta}>1$ (where $E_{\rm r}$ and E_{θ} are the meridional and circumferential elastic moduli, respectively), the shell retains its hard spring characteristic for larger curvatures. Novikov [66] also analyzed the nonlinear vibrations of spherical shells subjected to uniform normal pressure to determine lower bounds for their buckling loads. Shahinpoor and Balakrishnan [74] considered the nonlinear vibrations of a hyperelastic spherical shell made of an incompressible material such as rubber. Hui and Leissa [75,76] analyzed the effects of unidirectional [75] and bidirectional [76] imperfections upon the free vibrations of spherical shells. It was shown that, imperfections may either increase or decrease the frequency, depending upon the type of imperfection present, and whether a linear or nonlinear analysis is used.

Toroidal shells were studied by Tabaddor and Stafford [77]. Finite element incremental formulations were made for cord-reinforced inflatable shells made of materials having nonlinear constitutive equations.

5. CONCLUDING REMARKS

Nonlinear effects due to large vibratory amplitudes may be very important in determining free vibration natural frequencies and forced vibration response, and are worthy of the considerable attention given to them in recent years. Shells are particularly important structural elements, and more investigations of their nonlinear response should be conducted.

There do exist several theoretical approaches for dealing with nonlinear vibrations of plates and shells, and they are straightforwardly used in the literature. However, reliable, accurate results are generally lacking. Indeed,

considerable disagreement among existing published results is found. The resulting knowledge in many cases is therefore, at best, only qualitative. The writer would suggest two improvements in analysis to obtain reliable, quantitative understanding: (1) use of additional, independent functions to represent the modes (most studies to date have used single function representations of the vibration modes), (2) examination of residuals of the governing nonlinear differential equations to determine how accurately the latter are being satisfied.

Very little attention has been given to nonlinear problems arising due to nonlinear stress-strain relationships. This topic deserves more attention.

The presence of initial imperfections of flatness or curvature have been shown to be quite significant in determining free vibration frequencies. These problems may require the solution of nonlinear differential equations even for small amplitude vibration studies (e.g., in the case of initial stresses). Additional investigations, both theoretical and experimental, should be conducted on this topic in the coming years.

ACKNOWLEDGEMENT

The author wishes to acknowledge the important contribution of Mr. I. Jacob, a graduate student, in conducting the literature search in the abstract journals.

REFERENCES

- 1. A.W. LEISSA 1969 Vibration of Plates (NASA SP-160). Washington: U.S. Government Printing Office.
- 2. A.W. LEISSA 1979 The Ohio State University, Dept. of Engineering Mechanics. Short Course Notes: Vibrations of Beams, Plates and Shells.
- 3. A.W. LEISSA 1978 Shock and Vibration Digest 10, 21-35. Recent research in plate vibrations, 1973-1976; complicating effects.
- 4. A.W. LEISSA 1981 Shock and Vibration Digest 13, 19-35. Plate vibration research, 1976-1980: complicating effects.
- 5. C.Y. CHIA 1980 Nonlinear Analysis of Plates. McGraw-Hill International Book Co.
- 6. M. SATHYAMOORTHY 1979 Journal of Applied Mechanics, Trans. ASME $\underline{46}$, 215-217. Nonlinear vibration of rectangular plates.
- 7. TH. VON KARMAN 1910 Encyclopädie der Mathematischen Wissenschaften $\underline{4}$, 311-385. Festigkeitsprobleme im Maschinenbau.
- 8. H.M. BERGER 1955 Journal of Applied Mechanics 22, 465-472. A new approach to the analysis of large deflections of plates.
- 9. J.C. KENNEDY, JR. 1980 Journal of Mechanical Design, Trans. ASME 102, 405-411. Moderately large amplitude plate vibration modes.
- 10. H.N. CHU and G. HERRMANN 1956 Journal of Applied Mechanics 23, 532-540. Influence of large Amplitudes on free flexural vibrations of rectangular elastic plates.
- 11. B. BANERJEE and S. DATTA 1979 International Journal of Mechanical Sciences 21, 689-696. Large amplitude vibrations of thin elastic plates by the method of conformal transformation.

- 12. J.N. REDDY 1982 Journal of Sound and Vibration 83, 1-10. Large amplitude flexural vibration of layered composite plates with cutouts.
- 13. B. BANERJEE 1982 Journal of Sound and Vibration 82, 329-333. Large amplitude vibrations of a clamped orthotropic plate carrying a concentrated mass.
- 14. J. RAMACHANDRAN 1973 Journal of Applied Mechanics 95, 630-632. Large amplitude vibration of a rectangular plate carrying a concentrated mass.
- 15. M. SATHYAMOORTHY 1981 Computers and Structures 14, 129-134. Transverse shear and rotatory inertia effects on nonlinear vibration of orthotropic circular plates.
- 16. B.M. KARMAKER 1978 International Journal of Non-Linear Mechanics 13, 351-359. Amplitude-frequency characteristics of non-linear vibrations of clamped elliptic plates carrying a concentrated mass.
- 17. G. VENKATESWARA RAO and K. KANAKA RAJU 1980 Journal of Sound and Vibration 69, 175-180. Large amplitude axisymmetric vibrations of orthotropic circular plates elastically restrained against rotation.
- 18. J.N. REDDY, C.L. HUANG and I.R. SINGH 1981 International Journal of Numerical Methods in Engineering 17, 527-541. Large deflections and large amplitude vibrations of axisymmetric circular plates.
- 19. M. SATHYAMOORTHY and C.Y. CHIA 1980 Acta Mechanica 37, 247-258. Large amplitude vibration of orthotropic elliptical plates.
- 20. M. SATHYAMOORTHY 1980 Journal of Sound and Vibration <u>70</u>, 458-460. Nonlinear vibration of elliptical plates.
- 21. M. SATHYAMOORTHY 1978 International Journal of Solids and Structures $\underline{14}$, 869-880. Vibration of skew plates at large amplitudes including shear and rotary inertia effects.
- 22. M. SATHYAMOORTHY 1980 Journal of Applied Mechanics, Trans. ASME <u>47</u>, 675-677. Large amplitude vibration of skew orthotropic plates (brief notes).
- 23. S.K. CHAUDHURI 1981 Mechanics Research Communications <u>8</u>, 355-360. Large amplitude free vibrations of simply supported equilateral triangular plate using tri-linear co-ordinates.
- 24. A.K. NIYOGI and B.L. MEYERS 1981 International Journal of Non-Linear Mechanics $\underline{16}$, 401-408. A perturbation solution of non-linear vibration of rectangular orthotropic plates.
- 25. N.K. PESOTSKAYA 1980 Stroitel'naya Mekhanika i Raschet Sooruzhenii No. 2, 57-59. Vibrations of orthotropic plates during high deflections (in Russian).
- T.K. VARADAN and K.A.V. PANDALAI 1979 Journal of Sound and Vibration
 <u>67</u>, 329-340. Large amplitude flexural vibration of eccentrically stiffened
 plates.
- 27. G. PRATHAP and K.A.V. PANDALAI 1978 International Journal of Non-Linear Mechanics 13, 285-294. Non-linear vibrations of transversely isotropic rectangular plates.

- 28. M. SATHYAMOORTHY and C.Y. CHIA 1980 Journal of Applied Mechanics 47, 128-132. Effect of transverse shear and rotatory inertia on large amplitude vibration of anisotropic skew plates. Part 1 theory.
- 29. M. SATHYAMOORTHY and C.Y. CHIA 1980 Journal of Applied Mechanics 47, 133-138. Effect of transverse shear and rotatory inertia on large amplitude vibration of anisotropic skew plates. Part 2 Numerical results.
- 30. M. SATHYAMOORTHY 1981 Computers and Structures 14, 129-134. Transverse shear and rotatory inertia effects on nonlinear vibration of orthotropic circular plates.
- 31. M. SATHYAMOORTHY and C.Y. CHIA 1982 Ingenieur Archiv 52, 237-243. Nonlinear flexural vibration of moderately thick orthotropic circular plates.
- 32. M. SATHYAMOORTHY 1981 International Journal of Non-Linear Mechanics 16, 327-335. Effects of large amplitude, transverse shear and rotatory inertia on vibration of orthotropic elliptical plates.
- 33. T. NATH and R.S. ALWAR 1980 International Journal of Solids and Structures 16, 433-443. Nonlinear dynamic analysis of orthotropic circular plates.
- 34. G.V. RAO and K.K. RAJU 1980 Journal of Sound and Vibration 69, 175-180. Large amplitude axisymmetric vibrations of orthotropic circular plates elastically restrained against rotation.
- 35. J.N. REDDY and C.L. HUANG 1981 Journal of Sound and Vibration 79, 387-396. Large amplitude free vibrations of annular plates of varying thickness.
- 36. C. MASSALAS, K. SOLDATOS, and G. TZIVANIDIS 1979 Journal of Sound and Vibration 67, 284-288. Vibration and stability of a thin elastic plate resting on a nonlinear elastic foundation when the deformation is large.
- 37. L.J. PUTNICK, B.J. MATKOWSKY, and E.L. REISS 1981 Journal of the Acoustical Society of America 69, 1682-1687. Secondary states of vibrating plates.
- 38. M.M. BANERJEE and J.N. DAS 1979 Journal of the Indian Institute of Science 61, 51-56. A note on the nonlinear vibrations of rectangular plates with parabolically varying thickness.
- 39. M.M. BANERJEE, P.K. SARKER, and P. KAPOOR 1981 Journal of Sound and Vibration 74, 589-596. On the non-linear vibration of circular plates of variable thickness elastically restrained along the edges.
- 40. K. KANAKA RAJU and G. VENKATESWARA RAO 1979 Nuclear Engineering and Design 51, 417-421. Nonlinear vibrations of tapered circular plates elastically restrained against rotation at the edges.
- 41. N. SUGIMOTO 1981 Journal of Applied Mechanics 48, 377-382. Nonlinear theory for flexural motions of thin elastic plate, Part 1: Higher-order theory.
- 42. N. SUGIMOTO 1981 Journal of Applied Mechanics, Trans. ASME 48, 383-390. Nonlinear theory for flexural motions of thin elastic plate, Part 2: boundary-layer theory near the edge.

- 43. M. SATHYAMOORTHY 1978 Journal of Sound and Vibration $\underline{60}$, 308-311. Shear effects on vibration of plates.
- 44. K. KANAKA RAJU and E. HINTON 1980 International Journal for Numerical Methods in Engineering 15, 249-257. Nonlinear vibrations of thick plates using Mindlin plate elements.
- 45. M. SATHYAMOORTHY 1978 Journal of the Engineering Mechanics Division, Proc. ASCE 104, 1288-1293. Shear and rotatory inertia effects on plates.
- 46. C.Y. CHIA and M. SATHYAMOORTHY 1981 Journal of Sound and Vibration $\underline{78}$, 131-137. Non-linear vibration of circular plates with transverse shear and rotatory inertia.
- 47. M. SATHYAMOORTHY 1981 International Journal of Solids and Structures 17, 443-449. Large amplitude vibration of circular plates including transverse shear and rotatory inertia.
- 48. M. SATHYAMOORTHY 1982 Journal of Mechanical Design, Trans. ASME 104, 426-431. Large amplitude elliptical plate vibration with transverse shear and rotatory inertia effects.
- 49. Z. CELEP 1980 Journal of Applied Mechanics, Trans. ASME $\underline{47}$, 662-666. Shear and rotatory inertia effects on the large amplitude vibration of the initially imperfect plates.
- 50. A.W. LEISSA 1981 Composite Structures, I.H. Marshall, Editor, Applied Science Publishers, 312-334. Advances in vibration, buckling and post-buckling studies on composite plates.
- 51. J.M. WHITNEY 1968 Ph.D. Dissertation, The Ohio State University, Dept. of Engineering Mechanics. A study of the effects of coupling between bending and stretching on the mechanical behavior of layered anisotropic composite materials.
- 52. J.M. WHITNEY and A.W. LEISSA 1969 Journal of Applied Mechanics, Trans. ASME, 261-266. Analysis of heterogeneous anisotropic plates.
- 53. J.N. REDDY 1981 Virginia Polytechnic Institute and State University, ASME Paper No. 81-DET-144. Nonlinear vibration of layered composite plates including transverse shear and rotatory inertia.
- 54. J.N. REDDY and W.C. CHAO 1981 Computers and Structures 13, 341-347. Large-deflection and large-amplitude free vibrations of laminated composite-material plates.
- 55. J.N. REDDY and W.C. CHAO 1982 Journal of Applied Mechanics, Trans. ASME 49, 396-402. Nonlinear oscillations of laminated, anisotropic, rectangular plates.
- 56. D. HUI and A.W. LEISSA (to appear) Journal of Applied Mechanics. Effects of geometric imperfections on vibrations of biaxially compressed rectangular flat plates.
- 57. D. HUI (to appear) Journal of Sound and Vibration. Large amplitude axisymmetric vibrations of geometrically imperfect circular plates.
- 58. H. ABRAMOVICH, J. GIL, et.al. 1978 Technion-Israel Institute of Technology, Dept. of Aeronautical Engineering, TAE Report No. 332. Vibrations and buckling of radially loaded circular plates.

- 59. N. YAMAKI, K. OTOMO, and M. CHIBA 1981 Journal of Sound and Vibration 79, 23-42. Non-linear vibration of a clamped circular plate with initial deflection and initial displacement, Part I: Theory.
- 60. N. YAMAKI, K. OTOMO and M. CHIBA 1981 Journal of Sound and Vibration 79, 43-59. Non-linear vibration of a clamped circular plate with initial deflection and initial edge displacement, Part II: Experiment.
- 61. A.W. LEISSA 1973 Vibration of Shells (NASA SP-228). Washington: U.S. Government Printing Office.
- 62. A.W. LEISSA 1980 Shock and Vibration Bulletin <u>50</u>, 1-9. The relative complexities of plate and shell vibrations.
- 63. A.W. LEISSA and A.S. KADI 1971 Journal of Sound and Vibration 16, 173-187. Curvature effects on shallow shell vibrations.
- 64. C. MASSALAS and N. KAFOUSIAS 1979 Journal of Sound and Vibration 66, 507-512. Non-linear vibrations of a shallow cylindrical panel on a non-linear elastic foundation.
- 65. A.M. ILINA and A.M. KUZEMKO 1980 Soviet Applied Mechanics 15, 1221-1223. Nonlinear oscillation of a cylindrical panel bound to an elastic base.
- 66. V.V. NOVIKOV 1981 Journal of Applied Mechanics and Technical Physics 21, 574-576. Internal resonances and stability of elastic shells.
- 67. J. RAMACHANDRAN 1979 Journal of Sound and Vibration <u>64</u>, 97-106. Non-linear vibrations of cylindrical shells of varying thickness in an Incompressible fluid.
- 68. T. UEDA 1979 Journal of Sound and Vibration 64, -95. Non-linear free vibrations of conical shells.
- 69. J. SINGER and J. PRUCZ 1982 Journal of Sound and Vibration 80, 117-143. Influence of initial geometrical imperfections on vibrations of axially compressed stiffened cylindrical shells.
- 70. L. WATAWALA 1981 Ph.D. Thesis, University of Massachusetts. Influence of initial geometric imperfections on vibrations of thin circular cylindrical shells.
- 71. L. WATAWALA and W. NASH 1983 Computers and Structures $\underline{16}$, 1-4. Influence of initial geometric imperfections on vibrations of thin circular cylindrical shells.
- 72. P.S. KOVALCHUK and T.S. KRASNOPOLSKAYA 1980 Soviet Applied Mechanics 15, 867-872. Resonance phenomena in nonlinear vibrations of cylindrical shells with initial imperfections.
- 73. T.K. VARADAN and K.A.V. PANDALAI 1978 Computers and Structures 9, 417-425. Nonlinear flexural oscillations of orthotropic shallow spherical shells.
- 74. M. SHAHINPOOR and R. BALAKRISHNAN 1978 Iranian Journal of Science and Technology 7, 267-272. Large amplitude oscillations of thick hyperelastic spherical shells.

- 75. D. HUI and A.W. LEISSA (to appear) International Journal of Non-Linear Mechanics. Effects of uni-directional geometric imperfections on vibrations of pressurized shallow spherical shells.
- 76. D. HUI (to appear) AIAA Journal. Large amplitude vibrations of geometrically imperfect shallow spherical shells with structural damping.
- 77. F. TABADDOR and J.R. STAFFORD 1981 Computers and Structures 13, 737-743. Nonlinear vibration of cord-reinforced composite shells.

. Alexandra ...

NONSTATIONARY RANDOM RESPONSE OF NONLINEAR STRUCTURES
TO NONSTATIONARY RANDOM EXCITATION

C.W.S. To

Department of Mechanical Engineering The University of Calgary Calgary, Alberta, Canada T2N 1N4

ABSTRACT

For safety and economical reasons, the nonstationarity of excitation and response and nonlinearities of structures such as tall buildings, buildings that house nuclear reactors, naval and aerospace structures, and their components must be considered by the designers. This paper begins with an update review of the state of the art of techniques used for the random analysis of the response of general multi-degree-of-freedom (MDF) nonlinear mechanical systems to random excitation. Special attention is paid on methods applied to MDF nonlinear systems subjected to nonstationary random excitation. Their suitability to finite element analysis of complicated nonlinear structures with large deformation of finite strain is discussed. Then a new formulation for the analysis of response of discretized symmetric and asymmetric nonlinear structures, involving elastoplastic deformation, subjected to nonstationary random excitation represented as a product of an arbitrary time modulating function and a stationary process is proposed. Application of the method is made for the determination of time-dependent variance of response of a quarter-scale physical model of a class of mast antenna structures. Computed results are included graphically and discussion is made.

1. INTRODUCTION

For safety reasons, the designers of many modern structures such as tall buildings, buildings that house nuclear reactors, naval and aerospace structures, and their components must consider the effects of various intensive random excitations. The latter includes earthquake excitation, pressure waves of an explosion, and continuous atmospheric turbulence. For economic reasons, the use of the substantial reserve in strength inherent in most structures due to plastic effects is required. Consequently, for both safety and economic considerations, the nonstationarity of the excitation and response, and the non-linearities of the structure must be taken into account in the design procedure. This, in turn, requires the prediction of the nonstationary random response of nonlinear structures to nonstationary random excitation.

In the next section an update review of the state of the art of techniques used for the random analysis of the response of general multi-degree-of-freedom (MDF) nonlinear mechanical systems to random excitation is presented. Special attention is paid on methods applicable to MDF nonlinear systems subjected to nonstationary random excitation. Their suitability to finite element analysis of complicated nonlinear structures with large deformation of finite strain is discussed. Section 3 includes a new formulation for the analysis of response of discretized symmetric and asymmetric nonlinear structures, involving elastoplastic deformation subjected to nonstationary random excitation. The latter is represented as a product of an arbitrary time modulating function and a stationary process. This new approach essentially treats the governing nonlinear matrix equation of motion as a series of piecewise linear matrix equations between time steps. The piecewise linear matrix equations are solved by the existing method for MDF linear system proposed by To [1]. Application of the method is made in section 4 for the determination of the time-dependent variance of response of a quarter-scale physical model of a class of mast antenna structures. Computed results and discussions are included in section 5. Concluding remarks are presented in the final section.

A REVIEW OF EXISTING METHODS

The problem of predicting the response of MDF nonlinear systems to random excitations has received considerable attention in the last two decades. Chronologically, Bendat et al [2], Caughey [3], Iwan [4] and Roberts [5,6] have presented their comprehensive and excellent reviews. Recently, To [7] has carried out a detailed survey on existing methods involving non-parametric random excitations. As systems with parametric excitations were thoroughly reviewed by Ibrahim and Roberts [8], only non-parametric random excitations will be considered in this section.

At present, there are five basic methods for the determination of response of MDF nonlinear systems to random excitations. These are the statistical or equivalent linearization techniques, the Fokker-Planck-Kolmogorov equation or Markov vector approaches, the normal mode approaches, the perturbation techniques, and the simulation procedures.

2.1 Statistical or Equivalent Linearization Techniques

A number of generalized formulations for the steady-state solution of discrete MDF systems to stationary random excitation have been proposed by Caughey [3], Foster [9,10], Yang [11], Iwan and Yang [12], Iwan [13], Atalik [14], Spanos [15], Spanos and Iwan [16], Wen [17], Beaman and Hedrick [18-20], and Apetaur and Opicka [21]. The work of Beaman and Hedrick improved the accuracy of the Gaussian statistical linearization (SL) technique by making use of the Gram-Charlier expansion. In [21] the so-called "second-order" SL technique for MDF nonlinear systems was presented.

Formulations for response of MDF nonlinear systems to nonstationary excitation were presented by Iwan and Mason [22], Kimura and Sakata [23], Goto and Iemura [24], Kobari et al [25,26], Iwan and Gates [27], and Spanos [28]. The formulations in [23] and [28] apply to asymmetric MDF nonlinear systems.

The formulations by Iwan and Mason [22] and Spanos [28] may be considered the most general ones with regard to their suitability to the finite element analysis. However, they are not applicable to structures involving large deformation with finite strain.

2.2 Fokker-Planck-Kolmogorov or Markov Vector Approaches

These methods make use of the concept of Markov process and capable of providing exact solution of the transition probability density function. The response process is assumed to be Markovian or whose projection is Markovian.

Exact steady-state solution of MDF nonlinear systems to stationary excitation were given by Ariaratnam [29,30], Caughey [31,32], and Bolotin [33,34]. Recently, Caughey and Ma [35] obtained exact steady-state response of a wide class of MDF nonlinear systems to white noise excitation. They indicated that the approximate nonstationary response can be obtained by a perturbation analysis of Caughey and Payne [36]. The nonstationary solution of MDF nonlinear systems to nonstationary stochastic excitation has yet to be found.

In general, the Fokker-Planck-Kolmogorov equation approaches are difficult and computationally infeasible to be applied to structures discretized by the finite element method.

2.3 Normal Mode Approaches

The underlying idea of the normal mode approaches is to reduce a given set of generally coupled nonlinear second order stochastic differential equations to one which contains coupling only in the nonlinear terms. The reduced equations can be solved by using some approximate techniques. Grossmayer's two-state approach [37] belongs to this category. The major assumption in these approaches is the existence of normal modes of vibration. In the deterministic case, Rosenberg [38,39] has addressed on this subject. A rigorous stochastic equivalence has yet to be found.

These methods can be applied to nonlinear structures involing large deformation of finite strain in the context of finite element analysis. There are, however, two penalties. First, with structure discretized into a very large number of degrees of freedom such as one with tens of thousand degrees of freedom the task of finding accurate normal modes can be extremely difficult and expensive. The frontal or wave method of Irons [40], Melosh and Bamford [41], and Hellen [42] can be applied to improve this problem. The other penalty is associated with large deformation in which the eigenvalue solution for the governing matrix equation of motion has to be obtained at every discrete time step.

2.4 Perturbation Techniques

In these approaches [43-46] the stochastically excited nonlinear structures are treated in a similar manner as deterministically excited ones. The nonlinearity is assumed to be sufficiently small such that the solution may be represented as an expansion in powers of some small parameter which describes the size of the nonlinearity. In references [46] the transient response of MDF nonlinear system to stationary random excitation was presented. The methods hinge on the assumption that every sample function of the solution process can be represented by a convergent series on powers of the small parameter. The amount of algebraic effort in obtaining the solution is substantial as indicated by Tung [44].

2.5 Simulation Methods

Digital simulation of multi-dimensional and multi-variate processes of non-linear structures were presented by Vaicaitis et al [47], Shinozuka and Wen [48], Vaicaitis et al [49], and Harris [50]. These techniques can readily be applied to discrete MDF systems. The example problem in [50] indicated that to provide an accurate value such as the variance of the displacement response 5000 samples were required. This implies that for large number of degree of freedom systems, frequently encountered in the finite element analysis, the computational cost can be prohibitive. When the number of degrees of freedom is large and the excitation is nonstationary simulation is economically infeasible. It may seem logical to reduce the number of samples in the simulation. However, graphs included in [50] indicated that considerable discrepancy can occur between theoretical and simulated results with 2500 samples in the simulation.

3. A THEORY FOR THE ELASTIC-PLASTIC ANALYSIS

Consider the stochastic matrix equation of motion for the MDF nonlinear system

$$\underline{M} \ddot{x} + \underline{C} \dot{x} + \underline{K} \dot{x} + g(\dot{x}, \dot{x}) = e(t) w(t) = P(t)$$
(1)

where \underline{M} , \underline{C} and \underline{K} are the assembled linear mass, damping and stiffness matrices, respectively;

 \ddot{x} , \dot{x} and x are the stochastic acceleration, velocity and displacement response vectors of the MDF nonlinear system;

 $g(x,\dot{x})$ is the nonlinear term;

e(t) is the time-dependent deterministive vector;

and

w(t) is the Gaussian stationary process.

For asymmetric MDF nonlinear systems such as those involving the sloshing in liquid-filled tanks during earthquakes and in the vibration of trolley wires under wind loads,

$$g(x,\dot{x}) \neq -g(-x,-\dot{x}) \tag{2}$$

owing to the asymmetry, the solution of equation (1) may not have a zero mean value.

Equation (1) may be approximated as a series of piecewise linear systems between time steps such that

$$\underline{M} \overset{\mathbf{x}}{\mathbf{x}}_{S} + \underline{C} \overset{\mathbf{x}}{\mathbf{x}}_{S} + \underline{K} \overset{\mathbf{x}}{\mathbf{x}}_{S} = F_{S}$$
 (3a)

$$\underline{\mathbf{M}} \overset{\mathbf{x}}{\sim}_{s+1} + \underline{\mathbf{C}} \overset{\mathbf{x}}{\sim}_{s+1} + \underline{\mathbf{K}} \overset{\mathbf{x}}{\sim}_{s+1} = \overset{\mathbf{F}}{\sim}_{s+1} \tag{3b}$$

:

$$\underline{\mathbf{M}} \ \ddot{\mathbf{x}}_{N} + \underline{\mathbf{C}} \ \dot{\mathbf{x}}_{N} + \underline{\mathbf{K}} \ \mathbf{x}_{N} = \mathbf{F}_{N}$$

$$\mathbf{s} = 0, 1, 2, \dots, N;$$
(3c)

where

 x_s is the value of x at time step t_s ;

 x_{s+1} is the value of x at time step t_{s+1} such that $\Delta t = t_{s+1} - t_{s}$ and $t_{o} = 0$;

 Δt is the small time interval in which equation (3a), (3b), and (3c) can be considered as a linear matrix equation of motion;

$$\begin{aligned} \mathbf{F}_{S} &= \mathbf{P}(\mathbf{t}_{S}) - \mathbf{g}(\mathbf{x}_{S}, \dot{\mathbf{x}}_{S}) \\ &= \mathbf{e}(\mathbf{t}_{S}) \ \mathbf{w}(\mathbf{t}_{S}) - \mathbf{g}(\mathbf{x}_{S}, \dot{\mathbf{x}}_{S}). \end{aligned}$$

It is assumed that the step modulated random excitation $R(t_s)$ is Gaussian so that for the linear equations of motion the corresponding response process x_s is also Gaussian. Thus, the asymmetric MDF nonlinear system of equation (1) approximated by (3) imposes no further difficulty other than the solution of the individual linear equation. For structure discretized by the finite element method the total strain tensor $\{\epsilon\}$ may be expressed as

$$\{\varepsilon\} = \{\varepsilon_{\mathbf{e}}\} + \{\varepsilon_{\mathbf{p}}\} + \{\varepsilon_{\mathbf{\theta}}\} + \dots$$
 (4)

where the subscripts e, p, and θ denote elastic, plastic, and thermal parts of the total strain tensor, respectively. It should be noted that for large deformation involving finite strain equation (4) cannot be applied. Instead, the formulation given by Lubarda and Lee [51] should be applied.

Applying equation (4) and the finite element method [52], and assuming damping in the system is proportional then the terms $g(\chi_s, \dot{\chi}_s)$ reduce to $g(\chi_s)$

which is the equivalent nodal forces representing the effects of plastic action and elastic nonlinearity occurring in the structure. Equation (3) can then be written in a familiar form, for instance (3a) becomes

$$\underline{\underline{M}} \ddot{\chi}_{S} + \underline{\underline{C}} \dot{\chi}_{S} + \underline{\underline{K}} \chi_{S} = \underline{\underline{P}}(\underline{t}_{S}) + \underline{\underline{P}}_{Q}^{NL}(\underline{t}_{S}) + \underline{\underline{P}}_{p}^{L}(\underline{t}_{S}) + \underline{\underline{P}}_{p}^{NL}(\underline{t}_{S}),$$
 (5)

where $P_{q}^{NL}(t_s)$ represents a load vector arising from large deflections, $P_{p}^{L}(t_s)$ and $P_{p}^{NL}(t_s)$ are the load vectors due to the presence of plastic strains and are associated, respectively, with linear and nonlinear terms of the strain-displacement relations [53].

The piecewise linear equation (5) can readily be solved by making use of the results in [1]. For nonlinear structure involving elastic-plastic deformation \underline{M} , \underline{C} and \underline{K} are identical in every time step. Consequently, the computational effort can be drastically reduced.

The numerical solution procedure employed in this paper specifically focuses on elasto-plastic dynamic response of mast antenna structures involving small strains, strain-hardening and hysteresis. It is based on a numerical integration scheme corresponding to a marching forward process in the time domain. When the state of the structure is known or has been determined at time t_{s-1} , the state of the structure at $t_s = t_{s-1} + \Delta t$ is obtained, where Δt is a small increment of time. For brevity the detailed numerical strategy is not included here in this paper.

4. EXAMPLE

The formulation presented in the last section is applied in this section to find the time-dependent variance of response of the quarter-scale physical model, shown in Figure 1, of a class of mast antenna structures. The structure is assumed to be rigidly clamped at the base where the nonstationary random excitation is applied. Thus, the governing equation of motion is

$$\begin{bmatrix}
\frac{M}{yy} & \frac{M}{yx} \\
\frac{M}{xy} & \frac{M}{xx}
\end{bmatrix} \begin{pmatrix} \ddot{y} \\
\ddot{x} \end{pmatrix} + \begin{pmatrix} \frac{C}{yy} & \frac{C}{yx} \\
\frac{C}{xy} & \frac{C}{xx}
\end{pmatrix} \begin{pmatrix} \dot{y} \\
\dot{x} \end{pmatrix} + \begin{pmatrix} \frac{K}{yy} & \frac{K}{yx} \\
\frac{K}{xy} & \frac{K}{xx}
\end{pmatrix} \begin{pmatrix} y \\ x \end{pmatrix} = \begin{pmatrix} P \\ y \\ Q \end{pmatrix}$$
(6)

where \underline{M}_{xx} , \underline{C}_{xx} and \underline{K}_{xx} are the mass, damping and stiffness matrices of the constrained structure; \underline{x} and \underline{y} are the displacement response and prescribed displacement column matrices, respectively. It can be shown that

$$\underline{\underline{M}}_{xx} \ddot{\chi} + \underline{\underline{C}}_{xx} \dot{\chi} + \underline{K}_{xx} \chi = \underline{\xi}$$
 (7)

where $F = (K_{xy})$ y; note that the stiffness matrix in equation (6) contains the linear and nonlinear parts.

For simplicity and economy the physical model of the mast antenna structure was idealized by three elements, two beam elements and one discrete mass element. The beam and discrete mass elements used were TB5 and DM3 of reference [54]. The input data for the example are given in Table 1.

5. COMPUTED RESULTS AND DISCUSSION

For brevity only the variance of the elastic-plastic displacement response at the tip of the mast antenna structure subjected to a nonstationary random excitation having an exponential envelope modulating function was evaluated.

Various hardening parameters λ , that is the ratio of the tangential flexural rigidity to the flexural rigidity of the structure were considered. The computed results with 200 discrete points for the excitation duration of 1.25 sec are included in Figure 2. Note that in all the results it was assumed that the first two modes of the structure were excited, and the damping for each mode was 5% critical. Implicit in applying equation (7) is the omission of $\underline{\underline{M}}_{xy}$ $\ddot{\underline{y}}$ and $\underline{\underline{C}}_{xy}$ $\dot{\underline{y}}$ which have insignificant influence on the final results. The explanation for the observation is that the value of the elements in the stiffness matrix $\underline{\underline{K}}_{xy}$ for stiff structures is usually several orders higher than those of the mass and damping matrices.

With reference to Figure 2(b), the peak variance of displacement response at the tip of the mast atenna structure increases with decreasing hardening parameter. This is consistent with the finding for the deterministic excitation of a different example reported by Duffey and Krieg [55].

Finally, it may be appropriate to mention that for the example considered every curve presented in Figure 2(b) requires approximately 26 sec of execution time of CDC cyber 175 with NOS version 2 machine.

6. CONCLUDING REMARKS

An update review of the state of the art of techniques used for the random analysis of general MDF nonlinear mechanical systems to random excitation has been performed. A formulation with emphasis on its application to general nonlinear structures, discretized by the finite element method, subjected to a wide class of nonstationary random excitation has been presented. Results for an elastic-plastic nonlinear mast antenna structure involving deformation of small strain are included to demonstrate the versatility of the formulation proposed and capability of the digital computer program developed.

Applications of the present formulation to nonlinear structures involving material as well as geometrical nonlinearities are in progress.

ACKNOWLEDGEMENTS

The work reported in this paper was supported, in form of a senior fellow-ship, by the Natural Sciences and Engineering Research Council of Canada.

REFERENCES

- C.W.S. To 1984 Journal of Sound and Vibration 93(2). Time-dependent variance and covariance of responses of structures to nonstationary random excitations.
- 2. J.S. Bendat, L.D. Enochson, G.H. Klein and A.G. Piersol 1962 Chapter 9 in Advanced Concepts of Stochastic Processes and Statistics for Flight Vehicle Vibration Estimation and Measurements, Flight Dynamics Lab., Aeronaut. System Division, Air Force System Command, Wright-Patterson Air Force Base, Ohio, Tech. Rept. No. ASD-TDR-62-1973. The response of nonlinear systems to random excitation.
- 3. T.K. Caughey 1971 Advances in Applied Mechanics $\underline{11}$, 209-253. Nonlinear theory of Random Vibrations.
- 4. W.D. Iwan 1974 Applied Mechanics in Earthquake Engineering, Proc. of the Winter Meeting of A.S.M.E., ASME/AMD 8, edited by W.D. Iwan, 135-161. Application of nonlinear analysis techniques.

- 5. J.B. Roberts 1981 Shock and Vibration Digest 13 (4), 17-28. Response of nonlinear mechanical systems to random excitation, Part I: Markov Methods.
- 6. J.B. Roberts 1981 Shock and Vibration Digest 13 (5), 15-29. Response of nonlinear mechanical systems to random excitation, Part II: Equivalent linearization and other methods.
- 7. C.W.S. To 1983 Rept. No. 265, Department of Mechanical Engineering, The University of Calgary. On random response of nonlinear structures to random excitation.
- 8. R.A. Ibrahim and J.W. Roberts 1978 Shock and Vibration Digest 10 (5), 17-38. Parametric vibration, Part V: Stochastic problems.
- 9. E.T. Foster 1968 Journal of Applied Mechanics, Trans A.S.M.E. <u>35</u> (3), 560-564. Semilinear random vibrations in discrete systems.
- 10. E.T. Foster 1970 Proc. A.S.C.E., Journal of Engineering Mechanics Division 96 (EM 1), 41-67. Model for nonlinear dynamics of offshore towers.
- 11. I-M. Yang 1970 Ph.D. Thesis, California Institute of Technology, U.S.A. Stationary random response of multi-degree of freedom systems.
- 12. W.D. Iwan and I-M. Yang 1971 Proc. A.S.C.E., Journal of Engineering Mechanics Division 97 (EM 6), 1609-1623. Statistical linearization for non-linear structures.
- 13. W.D. Iwan 1973 International Journal of non-linear mechanics 8, 279-287. A generalization of the method of equivalent linearization.
- 14. T.S. Atalik 1974 Ph.D. Thesis, Duke University, U.S.A. Stationary random response of nonlinear multi-degree of freedom systems by a direct equivalent linearization technique.
- 15. P-T.D. Spanos 1976 EERL 76-04, California Institute of Technology, U.S.A. Linearization techniques for nonlinear dynamic systems.
- 16. P-T.D. Spanos and W.D. Iwan 1978 International Journal of Non-linear Mechanics $\underline{13}$ (2), 71-78. On the existence and uniqueness of solutions generated by Equivalent Linearization.
- 17. Y.K. Wen 1980 Journal of Applied Mechanics, Trans. A.S.M.E. <u>47</u> (1), 150-154. Equivalent linearization for hysteretic systems under random excitation.
- 18. J.J. Beaman 1978 Sc.D. Thesis, Massachusetts Institute of Technology, U.S.A. Statistical linearization for the analysis and control of nonlinear stochastic systems.
- 19. J.J. Beaman and J.K. Hedrick 1981 Journal of Dynamic Systems, Measurement, and Control, Trans. A.S.M.E. 103, 14-21. Improved statistical linearization for analysis and control of nonlinear stochastic systems, Part I: An extended statistical linearization technique.
- 20. J.J. Beaman and J.K. Hedrick 1981 Journal of Dynamic Systems, Measurement, and Control, Trans. A.S.M.E. 103, 22-27. Improved statistical linearization for analysis and control of nonlinear stochastic systems, Part II:

 Application to control system design.

- 21. M. Apetaur and F. Opicka 1983 Journal of Sound and Vibration 86 (4), 563-585. Linearization of non-linear stochastically excited dynamic systems.
- 22. W.D. Iwan and A.B. Mason, Jr. 1980 International Journal of Nonlinear Mechanics 15, 71-82. Equivalent linearization for systems subjected to non-stationary random excitation.
- 23. K. Kimura and M. Sakata 1981 Journal of Sound and Vibration 76 (2), 261-272. Non-stationary response of a non-symmetric, nonlinear system subjected to a wide class of random excitation.
- 24. H. Goto and H. Iemura 1973 Proc. Japanese Soc. Civil Engr. 212, 109-119. Linearization techniques for earthquake response of simple hysteretic structures.
- 25. T. Kobari, R. Minai and Y. Suzuki 1973 Bull. Disaster Prevention Institute, Kyoto University, Japan 23, 11-135. Statistical linearization techniques for hysteretic structures to earthquake excitations.
- 26. T. Kobari, R. Minai and Y. Suzuki 1974 Proc. 24th Japanese Natl. Congr. Appl. Mech., 143-152. Nonstationary random response of bilinear hysteretic systems.
- 27. W.D. Iwan and W.C. Gates 1979 Proc. A.S.C.E., Journal of Engineering Mechanics Division 105, 391-405. Estimated earthquake response of simple hysteretic structures.
- P-T.D. Spanos 1980 Journal of Applied Mechanics, Trans. A.S.M.E. <u>47</u>, 209-211. Formulation of stochastic linearization for symmetric or asymmetric M.D.O.F. nonlinear systems.
- 29. S.T. Ariaratnam 1960 Journal of Mechanical Engineering Science $\underline{2}$ (3), 195-201. Random vibrations of nonlinear suspensions.
- 30. S.T. Ariaratnam 1962 Journal of Applied Mechanics, Trans. A.S.M.E. 29, 483-485. Response of a loaded nonlinear spring to random excitation.
- 31. T.K. Caughey 1963 Journal of the Acoustical Society of America 35 (11), 1683-1692. Derivation and application of the Fokker-Planck equation to discrete nonlinear dynamic systems subjected to white random excitation.
- 32. T.K. Caughey 1964 Proc. Colloques Internationaux du Centre National de la Rechercher Scientifique, Marseille, France, No. 148, 392-402. On the response of a class of nonlinear oscillations to stochastic excitation.
- 33. V.V. Bolotin 1965 Proc. Intl. Conf. Dynam. Stability Struct., Northwestern University, Pergamon Press. Statistical aspects in the theory of structural stability.
- 34. V.V. Bolotin 1966 New York: Holden-Day. Statistical methods in structural mechanics.
- 35. T.K. Caughey and F. Ma 1982 Journal of Applied Mechanics, Trans. A.S.M.E. 49, 629-632. The steady-state response of a class of dynamical systems to stochastic excitation.
- 36. T.K. Caughey and H.J. Payne 1967 International Journal of Nonlinear Mechanics 2, 125-151. On the response of a class of self-excited oscillations to stochastic excitation.

- 37. R.L. Grossmeyer 1979 Journal of Sound and Vibration 65 (3), 353-379. Elastic-plastic oscillators under random excitation.
- 38. R.M. Rosenberg 1964 Quarterly of Appled Mathematics 22 (3), 217-234. On the existence of normal mode vibrations of nonlinear systems with two-degrees of freedom.
- 39. R.M. Rosenberg 1966 Advances in Applied Mechanics 9, 156-242. On non-linear vibrations of system with many degrees of freedom.
- 40. B.M. Irons 1970 Int. Journal for Numerical Methods in Engineering 2, 5-32. A frontal solution program for finite element analysis.
- 41. R.J. Melosh and R.M. Bamford 1969 Proc. A.S.C.E. Journal of Structural Division 95 (ST4), 661-676. Efficient solution of load-deflection equations.
- 42. T.K. Hellen 1969 Central Electricity Generating Board, Berkeley Nuclear Laboratories, Berkeley, Goucestershire, England, Rept. RD/B/N1459. A frontal solution for finite element technique.
- 43. S.H. Crandall 1963 Journal of the Acoustical Society of America 35 (1), 1720-1705. Perturbation techniques for random vibration of nonlinear systems.
- 44. C.C. Tung 1967 Journal of Sound and Vibration 5 (1), 164-172. The effects of runway roughness on the dynamic response of airplanes.
- 45. D.E. Newland 1965 J. Inst. Math. Applic. $\underline{1}$ (3), 199-207. Energy sharing in the random vibration of nonlinearly coupled modes.
- 46. S.R. Soni and K. Surrendran 1975 Journal of Applied Mechanics, Trans. A.S.M.E. 42, 891-893. Transient response of nonlinear systems to stationary random excitation.
- 47. R. Vaicaitis, C.M. Jan and M. Shinozuka 1972 American Institute of Aeronautics and Astronautics Journal 10 (7), 895-899. Nonlinear panel response from a turbuelnt boundary layer.
- 48. M. Shinozuka and Y.K. Wen 1972 American Institute of Aeronautics and Astronautics Journal $\underline{10}$ (1), 37-40. Monte Carlo solution of nonlinear vibrations.
- 49. R. Vaicaitis, M. Shinozuka and M. Takeno 1973 Proc. A.S.C.E., Journal of Structural Division 99 (ST 3), 453-468. Parametric study of wind loading on structures.
- 50. C.J. Harris 1979 Intl. J. Numer. Methods Engr. 14, 37-50. Simulation of multivariable non-linear stochastic systems.
- 51. V.A. Lubarda and E.H. Lee 1981 Journal of Applied Mechanics, Trans. A.S.M.E. 48, 35-40. A correct definition of elastic and plastic deformation and its computational significance.
- 52. O.C. Zienkiewicz 1977 The Finite Element Method. New York: McGraw-Hill.
- 53. R.W.H. Wu and E.A. Witmer 1974 Int. Journal of Solids and Structures 10, 243-260. The dynamical response of cylindrical shells including geometric and material nonlinearities.

- 54. C.W.S. To 1979 Journal of Sound and Vibration 63 (1), 33-50. Higher order tapered beam finite elements for vibration analysis.
- 55. T. Duffey and R. Krieg 1969 Int. Journal of Mech. Sc. <u>11</u>, 825-844. The effects of strain-hardening and strain-rate sensitivity on the transient reponse of elastic-plastic rings and cylinders.

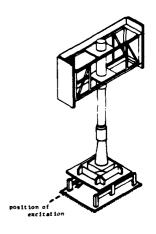


Figure 1. The Physical Model of Mast Aprenna Structure.

Table 1. Input data for the Example.

node number	Coordinate (m)
1	0.00
2	0.67370
3	1.34740

 $E = 2.07 \times 10^{11} \text{ N/m}^2$ $0 = 7860 \text{ kg/m}^3 \qquad \text{S}_{\text{max}} = 10^{-6} \text{ m}^2 \text{s}$

Mass attached at node 3 = 140 kg
Rotary inertia of attached
mass = 44.80 kg.m²

The cross-section area and area moment of inertia of the uniform beam are: $2.5844 \times 10^{-3} \text{ m}^2$ and $6.23 \times 10^{-6} \text{ m}^4$

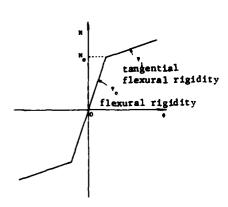
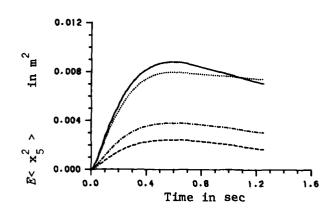


Figure 2(a). The Nonlinear Bending Moment Curvature Relation.





EXTENSION OF TRANSFER-MATRIX METHODOLOGY TO NONLINEAR PROBLEMS

J. W. David and L. D. Mitchell Virginia Polytechnic Institute and State University Blacksburg, Virginia 24061

1. INTRODUCTION

AD-P003 663

Transfer matrices have traditionally been used in the solution of linear mechanics problems, [4,2,3]. They have also been extensively used in the analysis of rotor systems, [4]. In current efforts to solve the dynamically-coupled nonlinear rotor mechanics equations, [5,6] it was necessary to extend the transfer-matrix technology to this class of nonlinear problems.

Hibner (7) has shown that transfer matrices can be used on certain classes of nonlinear problems. He incorporated the nonlinear stiffness and damping effects of a fluid-film bearing in the response analysis of rotor systems. However, his approach was essentially to linearize the bearing stiffness and damping about an operating point. Hence, his approach was unable to account for the multifrequency response that arises from certain system nonlinearities. Thus, a technique was sought which solved, in an approximate fashion, for the effects of system nonlinearities on response amplitude and frequency.

TRANSFER MATRICES

or

In general, the transfer matrix method is a procedure used to develop a set of algebraic equations which describe the response of a system in terms of its component physical characteristics. Differential equations are converted to algebraic equations by an assumption about the response in the time domain (i.e., harmonic). It also uses an initial-value approach in that, given the input components variables, the transfer matrix multiples the component input state vector producing the output state vector. Hence, a system may be modeled by appropriate multiplication of the transfer matrices for the individual system components and application of system boundary conditions. The reader is referred to Refs. 1, 2, and 3 for a more thorough discussion of transfer matrices. However, an example at this point may enhance understanding.

3. EXAMPLE: LINEAR TRANSFER MATRICES

This section is provided to acquaint the reader with transfer matrices and to highlight the development presented here. The reader who is familiar with transfer matrices may wish to proceed to the next section

Consider the system shown in Fig. 1. To model this system via transfer matrices, we begin with the individual system elements.

The free-body diagram for the spring is shown in Fig. 2. Application of Newton's second law of motion yields

$$N_{i+1} - N_i = 0 \tag{1}$$

$$N_{i+1} = N_i = N(t).$$
 (2)

For a linear spring, the force deflection relationship is

$$N_i = k(x_{i+1} - x_i) \tag{3}$$

which can be arranged as

$$x_{i+1} = x_i + N_i/k . (4)$$

Defining the state vector as

$$\underline{\mathbf{S}} = [\mathbf{x} \ \mathbf{N}]^{\mathrm{T}} \quad , \tag{5}$$

Eqs. 2 and 4 can be written as

which expresses the displacement and force on the right side of the spring as a function of the displacement and force on the left side and the spring stiffness k. For later use, one can "extend" the transfer matrix by including the identity equation to render Eq. 7 as

$$\left\{ \begin{matrix} x \\ N \\ 1 \end{matrix} \right\}_{i+1} = \begin{bmatrix} 1 & 1/k & 1 & 0 \\ \frac{0}{0} - \frac{0}{0} - \frac{1}{0} - \frac{0}{1} - \frac{0}{1} - \frac{1}{1} \\ \frac{N}{1} \end{bmatrix}_{i}
 \tag{7}$$

For the lumped mass of Fig. 1, the free-body diagram is shown in Fig. 3. Since this mass is assumed to exist at a point and displacements must be single-valued

$$x_{i+1} = x_i = x(t)$$
 (8)

Assuming the response to be harmonic at the excitation frequency

$$x(t) = x \sin(\omega t) , \qquad (9)$$

Newton's second law of motion yields the relationship

$$N_{i+1} - N_i + F_i = m_i \omega^2 x$$
 (10)

or rearranging

$$N_{i+1} = N_i - m_i \omega^2 x - F_i . {11}$$

Writing Eqs. 8 and 11 in matrix form yields

$$\left\{ \begin{array}{c} x \\ N \\ 1 \end{array} \right\}_{i+1} = \begin{bmatrix} 1 & 0 & 0 \\ -m\omega & -\frac{1}{0} & -F \\ -0 & -\frac{1}{0} & 1 \end{bmatrix} \begin{bmatrix} x \\ N \\ 1 \end{bmatrix}_{i} .
 \tag{12}$$

Note that "extending" the transfer matrices allowed the inclusion of the external excitation F $\sin(\omega t)$.

Hence, one can model the system of Fig. 1 by appropriate multiplication of the transfer matrices. Designating the spring as field 1 and the mass as field 2, one has

or

the boundary conditions for this system are

$$N_3 = 0; x_1 = 0.$$
 (15)

Hence, solving the equation for N_3 subject to the boundary conditions yields the nonzero initial value

$$N_1 = \frac{F}{1 - \frac{m\omega}{\kappa}} \tag{16}$$

and, substituting this into the Eq. 14 for x_3 yields

$$x_3 = \frac{\frac{F}{k}}{1 - \frac{m\omega}{k}}$$
 (17)

which is the well-known frequency response equation for an undamped harmonic oscillator.

4. EXTENSION TO NONLINEAR PROBLEMS

For the system of Fig. 1, if the force-deflection relationship of the spring is

$$N_{i} = k_{i} \{ (x_{i+1} - x_{i}) + \epsilon (x_{i+1} - x_{i})^{3} \}$$
 (18)

the system is nonlinear. However, following a procedure similar to that for a linear system, a transfer matrix can be developed for the spring.

As with linear transfer matrices, one begins with an assumption about the form of the response in the time domain. Here, however, this assumption must be used with the spring as well as the mass. For this system, the appropriate response is

$$x_{i+1}(t) - x_i(t) = x(t) = x1 \sin(\omega t) + x3 \sin(3\omega t)$$
. (19)

It should be pointed out that the correctness of the assumption concerning the harmonic content of the response is vital to obtaining an accurate solution [8]. In this case, the necessity of including the $\sin(3\omega t)$ term was found by initially assuming a harmonic response and noticing the higher-harmonic terms generated by the nonlinearity. Also, numerical simulation can be used in more difficult problems to aid in making the assumption concerning the harmonic components in the assumed solution.

Application of Newton's second law of motion to the spring yields

$$0 = mx = N_{i+1}(t) - N_i(t); N_{i+1}(t) = N_i(t).$$
 (20)

And, consistent with the assumed displacement response , the internal force is assumed to be of the form

$$N_{i+1}(t) - N_i(t) = N(t) = N1 \sin(\omega t) + N3 \sin(3\omega t)$$
 (21)

At this point, Eq. 19 and Eq. 21 are substituted into Eq. 18 and trigonometric identities used to reduce power and products of harmonic functions to simple harmonic functions. Next, all harmonic terms not in the assumed solution (i.e. $\sin(5\omega t)$, and $\sin(7\omega t)$) are ignored. This is the step that renders the solution approximate. Finally, applying the principle of harmonic balance (9,10) yields two nonlinear algebraic equations. For the coefficients of $\sin(\omega t)$

$$\frac{N1}{k} = x1 + \epsilon(3/4x1^3 - 3/4x1^2x^3 + 3/2x1x^3^2)$$
 (22)

and for the coefficients of $sin(3\omega t)$

$$\frac{N3}{k} = x3 + \epsilon(-1/4x1^3 + 3/2x1^2x3 + 3/4x3^3) . \tag{23}$$

Defining the state vector as

$$\underline{S} = [x1 \ N1 \ x3 \ N3|1]^{T},$$
 (24)

Eqs. 20, 22, and 23 can be written in matrix form as

$$\begin{pmatrix}
x1\\N1\\x3\\N3\\1
\end{pmatrix} = \begin{bmatrix}
1 & 1/k & 0 & 0 & | & NL1\\0 & 1 & 0 & 0 & | & 0\\0 & 0 & 1 & 1/k & | & NL3\\0 & 0 & 0 & -\frac{1}{0} & -\frac{1}{0} & -\frac{1}{1} & -\frac{0}{1}\\ & & & & & & & \\
1 & 1/k & 0 & 0 & | & NL1\\0 & 0 & 0 & 1 & 1/k & | & NL3\\0 & 0 & 0 & -\frac{1}{0} & -\frac{1}{0} & -\frac{1}{1} & -\frac{0}{1}\\
& & & & & & & \\
1 & & & & & & \\
1 & & & & & & \\
1 & & & & & & \\
1 & & & & & & \\
1 & & & & & & \\
1 & & & & & & \\
1 & & & & & & \\
1 & & & & & & \\
1 & & & & & & \\
1 & & & & & \\
1 & & & & & \\
1 & & & & & \\
1 & & & & & \\
1 & & & & & \\
1 & & & & & \\
1 & & & & & \\
1 & & & & & \\
1 & & & & & \\
1 & & & & & \\
1 & & & & & \\
1 & & & & & \\
1 & & & & & \\
1 & & & & & \\
1 & & & & & \\
1 & & & & & \\
1 & & & & & \\
1 & & & & & \\
1 & & & & & \\
1 & & & & & \\
1 & & & & & \\
1 & & & & & \\
1 & & & & & \\
1 & & & & & \\
1 & & & & & \\
1 & & & & & \\
1 & & & & & \\
1 & & & & & \\
1 & & & & & \\
1 & & & & & \\
1 & & & & & \\
1 & & & & & \\
1 & & & & & \\
1 & & & & & \\
1 & & & & & \\
1 & & & & & \\
1 & & & & & \\
1 & & & & & \\
1 & & & & & \\
1 & & & & & \\
1 & & & & & \\
1 & & & & & \\
1 & & & & & \\
1 & & & & & \\
1 & & & & & \\
1 & & & & & \\
1 & & & & & \\
1 & & & & & \\
1 & & & & & \\
1 & & & & & \\
1 & & & & & \\
1 & & & & & \\
1 & & & & & \\
1 & & & & & \\
1 & & & & & \\
1 & & & & & \\
1 & & & & & \\
1 & & & & & \\
1 & & & & & \\
1 & & & & & \\
1 & & & & & \\
1 & & & & & \\
1 & & & & & \\
1 & & & & & \\
1 & & & & & \\
1 & & & & & \\
1 & & & & & \\
1 & & & & & \\
1 & & & & & \\
1 & & & & & \\
1 & & & & & \\
1 & & & & & \\
1 & & & & & \\
1 & & & & & \\
1 & & & & & \\
1 & & & & & \\
1 & & & & & \\
1 & & & & & \\
1 & & & & & \\
1 & & & & & \\
1 & & & & & \\
1 & & & & & \\
1 & & & & & \\
1 & & & & & \\
1 & & & & & \\
1 & & & & & \\
1 & & & & & \\
1 & & & & & \\
1 & & & & & \\
1 & & & & & \\
1 & & & & & \\
1 & & & & & \\
1 & & & & & \\
1 & & & & & \\
1 & & & & & \\
1 & & & & & \\
1 & & & & & \\
1 & & & & & \\
1 & & & & & \\
1 & & & & & \\
1 & & & & & \\
1 & & & & & \\
1 & & & & & \\
1 & & & & & \\
1 & & & & & \\
1 & & & & & \\
1 & & & & & \\
1 & & & & & \\
1 & & & & & \\
1 & & & & & \\
1 & & & & & \\
1 & & & & & \\
1 & & & & & \\
1 & & & & & \\
1 & & & &$$

where

$$NL1 = -\epsilon(3/4x1^{3} - 3/4x1^{2}x3 + 3/2x1x3^{2})$$

$$NL3 = -\epsilon(-1/4x1^{3} + 3/2x1^{2}x3 + 3/4x3^{3})$$
(26)

Note that the nonlinear terms are not separated into left and right variables, but simply carried along in the extension column as a correction term. This transfer matrix is best understood as a set of nonlinear polynominals to which a solution must be found. This is in contrast to a standard transfer matrix which represents a set of simultaneous linear equations which can be explicitly solved. Hence, the solution using this matrix in effect seeks values of the system variables which satisfy the equations and the boundary conditions.

To develop the transfer matrix for the lumped mass, a similar procedure was followed. Again, since this is a point transfer matrix

$$x_{i+1} = x_i = x(t)$$
 (27)

Assuming the response to be consistent with that of the spring, i.e.,

$$x(t) = x l sin(\omega t) + x 3 sin(3\omega t)$$
 (19)

$$N(t) = N1\sin(\omega t) + N3\sin(3\omega t)$$
 (21)

Application of Newton's second law of motion and the principle of harmonic balance yields

$$N1 = N1 - m\omega^2 \times 1 - F$$
 (28)

and

$$N3 = N3 - 9m\omega^2 \times 3 . {(29)}$$

Again, Eqs. 27, 28, and 29 can be written in matrix form as

Hence, systems with these types of elements can be modeled by appropriate multiplication of transfer matrices and application of boundary conditions. However, one problem is quite noticeable. That is, the nonlinear terms in the extension column of the spring transfer matrix preclude an explicit solution. Hence, an iterative approach is employed.

5. ITERATIVE SOLUTION TECHNIQUE

As can be seen from the example problem, the unknown quantities which are needed to solve a problem are the nonzero components of the initial state vector. In linear transfer-matrix problems, application of the system boundary conditions to the assembled transfer matrix yields a system of n linear equations in n unknowns which can be explicitly solved for the nonzero components of the initial state vector. And, this initial state vector, when multiplied by the assembled transfer matrix, satisfies the output system boundary conditions.

In our iterative approach, we still desire the nonzero values of the initial state vector that will satisfy the system boundary conditions. Defining \underline{z}_n as the vector containing the components of the output state vector that are zero, we can express a correct solution as

$$\beta = \frac{Z}{n} \frac{T}{z_n} = 0 \tag{31}$$

where the underscore indicates a vector. Defining the nonzero components of the initial state vector as \underline{z}_1 . one can express \underline{z}_n as

$$\underline{Z}_{D} = [US]\underline{Z}_{1} + \underline{F} \tag{32}$$

where [US] is the appropriate submatrix of the assembled transfer matrix and \underline{F} is the appropriate subvector of the assembled transfer matrix extension column. Substituting Eq. 32 into Eq. 31 letting [US]^T [US] = [A] yields

$$\beta = \underline{Z_1}^T [A] \underline{Z_1} + \underline{Z_1}^T [US]^T \underline{F} + \underline{F}^T [US] \underline{Z_1} + \underline{F}^T \underline{F} = 0$$
 (33)

or

$$\beta = \sum_{i=1}^{n} \sum_{j=1}^{n} (a_{ij}Z_{1,i}Z_{1,j} + us_{ji}Z_{1,j}F_{j} + us_{ij}F_{i}Z_{1,j}) + F_{i}^{2} = 0$$
 (34)

is the ith component of the vector \underline{Z}_1 and \underline{F}_i is the ith component of vector \underline{F} . Equation 31 can be understood as an objective function for the where we have the distinct advantage of knowing the minimum value Fquation 34 is the objective function cast in terms of the initial \underline{F}_i . Hence, one can use standard optimization techniques to find \underline{Z}_i .

In the actual solution process, two optimization routines were used, both from the Harwell [11] library. The first, VAO9AD, uses a user supplier gradient while the second, VA10AD calculates the gradient numerically. Thus, one must consider obtaining the gradient of Eq. 34 in order to use VAO9AD.

)..

or

The gradient of the objective function can be calculated from Eq. 34 as

$$\frac{\partial \beta}{\partial Z_{1,k}} = \sum_{i=1}^{n} \sum_{j=1}^{n} a_{ij} \left(\frac{\partial Z_{1,i}}{\partial Z_{1,k}}\right) Z_{1,j} + Z_{1,i} \frac{\partial Z_{1,j}}{\partial Z_{1,k}}$$

$$+ us_{ij} \left(\frac{\partial F_{i}}{\partial Z_{1,k}}\right) Z_{j} + F_{i} \frac{\partial Z_{1,j}}{\partial Z_{1,k}} + us_{ij} \left(\frac{\partial Z_{1,i}}{\partial Z_{1,k}}\right) F_{j} + Z_{1,i} \frac{\partial F_{i}}{\partial Z_{1,k}}$$

$$+ 2F_{i} \frac{\partial F_{i}}{\partial Z_{1,k}}$$

$$(35)$$

where $\partial Z_{1,i}/\partial Z_{1,k}$ is the Kronecker delta δ_{ik} . All terms in Eq. 35 are readily calculated except for $\partial F_i/\partial Z_{1,k}$. Since this term is not, in general, an explicit function of the $Z_{1,k}^i$'s, extra consideration is necessary.

Each nonlinear element will have a transfer matrix of the form

$$\underline{\mathbf{S}}_{\mathbf{i}+1} = \begin{bmatrix} \mathbf{L}_{\mathbf{i}} & \mathbf{E}_{\mathbf{i}} \\ \mathbf{0} & \mathbf{1} & \mathbf{1} \end{bmatrix} \quad \underline{\mathbf{S}}_{\mathbf{i}}$$

where \underline{E}_i is the extension column containing the nonlinear correction terms. For each element, one can calculate $\partial E_{i,1}/\partial Z_{i+1,k}$. Since the state vector station i+1 can be written as

$$\underline{S}_{i+1} = \begin{bmatrix} \underline{L}_{n} & \underline{E}_{n} \\ 0 & 1 \end{bmatrix} \begin{bmatrix} \underline{L}_{n-1} & \underline{E}_{n-1} \\ 0 & 1 \end{bmatrix} \dots \begin{bmatrix} \underline{L}_{1} & \underline{E}_{1} \\ 0 & 1 \end{bmatrix} \underline{S}_{1}$$

$$\underline{S}_{i+1} = \begin{bmatrix} \underline{U}_{1} & \underline{G}_{1} \\ 0 & 1 \end{bmatrix} \underline{S}_{1} , \qquad (36)$$

one can determine $\partial Z_{i+1,k}/\partial Z_{1,k}$ approximately as $\Delta Z_{i+1,k}/\partial Z_{1,k}$ and hence

$$\frac{\partial E_{i,j}}{\partial Z_{1,k}} \sim \frac{\partial E_{i,j}}{\partial Z_{i+1,k}} \stackrel{\Delta Z_{i+1,k}}{\Delta Z_{1,k}} . \tag{37}$$

From here, one further extends the transfer matrix for each field as

$$\begin{bmatrix} L_{\underline{i}} & E_{\underline{i}} & J_{\underline{i}} \\ 0 & 1 & 1 \end{bmatrix}$$

where
$$[J_i] = \begin{bmatrix} \frac{\partial E_1}{\partial Z_{1,1}} & \frac{\partial E_1}{\partial Z_{1,2}} & \cdots & \frac{\partial E_n}{\partial Z_{1,n}} \\ \vdots & & \vdots \\ \frac{\partial E_n}{\partial Z_{1,n}} & \cdots & \frac{\partial E_n}{\partial Z_{1,n}} \end{bmatrix}$$
 (38)

In this fashion, when the overall transfer me ix is formed as

$$\begin{bmatrix} U & \vdots & F & \vdots & J \\ \hline -\bar{0} & -\bar{1} & -\bar{1} & -\bar{1} \end{bmatrix}$$

the matrix [J] will contain the partial derivatives $\partial F_i/\partial Z_{1,k}$ needed to evaluate the gradient (35).

6. RESULTS

In using VA09AD and Eq. 35 for the gradient of the objective function, good solutions were usually obtained. The objective function was usually reduced to 10^{-25} to 10^{-30} . However, in some regions, the routine would not reduce the objective function below $1 \rightarrow 10^{-1}$, even though the gradient was still nonzero.

The routine using VA10AD had greater areas of convergence than the one using VA09AD, though sometimes up the 800 iterations were required. Sometimes, however, this routine failed to converge to a good solution. These areas were where the response was a maximum, as will be shown in the next section. The reason for this nonconvergence is not known, but it is thought to be related to machine precision. For both routines used, variable changes of 10^{-15} were attempted before the convergence routine terminated. This is the practical limit using double precision on the IBM computer at Virginia Polytechnic Institute.

Comparing values of the gradient calculated by VA10AD and VA09AD using Eq. 35 showed little difference in the values. Thus, Eq. 24 is thought to give a good approximation to the gradient of the objective function.

7. COMPARISON OF PROPOSED SOLUTION TECHNIQUE WITH NUMERICAL SIMULATIONS

In order to compare the proposed transfer-matrix scheme with numerical simulations, damping was incorporated in the model. The procedure for deriving the transfer matrices is the same as presented in the previous section. The only difference is that assumed response contains sine and cosine terms.

The numerical simulations were performed using the IBM routine CSMP. The output data from the CSMP routine was Fourier transformed to obtain the harmonic components of the response.

The results of the analysis of the system depicted in Fig. 1 (with damping included) are shown in Fig. 4. The agreement between the transfer-matrix solution and the numerical integration is generally good. The largest discrepancy occurs in the region of $\omega=1/3$ rad/sec. This is because the cubic nonlinearity generates a response at 1/3 the shaking frequency in this region. In this case, this 1/3 frequency component is about an order of magnitude less than the other components.

In order to test this methodology on multi degree-of-freedom problems, the system shown in Fig. 5 was anlayzed, the results appearing in Figs. 6 and 7. There is generally good agreement between the two methods, except for the X3 component in the range of $\omega = 1.0$ rad/sec. The transfer-matrix routine had convergence problem in this area and this is thought to be the source of the error. Even the mapping in the amplitudes vary greatly at this point, the frequency range where the peak responses occur is accurately predicted by the transfermatrix routine.

CONCLUSIONS

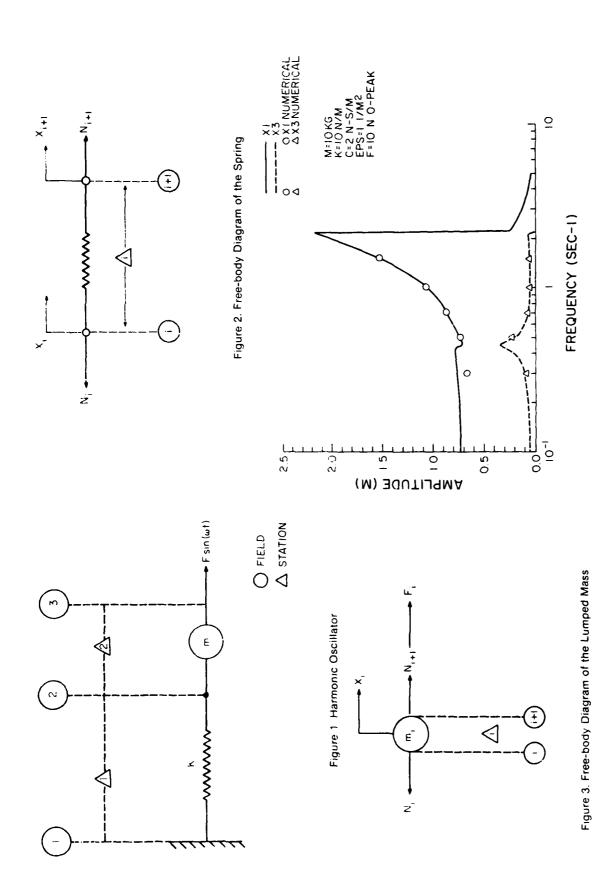
The previous examples illustrate that transfer matrices can be modified for use in solving nonlinear problems. This technique seems to be applicable to any nonlinear system for which the principle of harmonic balance can be used to obtain approximate solutions to the governing equations. For the problems investigated here, the nonlinear transfer-matrix approach appears to accurately predict system response except in small frequency regions where the numerical convergence indicates a residual error. This error indicator can be used to flag the regions where significant error can be expected. However, even in the error regions the results by the transfer matrix method show the trends of the solution thus showing areas of significant response.

ACKNOWLEDGEMENTS

The authors gratefully acknowledge the support of Dr. David Fleming of the NASA Lewis Research Center. We would also like to thank Dr. M. P. Kamat of Virginia Polytechnic Institute and State University for his assistance with the optimization problem.

REFERENCES

- E. C. Pestel and F. A. Leckie, 1963 Matrix Methods in Elastomechnics, New York: McGraw-Hill.
- 2. W. D. Pilkey, 1969, Manual for the Response of Structural Members, AD693141, Springifled, Va., National Technical Information Service.
- 3. W. D. Pilkey and P. Y. Chang, 1978, Modern Formulas for Statics and Dynamics, New York: McGraw-Hill.
- 4. J. W. Daws, 1978, Ph.D. Thesis, Virginia Polytechnic Institute and State University, An Analytical Investigation of Three-Dimensional Vibration in Gear-Coupled Rotor Systems.
- 5. L. D. Mitchell and J. W. David, 1983, ASME paper 83-DET-90, Proposed Solution Methodology for the Dynamically Coupled Nonlinear Sheared Rotor Mechanics Equations.
- 6. T. Yamamoto, 1954, Memoirs of the Faculty of Engineering, Nagoya University 6, No. 2, On the Critical Speeds of a Shaft.
- 7. D. H. Hibner, 1975, Journal of Aircraft 12, No. 4, Dynamic Response of Viscous Damped Multi-Shaft Jet Engines.
- 8. A. H. Nayfeh and D. T. Mook, 1979, Nonlinear Oscillations, New York: John Wiley and Sons.
- 9. W. J. Cunningham, 1958, Introduction to Nonlinear Analysis, New York: McGraw-Hill.
- 10. C. Hayashi, 1964, Nonlinear Oscillations in Physical Systems, New York; McGraw-Hill.
- 11. Harwell Subroutine Library, 1972, AERE Harwell, United Kingdom Atomic Energy Authority.



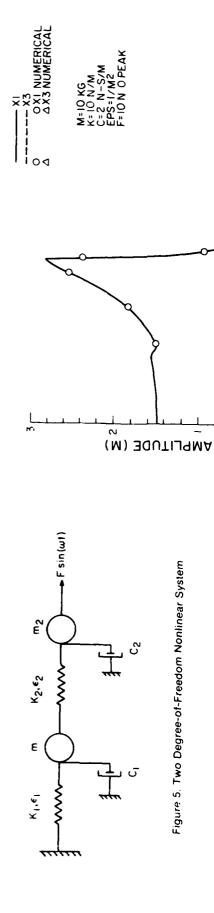


Figure 5. Two Degree-of-Freedom Nonlinear System

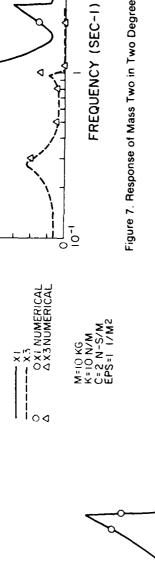
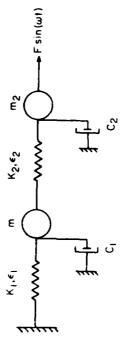


Figure 7. Response of Mass Two in Two Degree-of-Freedom System



205 AMPLITUDE (M) 5

Figure 6. Response of Mass One in Two Degree-of-Freedom System

FREQUENCY (SEC-1)

0.0

0.5



MODAL SYNTHESIS OF LARGE STRUCTURES WITH NONLINEAR JOINTS FROM VIBRATION TESTS

L. Jezequel

Département de Mécanique des Solides Ecole Centrale de Lyon Ecully - 69130 - FRANCE

AD-P003 664

INTRODUCTION

The fundamental idea of modal synthesis methods is to describe the movement of the structure assembly as a superposition of the lower modes of each substructure. The first method, proposed by Hurty, 41 by utilized the "fixed constraint modes" of each substructure obtained by clamping the internal boundaries. Initially, this method utilized constraint modes and rigid body modes to describe the movement at the connection points. Later, Craig and Bampton (2) showed that it was not necessary to differentiate between these two sets of modes and that both could be regarded as constraint modes. This substructure synthesis method is based on the Rayleigh-Ritz procedure. The other possibility is to utilize the free modes of each substructure and to impose the displacement boundary conditions (3.4). The coupling procedure can be implicit or explicit. The latter alternative corresponds to the utilization of Lagrange multipliers {5}. As Meirovitch and Hale clearly showed in recent studies, (6,7), the utilization of unconstrained modes leads to two basic problems. The first involves modal truncation and the second. the choice of the weighting functions which guarantee the compatibility conditions together with the residual methods. (5). The influence of modal truncation is to increase the calculated natural frequencies and thus compensate for the fact that the set of constraint functions is truncated in the case of continuous interfaces, according to the Weinstein method . [9].

The method of modal synthesis using the free modes, beyond its basic limitations, also converge less rapidly than the method utilizing the constraint modes as the former method does not allow a good description of the local structure rigidity near interface boundaries {10}. According to the classical acceleration mode method, the introduction of static responses induced by the boundary forces reduces the influence of the modal truncation {11,12}. Another alternative for increasing convergence is the use of branch modes as defined by Gladwell {13}. Thus, the hybrid method proposed by Mac Neal {14} utilizes the modes obtained with some boundary coordinates being free and others fixed. Similarly, Benfield and Hruda {15} utilize modes obtained by using stiffness and mass loadings at the interfaces.

In the case in which the modes are obtained from experimental tests, the basic limitations of the modal synthesis techniques are amplified. In effect, the number of modes obtained from vibration tests is necessarily low. When the assembly bring out a larger number of boundary coordinates, the substructure synthesis method utilizing constrained modes seems more appropriate. Thus, the Klosterman method uses fixed boundary and constraint modes {16}. It necessitates the difficult measurement of connection forces even if there are no redundant connection coordinates. The other alternative which consists of utilizing the unconstrained modes cannot lead to good results as the number of experimentally obtained mode shapes is too low to guarantee the compatibility conditions.

Hence, the two hybrid methods proposed in this study utilize two independent mode sets identified separately. The first is based on the Rayleigh-Ritz procedure and uses the "fixed constraint modes", the second is based on the

Weinstein method and uses the "free modes". Each of the two modal synthesis techniques defines boundary generalized coordinates by the help of branch modes obtained with mass loading at the interfaces.

These two hybrid substructure models can easily be extended to the case of damped structures by using a simple damping model. However, in many structure assemblies, the losses and the non-linear effects are primarily due to the slipping and clearances at the interfaces during forced vibrations. Many authors have studied the influence of partial slip on the dynamic behavior of joints {17,19}. An analysis based on the cyclic plastic laws allows the definition of standard joint models. But in the context of modal synthesis methods, it is very difficult to integrate such models in the case of riveted or bolted boundaries.

The present study proposes three methods allowing the identification of non-linear joint models from vibration tests. Each of three methods uses one of the two substructure models previously presented which describe the linear dynamic behaviour and define boundary generalized displacements. The first method uses the constrained mode set and is based on a dynamic transformation. It was applied to blade disk assemblies. The second method uses the notion of non-linear modes which take into account the non-linear coupling induced by the interface behavior. It is shown that the non-linear modes can be identified by a method based on the Ritz-Galerkin procedure. The last method permits the definition of a non-linear joint model from an identification of Volterra kernels with the help of a correlation analysis.

2. MODAL SYNTHESIS METHODS

Using certain classical hypotheses, the displacement μ of a continuous elastic structure subjected to force distributions f along a boundary Γ (Fig.1) is a solution to the following boundary value problem:

$$Lu = -\rho \frac{\partial^2 u}{\partial t^2}$$
 (1)

$$M \in \Gamma$$
 : $F_{\ell} (u(M)) = f_{i} \quad \ell \in \{m, 2m-1\}$ (2a)

$$M \in S_1 : F_{\ell} (u(M)) = 0 \quad \ell \in \{m, 2m-1\}$$
 (2b)

$$M \in S_2$$
: $D_0 (u(M)) = 0$ $l \in \{0, m-1\}$ (2c)

In equation (1), L is an elliptic differential operator of order 2m and ρ is the mass density. Boundary operators F_{ρ} and D_{ρ} are linear differential operators involving derivatives normal to the boundary and along the boundary of order through 2m-1 and m-1 respectively. Thus, the nature of the applied forces in Eq. (3) is dependant on the problem studied. For example, in the case of the flexural vibration of plates, force and moment distribution by unit of length are considered along boundary Γ . The following functional spaces are defined in accordance with the methods of modal synthesis.

$$E = \left\{ u \mid u \in H, M \in S_2 : D_{\varrho} u = 0 \ \ell \in \{0, m-1\} \right\}$$
 (3a)

$$E_0 = \left\{ u \mid u \in H, M \in S_2 \cup \Gamma : D_{\varrho} u = 0 \ \ell \in \{0, m-1\} \right\}$$
 (3b)

Space H corresponds to the space of the functions belonging to the field of definition of operator L. It is interesting to complete spaces E_0 and E with the help of the norm associated with the elastic energy so as to obtain a discrete model of the structure. In the case in which the part of boundary S_2 is empty, the quotient space with respect to the rigid body modes must be introduced. Since in the procedure for the functional completion the force boundary conditions are unstable, the Hilbert spaces E and E_0 obtained corroborate the inclusion relationship $E_0 \subset E$

Thus, it is possible to introduce the orthogonal complement of \overline{E}_0 in \overline{E} with respect to scalar product a(.,.) in relation to elastic energy.

$$R = \overline{E} - \overline{E}_0 \tag{4}$$

"Free boundary modes " x_{Fi} and " fixed boundary modes " x_{Ci} form complete bases for spaces E and E_0 respectively. By choosing the static displacement p induced by force distributions f_{Ci} and a function u in space E, one can integrate by parts the quantity a(u,p) to obtain

$$\mathbf{a}(\mathbf{u},\mathbf{p}) = (\mathbf{L}\mathbf{p}, \mathbf{u}) - \sum_{\ell=0}^{m-1} \left[\mathbf{f}_{\ell}, \mathbf{D}_{\ell} \mathbf{u} \right]$$
 (5)

In this equation, scalar product $\left[. \right]$ corresponds to an integration along boundary Γ

The first term of the second mem er of equation (5) is zero, as the static solution verifies that Lp = 0. When the functions u belonging to space \widetilde{E}_0 are considered, the second term is likewise zero. It appears clear that static solutions p belong to closed separable Hilbert space R. In accordance with Weinstein's method , finite space B_k engendered by k static solutions p and its orthogonal complement B_k are defined as follows

$$B_{k} = \overline{E} - R_{k}$$
 (7)

In fact we have

$$\overline{E} \supset \cdots \supset B_{k+1} \supset B_k \longrightarrow \overline{E}_0$$
 (8)

2.1 "Fixed-constraint mode"method

This method uses a variational formulation based on the theorem of virtual work. For example, the "free constraint modes" of each substructure are solutions of:

$$a(x_{Fi}, v) = \omega_{Fi}^{2}(\rho x_{Fi}, v) \Psi v \in \overline{E}$$
 (9)

Following the Rayleigh-Ritz discretisation method, the solution is sought in the space of finite dimension E_{nk} engendered by the n first "fixed constraint modes" and k independent static deflections p_i . As E_{nk} C \bar{E} , the n + k first resonance frequencies obtained are upper bounds. These approximated natural frequencies of the free substructure may be characterized by a Min - Max principle in discrete space E_{nk}

$$\omega_{m}^{2} = \min_{C_{m} \subset E_{nk}} \max_{u \in C_{m}} \left\{ \frac{\underline{\mathbf{a}}(\underline{\mathbf{u}},\underline{\mathbf{u}})}{(\rho \underline{\mathbf{u}},\underline{\mathbf{u}})} \right\}$$
(10)

During the coupling of the substructures, the compatibility conditions will only apply to the generalized interface coordinates associated with deflections p_i .

2.2. "Unconstrained mode"method

Fixed boundary modes x_i may be approximated by a function belonging to space B_k . Intermediate problems of the "first type" are thus defined by constraint equations of the following form

$$\mathbf{a}\left(\mathbf{u},\,\mathbf{p}_{\mathbf{i}}\right) = 0 \qquad \qquad \forall \mathbf{i} \in \left[1\,\,,\,\mathbf{k}\right] \tag{11}$$

The intermediate problem of order k is defined by the following

$$Q^{k} Gu = \omega^{-2} u \tag{12}$$

 Q^k is the orthogonal projection operator onto B_k . The compact operator G may be expressed by using the Green's function g(M,P) obtained when interface Γ is free

$$G u (M) = (u (P), g(M,P) \rho (P) u(P))$$
 (13)

As function $(G - Q^k G)u$ belongs to B_k , equation (12) may be written in the following manner

$$-\omega^{2}G u - u = \sum_{j=1}^{k} P_{j} \mu_{j}$$
 (14)

This equation is recognized as an integral equation of the second kind, and the unknowns μ_i as generalized forces. If ω^{-2} is not in the spectrum of operator G we can apply the resolvent $R_{\omega} = \begin{bmatrix} -\omega^2 & G + I \end{bmatrix}^{-1}$ to both sides of (14). We then have :

$$u = \sum_{j=1}^{k} R_{\omega} (P_{j}) \mu_{j}$$
 (15)

The resolvent R_{ω} may be expressed in the basis of the free modes, that is :

$$R_{\omega} (P_{j}) = P_{j} + \omega^{2} \sum_{i=1}^{\infty} \frac{a(P_{j}, x_{Fi}) x_{Fi}}{\omega_{i}^{2} (\omega_{i}^{2} - \omega^{2})}$$
 (16)

In accordance with the classical acceleration mode method, the influence of modal truncation may be reduced through the introduction of static solution P_i in the expression of the resolvent. Using orthogonality conditions (11), we obtain the following set of equations

$$a(u,p_{i}) = \sum_{j=1}^{k} a(p_{i}, R_{\omega}(P_{j})) \mu_{j}$$
 (17)

The approximated natural frequencies of the fixed interface modes correspond to values of ω which cancel out Weinstein's determinant, that is

$$det \left| \mathbf{a} \left(\mathbf{p_j} , \mathbf{R_{\omega}} \left(\mathbf{p_j} \right) \right) \right| = 0 \tag{18}$$

In the case in which the structure is artificially loaded along boundary Γ , such an analysis allows us to define a fictive structure for which the generalized coordinates of boundary λ_i are given by the following equation

$$\lambda_{i} = a(u, p_{i}) \tag{19}$$

By utilizing equation (16), we obtain

$$\lambda_{i} = \sum_{j=1}^{k} a(p_{i}, p_{j}) \mu_{j} + \omega_{j=1}^{2} \sum_{\ell=1}^{m} \frac{a(p_{i}, x_{F\ell}) a(p_{j}, x_{F\ell})}{\omega_{\ell}^{2} (\omega_{\ell}^{2} - \omega^{2})} \mu_{j}$$
 (20)

In these last equations, a modal truncation was introduced. Hence, it would appear interesting to explicitly point out the participations q. of the modes considered

$$\lambda_{\mathbf{i}} = \sum_{\mathbf{j}=1}^{\mathbf{n}} X_{\mathbf{i}\mathbf{j}} q_{\mathbf{j}} + \sum_{\mathbf{j}=1}^{\mathbf{k}} S_{\mathbf{R}\mathbf{i}\mathbf{j}} \mu_{\mathbf{j}}$$
 (21a)

$$(-\omega^2 + \omega_j^2) q_j = \sum_{i=1}^k X_{ij} \mu_i$$
 (21b)

with

$$X_{ij} = a(p_i, x_{Fj})$$
 (22a)

$$S_{Rij} = a(p_i, p_j) - \sum_{\ell=1}^{n} a(p_i, x_{F\ell}) a(p_j, x_{F\ell}) \omega_{\ell}^{-2}$$
 (22b)

Terms S_{Rij} correspond to the components of a first order residual flexibility matrix.

EXPERIMENTAL IDENTIFICATION OF SUBSTRUCTURE MODELS

The methods of experimental identification exposed in Ref. {20,21} permit an identification of the fixed or free constraint modes used in the modal synthesis methods. These experimental forms satisfy orthogonality relationships identical to those satisfied by actual normal modes.

$$\mathbf{a} \ (\mathbf{x_i}, \mathbf{x_j}) = \omega_{\mathbf{i}}^2 \ \delta_{\mathbf{ij}}$$

$$(\rho \ \mathbf{x_i}, \mathbf{x_j}) = \delta_{\mathbf{ij}}$$

$$(23a)$$

Static deflections p_i corresponding to interface loadings are difficult to obtain experimentally especially when the substructures are only supported by elastic supports which allow dynamic decoupling. Thus, we generate space R through the branch modes obtained by loading the boundaries with a known impedance. The simplest loading consists of a mass distribution along boundary Γ (Fig.2). Hence, by the use of independent vibratory tests, we identify k branch modes $x_{\rm Bi}$, verifying the dynamic equilibrium equation

$$L x_{Bi} = \bar{\omega}_{i}^{2} \rho x_{Bi}$$
 (24)

To each mode $x_{\rm Bi}$ is associated a force distribution along boundary Γ of the following type

$$\left\{ \mathbf{f_{j}} \right\}_{i} = - \bar{\omega}_{i}^{2} \left\{ \mathbf{J_{j}} \, \mathbf{D_{j}} \, (\mathbf{x_{Bi}}) \right\} \tag{25}$$

J, corresponds to the inertia distribution along boundary Γ relative to the boundary displacement governed by operator D. . Static deflection p_i corresponding to the boundary loading given in Eq. (25) satisfies the following integral equation: $P_i = x_{Bi} - \bar{\omega}_i^2 G x_{Bi}$ (26)

3.1. Model using "fixed-constraint modes"

The approximated solution u is sought in space E $_{nk}$ engendered by the n first "fixed-constraint modes" x $_{ci}$ and the k first-static deflections p $_{i}$. The Rayleigh-Ritz discretization is written in the following manner

$$u = \sum_{i=1}^{n} x_{ci} q_{i} + \sum_{i=1}^{k} p_{i} \lambda_{i}$$
 (27)

Modal coordinates q, and generalized boundary coordinates λ_{i} are solutions of the following matricial equation

$$\begin{bmatrix}
\Omega^{2} & 0 \\
0 & K_{pp}
\end{bmatrix}
\begin{cases}
q \\
\lambda
\end{cases}
+
\begin{bmatrix}
I & M_{cp} \\
M_{pc} & M_{pp}
\end{bmatrix}
\begin{Bmatrix}
q \\
\lambda
\end{cases}
=
\begin{Bmatrix}
f \\
\mu
\end{Bmatrix}$$
(28)

The identification procedure exposed in Ref. {20} allows the matrices involved in this equation to be obtained from vibratory tests. The procedure necessitates the projection of the branch modes on the "fixed-constraint modes" with respect to the scalar product associated with kinetic energy

$$M_{CBij} = \left(\rho \ x_{ci} \ x_{Bj} \right) \tag{29}$$

This scalar product may be approximated by using a mass matrix obtained by finite element method. If the mass matrix is not known, it is possible to make a projection by the least square method. This method of synthesis applied to plate assemblies has given good results, even in highly damped cases {20}.

3.2 Model using "free constraint modes"

This method requires the calculation of the displacements $R(p_i)$ induced by the boundary distribution given in Eq. (25) and for a given frequency ω . The number of free modes obtained by tests being finite, it is necessary to truncate the series which appears in Eq.(16)

$$R_{\omega} (P_{i}) = p_{i} + \omega^{2} \sum_{j=1}^{n} \frac{\alpha_{ij} x_{Fj}}{(\omega_{j}^{2} - \omega^{2})}$$

$$(30)$$

with

$$\alpha_{ij} = (\rho p_i, x_{Fj})$$
 (31)

This truncation penalizes much less than the modal truncation employed in the Rayleigh-Ritz models as the series convergence is improved by using the static solutions p. Coefficients $\alpha_{i,j}$ are calculated with the help of relation (9) and of the boundary loading given in Eq.(25)

$$\alpha_{ij} = \frac{\overline{\omega}_{i}^{2}}{\omega_{j}^{2}} \sum_{\ell=1}^{m-1} \left[J_{\ell} D_{\ell} (\mathbf{x}_{Bi}), D_{\ell} (\mathbf{x}_{Fj}) \right]$$
(32)

When the interface loading is induced by rigid bodies - Fig.2 - the scalar products are replaced by the finite sums of terms associated with the displacements and rotations at points distributed along boundary Γ . In the case in which the measurement of forces and displacements along the boundary is difficult, it is possible - as with the "fixed-constraint mode" method - to identify the model from the measurement of the modal displacements at particular points defined by a grid of the finite element type.

The branch modes can then be expressed in the base of the unconstrained modes

$$\mathbf{x}_{\mathrm{Bi}} = \sum_{j=1}^{\infty} \theta_{i,j} \ \mathbf{x}_{\mathrm{F},j}$$
 (33)

with

$$\theta_{i,j} = (\rho x_{Bi}, x_{F,j})$$
 (34)

These coefficients are approximated with the help of the mass matrix obtained by the finite element method. Thanks to this series, it is possible to express the static solutions given in equation (26)

$$p_{i} = x_{Bi} - \overline{\omega}_{i}^{2} \sum_{j=1}^{\infty} \theta_{ij} K x_{Fj}$$
 (35)

According to the Hilbert-Schmidt theorem, the series appearing in this equation converges uniformly. Coefficients α_{ij} given in equation (31) can be deduced from this expression of the static deflections. A very simple result is obtained

$$\alpha_{ij} = \theta_{ij} \left(I - \overline{\omega}_{i}^{2} / \overline{\omega}_{j}^{2} \right) \tag{36}$$

On the other hand, the calculation of terms $a(p_i, p_j)$ brings into play the truncation at order N of the series appearing in Eq.(33)

$$\mathbf{a} \left(\mathbf{p_{i}}, \mathbf{p_{j}}\right) = \left(\frac{\overline{\omega_{i}^{2}} + \overline{\omega_{i}^{2}}}{2}\right) \left(\delta_{ij} - 2\sum_{\ell=1}^{N} \theta_{i\ell} \quad \theta_{j\ell}\right) \tag{37}$$

$$+ \quad \overline{\omega}_{\mathbf{j}}^{2} \quad \overline{\omega}_{\mathbf{j}}^{2} \quad \sum_{\ell=1}^{N} \quad \frac{\theta_{\ell} \quad \theta_{\ell}}{\omega^{2}_{\ell}}$$

TABLE 1

Natural frequency of a simply supported rectangular steel plate (0,6mx0,4mx0,005)

N° of modes	1	2	3	4	5
Eigenvalue of branch modes H Z	15.97	44.54	80.62	X	Х
Estimated Eigenvalue H =	114.7	221.5	354.1	401.8	465.5
Exact Eigenvalue H Z	114.5	220.2	352.3	396.3	458.0

Table 1 shows the resonance frequencies of a simply supported plate calculated by this method from unconstrained modes \mathbf{x}_{Fi} obtained by freeing one of its sides and branch modes obtained by adding masses along this same side in the case k=3, n=8 and N=10.

4. EXTENSION TO NON-LINEAR CASES

The methods of modal synthesis derived from vibration tests presented previously can easily be extended to the case of damped linear structures. Thus, in Ref. {20} a synthesis of the damping using the "fixed-constraint modes" in the case of assemblies of strongly damped sandwich plates is presented. If the synthesis method using free modes is utilized, the damping may easily be introduced by replacing the normal modes in the expression of the resolvent given in Eq. (16) by the complex modes by supposing a purely viscous or frequency-independent hysteretic damping. On the other hand, the introduction of non-linear terms in the structures assemblies leads to serious complicatications in the utilization of the modal synthesis methods. These difficulties are principally due to the non-linear coupling among the normal modes and to the existance of several forced solutions for the same forcing frequency.

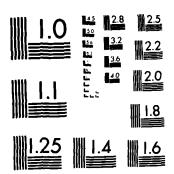
The sources of non-linear terms in structures's assemblies are numerous and it is often difficult to make a choice of the non-linear model best describing them. It has often been observed that the principal cause of large structure damping is the relative interfacial slip in the joints {22}. Numerous authors have clearly shown the influence of the microslip mechanism on the dynamic behavior of the joints {23 - 25}. Such a mechanism may be represented by a generalized kinematic hardening model often used in cyclic plasticity theories. In the case of structures with geometric non-linearity, several authors have shown that the dynamic behavior of the structure may be described satisfactorily by polynomial series truncated at the third order {26-27}.

Once the non-linear models are chosen, they must be identified from vibration tests. The diverse methods allowing the identification of non linear systems may be divided into two families.

- Parametric identification These methods attempt to narrow the gap between the non-linear model and the experimental results through an optimal choice of the model parameters. Research may be done based on the transient or frequency-response data {26-28}. Some methods use models obtained after linearization of the equilibrium equations with the help of an averaging or harmonic balance technique {29}. In particular, the trials with constant modal coordinate amplitude allow the derivation of impedance curves approaching those obtained in linear cases. However, the latter procedure can only be applied to systems with weak non-linearity and in the case of isolated modes.
- Nonparametric identification The non-linear model is sought in the form of a series of particular functions. Thus, the method proposed in Ref. {30} uses the Chebyshev polynomials. Another possibility is the utilization of a decomposition of the system response into non-linear subsystems. Hence, certain methods utilize a finite Fourier series and an identification based on frequency-response measurements {31} and still others a decomposition into Volterra or Wiener series {32 33}. Yet, these latter methods which have the advantage of separating the identification of the linear part from that of the non-linear joint can only be applied in the case of zero memory non-linear elements.

The three methods for analysis of non-linear structure assembly behavior proposed in this study utilize an identification technique related to both these families and each corresponding to an extention in the non-linear case of modal synthesis methods from the vibrations tests described previously.

RD-R143 300 PROCEEDINGS OF THE INTERNATIONAL CONFERENCE ON RECENT ADVANCES IN STRUCTU. (U) SOUTHENPTON UNITY (ENGLAND). INST OF SOUND AND VIBRATION RESEAR. H PETY ET AL. 1984 4/5 UNCLASSIFIED NL.



MICROCOPY RESOLUTION TEST CHART NATIONAL BUREAU OF STANDARDS-1963-A

4.1. Method using non-linear modes

By using a modal synthesis method, the dynamic behavior of a continuous non-linear structure subjected to a harmonic forcing function is obtained in the following form

$$\dot{q}^{\cdot} + \Omega^{2} q + H(q, \dot{q}) = f_{0} e^{iwt}$$
 (38)

The spectral matrix Ω^2 is constituted by the squares of the natural frequencies. The displacement of the structure is approximated by

$$u = \sum_{i=1}^{n} q_i x_i$$
 (39)

Linear modes x are calculated in the case of low amplitude. In Ref. {34},non-linear matrix H^1 is expressed in the case of a cantilever plate possessing slipping joints on its boundary. It is obtained from in-plane forces N , N and N induced by the displacement field given in Eq.(39) and calculated by the finite element method, that is

$$H_{i,j}(q, \dot{q}) = -(B(N, x_i), x_j) q_j$$
 (40)

with $B(N, \mathbf{x_i}) = N_x \frac{\partial^2 \mathbf{x_i}}{\partial x^2} - 2N_{xy} \frac{\partial^2 \mathbf{x_i}}{\partial x \partial y} + N_y \frac{\partial^2 \mathbf{x_i}}{\partial y^2}$ (41)

In the case of weak non-linearities, the solution for modal coordinate q_i is assumed in the form of an harmonic function of time

$$q_{i} = q_{in} e^{iwt}$$
 (42)

By using a linearization method, the modal amplitudes are a solution of the following matrix system

For example, if the K.B.M. method is used, the non-linear stiffness and damping matrices are given by

$$\psi_{\mathbf{i}\mathbf{j}} = \frac{1}{2\pi} \int_{0}^{2\pi} H_{\mathbf{i}\mathbf{j}} \left(1 - \cos 2 \phi\right) d\phi \tag{44}$$

$$\phi_{ij} = \frac{1}{2\pi} \int_{0}^{2\pi} H_{ij} \sin 2\phi \ d\phi$$
 (45)

If the non-linear stiffness matrix ψ is symmetrical, the non linear modes can be defined by the following equations

$$u = q_{i_0} x_i (q_{i_0}) = q_{i_0} \sum_{j=1}^n a_{ij} (q_{i_0}) x_j$$
 (46)

with $\left[-\frac{\mathbf{v}_{i}^{2}}{\omega_{i}^{2}}\mathbf{I} + \Omega^{2} + \Psi\right] \mathbf{a}_{ij} = 0$ (47)

$$\mathbf{a_{i\,i}} = 1 \qquad \mathbf{x_{i}}(0) = \mathbf{x_{i}} \qquad (48a,b)$$

These modes correspond to the non-linear modes defined by Rosenberg $\{35\}$ in the case in which the latter are considered as disturbed lines modes and are calculated by linearization method. The solutions of the eigenvalue problem defined by equations (46), (47) and (48a,b) are obtained by increasing modal coordinate q_i step by step from zero.

Only the solution approaching linear mode is retained. In the case of weak non-linearities, the n non-linear modes x_i utilized remain close to the n linear modes x_i and their stability is assured. As Szempliska-Stupnicka {36} has clearly shown, the deflection at the resonance is close to a non-linear mode in the case of weak damping.

 $\label{eq:modal_coordinates} \ \mathbf{q_i} \ \ \mathbf{are} \ \ \mathbf{given} \ \ \mathbf{by} \ \ \mathbf{the} \ \ \mathbf{following} \ \ \mathbf{expression}$

$$(-M_{i}\omega^{2} + \omega_{i}^{2}(\alpha_{i} + j\beta_{i}))q_{i_{0}} = \hat{f}_{i_{0}}$$
 (49)

avec

$$\widetilde{M}_{i} (q_{i_0}) = \sum_{j=1}^{n} a_{ij}^{2} (q_{i_0}) \widetilde{f}_{i_0} = \sum_{j=1}^{n} a_{ij}^{2} (q_{i_0}) f_{i_0}$$

$$\tilde{\omega}_{i}^{2} \quad (q_{i_{0}}) = \alpha_{i} \quad \omega_{i}^{2} / \tilde{M}_{i}$$
 (50a,b,c)

The loss factor β is obtained by calculating the energy loss per cycle. In the case of a cantilever plate with a sliding point, the values of α and β as a function of the modal amplitude relative to the first mode are given in Ref.{37} Although the existance of non-linearities excludes the superposition of solutions we have observed in numerous examples that the forced response of a non-linear structure is well described by the following modal décomposition

$$u = \sum_{i=1}^{n} x_{i} \left(-M_{i} \omega^{2} + \omega_{i}^{2} \left(\alpha_{i} + j\beta_{i}\right)\right)^{-1} f_{i_{0}}$$
 (51)

The identification method described in Ref. $\{20\}$ allows one to obtain non-linear modes for several values of modal coordinates q_i . It is advantageous to choose a simple analytical expression for these coefficients. Based on experimental analyses, it appears judicious to choose the following form

$$a_{ij} = b_{ij} q_{i0} + c_{ij} q_{i0}^2$$
 $i \neq j$ (52)

coefficients b and c are calculated by the mean square method.

4.2. Dynamic transformation method

The utilization of the non-linear modes does not take advantage of the knowledge of the location of the non-linearities when they originate in the joints. In the case of a modal synthesis using the free modes, the non-linear terms only come into play in flexibility matrix S_R . The equation giving the vibration frequency as a function of the displacement amplitude is analogous to that obtained by Dowell who uses the lagrange multipliers {38}. If the method used fixed constraint modes is adopted, in Eq.(28) the non-linear terms only come into play in the constrained stiffness and damping matrices K et H pp

$$\begin{bmatrix} \Omega^{2} & 0 \\ 0 & K_{pp} \end{bmatrix} - \omega^{2} \begin{bmatrix} I & M_{cp} \\ M_{pc} & M_{pp} \end{bmatrix} + \dot{J} \begin{bmatrix} \eta & \Omega^{2} & 0 \\ 0 & H_{pp} \end{bmatrix} \begin{pmatrix} q_{0} \\ \lambda_{0} \end{pmatrix} = \begin{pmatrix} f_{0} \\ \mu_{0} \end{pmatrix}$$
(53)

The boundary coordinate amplitudes λ_0 are related linearly to the modal coordinate amplitudes q_0

with
$$q_0 = \omega^2 Z (\omega) M_{cp} \lambda_0 + Z (\omega) f_0$$

$$Z (\omega) = \begin{bmatrix} -\omega^2 I & \phi \\ 0 & + \Omega \end{bmatrix} + J (0) f_0$$
(54)

By using the relationship, linearized equilibrium equation (53) may be condensed on the boundary degrees of freedom

$$\left[K_{pp} + j H_{pp} - \omega^2 \vec{M}\right] \lambda_0 = F_0 \qquad (56)$$

with

$$\overline{M} = M_{pp} + \omega^2 M_{pc} Z M_{cp}$$
 (57a)

$$F_0 = \mu_0 + M_{DC} Z f_0$$
 (57b)

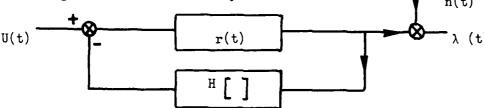
The "mass" matrix \overline{M} and the generalized force vector F_0 depend on pulsation ω The non-linear terms can be obtained from vibration tests through the use of a parametric identification method.

4.3. Method utilizing the Volterra series

The preceding methods define non-linear models identified through a linearization of the structure responses subjected to harmonic forces. Yet, in the case in which the non-linearities are at zero-memory and localized at links, it is possible with the help of random excitations to identify separately the linear part of the structure and the non-linear joint model. Although this study could be extended to the multidimensional case, we shall limit ourselves to the study of an assembly of two structures whose interface behavior only brings a single generalized displacement coordinate into play - Fig.3 - The joint possesses an elasticity in parallel with an assumed non-linear element of the following form

$$\mu = H \left[\lambda \right] = \sum_{i=2}^{n} \gamma_{i} \lambda^{i}$$
 (58)

The dynamic equilibrium of the two assembled structures may be represented by the following non-linear feedback system



r (t) is the impulse response of the assembled linear system which takes the linear stiffness of the joint into account. Input U corresponds to the intensity of two balanced forces acting on the two extremities of the joint - Fig.3 - In general, this input is linked to forces applied to the structures by transfer functions which we have purposely not expressed so as to simplify the dynamic equilibrium equation. The latter is written as follows

$$\lambda (t) = r (t) \not\models (U (t) - H [\lambda])$$
 (59)

response λ may be divided into Volterra series

$$\lambda (t) = \sum_{i=1}^{\infty} w_i (t) + n (t)$$
 (60)

with

$$w_{\mathbf{i}}(t) = \int \dots \int U(t - \tau_{\mathbf{i}}) \dots U(t - \tau_{\mathbf{i}}) \omega_{\mathbf{i}}(\tau_{\mathbf{i}} \dots \tau_{\mathbf{i}}) d\tau_{\mathbf{i}} \dots d\tau_{\mathbf{i}}$$
(61)

The Volterra kernels ω_i may be expressed as a function of the subsystems' characteristics. In the case of a separable white gaussian input process U(t) crosscorrelation function C_{uw_1} (t) verifies the following relation

$$C_{uw_1}(t) = r(t) = \omega_1(t)$$
 (62)

with

$$C_{m}(t) = \delta(t) \tag{63}$$

Unlike systems in cascade, the invariance property of the separable process cannot be used and it is therefore necessary to determine $^{\text{C}}_{\text{uwi}}$ from measurement of $^{\text{C}}_{\text{u}\lambda}$ for several input levels. As noise term $^{\text{C}}_{\text{un}}$ to zero when n(t) is zero mean and independent of the input, we obtain

$$c_{\alpha_{j} u\lambda}(t) = \sum_{i=1}^{N} \alpha_{i}^{i} c_{uw_{i}}(t)$$
 (64)

In these last equation, a truncation of Volterra series was introduced. By using N equations with α , $\neq \alpha_k$, ψ , $\neq k$, the impulse response r(t) for the linear subsystem can be determined

$$\begin{cases}
\mathbf{r}(\mathbf{t}) \\
\vdots \\
\mathbf{c}_{\mathbf{u}\mathbf{w}_{\mathbf{N}}}
\end{cases} = \begin{bmatrix} \alpha & \mathbf{i} \\
\mathbf{j} \end{bmatrix}^{-1} \qquad
\begin{cases}
\mathbf{c}_{\alpha_{\mathbf{1}}}\mathbf{u}\lambda \\
\vdots \\
\mathbf{c}_{\alpha_{\mathbf{N}}}\mathbf{u}\lambda
\end{cases}$$
(65)

Modal identification of the linear structure can be obtained by a curve fitting procedure $\{39\}$. Knowing r(t) allows the parameters of the non-linear subsystem to be identified. Indeed, displacement λ is linearly linked to coefficients γ_i which appear in equation (57)

$$\begin{array}{cccc} \mathbf{A} & & \\ \mathbf{Z} & = & \mathbf{\theta} \ \mathbf{Y} \end{array} \tag{66}$$

is a vector composed of displacements calculated at m different moments t (m >> n), θ is a known matrix which brings input U(t) into play. Parameter vector γ is obtained by the least squares method

$$\gamma = \begin{bmatrix} e^{T} & e^{T} \end{bmatrix} \quad e^{T} Z \tag{67}$$

Vector Z is composed of displacement values measured at moments t. This procedure has been successfully tested on analog computer results.

5. CONCLUSIONS

The modal synthesis methods from vibration tests proposed in this study allow the assembly of structures along continuous boundaries. The extensions to non-linear cases which were proposed allow the identification of non-linearities internal to the structures and non-linearities localized at the joints. The experimental procedures utilized necessitate the identification of two mode sets and the search for non-linear models with the help of delicate techniques. Nonetheless, the methods' complexity is justified by very difficulty of the problems treated.

6. REFERENCES

- 1. W.C. HURTY 1965 American Institute of Aeronautics and Astronautics Journal 3, 678 -685. Dynamic analysis of structural systems using component modes.
- 2. R. CRAIG and M.C.C. BAMPTON 1968 American Institute of Aeronautics and Astronautics Journal 6, 1313-1321. Coupling of substructures for dynamic analysis.
- 3. R.L. GOLDMAN 1969 American Institute of Aeronautics and Astronautics Journal 7, 1152-1154. Vibrations analysis by dynamic partitioning.
- 4. S.N. HOU 1969 Shock and Vibration Bulletin 40, 25-20 . Review of modal synthesis techniques and a new approach.
- 5. E.H. DOWELL 1972 Journal of Applied Mechanics 39, 727-732. Free vibrations of an arbitrary structure in terms of component modes.
- 6. L. MEIROVITCH and A.L. HALE 1981 American Institute of Aeronautics and Astronautics Journal 19, 940-947. On the substructure synthesis method.
- 7. A.L. HALE and L. MEIROVITCH 1982 American Institute of Aeronautics and Astronautics Journal 20, 1128-1136. A procedure for improving discrete substructure representation in dynamic synthesis.
- 8. L. MEIROVITCH 1980 Computational Methods in Structural Dynamics. Alphen aan den Rijn, The Netherlands Lijthoff-Noordhoff International Publishers.
- 9. A. WEINSTEIN and W. STENGER 1972 Methods of Intermediate Problems for Eigenvalues. New York and London: Academic Press.
- 10. J.D. COLLINS, J.C. HART and W.C. HURTY 1971 Computer and Structure 1, 535-563. Dynamic analysis of large structures by modal synthesis techniques.
- 11. S. RUBIN 1975 American Institute of Aeronautics and Astronautics Journal 13, 996-1006. Improved Component- mode representation for structural dynamic analysis.
- 12. B.P. WANG and F.H. CHU 1981 Shock and Vibration Bulletin 51, 73-79. Effective dynamic reanalysis of large structures.
- 13. G.M.L. GLADWELL 1964 Journal of Sound and Vibration 1, 41-59. Branch mode analysis of vibrating systems.
- 14. R.H. MAC NEAL 1971 Computers and Structures 1, 581-601. A hybrid method of component mode synthesis.
- 15. W.A. BENFIELD and R.F. HRUDA 1971 American Institute of Aeronautics and Astronautics Journal 9, 1255-1261. Vibration analysis of structures by component mode substitution.
- 16. A.L. KLOSTERMAN 1971 Ph.D.Dissertation, University of Cincinnati. On the experimental determination and use of modal representations of dynamic characteristics.
- 17. R.D. MINDLIN, W.P. MASON and T.F. OSMER 1952 Proceeding of International Congress of Applied Mechanics ASME New York. The effects of an oscillating tangential force on the contact surfaces of elastic spheres.
- 18. S.W. EARLES and M.G. PHILPOT 1967 Journal of Mechanical Engineering Science 9, 86-95. Energy dissipation at plane surfaces in contact.
- 19. M. MASUKO, Y. ITO and T. KOIZUMI 1974 Bulletin of the JSME 17,1494-1501. Horizontal stiffness and micro-slip on a bolted joint.
- 20. L. JEZEQUEL 1980 Journal of Mechanical Design American Society of Mechanical Engineers 102, 286-294. A method of damping synthesis from substructure tests.

- 21. T.K.HASSELMAN 1976 American Institute of Aeronautics and Astronautics 1409-1418. Damping synthesis from substructure tests.
- 22. C.F. BEARDS 1983 Journal of Vibration Digest 11, 35-41. Damping in structural joints.
- 23. C.F. BEARDS 1983 Journal of Vibration, Acoustics, Stress, and Reliability in Design ASME, 369-373. The damping of structural vibration by controlled interfacial slip in joints.
- 24. R.S.H. RICHARDSON and H. NOLLE 1977 Journal of Sound and Vibration 54, 577-588. Energy dissipation in rotary structural joints.
- 25. L. GAUL 1981 Design Engineering Technical Conference, Hartford, Paper 81-DET 17. Wave transmission and energy dissipation at structural and machine joints.
- 26. G. MAYMON 1978 Israel Journal of Technology 16, 64-69. Experimental determonation of linear damping coefficients in elastic structures with geometric non linearity.
- 27. W.J. PARZYGNAT 1978 International Journal of Engineering Sciences 16, 999-1017. Resonance phenomène in the non linear vibration of plates governed by Duffing's equation.
- 28. N. DISTEFANO and A. RATH 1975 Computer Methods in Applied Mechanics and Engineering 5, 353-372. System identification in non linear structural seismic dynamics.
- 29 Y.A. TUMANOV, V.Y. LAVROV and Y.G. MARKOV 1982 Journal of Soviet Applied Mechanics 17, 106-110. Identification of non linear mechanical systems.
- 30. S.F. MASRI, H. SASSI and T.K. CAUGHEY 1982 Journal of Applied Mechanics 49, 619-629. Nonparametric identification of nearly arbitrary non linear systems.
- 31. E.M. WYSOCKI and W.J. RUGH 1979 International Journal of Control 29, 113-123. An Approximation approach to the identification of non linear systems based on frequency response measurements.
- 32. P.J. LAWRENCE 1981 IEE Proceedings 128, 206-210. Estimation of the Volterra functional series of a non linear system using frequency response data.
- 33. S.A. BILLINGS and S.Y. FAKHOURI 1978 IEE Proceedings 125, 1051-1058. Theory of separable processes with applications to the identification of non linear systems.
- 34. L. JEZEQUEL 1981 Design Engineering Technical Conference, Hartford 81 DET-139 . Structural damping by slip in joints.
- 35. R.M. ROSENBERG 1962 Journal of Applied Mechanics ASME , 7-14. The normal modes of non linear n.degree of freedom systems.
- 36. W. SZEMPLINSKA STUPNICKA 1979 Journal of Sound and Vibration 63, 475-489. The modified single mode method in the investigations of the resonant vibrations of non linear systems.
- 37. L. JEZEQUEL 1982 Mécanique Matériaux Electricité 394-395,451-460 Amortissement des plaques rivetées ou boulonnées dans le domaine des basses fréquences.
- 38. E.H. DOWELL 1982 Journal of Sound and Vibration 80, 233-246. Component mode analysis of a simple nonlinear, non conservative system.
- 39. S.R. IBRAHIM and E.C. MIKULCIK 1977 Shock and Vibration Bulletin 47, 183-198. A method for the direct identification of vibration parameters from the free response.

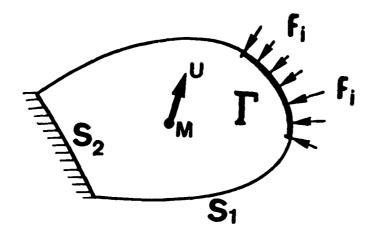


Figure 1 - Substructure model definition

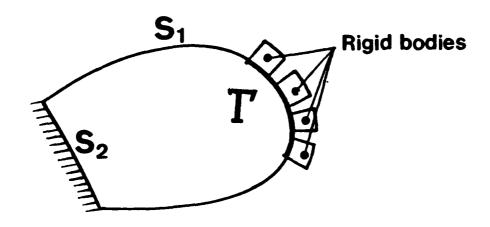


Figure 2 - Substructure with mass loading

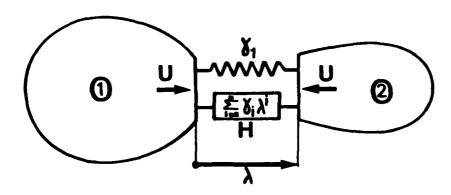


Figure 3 - Substructure assembly with a simple non-linear joint

AN AVERAGING TECHNIQUE FOR THE ANALYSIS OF OSCILLATIONS IN ABRUPTLY NONLINEAR SYSTEMS



Richard K. Miller and Mohammad A. Heidari

Department of Civil Engineering University of Southern California Los Angeles, California 90089-1113

AD-P003 665 ·

ABSTRACT

An approximate technique, ba on a new generalization of the method of equivalent linearization, is presented for analysis of oscillations in such abruptly nonlinear systems as those involving vibroimpact between adjacent structures. The new method introduces a weighting function into the averaging integrals used in the familiar method of equivalent linearization. The weighting function is chosen such that the free vibration backbone curve of the approximate solution matches that of the exact solution at an arbitrary number of preselected amplitudes. Both one- and two-degree-of-freedom (DOF) examples involving periodic motion of colliding oscillators are presented to illustrate the nature of the results. Contact forces are modeled both by a unilateral linear spring and dashpot and by impulse/momentum and coefficient of restitution approaches. It is shown that an approximate amplitude-frequency response curve of adequate accuracy can be obtained with a computational effort several orders of magnitude less than that required by direct numerical simulation.

2. INTRODUCTION

When intermittent contact between structures, pipes, or machine parts occurs during structural vibrations, the effective stiffness and damping of the system undergo abrupt changes. Such changes also occur in cable-stayed structures when the amplitude of vibration is large enough to cause one or more of the cables to go slack and then snap back into a taut configuration. The dynamic analysis of such systems is seriously complicated by these abrupt changes in system characteristics which occur at various amplitudes of vibration. Probably the most common approach for analysis is to use a direct numerical simulation of the equations of motion, but difficulties can arise because of sudden large changes in system eigenvalues, or in the order of the governing equations. Hence, such simulations can be quite tedious and expensive. The use of such approximate analytical techniques as those based on small perturbations is limited by the severely nonlinear nature of the problem. Furthermore, the accuracy of the approximate solutions generated by the familiar methods of energy balance, harmonic balance, equivalent linearization, and slowly varying parameters is generally unacceptable for engineering purposes. However, presented herein is an improvement to the method of equivalent linearization, which substantially improves the accuracy of the approximate solution while retaining the computational efficiency which is characteristic of methods based on averaging.

3. WEIGHTED EQUIVALENT LINEARIZATION FOR SDOF OSCILLATORS

Consider a single-degree-of-freedom (SDOF) oscillator with a symmetric non-linear restoring force element $F(x,\dot{x})$ as depicted in Fig. 1 a. The equation of motion for this system under excitation f(t) is

$$m\ddot{x} + F(x,x) = f(t). \tag{1}$$

Due to the nonlinear term $F(x,\dot{x})$ the solution of this equation is often quite difficult to obtain, particularly when the nonlinearity is hysteretic in nature, or when abrupt changes in system characteristics occur at a particular amplitude of

response. Thus, for computational convenience we consider an equivalent linear replacement system shown in Fig. 1 b. The equation of motion for this linear replacement system under the same excitation f(t) is

$$m \ddot{x} + c \dot{x} + k \dot{e} = f(t)$$
 (2)

Clearly, the extent to which the solution $x_e(t)$ of Eq. (2) resembles the solution x(t) of Eq. (1) depends heavily on the selection of the parameters k_e and c_e .

In the special case when the steady-state (periodic) response to a sinusoidal excitation of the form

$$f(t) = F_0 \cos(\omega t + \phi)$$
 (3)

is sought, an appropriate choice of c_e and k_e which minimizes (in a mean-squared sense) the equation difference between Eqs. (1) and (2) over the class of linear solutions x_e may be expressed as [1]

$$k_{e} = \frac{\mathcal{A}[x_{e}F(x_{e},\dot{x}_{e})]}{\mathcal{A}[x_{e}^{2}]} ; c_{e} = \frac{\mathcal{A}[\dot{x}_{e}F(x_{e},\dot{x}_{e})]}{\mathcal{A}[\dot{x}_{e}^{2}]}$$
(4)

where the operator $\mathcal{A}[\cdot]$ represents the time-average over one period of oscillation $T=2\pi/\omega$ of the linearized response x_e . The integrals implied in Eqs. (4) are relatively simple to evaluate for a broad class of nonlinearities, even including hysteresis [2-5] due to the fact that while $F(x_e,\dot{x}_e)$ may be a functional of the entire time history of x_e (t) it is a single-valued function of time for sinusoidal x_e (t), as implied in the integrals.

In the slightly more interesting case when the nonlinear term $F(x,\dot{x})$ is asymmetric (i.e., the restoring force for positive displacements x is different in character than that for negative x), an appropriate form for x is that of a constant or bias term together with a sinusoidal term [6] such as

$$x_{e}(t) = x_{o} + A \cos(\omega t) . \qquad (5)$$

The constant x_0 may be evaluated by substituting $x_e(t)$ from Eq. (5) into Eq. (1), and then requiring the resulting left-hand-side to equal the right-hand-side in time-average over one period of oscillation. After having so obtained x_0 , the amplitude-dependent parameters k_e and c_e may be obtained from Eqs. (4).

The parameters k_e and c_e so obtained are, in general, functions of the response amplitude A, so that the solution of Eq. (2) generally involves an iterative technique. However, very substantial savings in computational effort are achieved since the original nonlinear differential equation (1) is effectively replaced by a simpler set of nonlinear algebraic equations.

While this approach is quite useful for a broad class of engineering problems, it provides an approximate solution whose accuracy may not be acceptable in all cases. This is particularly true of some problems involving strong nonlinearities.

In order to provide a mechanism for improving the accuracy of the resulting approximate solution, consider a slight generalization of the approach outlined above. The generalization is obtained by including a weighting function w(x) of the form

$$w(x) = 1 + \sum_{k=1}^{N} \alpha_k x^k$$
 (6)

in the averages of Eqs. (4). The N parameters α_k are to be determined by requiring the "backbone curve," or free vibration amplitude-frequency behavior, of the approximate solution to match that of the exact solution at N preselected amplitudes. This results in N linear algebraic equations which may be solved for the N unknown parameters α_k . (Note that the familiar unweighted form of equivalent linearization may be recovered by simply requiring α_k = 0 for every k).

The backbone curve of a SDOF oscillator may be interpreted as the amplitude dependence of the period of free vibration. The period of free ibration of <u>any</u> conservative nonlinear SDOF oscillator may be obtained directly from a first integral of the equation of motion, as shown on page 18 of Stoker's text [7]. The integral often requires evaluation by numerical quadrature. However, the proposed method has been constructed to conveniently accommodate this most general case, since only N points on the backbone curve are required, and hence N evaluations by numerical quadrature suffice. A closed-form expression for the backbone curve is not necessary.

The order N of the weighting function w(x) must be selected to be large enough to obtain an adequate polynomial fit to the backbone curve, but small enough to avoid excessive computation. In the examples which follow, different values of N between 10 and 20 provided results which were indistinguishable on the plots.

4. EXAMPLE: ONE-SIDED VIBROIMPACT OF A SDOF OSCILLATOR

As an example of application of the approach just described, consider a SDOF oscillator whose motion in one direction is limited by the presence of a stiff but dissipative barrier, as shown in Fig. 2. When the mass is at rest, a gap of width d exists between the mass and the barrier of stiffness K and viscous damping coefficient C.

The equation of motion for steady forced vibration of the system shown in Fig. 2 may be written as

$$m\ddot{\mathbf{x}} + c\dot{\mathbf{x}} + k\mathbf{x} + \mathbf{\mathcal{F}}(\mathbf{x}, \dot{\mathbf{x}}) = \mathbf{F}_{0} \cos(\omega t + \phi) \tag{7}$$

where $\mathscr{F}(x,x)$ represents the force on the oscillator mass from the barrier, which may be expressed as

$$\mathcal{F}(\mathbf{x}, \dot{\mathbf{x}}) = \begin{cases} K(\mathbf{x} - \mathbf{d}) + C\dot{\mathbf{x}} & ; \mathbf{x} > \mathbf{d} \text{ and} \\ K(\mathbf{x} - \mathbf{d}) + C\dot{\mathbf{x}} \ge 0 \\ 0 & ; \text{ otherwise.} \end{cases}$$
 (8)

Since the aggregate restoring force is piecewise linear, an exact solution for the amplitude-frequency behavior of the system may be obtained [8]. Assuming the response to be periodic motion with one impact per cycle of excitation, the determination of the amplitude-frequency behavior may be reduced to the problem of finding the root of a single transcendental equation.

The equivalent linear model for the system is governed by the equation of motion $\ensuremath{\mathsf{T}}$

$$m\ddot{x} + c_{e}\dot{x} + k_{e}x = F_{o}\cos(\omega t + \phi)$$
 (9)

where $c_{\mbox{\footnotesize e}}$ and $k_{\mbox{\footnotesize e}}$ are the equivalent stiffness and damping parameters previously described.

Let the approximate solution take the form

$$x(t) = x_0 + \tilde{x}(t) = x_0 + A \cos(\omega t)$$
 (10)

Substituting Eq. (10) into Eq. (7) and averaging over one cycle of oscillation provides the relation

$$2\pi kx_0 + K(x_0 - d)(\theta_1 + \theta_2) + KA(\sin\theta_1 + \sin\theta_2) + \omega CA(\cos\theta_1 - \cos\theta_2) = 0$$
 (11)

where

$$\theta_{1} = \tan^{-1}(K/\omega C) - \sin^{-1}\left[\frac{d-x_{o}}{A\sqrt{1+\left(\frac{\omega C}{K}\right)^{2}}}\right]$$

$$\theta_{2} = \cos^{-1}\left(\frac{d-x_{o}}{A}\right) . \tag{12}$$

Determination of k_e and c_e by the weighted equivalent linearization procedure requires N points on the exact backbone curve of the system. Thus, we consider the amplitude-frequency behavior for free vibrations of the system obtained by setting c=C=0. In this special case, the exact period of vibration of the resulting conservative system may be obtained in closed-form. The resulting natural frequency ω_n is dependent on the peak displacement (for example) during one complete cycle of oscillation. However, since the system shown in Fig. 2 has an asymmetric restoring force, the peak positive displacement is smaller than the peak negative displacement. For convenience, let the absolute value of the peak negative displacement be A_{max} , and regard ω_n as dependent upon A_{max} . Then, it can be shown that

$$\omega_{n}(A_{\text{max}}) = \frac{\sqrt{k/m}}{B(A_{\text{max}})}$$
 (13)

where

$$B(A_{\text{max}}) = \begin{cases} \frac{1}{2} \left[\frac{1}{\sqrt{1 + \left(\frac{K}{k}\right)}} + 1 \right] + \frac{1}{\pi} \left\{ \sin^{-1} \left(\frac{d}{A_{\text{max}}} \right) \right. \\ \left. - \frac{1}{\sqrt{1 + \left(\frac{K}{k}\right)}} \sin^{-1} \left(\frac{d}{\sqrt{A_{\text{max}}^2 \left(1 + \frac{K}{k} \right) - d^2 \left(\frac{K}{k} \right)}} \right) \right\}; A_{\text{max}} > d \end{cases}$$

$$\begin{cases} 1 : A_{\text{max}} \leq d \end{cases}$$

$$\begin{cases} 1 : A_{\text{max}} \leq d \end{cases}$$

Because a closed-form solution is possible in this special case $k_{\rm e}$ may be chosen such that the backbone curve of the equivalent linear system matches the exact backbone curve at every amplitude. This fortunate choice of $k_{\rm e}$ is

$$k_e(A) = m \omega_n^2(A_{max})$$
 (15)

where, in the approximate solution from Eq. (10),

$$A_{\text{max}} = A + |x_0| . \tag{16}$$

Although consideration of the weighting function w(x) was not required for the specification of the stiffness parameter k_e , it must be considered now in defining the damping parameter c_e . This may be accomplished by first selecting (arbitrarily) a global maximum peak response amplitude A^* which is intended to bound from above the response amplitude A_{max} which will later emerge as the approximate solution to the forced vibration problem. Then select (arbitrarily) N values $\{A_{max}, i = 1, 2, \ldots, N\}$ such that

$$d \leq A_{\max_{1}} < A_{\max_{2}} < \dots < A_{\max_{N}} \leq A^{*}. \tag{17}$$

For example, the A_{max} values may be equally spaced in the interval [d,A*].

For each value of A_{\max_i} Eqs. (11), (12), and (16) may be used to decompose A_{\max_i} into an equivalent static offset x_0 and a harmonic amplitude A_i .

Requiring the backbone curve of the weighted equivalent linear system to coincide with the exact backbone curve at each of the N amplitudes just described, one finds that

$$\frac{k_{e}(A_{i})}{m} = \frac{\mathcal{A}[A_{i}\cos\theta \ w(A_{i}\cos\theta)F(x_{o_{i}} + A_{i}\cos\theta, -\omega A_{i}\sin\theta)]}{m \ \mathcal{A}[A_{i}^{2}\cos^{2}\theta \ w(A_{i}\cos\theta)]} = \omega_{n}^{2}(A_{i})$$
(18)

for i = 1, 2, ..., N, where

$$F(x,\dot{x}) \equiv kx + c\dot{x} + \mathscr{F}(x,\dot{x}) \tag{19}$$

and $\mathcal{F}(x,\dot{x})$ is described in Eq. (8). Substituting from Eq. (6) into Eq. (18) and rearranging,

$$\sum_{k=1}^{N} a_{ik} \alpha_{k} = b_{i} ; i = 1, 2, ..., N$$
 (20)

where

$$a_{ik} = \mathcal{A}[A_i^{k+1}\cos^{k+1}\theta \ F(x_{o_i} + A_i\cos\theta, -\omega A_i\sin\theta)] - m \omega_n^2(A_i) \mathcal{A}[A_i^{k+2}\cos^{k+2}\theta]$$
 (21)

$$b_{i} = \mathcal{A}[A_{i}\cos\theta F(x_{o_{i}} + A_{i}\cos\theta, -\omega A_{i}\sin\theta)] - m \omega_{n}^{2}(A_{i})\mathcal{A}[A_{i}^{2}\cos^{2}\theta] . \qquad (22)$$

After evaluating the coefficients in Eqs. (21) and (22), the N linear algebraic equations (20) may be solved (numerically) for the set $\{\alpha_k;\ k=1,\ 2,\ldots,\ N\}$ which then defines the weighting function.

The method as just described requires the recalculation of the $\alpha_{\bf k}$'s for each excitation frequency ω , because of the dissipative term in the restoring force. An alternative, which was employed in the numerical examples presented herein, is to use only the conservative portion of the restoring force for purposes of determining the $\alpha_{\bf k}$'s. Then the tedious calculation of the $\alpha_{\bf k}$'s need be performed only once and the results stored.

The equivalent damping parameter $c_{\mbox{\it e}}$ may then be obtained as

$$c_{e}(A) = \frac{\sqrt{[-\omega A \sin\theta w(A\cos\theta)F(x_{o} + A\cos\theta, -\omega A\sin\theta)]}}{\sqrt{[\omega^{2}A^{2}\sin^{2}\theta w(A\cos\theta)]}}$$
(23)

where Eq. (11) is again used to eliminate \mathbf{x}_{o} in favor of A.

Finally, the steady-state amplitude-frequency behavior of the equivalent linear system is determined by

$$\omega^{2}(A) = \frac{k_{e}}{m} - \frac{c_{e}^{2}}{2m^{2}} \pm \sqrt{\left(\frac{F_{o}}{mA}\right)^{2} - \frac{c_{e}^{2}}{2m^{2}} \left(2 \frac{k_{e}}{m} - \frac{c_{e}^{2}}{2m^{2}}\right)}$$
(24)

where the dependence of k_e and c_e on the amplitude A of response is implied in Eqs. (15) and (23) respectively. The approximate forced response of the system is then obtained by solving the four nonlinear algebraic Equations (11), (15), (23) and (24) simultaneously.

Shown in Fig. 3 is a comparison of curves depicting the amplitude-frequency behavior of the forced vibration of the system shown in Fig. 2. The curve labeled "exact" was obtained by the method of Ref. 7. The curve labeled "Wtd. Equiv. Lin" was obtained by the weighted equivalent linearization approach presented herein. The curve labeled simply "Equiv. Lin." was obtained by the method of Ref. 2, which is a special case of weighted equivalent linearization with $\alpha_{\rm L}=0$.

The curves in Fig. 3 illustrate the substantial improvement in accuracy obtained by the proposed method over that of "unweighted" equivalent linearization. After a one-time effort to obtain the coefficients $\alpha_{\bf k}$ and develop an algorithm for ${\bf k}$ and c from Eqs. (15) and (23), the weighted equivalent linearization algorithm is computationally the same as the equivalent linearization method [2]. Hence, the computational costs for both are quite similar. This is a significant advantage for more complicated examples where an exact solution is not available, because direct numerical simulation from Eq. (1) is typically two or three orders of magnitude more expensive than the solution of the equivalent linear problem as outlined herein.

5. EXTREME CASE OF SDOF VIBROIMPACT WITH A RIGID WALL

As an example of a problem with a severe nonlinearity, consider the vibro-impact of a SDOF oscillator with a rigid wall as indicated in Fig. 4. The equation of motion for this system is again Eq. (7) where, in this case, the nonlinear restoring force $\mathscr{F}(x)$ is as shown in Fig. 5.

The rigid barrier may be regarded physically as a limiting case of the spring-dashpot assembly of Fig. 2 as $K \to \infty$. In the limit, the spring-dashpot assembly produces a force-displacement behavior as shown in Fig. 5. Note that F becomes conservative in this limit, and the collisions between the oscillator mass and the wall occur instantaneously, impulsive forces of interaction are generated, and energy is conserved. Thus, an appropriate technique for generating an exact solution in this case may be based on impulse-momentum considerations. This approach applied to vibroimpact is presented in Ref. 9, and was used to generate the exact solutions discussed later in this section.

It is interesting that, even in this limiting case as K $\rightarrow \infty$, the equivalent linearization technique yields an equivalent stiffness k_e which is finite. In fact, from Eqs. (13), (14), and (15), one finds that

$$k_{e^{\infty}} = \lim_{K \to \infty} k_{e} = \begin{cases} k; & A_{\text{max}} \leq d \\ \frac{k}{\left[\frac{1}{2} + \frac{1}{\pi} \sin^{-1} \left(\frac{d}{A_{\text{max}}}\right)\right]^{2}}; A_{\text{max}} > d \end{cases}$$
 (25)

for the <u>weighted</u> equivalent linear stiffness in this limiting case. Similarly, it can be shown using the unweighted equivalent linearization approach that

$$\hat{k}_{e^{\infty}} = \begin{cases} k & ; & A_{\max} \leq d \\ k \left(3 - \frac{4d}{A_{\max} + d}\right) ; & A_{\max} > d \end{cases}$$
 (26)

Note from Eq. (25) that as A $\rightarrow \infty$, k $_{e^{\infty}} \rightarrow 4k$, while from Eq. (26) k $_{e^{\infty}} \rightarrow 3k$. Hence, the weighted equivalent linear stiffness (which yields the correct period of oscillation for free vibrations) is substantially larger than the unweighted equivalent linear stiffness.

Both the weighted and unweighted equivalent linearization algorithms yield the result

$$c_{e^{\infty}} = \lim_{K \to \infty} c_{e} = c.$$
 (27)

This result is consistent with the fact that as the wall becomes rigid no deformation of the viscous damped C occurs, and hence no additional energy dissipation occurs.

Furthermore, it can be shown that

$$\lim_{K \to \infty} x_0 = d - A. \tag{28}$$

The equivalent linear solution in this case may then be constructed by simultaneously solving Eqs. (24), (27), (28), and either (25) or (26).

Presented in Fig. 6 is a comparison of curves which represent the amplitude frequency behavior for the forced vibration of the system shown in Fig. 4. The excitation level and linear oscillator parameters are the same as those used to construct Fig. 3. Again it is found that the weighted equivalent linear solution is substantially more accurate than the unweighted solution. In fact, the weighted approximate solution is found to be remarkably accurate in predicting all features of the response except the very peak of the curve.

6. APPLICATION TO MULTIDEGREE-OF-FREEDOM (MDOF) SYSTEMS

In order to investigate the validity of the weighted equivalent linearization approach for MDOF systems, the simple 2 DOF system of Fig. 7 is considered. The system is piecewise linear and sufficiently simple that an exact solution is obtainable for calibration of the approximate results. The system consists of two adjacent linear SDOF oscillators separated by a gap of width d. Collision between masses is cushioned by stiffness K and viscous damping C. Excitation is provided by simultaneous support acceleration $\ddot{z}(t)$ of both walls. The system response is that of uncoupled SDOF oscillators as long as $(y_2-y_1)>d$. However, the variable x defined as $x=y_2-y_1$ always displays two degrees of freedom regardless of response level, and provides a convenient description of overall impact behavior of the system.

For the case when the base excitation has displacement amplitude z and driving frequency ω , an exact solution for the steady-state periodic motion of the system was obtained by numerical integration of the equations of motion with appropriate periodicity conditions.

Two approximate solutions for the steady-state response were also obtained by the method of equivalent linearization. In each case the nonlinear restoring force was replaced by an equivalent linear stiffness and damping term as previously discussed. The approximate solutions for \mathbf{y}_1 and \mathbf{y}_2 (and hence also \mathbf{x}) were assumed to consist of a constant bias term together with a sinusoidal term,

as in Eq. (2). In each case the equivalent linear stiffness was obtained from the SDOF analysis replacing k with the effective stiffness of the system in Fig. 7 for equal and opposite forces applied to the masses.

Shown in Fig. 8 is a comparison of approximate and exact amplitude-frequency curves for the system shown in Fig. 7. Again it is found that the weighted equivalent linearization approach results in a substantial improvement in the accuracy of the approximate solution.

ACKNOWLEDGMENT

Portions of this research were supported by a grant from the National Science Foundation.

REFERENCES

- 1. W.D. IWAN 1973 International Journal of Non-Linear Mechanics 8, 279-287. A Generalization of the Concept of Equivalent Linearization.
- 2. T.K. CAUGHEY 1960 Journal of Applied Mechanics 27, 640-643. Sinusoidal Excitation of a System with Bilinear Hysteresis.
- 3. W.D. IWAN 1966 Journal of Applied Mechanics 33, 893-900. A Distributed Element Model for Hysteresis and Its Steady-State Dynamic Response.
- 4. W.D. IWAN 1965 Journal of Applied Mechanics 32, 921-925. The Steady-State Response of the Double Bilinear Hysteretic Model.
- 5. W.D. IWAN 1968 Journal of Applied Mechanics 35, 322-326. Steady-State Dynamic Response of a Limited Slip System.
- 6. P.T.D. SPANOS and W.D. IWAN 1979 Journal of Dynamic Systems, Measutement and Control 101, 31-36. Harmonic Analysis of Dynamic Systems with Nonsymmetric Nonlinearities.
- 7. J.J. STOKER 1950 Nonlinear Vibrations in Mechanical and Electrical Systems. New York: Interscience Publishers, Inc.
- 8. S.F. MASRI 1978 Journal of Mechanical Design 100, 480-486. Analytical and Experimental Studies of a Dynamic System with a Gap.
- 9. R.K. MILLER 1980 Proceedings of the Seventh World Conference on Earthquake Engineering, Istanbul, Turkey, <u>6</u>, 57-64. Steady Vibro-impact at a Seismic Joint Between Adjacent Structures.

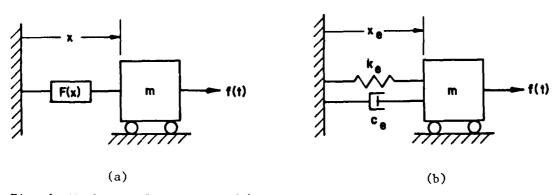


Fig. 1 Nonlinear SDOF system (a) and equivalent linear replacement system (b).

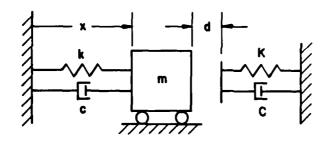


Fig. 2 SDOF vibroimpact model.

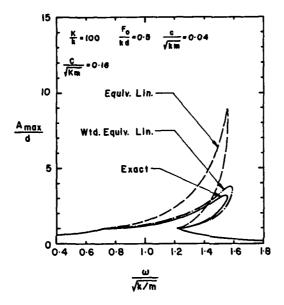


Fig. 3 Amplitude-frequency response of the SDOF system shown in Fig. 2, as determined by an exact and two approximate analyses.

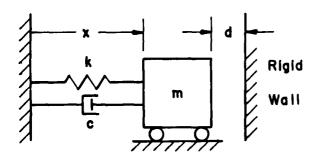


Fig. 4 SDOF vibroimpact model with rigid wall.

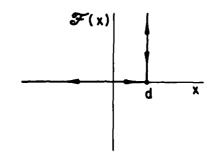
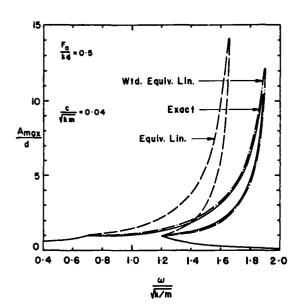


Fig. 5 Force-displacement relation for nonlinear term in rigid vibroimpact model.

Fig. 6 Amplitude-frequency response of the system shown in Fig. 4, as determined by an exact and two approximate analyses.



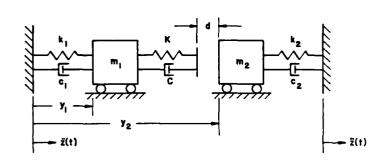
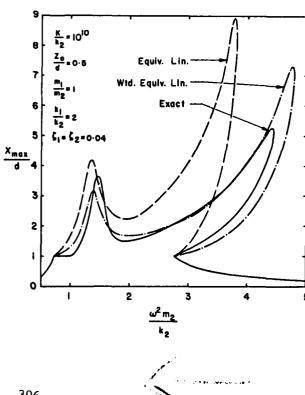


Fig. 7 Two DOF vibroimpact model with base excitation.

Fig. 8 Amplitude-frequency response of the 2 DOF system shown in Fig. 7, as determined by an exact and two approximate analyses.





THE NUMERICAL SOLUTION OF DISCONTINUOUS STRUCTURAL SYSTEMS

W.K.D. Borthwick

Department of Mechanical Engineering University of Dundee

INTRODUCTION

This paper presents a numerical method, based on the classical fourth order Runge-Kutta process which is suitable for the solution of systems of ordinary differential equations with discontinuous right hand sides. These could, for example, include structural systems with discontinuous stiffness, mass or damping or indeed any system whose discontinuous characteristics may be expressed in terms of discontinuity functions. There is no restriction on the size of the system or on the number of discontinuity conditions. Typically the solutions to such systems consist of continuous pieces, which may be integrated quite satisfactorily by the basic Runge-Kutta process (or other convergent integration algorithm). Difficulties arise, however, when one or more components of the solution encounters a discontinuity. Generally, the timing of these discontinuities cannot be predicted in advance of the solution. Therefore timing errors in switching the system parameters are in general introduced unless all discontinuities occur at mesh points of the discrete solution. These timing errors generally have a catastrophic effect on the global accuracy of the numerical solution, with the order of convergence collapsing to one after only one discontinuity traversal. The practical significance of this is demonstrated in Section 2, using a simple discontinuous structural problem.

The structural dynamics literature contains many examples of systems with discontinuities. Grubin [1] describes impact dampers which have jump discontinuities in velocity. Masri [2] studied a two-degree-of-freedom system with discontinuous stiffness and damping. Mounting systems for vital equipment in buildings and ships are often required to satisfy the conflicting requirements of shock protection and noise isolation. This can be achieved through use of mounts with piecewise linear stiffness, as in Iwan [3]. Similar snubber-support systems are described by Lashkari and Weingarten [4], for complex pipe net-works. Stiffness discontinuities are also found in rotating machinery (blade rubs in turbines) and electrical switching mechanisms. Systems, such as the nonlinear vibratory conveyor studied by Leckie and Barr [5], which incorporate connections by Coulomb friction, may give rise to equations with discontinuous mass. Discontinuous problems range from very large (finite element based) systems with discontinuities in some components, to small two- and three-degree-of-freedom problems. Except in certain trivial cases, closed-form analytical solutions are not obtainable.

2. BACKGROUND THEORY

The solution by direct numerical integration of large continuous non-linear problems in structural dynamics is now relatively commonplace. There exists a considerable number of sophisticated library programs, as surveyed by Noor [6]. The options available for numerical integration are generally confined to fixed-step low order algorithms such as the familiar Newmark, Park, Wilson-0, or Houbolt algorithms. This perhaps reflects Dahlquist's [7] celebrated theorem on the A-stability of linear multistep methods (LMM), which states that the maximal order of any LMM, consistent with A-stability (i.e. unconditional on stepsize h), is two. In fact, the numerical analysis literature contains several classes of algorithms which circumvent Dahlquist's "barrier" (see Lambert [8]). However all A-stable algorithms are implicit in some sense, and all require matrix inversion, which can be a major computational deterrent. The literature contains conflicting

views on the relative efficiency of explicit versus implicit algorithms. Belytschko et al [9], and Braekhus and Aasen [10], have favoured explicit algorithms, particularly when accurate integration of medium/high modes is sought. This is significant for discontinuous systems where sudden changes in system parameters and/or shock excitation are likely to perpetuate the high mode response. Furthermore in transient response calculations of discontinuous systems, it can be critical to the global accuracy that the relative phase relationships between the various modes are faithfully reproduced (this is demonstrated in Section 2.3). These factors, combined with ease of implementation, justify consideration of the explicit classical fourth-order Runge-Kutta algorithm as a suitable basis for a numerical method for discontinuous systems.

2.1 Loss of order of convergence on discontinuous systems.

Consider the initial value problem

$$y' = f(t,y) ; y(0) = \eta$$
 (1)

Solution of equation (1) by direct numerical integration over the interval t = [0,b], involves stepwise computation of the sequence $\{y_n\}$, n = 1,2,...,b/h, where y_n is an approximation to $y(t_n)$, the exact solution. Each value y_n is computed by a recurrence formula, or algorithm. From classical numercial analysis theory (Lambert [8]), the traditional results on convergence, order, derivation of asymptotic formulas for the error, etc., are only guaranteed for an algorithm, when the function f(t,y) in equation (1) satisfies the Lipschitz condition

$$||f(t,y) - f(t,y^*)|| \le L||y - y^*||$$
 (2)

where y, and y* are two distinct values lying in a bounded region of the solution space. The order of convergence of an integration algorithm may be formally defined as the largest integer p which satisfies

$$\lim_{h\to 0} ||y(t_n) - y_n|| = O(h^p)$$

$$h \to 0$$

$$h \to t$$
(3)

Feldstein and Goodman [11] have proved that if any algorithm of design order $p \ge 1$ is applied to a differential equation (1) which does not satisfy the Lipschitz condition (2), its order of convergence in general collapses to p = 1 after only one discontinuity traversal. This is demonstrated numerically in Section 2.3, and the consequences for problems in structural dynamics are considered.

2.2 Discontinuous test problem

Consider the two degree-of-freedom system illustrated in Fig. 1(a). For displacements exceeding the gap condition, the mass m_1 contacts precompressed snubber springs. The resulting stiffness characteristic for the spring connecting the mass m_1 to the base is illustrated in Fig. 1(b). It can be seen that as m_1 contacts the snubber spring, there is a jump discontinuity in the spring force as well as the spring stiffness.

This system may be non-dimensionalised with respect to displacement by making the substitution x = u/u. Non-dimensionalisation with respect to time is accomplished by the substitution

$$\frac{d^2 u}{d\tau^2} = \frac{d^2 x}{dt^2} = \omega_1^2 \ddot{x}; \text{ where } \omega_1^2 = \frac{k_1}{m_1}$$

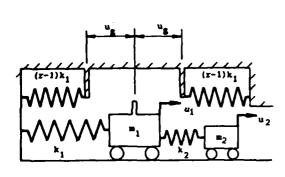
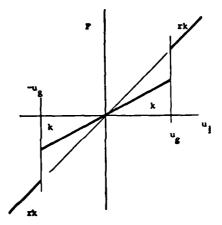


FIG. 1(a) Discontinuous System



Pig. 1(b) Stiffness Characteristic

Making the additional substitutions

$$\omega_2^2 = \frac{k_2}{m_2}$$
; $\Omega = \frac{\omega_2}{\omega_1}$; $m = \frac{m_2}{m_1}$

enables the equations of motion to be expressed in non-dimensional form

$$\ddot{x} = \kappa x \text{ where } \kappa = -M^{-1}(K + HK)$$
 (4)

and where the various matrices M, K, H, K are defined

$$M = \begin{pmatrix} 1 & 0 \\ 0 & m \end{pmatrix} \qquad K = \begin{pmatrix} 1 + m\Omega^2 & -m\Omega^2 \\ -m\Omega^2 & m\Omega^2 \end{pmatrix} \qquad (5a,b)$$

$$H = \begin{pmatrix} H(x_1) & 0 \\ 0 & 0 \end{pmatrix} \qquad \tilde{K} = \begin{pmatrix} (r-1) & 0 \\ 0 & 0 \end{pmatrix}$$
 (5c,d)

Thus K is a matrix of stiffness increments whose accumulation is controlled by the matrix H which contains Heaviside functions. Thus the element $H(x_1)$ in (5c) is defined

$$H(x_1) = \begin{cases} 0 \text{ for } |x_1| \leq 1\\ 1 \text{ otherwise} \end{cases}$$
 (6)

Let $y = x_1$; $y = x_2$; $y = x_2$; $y = x_1$; $y = x_2$ (the superscripts denote component numbers of y). Equation (4) may now be written in first-order form

$$y' = \alpha y$$
; where $\alpha = [A + HA]$ (7)

The partitioned matrices A, and A are obtained from the matrices in (5)

$$A = \begin{pmatrix} 0 & 1 \\ -M^{-1}K & 0 \end{pmatrix} \qquad \stackrel{\sim}{A} = \begin{pmatrix} 0 & 1 \\ -M^{-1}K & 0 \end{pmatrix}$$

For larger systems advantage must be taken of the sparseness. In view of the Heaviside function (6), which switches the jump discontinuity in force, the first-order system (7) does not satisfy the Lipschitz condition (2) at |1y|=1. The system (7) provides a suitable test equation for discontinuous problems in structural dynamics, for it is possible to obtain an analytical solution (see Appendix I). The jump discontinuity causes an instantaneous change in the modal

spectrum.

2.3 Fixed-step integration of the discontinuous test problem.

The loss of order of convergence after only one discontinuity is demonstrated numerically using the classical fourth-order Runge-Kutta process.

$$y_{n+1} = y_n + \frac{h}{6}(k_1 + 2k_2 + 2k_3 + k_4)$$
where $k_1 = f(t_n, y_n)$ $k_3 = f(t_n + \frac{1}{2}h, y_n + \frac{1}{2}hk_2)$

$$k_2 = f(t_n + \frac{1}{2}h, y_n + \frac{1}{2}hk_1)$$
 $k_4 = f(t_n + h, y_n + hk_3)$ (8)

This Runge-Kutta process is applied to the discontinuous test problem (7) with the particular choice of parameters $r=11.5,\,m=0.1,\,\Omega=4.582576.$ For $\left|\begin{smallmatrix}1\\y\end{smallmatrix}\right|\leq 1$, the eigenvalues are $\mu_1=0.951516,\,\mu_2=4.816079,$ whereas for $\left|\begin{smallmatrix}1\\y\end{smallmatrix}\right|>1,\,\mu_1=\overline{3}.114166,\,\mu_2=4.990190.$ The system is subject to the initial conditions $\begin{smallmatrix}1\\y\end{smallmatrix}(0)=1.5,\,\begin{smallmatrix}2\\y\end{smallmatrix}(0)=\stackrel{4}{3}y(0)=\stackrel{4}{3}y(0)=0.$ The results of numerical experiments to determine the order of convergence are presented graphically in Fig. 2(a) and (b). In each Figure, the ordinate is the uniform norm for the first displacement component

$$\lim_{j} \| \mathbf{y}_{j} - \mathbf{y}(\mathbf{t}_{j}) \|$$
; $j = 1, 2, ..., n_{s}$

evaluated at the fixed station $t = n_s h$. This is plotted as a function of h.

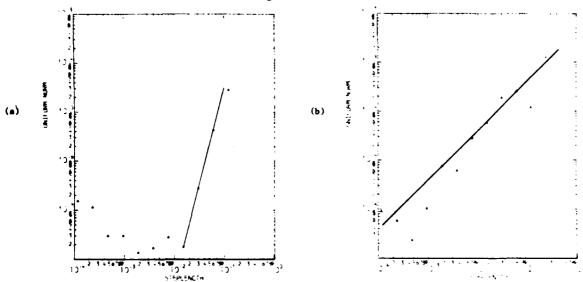
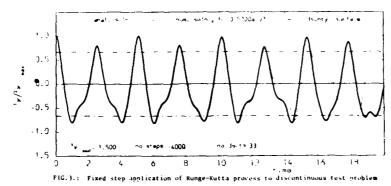


Fig. 2: Fixed station convergence at (a) t = 0.12 (before discontinuity); (b) t = 0.24 (after discontinuity).

In Fig. 2(a) the fixed station is t=0.12 and n_s assumes the values 2^0 , 2^1 , ... 2^{12} . The trend line on this log-log plot has gradient four, corresponding to the design order of convergence p=4 of algorithm (8). This is as expected over the initial continuous piece of solution, prior to the first discontinuity at t=0.2298. The effects of rounding errors are clearly evident for h<0.01. Both the exact solution $l_y(t)$ and the numerical approximation were computed in single precision arithmetic. Fig. 2(b) shows the fixed station convergence at t=0.24 after the first discontinuity, with h taking the same values as before. The trend line shown, which is drawn through the upper set of points, has slope

one. Isolated points of high accuracy are therefore ignored, as they correspond to a discretisation where a mesh point nearly coincides with the discontinuity. Comparing values for the uniform norm in the two plots at, for example, h = 0.03 shows that the error after the discontinuity is a factor of \sim 680 times greater than before. For continuous problems one would not expect the error to grow more than linearly with the total number of steps.

This section is concluded with a practical demonstration of how costly it would be to obtain a converged solution over a lengthy interval. The discrete solution $\{^1y_n\}$ obtained by applying the Runge-Kutta process with the fixed stepsize h = 0.005 is shown in Fig. 3 superimposed on the exact solution $^1y(t)$ (fainter line). The discontinuity surface is represented by the chain dotted lines $|^1y|=1$. Although the stepsize corresponds to $^{\circ}$ 250 integration steps per period of the highest frequency present, the numerical solution starts to diverge around t = 13. Considerable errors in the phase of the lower mode then become evident. The poor performance of the Runge-Kutta process on this relatively simple test problem provides the motivation for the development of special procedures for locating points of discontinuity.



3. SPECIAL DISCONTINUITY SEARCH PROCEDURES

The problem of locating points of discontinuity may be formulated as the algebraic problem of solving for the roots of the equations

$$j_{\gamma}(t,y(t)) = 0; j = 1,2,...,r$$
 (9)

where $^j\gamma$ denotes the jth component of the discontinuity function $\gamma(t,y(t))$. In applications, the numerical solution $\{y_n\}$ replaces the exact solution y(t). The general case has r distinct discontinuity conditions (9). The discontinuous test problem (7) has the single discontinuity condition $\gamma(t,y(t)) = |^1y(t)| - 1$. A discontinuity is detected in the jth component of γ in any integration step $y(t) = |^1y(t)| + 1$. Which satisfies the bracketting condition

$$j_{\gamma_n} \cdot j_{\gamma_{n+1}} < 0 \tag{10}$$

The overbar notation signifies here that the function parameters have not been switched in accordance with y_{n+1} .

The formulation (9) provides the flexibility necessary for handling problems with discontinuous stiffness, mass, or damping. Similar formulations have been used by O'Regan [12], in a variable weight Runge-Kutta process, and by Hay et al. [13], who proposed a general computer program structure for handling discontinuous systems. This program could be adapted to accommodate virtually any combination of integration algorithm and direct interpolation scheme, although the example given is essentially equivalent to the Regula Falsi method. Clearly it is possible

to adapt most of the standard procedures for the solution of equations (9). Newton iteration is widely favoured because of its rapid convergence. Making the substitutions

$$\bar{\psi}(t) = j_{\gamma(t,\bar{y})}$$
 (11)

and applying Newton's method to equation (9) in the bracketting step J_n one obtains

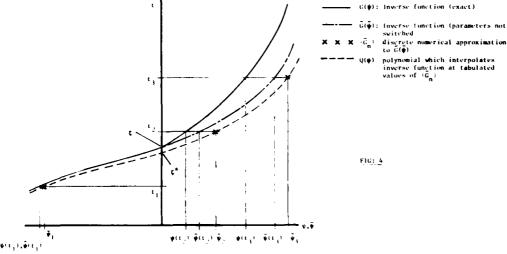
$$t^{[\nu+1]} = t^{[\nu]} - \frac{\overline{\psi}(t^{[\nu]})}{\overline{\psi}'(t^{[\nu]})}$$
(12)

where the superscript ν denotes the iteration number, and the overbars indicate that the function is not switched. It is necessary to insert an integration step (with stepsize $t^{[\nu]} - t_n$) between iteration steps to update \bar{y} and, through (12), $\bar{\psi}(t^{[\nu]})$. A disadvantage of Newton's method is the need for evaluation of the derivative of the discontinuity function $\bar{\psi}' = \bar{j}\bar{\gamma}'$.

Mannshardt [14] has proposed transition methods for discontinuous systems based on algorithms of Runge-Kutta type. The increment function of the one-step algorithm is incorporated directly into a modified Newton iteration scheme, in which the derivative is evaluated only once at the start point t_n . This eliminates the prodigious effort involved in evaluating the derivative of the increment function at each iteration step.

3.1 Construction of a New Inverse Interpolation Scheme

The search procedure now proposed has comparable rate of convergence to Newton's method, but avoids differentiation of the discontinuity function. The procedure is based on quadratic inverse interpolation of the discontinuity function. The inverse interpolation problem is illustrated in Fig. 4.



The curve $t = G(\psi)$ (where $\psi(t) = j$ (t,y(t)) represents the exact trajectory of the inverse discontinuity function. Let $\zeta = G(0)$ be the exact value of the switching point. The inverse function $\overline{G}(\overline{\psi})$ represents the exact solution if the function parameters are not switched at ζ . In the numerical solution the inverse function $\overline{G}(\overline{\psi})$ is approximated by the discrete solution $\{\overline{G}_n\}$. This enables the polynomial $Q(\overline{\psi})$ of degree s to be constructed which interpolates (s+1) tabulated values of $\{\overline{G}_n\}$. Evaluating $Q(0) = \zeta^*$, provides the desired approximation to the switching point.

The new scheme avoids the wasteful computation involved in continuing the solution beyond the bracketting step for (s-1) additional points (or alternatively storage of back values). The interpolation points are instead confined to the

bracketting step. The basic integration over the continuous pieces is performed by the Runge-Kutta process (8). At each step the discontinuity functions (9) are evaluated. The end points of a step J_n satisfying the bracketting condition (10) therefore provide two interpolation points. The third interpolation point is provided by the approximation

$$y_{n+\frac{1}{2}} = y_n + \frac{h}{4}(k_1 + k_2) \tag{13}$$

The global error at the two end points y_n , y_{n+1} is $O(h^4)$, the design order of the algorithm (8). The local error at the midpoint is obtained for the scalar equation y' = f(t,y) by making the usual localising assumption $y_n = y(t_n)$. Expanding $y(t_n + \frac{1}{2}h)$ in a Taylor series about $y(t_n)$, and k_2 in a Taylor series about $f(t_n, y_n)$

$$y(t_n + \frac{1}{2}h) - (y_n + \frac{h}{4}(k_1 + k_2)) = \frac{h^3}{96}(2Ff_y - G) + O\left[\left(\frac{h}{2}\right)^4\right]$$
 (14)

where $F = (f_t + ff_y)$; $G = (f_{tt} + 2ff_{ty} + f^2f_{yy})$

The error in the approximation (13) is therefore $O(h^3)$, the same order as the error in quadratic interpolation.

For notational convenience, the subscripts n, $n+\frac{1}{2}$, n+1, will be replaced by the numbers 1, 2, 3. The three interpolation points become

$$Q(\bar{\psi}_{1}) = t_{1}; \quad Q(\bar{\psi}_{2}) = t_{2}; \quad Q(\bar{\psi}_{3}) = t_{3}$$
where $\bar{\psi}_{1} = {}^{j}\gamma(t_{n}, \bar{y}_{n}); \quad \bar{\psi}_{2} = {}^{j}\gamma(t_{n+\frac{1}{2}}, \bar{y}_{n+\frac{1}{2}}); \quad \bar{\psi}_{3} = {}^{j}\gamma(t_{n+1}, \bar{y}_{n+1})$
(15)

The interpolating polynomial Q is constructed using Aitken's algorithm (see Henrici [15], p.210). Evaluating the polynomial at $\bar{\psi}$ = 0, Aitken's scheme is set out

$$t_{j,1} = t_{j} \quad (j = 1,2,3)$$

 $k = 1,2,..., j-1$

For

$$t_{j,k+1} = \frac{\bar{\psi}_j t_{k,k} - \bar{\psi}_k t_{j,k}}{\bar{\psi}_j - \bar{\psi}_k}$$
(16)

Aitken's algorithm enables polynomials of higher degree to be constructed recursively from polynomials of lower degree. The final approximation to the root is given by $\zeta = t_3$. The Runge-Kutta process (8) is then applied again at t = t with the fractioned stepsize $h_f = (\zeta - t_n)$. The process is repeated as often as is necessary until the switching condition

$$|\overline{\psi}(\zeta^*)| \leq \varepsilon \tag{17}$$

is satisfied. The function parameters may then be switched and the algorithm applied again at ζ^* over the residual piece of the original step J_n .

4. ACCURACY OF THE INVERSE INTERPOLATION SCHEME

A formula for the error in inverse interpolation is given by Ostrowski [16]. Applying this formula to the 3-point scheme (16) gives the estimate for the error in approximating the switching point

$$\zeta - \zeta^* = \frac{\bar{G}^{(3)}(\xi)}{3!} (-1)^3 \bar{\psi}_1 \bar{\psi}_2 \bar{\psi}_3$$
 (18)

where ξ lies in $(\bar{\psi}_1,\bar{\psi}_3)$ and () denotes differentiation with respect to $\bar{\psi}$. If all interpolation points are close to the root, the product $\bar{\psi}_1\bar{\psi}_2\bar{\psi}_3$ means that the error (18) will be small. This is one advantage of confining the inverse interpolation to the bracketting step. Assume (i) that $\bar{\psi}(t)$ is sufficiently differentiable on J_n and (ii) that the root $\bar{\zeta}$ of $\psi(t)$ lies in J_n such that

 $\zeta=t_n+\eta h,0<\eta<1$. Taking account of the global error in the interpolation points $(\bar{\psi}_1=\psi(t_1)+0(h^4),$ etc.), and expanding these in Taylor series about the switching point $\zeta=t_n+\eta h$

$$\overline{\Psi}_{1} = \overline{\Psi}(\zeta - \eta h) + O(h^{4}) = \overline{\Psi}(\zeta) - \eta h \overline{\Psi}'(\zeta) + \frac{(\eta h)^{2}}{2} \overline{\Psi}''(\zeta) + O(h^{3})$$

$$\overline{\Psi}_{2} = \overline{\Psi}(\zeta + (\frac{1}{2} - \eta) h) + O(h^{3}) = \overline{\Psi}(\zeta) + (\frac{1}{2} - \eta) h \overline{\Psi}'(\zeta) + \frac{(\frac{1}{2} - \eta)^{2} h^{2}}{2} \overline{\Psi}''(\zeta) + O(h^{3})$$

$$\overline{\Psi}_{3} = \overline{\Psi}(\zeta + (1 - \eta) h) + O(h^{4}) = \overline{\Psi}(\zeta) + (1 - \eta) h \overline{\Psi}'(\zeta) + \frac{(1 - \eta)^{2} h^{2}}{2} \overline{\Psi}''(\zeta) + O(h^{3})$$
(19)

Noting that, by definition, $\bar{\psi}(\zeta)=0$, and substituting from equations (19) for the product $\bar{\psi}_1\bar{\psi}_2\bar{\psi}_3$ into equation (18) and writing $\bar{G}^{(3)}(\zeta)$ as a polynomial in $\bar{\psi}'(t)$ and its derivatives (Ostrowski [16]) enables the expression (18) to be rewritten

$$\zeta - \zeta^* = (2\eta^3 - 3\eta^2 + \eta) \left(-\overline{\psi}'''(t_{\xi}) \overline{\psi}'(t_{\xi}) + 3\overline{\psi}''(t_{\xi})^2 \right) \frac{h^3}{12} \frac{\overline{\psi}'(\zeta)^3}{\overline{\psi}'(t_{\xi})^5} \mathcal{O}(h^4)$$
 (20)

where 'denotes differentiation with respect to t, and $\overline{G}(\xi) = t_{\xi}$ is some intermediate point of J_n . Equation (20) shows that the error in the inverse interpolation scheme (16) is normally $O(h^3)$ but may become large if $(i)\overline{\psi}'(\zeta) >> \overline{\psi}'(t_{\xi})$, which is unlikely in J_n , or $\overline{\psi}'(\zeta) = \overline{\psi}'(t_{\xi}) << 1$, which corresponds to the critical case when the solution trajectory is tangential to the switching surface. In this situation inverse interpolation is unreliable (as is Newton iteration). It is then necessary to resort to the straightforward bisection method.

TOLERANCE ON LOCATING THE SWITCHING POINT

Preliminary numerical experiments with one-degree-of-freedom systems more or less confirm Mannshardt's theory that to maintain global order of convergence p, all points of discontinuity must be located with accuracy $O(h^q)$, where $q \ge p-1$. Therefore specifying $\varepsilon = O(h^q)$ in equation (17) should be sufficient for the Runge-Kutta process with the search procedure (16). However, the theory is based on the tacit assumption $h \to 0$, whereas it is generally the aim of structural dynamicists to use moderate values of h. In practice it is found that a tolerance $\varepsilon = O(h^q)$ with $q \ge p$ yields improved global accuracy, (especially for systems). There is a need for methods which automatically match the stepsize and switching tolerance to the problem being solved.

6. COMPARISON OF THE INVERSE INTERPOLATION SCHEME WITH NEWTON'S METHOD

The Runge-Kutta process (8) has been applied in conjunction with Newton's method (12), to the test problem with stepsize h = 0.04, and switching tolerance ϵ = 5.0 x 10 $^{-7}$ (\cong h $^{-7}$ 5), the minimum practicable for single precision implementation. The basic discretisation corresponds to \sim 31 steps per period of the highest frequency present. The results are presented in Fig. 5(a), which shows the displacement-time curve for the component y, scaled by $y_{max} = 1.5$. The numerical solution $\{1y_n/1y_{max}\}$ is superimposed on the continuous line which represents the exact solution $y(t)/y_{max}$. Both solutions are in very close agreement up to t = 19, where they start to diverge.

This solution may be compared with that in Fig. 5(b) generated by the Runge-Kutta process with the new search procedure (16). The same parameters have been used in both cases. Both search procedures yield virtually identical approximations, and the computational costs are comparable. The new search procedure required an average of 6.31 step changes per discontinuity. This compares with 5.07 for Newton's method. This slight cost disadvantage must be weighed against the need for evaluation of the derivative of the discontinuity function $\bar{\psi}'(t) = \bar{J}\gamma'(t,\bar{y})$ in Newton's method. Very considerable savings are achieved by either search procedure when compared with the fixed step solution

in Fig. 3, which required 5.9 times as many steps and is less accurate.

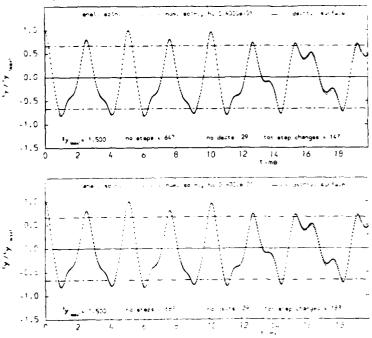


FIG. 5: Runge-Kutta process (8) applied with discontinuity search procedures
(a) Newton iteration; (b) new inverse interpolation scheme.

CONCLUSIONS

The inverse interpolation scheme proposed offers certain advantages when compared with the more usual form of inverse interpolation. The interpolation points are confined to the initial bracketting step, thus avoiding unnecessary storage of back values. This is also an advantage when multiple discontinuities occur at intervals of comparable length to the integration step. Furthermore the error analysis showed that the error is small when all the interpolation points are close to the root. The scheme has been demonstrated in practice to have comparable rate of convergence to Newton's method, but avoids explicit differentiation of the discontinuity function. In experiments, both the new scheme and Newton's method have considerably better convergence properties than straightforward linear interpolation, especially when a stringent switching tolerance is specified. The fact that the basic algorithm is not A-stable may not be a disadvantage. In many cases the discontinuities may perpetuate significant high mode response, accurate simulation of which can often be achieved more cheaply using conditionally stable algorithms. The use of implicit A-stable algorithms and the concomitant increased stepsizes may even result in the solution 'skipping over' discontinuities.

APPENDIX I: Exact Solution to the Discontinuous Test Problem

In the ith sub-interval $[t_d, t_d, i+1]$, where the solution is continuous, equation (4) may be uncoupled using the transformation $x^i = Z^i q^i$, where Z^i is the local matrix of eigenvectors. The uncoupled problem may be written in terms of the local principal co-ordinates $q^i = [1q^i \ 2q^i]^T$,

$$\begin{array}{lll} q^{i} & = & \Lambda^{i}q^{i} & & & \\ \text{where } \Lambda^{i} & = & & (Z^{i})^{-1} \kappa Z^{i} \text{ is the diagonal matrix of eigenvalues} & & \mu_{1}^{i^{2}}, & \mu_{2}^{i^{2}} \text{ of } \kappa \\ & & \mu_{1}^{i^{2}} \\ & & \mu_{2}^{i^{2}} \end{array}$$

$$= & \frac{1}{2} \{ -(1 + (r-1)H(x_{1}^{i}) + (m+1)\Omega^{2}) \pm [(1 + (r-1)H(x_{1}^{i}) + (m+1)\Omega^{2})^{2} \\ & & \mu_{2}^{i^{2}} - 4\Omega^{2}(1 + (r-1)H(x_{1}^{i}))]^{\frac{1}{2}} \} \end{array}$$

$$(a)$$

The solution to an individual component of the uncoupled system (a) becomes

$$j_{q^{i}(t^{i})} = j_{q^{i}_{0}} \cos \mu_{j}^{i} t^{i} + \frac{j_{q^{i}_{0}}^{i}}{\mu_{j}^{i}} \sin \mu_{j}^{i} t^{i}; j = 1,2$$

where $t^i = t - t_{d,i}$, and q^i_0 , q^i_0 are obtained from the conditions at the end of the (i-1)st sub-interval). The solution in local generalised co-ordinates is obtained using the transformation $x^i = Z^i q^i$. This is computed at steps of length q^i . The time points of discontinuities are located by Newton iteration.

REFERENCES

- 1. C. GRUBIN 1956 Trans ASME, Journal of Applied Mechanics 23. On the theory of the acceleration damper.
- 2. S.F. MASRI 1972 International Journal of Non-Linear Mechanics 7, 663-674. Forced vibration of a class of non-linear two-degree-of-freedom oscillators.
- 3. W.D. IWAN 1978 Earthquake Engineering and Structural Dynamics, 6,523-534. The earthquake design and analysis of equipment isolation systems.
- 4. M. LASHKARI and V.I. WEINGARTEN 1981 Journal of the Structural Division, Proc. ASCE, 107, No. ST8, 1443-1463. Continuum solution of simulated pipe whip problem.
- 5. G.G. LECKIE and A.D.S. BARR 1971 Proc. IMech.E., 185 79/71. A study of the performance of a non-linear resonant vibratory conveyor.
- 6. A.K. NOOR 1981 Computers and Structures 13, 425-465. Survey of computer programs for solution of nonlinear structural and solid mechanics problems.
- 7. G. DAHLQUIST 1963 BIT, 3, 27-42. A special stability problem for linear multistep methods.
- 8. J.D. LAMBERT 1973 Computational Methods in Ordinary Differential Equations. John Wiley and Sons, Ltd.
- 9. T. BELYTSCHKO, R.L. CHIAPETTA and H.D. BARTEL 1976 International Journal for Numerical Methods in Engineering 10, No. 3, 579-596. Efficient large scale non-linear transient analysis by finite elements.
- 10. J. BRAEKHUS and J.O. AASEN 1981 Computers and Structures 13, 91-96. Experiments with direct integration algorithms for ordinary differential equations in structural dynamics.
- 11. A. FELDSTEIN and R. GOODMAN 1973 Numerische Mathematik 21, 1-13. Numerical solution of ordinary and retarded differential equations with discontinuous derivatives.
- 12. P.G. O'REGAN 1970 Computer Journal, 13, No. 4, 401-404. Step size adjustment at discontinuities for fourth order Runge-Kutta methods.
- 13. J.L. HAY, R.E. CROSBIE and R.I. CHAPLIN 1974 Computer Journal 17, No. 3. 275-278. Integration routines for systems with discontinuities.
- 14. R. MANNSHARDT 1978 Numerische Mathematik 31, 131-152. One-step methods of any order for ordinary differential equations with discontinous right-hand sides.
- 15. P. HENRICI 1964 Elements of Numerical Analysis. John Wiley & Sons Inc.
- 16. A.M. OSTROWSKI, 1960 Solutions of Equations and Systems of Equations. Academic Press Inc., London.

6. NON LINEAR DYNAMICS OF BEAMS



A FINITE ELEMENT METHOD FOR NONLINEAR FORCED VIBRATIONS OF BEAMS

Chuh Mei and Kamolphan Decha-Umphai

Department of Mechanical Engineering and Mechanics Old Dominion University, Norfolk, Virginia, USA

INTRODUCTION

Many optimum or minimum-weight designed structural components are under severe operational conditions. In many cases, the small deflection linear structural theory is no longer applicable. Considerable research effort has been devoted to obtain the approximate solutions for nonlinear response of beam structures under harmonic excitation. The common approach is to assume some form for the spatial solution, usually a linear mode shape, and then solve the governing nonlinear partial differential equation using Galerkin's This reduces the governing equation to a nonlinear ordinary differential equation of the Duffing type. Most of the investigations have been concerned with beams of simply supported ends (e.g., [1] and [2], plus others too numerous to mention).

Bennett and Eisley [3] used a multiple mode (3 modes) Galerkin approach and the Wegstein iteration scheme in investigation of nonlinear forced response of a clamped beam subjected to a concentrated harmonic force. Busby and Weingarten [4] employed the finite element technique to obtain the nonlinear differential equations of motion with 2-mode participation for beams of simply supported and clamped boundary conditions. The method of averaging is then used to obtain an approximation solution. A numerical-perturbation technique for the nonlinear forced response of general structural elements was proposed by Nayfeh, Mook and Lobitz [5]. The problem is represented as a nonlinear temporal problem and a linear spatial problem. The spatial problem can be treated by using either finite-difference or finite element technique, while the temporal problem is solved by the method of multiple scales. Large amplitude forced vibrations of a hinged-clamped beam having a discontinuous cross section was investigated.

In this paper, a finite element formulation is presented for nonlinear vibrations of beam structures subjected to harmonic excitation. Longitudinal deformation and longitudinal inertia effects are both included in the These effects were not considered in existing finite element nonlinear vibration of beam and plate structures [6], [7]. A harmonic force matrix is developed for nonlinear oscillations of a beam element under uniform harmonic excitation. Formulation of the harmonic force matrix follows the mathematical basis [8] that the simple harmonic forcing function ($P_{c}\cos \omega \tau$) is simply the first order approximation of the Jacobian elliptic forcing function (BA cn (ρτ, k)). Also the well-known perturbation solution of a Duffing system to a simple harmonic forcing function is the first order approximate solution of the simple elliptic response. Derivation of the harmonic force and nonlinear stiffness matrices are given. Nonlinear forced response to uniform harmonic excitation and improved nonlinear free vibration results are presented for beams with various boundary conditions. Finite element results of simply supported and clamped beams with inplane movements restrained at both ends are compared with solutions of simple elliptic response, approximate perturbation methods and other approximate numerical approaches.

2. FINITE ELEMENT FORMULATION

The strain energy of a beam element shown in Fig. 1 is given by

$$U = \frac{1}{2} \int_{0}^{\ell} \left[ES \left(\frac{\partial u}{\partial x} + f \frac{\partial w}{\partial x} \right)^{2} + EI \left(\frac{\partial^{2} w}{\partial x^{2}} \right)^{2} \right] dx = U_{L} + U_{NL}$$
 (1)

where l is the beam element length, E is the Young's modulus, S is the area of cross section, and I is the moment of inertia. The linearizing function f is defined as

$$f = \frac{1}{2} \frac{\partial w}{\partial x} \tag{2}$$

This type of linearization has been used efficaciously in earlier studies of nonlinear free vibration problems. As will become evident later, this linearizing function is displacement dependent and actually evaluated at the corresponding deflection shape of the beam. The linear strain energy in Eq. (1) is

$$U_{L} = \frac{1}{2} \int_{0}^{\ell} \left[ES \left(\frac{\partial u}{\partial x} \right)^{2} + EI \left(\frac{\partial^{2} w}{\partial x^{2}} \right)^{2} \right] dx$$
 (3)

which leads to the element linear stiffness matrix [k].

The kinetic energy of the beam element executing harmonic oscillations is

$$T = \frac{1}{2} \rho S \int_{0}^{\ell} (\dot{u}^{2} + \dot{w}^{2}) dx$$
 (4)

where ρ is the mass density. It yields the element consistant mass matrix [m]. Both [k]_L and [m] are standard matrices available explicitly in literature[9].

The displacement functions for the beam element are chosen as

$$w = a_1 + a_2 x + a_3 x^2 + a_4 x^3 \quad u = a_5 + a_6 x$$
 (5)

The element nodal displacements at the two end nodes are

$$\left\{\delta\right\}^{\mathbf{T}} = \begin{bmatrix} \mathbf{w}_1 & \mathbf{\theta}_1 & \mathbf{w}_2 & \mathbf{\theta}_2 & \mathbf{u}_1 & \mathbf{u}_2 \end{bmatrix} \tag{6}$$

and are expressed in terms of generalized displacements

$$\{a\}^{T} = [a_1 \ a_2 \ a_3 \ a_4 \ a_5 \ a_6]$$
 (7)

$$\{a\} = \begin{bmatrix} 1 & 0 & 0 & 0 & 0 & 0 & 0 \\ 0 & 1 & 0 & 0 & 0 & 0 & 0 \\ -3/\ell^2 & -2/\ell & 3/\ell^2 & -1/\ell & 0 & 0 \\ 2/\ell^3 & 1/\ell^2 & -2/\ell^3 & 1/\ell^2 & 0 & 0 \\ 0 & 0 & 0 & 0 & 1 & 0 \\ 0 & 0 & 0 & 0 & -1/\ell & 1/\ell \end{bmatrix} \{\delta\} = [T]\{\delta\}$$
(8)

The nonlinear strain energy in Eq. (1) is

$$U_{NL} = \frac{ES}{2} \int_{0}^{1} \left[2f \frac{\partial u}{\partial x} \frac{\partial w}{\partial x} + f^{2} \left(\frac{\partial w}{\partial x} \right)^{2} \right] dx$$
 (9)

The terms in Eq. (9) can be expressed as

$$\frac{\partial u}{\partial x} = [0 \ 0 \ 0 \ 0 \ 1] \{a\} = [C][T]\{\delta\}$$
 (10)

$$\frac{\partial w}{\partial x} = [0 \ 1 \ 2x \ 3x^2 \ 0 \ 0] \ \{a\} = [D][T]\{\delta\}$$
 (11)

Substituting Eqs. (10) and (11) in Eq. (9) yields the element nonlinear stiffness matrix

$$[k]_{NL} = ES [T]^{T} \int_{0}^{\lambda} (f [C]^{T}[D] + f [D]^{T}[C] + f^{2}[D]^{T}[D]) dx [T]$$
 (12)

in which the linearizing function f is evaluated from the expression

$$f = \frac{1}{2} [D] [T] \{\delta\}$$
 (13)

where the element displacements $\{\delta\}$ are obtained from the beam deflection discussed in Section 3. This indicates clearly that the nonlinear stiffness matrix depends on the deflection of beam.

With a standard beam deflection $w=Rq(t)\phi(x)$ where R is the radius of gyration of the cross-sectional area, Hsu [8] presented both the exact and approximate solutions of a Duffing system to forced vibration $q,_{\tau\tau}+q+\beta q=F(\tau)$. With a simple elliptic forcing function BA cn $(p\tau,\,k)$ = Bq as the external excitation to the system, an elliptic response q = A cn $(p\tau,\,k)$ is obtained as the exact solution. When the forcing function $F(\tau)$ is a simple harmonic P cos $\omega\tau$, an approximate solution obtained from the perturbation method is the well-known result

$$\left(\frac{\omega^{2}}{\omega_{L}}\right) = 1 + \frac{3}{4} \beta A^{2} - \frac{P_{o}}{A}$$
 (14)

Expanding the elliptic forcing function into the Fourier series and comparing the orders of magnitude of the various harmonic components, Hsu concluded that the simple harmonic forcing function and the corresponding perturbation solution are simply the first order approximation of the simple elliptic forcing function and the associated elliptic response. In obtaining the exact solution, the simple elliptic forcing function is treated as a linear spring force. The potential energy of a beam element due to the uniform harmonic forcing function can thus be approximated by

$$V = \frac{B}{2} \int_{0}^{R} w^{2} dx \tag{15}$$

Examining Eqs. (4) and (15), the element harmonic force matrix under uniform loading \mathbf{F}_{O} cos $\omega \mathbf{t}$ is

the actual applied force intensity F $_{\rm O}$ (N/m or lb/in.) is related to the dimensionless forcing parameter P $_{\rm O}$ and the dimensionless forcing amplitude factor B by

$$B = \frac{P_o}{A} = \frac{c F_o}{AR_0 S \omega_L^2}$$
 (17)

where c is a constant given by $c = \int_{0}^{L} dx / \int_{0}^{L} dx$, which is simply the ratio of areas under beam mode shape and square of mode shape. The harmonic force matrix depends on the maximum beam amplitude $A = w_{max}/R$ and P_{o} .

The application of the Lagrange's equation leads to the stiffness equation of motion for a beam element under the influence of inertia, elastic, large deflection and uniform harmonic excitation forces as

$$[m] \{\ddot{\delta}\} + ([k]_L + [k]_{NL} - [h])\{\delta\} = 0$$
 (18)

Nonlinear free vibration is a special case of the more general forced vibration problem with P_0 or [h] = 0 in Eq. (18).

3. SOLUTION PROCEDURE

Equation (18) is solved using an iterative procedure outlined as follows. First, the linear free vibration problem of a given beam is solved

$$\omega_{L}^{2}[M] \{\phi\}_{o} = [K]_{L}\{\phi\}_{o}$$
(19)

where [M] and [K]_L are the system mass and linear stiffness matrices, respectively, and ω_L is the fundamental linear frequency, $\{\phi\}_O$ is the corresponding linear mode shape. The mode shape is then normalized with respect to the maximum beam amplitude A, and is used to obtain the element nonlinear stiffness matrix [k]_NL through Eqs. (12) and (13). The element harmonic force matrix is obtained through Eq. (16) for given P_O . The nonlinear forced beam vibration is approximated by a linearized eigenvalue equation of the form

$$\omega^{2}[M] \{\phi\}_{1} = ([K]_{L} + [K]_{NL} - [H]) \{\phi\}_{1}$$
 (20)

where ω is the fundamental nonlinear frequency and $\{\phi\}_1$ is the corresponding mode shape of the first iteration associated with amplitude A and force P_0 . The iterative process can now be repeated until a convergence criterion is satisfied. Three displacement convergence criteria proposed by Bergan and Clough [10] and a frequency convergence criterion are used in the present study. The three displacement norms are the modified absolute norm, the modified Euclidean norm and the maximum norm. The frequency norm is defined as $\left|\Delta\omega_1\right|/\omega_1$, where $\Delta\omega_1$ is the change in nonlinear frequency during the i-th iteration cycle. A typical plot of the four norms versus number of iterations for a simply supported beam of slenderness ratio L/R = 100 with immovable

axial end supports subjected to an uniform harmonic force of P_0 = 2.0 at A = 4.0 is shown in Fig. 2. The results presented in the following section, convergence is considered achieved whenever any one of the norms reaches a value of 10^{-5} .

RESULTS AND DISCUSSION

4.1 Immovable Axial End Supports

The fundamental frequency ratios ω/ω_L of free vibration at various amplitude for a simply supported beam (L/R = 100) with both ends restrained from longitudinal movement are shown in Table 1. Due to symmetry only one-half of the beam which is divided equally into six elements is used. Results with and without considering effects of longitudinal deformation and inertia (ELDI) in the analyses are both given. It shows that the improved finite element results by including ELDI in the formulation are to reduce the nonlinearity. The elliptic function solution [8], [11] is also given to demonstrate the closeness of the earlier finite element results without ELDI. Raju et al. [12] used the Rayleigh-Ritz method in investigation of the effects of inplane deformation and inertia on large amplitude flexual vibration of slender beams. Appropriate frequency-amplitude relationship using Rayleigh-Ritz method is also given in Table 1. This clearly demonstrates the remarkable agreement between the improved finite element and Rayleigh-Ritz solutions.

A	Without ELDI ^a			With ELDI (L/R = 100)		
	Elliptic Function Solution [11]	Finite Element		Rayleigh	Finite Element	
		First Iteration	Final Result	Ritz Solution [12]	First Iteration	Final Result
1.0	1.0892	1.0895	1.0888	1.0607	1.0613	1.0613(3) ^b
2.0	1.3178	1.3203	1.3119	1.2246	1.2270	1.2269(4)
3.0	1.6257	1.6295	1.6022	1.4573	1.4620	1.4617(4)
4.0	1.9760	1.9761	1.9216	1.7309	1.7383	1.7375(6)
5.0	2.3501	2.3396	2.2544	2.0289	2.0393	2.0378(7)

- a. Effects of longitudinal deformation and inertia
- b. Number in brackets denotes the number of iterations to get a converged solution.

Table 2 shows the frequency ratios of the same simply supported beam subjected to an uniform harmonic force of $P_0=2.0$. It demonstrates the closeness between the earlier finite element results without ELDI, the simple elliptic response [8] and the perturbation solution. The present improved finite element results indicate clearly that the effects of longitudinal deformation and inertia are to reduce the nonlinearity.

TABLE 2 Forced Vibration Frequency Ratios ω / ω $_L$ for a Simply Supported and a Clamped Beam with Immovable Axial Ends

_		With ELDI				
A	Simple	Perturbation	Finite Element		Finite Element	
	Elliptc Response [8]	Solution	First Iteration	Final Result	Final Result	
	Simply Supp	orted Beam Subje	cted to P =	2.0 (F _o =	1322 lb/in.)	
- 1.0	1.7852	1.7854	1.7852	1.7856	1.7682(3) ^b	
± 2.0	0.8472	0.8660	0.8621	0.8460	0.7108(4)	
	1.6557	1.6583	1.6563	1.6512	1.5829(4)	
± 3.0	1.4003	1.4216	1.4102	1.3760	1.2123(4)	
	1.8217	1.8314	1.8226	1.8002	1.6743(4)	
± 4.0	1.8413	1.8708	1.8453	1.7846	1.5871(6)	
	2.1013	2.1213	2.0988	2.0495	1.8759(6)	
± 5.0	2.2606	2.2995	2.2525	2.1619	1.9371(7)	
	2.4361	2.4673	2.4236	2.3432	2.1337(7)	
	Clamped	Beam Subjected	to P _o = 1.0	$(F_0 = 327)$	7 lb/in.)	
± 1.0	0.2118	0.2165	0.2096	0.2091	0.1772(3)	
	1.4307	1.4307	1.4297	1.4297	1.4251(3)	
± 2.0	0.8279	0.8292	0.8215	0.8203	0.7905(4)	
	1.2987	1.2990	1.2942	1.2936	1.2743(4)	
± 3.0	1.0401	1.0433	1.0279	1.0239	0.9726(5)	
	1.3232	1.3248	1.3127	1.3099	1.2694(5)	
± 4.0	1.2183	1.2247	1.1979	1.1888	1.1151(6)	
	1.4101	1.4142	1.3910	1.3836	1.3197(6)	
± 5.0	1.3938	1.4042	1.3619	1.3457	1.2513(8)	
	1.5322	1.5401	1.5016	1.4874	1.4014(8)	

a. Effects of longitudinal deformation and inertia.

b. Number in brackets denotes the number of iterations to get a converged solution.

Similar results of a clamped beam (L/R = 100) with immovable axial end supports subjected to an uniform harmonic force of P_0 = 1.0 are also given in Table 2.

4.2 Movable Axial End Support

Figures 3(a) and (b) show the |A| versus ω / ω for a simply supported beam of slenderness ratio L/R = 100 and 20, respectively. One of the end supports (x = L) is assumed to be free to move in the axial direction. For a highly slender beam (L/R > 100), the hard spring type nonlinearity due to large deflection is so small as shown in Fig. 3(a), therefore, it can be practically neglected. Longitudinal deformation and inertia effects are more pronounced in a short beam than a long one. As a consequence, the reduction of nonlinearity due to longitudinal deformation and inertia, from the nearly small deflection linear case in Fig. 3(a), leads to a situation that the beam eventually exhibits slightly soft spring type nonlinearity as shown in Fig. 3(b). Atluri [13] also obtained similar nonlinearity of softening type in his investigation.

CONCLUSIONS

The finite element method has been extended to analyze nonlinear forced vibration problems. A harmonic force matrix was developed for a beam element subjected to uniform harmonic excitation. Improved finite element results on nonlinear free flexural vibration of slender beams are achieved by considering longitudinal deformation and inertia effects in the formulation. Nonlinear free vibration can be simply treated as a limiting case of the more general forced vibration problem by setting the harmonic force matrix equal to zero. The effect of midplane stretching due to large deflection is to increase the nonlinearity, however, the effects of longitudinal deformation and inertia are to reduce nonlinearity. For beam with end supports restrained from axial movement, only hardening type nonlinearity is observed. For beams of large slenderness ratio with a movable axial end support, the increase in nonlinearity due to large deflection is partially compensated by the reduction in nonlinearity due to longitudinal deformation and inertia. This leads to a negligible hardening type nonlinearity, and thus small deflection linear solution can be used. For beams of small slenderness ratio, however, softening type nonlinearity is observed.

ACKNOWLEDGEMENT

The work reported herein was sponsored by NASA-Langley Research Center under Grant NAG-1-301. The authors would like to thank their technical monitors Dr. Jerrold M. Housner and Joseph E. Walz, Structural Dynamics Branch, Structures and Dynamics Division, NASA-Langley for their encouragement and many helpful discussions.

REFERENCES

- 1. W. Y. TSENG and J. DUGUNDJI 1971 Journal of Applied Mechanics, 467-476. Nonlinear Vibrations of a Beam Under Harmonic Excitation.
- 2. C. L. LOU and D. L. SIKARSKIE 1975 ASME Paper No. 75-APMW-10. Nonlinear Vibrations of Beam Using a Form-Function Approximation.
- 3. J. A. BENNETT and J. G. EISLEY 1970 AIAA Journal, 734-739. A Multiple Degree-of-Freedom Approach to Nonlinear Beam Vibrations.

- 4. H. R. BUSBY and V. I. WEINGARTEN 1972 International Journal Non-Linear Mechanics, 289-303. Nonlinear Response of a Beam to Periodic Loading.
- 5. A. H. NAYFEH, D. T. MOOK and D. W. LOBITZ 1974 AIAA Journal, 1222-1228. A Numerical-Perturbation Method for the Nonlinear Analysis of Structural Vibrations.
- 6. G. PRATHAP and G. R. BHASHYAN 1980 AIAA Journal, 733-734. Comments on the Nonlinear Vibrations of Immovably Supported Beams by Finite Element Method.
- 7. C. MEI, M. H. SHEN and F. M. CUNNINGHAM 1983 24th Structures, Structural Dynamics and Materials Conference Part 2 AIAA CP 832, 685-692. Large Amplitude Vibration of Laminated Composite Plates of Arbitrary Shape.
- 8. C. S. HSU 1960 Quarterly Applied Mathematics 393-407. On the Application of Elliptic Functions in Nonlinear Forced Oscillations.
- 9. J. S. PRZEMIENIECKI 1968 Theory of Matrix Structural Analysis. New York: McGraw-Hill.
- 10. P. G. BERGAN and R. W. CLOUGH 1972 AIAA Journal, 1107-1108. Convergence Criteria for Iterative Process.
- 11. S. WOINOWSKY-KRIEGER 1950 Journal of Applied Mechanics, 35-36. The Effect of An Axial Force on the Vibration of Hinged Bars.
- 12. I. S. RAJU, G. V. RAO and K. K. RAJU 1976 Journal Sound and Vibration, 415-422. Effect of Longitudinal or Inplane Deformation and Inertia on the Large Amplitude Flexural Vibrations of Slender Beams and Thin Plates.
- 13. S. ATLURI 1972 ASME Paper No. 72-APM-51. Nonlinear Vibrations of a Hinged Beam Including Nonlinear Inertia Effects.

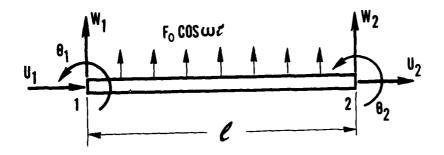


Fig 1. Beam element

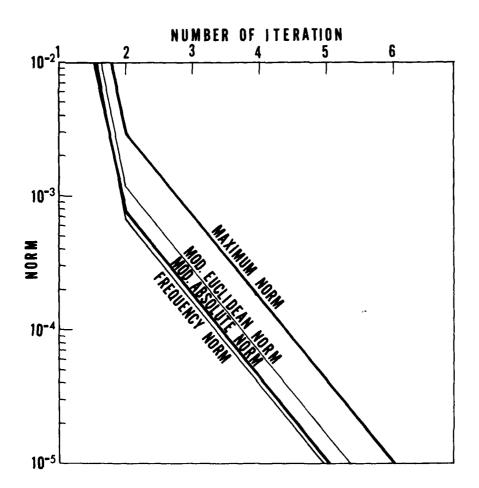


Fig 2. Convergence characteristics

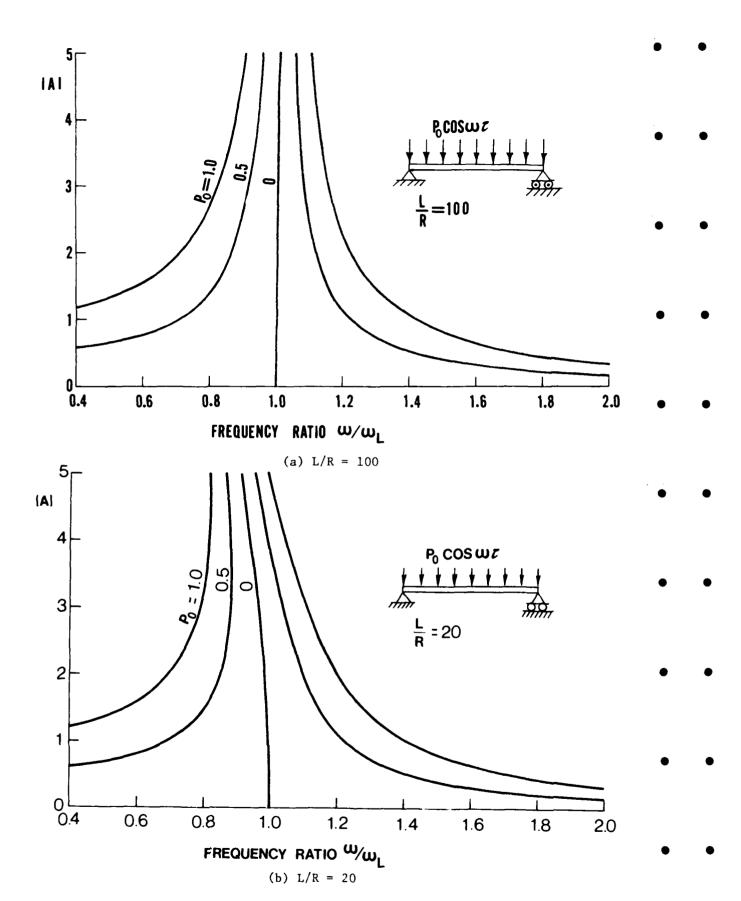


Fig 3. Amplitude versus frequency for a simply supported beam with a movable axial end support at $P_0 = 0$, 0.5 and 1.0



SNAP-THROUGH OF INITIALLY BUCKLED BEAMS UNDER UNIFORM RANDOM PRESSURE

Paul Seide Department of Civil Engineering University of Southern California

AD-P003 668

1. INTRODUCTION

Aircraft structural components such as engine air intake ducting and rear fuselage and empennage structures which are located in the vicinity of jet engine exhausts experience combined heating and random dynamic excitation which result from the acoustic or pseudoacoustic noise emitted by the jet efflux. A program to obtain a measure of the effects of the thermal-acoustic environment has been described in reference [1]. Among the qualitative phenomena which have been revealed experimentally by that investigation is that there are limited ranges of temperature and acoustic environment which cause violent oilcanning vibrations of plate structures. If the sound pressure level of the random acoustic environment is kept constant and the steady-state temperature is increased, the RMS strain response was observed to increase slowly until some "critical" temperature was reached beyond which oil-canning vibrations occurred and the RMS strain response increased rapidly at first. As the steadystate temperature was further increased, the RMS strain response reached a peak value and then decreased rapidly to some value lower than the pre-critical level. The large stress reversals that occur during oil-canning vibrations in sufficiently high intensity acoustic environments can lead to early fatigue failure. Although the experimental data obtained in reference [1] were used to define a region of instability, the data are insufficient to inspire confidence in the accuracy or reasonableness of the semi-empirical criterion.

A perusual of the literature indicates that the only analytical investigation of a similar problem is available in reference [2]. Here the interest centers on the time required for the maximum deflection of a simply supported arch to first reach or exceed a certain critical value. The method used in reference [2] can be described as an "experimental" one since the equation of motion of the arch, represented by that for an equivalent single-degree-offreedom system, is integrated numerically for loadings given by a random-number generator. Enough of these numerical experiments are conducted to yield a curve of the probability of first-passage snap-through at a given time as a function of time. The response of axially compressed initially buckled beams to deterministic transverse load has been discussed in a number of papers. The buckling and snap-through behavior of steep buckled simply supported beams under concentrated and uniform static transverse loading is investigated in reference [3]. The snap-through of shallow buckled clamped beams due to harmonic support excitation was studied in reference [4]. In references [5] to [8] results for the small large amplitude free vibrations of buckled beams are given. The response of such structures to random loading has not been studied however.

In view of the meager available literature on the problem, an investigation of the response of initially buckled beams was undertaken through Air Force Office of Scientific Research Grant No. 79-0013 with the University of Southern California. The present paper describes a part of the work done toward further understanding of the phenomenon.

2. EQUATION OF MOTION

The equation of motion of an initially buckled beam is derived under the assumption of small strains, moderately large deflections, and negligible longitudinal inertia. Consider an initially straight beam (Fig. 1) whose ends are brought together a certain amount, d. If d is less than a critical value d the beam is compressed only and does not bend. The axial compressive load $^{\rm Cr}$, in the beam is less than the Euler buckling load and is given by

$$N_{O} = EA_{\overline{L}}^{\underline{d}} .$$
(1)

where E is Young's modulus of the beam material and A the beam cross-sectional area. If, however, d is greater than ${\rm d}_{\rm cr}$, the beam buckles with a deflection ${\rm w}_{\rm s}({\rm x})$. For relatively small buckle amplitudes the axial compressive load N remains constant at the Euler buckling load N cr.

For a simply supported beam the Euler buckling load is given by

$$N_{cr} = \frac{\pi^2 EI}{I^2}$$
 (2)

where I is the centroidal axis moment of inertia of the beam cross section. The initial buckled shape is a half sine wave

$$w_s = w_0 \sin \frac{\pi x}{L} \tag{3}$$

with an amplitude given by

$$w_0 = \frac{2}{\pi} \sqrt{L(d-d_{cr})}$$
 (4)

and

$$d_{cr} = \frac{\pi^2 I}{\Delta I^2} \tag{5}$$

With the ends of the beam now fixed in the compressed position, the beam is next subjected to uniformly distributed time dependent loading (Fig. 1). The equation of motion of the beam, including viscous damping with a damping coefficient β , is given by

$$EI \frac{\partial^{4}(w+w_{s})}{\partial x^{4}} + N \frac{\partial^{2}(w+w_{s})}{\partial x^{2}} + A \frac{\partial^{2}w}{\partial t^{2}} + \beta \frac{\partial w}{\partial t} + p = 0$$
 (6)

where w is the additional beam deflection, N is the axial compressive force exerted on the beam by the supports, and \circ is the density of the beam material.

The change in the axial compessive force from its initial value $\rm N_0$ is determined by the additional stretching or compression the beam undergoes during its motion. The amount by which the ends of the beam move together prior to motion is equal to the sum of the change of length due to the critical load and the amount by which the ends move together due to beam bending. Thus

$$\Delta L_0 = \frac{N_0 L}{EA} + \frac{1}{2} \int_0^L \left(\frac{dw_s}{dx}\right)^2 dx \tag{7}$$

where w_s vanishes if N_0 is less than $N_{\rm cr}$. With w_s given by Eq. (3), Eq. (7) yields the result of Eq. (5). When the beam deflects from its static position, the beam ends would tend to move, were they not fixed in position, an additional amount equal to

$$\Delta L = \frac{1}{2} \int_{0}^{L} \left\{ \left[\frac{\partial}{\partial x} (w + w_{s}) \right]^{2} - \left(\frac{dw_{s}}{dx} \right)^{2} \right\} dx$$
 (8)

This change of position must be negated by stretching the beam by an axial tensile force given by

$$\Delta N = \frac{EA\Delta L}{L} = \frac{EA}{2L} \int_{0}^{L} \frac{\partial w}{\partial x} \left(\frac{\partial w}{\partial x} + 2 \frac{dw}{dx} \right) dx$$
 (9a)

Thus

$$N = N_0 - \frac{EA}{2L} \int_0^L \frac{\partial w}{\partial x} \left(\frac{\partial w}{\partial x} + 2 \frac{dw}{dx} \right) dx$$
 (9b)

Let the additional dynamic deformation be assumed to be symmetric and to be given by

$$w = \sum_{m=1}^{\infty} w_m \sin \frac{(2m-1)\pi_X}{L}$$
 (10)

Then the equations for the time dependence of the coefficients \mathbf{w}_{m} may be obtained by substitution in Eq. (6) to yield, in nondimensional form,

$$\frac{d^{2}\overline{w}_{m}}{dT^{2}} + \overline{\mu} \frac{d\overline{w}_{m}}{dT} + [(2m-1)^{2} - \overline{N}] (2m-1)^{2} (\overline{w}_{m} + \overline{w}_{0} \delta_{m1}) = -\frac{\overline{p}}{2m-1}$$

$$m = 1, 2, ... \qquad (11a)$$

with

$$\bar{N} \approx \bar{N}_0 + \frac{1}{4} \bar{w}_0^2 - \frac{1}{4} \sum_{n=1}^{\infty} (2n-1)^2 (\bar{w}_n + \bar{w}_0 \delta_{n1})^2$$
 (11b)

Here

$$\overline{w}_{m} = w_{m} / \sqrt{I/A}$$
 (12a) $\overline{p} = \frac{4}{\pi^{5}} \frac{pL^{4}}{EI} \frac{A}{I}$ (12d)

$$T = \frac{\pi^2}{L^2} = \frac{EI}{\rho A} t$$
 (12b) $\bar{N} = NL^2/\pi^2 EI$ (12e)

$$\bar{\mu} = \frac{\beta L^2}{\pi^2 \sqrt{0 AEI}}$$
 (12c) $\bar{N}_0 = N_0 L^2 / \pi^2$ EI (12f)

$$\delta_{pq} = \begin{cases} 0 & p \neq q \\ 1 & p = q \end{cases}$$
 (12g)

The nature of the equations is best illustrated by considering only the term for m equal to unity. Then Eqs. (11) reduce to

$$\frac{d^{2}\bar{w}_{1}}{dT^{2}} + \bar{\mu} \frac{d\bar{w}_{1}}{dT} + \frac{1}{4}\bar{w}_{1} (\bar{w}_{1} + \bar{w}_{0})(\bar{w}_{1} + 2\bar{w}_{0}) = -\bar{p}$$
 (13)

which is of the form of the equation of motion of a mass-spring system with a nonlinear spring stiffness. The restoring spring force is shown as a function of $\bar{\mathbf{w}}_1/\bar{\mathbf{w}}_0$ in Fig. 2. The spring resistance is of the softening type as $\bar{\mathbf{w}}_1$ decreases from 0 and is actually destabilizing when the beam becomes susceptible to snap-through from the buckled position on one side of the initially straight axis to the buckled position on the other side. Thus the beam would be expected to vibrate about the static buckled position for small excitations but to snap back and forth between the two equilibrium positions for larger excitations.

DYNAMIC STABILITY OF INITIALLY BUCKLED BEAMS UNDER UNIFORM RANDOM PRESSURE

An important consideration in the study of critical random loading of initially buckled beams is the definition of what constitutes instability and the method of calculation of that critical loading. If it is supposed that for low levels of spectral density of loading the beam vibrates about its buckled equilibrium position while at high levels of spectral density the beam snaps through repeatedly and vibrates about its straight zero-deflection position, then presumably there is a critical value or range of spectral density value for which snap-through is first initiated.

A description of the behavior of the initially buckled beam can be based on time averages of the response. A computer program was developed to calculate the response of a compressed beam, buckled or unbuckled, over any desired length of time and to obtain time averages of various quantities at stated intervals.

To integrate the nonlinear equations of motion, a fourth-order Runge-Kutta method of numerical integration reference [9] was used. A random loading function having a Gaussian distribution with a mean of zero and a specified deviation \bar{c}_0 was generated. The loading function consists of steps which are constant over a given constant increment of time ΔT . A typical generated time history of loading is shown in Fig. 3. The statistics of the distribution have been studied in references [2] and [10] from which the value of the power spectral desnity parameter can be determined as

$$\bar{s}_0 = \bar{\sigma}_0^2 \Delta T \tag{14}$$

In the numerical integration process, the constant integration time step was taken as some integral division of ΔT , generally $\Delta T/5$. The number of terms in the Fourier series expansion of the deflection function was taken as three in all cases.

The primary object of investigation is the average frequency of snapthrough, defined as the number of zero crossings N(T) of the maximum deflection divided by the time T, i.e.,

$$\mathcal{F} = \underset{T \to \infty}{L} \frac{N(T)}{T} \tag{15}$$

The number of crossings of the zero axis of the maximum deflection function, both from above and from below, was counted during the calculation procedure. At stated intervals, a time average of the crossing rate was calculated. It was observed that this calculated rate was reasonably constant when the time was sufficiently long, and that different loading sequences led to essentially the same result. Some of the results are shown in Table 1. The time averages shown for $\bar{\mathbf{w}}_0$ equal to 10 suggest the calculation of a critical spectral der \mathbf{y} parameter based on the average frequency vanishing or becoming very small, since for $\bar{\mathbf{v}}_0$ equal to 10 the average frequency is zero whereas for $\bar{\mathbf{v}}_0$ equal to 100 the average frequency of snap-through is 1.56. Additional caluculations were made for various combinations of values of $\bar{\mathbf{w}}_0$, $\bar{\mathbf{\mu}}$, $\Delta \mathbf{T}$, and $\bar{\mathbf{v}}_0$.

Some correlating parameters may be deduced from the following considerations. If only one term is retained in Eqs. (11) and the resulting Eq. (12) is divided by $\overline{\mathbf{w}}_0^3$, the following is obtained.

$$\frac{d^{2} \frac{\overline{w}_{1}}{\overline{w}_{0}}}{d(\overline{w}_{0}^{T})^{2}} + \frac{\overline{\mu}}{\overline{w}_{0}} \frac{d^{2} \frac{\overline{w}_{1}}{\overline{w}_{0}}}{d(\overline{w}_{0}^{T})} + \frac{1}{4} \frac{\overline{w}_{1}}{\overline{w}_{0}} \left(1 + \frac{\overline{w}_{1}}{\overline{w}_{0}}\right) \left(2 + \frac{\overline{w}_{1}}{\overline{w}_{0}}\right) = -\frac{\overline{p}}{\overline{w}_{0}^{3}}$$
(16)

Since the first term predominates in the series, the above equation indicates that initially buckled beams having the same modified loading function \bar{p}/\bar{w}_0^3 as a function of modified time \bar{w}_0^T will have nearly identical deflection ratios \bar{w}_1/\bar{w}_0 . Since the standard deviation $\bar{\sigma}_0$ of the random loading is a measure of load intensity, these results suggest that random loadings having the spectral density value of

$$\left(\frac{\overline{\sigma}_0}{\overline{w}_0^3}\right)^2 \overline{w}_0 \Delta T = \frac{\overline{s}_0}{\overline{w}_0^5}$$
(17)

should yield nearly identical average responses.

In addition, the investigation of reference [11] indicates that the primary white noise spectral density parameter is

$$\bar{S} = \frac{\bar{\sigma}_0^2 \Delta T}{8\bar{u}} = \frac{\bar{S}_0}{8\bar{u}} \tag{18}$$

The results of reference [11] were also found to be insensitive to the parameter $\bar{\mu}$. It is possible then that beams of different initial amplitudes having the same value of

$$\frac{1}{8} \frac{\bar{s}_0}{\bar{w}_0^5} / \frac{\bar{\mu}}{\bar{w}_0} = \frac{\bar{s}}{\bar{w}_0^4}$$
 (19)

would have similar average response.

These conjectures are tested in Fig. 4 where the various frequency results for initially buckled beams are plotted as a function of the spectral density parameter \bar{S}/\bar{w}_0^4 . The frequency has been modified by division by \bar{w}_0 , since the results should depend on \bar{w}_0^T . It will be seen that the results for the beams of different initial buckle amplitudes appear to nearly coincide in the vicinity

of region of vanishing frequency of zero-crossing. Thus an estimate of the critical spectral density parameter for snap-through and subsequent oscillation between buckled equilibrium positions is given by

$$\bar{s} = 0.001 \, \bar{w}_0^4$$
 (20)

4. RMS RESPONSE OF INITIALLY BUCKLED BEAMS UNDER UNIFORM RANDOM PRESSURE

(a) Numerical Integration Results

Although knowledge of the critical spectral density of loading is useful, it is also of interest to determine the expected average and root-mean-square (RMS) deflections and stresses of the beam since these affect the fatigue life of the structure. During the integration process which led to the result of the maximum preceding chapter, a record was kept of the RMS deflections and stresses at the beam center. The integrated deflections and stresses and their squares over the time period were calculated using an extended Simpson's Rule formula (reference [14]).

As stated times the RMS center deflection and outer fiber stresses were calculated. It was observed that after a sufficiently long time period the averaged values became reasonably constant. The mean values calculated at the end of the maximum time period in each case are plotted in Figs. 5 and 6, together with some theoretical results which will be discussed later. Only the RMS stress having the greatest magnitude is given. For sufficiently large values of the parameter $\overline{\bf S}$ the two values of stress were essentially the same.

The results exhibit remarkably little scatter and thus indicate the primary importance of the spectral density parameter \bar{S} and the lesser importance of the damping parameter $\bar{\mu}$. The results also indicate, as would be expected, that the effect of initial buckling becomes less important as the spectral density parameter \bar{S} increases. The deflections and stresses are then large enough for the beam behavior to be similar to that of an unbuckled beam under large loading. The RMS deflections appear to first decrease as the spectral density parameter increases and to then increase. This phenomenon is explainable as the result of a shift in the average deflection from the buckled position to the unbuckled beam reference axis. The mean position of the buckled beam would tend to shift toward the straight reference axis because of the softening spring characteristic for inward deflections and hardening spring characteristic for outward deflections exhibited in Fig. 2: Unfortunately, the few results obtained for the variation of the average deflection with \bar{S} are insufficient to define the shift.

(b) Approximate Analytical Investigation

The computation effort involved in these calculations is very great, so great as to motivate an approximate analytical treatment of the problem. The method of equivalent linearization (reference [13]) which was used in reference [11] for unbuckled beams suggests itself as a possible means of obtaining an approximate solution which can be compared to the numerical integration results for an accuracy check. There are certain complications in the present case, however, the method of equivalent linerization has been applied successfully in cases on nonlinearities which imply a zero mean displacement. In the present case, however, the restoring force is reasonably symmetrical only for small motion about the buckled equilibrium position and for large snap-through motion about the straight reference position. Between these two extremes the

mean displacement shifts from the buckled to the unbuckled position.

The two extreme cases are considered herein as providing possible bounds on the RMS displacements and stresses. The method of equivalent linearization involves replacing the nonlinear terms in each of Eqs. (11) by an equivalent linear term. The equivalent linear term is determined by requiring that the mean-square error be a minimum. For small motion about the buckled equilibrium position the nonlinear terms in each of Eqs. (11) are replaced by a term of the form $k_m w_m$. When motion about a mean straight reference position is considered, the nonlinear terms in Eqs. (11) are replaced by equivalent linear expressions $k_m (\bar w_m + \bar w_0 \dot s_m)$. The procedure is similar to that of reference [11] and leads to the curves of Figs. 5 and 6.

(c) Comparison of Simulated and Equivalent Linearization Results

It will be noted that the deflections obtained by the numerical integration are reasonably bracketed by the two sets of approximate curves. The RMS deflections with respect to the straight reference position approach the static buckle deflection for small excitation and merge with the curve for large snapthrough deflections about the straight reference position as the excitation increases. For an unbuckled beam ($\bar{\mathbf{w}}_0 = \bar{\mathbf{N}}_0 = 0$) the equivalent linearization results reduce to a single curve. In this case the numerical integration and equivalent linearization results are in very good agreement over a quite large range of the parameter $\bar{\mathbf{S}}$.

In agreement with the numerical integration results, the deflection for all values of \bar{w}_0 tend to become equal. . The equivalent linearization deflections appear to become increasingly larger than those obtained by numerical integration for large \bar{s} . This disagreement is possibly due to use of the method of equivalent linearization beyond its range of applicability (see, however, reference [14]). Certainly the beam is very highly nonlinear for large deformations. It is also possible that the constant time increment used in the simulation process for the random loading is too large. The average period of vibration about the straight position decreases as the excitation increases, whereas the time increment over which the loading remains constant was not decreased. This could conceivably result in decreased deflections. Additional calculations to prove or disprove this contention would be quite costly, however.

Also shown in Fig. 5 are the critical values of the spectral density parameter \bar{S} given by Eq. (20). The RMS deflections only appear to first depart significantly from the static value at this point rather than to have an abrupt discontinuity.

Similar agreement is found for simulated and equivalent linearization stress results in Fig. 6. There is again a transition of the simulated stresses from those given for vibrations about the buckled position to vibrations about the unbuckled position. The somewhat strange behavior of the approximate theoretical results consisting of the stress of the two approximate results crossing for large $\overline{\mathbf{w}}_0$, but not for $\overline{\mathbf{w}}_0$ of unity, is confirmed by the simulated results.

Again the stresses given by equivalent linearization deviate from the simulated results for large \overline{S} . The approximate results are conservative, however, and are thus useful. Indeed, they may be more reliable for the reasons discussed earlier.

CONCLUSIONS

The present investigation serves to cast some light in the behavior of initially buckled beams under random loading. A reasonable indication of the critical spectral density of loading required for beam snap-through appears

to be the vanishing of the average zero-crossing frequency of the beam. While this criterion does not lead to a completely precise value, due to the lengthy calculations required, an estimate of the critical power spectral density parameter has been obtained as

$$\bar{S} = 0.001 \, \bar{w}_0^4$$

An investigation of the RMS response of initially buckled simply supported beams does not reveal any drastic change in the vicinity of the critical spectral density. The onset of snap-through does herald the possibility of stress reversal, however.

Bounds on the RMS response have been obtained by considering vibrations about the initial buckled position as an average and about the straight reference position as an average, together with the method of equivalent linearization. The results obtained by numerical simulation of random loading indicate a smooth transition from the first to the second type of behavior and in the limit are in good agreement with the approximate analytical values.

The results obtained suggest the need for better analytical techniques to furnish the required data. While useful results have been obtained by numerical load simulation and integration of the differential equations of motion, the calculations are quite costly and time consuming. Further studies on methods for estimating the response of highly nonlinear structures for random loading are thus required.

6. REFERENCES

- M. J. Jacobson and P. E. Finwall 1974 Report No. AFFDL-TR-73-56, Air Force Flight Dynamics Laboratory, Wright-Patterson AFB, Ohio Effects of Structural Heating on the Sonic Fatigue of Aerospace Vehicle Structures.
- H. N. Pi, St. T. Ariaratnam, and W. C. Lennox 1971 J. Sound Vib., 14, 375-384. First-Passage Time for the Snap-through of a Shell-type Structure
- 3. J. V. Huddleston 1970 J. Appl. Mech., 37, 984-994. Behavior of a Steep Prestressed Arch Made from a Buckled Strut
- 4. W. Y. Tseng and J. Dugundji 1971 J. Appl. Mech., 38, 467-476.

 Nonlinear Vibrations of a Buckled Beam under Harmonic Excitation
- 5. D. Burgreen 1951 J. Appl. Mech. 18, 135-139.
 Free Vibrations of a Pin Ended Column with Constant Distance Between Ends
- 6. R. L. Bisplinghoff and T. H. H. Pian 1957 Proc. IX Int. Cong. Appl. Mech., 7, 307-318. On the Vibration of Thermally Buckled Bars and Plates
- 7. J. G. Eisley 1964 Z. Agnew. Math. Phys., 15, 167-174. Nonlinear Vibrations of Beams and Rectangular Plates
- 8. J. G. Eisley 1964 AIAA J., 2, 2207-2209. Large Amplitude Vibrations of Buckled Beams and Rectangular Plates
- 9. M. D. Greenberg 1978 New Jersey: Prentice-Hall, Inc. Foundations of Applied Mathematics

- S. J. Stott and S. F. Masri 1978 Report No. NUREG/CR-0361, CE78-8,
 U. S. Nuclear Regulatory Commission, Washington, D.C.
 Random Vibration of a Nonlinear Two-Degree-of-Freedom Oscillator
- 11. P. Seide 1976 J. Eng. Ind., 98, 1014-1020. Nonlinear Stresses and Deflections of Beams Subjected to Random Time Dependent Uniform Pressure
- 12. M. Abramowitz and I. A. Stegun 1964 Handbook of Mathematical Functions Washington, D.C.: National Bureau of Standards
- 13. Y. K. Lin 1967 Probabilistic Theory of Structural Dynamics. New York: McGraw-Hill

Table 1. Effect of Seed Value and Maximum Integration Time on Zverage Zero-Crossing Frequency ($\bar{\mu} = \Delta T = 0.1$)

w _o	w ₀ 1.0		10.0				
σ ₀ 10		00	100		10		
Seed Value	999999999	123456789	999999999	369121518	999999999	369121518	
T	N(T)/T	N(T)/T	N(T)/T	N(T)/T	N(T)/T	N(T)/T	
3141.6	1.980	1.909	1.548				
6283.2	1.945	1.916	1.579	1.55	0.000	0.000	
9424.8	1.947	1.926	1.551				
12566.4	1.948	1.935	1.555	1.55	0.000	0.000	
15708.0	1.953	1.935	1.556				
18849.6	1.957		1.552	1.54	0.000	0.000	
21991.2	1.961		1.555		ļ 		
25132.8	1.969		1.547	1.55	0.000	0.000	
28274.4	1.957		1.550		 		
31416.0	1.955		1.550	1.56	0.000	0.000	

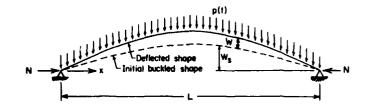


Fig. 1 Buckled Beam Subjected to Uniform Pressure

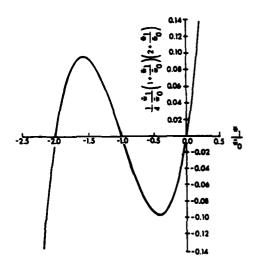


Fig. 2 One Mode Approximation to Beam Restoring Force

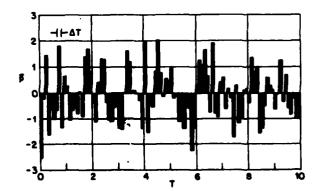


Fig. 3 Typical Generated Random Pressure Variation with Time

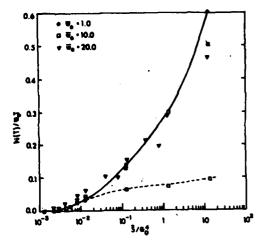


Fig. 4 Variation of Modified Zero-Crossing Frequency with Modified Spectral-Density Parameter

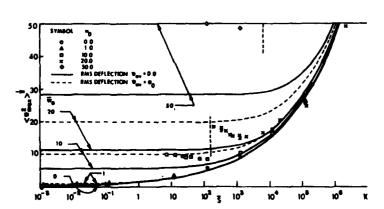


Fig. 5 Comparison of Analytical and Simulated RMS Deflections

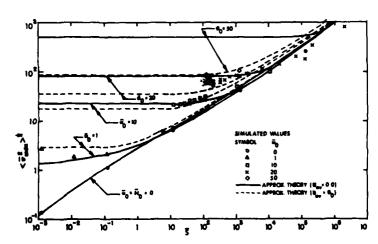


Fig. 6 Comparison of Analytical and Simulated RMS Results



ACCURATE NONLINEAR EQUATIONS AND A PERTURBATION SOLUTION FOR THE FREE NONPLANAR VIBRATIONS OF INEXTENSIONAL BEAMS

A. Luongo (*), G. Rega (**), F. Vestroni (**)

- (*) Istituto di Scienza delle Costruzioni, University of Rome, Italy
- (**) Istituto di Scienza delle Costruzioni, University of L'Aquila, Italy

1. INTRODUCTION

Many works on what is generally termed nonlinear structural vibration problems have appeared in the literature. Most of them concern the dynamic behaviour of single beams having various support conditions and forces with different appro ximations regarding the kinematics of the beam model, the ordering of the elastic nonlinear terms and the accounting for the inertia terms [1]. Relatively few work were devoted to the study of nonplanar motions, for which the introduction of sim plifying assumptions is less easy and more questionable. The axially restrained simply-supported beam was considered in reference [2] in absence of torsional motions and assuming linear curvature of the beam. The same assumption had already been made in reference [3] for a base-excited inextensible cantilever beam, notwithstanding in this case large curvature can occur. This problem was successively treated in references [4] and [5] including nonlinear inertia and nonlinear curva ture; in particular in the former the general order-three nonlinear differential equations of a compact beam are derived considering bending about two principal axes and torsion, while the study of the forced motion of a fixed-free beam is developed under the assumption the torsional frequency is much greater than the flexural ones.

In the present work free nonplanar motions of an inextensional elastic beam with no warping and shear deformation, supported in an arbitrary manner but no axially restrained, are studied without introducing simplifying assumptions. The kinematically nonlinear beam model is derived within the theory of rods from a continuum mechanics point of view Although elsewhere the usefulness of such model is not recognized, it has been followed here because its major generality; indeed it permits an unitary approach for both cases of inextensional and deformable beam [7].

After introducing the conditions of inextensionality and shear indeformability, the exact equations of motion are explicitly obtained through the extended Hamilton's principle. The equations are then expanded up to order-three nonlinearities without any ordering assumption with respect to the configuration variables. A system of three partial integro-differential equations are obtained which are accurate for studying moderately large oscillations of a beam having two flexural and one torsional components of equal order.

Three ordinary differential equations are derived via a Galerkin procedure adopting three eigenfunctions of the system as spatial shapes of the three configuration variables, and are analysed by the multiple time scale perturbation technique. The conditions involving the linear frequencies under which internal resonance occurs are examined and various cases of resonance are evidenced. The solution of the equations in absence of internal resonance, which allows to study the nonlinear coupling phenomena among the three modes considered, is accomplished.

The complete analytical developments of the equations and solution presented here are contained in reference [8].

2. INEXTENSIONAL BEAM NONLINEAR MODEL

The kinematical behaviour of an indeformable beam is described referring to a one-dimensional polar continuum beam model [6] in which the conditions of internal constraint are introduced.

Let the initial static equilibrium configuration C_0 (at time t_0) of the beam B be straight. By assigning to each point $P \in B$ an abscissa s on C_0 , the initial configuration is defined by a position vector $\vec{r}(s,t_0)$ and an orthonormal basis $\beta(s,t_0) \equiv \beta_0 \equiv \{\vec{b_1},\vec{b_2},\vec{b_3},\vec{b_3}\}$. In the following β_0 is the inertia principal basis, $\vec{b_1}(s,t_0)$ being aligned with the beam axis.

Let C be the beam configuration at time t, defined by $\vec{r}(s,t)$ and $\beta(s,t) \equiv \{\vec{b}_1, \vec{b}_2, \vec{b}_3, \vec{b}_4, \vec{b}_5, \vec{b}_7, \vec{b}_8, \vec{b}_8\}$ b2, b3}. By assuming the initial configuration as the reference configuration, the referential description of the beam motion from C_0 to C is given by:

$$\vec{u}(s,t) = \vec{r}(s,t) - \vec{r}(s,t_0)$$
 $\vec{b}_i(s,t) = R(s,t) \vec{b}_i(s,t_0)$ $(1_{1,2})$

where \vec{u} is the displacement vector field and R is the rotation tensor field. The rigid rotation R of the cross section at s is described as the composition of three successive elementary rotations R_1 , R_2 , R_3 which lead the triad β_0 to match the triad β ; their amplitudes are the angles $\theta_1(s,t)$, $\theta_2(s,t)$, $\theta_3(s,t)$.

Define now the deformation field with respect to the reference configuration. If $\vec{q}(s,t_0)$ is a material vector solid with basis β_0 , the corresponding vector $\vec{q}(s,t)$ is given by the relationship:

$$\overrightarrow{q}(s,t) = R(s,t) \overrightarrow{q}(s,t_0)$$
 (2)

The curvature tensor field C defined by the equation [6]:

$$\vec{q}'(s,t) = C(s,t) \vec{q}(s,t)$$
 (3)

is assumed as a measure of the flexural and torsional deformation of beam, where ()' = $\partial/\partial s$. By deriving Eq.(2) with respect to s, accounting for $C(s,t_0) \equiv 0$, eliminating $\vec{q}(s,t_0)$ through Eq.(2) and equating the resulting expression to Eq.(3), it follows:

$$C = R^{\dagger}R^{T}$$
 (4)

where the orthogonality property of R was accounted for; C is a skew tensor. The shear and axial indeformability of the beam is expressed as:

$$\vec{r}'(s,t) = R \vec{r}'(s,t_0)$$
 (5)

The spin tensor field W is defined by the relationship:

$$\dot{\vec{q}}(s,t) = W(s,t) \dot{\vec{q}}(s,t)$$
 (6)

analogous to Equation (3), being ($\dot{}$) = $\partial/\partial t$, from which it follows:

$$W = \hat{R} R^{T}$$
 (7)

Introduce now the scalar components of the previous quantities. The components of \vec{u} with respect to basis β_0 will be denoted as $\underline{u}(s,t) = \{u_1, u_2, u_3\}^T$; the representation of R in such a basis is given by the matrix $R = R_1 R_2 R_3$, whose j-th line gives the components of the unit vectors $\vec{b}_1(s,t)$, (i=1,2,3), on the axis of unit vector \vec{b} (s,t₀). The components of C and W with respect to the basis β are:

$$\underline{C} = \underline{R}^{T} \underline{R}' \qquad \underline{W} = \underline{R}^{T} \dot{\underline{R}}$$
 (8,9)

Eq. (8) gives the expressions of the three independent components c_{12} , c_{13} , c_{23} of the skew tensor C with respect to the basis β . The quantities:

$$\mu_{1} = -c_{23} = \theta_{1}^{\prime} \cos \theta_{2} \cos \theta_{3} + \theta_{2}^{\prime} \sin \theta_{3}$$

$$\mu_{2} = c_{13} = -\theta_{1}^{\prime} \cos \theta_{2} \sin \theta_{3} + \theta_{2}^{\prime} \cos \theta_{3}$$

$$\mu_{3} = -c_{12} = \theta_{1}^{\prime} \sin \theta_{2} + \theta_{3}^{\prime}$$
(10)

are defined as torsional and flexural curvatures of the beam in a finite deforma tion. The expressions for the components of the angular velocity $\widetilde{\omega}(s,t)$ of the basis β are obtained from Equations (10) by substituting the prime with the dot.

The representation of Equation (5) on the basis β_0 is given by three scalar equations, from which the relationships follow:

$$\tan \theta_2 = \frac{u_2^* \sin \theta_1 - u_3^* \cos \theta_1}{1 + u_1^*} \tag{11}_1)$$

$$\tan \theta_3 = \frac{u_2' \cos \theta_1 + u_3' \sin \theta_1}{\left[(1 + u_1')^2 + (u_2' \sin \theta_1 - u_3' \cos \theta_1)^2 \right]_{\frac{1}{2}}}$$
(11₂)

$$(1+u_1^*)^2 + u_2^{*2} + u_2^{*2} = 1 (12)$$

To identify the beam configuration at time t with respect to the reference configuration the six variables u_1 , u_2 , u_3 , θ_1 , θ_2 , θ_3 have been introduced. The internal constraint conditions (11), (12) allow to reduce to three the number of configuration variables. However, Eqs.(11) give directly θ_2 and θ_3 in terms of the other four configuration variables, while an integral relationship only between u_1 and u_2' , u_3' can be obtained from Eq.(12). This entails that when obtaining exact equations of motion by variational procedure, Eqs.(11) will be accounted for at once while Eq.(12) will be added through a Lagrangian multiplier. In a second stage, in which three approximate nonlinear equations of motion in the variables u_2 , u_3 , θ_1 amenable to a perturbation analysis are obtained, the following order-three expansions will be used to eliminate θ_2 , θ_3 , u_1 :

$$\theta_{2} = -u_{3}^{"} + (u_{1}^{"}u_{3}^{"} + u_{2}^{"}\theta_{1}^{"}) + (\frac{1}{3}u_{3}^{"}^{"} - u_{1}^{"}u_{2}^{"}\theta_{1}^{"} - u_{1}^{"}^{"}u_{3}^{"} + \frac{1}{2}u_{3}^{"}\theta_{1}^{"}) + O(\|u\|^{4})$$

$$\theta_{3} = u_{2}^{"} + (u_{3}^{"}\theta_{1} - u_{1}^{"}u_{2}^{"}) + (-\frac{1}{3}u_{2}^{"} - u_{1}^{"}u_{3}^{"}\theta_{1}^{"} + u_{1}^{"}^{"}u_{2}^{"} - \frac{1}{2}u_{2}^{"}\theta_{1}^{"} - \frac{1}{2}u_{3}^{"}u_{2}^{"}) + O(\|u\|^{4})$$

$$u_{1}^{"} = -\frac{1}{2}(u_{2}^{"} + u_{3}^{"}^{"}) + O(\|u\|^{4})$$

$$(13_{1})$$

3. EQUATIONS OF MOTION

3.1 Exact equations

The equations of motion are obtained through Hamilton's principle. Referring to basis β_0 which is taken coincident with the principal basis of the constitutive law, the Lagrangian ℓ per unit length of beam is as follows:

$$\mathcal{L} = \frac{1}{2} \, m \, \sum_{1}^{3} \, \dot{u}_{1}^{2} + \frac{1}{2} \, \sum_{1}^{3} I_{1} \, \omega_{1}^{2} - \frac{1}{2} \, \sum_{1}^{3} E_{1} \mu_{1}^{2}$$
(15)

where m is the mass per unit lenght, $I_{\underline{i}}$, $J_{\underline{i}}$ are the principal mass moments and geometric moments of inertia of the beam, $E_1 = GJ_1$ is the torsional stiffness, $E_2 = EJ_2$, $E_3 = EJ_3$ are the flexural stiffnesses, with E elastic modulus.

The extended expression of the Hamiltonian reads:

$$H = \int_{t_1}^{t_2} \int_{0}^{\chi} \left\{ \mathcal{L} + \frac{1}{2} \lambda \left[1 - \left(1 + u_1^{\dagger} \right)^2 - u_2^{\dagger 2} - u_3^{\dagger 2} \right] \right\} ds dt$$
 (16)

 ℓ being the beam length, from which it follows:

$$\delta H = \begin{cases} t_2 \\ t_1 \end{cases} \begin{cases} \delta \mathcal{L} + \frac{1}{2} \delta \lambda \left[1 - (1 + u_1^{\dagger})^2 - u_2^{\dagger 2} - u_3^{\dagger 2} \right] + \\ - \lambda \left[(1 + u_1^{\dagger}) \delta u_1^{\dagger} + u_2^{\dagger} \delta u_2^{\dagger} + u_3^{\dagger} \delta u_3^{\dagger} \right] \end{cases} ds dt$$
 (17)

where it is:

$$\delta \mathcal{L} = m \sum_{i=1}^{3} \dot{\mathbf{u}}_{i} \quad \delta \dot{\mathbf{u}}_{i} + \sum_{i=1}^{3} \mathbf{I}_{i} \dot{\mathbf{u}}_{i} \quad \delta \omega_{i} - \sum_{i=1}^{3} \mathbf{E}_{i} \mu_{i} \quad \delta \mu_{i}$$

$$\tag{18}$$

$$\delta\omega_{i} = \sum_{i,j}^{3} \frac{\partial\omega_{i}}{\partial\theta_{j}} \delta\theta_{j} + \sum_{i,j}^{3} \frac{\partial\omega_{i}}{\partial\dot{\theta}_{j}} \delta\dot{\theta}_{j}$$
(19)

$$\delta\mu_{i} = \sum_{1j}^{3} \frac{\partial\mu_{i}}{\partial\theta_{j}} \delta\theta_{j} + \sum_{1j}^{3} \frac{\partial\mu_{i}}{\partial\theta_{j}^{*}} \delta\theta_{j}^{*}$$
(20)

and $\lambda(s,t)$ is a Lagrangian multiplier with the meaning of an axial force. The

virtual variations $\delta\theta_2$, $\delta\theta_3$ in equations (19), (20) will be expressed in terms of the variations of the remaining configuration variables through the relationships:

$$\delta\theta_{j} = \sum_{i=1}^{3} \frac{\partial\theta_{i}}{\partial u_{k}^{i}} \left(1 - \delta_{j}^{1}\right) \delta u_{k}^{i} + \frac{\partial\theta_{j}}{\partial\theta_{1}} \delta\theta_{1} \qquad (j = 1, 2, 3)$$
(21)

where the derivatives $\partial\theta_{i}/\partial u_{k}^{i}$, $\partial\theta_{i}/\partial\theta_{1}$, (j=2,3) are obtained from equations (11) and $\delta_{i,j}$ is the Kronecker symbol.

By substituting Eqs.(18)-(21) into (17), performing a few integration by parts with respect to both time and space and imposing δ H=0 for each δ u. (i=1,2,3), $\delta\theta_1$ kinematically admissible and for each $\delta\lambda$, the following differential equations describing the free finite motion of beam:

$$G_{k}' = \{ \sum_{i=1}^{3} [B_{j} - A_{j}] \frac{\partial \theta_{j}}{\partial u_{k}'} (1 - \delta_{j1}) + \lambda (\delta_{k1} + u_{k}') \}' = m\ddot{u}_{k}$$
 (k=1,2,3) (22₁)

$$\sum_{i,j}^{3} \begin{bmatrix} B_{i} - A_{j} \end{bmatrix} \frac{\partial \theta_{i}}{\partial \theta_{1}} = 0$$
 (22₂)

$$[1-\sum_{1}^{3}(\delta_{k1}+u'_{k})(\delta_{k1}+u'_{k})] = 0$$
 (22₃)

are obtained; the relevant boundary conditions read:

$$\left\{-\sum_{1}^{3} G_{k} \delta \mathbf{u}_{k} - \sum_{1}^{3} H_{k} \delta \mathbf{u}_{k}^{\dagger} - H_{\theta} \delta \theta_{1}\right\} \Big|_{0}^{\ell} = 0$$

$$(23)$$

being

$$H_{\mathbf{k}} = \sum_{1}^{3} \sum_{1}^{3} \mathbf{E}_{\mathbf{i}} \mu_{\mathbf{i}} \frac{\partial \mu_{\mathbf{i}}}{\partial \theta_{\mathbf{j}}^{\mathbf{i}}} \frac{\partial \theta_{\mathbf{j}}}{\partial \mathbf{u}_{\mathbf{k}}^{\mathbf{i}}} (1 - \delta_{\mathbf{j}1}) \qquad H_{\theta} = \sum_{1}^{3} \sum_{1}^{3} \mathbf{E}_{\mathbf{i}} \mu_{\mathbf{i}} \frac{\partial \mu_{\mathbf{i}}}{\partial \theta_{\mathbf{j}}^{\mathbf{i}}} \frac{\partial \theta_{\mathbf{j}}}{\partial \theta_{\mathbf{i}}}$$
(24)

In equations (22), (23) it is:

$$A_{j} = \sum_{i=1}^{3} E_{i} \mu_{i} (\partial^{2} \mu_{i} / \partial s \partial \theta_{j}^{!} - \partial \mu_{i} / \partial \theta_{j}^{!}) + \sum_{i=1}^{3} E_{i} \mu_{i}^{!} \partial \mu_{i} / \partial \theta_{j}^{!}$$
(25)

$$B_{j} = \sum_{i=1}^{3} I_{i} \omega_{i} (\partial^{2} \omega_{i} / \partial t \partial \dot{\theta}_{j} - \partial \omega_{i} / \partial \dot{\theta}_{j}) + \sum_{i=1}^{3} I_{i} \dot{\omega}_{i} \partial \omega_{i} / \partial \dot{\theta}_{j}$$

$$(26)$$

By substituting the functions μ_1 , ω_1 , $\partial\theta_1/\partial u_k'$, $\partial\theta_1/\partial\theta_1$ and considering θ_2 , θ_3 as functions of the remaining four configuration variables u_1 , u_2 , u_3 , θ_1 to be expressed via equations (11), exact explicit equations of motion and boundary conditions can be obtained [8].

3.2 Equations with order-three nonlinearities

The exact equations (22) are valid for arbitrarily large deformations of the beam. They are not amenable however to an analytical solution still able to give information on the nonlinear coupling and resonance phenomena which occur in moderately large deformations of the beam as well. Therefore a set of five approximate differential equations of motion in the variables u_1 , u_2 , u_3 , θ_1 , λ with nonlinear terms up to third order - which still retain relevant information about the motion - is obtained by developing all terms in equations (22) in Taylor series and substituting the order-three expansions (13) for θ_2 and θ_3 . Besides, taking into account that the axial displacement u_1 is a second-order variable with respect to u_2 , u_3 , λ is obtained as second-order variable as well through integration of the axial equation of motion. By substituting u_1 and λ in the transverse and tor sional equations, the following system of order-three integro-differential equations with the unknowns u_2 , u_3 , $\theta \equiv \theta_1$ is obtained:

$$\begin{split} G_{2}^{\prime} &= \left\{ I_{3} \left[\ddot{u}_{2}^{\prime} + u_{2}^{\prime} \dot{u}_{2}^{\prime}^{\prime}^{2} + u_{2}^{\prime}^{\prime} \ddot{u}_{2}^{\prime} \right] + I_{1} \left[\dot{u}_{3}^{\prime} \dot{\theta} + u_{2}^{\prime} \theta \ddot{\theta} \right] + I_{2} u_{2}^{\prime} u_{3}^{\prime} \ddot{u}_{3}^{\prime} - (I_{2} - I_{3}) \left[(\dot{u}_{3}^{\prime} \theta)^{\circ} - \ddot{u}_{2}^{\prime} \theta^{2} + 2\dot{u}_{2}^{\prime} \dot{\theta}^{\prime} \right] - (I_{1} - I_{2}) u_{2}^{\prime} \dot{u}_{3}^{\prime}^{\prime}^{2} - E_{3} \left[u_{2}^{\prime\prime\prime} + u_{2}^{\prime} u_{2}^{\prime\prime}^{2} + u_{2}^{\prime}^{\prime} u_{2}^{\prime\prime\prime} \right] - E_{1} \left[u_{3}^{\prime\prime} \theta^{\prime} + u_{2}^{\prime} \theta \theta^{\prime\prime} \right] - E_{2} u_{2}^{\prime} u_{3}^{\prime\prime\prime}^{\prime\prime\prime} + + (E_{2} - E_{3}) \left[(u_{3}^{\prime\prime} \theta)^{\prime} - u_{2}^{\prime\prime\prime}^{\prime\prime} \theta^{2} - 2 u_{2}^{\prime\prime} \theta \theta^{\prime\prime} \right] + (E_{1} - E_{2}) u_{2}^{\prime} u_{3}^{\prime\prime\prime}^{2} - 1/2 \, \text{m} \, u_{2}^{\prime\prime} \, \int_{0}^{s} \left(u_{2}^{\prime\prime}^{2} + u_{3}^{\prime\prime}^{2} \right)^{\prime\prime\prime} \, ds \, ds + m \, u_{2}^{\prime\prime} \, \int_{0}^{s} \ddot{u}_{1}(0) \, ds + u_{2}^{\prime\prime} G_{1}(\ell) \right\}^{\prime} = m \, \ddot{u}_{2} \end{split} \tag{27}_{1}$$

$$\begin{split} G_3^{\prime} &= \big\{ I_2 \left[\ddot{u}_3^{\prime} + \dot{u}_2^{\prime 2} u_3^{\prime} + u_2^{\prime} \ddot{u}_2^{\prime} u_3^{\prime} + u_3^{\prime} \dot{u}_3^{\prime 2} + u_3^{\prime 2} \ddot{u}_3^{\prime} \big] - I_1 \left[+ \left(u_2^{\prime} \dot{\theta} \right)^{^{\prime}} + u_3^{\prime} \theta \ddot{\theta} - 2 u_2^{\prime} \dot{u}_2^{\prime} \dot{u}_3^{\prime} - u_2^{\prime 2} \ddot{u}_3^{\prime} \right] + \\ &- \left(I_2 - I_3 \right) \left[\left(\dot{u}_2^{\prime} \theta \right)^{^{\prime}} + \ddot{u}_3^{\prime} \theta^2 + 2 \dot{u}_3^{\prime} \theta \dot{\theta} \right] - E_2 \left[u_3^{\prime\prime\prime} + u_2^{\prime\prime\prime} u_3^{\prime} + u_2^{\prime} u_2^{\prime\prime\prime} u_3^{\prime} + u_3^{\prime} u_3^{\prime\prime\prime} + u_3^{\prime\prime}^2 u_3^{\prime\prime\prime} \right] + \\ &+ E_1 \left[\left(u_2^{\prime} \theta^{\prime} \right)^{\prime} + u_3^{\prime} \theta \theta^{\prime\prime} - 2 u_2^{\prime} u_2^{\prime\prime} u_3^{\prime\prime\prime} - u_2^{\prime 2} u_3^{\prime\prime\prime} \right] + \left(E_2 - E_3 \right) \left[\left(u_2^{\prime\prime} \theta \right)^{\prime} + u_3^{\prime\prime\prime} \theta^2 + 2 u_3^{\prime\prime} \theta \theta^{\prime} \right] + \\ &- 1/2 \, m \, u_3^{\prime} \, \int_{0}^{S} \int_{0}^{S} \left(u_2^{\prime 2} + u_3^{\prime 2} \right)^{\prime\prime} ds \, ds + m \, u_3^{\prime\prime} \int_{0}^{S} \ddot{u}_1 \left(0 \right) \, ds + u_3^{\prime\prime} G_1 \left(\ell \right) \right\}^{\prime\prime} = m \, \ddot{u}_3 \qquad (27_2) \end{split}$$

$$G_{\theta} = \{ I_{1} [\ddot{\theta} - u_{2}^{1}\ddot{u}_{3}^{1} + \ddot{u}_{2}^{1}u_{2}^{1}\theta + 2u_{2}^{1}\dot{u}_{2}^{1}\dot{\theta} + u_{2}^{1}^{2}\ddot{\theta} - u_{3}^{1}\ddot{u}_{3}^{1}\theta - 2u_{3}^{1}\dot{u}_{3}^{1}\dot{\theta} - u_{3}^{1}^{2}\ddot{\theta}] - (I_{1} - I_{2} + I_{3})$$

$$[\dot{u}_{2}^{1}\dot{u}_{3}^{1} - \dot{u}_{2}^{1}^{2}\theta + \dot{u}_{3}^{1}^{2}\theta] - E_{1} [\theta'' - u_{2}^{1}u_{3}^{1}' + u_{2}^{1}' u_{2}^{1}\theta + 2u_{2}^{1}u_{2}^{1}\theta' + u_{2}^{1}^{2}\theta'' - u_{3}^{1}u_{3}^{1}'\theta - 2u_{3}^{1}u_{3}^{1}\theta' + u_{2}^{1}^{2}\theta''] + (E_{1} - E_{2} + E_{3}) [u_{2}^{1}u_{3}^{1} - u_{2}^{1}^{2}\theta + u_{3}^{1}^{2}\theta] \} = 0$$

$$(27_{3})$$

As regards the boundary conditions, by using Eq. (14) to write $\delta u_1'$ in terms of $\delta u_2'$, $\delta u_3'$, expanding H_k in power series and eliminating θ_2 , θ_3 , u_1 , the following explicit conditions are obtained:

$$G_1 \delta u_1 \Big|_{\mathfrak{Q}}^{\mathfrak{L}} = 0 \qquad G_2 \delta u_2 \Big|_{\mathfrak{Q}}^{\mathfrak{L}} = 0 \qquad G_3 \delta u_3 \Big|_{\mathfrak{Q}}^{\mathfrak{L}} = 0 \qquad (28_{1,2,3})$$

$$H_2 \stackrel{*}{\delta} u_2^{\dagger} \Big|_{0}^{\ell} = 0 \qquad H_3 \stackrel{*}{\delta} u_3^{\dagger} \Big|_{0}^{\ell} = 0 \qquad H_{\theta} \stackrel{*}{\delta} \theta \Big|_{0}^{\ell} = 0 \qquad (28_{4,5,6})$$

where:

$$H_{2}^{**} = H_{2} - u_{2}^{*}H_{1} = E_{3}[u_{2}^{"} + u_{2}^{"}u_{2}^{"}] + E_{1}u_{2}^{"}\theta\theta' + E_{2}u_{2}^{"}u_{3}^{"}u_{3}^{"} - (E_{2} - E_{3})[u_{3}^{"}\theta - u_{2}^{"}\theta^{2}]$$
(29₁)

$$H_{3}^{*} = H_{3} - u_{3}^{*}H_{1} = E_{2}[u_{3}^{"} + u_{2}^{'}u_{2}^{"}u_{3}^{"} + u_{3}^{"}^{2}u_{3}^{"}] - E_{1}[u_{2}^{"}\theta' + u_{3}^{"}\theta\theta' - u_{2}^{"}^{2}u_{3}^{"}] - (E_{2} - E_{3})[u_{2}^{"}\theta + u_{3}^{"}\theta^{2}] (29_{2})$$

$$H_{\theta} = E_{1}[\theta' - u_{2}'u_{3}'' + u_{2}'u_{2}''\theta + u_{2}'^{2}\theta' - u_{3}'u_{3}''\theta - u_{3}'^{2}\theta']$$
(29₃)

Eq. (28_1) is used to determine $u_1(0)$ and $G_1(\ell)$. The remaining Eqs. (28_2) - (28_6) are the boundary conditions for the nonlinear system (27), which allows to study moderately large oscillations of a beam having two flexural and one torsional components of equal order; the system and the boundary conditions show both quadratic and cubic nonlinearities.

If beams with high torsional rigidity are referred to (compact beams), the previous system can be simplified by neglecting the torsional and flexural inertia terms. From Eq. (27_3) it ensues that θ is a second-order variable as well, which can be related to u_2 , u_3 by neglecting terms of order higher than three in that equation, and integrating it. Successively substituting θ into Eqs. $(27_{1,2})$ two integro-differential equations in the variables u_2 , u_3 are obtained, which contain cubic nonlinearities only. They were deduced already by Crespo da Silva and Glynn [4] referring to a fixed-free beam and are accurate for studying flexural-flexural

oscillations of compact beams in which the angle of twist θ is forced statically. As regards the boundary conditions, it is worthwhile to notice that, for compact beams, the nonlinear conditions are satisfied by the corresponding linearized ones for many constraints of practical interest [8].

4. PERTURBATION EQUATIONS

In the following development reference will be made to the general system (27), since it allows for studying the effects of nonlinear coupling between flexural and torsional oscillations of the beam.

The following non-dimensional quantities are introduced:

$$\tilde{u}_2 = u_2/\ell \qquad \tilde{u}_3 = u_3/\ell \qquad \tilde{s} = s/\ell \qquad \tau = \omega t \tag{30}$$

 ω being whatever real frequency of the beam, and the solutions to the equations of motion are approximated by one mode as:

$$\theta_1 = f_1(s)q_1(\tau)$$
 $u_2 = f_2(s)q_2(\tau)$ $u_3 = f_3(s)q_3(\tau)$ $(31_{1,2,3})$

where $f_{\cdot}(s)$ are the eigenfunctions of the linearized problem and $q_{\cdot}(\tau)$ are unknown time functions. The Galerkin procedure is used to transform the partial differential equations into three ordinary equations with quadratic and cubic nonlinearities:

$$m_{1}\ddot{q}_{1} + k_{1}q_{1} = F(\dot{q}_{2}\dot{q}_{3}, q_{2}\ddot{q}_{3}, q_{2}q_{3}, q_{1}\dot{q}_{2}^{2}, q_{1}\dot{q}_{3}^{2}, q_{1}q_{2}\ddot{q}_{2}, \dot{q}_{1}q_{2}\dot{q}_{2}, \ddot{q}_{1}q_{2}^{2}, q_{1}q_{3}\ddot{q}_{3}, \dot{q}_{1}q_{3}\ddot{q}_{3}, \\ \ddot{q}_{1}q_{2}^{2}, q_{1}q_{2}^{2}, q_{1}q_{3}^{2})$$

$$(32_{1})$$

$$m_{2}\ddot{q}_{2} + k_{2}q_{2} = F(\dot{q}_{1}\dot{q}_{3}, q_{1}\ddot{q}_{3}, q_{1}q_{3}, q_{2}\dot{q}_{2}^{2}, q_{1}\ddot{q}_{1}q_{2}, q_{1}^{2}\ddot{q}_{2}, q_{1}\dot{q}_{1}\dot{q}_{2}, q_{2}\dot{q}_{3}^{2}, q_{2}^{2}\dot{q}_{3}^{2}, q_{1}^{2}q_{2}, q_{2}q_{3}^{2},$$

$$q_{2}q_{3}\ddot{q}_{3}, q_{2}^{2}\ddot{q}_{2})$$

$$(32_{2})$$

$$m_{3}\ddot{q}_{3} + k_{3}q_{3} = F(\dot{q}_{1}\dot{q}_{2}, q_{1}\ddot{q}_{2}, \ddot{q}_{1}q_{2}, q_{1}q_{2}, \dot{q}_{2}^{2}q_{3}, q_{2}\ddot{q}_{2}q_{3}, q_{3}\dot{q}_{3}^{2}, q_{1}^{2}\ddot{q}_{3}, q_{1}\dot{q}_{1}\dot{q}_{3}, q_{1}\ddot{q}_{1}q_{3},$$

$$q_{2}\dot{q}_{2}\dot{q}_{3}, q_{2}^{2}\ddot{q}_{3}, q_{3}^{2}q_{3}, q_{3}^{2}q_{3}, q_{3}^{2}\ddot{q}_{3})$$

$$(32_{3})$$

The dot now denotes the derivative with respect to τ . The coefficients of the 1i near and nonlinear terms depend on the elastic, geometric and inertial properties of the beam and on numerous integrals of products of the eigenfunctions f as well as on the boundary values of such products. F means function of the arguments.

Analysis of the nonlinear terms in Eqs. (32) gives some general indications with regard to the phenomena which can occur in the finite free dynamics of the beam. The occurrence of nonlinear terms of pure nature (q_2^2, q_3^3) in the equations for the flexural variables assures that the corresponding monofrequent oscillations can exist under particular initial conditions for the remaining variables, with frequency dependent on the amplitude of oscillation and temporal law different from the linear one; instead the torsional monofrequent oscillation is always coincident with the linear oscillation. This is bound up with the torsional curvature μ_1 being linear in the angle of twist θ_1 and with the relevant constitutive law having been assumed linear as well. A more correct analysis of oscillations having a prevailing torsional component would require consideration of a nonlinear constitutive law between torque and torsional curvature. However Eqs. (32) are ac curate for studying cases in which either q_1,q_2,q_3 are of the same order or q_1 is of order higher than q_2,q_3 . In such cases phenomena of modal coupling and internal resonance among the three variables can be analysed. In the first case the beam can undergo flexural-flexural-torsional vibrations, in the second case flexuralflexural vibrations in which the angle of twist is forced dynamically at an higher order.

To obtain the solution to system (32) the multiple scale method [1] is adopted. A perturbation parameter ϵ of the order of the amplitude is introduced and the variables q are considered functions of a sequence of independent time scales T_0 , T_1 ,... T_n , which are related to τ by the expressions $T_n = \epsilon^n \tau$, and are expanded in power of ϵ :

$$q_i = \epsilon q_{i_1} (T_0, T_1, T_2) + \epsilon^2 q_{i_2} (T_0, T_1, T_2) + \epsilon^3 q_{i_3} (T_0, T_1, T_2) + O(\epsilon^4 \tau)$$
 (33)

By expressing the time derivatives in terms of the T_n variables and substituting Eqs. (33) into Eqs.(32), a system of three partial differential equations with the unknowns q_{ij} is obtained; from this, equating coefficients of like powers of ε , a sequence of three linear systems is obtained – at the orders ε , ε^2 , ε^3 – in each of which the non-linear part is known from the lower-order solutions [8]. The problem is completed with the initial conditions:

$$q_i(0) = \varepsilon \overline{q}_i$$
 $\dot{q}_i(0) = \varepsilon \dot{\dot{q}}_i$ (34)

from which, accounting for Eqs. (33), the conditions to be associated with each system of the above mentioned sequence are obtained.

5. STUDY OF THE EQUATIONS AND SOLUTION IN ABSENCE OF INTERNAL RESONANCE

The periodic solution

$$q_{j1} = A_{j}(T_{1}, T_{2})e^{i\omega jT_{0}} + c.c.$$
 (35)

is adopted as the solution (generating solution) to the system of equations at the ε -order. In Eqs. (35) $\omega_j = \sqrt{k_j/m_j}$ is the frequency of the beam over the dimensionless time scale τ , $A_j(T_1,T_2)$ is an unknown complex function, c.c. and the overbar (e.g., $\overline{A_j}$) indicate the complex conjugate. Substitution of Eqs. (35) into the system at the ε^2 -order gives:

$$D_{00}q_{12} + \omega_{1}^{2}q_{12} = F[A_{2}A_{3}e^{i(\omega_{2}+\omega_{3})T_{0}}, \overline{A_{2}A_{3}}e^{i(\omega_{3}-\omega_{2})T_{0}}, iD_{1}A_{1}e^{i\omega_{1}T_{0}}] + c.c.$$
 (361)

$$D_{00}q_{22} + \omega_2^2 q_{22} = F[A_1A_3 e^{i(\omega_1 + \omega_3)T_0}, A_1\overline{A_3} e^{i(\omega_1 - \omega_3)T_0}, iD_1A_2 e^{i\omega_2T_0}] + c.c.$$
 (36₂)

$$D_{00}q_{32} + \omega_3^2 q_{32} = F[A_1 A_2 e^{i(\omega_1 + \omega_2)T_0}, A_1 A_2 e^{i(\omega_1 - \omega_2)T_0}, iD_1 A_3 e^{i\omega_3 T_0}] + c.c.$$
 (36₃)

where the notations $D_i = \partial/\partial T_i$ and $D_{ij} = \partial^2/\partial T_i \partial T_j$ are used for the sake of simplicity.

Analysis of system (36) shows that internal resonance occurs at the order ϵ^2 if the linear frequencies of the three components verify the conditions:

$$\omega_{j} + \omega_{h} = \omega_{k}$$
 (j,h,k = 1,2,3; j\neq h\neq k) (37)

All three components of the motion are involved in the energy exchange phenomenon which characterizes this internal resonance situation.

The case q_1 of order higher than q_2 and q_3 is now examined; in this case the generating solution (35) has two non-zero components only, i.e. $A_1(T_1,T_2)\equiv 0$. Equation (36₁) shows that, in absence of internal resonance, a torsional component of order ε^2 is forced dynamically from the flexural components provided these are both different from zero; this constitutes a classical phenomenon of nonlinear modal coupling. The same equation shows that a monofrequent planar flexural vibration can occur in conditions of internal resonance as well, with no torsional component, since zeroing of the secular term in Eq. (36₁) entails $A_2A_3=0$ and thus either $A_2=0$ or $A_3=0$. However flexural frequencies do not change at this order.

5.1 Absence of internal resonance at the ε^2 -order

Coming back to the case q_1 , q_2 , q_3 of the same order, zeroing of the secular terms in Eqs. (36) gives $A_j=A_j(T_2)$ showing no frequency correction occurs at this order for the j-th component. The solution to system (36) is then obtained. By substituting it and the generating solution into the system of perturbation equations at the order ε^3 , the following equations are obtained:

$$D_{00}q_{13} + \omega_1^2 q_{13} = F[A_1 A_2^2 e^{i(\omega_1 + 2\omega_2)T_0}, \overline{A_1} A_2^2 e^{i(2\omega_2 - \omega_1)T_0}, A_1 A_3^2 e^{i(\omega_1 + 2\omega_3)T_0},$$

$$\overline{A}_{1}A_{3}^{2}e^{i(2\omega_{3}-\omega_{1})T_{0}}, (A_{2}B_{3}+A_{3}B_{2})e^{i(\omega_{2}+\omega_{3})T_{0}}, (\overline{A}_{2}B_{3}+A_{3}\overline{B}_{2})$$

$$e^{i(\omega_{3}-\omega_{2})T_{0}}, (A_{1}A_{2}\overline{A}_{2}, A_{1}A_{3}\overline{A}_{3}, iD_{2}A_{1})e^{i\omega_{1}T_{0}}] + c.c. (38_{1})$$

$$D_{00}q_{23} + \omega_{2}^{2}q_{23} = F[A_{2}^{3}e^{3i\omega_{2}T_{0}}, A_{1}^{2}A_{2}e^{i(\omega_{2}+2\omega_{1})T_{0}}, A_{1}^{2}\overline{A}_{2}e^{i(2\omega_{1}-\omega_{2})T_{0}},$$

$$A_{2}A_{3}^{2}e^{i(\omega_{2}+2\omega_{3})T_{0}}, \overline{A}_{2}A_{3}^{2}e^{i(2\omega_{3}-\omega_{2})T_{0}}, (A_{1}B_{3}+A_{3}B_{1})e^{i(\omega_{1}+\omega_{3})T_{0}},$$

$$(\overline{A}_{1}B_{3}+A_{3}\overline{B}_{1})e^{i(\omega_{3}-\omega_{1})T_{0}}, (A_{2}^{2}\overline{A}_{2},A_{1}\overline{A}_{1}A_{2}, A_{2}A_{3}\overline{A}_{3},iD_{2}A_{2})$$

$$e^{i\omega_{2}T_{0}}] + c.c.$$

$$(38_{2})$$

$$D_{00}q_{33} + \omega_{3}^{2}q_{33} = F[A_{3}^{3}e^{3i\omega_{3}T_{0}}, A_{2}^{2}A_{3}e^{i(\omega_{3}+2\omega_{2})T_{0}}, A_{2}^{2}\overline{A}_{3}e^{i(2\omega_{2}-\omega_{3})T_{0}}, A_{1}^{2}A_{3}$$

$$e^{i(2\omega_{1}+\omega_{3})T_{0}}, A_{1}^{2}\overline{A}_{3}e^{i(2\omega_{1}-\omega_{3})T_{0}}, (A_{1}B_{2}+A_{2}B_{1})e^{i(\omega_{1}+\omega_{2})T_{0}},$$

$$(\overline{A}_{1}B_{2}+A_{2}\overline{B}_{1})e^{i(\omega_{2}-\omega_{1})T_{0}}, (A_{3}^{2}\overline{A}_{3}, A_{2}\overline{A}_{2}A_{3}, A_{1}\overline{A}_{1}A_{3}, iD_{2}A_{3})$$

$$e^{i\omega_{3}T_{0}} + c.c.$$

$$(38_{3})$$

The amplitudes B_j of the homogeneous solution to system (36) appear in Eqs.(38), for which the same dependance on T_1 and T_2 as for the amplitudes A_j is assumed.

Analysis of system (38) gives the conditions under which internal resonance occurs at the order ε^3 . Since conditions (37) were excluded, it occurs if:

$$\omega_{i} = \omega_{k}$$
 (j,k = 1,2,3) (39)

In this case two components of the motion only are involved in the resonance phenomenon; as a particular case, resonance involving all three components can still occur if $\omega_1 = \omega_2 = \omega_3$.

The resonance between the two flexural components, which occurs if $\omega_2 = \omega_3$, was studied by Crespo da Silva and Glynn [9] referring to a fixed-free beam with high torsional rigidity; in that case the torsional component is simply forced statically by the flexural variables, i.e. it oscillates with the nonlinear frequency $\omega_2 = \omega_3$. Instead, when the system with three components is considered (beams with low torsional rigidity), the torsional variable lives in the beam oscillation with a constant amplitude and with its natural frequency modulated on the slow scale T_2 by the amplitudes of the remaining two variables.

If the case q_1 of order higher than q_2 , q_3 is examined, Eq. (38₁) shows that the angle of twist is never forced at the ϵ^3 -order, which entails some interesting consequences.

In absence of whatever resonance, a motion with prevailing flexural components having frequencies dependent on the two amplitudes occurs, in which a forced torsional component of order ϵ^2 exists. If either $A_2\equiv 0$ or $A_3\equiv 0$ as well, corrected plane flexural monofrequent oscillations occur.

In conditions of resonance at the ε^3 -order involving the torsional frequency, two distinct cases can be considered. a) If one flexural frequency only is involved (e.g., $\omega_1=\omega_2\neq\omega_3$), the same motions as in absence of whatever resonance occur, i.e. either a prevailing flexural vibration with two components having nonlinear frequencies or, in particular, flexural monofrequent vibrations. b) If both flexural frequencies are involved ($\omega_1=\omega_2=\omega_3$), resonance occurs between the two flexural variables, the ε^2 -order forced torsional component always being present in the oscillation.

5.2 Absence of internal resonance at the ε^3 -order

Considering again q_1 , q_2 , q_3 of the same order, the zeroing of the secular terms in Eqs. (38), when the polar forms:

$$A_k(T_2) = a_k(T_2)/2 e^{i\phi_k(T_2)}$$
 (40)

are introduced and the real and imaginary parts are separated, provides a differential system with respect to time scale T_2 having the unknowns a_k , ϕ_k , whose solution reads:

$$a_k = cost$$
 $\phi_k = \hat{\phi}_k \tau + \phi_k^0$ (k=1,2,3) (41) (42)

The functions $\hat{\phi}_k$ depend on the amplitudes a_k and the linear frequencies of the three components. The values of a_k and $\varphi_k^0 = \varphi_k(0)$ are determined by means of the initial conditions at the ϵ -order. The solution to system (38) is then obtained.

To write the temporal laws of motion in circular form, the amplitude B_j and C_i of the homogeneous solutions to systems (36) and (38) are written as:

$$B_{j}(T_{2}) = b_{j}/2 e^{i\psi} j^{(T_{2})}$$
 $C_{j}(T_{2}) = c_{j}/2 e^{i\chi} j^{(T_{2})}$ (43_{1,2})

where the phases ψ_i , χ_i depend on T_2 like the phases ϕ_i :

$$\psi_{\mathbf{j}} = \widehat{\phi}_{\mathbf{j}} \tau + \psi_{\mathbf{j}}^{0} \qquad \qquad \chi_{\mathbf{j}} = \widehat{\phi}_{\mathbf{j}} \tau + \chi_{\mathbf{j}}^{0} \qquad (44_{1,2})$$

The values of the amplitudes b_j , c_j and of the initial phases ψ_j^0 , χ_j^0 are determined by means of the initial conditions at the order ϵ^2 and ϵ^3 respectively. The following expressions are finally obtained for the temporal laws of the motion:

$$\begin{aligned} \mathbf{q}_{1} &= \varepsilon \mathbf{a}_{1} \cos \Phi_{1} + \varepsilon^{2} \{ \mathbf{F} \left[\mathbf{a}_{2} \mathbf{a}_{3} \cos \left(\Phi_{3} \pm \Phi_{2} \right), \mathbf{b}_{1} \cos \Psi_{1} \right] \} + \varepsilon^{3} \{ \mathbf{F} \left[\mathbf{a}_{1} \mathbf{a}_{2}^{2} \cos \left(2 \Phi_{2} \pm \Phi_{1} \right), \mathbf{a}_{1} \mathbf{a}_{3}^{2} \cos \left(2 \Phi_{3} \pm \Phi_{1} \right), \mathbf{a}_{2} \mathbf{b}_{3} \cos \left(\Psi_{3} \pm \Phi_{2} \right), \mathbf{a}_{3} \mathbf{b}_{2} \cos \left(\Psi_{2} \pm \Phi_{3} \right), \mathbf{c}_{1} \cos \mathbf{X}_{1} \} \end{aligned}$$

$$q_{2} = \varepsilon a_{2} \cos \Phi_{2} + \varepsilon^{2} \{ F[a_{1} a_{3} \cos(\Phi_{3} \pm \Phi_{1}), b_{2} \cos \Psi_{2}] \} + \varepsilon^{3} \{ F[a_{2}^{3} \cos 3\Phi_{2}, a_{2} a_{1}^{2} \cos(2\Phi_{1} \pm \Phi_{2}), a_{2} a_{3}^{2} \cos(2\Phi_{3} \pm \Phi_{2}), a_{1} b_{3} \cos(\Psi_{3} \pm \Phi_{1}), a_{3} b_{1} \cos(\Psi_{1} \pm \Phi_{3}), c_{2} \cos X_{2}] \}$$

$$(45)$$

$$\begin{aligned} \mathbf{q}_{3} &= \varepsilon \mathbf{a}_{3} \cos \Phi_{3} + \varepsilon^{2} \{ \mathbf{F} \left[\mathbf{a}_{1} \mathbf{a}_{2} \cos \left(\Phi_{2} \pm \Phi_{1} \right), \mathbf{b}_{3} \cos \Psi_{3} \right] \} + \varepsilon^{3} \{ \mathbf{F} \left[\mathbf{a}_{3}^{3} \cos 3\Phi_{3}, \mathbf{a}_{2}^{2} \mathbf{a}_{3} \cos \left(2\Phi_{2} \pm \Phi_{3} \right), \mathbf{a}_{1}^{2} \mathbf{a}_{3} \cos \left(2\Phi_{1} \pm \Phi_{3} \right), \mathbf{a}_{1}^{2} \mathbf{b}_{2} \cos \left(\Psi_{2} \pm \Phi_{1} \right), \mathbf{a}_{2}^{2} \mathbf{b}_{1} \cos \left(\Psi_{1} \pm \Phi_{2} \right), \mathbf{c}_{3} \cos X_{3} \} \end{aligned}$$

In equations (45) the phases Φ_i , Ψ_i , X_i read:

$$\Phi_{i} = \overline{\omega}_{i}\tau + \phi_{i}^{0} \qquad \Psi_{i} = \overline{\omega}_{i}\tau + \psi_{i}^{0} \qquad X_{i} = \overline{\omega}_{i}\tau + \chi_{i}$$
 (46)

 $\overline{\omega}_{i}$ being the nonlinear frequencies of the three configuration variables:

$$\overline{\omega}_{1} = \omega_{1} \left[1 + \frac{1}{8\omega_{1}^{2}} \left(\tilde{d}_{133} a_{3}^{2} - \tilde{d}_{122} a_{2}^{2} \right) \varepsilon^{2} \right]
\overline{\omega}_{2} = \omega_{2} \left[1 + \frac{1}{8\omega_{2}^{2}} \left(\tilde{d}_{233} a_{3}^{2} - \tilde{d}_{222} a_{2}^{2} - \tilde{d}_{112} a_{1}^{2} \right) \varepsilon^{2} \right]
\overline{\omega}_{3} = \omega_{3} \left[1 + \frac{1}{8\omega_{3}^{2}} \left(-\tilde{d}_{333} a_{3}^{2} - \tilde{d}_{223} a_{2}^{2} + \tilde{d}_{113} a_{1}^{2} \right) \varepsilon^{2} \right]$$
(47)

The coefficients d which appear in Eqs. (47) depend on the linear frequencies ω and on the beam properties.

6. CONCLUDING REMARKS

Accurate equations for studying flexural-flexural-torsional vibrations of inextensional beams have been obtained and a perturbation analysis up to ϵ^3 order has been developed. After identifying the conditions of internal resonance, the laws of motion (45) of the beam in absence of resonance have been obtained which allow to study modal coupling phenomena among the three configuration variables.

The equations put into light a strong modification of the temporal laws with respect to the linear ones. Indeed the motion of the i-th component is described by the superposition of several harmonics with frequencies combinations of the three nonlinear fundamental frequencies (47):

$$\overline{\omega}_{i}$$
, $\overline{\omega}_{j}^{\pm}\overline{\omega}_{k}$, $\overline{\omega}_{i}^{\pm}2\overline{\omega}_{j}$, $\overline{\omega}_{i}^{\pm}2\overline{\omega}_{k}$ (i,j,k=1,2,3;i\neq j\neq k)

 $3\overline{\omega}_{i}$ (i=2,3)

Harmonics having the same frequency $(\overline{\omega}_1, \overline{\omega}_1, \overline{\omega}_2)$ but different phases occur; such differences however reduce to zero if the particular case of zero initial velocity for all components is considered.

The relations (47) show that the nonlinear frequency of each variable depends on the squares of both its own amplitude of oscillation and the amplitudes of the remaining two variables. The dependance on its own amplitude does not occur for the frequency of torsional vibration, which is always coincident with the linear one in the monofrequent vibration.

7. REFERENCES

- 1. A.H. NAYFEH and D.T. MOOK 1979 Nonlinear Oscillations. New York; J. Wiley and Sons.
- 2. C. HO, R.A. SCOTT and J.G. EISLEY 1976 Journal of Sound and Vibration 47, 333-339. Non planar, non-linear oscillations of a beam. II. Free motions.
- 3. E.C. HAIGHT and W.W. KING 1971 J. of the Acoustical Society of America 52, 899-911. Stability of nonlinear oscillations of an elastic rod.
- 4. M.R.M. CRESPO da SILVA and C.C. GLYNN 1978 J. of Structural Mechanics 6, 437-461. Nonlinear flexural-flexural-torsional dynamics of inextensional beams. I Equations of motion. II Forced motions.
- 5. M.W. HYER 1978 Virginia Polytechnic Institute and State University, Dept. of Engineering Science and Mechanics, Report VPI-L-78-28. The effect of non linear curvature and inertia on the predictions for the planar response and stability of an inextensible base-excited cantilever.
- 6. A. DI CARLO and A. TATONE 1980 Proc. of the 5th Italian Congress of Theoretical and Applied Mechanics, AIMETA 2, 161-170. A rational beam model for the analysis of equilibrium bifurcation of beam systems in 3D (in Italian).
- 7. A. LUONGO, G. REGA, A. TATONE and F. VESTRONI 1982 Proc. International Conference on Finite Element Methods. Gordon and Breach, Science Publishers, New York. (Editors H. Guangqian and Y. K. Cheung) 2, 70-75. A finite element perturbational approach for the study of nonlinear free oscillations of a beam.
- 8. A. LUONGO, G. REGA and F. VESTRONI 1983 University of L'Aquila, Istituto di Scienza delle Costruzioni Report No. 69. Accurate nonlinear equations and a perturbation solution for the free nonplanar vibrations of inextensional beams.
- 9. M.R.M. CRESPO da SILVA and C.C. GLYNN 1979 Int.J. of Solids and Structures 15,209-219. Non-linear non-planar oscillations in fixed-free beams with support asymmetry.



PARAMETRIC VIBRATION IN LARGE BLADES ROTATING IN A GRAVITATIONAL FIELD

A.D.S. Barr¹ and T. Webster²

¹Department of Mechanical Engineering, University of Dundee, Scotland ²Yarrow Shipbuilders, Glasgow, Scotland

1. INTRODUCTION

Parametric vibration of structures is a generic term which relates to their motion when they are modelled by differential equations which include coefficients which are explicit functions of time. In fact the term is often reserved for situations in which the oscillation of the structure is effectively due to this time variation of parameters. The condition may then be referred to as parametric instability or as parametric resonance. However such structures will also in general be subjected to forced excitation in the usual way that is, by non-homogeneous terms in the describing differential equations. This sort of excitation is important in parametric structures just as it is in structures modelled with constant coefficients. A review of the literature of the field of parametric vibration can be found in references [1].

The basic problem considered in this paper is that of a long flexible elastic beam rotating about a horizontal axis passing through one end normal to its centre line. Such a beam is subjected to gravitational forces which vary from an effective compression when the beam is above its axis of rotation to a tension when it is below. The beam thus undergoes a time dependent variation in axial force. The lateral or bending motion of the beam is influenced by such axial loads, the bending frequencies tend to be reduced by axial compression and raised by axial tension. Thus the equations of motion for bending of the beam will include time dependent terms which account for the axial force. These terms are explicitly time dependent if the angle of rotation of the beam is regarded as given and if axial vibration of the beam is neglected.

The beam is therefore an example of a structure undergoing parametric excitation. If the rotation rate about the axis is constant the parametric excitation is periodic. This is not a necessary condition for periodicity but will be assumed to be true for simplicity in what follows.

As well as the lateral natural frequencies of the beam being influenced periodically by the gravitational loading they are also altered by the centrifugal field due to the rotation. This can be thought of as a tension field rotating with the beam and acting to stiffen it flexurally. The stiffening effect depends on the angle of the plane of flexure of the beam relative to the plane of rotation. For instance vibration in a direction normal to the plane of rotation is generally much more affected by the centrifugal field than bending vibration occurring in the plane of rotation. In any event, the centrifugal field for increasing rotational speeds very quickly dwarfs the relatively small periodic changes due to the varying gravitational field and this makes the problem somewhat different from the usual class of problems in parametric structural vibration. In fact it may make it virtually impossible for parametric instability to occur at all.

The problem is interesting in its own right but it clearly is directly relevant to the oscillation of the blades of large wind turbine generators.

2. EQUATIONS OF MOTION

For the purpose of analysis the simple one dimensional Bernoulli-Euler

level of modelling of the beam dynamics will be considered adequate, that is, the effects of shear and rotatory inertia and so forth will be neglected. While equations will be derived for a general beam element further discussion of the motion will usually be restricted for simplicity to the case of a lumped mass at the end of a weightless beam. It is thought that this rather drastic specialisation will not lose any of the essential features of the dynamics at least for the first mode. Flexural vibration along one principal direction only is considered. More general theories including pretwist and torsion are feasible but confusing for present purposes.

2.1 Beam Bending in Direction α from Axis of Rotation

The beam is taken as having mass per unit length m and stiffness EI in the direction of bending. If a triad of moving unit vectors, \vec{i} , \vec{j} , \vec{k} is taken at the base of the beam, that is at the axis, with \vec{i} directed along the axis of the beam and \vec{k} along the axis of rotation, the situation for an element dx of the beam at a typical angle $\theta(t)$ from the vertical is as shown in Fig. 1.

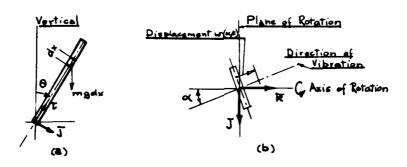


Fig. 1. Beam element (a) configuration and axes
(b) cross-section and direction of motion

In terms of the moving vectors \vec{i} , \vec{j} , \vec{k} the position vector \vec{r} of the typical element is $\vec{r} = x\vec{i} + (-w\sin\alpha)\vec{j} + (w\cos\alpha)\vec{k}$ while the angular velocity of the vector system is $\vec{\omega} = \theta \vec{k}$ where the dot signifies the time rate as usual. The acceleration of the element can be evaluated and is

$$\frac{\ddot{x}}{\ddot{r}} = [\ddot{x} - x\dot{\theta}^2 + 2\dot{w}\dot{\theta}\sin\alpha + w\ddot{\theta}\sin\alpha]\ddot{i} + [-\ddot{w}\sin\alpha + w\dot{\theta}^2\sin\alpha + 2\dot{x}\dot{\theta} + x\dot{\theta}]\ddot{j} + [\ddot{w}\cos\alpha]\ddot{k}$$

If equation (1) is rewritten as $\bar{r} = a_1 \bar{i} + a_2 \bar{j} + a_3 \bar{k}$ then the equations of motion of the beam element defined by planes normal to the x axis and dx apart as indicated in Fig. 2 can be written, assuming deflections and slopes to be small, as follows.

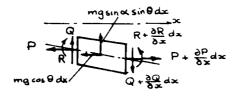


Fig. 2. Forces P and Q and moment R on beam element

$$\text{ma}_{1} = \frac{\partial P}{\partial x} - \text{mgcos}\theta; \quad m(a_{3}\cos\alpha - a_{2}\sin\alpha) = \frac{\partial Q}{\partial x} - \text{mgsin}\alpha\sin\theta; \\
 0 = \frac{\partial R}{\partial x} - Q + P\frac{\partial w}{\partial x}$$
(2)

Along with equations (2) we have the usual moment-curvature relation R = -EIw'' where dashes indicate differentiation with respect to x. Using the acceleration components (1) the equations (2) become

$$\frac{\partial P}{\partial x} = m(\ddot{x} - x\dot{\theta}^2 + 2\dot{w}\dot{\theta}\sin\alpha + w\ddot{\theta}\sin\alpha) + mg\cos\theta$$

$$\frac{\partial Q}{\partial x} = m(\ddot{w} - w\dot{\theta}^2\sin^2\alpha - 2\dot{x}\dot{\theta}\sin\alpha - x\dot{\theta}\sin\alpha) + mg\sin\alpha\sin\theta$$

$$\frac{\partial R}{\partial x} = Q - P\partial w/\partial x$$

$$\frac{\partial^2 w}{\partial x^2} = -R/EI$$
(3)

The moment R and the shear Q can be eliminated from (3) if desired to give the two equations

$$(EIw'')'' - (Pw')' + m(\ddot{w} - w\dot{\theta}^2 \sin^2 \alpha - 2\dot{x}\dot{\theta}\sin \alpha - x\theta\sin \alpha) = -mg\sin\alpha\sin\theta$$

$$P' = m(\ddot{x} - x\dot{\theta}^2 + 2\dot{w}\dot{\theta}\sin\alpha + w\theta\sin\alpha) + mg\cos\theta$$

$$(4)$$

The second equation of (4), neglecting the term \ddot{x} , can be integrated from x to the far end of the beam $x=\ell$ and substitution for P(x) and P'(x) made in the first equation. The result is a very complicated nonlinear integro-differential equation in w with time dependent coefficients depending on $\theta(t)$. If we simplify this equation by neglecting \mathring{x} , $\mathring{\theta}$, $P(\ell)$ and all nonlinear terms then the governing equation for w is

$$(EIw'')'' + (g\cos\theta) \int_{X}^{\ell} mdx - \dot{\theta}^{2} \int_{X}^{\ell} mxdx)w'' - (mg\cos\theta - mx\dot{\theta}^{2})w'$$

$$+ m(\ddot{w} - w\dot{\theta}^{2}\sin^{2}\alpha) = -mg\sin\alpha\sin\theta.$$
 (5)

An approximate solution of equation (5) could be obtained by for instance expanding w in a sum of the eigenfunctions of the non-rotating beam and applying Galerkin's method. Here however it is preferred, hopefully without losing any of the essential mechanics of the problem, to simplify matters considerably by taking a mass distribution in the form of a point mass at the free end of a massless beam. Hence the problem is specialised to the case $m(x) = M\delta(x-\ell)$ where M is the point mass at $x = \ell$, located by the δ -function.

The equation of motion for M is most directly obtained by using equations (3). The lateral displacement of M is denoted by W. Integrating the first two of equations(3) and using the end conditions $P(\ell) = Q(\ell) = 0$ gives, neglecting \dot{x} and \ddot{x} terms

$$P(x) = -Mg\cos\theta - M(\ell\theta^2 + 2\theta\theta\sin\alpha + W\theta\sin\alpha)$$

$$Q(x) = -Mg\sin\alpha\sin\theta - M(W - W\theta^2\sin^2\alpha - \ell\theta\sin\alpha)$$
(6)

It is clear from these equations that P and Q are not functions of x. The third and fourth of equations (3) can be used to eliminate the bending moment R and give the differential equation for the beam displacement shape in terms of P and Q and the end deflection W. Thus, $w'' - (P/EI)w = -(P/EI)W + Q(\ell - x)EI$, and this equation is easily solved incorporating the end conditions $w(\ell) = W$, w(0) = w'(0) = 0. The last two conditions are those appropriate to a cantilever fixing at x = 0. This solution provides an expression for Q in terms of W and P, in fact $Q/W = (P/\ell)/[1 - (\tanh 2/4\ell)]$, where $a^2 = (P/EI)$. This can be approximated by the expression $Q/W \cong (3EI/\ell^3) + (6P/5\ell)$.

Substituting from this in the second of equation (6) and substituting for P from the first gives the final differential equation for W. This takes the form

$$\frac{3EI}{\hbar W} + {\frac{3EI}{\ell^3} + M\dot{\theta}^2 (\frac{6}{5} - \sin^2 \alpha) - \frac{6}{5\ell} Mg\cos\theta}W = M\ell\theta\sin\alpha - Mg\sin\alpha\sin\theta}
+ \frac{12M}{5\ell} \sin\alpha W\dot{\theta}\dot{\theta} + \frac{6M}{5\ell} \sin\alpha W^2\dot{\theta}.$$
(7)

If the rotation rate $\dot{\theta}$ is taken as a constant Ω and if the nonlinear term WW is ignored, equation (7) takes on the simple form

$$\frac{3EI}{MW} + \{\frac{3EI}{\ell^3} + M\Omega^2(\frac{6}{5} - \sin^2\alpha) - \frac{6Mg}{5\ell}\cos\Omega t\}W = - Mg\sin\alpha\sin\Omega t$$

The extreme cases of this equation are for $\alpha = 0$ and for $\alpha = \pi/2$. Thus for $\alpha = 0^{\circ}$; motion out of plane of rotation

$$M\ddot{W} + \{\frac{3EI}{L^3} + \frac{6}{5}M\Omega^2 - \frac{6}{5}\frac{Mg}{L}\cos\Omega t\}W = 0$$
 (8)

for $\alpha = 90^{\circ}$; motion in plane of rotation

$$M\ddot{W} + \left\{\frac{3EI}{\ell^3} + \frac{1}{5}M\Omega^2 - \frac{6}{5}\frac{Mg}{\ell}\cos\Omega t\right\}W = -Mg\sin\Omega t$$
 (9)

Examination of these equations shows that the non-rotating flexural stiffness $(3EI/\ell^3)$ is increased by the centrifugal stiffening to an extent which is much greater for out of plane motion. The parametric excitation is due to the gravity field while in the case of in-plane motion gravity also provides a non-homogeneous or forcing term -Mgsin Ω t.

2.2 Beam not Normal to Axis of Rotation

As a slight extension of the problem considered in 2.1 we now examine briefly what additional terms are introduced by having the beam's free centreline set at angle β to the plane of rotation which is still considered to be vertical. The undistorted beam or blade would then describe a cone of half angle $(\pi/2)$ - β about the horizontal axis of rotation (see Fig. 3).

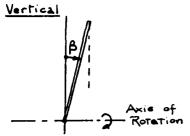


Fig. 3. Blade set at β

to rotation plane.

Restricting attention to the case of out of 'plane' motion (α = 0°) and taking again the simple case of an end mass on a light beam, the equation for this case, corresponding to equation (8) for β =0 is

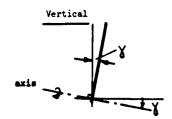
$$M\ddot{W} + \{(\frac{3EI}{\ell^3}) + \frac{6}{5}M\Omega^2\cos^2\beta - M\Omega^2\sin^2\beta - \frac{6}{5}\frac{Mg}{\ell}\cos\beta\cos\Omega t\}W =$$

$$Mgsin\beta cos\Omega t - M\Omega^2 lsin\beta cos\beta$$
 (10)

The angle β has therefore very slightly altered the centrifugal stiffening and the parametric excitation but it has introduced on the right hand side a DC and a periodic forcing term.

2.3 Beam's Plane of Rotation Inclined to Vertical

As a different variation on the problem of 2.1, the plane of rotation is now taken to be at an angle γ to the vertical so that the axis of rotation is also at γ to the horizontal (see Fig. 4).



In this case, again for the one degree of freedom problem vibrating out of the plane of rotation the equation of motion is

$$M\ddot{W} + \left\{ \frac{3EI}{\ell^3} + \frac{6}{5} M\Omega^2 - \frac{6}{5} \frac{Mg}{\ell} \cos \gamma \cos \Omega t \right\} W = Mg \sin \alpha \qquad (11)$$

Fig. 4. Blade rotating which is similar to equation (8) but with a slight modification of the parametric excitation term and the addition of a DC term to the right hand side.

PARAMETRIC INSTABILITY

The differential equations derived above all include a periodic coefficient on the bending deflection W. The deflection is thus under parametric excitation and for some values of the parameters a growing oscillation or parametric instability of W might be expected. To investigate this further the equation can be rewritten in a way that will allow its easy comparison with the Mathieu equation for which the stability properties are well documented.

Thus if the homogeneous equation (8) for out of plane vibration is considered for example, it can be rewritten in the form

$$\ddot{\mathbf{W}} + \omega_{\mathbf{r}}^2 (1 - \varepsilon_{\mathbf{r}} \cos \Omega \mathbf{t}) \mathbf{W} = 0$$
 (12)

The quantity $\boldsymbol{\epsilon}_{\boldsymbol{0}}$ is the magnitude of the parametric excitation when the rotation speed is negligible compared with $\omega_{\rm O}$. For finite Ω the parameter is $\epsilon_{\rm r}$ which is less than ε_0 .

This equation (12) is a typical form for a parametrically excited structure but it differs from the usual situation in that the natural frequency ω_r is an increasing function of the parametric excitation frequency Ω . Further, the excitation parameter ε_r is a decreasing function of Ω . These two features completely change the stability of equation (12) and some of the instability zones which would normally be associated with it may be unattainable.

To see this more clearly the equation (12) can be changed to the canonical Mathieu form by making the transformations

$$z = \Omega t/2$$
, $a = (2 \omega_r/\Omega)^2$, $q = \frac{1}{2} (2\omega_r/\Omega)^2 \varepsilon_r$ (14)

so that equation (12) becomes

$$\frac{\mathrm{d}^2 W}{\mathrm{d}z^2} + (a - 2q\cos 2z)W = 0 \tag{15}$$

The a, q, plane of equation (15) is divided into stable and unstable areas, maps and details of the structure of the regions can be found in references[2] and [3]. For engineering purposes it is more meaningful to have the stability regions on the plane of $(\Omega/2\omega_r)$ against ϵ_r which can be arranged using the transformation in (14).

The stability map is indicated in Fig. 5. For a given system ε_r starts as ε_0 on the abscissa where Ω = 0. For increasing Ω , ε_r reduces along the curve given by equations(13). Such curves are shown as dotted lines. The relationship is

$$\varepsilon_{\mathbf{r}} = \varepsilon_{\mathbf{0}} [1 - 4k(\Omega/2\omega_{\mathbf{r}})^2]$$
 (16)

where k is the rotation augmentation factor of the natural frequency being (6/5) for out-of-plane vibration (equation (13)) and (1/5) for in-plane vibration. In general $k = (6/5) - \sin^2\alpha$ for a concentrated mass moving at α to the axis of rotation, see section 2.1. It can be seen that $\epsilon_r \to 0$ for $(\Omega/2\omega_r) = 1/2\sqrt{k}$ which is 0.4564 for out-of-plane motion and about 1.118 for in-plane motion. This is also the maximum value that can be reached by the parameter $(\Omega/2\omega_r)$ for very large Ω . It can be noted that the excitation parameter ϵ_0 is related to the static buckling load of the blade. If the Euler buckling load is $P_E = (\pi^2 EI/4\ell^2)$ and the gravity load Mg = κP_E where κ is a number then ϵ_O = $(\pi^2 \kappa/10)$. For $\kappa = 1$, ϵ_0 has a value of about 0.987.

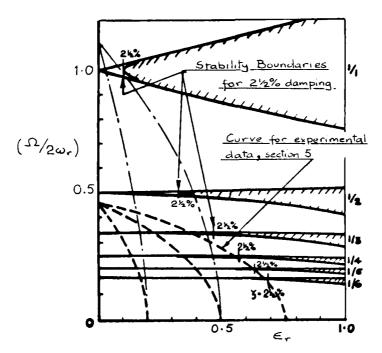


Fig.5. Stability diagram for rotating blade. Typical operating characteristics; ---- α = 0°,— - — α = 90°

The unstable zones are the shaded areas of Fig. 5. They emanate at $\varepsilon_{\mathbf{r}}=0$ from the points 1, 1/2, 1/3, 1/4, etc. and become progressively narrower. It can be seen that the out-of-plane motion broken curves cross only the higher order regions and never reach the really significant instabilities around $\frac{1}{2}$ and 1. The in-plane curves cross all the unstable zones. For intermediate cases instability zones are included up to $(\Omega/2\omega_{\mathbf{r}})=0.4564/\sqrt{(1-\frac{1}{6}\sin^2\alpha)}$. Thus if attention is restricted to out-of-plane motion there are only a few narrow speed zones in which parametric instability might arise. Further, in the presence of damping the instability zones retreat from the $(\Omega/2\omega_{\mathbf{r}})$ axis and this effect is greater for the higher order zones. If the damping ratio is ζ the unstable zone associated with $(\Omega/2\omega_{\mathbf{r}})=1/k$ starts at approximately $\varepsilon_{\mathbf{r}}=(4\zeta)^{1/k}$.

Experimental work simulating this case did show significant amplitudes of motion in the neighbourhood of the rotational speeds $(\Omega/2\omega_r)$ = 1/6, 1/5, 1/4. Such motion may however be associated also with forced vibration and this question is examined theoretically in the following section.

4. FORCED VIBRATION

Equation (10) covers the case of the flexural motion at $\alpha=0$ of a blade which is slightly inclined at angle β to the rotation plane. It thus simulates very roughly any initial lack of straightness of the blade. The homogeneous part of the equation has the same structure as before but there are now non-homogeneous terms, one constant or DC, and the other periodic at frequency Ω .

The equation can be written

$$\ddot{W} + \{\omega_0^2 + \Omega^2 (\frac{6}{5}\cos^2\beta - \sin^2\beta) - \frac{6g}{5l}\cos\beta\cos\Omega t\}W = g\sin\beta\cos\Omega t - \Omega^2 l\sin\beta\cos\beta$$
 (17)

where ω_0^2 is as defined in equation (13). The rotating gravity-free blade now has frequency $\omega_{_{T}}$ given by

$$\omega_{r}^{2} = \omega_{o}^{2} + k\Omega^{2} = \omega_{o}^{2} + (\frac{6}{5}\cos^{2}\beta - \sin^{2}\beta)\Omega^{2}$$
 (18)

If the following transformations are incorporated in equation (17),

$$\varepsilon_{o} = (6g\cos\beta/5l\omega_{o}^{2}), \quad \varepsilon_{r} = \varepsilon_{o}\omega_{o}^{2}/\omega_{r}^{2}$$

$$z = (\Omega t/2), \quad a = (2\omega_{r}/\Omega)^{2}, \quad 2q = (2\omega_{r}/\Omega)^{2}\varepsilon_{r}$$

$$y = (W/l)$$
(19)

then it is found to reduce to the form,

$$\frac{d^2y}{dz^2} + (a - 2q\cos 2z)y = A\cos 2z + B$$
 (20)

where A =
$$\frac{5}{3}$$
qtan β , B = $-2\sin 2\beta$

Equation (20) is a non-homogeneous Mathieu equation. In general we are interested in the steady-state response of y to the input on the right hand side but in particular we wish to establish whether there are resonance responses at relatively low values of $(\Omega/2\omega_{\text{T}})$ perhaps in the vicinity of the instability zones of Fig. 5.

Now the Mathieu equation on the left of (20) does not 'recognise' either the sinusoidal or the constant input of the right, that is B and Acos2z are not 'natural' functions for it. It is analogous to an input of say a periodic square wave into a simple linear oscillator. The square wave is not natural to the equation but it is possible to break it down into a series of functions which are, that is to carry out a Fourier analysis of it. In the same way here, the quantity $A\cos 2z + B$ which is periodic of minimum period π can be written in terms of Mathieu functions of the same period.

It is therefore assumed that the terms of the right of (20) can be written in the form

$$A\cos 2z + B = F_0 ce_0(z,q) + F_2 ce_2(z,q) + F_4 ce_4(z,q) + \dots$$
 (21)

where $ce_m(z,q)$ signifies the cosine type of Mathieu function of order m and the F_m are constants. The means of establishing these constants will be returned to below.

Also, to give a more realistic modelling of the system through any resonance a damping term proportional to $\frac{dy}{dz}$ is introduced. The equation to be solved for steady state motion is thus

$$\frac{d^2y}{dz^2} + 2\mu \frac{dy}{dz} + (a - 2q\cos 2z)y = \sum_{s} F_s ce_s(z,q).$$
 (22)

The solution can be expected to be expressible as a series in the even order Mathieu functions, we thus take the steady-state solution in the form,

$$y = \sum_{p=0}^{\infty} [C_{2p} ce_{2p}(z,q) + S_{2p} se_{2p}(z,q)]$$
 (23)

The even order sine type of Mathieu functions $\sec_{2n}(z,q)$ have been included because of the damping term, that is effectively they accommodate the associated phase shift. With the parametric excitation q zero the functions would revert to cosine and sine as could be expected in the solution of (22) with q = 0.

Substituting from (23) in (22) and bearing in mind that the function ce_r is a solution of $y'' + (a_r - 2q\cos 2z)y = 0$ and that se_r is a solution of $y'' + (b_r - 2q\cos 2z)y = 0$ where a_r and b_r are the characteristic numbers, functions of q, associated with ce_r and se_r respectively, equation (22) becomes (r = 2p),

$$\sum_{p=0}^{\infty} C_r(a - a_r) c e_r + \sum_{p=0}^{\infty} S_r(a - b_r) s e_r + 2\mu \sum_{p=0}^{\infty} (C_r c e_r' + S_r s e_r') = \sum_{p=0}^{\infty} F_r c e_r$$
 (24)

If this equation is multiplied by ce_s and integrated from 0 to 2π then by virtue of the orthogonality properties of the Mathieu functions and assuming them to be normalized to π , that is

$$\int_{0}^{2\pi} ce^{2} s dz = \int_{0}^{2\pi} se^{2} s dz = \pi$$

there results

$$\pi C_{s}(a - a_{s}) + 2\mu \sum_{p=0}^{\infty} S_{r}K_{rs} = \pi F_{s}$$
 (25)

where $K_{rs} = \int_{0}^{2\pi} se'_{r} ce_{s} dz$ and r and s are even, r = 2p.

Multiplying instead by se_s and integrating as before similarly leads to

$$\pi S_s(a - b_s) - 2\mu \sum_{p=0}^{\infty} C_r K_{sr} = 0,$$
 (26)

where
$$K_{sr} = \int_{0}^{2\pi} se'_{s} ce_{r} dz = -\int_{0}^{2\pi} ce'_{r} se_{s} dz$$
.

The quantities $K_{\rm ST}$ are functions of the parametric excitation q and can be calculated from series expansions for the Mathieu functions. Equations (25) and (26) then formally provide a basis for the calculation of the various coefficients $C_{\rm r}$ and $S_{\rm r}$ of the solution in terms of those $F_{\rm S}$ of the excitation. In fact if the series

$$ce_{2m} = \sum_{r=0}^{\infty} A_{2r}^{(2m)} cos2rz$$
 and $se_{2n+2} = \sum_{r=0}^{\infty} B_{2r+2}^{(2n+2)} sin(2r+2)z$

are used, the coefficients K_{sr} can be evaluated. The coefficients $A_{2r}^{(2m)}$ and $B_{2r+2}^{(2n+2)}$ are known as series expansion on the variable q (see for instance reference [3]).

Finally, the values of the coefficients F_s in equation (21) can be established by substituting the Fourier expansion for ce_{2m} given above in equation (21) and comparing coefficients on either side.

5. EXPERIMENTAL

Some experimental work has been carried out to establish the nature of the oscillatory behaviour of a model blade in the laboratory. Two identical strips of spring steel 25.4 mm x 1.52 mm x 0.868 m long were attached diametrically opposite each other on a small diameter hub. They were oriented so that the flexible bending direction was normal to the plane of rotation (i.e. α = 0°). End masses were bolted to the blades.

The hub was driven by a $\frac{1}{2}$ hp servo-controlled motor and the whole assembly was mounted on a rigid pillar with the axis of rotation horizontal. The motion of the blades was monitored through the signal from a strain gauge attached about 150 mm from the root and feeding into a strain meter through a precision slip-ring. The strain output was filtered to remove high frequency noise and was displayed on a recording oscilloscope. An accurate signal generator provided a timing signal to go along with the strain trace while a non-contacting magnetic probe was set up to give three blips per rotation from which the position angle θ of the blade at any stage could be determined.

With the parameters used, the blade mass was 0.280 Kg and the end mass 0.201 Kg, the natural frequency of the non-rotating blade was determined for a range of position angles θ and was found to vary approximately sinusoidally from about 22.2 cycles per minute (cpm) in the vertically upward position

 θ = 0°, through 39.7 cpm in the horizontal position to 55.8 cpm at θ = 180°.

The variation of the average vibration frequency with the rotation speed was found by giving the blade a disturbance at each chosen Ω . This was accomplished by the somewhat inelegant but effective means of attaching a loose length of string to the end mass and giving it a judicious pull. The resulting decaying oscillation provided a natural frequency ω_r and an approximate damping ratio.

It was found that ω_r varied with Ω almost exactly according to the theoretical result for a concentrated mass $\omega_r^2 = \omega_0^2 + 6\Omega^2/5$.

The mean damping appeared to be very low at zero speed (θ = 90°) about 0.37% in fact, but it rose rapidly with Ω then levelled off beyond about Ω = 10 rpm to a value between $2\frac{1}{2}\%$ and 3%.

The oscillation of the blade was recorded over a range of rotating speeds up to around 40 rpm which is just over $(2/3)\omega_r$. At certain speeds large amplitude oscillations built up and these were particularly noticeable in the vicinity of $(\Omega/2\omega_r)$ equal to 1/6 and 1/4 and to a lesser extent at 1/5. No significant oscillation was found near $(\Omega/2\omega_r) = 1/3$.

Typical records are shown in Fig. 6. The timing trace frequency is 5 Hz. The lowest trace in each case is the output from the magnetic probe and this provides the relative phasing. The point relating to θ = 0° is indicated. The maximum peak to peak amplitude for each case is also stated.

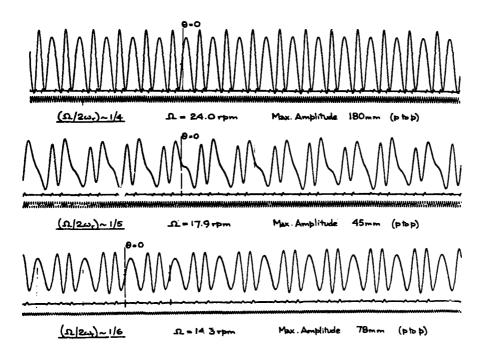


Fig. 6. Experimental Responses

The gravity load on the vertical blade is estimated to be about 0.77 of the buckling load so that $\varepsilon_0 \cong 0.76$. For the lowest speed trace of Fig. 6, Ω = 14.30 rpm and $\varepsilon_r \cong 0.66$, thus a $\cong 36$, q $\cong 12$, For a damping factor of 0.025 of critical, the estimated cut-off for the 1/6 zone is $\sqrt[6]{0.1} = 0.68$. This is however approximate but it shows that conceivably the 1/6 order instability zone might just be entered. The beam used had also a definite initial lack of straightness which as has been shown, would induce a forced input at that speed.

It is difficult to separate forced from unstable motion. The unstable motion theoretically grows without limit but nonlinear factors intervene and limit the amplitude.

Similar comments apply to the motion at 1/4, i.e. 24.00 rpm for which ε_r = 0.53, a = 16, q = 4.25. The limiting ε for that case is estimated from 74ζ = 0.53 so it is just possible that the operating point is in the unstable region (see Fig. 5). Again forcing is possible due to the lack of straightness with a resulting motion of the form of $se_{\lambda}(z,q)$.

The intermediate trace near 1/5 has however no theoretical forced excitation. The operating point on the $(\Omega/2\omega_T)$ versus ϵ_T plane must be within the unstable 1/5 boundary but again with amplitude limited by nonlinear factors. It is noted that the amplitude obtained in this zone is typically less than in either the 1/4 or 1/6 zones suggesting that in these other cases the unstable motion was augmented by the forced motion.

No evidence of motion in the 1/3 region was found. Around this zone $\varepsilon_r \approx 0.35$ while the front of the stability zone is at $\sqrt[7]{0.1} = 0.464$ which indicates that the operating point is clearly outise the unstable zone while in addition no forced oscillation of the odd functions is predicted.

These results and observations are very preliminary and much further work remains to be done before the problem could be said to have been properly researched. The results do however appear to agree more or less with what was anticipated qualitatively and give some encouragement for further effort.

6. CONCLUSIONS

The linearised equations of motion for a slender beam rotating in a gravitational field have been derived and examined in some detail for the special case of a light beam carrying an end mass. It has been shown that the zones of parametric instability of the beam may or may not be crossed as the rotational speed is increased depending on both the direction of the vibratory motion relative to the plane of rotation and the damping.

Initial lack of straightness of the beam also occasions forced motion which should result in resonance near the even order instability boundaries.

The experimental results presented do show the existence of large amplitude motion at the speeds predicted but separation of the unstable from resonant behaviour would require much more work including an analysis of the system's nonlinear behaviour.

REFERENCES

- 1. R.A. IBRAHIM et al. 1978 The Shock and Vibration Digest, 10 (1),15-29. Parametric vibration, Part I: Mechanics of linear problems. 10(2),9-24. Parametric vibration, Part II: Mechanics of nonlinear problems. 10(3), 41-57. Parametric vibration, Part III: Current problems. 10(4), 19-47. Parametric vibration, Part IV: Current problems (2).
- 2. N.W. McLACHLAN 1947 Theory and Application of Mathieu Functions. Clarendon Press, Oxford.
- 3. M. ABRAMOWITZ and I.A. STEGUN (Editors) 1964 Handbook of Mathematical Functions, National Bureau of Standards, Washington, D.C.





H. Wißbrok

Institut für Mechanik, Universität Hannover

Hannover, West Germany

1. INTRODUCTION

In many cases welded structures like machine frames have a very small inherent damping capacity. In general this leads to an unfavourable noise and vibration behaviour. Some methods to increase the damping are known:

- visco-elastic lavers.
- discrete viscous dashpots,
- admission of sliding friction by decrease of the interface pressure in joints.

The application of these methods to machine tool frames is restricted by some disadvantages. Visco-elastic layers must be very thick. Discret dashpots are more suitable for the reduction of local vibrations. The optimization of friction damping in the joints requires a non-acceptable loss of stiffness. This paper is concerned with the idea of avoiding this stiffness reduction by additional frictional interfaces. Such interfaces are formed by fastening additional e.g. beam-like elements on the vibrating frame regions. These so-called frictional ledges (Fig.) can be fixed with an interface pressure for maximal damping without any reduction of the machine stiffness.

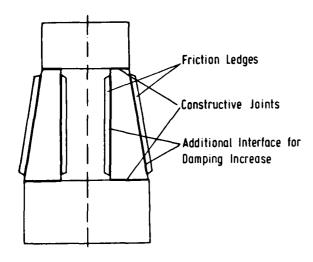


Figure 1 Forge hammer frame damped by frictional ledges

Due to the friction nonlinearity the general knowledge about the vibrational behaviour of structures damped by dry Coulomb friction is small. Therefore practical application of the frictional ledge concept needs research in some open questions. The most important point is the dependence of the maximal frictional damping on the corresponding interface pressure. For the investigation of these questions the following simple model of a structure damped by frictional ledges is used: A cantilever double beam has a frictional interface in the neutral axis, which is prestressed by bolts. I shall present some numerical and experimental results of the system behaviour contributing to the solution of the unsolved problems.

2. THEORETICAL CONSIDERATIONS

The treated system (Fig. 2) consists of two bars, which are connected by 10 equidistant bolts in long-holes. Because of this screwing design relative motion of the bars is restricted only by the tangential friction forces in the interface and not by the shear resistance of the bolts. To avoid friction between bar and nuts roller cages are built in.

Here the bending vibrations of the jointed beam and the friction coupled longitudinal motions are considered.

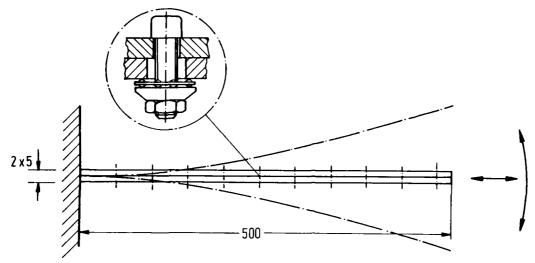


Figure 2 Analysed system

2.1 Computational Model

Using the finite element method the two rods are modelled by 12 usual beam elements with cubic shape function in lateral and linear shape function in longitudinal direction (Fig. 3).

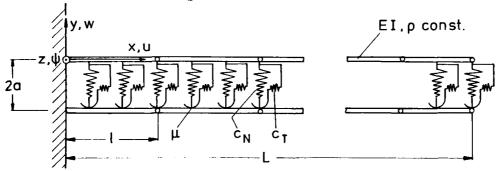


Figure 3 Computational mode.

The normal behaviour of the prestressed interface is determinated by the characteristics of the rough bar surfaces and of the bolts (Fig. 4). The interface without bolts does not transmit tensile forces. In the compressive region the strong progressive stiffness can be approximated by an exponential function

$$|f_{\mathsf{T}}| = C \cdot |\Delta W|^{\mathsf{B}} . \tag{1}$$

The experimentally determinated parameters B and C depend on the materials and the surface roughness [1]. Tensile forces are transmitted by the screwing. The bolt stiffness is linear and assumed to be constant distributed over the whole beam length. The resulting stiffness follows by parallel connection of the interface and the screwing, which means mathematically superposition of the two spring characteristics. This nonlinear normal stiffness is linearized in the working point, which results from the prestress. Assuming a linear distribution over one beam element the linearized normal interface stiffness is reduced to static equivalent nodal springs.

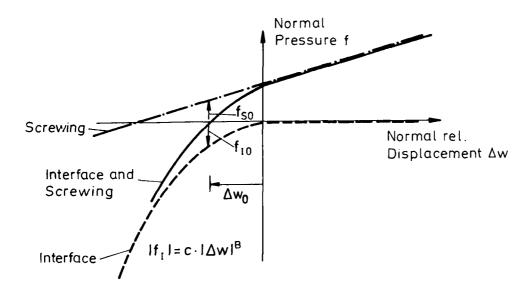


Figure 4 Normal interface characteristic

Tangential forces in the interface are transmitted by Coulomb friction. Two contact conditions are possible during motion: sticking and sliding. When the actual tangential force between two opposite interface points is less than the maximal possible sliding force, sticking friction occurs. Inspite of this friction of rest in the interface longitudinal relative motion of the beam axes is possible because of the beam shear flexibility. In the computational model this effect is taken into account by a series connection of sliding friction elements and a linear tangential stiffness \mathbf{c}_{T} . For determination of \mathbf{c}_{T} a bending beam loaded by an additional distributed tangential force T is considered (Fig. 5). The evaluation of the shear stress distribution [2] yields

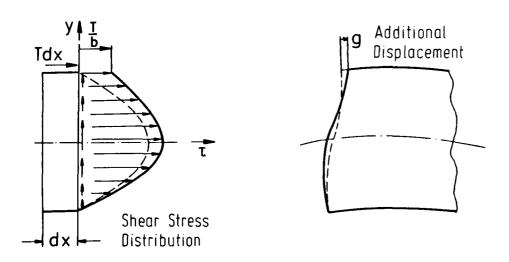


Figure 5 Tangential interface characteristic

a parabolic function with the value

$$\tau = \frac{T}{b}$$
 (b width of the beam) (2)

on the forced side of the beam. The tangential load T leads to an additional displacement of the amount g at the beam edge. The tangential interface stiffness $c_{_{\rm T}}$ is defined

$$c_{T} = \frac{T}{2g} . ag{3}$$

With the above relations follows

$$c_T = \frac{4}{5} \frac{Gb}{h}$$
 (G shear modulus h height of the beam). (4)

The continuous tangential interface behaviour of the physical system is figured in the computational model by discret tangential springs c_T^* between opposite nodes in the case of sticking friction and by discret friction forces at the nodes in the case of sliding.

2.2 Equation of Motion

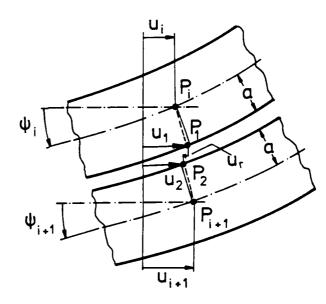
The tangential relative displacement u_r between two opposite nodes i and i+1 (Fig. 6) is defined as

$$u_r = u_2 - u_1$$
,
 $u_r = u_{i+1} - u_i - a(\psi_{i+1} + \psi_i) + 2g.$
(5)

Sticking contact yields with

$$\Delta u_r = 0,$$

$$\Delta(2g) = -\Delta[u_{i+1} - u_i - a(\psi_{i+1} + \psi_i)]$$
(6)



an incrementally valid stiffness relation between the contact forces and the Figure 6 Tangential relative disteam displacements (Fig. 7):

placement u_r

$$\Delta N_{i} = c_{T}^{*} \Delta(2g),$$

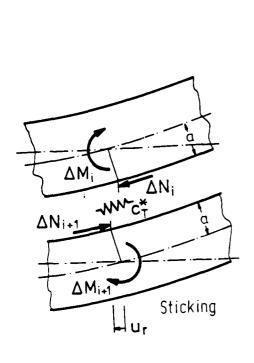
$$\Delta N_{i} = -c_{T}^{*} \Delta[u_{i+1} - u_{i} - a(\psi_{i+1} + \psi_{i})].$$
(7)

The excentric origion of the tangential contact forces leads to moments

$$\Delta M_{i} = a \cdot \Delta N_{i} . \tag{8}$$

The complete stiffness relation for a node pair in sticking contact can be formulated:

$$\Delta \begin{pmatrix} N_{i} \\ M_{i} \\ N_{i+1} \\ M_{i+1} \end{pmatrix} = -c_{T}^{*} \begin{bmatrix} 1 & a & -1 & a \\ a & a^{2} - a & a^{2} \\ -1 & -a & 1 & -a \\ a & a^{2} - a & a^{2} \end{bmatrix} \cdot \Delta \begin{pmatrix} u_{i} \\ \psi_{i} \\ u_{i+1} \\ \psi_{i+1} \end{pmatrix}$$
(9)



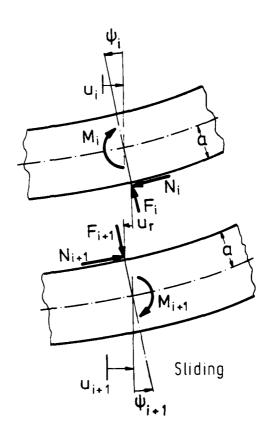


Figure 7 Contact forces

In sliding contact the tangential springs persist in their excursion, if the normal contact forces do not change. The absolute value of the tangential interface forces is determinated by the normal interface forces F_i and the coefficient of friction μ (Fig. 7). The sliding friction forces act always in opposite direction of the tangential relative velocity $\mathring{\mathbf{u}}_r$:

$$\begin{pmatrix}
N_{i} \\
M_{i} \\
N_{i+1} \\
M_{i+1}
\end{pmatrix} = \mu \cdot F_{i} \cdot \operatorname{sgn} \dot{u}_{r} \cdot \begin{pmatrix} 1 \\ a \\ -1 \\ a \end{pmatrix} .$$
(10)

For numerical solution by a step-by-step integration procedure the equation of motion is formulated for both contact cases in incremental form. The following notation is used:

- {u} displacement vector,
- [M] mass matrix,
- $[K_R]$ stiffness of the beams,
- $[K_N]$ linearized normal interface stiffness,
- $[K_T]$ tangential interface stiffness,
- {F_{Sp}} elastic forces vector,
- $\{F_{\mathbf{F}}\}$ friction forces vector,
- {P} external load vector.

Equilibrium at an arbitrary time $t+\Delta t$ requires:

sticking
$$[M]\{\ddot{u}\}_{t+\Delta t} + \{F_{Sp}\}_{t} + ([K_B]+[K_N]+[K_T])\Delta\{u\} = \{F_F\}_{t} + \{P\}_{t+\Delta t}$$
 (11)

sliding
$$[M]\{\ddot{u}\}_{t+\Delta t} + \{F_{Sp}\}_{t} + ([K_B]+[K_N])\Delta \{u\} = \{F_F\}_{t+\Delta t} + \{P\}_{t+\Delta t}$$
. (12)

The inertia forces $[M]\{\ddot{u}\}_{t+\Delta t}$, the nonlinear elastic forces $\{F_{Sp}\}_t$, the spring forces increment of the beam stiffness and of the linearized normal stiffness $([K_B]+[K_N])$ $\Delta\{u\}$ and the external loads $\{P\}_{t+\Delta t}$ are identical in both contact cases. Differences exist in the terms of friction. During sticking contact the tangential stiffness $[K_T]$ acts in the system. This matrix is filled with one tangential element stiffness matrix (eq.(9)) for each sticking node pair. The tangential springs T are loaded by the preceding motions. This tangential spring forces at the time t appear in the vector $\{F_F\}_t$. During sliding contact the tangential stiffness vanishes, on the right hand side are now the sliding friction forces (eq.(10)) at the considered time of equilibrium $t+\Delta t$. In general the equation of motion is of mixed typ, because the contact conditions are changed for each single node pair, if necessary.

2.3 Numerical Procedure

The integration of the equation of motion is carried out with the Newmark method [3]. This integration scheme is used because of some advantages in this case. It is unconditionally stable, even if the step length is greater than the period length of higher frequency vibration parts. The Newmark method is an one-step-scheme. More-step-algorithms would considerably complicate the friction change-over. Similar integration schemes always have solution errors, represented as period elongation and amplitude decay [3]. The Newmark method has a relative small period elongation and no amplitude decay, which is of particular interest for damping investigations.

For application in the present case the Newmark integration scheme must be coupled with an alogorithm for control and change-over of the frictional contacts in the interface. The following procedure has been found to be most advantageously: The known contact conditions of all node pairs at the time t are assumed to be valid during the following time step Δt . With these frictional conditions the integration over this time step is carried out by the Newmark algorithm. In the case of sliding contact previously the sliding forces $\{F_F\}_{t+\Delta t}$ are evaluated by cubic extrapolation from their preceding values. After calculation of all required values at the time $t+\Delta t$ a control of the contact conditions at all node pairs is performed. The change-over decision bases on the principle: Sticking is true, where and when ever possible. Thus the question is, whether a sliding assumed node pair would also be possible with sticking contact, or whether a node pair in sticking contact at the time t retains its contact condition at the time $t+\Delta t$. In the change-over decision the amount of the transferable tangential force $|N_{T^T t+\Delta t}|$ and the amount of the sum of the tangential force N_t at the time t and the tangential force increment for sticking friction ΔN_{St} are compared:

$$|N_t + \Delta N_{St}| \lesssim |N_{Tr_{t+\Delta t}}|$$
 sticking friction . (13)

The tangential force increment for friction of rest ΔN_{St} is also calculable in sliding contact. For that purpose the assumption is made, that a charge-over of only this one node pair to sticking contact at the time t would result

only in a small change of the relative displacement increment in the interface $\Delta \textbf{u}_{\textbf{r}}$:

$$\Delta N_{St} = c_T^* \cdot \Delta u_r \tag{14}$$

If the contact conditions evaluated in this way agree with the assumed contact conditions at all nodes, the solution increment is true and the next time step can be calculated. If the assumed contact conditions do not agree with the calculated ones at one or more node pairs, the procedure returns to the starting time t . For a more accurate evaluation of the real change-over time than the time step Δt is divided into n smaller time steps $\Delta t^{*}\colon$

$$\Delta t = n \cdot \Delta t^*. \tag{15}$$

The calculation of the displacement increment Δu and the control of the contact conditions now are carried out as before with the time step Δt . The change-over of the friction contact works during the smaller time step size Δt^* different in two program versions: in the first version the change-over takes place at the beginning of the time step, in which the change-over criterion is reached. In the other version only the next time step is computed with the new contact conditions. Sufficient agreement of the numerical solutions computed by both versions is criterion for the size of the time step Δt^* .

2.4 Numerical Results

2.4.1 Free Vibrations

After some investigations concerning stability, accuracy and computation time optimization of the developed procedure first free vibrations of the frictional damped beam are considered. Figure 8 shows the computed free vibration of the cantilever beam after deflection by a single force F at the free end.

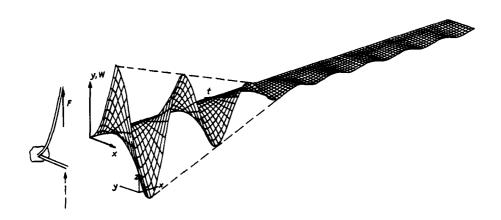


Figure 8 Friction damped free vibration

The enlarged deflection w is plotted versus beam length coordinate x and time t. Two distinct regions appear: in the beginning a hard damped section of about 3 periods followed by a stationary vibration with small amplitude. The shape of the static bending line is similar to the first vibration mode of the cantilever beam. Therefore essentially the fundamental oscillation appears and the damped section shows a linear envelope, which is typical for systems with Coulomb friction. Figure 9 shows the lateral deflection w, the longitu-

dinal motion u and the tangential relative displacement u_r at the beam length coordinate x = 0.5 L versus time t. The longitudinal displacement u

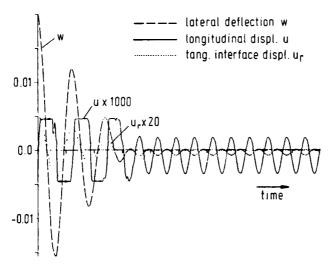


Figure 9 Displacements at x = 0.5 L

is caused by the friction forces. In the damped region its magnitude is limited by the change-over to sliding contact. The following stationary region is governed by continuous sticking contact. Here the relative displacement $\mathbf{u_r}$ becomes constant and the flexural and logitudinal motions \mathbf{w} and \mathbf{u} become harmonic because of the now linear character of the system. The potential energy of the jointed beam (Fig. 10) is maximal in the cusps of the vibration, where also the short sticking intervals appear. This short conservative behaviour

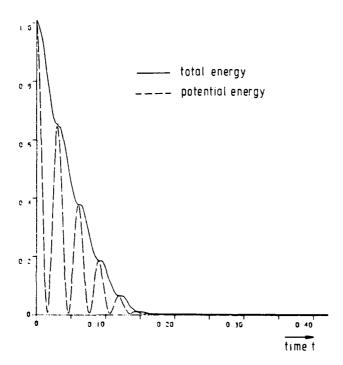


Figure 10 Energy of the free vibration

causes the saddle points of the total energy curve. The following undamped vibration contains in this example less than one percent of the initial total energy.

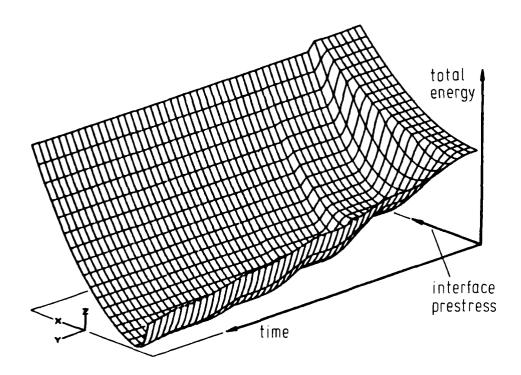


Figure 11 Influence of the interface prestress on the damping

The main purpose of the vibration analysis with interface damping becomes evident in figure 11. Here the total energy-time-relation is plotted against the beam interface pressure. During vanishing interface prestress no friction forces act and thus no damping occurs. At high prestresses no energy dissipation occurs, because all the time the tangential interface forces are transmitted by friction of rest. Between these extremes a region of interface pressure is optimal in the sense of a damping maximum. Inside this optimal region higher values of interface pressure lead to strong initial damping with a following stationary vibration of higher amplitude. On the other hand lower values lead to a smaller energy dissipation, but to a following motion of smaller amplitude.

In a number of parametric variations different influences on the optimal interface pressure and on the arising damping factor were investigated. Here just one result: The optimal interface pressure for maximal damping is proportional to the initial static deflection.

2.4.2 Forced Vibrations

Besides free vibrations the behaviour of the jointed beam excited by a harmonic load at the free end is considered. Because the numerical integration always yields the complete solution, the simulation time must be choosen long enough for complete dying-out of the transient vibration. The resonance curves for angular frequencies

 $\Omega \leq 1200 \text{ sec}^{-1}$

are computed for different interface prestresses and presented in figure 12.

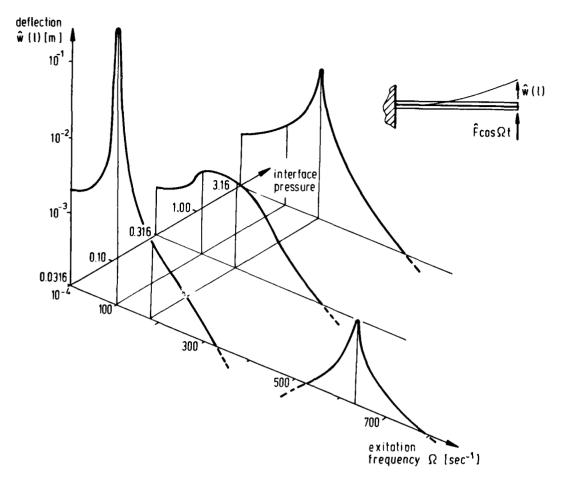


Figure 12 Resonance curves at different interface prestresses

Analogue to free vibrations no friction forces occur if the interface pressure vanishes. In this case the resonance curve passes into the amplitude characteristic of a single linear beam with the two lowest angular eigenfrequencies

$$\omega_{1s1} = 100 \text{ sec}^{-1}$$
 , $\omega_{2s1} = 640 \text{ sec}^{-1}$.

At high interface prestresses even largest tangential forces are transmitted by friction of rest. The resonance curve again has linear shape, but now with resonance in the natural frequencies of a nearly double thick beam

$$\omega_{1st} = 190 \text{ sec}^{-1}$$
, $(\omega_{2st} = 1216 \text{ sec}^{-1})$.

Between these extremes exists a region of interface pressure with smaller resonance amplitudes caused by the frictional damping. In this optimal pressure region the linear character of the resonance curve is lost due to the Coulomb friction. The resonance peak of the fundamental vibration is depressed and inclined to lower frequencies. This inclination can be explained by the degressive characteristic of the tangential springs c_T and the Coulomb friction elements jointed by a series connection [4]. Analogue to free vibrations parametric variations yield as one result a proportionality between the optimal interface pressure for maximal damping and the excitation force amplitude.

3. EXPERIMENTAL ANALYSIS

3.1 Test System

Parallel to the theoretical considerations presented in the last chapter experiments are carried out. The arrangement of the experimental rig is shown in figure 13. The theoretically rigid clamping is approached by a stiff hydraulic clamping device. Two transducers are mounted on the test beam. The strain near the fixed end of the beam is measured by strain gauges. An opto-electronic displacement transducer measures the lateral deflection near the free end. Both signals are amplified and recorded. In the case of free vibration measurements the shaker for harmonic excitation is exchanged by a device for static deflection.

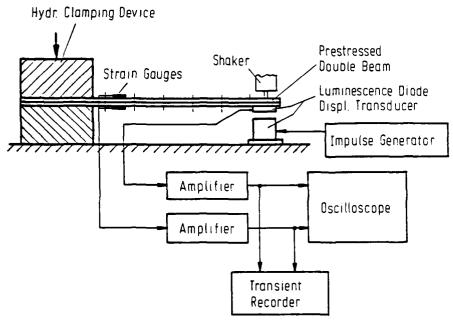


Figure 13 Arrangement of the test rig

3.2 Experimental Results

Figure 14 shows the computed and the measured deflection of the free end of the beam versus time. The first frictional damped periods agree qualitative in numerical computation and experiment. The amplitude of the calculated

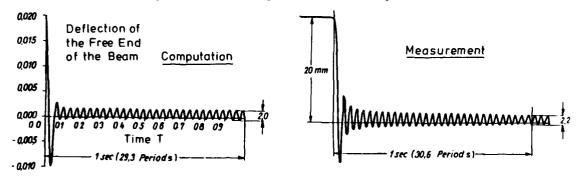


Figure 14 Comparison Computation - Measurement

vibration after one second is 1mm. In the measurement a weakly damped vibration (material damping) with an amplitude of 1.1mm at time T = 1sec appears.

A counting of the periods over the first second yields a mean value of frequency of 29.3 Hz in the computation and 30.6 Hz in the experiment. A value for comparison: the undamped fundamental bending frequency of a beam with equal dimensions, but without interface is 32.6 Hz. More experiments and corresponding computations with initial static deflection as well as harmonic excitation are carried out. In all these cases a comparison between measurements and calculations yields sufficient agreements.

6. CONCLUSIONS

A computational model and an integration procedure for the computation of frictional damped vibrations of structures with interfaces are developed. Model and calculation algorithm lead to physical plausible results in all possible contact conditions, like sliding friction or friction of rest, vanishing or high interface pressure.

Corresponding experiments are carried out. Considering the large range of the friction coefficient and of the other parameters of important influence on the system behaviour, measurement and numerical computation show an acceptable agreement. Consequently the developed computation model and numerical procedure are suitable for vibration computation of the investigated double beam and other similar structures with frictional interfaces.

A distinctive maximum of the frictional damping exists at an optimal interface pressure. Thus the frictional ledge concept is a useful method of damping increase.

REFERENCES

- 1. C. ANDREW, J.A. COCKBURN and A.E. WARING 1967/68 Proc. Inst. Mech. Eng. 182, 91-100. Metal Surfaces in Contact under Normal Forces: Some Dynamic Stiffness and Damping Characteristics.
- 2. J.P. DEN HARTOG 1949 Strength of Materials. New York: McGraw-Hill.
- 3. K.J. BATHE and E.L. WILSON 1976 Numerical Methods in Finite Element Analysis. Englwood Cliffs, New Jersey: Prentice-Hall.
- 4. J.J. STOKER 1950 Nonlinear Vibrations. New York: Interscience Publishers.



THE EFFECT OF SMALL CLEARANCES AND FRICTION-LOADED CONSTRAINT POINTS ON BENDING WAVE ENERGY TRANSMISSION IN A LONG BEAM

M.J.H. Fox

CEGB, Berkeley Nuclear Laboratories

1. INTRODUCTION

Many different classes of structure contain beam or shell-like components which efficiently transmit mechanical vibration in the form of bending waves from one part of the structure to another. Studies of the effect of various forms of constraint and structural discontinuity in attenuating such waves have been carried out. For example, discontinuities in structural material and cross section have been considered ([1], V1, 2). Joints ([2], [3]), 'blocking' masses, and sequences of regularly spaced masses or pinned supports | 1 |, V4, 5 form further examples of attenuation mechanisms. Many of the investigations have considered the beams, or plates, to be sections of infinite systems with bending waves incident on the constraint or discontinuity being reflected and transmitted in various proportions. The radiated waves are assumed to travel out of the region of interest in the problem and have no further influence on it. This assumption may be seen to be physically realistic in some applications, as for instance where sound transmission from a concentrated source region is being considered, with sufficient structural damping for multiple reflection to be ignored. It may also lead to useful results in systems subjected to distributed random forcing, to be treated by the methods of Statistical Energy Analysis. Here, the results for coupled infinite systems may be used to define a mean 'transmission loss factor' for assessing relative vibration levels in different parts of the structure, [4], [5].

This paper considers the effect on bending wave energy transmission in an infinite beam of constraints in the form of nonlinear force/displacement or force/velocity relationships. A point receptance method is used, whereby the linear (Euler beam theory) equations for the beam in the absence of the constraints are used to derive explicit expressions for displacement or velocity at the points where constraints are to be applied, in terms of applied forces at these points. Substitution of the chosen forms of these forces then lead to (nonlinear) integral equations determining displacement or velocity at the constraint points. In this way the infinite number of degrees of freedom of the original problem have been reduced to a number equal only to the number of nonlinear constraints, for numerical solution. This is analogous to the process adopted by Dowell [6] for finite systems.

2. SINGLE STICK-SLIP CONSTRAINT

The numerical solution is carried out, firstly, for a force-velocity relationship modelling stick-slip behaviour at a single constraint. For very small values of velocity the force is assumed to increase linearly with velocity up to a limiting value. In this 'sticking' phase the force can take any value required for overall equilibrium up to the limiting value, the associated velocity being negligible in the context of the whole system. When the limiting force value has been reached, the force remains constant for all further velocity increments, allowing 'slip' until velocity returns below the limiting value, when 'stick' is re-established. Solutions are found modelling steady state periodic response to an incoming harmonic wave, for different values of the ratio: limiting applied force/shear force amplitude of incident wave.

2.1 Equations of Motion

The beam is taken to lie along the x-axis with transverse displacement in the y-direction. The velocity field produced by a harmonic incoming wave of frequency ω from a negative x-direction, together with the onward travelling and reflected waves generated at that frequency, is shown in figure 1. k is the wavenumber of the waves, given by Euler beam theory as $k^4=\omega^2\rho/EI$, ρ being the mass/unit length and EI the bending stiffness of the beam. The nonlinear nature of the force/velocity relationship to be applied at x=0 will result in waves at harmonics of the incoming frequency being generated, these will be superimposed on the fundamental reflected and transmitted waves to produce a more complex waveform. The higher harmonics will each produce a velocity field as shown in figure 1, each with its appropriate k-value, but without an incoming wave component.

The continuity equations at x=0 may now be written in the frequency domain as:

$$i\omega U_{0}$$
 + a + b - c - d = 0
 $k\omega U_{0}$ + ka + ikb + kc + ikd = 0 (1)
 $-k^{2}i\omega U_{0}$ + $k^{2}a$ - $k^{2}b$ - $k^{2}c$ + $k^{2}d$ = 0
 $-k^{3}\omega U_{0}$ + $k^{3}a$ - i $k^{3}b$ + $k^{3}c$ - i $k^{3}d$ =i $\omega F/EI$

for continuity of velocity, angular velocity and bending moment, and equality of discontinuity in rate of change of shear force to rate of change of external applied force, respectively. $i\omega U_0$ is now understood to be the time Fourier transform of the incoming velocity field at x=0 and F the time Fourier transform of the applied force. The equations may be solved for the Fourier components of standing, reflected and transmitted waves at frequency ω to give:

$$a = c = -i\omega F/4EIk^3$$
, $b = \omega F/4EIk^3$, $d = i\omega U_O + \omega F/4EIk^3$

and so the Fourier transform of velocity at x=0 is

$$i\omega U(0,\omega) = i\omega U_0 - (1+i)i\omega F/4EIk^3$$

Reverting to the time domain, the velocity at x=0 is:

$$\frac{dU}{dt} (0,t) = 2 \operatorname{Re} \int_{0}^{\infty} \left\{ i\omega \widetilde{U}_{0} - \frac{(1+i)i\omega}{4EIk^{3}} \right\} \widetilde{F} (\omega) e^{i\omega t} d\omega$$

$$= \frac{dU_o}{dt} (t) - \frac{2}{8\pi (EI)^{1/4} \rho^{3/4}} \int_{-\infty}^{\infty} F(\tau) Re \left\{ \int_{0}^{\infty} (1+i)i\omega^{-1/2} e^{i\omega(t-\tau)} d\omega \right\} d\tau$$

using the beam bending wave characteristics, $EIk^4 = \rho\omega^2$, and the explicit expression for the Fourier transform $F(\omega)$ in terms of the time-history of the force. $\frac{dV_0}{dt}(t)$ is the velocity associated with the incoming wave field at x=0. The inner integral may be evaluated explicitly [7] to give

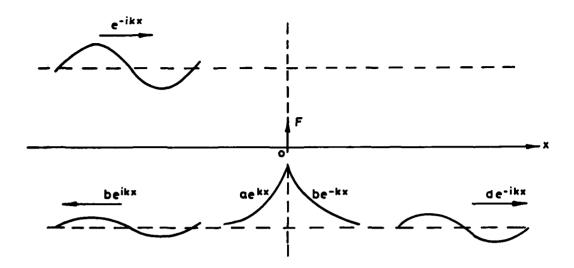
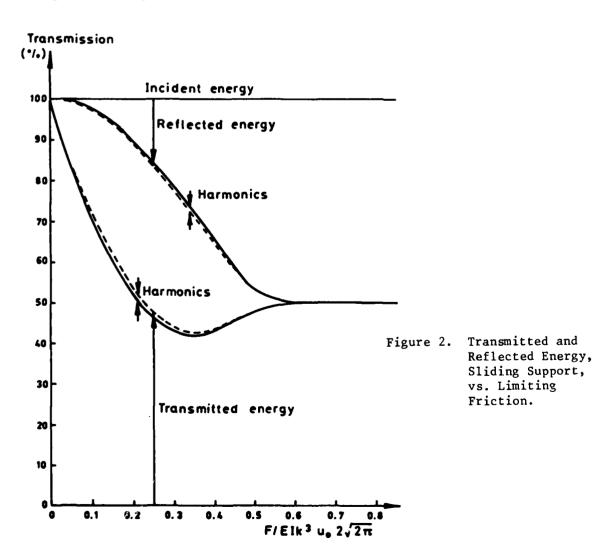


Figure 1. Single Interaction Point: Velocity/Displacement Field.



Re
$$\int_{0}^{\infty} (1+i) i\omega^{-1/2} e^{i\omega(t-\tau)} d\omega = -\sqrt{\frac{2\pi}{t-\tau}}$$
 $t > \tau$

which leads to an integral equation for $\frac{du}{dt}$ (0,t)

$$\frac{du}{dt}(0,t) = \frac{dU_0}{dt}(t) + \frac{1}{2/2\pi(EI)^{1/4}} \int_{0}^{t} \frac{F(\tau)}{\sqrt{(t-\tau)}} d\tau$$
 (2)

2.2 Solution Technique

The equation was solved using a step-by-step timewise integration until the difference between successive cycles of response was less than some pre-set small value, starting from a state of rest at t=0. As the assumed force-velocity relationship:

$$F = -a \frac{du}{dt}/b$$

$$= -a \frac{du}{dt} > b$$

$$= du + b$$

$$= du + dt$$

$$= a \frac{du}{dt} < -b$$
(3)

is piecewise linear an implicit integration scheme, with its advantage of enhanced numerical stability permits extraction of explicit expressions for du/dt at the current time step from (2). Here a is the limiting friction force, while a/b is the slope of the force-velocity curve modelling the 'sticking' phase of the motion, b being a small quantity.

2.3 Results

Having found the steady-state response of velocity, and hence applied force, in the time domain, a Fourier transform routine was applied to recover the frequency-domain coefficients a, b, c, d of standing, reflected and transmitted waves for the fundamental (incoming wave) frequency, and harmonics. Figure 2 shows the proportions of energy reflected and transmitted, as a function of the ratio of limiting friction a, to $\omega^{3/2} U_{\rm o}/A$, which is a measure of the internal shear-force amplitude associated with the incoming wave. The vertical distance between the two broken lines is a measure of the rate of energy dissipation in sliding. At zero limiting friction there is no constraint on beam motion, and all the incoming energy is transmitted. As limiting friction is increased there is a minimum on the transmission curve near a limiting friction of 0.35 $\omega^{3/2} U_{\rm o}/A$, and the curve rises again to a value of 50% transmission as friction is further increased. This 50% value is that obtained for transmission past a single pinned support on an infinite beam, and represents the situation in which sliding motion has been prevented by the friction force.

3. SINGLE CLEARANCE CONSTRAINT

The equations are next solved for a displacement-dependent force modelling beam motion in a clearance which has no influence on the beam until the displacement exceeds a certain value. A simplified model of the impact process is used in which a stiff spring relationship between force and displacement is assumed once the latter exceeds the clearance value. Again, solutions

representing steady-state response to an incoming harmonic wave are sought, and the interest is now in finding the dependence of onward transmitted energy on the incoming wave ampliltude/clearance ratio.

3.1 Equations of Motion and Solution Technique

The applied force is taken to have the form:

$$F = 0 \qquad |u| < a$$

$$= -K(u-a) \qquad u > a \qquad (4)$$

$$= -K(u+a) \qquad u < -a$$

at x=0, where a is the clearance, and K the stiff spring rate providing a restoring force after impact. As the force is displacement, rather than velocity, dependent, modifications must be made to the previous solution technique. It proved most convenient, for the numerical integration, to use (2) for the time-stepping equation, with a simultaneous integration of du/dt being carried out to obtain the current value of u, and hence F.

3.2 Results

Figure 3 shows the proportion of incident energy transmitted onward past the clearance, as a function of the ratio clearance/incoming wave amplitude. As the applied force is conservative, no energy is dissipated in the clearance, and the reflected energy is represented by the deficit in transmission. At zero clearance, the effect is that of a pinned support and 50% of incident energy is transmitted. As the clearance is increased the proportion of transmitted energy reduces, to a minimum of around 30% at clearances of around 0.3-0.4 of the incoming wave amplitude, with an increasing proportion of this energy appearing in harmonics generated by the impacting. The transmission then starts to increase again, but only to a value of 70% for a clearance equal to the wave amplitude. For clearances greater than this a solution in which the wave continues through the clearance unaffected by its presence is clearly possible, and it is this solution that is found by the numerical technique. It is possible that there is a range of clearances greater than one wave amplitude for which a second, contacting solution also exists; this would give a continuous branch to the transmission curve rising to 100% at a value greater than 1.

4. TWO STICK-SLIP CONSTRAINTS

The cases for two constraint points on a beam are considered next, to permit the investigation of the dependence of transmitted energy on separation of the points. The force at each constraint point is related to the local velocity by the forms (3) used for a single point.

4.1 Equations of Motion

The notation used for the various standing and travelling wave components in this case is indicated in figure 4. Frequency-domain equations to determine the corresponding coefficients are set up as in section 2.1, but now considering continuity and force-balance conditions at each of the two clearances. These result in the solutions:

$$a = -i\omega(\widetilde{F}_1 + \widetilde{F}_2 e^{-k\ell})/4EIk^3$$

$$b = \omega(\widetilde{F}_1 + \widetilde{F}_2 e^{-ik\ell})/4EIk^3$$

$$A = -i\omega\widetilde{F}_2/4EIk^3$$

$$B = \omega\widetilde{F}_2/4EIk^3$$

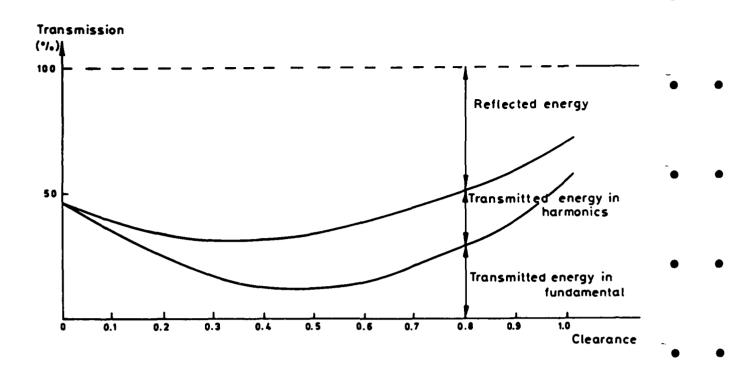


Figure 3. Transmitted Energy through Clearance vs. Clearance.

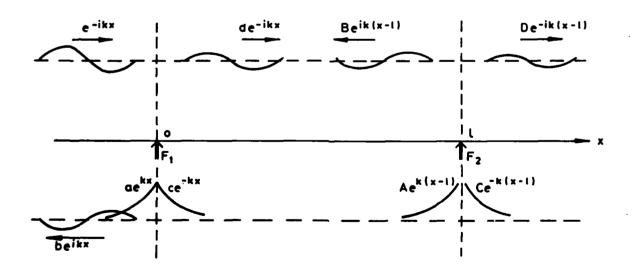


Figure 4. Two Interaction Points: Velocity/Displacement Field.

$$c = -i\omega \widetilde{F}_1/4EIk^3$$

$$C = -i\omega (\widetilde{F}_2 + \widetilde{F}_1 e^{-k\ell})/4EIk^3$$

$$d = i\omega \widetilde{U}_0 + \omega \widetilde{F}_1/4EIk^3$$

$$D = i\omega \widetilde{U}_0 e^{-ik\ell} + \omega (\widetilde{F}_2 + \widetilde{F}_1 e^{-ik\ell})/4EIk^3$$

The time dependence of velocity at the second constraint point x=1 is

$$\frac{du}{dt}(\ell,t) = \frac{dU_{\ell}}{dt}(t) - \frac{1}{4\pi\rho^{3/4}(EI)^{1/4}} \int_{-\infty}^{\infty} \{F_{1}(\tau)A(t,\tau) + F_{2}(\tau) B(t,\tau)\}d\tau$$
at x = 0 (5)

$$\frac{dU}{dt} (0,t) = \frac{dU_0}{dt} (t) - \frac{1}{4\pi o^{3/4} (EI)^{1/4}} \int_{-\infty}^{\infty} \{F_1(\tau)B(t,\tau) + F_2(\tau)A(t,\tau)\} d\tau (6)$$

where $\frac{dU_{\ell}}{dt}$ (t) is the velocity of the incoming wave field at x=1,

$$A(t,\tau) = \text{Re i} \int_{0}^{\infty} \omega^{-1/2} (e^{i\omega(t-\tau)} - \omega^{1/2}L + ie^{i\omega(t-\tau)} - i\omega^{1/2}L)_{d\omega}$$

where $L = \rho^{1/4} (EI)^{-1/4} l$, so that $kl = \omega^{1/2} L$

 $B(t,\tau) = -\sqrt{(2\pi/t-\tau)}$, the kernal for the single support case. After some substitution, A may be reduced to [7]:

$$A(t,\tau) = -\sqrt{\frac{2\pi}{t-\tau}} \left(\cos\left(\frac{L^2}{4(t-\tau)}\right) + \sin\left(\frac{L^2}{4(t-\tau)}\right)\right) t > \tau$$

$$= 0 \qquad \qquad t < \tau$$

4.2 Solution Technique

A becomes singular as $t-\tau$, with an increasingly rapid oscillatory behaviour. This is because A, representing the response at the second constraint point due to the force applied at the first constraint point is, at very small time-differences dominated by the high frequency components which have the necessary high propagation speeds to travel between the support points on such a short timescale. To overcome this problem in integrating (5) and (6) the forces are approximated by linear functions in each time interval $(t-(n+1)\varepsilon, t-n\varepsilon)$ and the resulting products with A, B integrate to give weighting factors for the values of F_1 , F_2 at the ends of the interval in terms of trigonometric functions and Fresnel integrals [7], which are available from computer numerical algorithm packages [8].

This gives a pair of implicit, but piecewise linear, equations for the values of du/dt at the two constraint points, for the current time step. These may again be inverted to obtain explicit expressions for du/dt at the constraints.

4.3 Results

Figure 5 shows the dependence of transmitted energy (including that in harmonics) as a function of the ratio: constraint separation/wavelength, for three different values of limiting friction, covering the range of values for which sliding was seen in the single-point analysis. Also shown for comparison is the curve obtained for the case of two simple pinned supports at the constraint points, from a linear theory. At the lowest friction value the

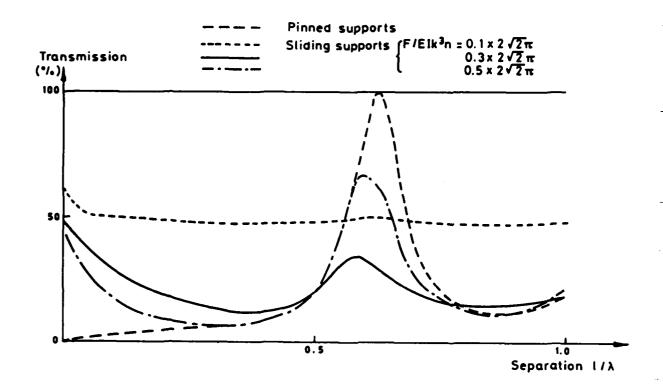


Figure 5. Transmission through Two Sliding Supports vs. Separation.

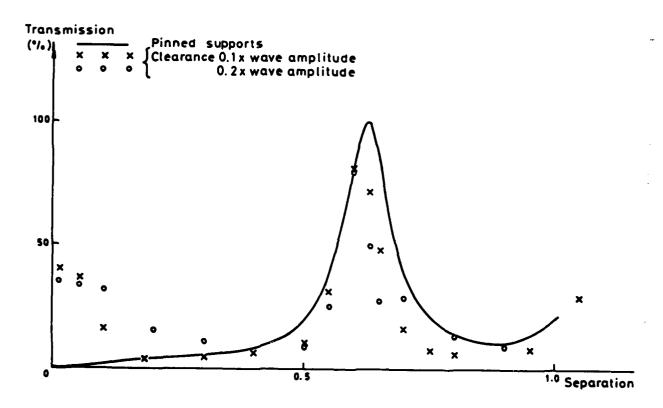


Figure 6. Transmission through Two Clearances vs. Separation.

sliding forces dissipate about half the incident energy independently of the constraint separation. As the friction is increased, however, the additional constraining force is sufficient to reproduce the feature seen in the pinned-support curve of a resonance near a separation of 0.6 wavelengths where a peak in transmission levels is found. A qualitative difference in the forms of the pinned support curve and of the higher friction value curves is seen at low separations. The effect of two pinned supports being moved together on a beam, is equivalent to introducing a clamped condition there, preventing all energy transmission. This is only achieved because an idealised pinned support can resist an arbitrarily large lateral force, so that the pair can, by means of equal and opposite lateral forces, apply the required moment on the beam even as their separation tends to zero. This is not true for stick-slip constraints: however large the limiting friction there will come a point at which, as the constraints are moved together, the limit is exceeded and slip will occur at one of them, allowing energy transmission.

5. TWO CLEARANCE CONSTRAINTS

The case of a beam with two clearance points is treated as in the previous section, where the forces at the two constraint points are now governed by the local displacements according to (4). As described in section 3.1, additional integration steps are required to derive the displacements from calculated velocities.

The transmitted energy vs. separation/wavelength results for clearances 0.1 and 0.2 x incoming wave amplitude (figure 6) again show a similar form to those for pinned supports, with the pinned support curve as an upper bound, except at small separations. At small separations the clamping effect of two pinned supports is not seen, as even very small clearances allow some rotation of the beam as they are brought together. For larger clearance values (e.g. 0.5 x wave amplitude) impacting at the first constraint point reduces the amplitude sufficiently to prevent contact at the second, and so transmission is separation-independent.

6. CONCLUSIONS

This paper has considered theoretically the effect on bending wave energy transmission along an infinite beam of nonlinear constraints modelling friction loaded 'stick-slip' support points and small clearances. Single constraints of either type are found to produce a similar degree of attenuation (about 50%) to that produced by a pinned support, provided that either the friction is high enough, or the clearance is small enough, to provide a significant degree of interaction between support and beam.

Higher attenuation may be obtained with two such constraints provided the separation is correctly chosen. As for two pinned supports, a separation of around 0.6 wavelengths introduces a resonant effect, giving comparatively low attenuation. Unlike idealised pinned supports, however, which clamp the beam as they are brought together, friction loaded supports and clearances suffer a loss in attenuation potential as they approach each other. The optimum separation, for most significant friction levels and for small clearances, appears to lie in the range 0.2 - 0.4 wavelengths.

ACKNOWLEDGEMENT

This paper is published by permission of the Central Electricity Generating Board.

REFERENCES

- 1. L. CREMER, M. HECKL and E.E. UNGAR 1973 Structure-Borne Sound. Berlin: Springer Verlag.
- 2. K.H. YONG and K.J. ATKINS 1983 J. Sound and Vibration 88, 431-436, Generation of Elastic Stress Waves at a T junction of square rods.
- 3. P.G. CRAVEN and B.M. GIBBS 1981 J.Sound and Vibration 77, 417-427. Sound Transmission and Mode Coupling at junctions of Thin Plates.
- 4. P.J. REMINGTON and J.E. MANNING 1975 J. Acoustical Soc.Am. <u>57</u>, 374-Comparison of Statistical Energy Analysis power flow predictions with an 'exact' calculation.
- 5. W. WOHLE, Th. BECKMANN and H. SCHRECKENBACH 1981 J. Sound and Vibration 77, 323-334, Coupling Loss Factors for Statistical Energy Analysis of Sound Transmission at rectangular structural slab joints.
- 6. E.H. DOWELL 1980 J. Applied Mechanics, Trans. ASME 47, 172-176, Component mode analysis of Nonlinear and Nonconservative Systems.
- 7. I.S. GRADSHTEYN and I.M. RYZHIK 1965 Tables of Integrals, Series and Production: Academic Press.
- 8. NUMERICAL ALGORITHMS GROUP: FORTRAN Library Manual Mk. 8.

REVIEW OF AIR-BLAST RESPONSE OF BEAMS AND PLATES

4

J. Ari-Gur*, D.L. Anderson and M.D. Olson

Department of Civil Engineering University of British Columbia Vancouver, B.C., V6T 1W5, Canada

1. INTRODUCTION

The objective of the present study is to provide a comprehensive review of the behaviour of beams and plates which are subjected to air blast loadings. Since this is a compilation and analysis of published research results, it will also serve as a guide to the needs for future research.

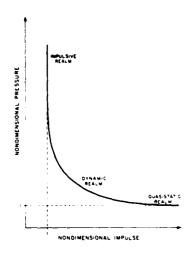
At first, loading characteristics and material properties are discussed. Then the responses of beams and plates are considered for various ranges of loading. Throughout the study nondimensional parameters which best represent the structural behaviour are presented. The selection of these parameters is determined by the requirement of most complete presentation with minimum variables. Also, similarities between beams and plates are derived and areas of deficient knowledge are pointed out. The presentation here is necessarily brief, but full details are available in [1]

2. LOADING CHARACTERISTICS

A typical pressure wave from an explosion has an overpressure phase and then an underpressure phase. If the source is a conventional explosion and not too far from the target, the peak over-pressure p_m is much larger than the peak underpressure. Hence, in practice, the negative phase is often neglected. Also, since the rise time is very short compared to the total duration of positive loading τ_0 , a zero rise time is often assumed. For blasts in air the peak pressure p_m , duration of load τ_0 , and impulse per unit area I, which is the integral of the pressure time history, are usually expressed as a function of the scaled distance $R_0/W^{1/3}$ from the explosion. Here R_0 is the distance from the explosion and W is the equivalent TNT weight of explosive. Empirical charts are available which give data for both incident or reflected pressures, and side on pressures. See for example, [2] (Ch. 4).

The response of a structure to a blast load is highly dependent on the duration of loading. This is best described by an iso-response plot [2] (Ch. 2), as presented in Fig. 1. The plot presents the combinations of pressure and impulse which, when applied on a certain structure, result in a similar specified The response may be a displacement at a point, the elastic limit stress, tensile failure or any qualitative or quantitative response as desired. The iso-response curve shows that there are minimum values of pressure and impulse which are necessary to obtain the required response. In the quasi-static realm, the load is applied slowly and therefore the impulse is very large, but, since the response is dominated by the load level, the desired response will be obtained only if the minimum pressure is applied. In the impulsive realm, a high level of load is applied during a very short period. Here, the impulse is the dominant loading parameter, and regardless of the magnitude of pressure, if the impulse is below the minimum, the iso-response is not reached. In these two extreme realms, the history of loading is not important, and the peak pressure $\mathbf{p}_{\mathbf{m}}$ or the maximum positive impulse I, respectively, are the only significant loading characteristics.

^{*} Now with Armament Development Authority, Israel.



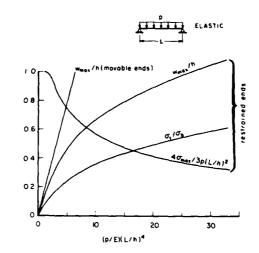


Fig. 1. Iso-Reponse Curve.

Fig. 2. Simply Supported Beam Results With Axial Restraint.

The period T of the linear natural frequency of the structure in the particular mode of response relative to the duration of loading τ_0 provides a criterion to determine the loading realm. When $\tau_0/T<0.2$, an impulsive approach provides a fairly good estimate of the response, whereas for $\tau_0/T>>1$, a stepload approximation becomes reasonable.

In the dynamic realm, the entire history of loading p(t) affects the response. The most severe response is obtained when the external load follows the natural response of the structure. There have been attempts to eliminate the need to investigate separately the responses to each pulse shape. The idea is to find the response to a certain shape and then to correlate other load histories to that with the known response. See for example Youngdahl [3] and Robinson [4]. However this approach has not been pursued thoroughly and much more work is required before definitive results will be available.

3. MATERIAL PROPERTIES

The most commonly used stress-strain relations are bilinear elastic-plastic. When the response is deep inside the plastic domain, a rigid-plastic behaviour is commonly assumed. Materials that exhibit weak strain-hardening are usually assumed to be perfectly plastic.

Yield criteria are required to define the limits of elasticity and the onset of plastic flow. The Tresca and the von Mises yield criteria as well as the square Johansen criterion have all been used for the principal bending moments in a plate. The results obtained using the various criteria differ from each other by approximately 10% or less, with Johansen's criterion always giving the highest loads.

When the loading conditions involve bending moments M and in-plane forces N or when transverse shear forces Q are included, the yield criteria have to combine these forces to provide acceptable results. For example, for rectangular beams with restrained axial motion at the supports, the yield condition

$$\left|\frac{M}{M_{o}}\right| + \left(\frac{N}{N_{o}}\right)^{2} \le 1 \tag{1}$$

was employed in [5], whereas the square-type condition

$$(\left|\frac{M}{M_{0}}\right|-1)(\left|\frac{Q}{Q_{0}}\right|-1) \le 0$$
 (2)

was used in [6], where $\rm M_{\odot}$, $\rm N_{\odot}$ and $\rm Q_{\odot}$ are the appropriate independent plastic limiting quantities.

For materials that exhibit strain rate sensitivity (like mild steel), the plastic domain for a high strain rate may be at a stress level two times that of the static one. In a typical blast test on a structure, the strain rates are time dependent and, in principle, the material behaviour at the plastic range should be updated continuously. In practice, fairly good predictions have been obtained for models where the yield level is assumed to correspond to the yield level at the highest strain rate, and then held constant (see, for example, [7-8]). The justification is that most of the energy is absorbed by plastic deformation at the highest level of stress.

4. BEAMS

The collapse pressure under a static load is an important quantity in the quasistatic realm of loading, and is an important parameter used in nondimensionalizing the dynamic results. Consider a beam of rectangular cross section, either a cantilever or a symmetrically supported bar, of length L, loaded by a slowly increasing uniform lateral pressure p. At a load level p_{γ} , an extreme fibre reaches the yield stress σ_{γ} and for $p\!>\!p_{\gamma}$, plastic deformation occurs. The bending moment per unit width at the cross-section of incipient yield is

$$M_{Y} = \sigma_{Y}h^{2}/6 \tag{3}$$

where h is the beam depth. Therefore the yield load is given by

$$p_{Y} = \alpha_{1}\sigma_{Y} h^{2}/L^{2}$$
 (4)

where α_1 = 1/3, 4/3, and 2 for a cantilever, simply supported and clamped beam, respectively. For a perfectly plastic material, the maximum bending moment per unit width is:

$$M_0 = \sigma_v h^2 / 4 \tag{5}$$

and the ultimate or collapse pressure \mathbf{p}_{o} is given by:

$$p_o = \alpha_2 \sigma_Y h^2 / L^2$$
 (6)

where $\alpha_2 = 1/2$, 2 and 4 for the above three cases, respectively.

When the ends of the simply supported and clamped beams are held fixed against in-plane motion, tensile forces along the beams change the deflection and the stress distribution through the thickness. The higher the deflection, the poorer the results obtained by the pure bending approximation. These effects are illustrated in Fig. 2 for the simply supported beam, where $\sigma_{\rm t}$ is the stress due to maximum membrane force and $\sigma_{\rm b}$ is the maximum bending stress. It is clear that once the deflection reaches an appreciable fraction of the beam depth, then nonlinear effects play a significant role.

4.1 Dynamic Response of Cantilevers

Baker et al. summarized in [9] and [2] (Ch. 7) test results on cantilevers loaded in the dynamic and impulsive realms. For cantilevers that responded

elastically, bending strains $\epsilon_{\hat{b}}$ were measured at the root, but for higher impulsive loads measurements were not taken during the tests and only the final tip deflections w_{tip} were measured.

In the impulsive realm, the loading is expressed by the impulse I. The plastic deformation results of the impulsive loading tests are presented in Fig. 3 as a function of the parameter $I/L\sqrt{\sigma_Y\rho}$, which contains a plastic material property, instead of $I/L\sqrt{E\rho}$ as used by Baker et al. For the response in the plastic range, the yield stress σ_Y is considered to be a more appropriate parameter than the elastic modulus E. The impulse required for incipient yielding is given by

$$\frac{I}{L\sqrt{\sigma_{\mathbf{v}}\rho}} = \frac{\sqrt{\varepsilon_{\mathbf{Y}}} h}{\sqrt{6} L}$$
 (7)

where ϵ_Y is the yield strain corresponding to the yield stress σ_Y . The test results agree well with this estimate in that no appreciable permanent deformation occurred until the impulse exceeded this elastic limit.

The significance of the elastic response part decreases for higher impulses. A simple analysis for a rigid-plastic material with a single plastic hinge at the root gives the relation

$$\sin^{-1}\left(\frac{\mathbf{w}_{tip}}{L}\right) = 2\left(\frac{L}{h}\right)^3 \frac{I^2}{L^2 \sigma_{\mathbf{v}}^{\rho}} \tag{8}$$

which, as shown in Fig. 3, overpredicts the deflections. However, if the elastic energy for incipient yield is subtracted from the input kinetic energy, this equation becomes

$$\sin^{-1}\left(\frac{w_{tip}}{L}\right) = 2\left(\frac{L}{h}\right)^3 \frac{I^2}{L^2 \sigma_{yp}} - \frac{1}{3} \frac{L}{h} \varepsilon_{y} \tag{9}$$

Eq. (9) is also shown in Fig. 3 and it clearly gives a much better representation than Eq. (8).

4.2. Dynamic Response of Symmetrically Supported Beams

Symonds [10] obtained the permanent response of simply supported and clamped beams with no axial constraint subjected to rectangular pressure pulses. It is possible to write the deflection equation for both beams in a single equation:

$$\frac{2\rho h}{p_{o}^{\tau_{o}^{2}}} w_{max} = \begin{cases} \frac{3}{2} & \frac{p_{m}}{p_{o}} \left(\frac{p_{m}}{p_{o}} - 1\right) & , & 3 > \frac{p_{m}}{p_{o}} > 1 \\ \frac{4}{3} & \frac{p_{m}}{p_{o}} \left(\frac{p_{m}}{p_{o}} - \frac{3}{4}\right) & , & \frac{p_{m}}{p_{o}} > 3 \end{cases}$$
(10)

where p_0 is the static collapse pressure given by Eq. (6).

With the following definitions of nondimensional impulse I and pressure p:

$$\bar{\mathbf{I}} \equiv p_{m} \tau_{o} / \sqrt{1.5 p_{o} \rho h w_{max}}, \qquad \bar{\mathbf{p}} \equiv p_{m} / p_{o}$$
 (11)

PROCEEDINGS OF THE INTERNATIONAL CONFERENCE ON RECENT ROYANCES IN STRUCTU. (U) SOUTHAMPTON UMIV (ENGLAND) INST OF SOUND AND VIBRATION RESEAR. M PETYT ET AL. 1984 ND-8143 300 5/5 UNCLASSIFIED



MICROCOPY RESOLUTION TEST CHART NATIONAL BUREAU OF STANDARDS-1963-A

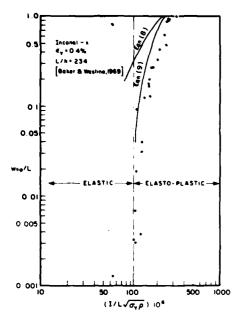


Fig. 3. Permanent Rotation of Cantilever.

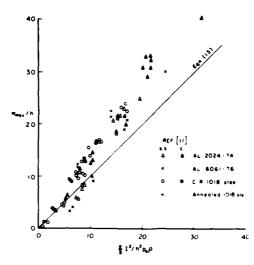


Fig. 4. Permanent Deflection of Simply Supported Beam - No Axial Restraint.

Eq. (10) can be written as:

$$1 = \begin{cases} \frac{9}{8} \overline{1}^2 (1 - 1/\overline{p}) & , & 3 > \overline{p} > 1 \\ \overline{1}^2 (1 - 3/4\overline{p}) & , & \overline{p} > 3 \end{cases}$$
 (12)

Eq. (12) may be plotted as a single iso-response curve of \bar{p} vs. \bar{I} . In the impulsive loading realm, $\bar{p} \rightarrow \infty$ and $\bar{I} \rightarrow 1$ or

$$\frac{w_{\text{max}}}{h} \approx \frac{2}{3} \frac{I^2}{h^2 p_0 \rho} \tag{13}$$

where $I = p_m \tau_o$.

In an extensive experimental study, Florence and Firth [11] tested the response of beams to impulsive uniform lateral pressure. The boundary conditions approximated clamped (c.) and simply supported (s.s.) edges with free axial motion. All of the results are plotted together in Fig. 4 in the form of normalized maximum permanent deflection w_{max}/h versus the impulsive loading parameter $I^2/h^2p_0\rho$. The impulsive load result of Eq. (13) is also shown for comparison. The experimental data appears to agree with the prediction at low levels ($w_{max}/h \le 10$), but deviates significantly from it at high levels.

Symonds and Mentel [5] extended the solution for the rigid-plastic beams to include effects of axial tension for the case of impulsive loading. It results in a nonlinear correction term for Eq. (13) in the form

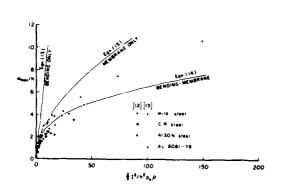
$$\frac{w_{\text{max}}}{h} + \frac{4}{3} \left[\frac{p_0(s \cdot s \cdot)}{p_0} \right]^2 \left(\frac{w_{\text{max}}}{h} \right)^3 = \frac{2}{3} \frac{1^2}{h^2 p_0 \rho}$$
 (14)

where $p_0(s.s.)$ is the static collapse load for the simply supported beam. This result is valid for $w_{max}/h \le 0.5$. For response beyond this limit, the membrane force reaches its maximum value with resulting zero moment, and the beam responds as a taut string. Using an approximate analysis to this problem, Symonds and Mentel [5] give the following estimate of the maximum permanent deflection

$$\frac{w_{\text{max}}}{h} = \frac{IL}{2h^2\sqrt{\sigma_V\rho}} - \frac{1}{4} \frac{p_0}{p_0(s \cdot s \cdot)}$$
 (15)

Because of the nature of the approximations, Symonds and Mentel estimate that Eq. (15) should provide an upper bound for the permanent deflection.

The clamped beam test results processed from the experiments of Humphreys [12] and Jones, Griffin and Van Duzer [13] are presented in Fig. 5 along with the predictions of Eqs. (13), (14) and (15). It appears that Eq. (15) fits the aluminum specimen data fairly well but is significantly above the steel results. Much of this difference can probably be attributed to the rate sensitivity of the latter. It is also clear that Eq. (14) lies close to the experimental data for low loads but lies significantly below it at high loads. Symonds and Mentel [5] have noted this and suggested that for high loads the deflection should vary linearly with impulse as given by Eq. (15) but that the result should fall between Eqs. (14) and (15).



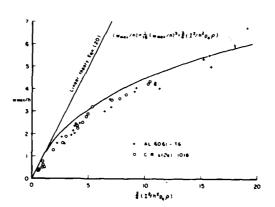


Fig. 5. Permanent Deflection of Clamped Beam With Axial Restraint.

Fig. 6. Permanent Deflection of Simply Supported Circular Plates.

5. PLATES

The deflected shape of a plate is generally not a developable surface and so stretching occurs even when free in-plane motion is allowed at the edges. Therefore, pure bending theory is restricted not only to thin plates, but also to small deflections.

For a perfectly plastic material, the static uniform lateral pressure capacity of a circular plate [14] is given by

$$p_0 = \frac{3}{2} \sigma_Y(\frac{h}{R})^2 = 6 \frac{M_0}{R^2}$$
 (16)

and

$$p_0 = 2.815 \sigma_Y(\frac{h}{R})^2 = 11.26 \frac{M_0}{R^2}$$
 (17)

for simply supported and clamped edges, respectively, where ${\rm M}_{\rm O}$ is given by Eq. (5), h is the plate thickness, and the Tresca yield criteria is used.

For rectangular plates, the solutions depend also on the aspect ratio a/b, where a is the length of the plate and b is its width (a>b). The static collapse pressure for simply supported edges is:

$$p_o = \frac{3}{2(3-2\beta)} \sigma_Y \left(\frac{2h}{b}\right)^2 = \frac{6M_o}{(b/2)^2(3-2\beta)}$$
 (18)

where the aspect ratio parameter β is given by [15]:

$$\beta = (b/a) [\sqrt{3 + (b/a)^2 - b/a}]$$
 (19)

For a clamped plate, p_0 is 1.9 to 2.0 times larger than that given by Eq. (18), depending on the yield criterion used in the analysis.

Linear pure bending theory is adequate when w/h < 0.4 for simply supported plates or w/h < 0.5 for clamped plates. Larger deflections require inclusion of the membrane stresses which as a result yields nonlinear equations for w_{max}/h .

5.1 Dynamic Response of Circular Plates

The permanent deflection of circular plates due to a pressure pulse of magnitude p_m and duration τ_0 was studied by Hopkins and Prager [16] and Florence [17] for simply supported and clamped edges, respectively. They used linear pure bending theory with rigid-plastic material obeying the Tresca yield criterion. Their solutions may be written together as

$$\frac{2\rho h}{p_{o}^{T}o^{2}} w_{max} = \begin{cases} 2 \frac{p_{m}}{p_{o}} {p_{m} \choose p_{o}} - 1 & , & 2 > \frac{p_{m}}{p_{o}} > 1 \\ \frac{3}{2} \frac{p_{m}}{p_{o}} {p_{m} \choose p_{o}} - \frac{2}{3} & , & \frac{p_{m}}{p_{o}} > 2 \end{cases}$$
(20)

where p_0 is given in Eqs. (16) and (17) for the two boundary conditions.

Florence [18] obtained test results for circular plates and these are replotted in Fig. 6. The linear prediction of Eq. (20) for $p_m/p_0 \rightarrow \infty$ and $\tau_0 \rightarrow 0$ is also shown for comparison, and is clearly not very good. Jones [19] improved the theoretical predictions by including both bending and membrane effects, but his results are in a form that cannot be easily presented.

Here we propose an empirical curve of the form of Eq. (14) for beams. The result is plotted in Fig. 6 where the 1/16 coefficient of the cubic term was obtained simply by adjusting the curve downward until it gave a close upper bound to the data.

5.2 Dynamic Response of Rectangular Plates

The permanent response of a rigid-plastic rectangular plate to a uniform pressure pulse was studied by Jones [15]. He assumed deflection shapes similar to the static ones even for large dynamic pressures for which an initial flat area in the centre was observed in tests [20]. His solution for a rectangular pulse shape may be written for simply supported and clamped plates as:

$$\frac{2\rho h}{p_0 \tau_0^2} w_{\text{max}} = \frac{3-\beta}{2-\beta} \cdot \frac{2}{\gamma^2 \tau_0^2} \cdot \left\{ \left[1 + 2\bar{p}(\bar{p} - 1)(1 - \cos \gamma \tau_0) \right]^{1/2} - 1 \right\}$$
 (21)

where p_0 is the static collapse pressure of Eq. (18), $\bar{p} = p_m/p_0$ and the parameter γ is defined by

$$\gamma^2 = \frac{24 \sigma_{\rm Y}}{\rho b^2} \cdot (1 - \beta + \frac{1}{2-\beta})/(3 - 2\beta) \tag{22}$$

Note that γ has the units of frequency and hence it provides a second natural time scale of the structure. Unfortunately Eq. (21) does not include the effect of membrane stresses.

Experimental results [21] of the permanent deflection at the centre of built-in rectangular plates (a/b=1.69) under impulsive lateral pressure are presented in Fig. 7. (The data with edge slippage were not included.) Note that the results for the mild steel specimens fall significantly below the the aluminum ones which is consistent with the fact that the mild steel is much more strain rate sensitive than the aluminum. Two theoretical curves are also shown for comparison. The linear prediction of

$$\frac{w_{\text{max}}}{h} = \frac{4 - \beta}{2(3 - \beta)} \frac{I^2}{h^2 p_0 \rho}$$
 (23)

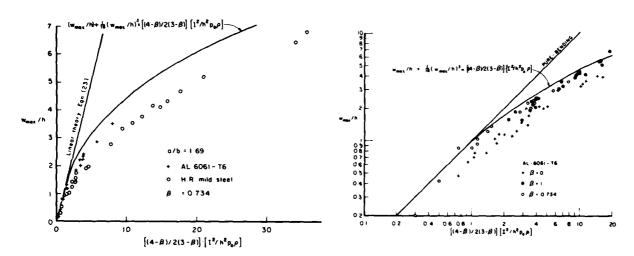


Fig. 7. Permanent Deflection of Clamped Rectangular Plates.

Fig. 8. Combined Results, Beams and Plates.

which was derived in [1] for impulsive loading appears to be adequate only for $w_{max}/h \le 1$. The other curve is the empirical nonlinear upper bound curve of Fig. 6 with appropriate modifications for aspect ratio for rectangular plates. Again it appears to provide a reasonable upper bound.

6. COMBINED RESULTS

In considering the response of structures to lateral blast loading, it is common to present the permanent response of beams and plates separately. The method proposed here, which includes effects of aspect ratio, combines and unifies the presentation of results for all impulsively loaded flat structures. Thus, the test results for clamped beams, simply supported circular plates and clamped rectangular plates are presented together in Fig. 8 in a log-log plot. Only the aluminum 6061-T6 specimen data are shown in order to emphasize the structural effects and minimize the material property effects. The maximum permanent deflections of the beams are slightly lower than those of the plates. Note, however, that the edges of the circular plates were without in-plane restraints. It is seen from Fig. 8 that all the experimental data are effectively collapsed together and the fitted curve provides a reasonable upper bound for all the data.

7. CONCLUDING REMARKS

The iso-response plot has not been included herein because of the lack of experimental results and theoretical solutions over the full duration of loading. The $\bar{p}-\bar{1}$ relations discussed in [1], were obtained for pure-bending and rigid-plastic approximations which introduce two major disadvantages: 1) with the exception of beams which are not axially restrained, the pure-bending solutions are restricted to small deflections, and 2) the rigid-plastic approximation does not correctly model the natural frequency of the structure, and hence the solutions are only valid for durations of loading well removed from the natural period of the structure. Hence, these equations have little practical significance.

Another assumption in these solutions, and also in their nonlinear extensions, is the rectangular shape of the history of loading. When the loading is not impulsive, the response depends on the history of loading and therefore the iso-response plot obtained with the rectangular assumption will differ from reality. Correlation parameters between different shapes of loading may provide the means to apply iso-response plots of the rectangular pulse to other shapes, but these parameters have yet to be verified.

Further research is needed to establish realistic iso-response plots even for simple shapes of loading. These require nonlinear theoretical solutions and extensive test programs that cover the dynamic loading realm. At present, even the simplified rigid-plastic approximate solutions are incomplete in that for beams and circular plates the solutions are for impulsive loading only. The nonlinear analysis of rectangular plates reviewed herein, did not allow for deflection modes other than the static one. It appears from the analytical complications which arise even for the most simplified structural and material approximations that one has to resort to numerical methods in order to obtain more realistic results for the entire range of loading.

Further research is also required to investigate the effect of different shapes of loading. Hopefully correlation parameters can be found to cover such effects and thereby reduce the number of iso-response plots required to cover all loading shapes. The area of stiffened plates and anisotropic plates has hardly been touched and much work is needed here [1].

8. ACKNOWLEDGEMENT

This work was supported by the Canadian Department of National Defence through a contract from the Defence Research Establishment Suffield.

9. REFERENCES

- J. ARI-GUR, D.L. ANDERSON and M.D. OLSON 1983 Dept. of Civil Eng., Struc. Res. Series Rept. No. 30, U.B.C., Vancouver, Canada. Air-Blast Response of Beams and Plates.
- 2. W.E. BAKER, P.S. WESTINE and F.T. DODGE 1973 Similarity Methods in Engineering Dynamics, Spartan Books, Hayden Book Company, New Jersey.
- 3. C.K. YOUNGDAHL 1970 J. of Applied Mechanics 37(3), Trans. ASME, Sept., 744-752. Correlation Parameters for Eliminating the Effect of Pulse Shape on Dynamic Plastic Deformation.
- 4. D.N. ROBINSON 1970 J. of the Mechanics and Physics of Solids, 18(1),

- February, 65-80. Displacement Bound Principle for Elastic-Plastic Structures Subjected to Blast Loading.
- 5. P. SYMONDS and P. MENTEL 1958 J. of the Mechanics and Physics of Solids, 6(3), 186-202. Impulsive Loading of Plastic Beams with Axial Constraints.
- 6. T. NONAKA 1977 Inginieur-Archiv, 46(1), February, 35-52. Shear and Bending Response of a Rigid-Plastic Beam to Blast-Type Loading.
- 7. M.J. FORRESTAL and M.J. SAGARTZ 1978 J. of Applied Mechanics, 45(3), Trans. ASME, September, 685-687. Elastic-Plastic Response of 304 Stainless Steel Beams to Impulse Loads.
- 8. M.J. FORRESTAL and D.L. WESENBERG 1977 J. of Applied Mechanics, 44(4), Trans. ASME, December, 779-780. Elastic-Plastic Response of Simply-Supported 1018 Steel Beams to Impulse Loads.
- 9. W.E. BAKER and P.S. WESTINE 1969 AIAA J., 7(5), May, 951-959. Modelling the Blast Response of Structures Using Dissimilar Materials.
- 10. P.S. SYMONDS 1962 Proc. of the Second U.S. National Congress of Applied Mechanics, ASME, 505-515. Large Plastic Deformations of Beams Under Blast Type Loading.
- 11. A.L. FLORENCE and R.D. FIRTH 1965 J. of Applied Mechanics, 32(3), Trans. ASME, September, 481-488. Rigid Plastic Beams Under Uniformly Distributed Impulses.
- 12. J.S. HUMPHREYS 1965 J. of Applied Mechanics, 32(1), Trans. ASME, March, 7-10. Plastic Deformation of Impulsively Loaded Straight Clamped Beams.
- 13. N. JONES, R.N. GRIFFIN and R.E. VAN DUZER 1971 Int. J. of Mechanical Sciences, 13(8), August, 721-735. An Experimental Study into the Dynamic Plastic Behaviour of Wide Beams and Rectangular Plates.
- 14. H.G. HOPKINS and W. PRAGER 1953 J. of the Mechanics and Physics of Solids, 2(1), 1-13. The Load Carrying Capacities of Circular Plates.
- 15. N. JONES 1971 Int. J. of Solids and Structures, 7, 1007-1029. A Theoretical Study of the Dynamic Plastic Behaviour of Beams and Plates with Finite-Deflections.
- 16. H.G. HOPKINS and W. PRAGER 1954 ZAMP (J. of Applied Mathematics and Physics), 5, 317-330. On the Dynamics of Plastic Circular Plates.
- 17. A.L. FLORENCE 1966 J. of Applied Mechanics, 33(2), Trans. ASME, June, 256-260. Clamped Circular Rigid-Plastic Plates Under Blast Loading.
- 18. A.L. FLORENCE 1966 Int. J. of Solids and Structures, 2(1), 37-47. Circular Plates Under a Uniformly Distributed Impulse.
- 19. N. JONES 1968 J. of Applied Mechanics, 35(1), Trans. ASME, March, 59-65. Impulsive Loading of a Simply Supported Circular Rigid Plastic Plate.
- 20. C.A. ROSS, W.S. STRICKLAND and R.L. SIERAKOWSKI 1977 Shock and Vibration Digest, 9(12), December, 15-26. Response and Failure of Simple Structural Elements Subjected to Blast Loadings.
- 21. N. JONES, T.O. URAN and S.A. TEKIN 1970 Int. J. of Solids and Structures, 6, 1499-1512. The Dynamic Plastic Behaviour of Fully Clamped Rectangular Plates.

SEZ